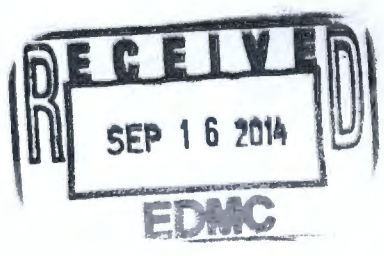


1226906
[0083701]

WCH-520
Rev. 1

River Corridor Closure Contract

Performance Assessment for the Environmental Restoration Disposal Facility, Hanford Site, Washington



August 2013

For Public Release

*cross ref -
1226903
1226904
1226905*

Washington Closure Hanford
Prepared for the U.S. Department of Energy, Richland Operations Office
Office of Assistant Manager for River Corridor



570 pgs

100-100000

TRADEMARK DISCLAIMER

Reference herein to any specific commercial product, process, or service by trade name, trademark, manufacturer, or otherwise, does not necessarily constitute or imply its endorsement, recommendation, or favoring by the United States Government or any agency thereof or its contractors or subcontractors.

This report has been reproduced from the best available copy.

Printed in the United States of America

RECEIVED
SEP 1 1952

100-100000

DOCUMENT
CONTROL

8/28/2013

WCH-520
Rev. 1

STANDARD APPROVAL PAGE

Title: Performance Assessment for the Environmental Restoration Disposal Facility,
Hanford Site, Washington

Author Name: S. Mehta, W. J. McMahon, R. Khaleel, S. M. Baker, B. Sun, C. Courbet,
N. Hasan

Approval: W. A. Borlaug, Waste Operations Project Engineer

W.A. Borlaug
Signature

8/27/2013
Date

The approval signature on this page indicates that this document has been authorized for information release to the public through appropriate channels. No other forms or signatures are required to document this information release.

**River Corridor
Closure Contract** 

**Performance Assessment for the
Environmental Restoration
Disposal Facility, Hanford Site,
Washington**

August 2013

Authors:

**S. Mehta
W. J. McMahon
R. Khaleel
S. M. Baker**

**B. Sun
C. Courbet
N. Hasan**

For Public Release

Washington Closure Hanford

Prepared for the U.S. Department of Energy, Richland Operations Office
Office of Assistant Manager for River Corridor



EXECUTIVE SUMMARY

This document provides a performance assessment (PA) analysis of the Environmental Restoration Disposal Facility (ERDF), located within the Central Plateau of the Hanford Site in southeastern Washington (Figure ES-1). The projected impacts of disposal of radionuclides to the environment are compared with applicable U.S. Department of Energy (DOE) and U.S. Environmental Protection Agency (EPA) standards as per DOE O 435.1 Chg 1, *Radioactive Waste Management*¹. Occupational radiological doses and impacts of nonradioactive, hazardous constituents are beyond the scope of this radiological PA.

The fundamental objective of the ERDF is to support the timely removal and disposal of Hanford Site remediation waste, primarily from cleanup of contaminated waste sites. However, disposal of investigation-derived waste; decontamination and decommissioning waste; waste from *Resource Conservation and Recovery Act of 1976 (RCRA)* past-practice operable units and closures; and non-RCRA waste from inactive treatment, storage, and disposal units is also allowed.

Beginning in 1996, ERDF started accepting low-level radioactive, hazardous, and mixed wastes that were generated during the cleanup activities at the Hanford Site. Designed to be expanded as needed, ERDF is composed of a series of cells or disposal areas. For cells 1 through 8, each cell is 21 m (70 ft) deep and 152 m (500 ft) by 152 m (500 ft) at the base. Cells 9 and 10 are "supercells" and each are equal to two regular cells in extent (152 m [500 ft] by 305 m [1,000 ft] at the base) but have the same depth of 21 m (70 ft). Figure ES-2 illustrates the ERDF site during its construction phase. As of July 2013, approximately 13.6 million metric tons of waste has been disposed at ERDF, which occupies approximately 6.5 million m³ of volume. The ERDF is intended to continue operations until the remediation efforts are completed per the record of decision (ROD), which was approved in 1995. Another two decades of waste receipt is expected from *Comprehensive Environmental Response, Compensation, and Liability Act of 1980 (CERCLA)* waste site remediation efforts across the Hanford Site. No offsite (non-Hanford Site) waste is permitted in ERDF.

¹ DOE O 435.1 Chg 1, 2001. *Radioactive Waste Management*, U.S. Department of Energy, Washington, D.C.

Figure ES-1. Hanford Site and Environmental Restoration Disposal Facility Location
(see Figure ES-2 for ERDF Details).

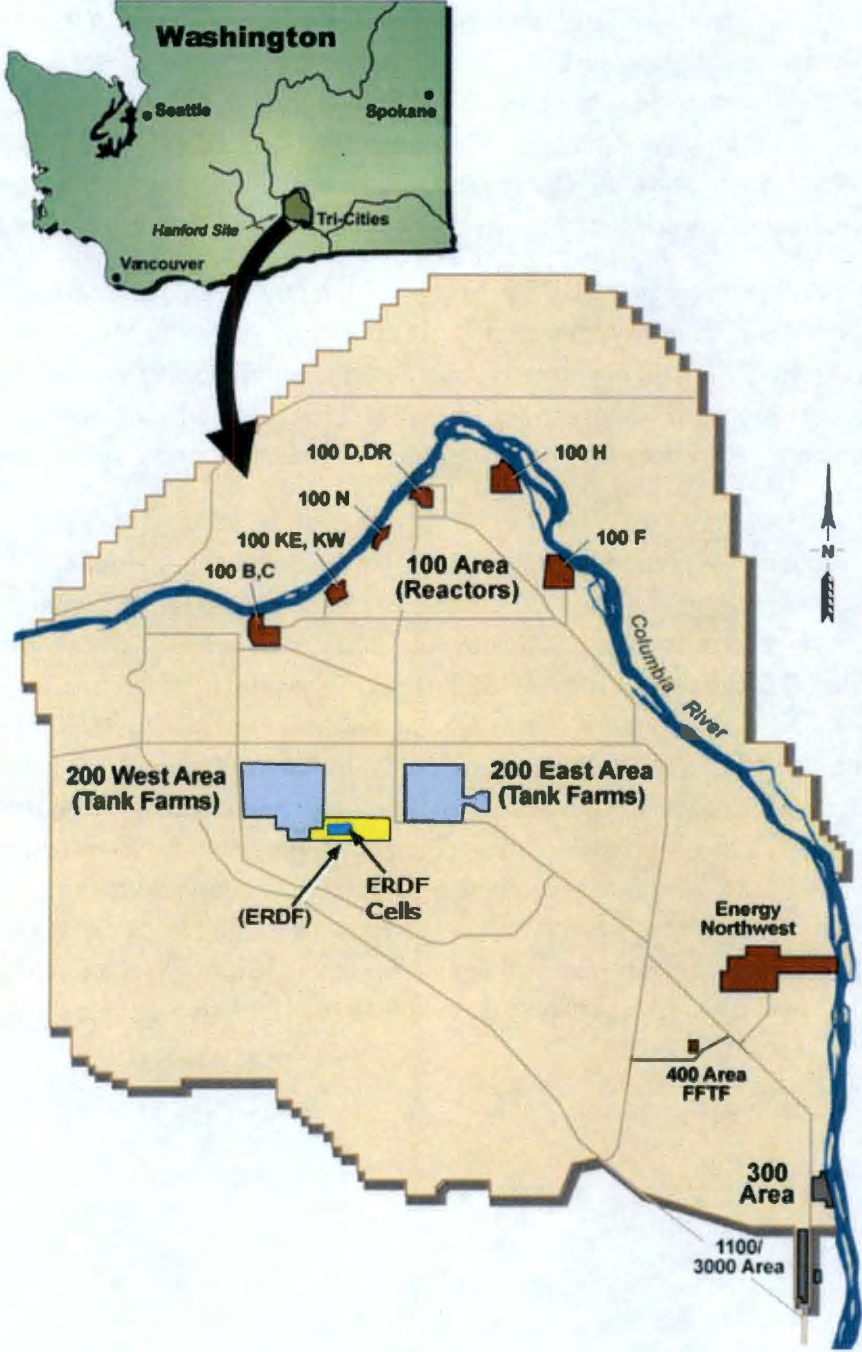


Figure ES-2. Environmental Restoration Disposal Facility Site During Its Construction Phase (August 2010).

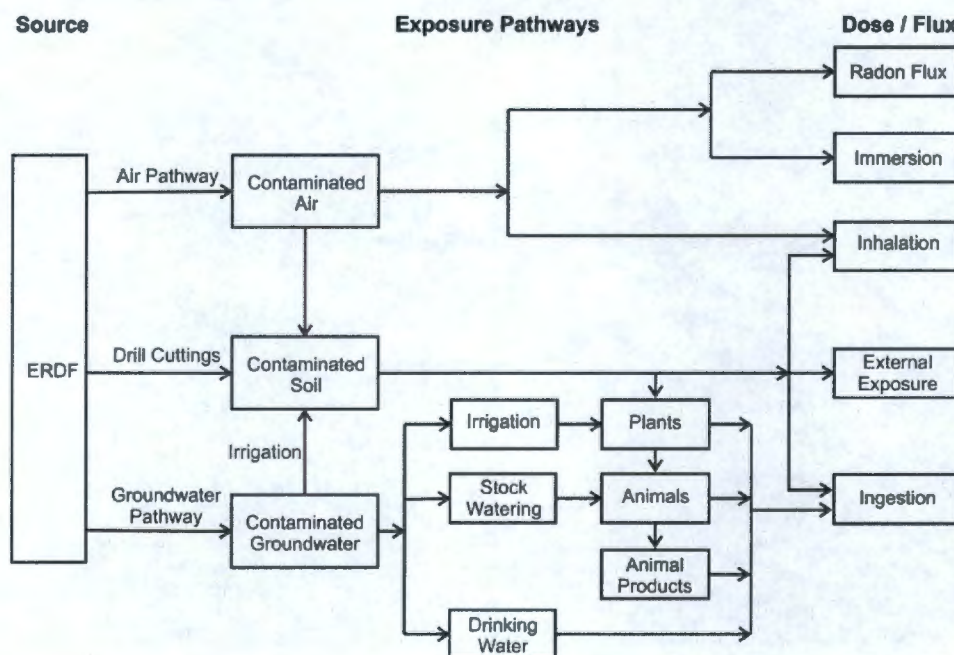


The various pathways of possible exposure are illustrated in Figure ES-3. The major pathways for contamination entering the environment are the groundwater pathway, the air pathway, and an inadvertent intruder pathway (through drill cuttings brought to the surface). The most important exposure pathway for hydrologic transport is groundwater use for drinking water, irrigation, livestock watering, and biotic transport. Under the groundwater pathway, it is assumed that moisture from rain and snowfall enters the subsurface, contacts waste, and carries dissolved contaminants through the thick heterogeneous vadose zone to the unconfined aquifer. Therefore, a primary focus of the PA is estimating the groundwater all-pathways dose to a hypothetical member of the public (i.e., receptor) who

- Consumes contaminated groundwater, leafy vegetables, and produce that were irrigated with contaminated groundwater, and
- Consumes milk and meat from animals that in turn consume contaminated water and fodder that was irrigated with contaminated groundwater (Figure ES-3).

During the compliance and post-compliance periods, the receptor is assumed to reside 100 m downgradient from the eastern edge of the facility, which is assumed to be the edge of the ERDF berm. The surface water pathway is not a possible exposure pathway for the disposal facility because surface water is not present near ERDF, and is too limited on the Hanford Site Central Plateau in quantity to be used domestically.

Figure ES-3. Overview of the Analysis of Performance for the Environmental Restoration Disposal Facility Performance Assessment.



For the purpose of assessing the long-term performance, a closure date of year 2035 is assumed for ERDF. In the post-closure assessment, four time periods are considered: (1) a 100-year institutional control period when the surface cover and double leachate liner are working to their full barrier capability resulting in effectively zero recharge rate under the base of ERDF; (2) a 400-year degraded liner period (from 100 years to 500 years following closure) within which the double leachate liner is assumed to be effectively degraded but the surface cover remains intact; (3) the time period from 500 years after closure up to the DOE O 435.1-defined compliance time period of 1,000 years, during which the surface cover barrier function is assumed to be fully degraded at the start of the time period (assuming a design life of 500 years); and (4) the post-compliance period (beyond 1,000 years) up to 10,000 years for the purpose of evaluating uncertainty and sensitivity on dose estimates. Maximum dose from long-lived mobile contaminants occurs within this time period.

The ERDF PA methodology includes deterministic calculations of the estimated impacts from the proposed closure action. The dose impacts are calculated with the numerical models and a set of input values and assumptions that are most representative of the disposal system. This case is referred to as the *compliance* case. The compliance case provides the “expected” estimate for how the system may perform given the information available; it is assumed to provide a reasonable estimate of the expected performance. Uncertainty and sensitivity analyses are performed to understand the importance of key input parameters on transport behavior and dose.

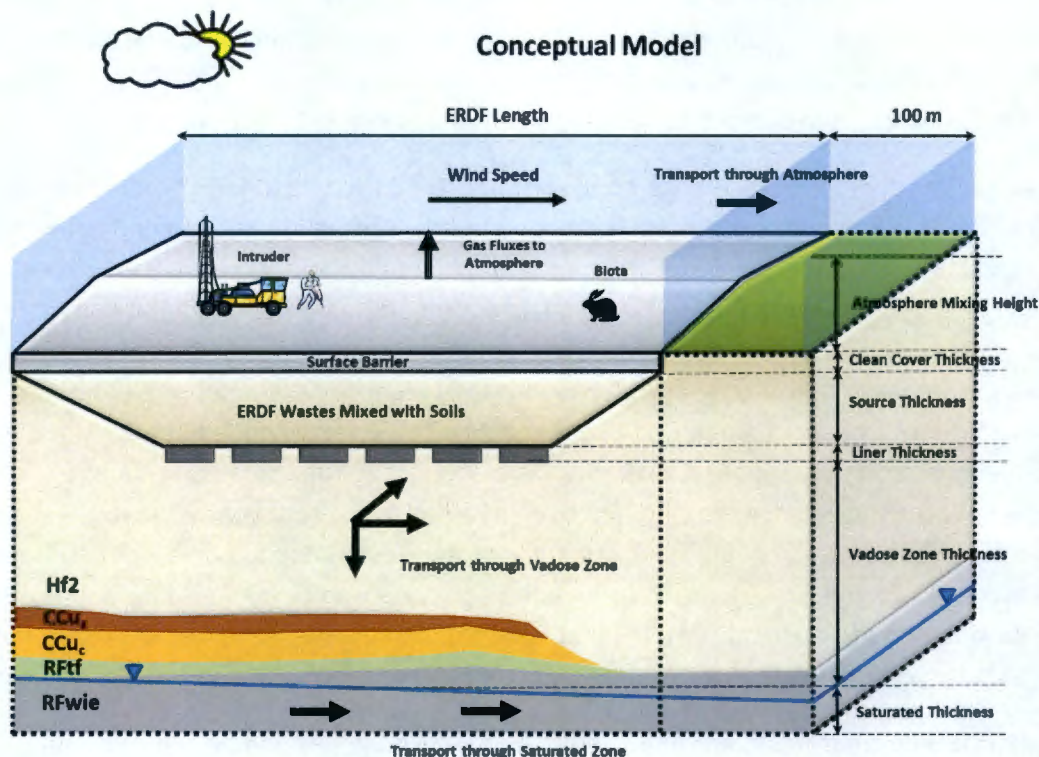
All disposed radionuclides at ERDF with relatively long half-lives (>6 years) and/or non-negligible inventories (>1 Ci) are considered for the purpose of the PA. Few radionuclides, regardless of inventory, that were deemed important to PA analysis dose estimates are also included in this group (e.g., radium-226, iodine-129). In addition, certain radionuclides are added to the list for which no current inventory is available but that may in-grow from the decay of parent radionuclides. A total of 46 radionuclides are evaluated in the ERDF PA.

The source term for the compliance case analysis considered two waste forms present in ERDF for all radionuclides, except for carbon-14: untreated waste (contaminated soil) and activated metals. Some waste emplaced at ERDF is grouted waste, but the fraction is very small and conservatively included as part of the untreated waste. For carbon-14, most of the inventory (93%) is associated with insoluble waste (derived from graphite blocks) with the remaining inventory associated with activated metals (predominantly steel components) and untreated waste (derived from disposal of reactor gas condensate). The inventory used in the source term model includes the currently disposed inventory (as of August 2010) and the forecasted inventory from waste sites where cleanup has been planned from fiscal year 2011 to the closure time (year 2035). The majority of the forecasted inventory is estimated to come from 100 Area reactor buildings (including pipelines with associated soil, solid waste, and building debris), remaining solid waste sites (e.g., 118-K-1 Burial Ground), and the two solid waste sites in the 300 Area (618-10 and 618-11 Burial Grounds that contain uranium metals and research waste).

Radionuclides in untreated waste are assumed to be mixed homogeneously in the soil and readily leachable (soluble) in the presence of infiltrating water. The inventory of carbon-14 associated with insoluble waste and the small fraction associated with activated metal is released based on graphite leach rates. For other activated metal, such as niobium-94, nickel-59, and nickel-63, a conservative solubility limit based on solubility of hydrous ferric oxide is imposed for source-term release assuming congruent dissolution.

The ERDF conceptual model is composed of manmade as well as natural components (Figure ES-4). The manmade components of the system that influence contaminant migration include a closure surface barrier, a double-liner leachate collection system, the ERDF cells and infrastructure, and the distribution of waste in the subsurface. The natural components of the system that influence contaminant migration are the several underlying nearly horizontal stratigraphic layers within the vadose zone and the unconfined aquifer. The PA modeling considered reduction of net infiltration from the presence of a double leachate collection liner system at the base and an engineered cover (surface barrier) over ERDF. The liner system is installed during construction of the cells, and the surface barrier is assumed to be installed on ERDF at closure in 2035. The surface barrier and double leachate collection liner system are assumed to remain intact and allow only negligible amounts of net infiltration for the first 100 years (i.e., 2035 to 2135), coinciding with the institutional control time period.

Figure ES-4. Schematic Conceptual Representation of the ERDF Site and Various Pathways.



During the next 400 years (i.e., 2135 to 2535), the capability of the double-liner system is assumed to degrade, but the capability of surface barrier is assumed to remain intact. Net infiltration leading to recharge is estimated to be 0.50 mm/yr during this time. After this time (i.e., 500 years after post-closure), the capability of the surface barrier to limit net infiltration is assumed to be diminished also, leading to a maximum infiltration rate of 1 mm/yr (for compliance case calculations) for the remaining duration.

Based on the conceptual models for different pathways, numerical models were developed to estimate the contaminant concentrations within water, air, or soil as a function of time. A three-dimensional flow and transport model was developed using the Subsurface Transport Over Multiple Phases (STOMP) code developed by Pacific Northwest National Laboratory to evaluate the impact to the environment from the groundwater pathway. The model assumed that infiltration of moisture from precipitation eventually enters the facility, but most of the moisture is diverted around ERDF during operations and for the first 100 years after closure. Once the double liner is assumed to be degraded, the contaminants, based on their relative inventories associated with a given waste form type, are released into the vadose zone by contact with recharge water (the release of carbon-14 inventory associated with graphite and activated metals is based on the graphite leaching rate). The infiltrating moisture, along with

contaminants, travels through the vadose zone, with the contaminant transport times influenced by the equilibrium sorption characteristics (determined by the distribution coefficient [K_d]). The contaminants travel through the vadose zone until they reach the water table and the unconfined aquifer. The contaminant breakthrough curves (contaminant concentration in groundwater versus time) are obtained for different radionuclides. Exposure scenario dose coefficients specific to the chosen exposure scenario are then applied to transform groundwater concentrations to dose quantities to determine total effective dose equivalent on a per-year basis.

All-pathway dose calculations are performed by evaluating the long-term release of radionuclides from ERDF along the groundwater and atmospheric pathways. The groundwater pathway modeling analysis is the most complex and included the following:

- (a) An initial one-dimensional screening analysis to identify radionuclides that cannot provide calculable groundwater contamination over the duration of the simulation and thus can be screened out from detailed three-dimensional calculations. Using conservative recharge rates and hydraulic properties it was determined that radionuclides with a $K_d > 0.1$ mL/g require no detailed analysis for the 1,000-year compliance time frame, and radionuclides with a $K_d > 0.9$ mL/g require no detailed analysis for the 10,000-year post-compliance period. As a result of the screening, radionuclides with $K_d > 0.9$ mL/g are excluded from further consideration in the groundwater pathway calculations.
- (b) A three-dimensional flow and transport analyses for the compliance case with the parameter values set at their expected values. This involved determining the appropriate boundary conditions under steady-state conditions that are expected in the future. No breakthrough of contaminant was observed within the 1,000-year compliance time period at the 100-m downgradient compliance location in the saturated zone. The first breakthrough of nonretarded contaminants occurred after 2,000 years.
- (c) One-dimensional abstraction models for performing uncertainty analyses and multiple parameter sensitivity analyses. For the uncertainty analysis, including evaluation of the coupled effects of uncertainty in source term, engineered system, and natural system, a PA abstraction model was developed. A full uncertainty analysis using the Monte Carlo sampling methodology was undertaken by developing stochastic inputs and performing multi-realization simulations. Uncertainty in the dose estimates are calculated for the compliance and post-compliance time periods. Most important, stochastic parameters that contribute significantly to the uncertainty in total dose for the groundwater pathway are saturated hydraulic conductivity, flow velocities (flow-field selector) in the vadose zone, and K_d of technetium-99. For the sensitivity phase, model input parameters were varied one at a time.

Under the atmospheric pathway, for a limited number of radionuclides that can partition into the gas phase from dissolved phase (e.g., carbon-14, hydrogen-3, iodine-129, and radon-222), a conservative one-dimensional modeling is performed to estimate diffusive release from the ERDF into the atmosphere across the modified RCRA-compliant closure cover (Figure ES-4).

The results indicate that the atmospheric carbon-14 release is the dominant release in comparison to other radionuclides. It is sustained by a slow continuous release from the source term as a function of the graphite leaching rate.

Under the intruder scenarios, a well is drilled through the emplaced ERDF waste all the way to the water table and the contamination is then brought to the surface as part of the drill cuttings where it can cause human exposure (Figure ES-4). One acute well drilling and three chronic inadvertent intruder (commercial farm, rural pasture, and suburban garden) scenarios were evaluated. Although the likelihood of an inadvertent intrusion at ERDF is very small in the foreseeable future, for the purpose of compliance calculations, passive and active institutional controls are assumed to be ineffective in preventing temporary intrusion after 100 years following closure. In other words, loss of institutional controls is assumed after 100 years following closure and peak dose is evaluated assuming inadvertent intrusion occurs immediately after the loss of institutional controls.

The PA results of the all-pathways, atmospheric, radon flux, inadvertent intruder, and groundwater (water resources) protection analyses are shown in Table ES-1 for the compliance and post-compliance periods. Only the peak values of the effective dose equivalent or peak concentrations are compared to the standards. The only dose calculated in the all-pathways analysis within the 1,000-year compliance time period is from the air pathway; there are no impacts to groundwater during this period. For the all-pathway dose calculations, the peak dose within the compliance time period (1.02 mrem/yr) is predominantly from the carbon-14 atmospheric pathway, while for the post-compliance time period the peak dose of 1.88 mrem/yr is predominantly from technetium-99 from the groundwater pathway. The PA results indicate that the performance objectives and measures for atmospheric, all-pathways, radon, inadvertent intruder, and groundwater protection are met for both the 1,000-year compliance time period (2035 to 3035) and the post-compliance period (3035 to 12035). Therefore, there is a reasonable expectation that performance objectives and measures established for the long-term protection of the public and the environment will not be exceeded following closure of ERDF.

Note that, for the post-compliance time period, Table ES-1 shows the all-pathway dose to be 1.88 mrem/yr and the groundwater protection dose to be 3.3 mrem/yr. This apparent difference is due to usage of latest DOE effective dose coefficient for ingested water (DOE-STD-1196-2011, *DOE Standard Derived Concentration Technical Standard*²) for the all-pathway dose calculation while using the EPA maximum contaminant level (40 CFR 161³) for the groundwater protection calculation.

² DOE-STD-1196-2011, 2011, *DOE Standard Derived Concentration Technical Standard*, U.S. Department of Energy, Washington, D.C.

³ 40 CFR 61, "National Emission Standards for Hazardous Air Pollutants," *Code of Federal Regulations*. Available at: <http://www.gpo.gov/fdsys/pkg/CFR-2010-title40-vol8/xml/CFR-2010-title40-vol8-part61.xml>.

Table ES-1. Comparison of Performance Objectives and the Environmental Restoration Disposal Facility Performance Assessment Results for the Compliance and Post-Compliance Periods.

Performance Objective and/or Measure	Standard	Performance Assessment Results	
		Compliance Period (2035-3035) ^a	Post-Compliance Period (3035-12035) ^a
All pathways (DOE O 435.1 Chg 1)	25 mrem/yr EDE	1.02 mrem/yr	1.88 mrem/yr
Atmospheric (40 CFR 61, Subpart H)	10 mrem/yr EDE	1.02 mrem/yr	0.51 mrem/yr
Atmospheric (40 CFR 61, Subpart Q)	20 pCi.m ⁻² .s ⁻¹ radon flux (at surface of disposal facility)	0.11 pCi.m ⁻² .s ⁻¹	0.08 pCi.m ⁻² .s ⁻¹
Acute inadvertent intruder (DOE O 435.1 Chg 1)	500 mrem EDE ^b	5.51 mrem ^f	NA
Chronic inadvertent intruder (DOE O 435.1 Chg 1)	100 mrem/yr EDE ^b	9.27 mrem/yr ^f	NA
Groundwater protection (water resources) (40 CFR 141)	Beta-gamma dose equivalent ≤ 4 mrem/yr	0 mrem/yr	3.3 ^c mrem/yr
	Gross alpha activity concentration (excluding radon and uranium) ≤ 15 pCi/L	0 pCi/L	1E-10 ^d pCi/L
	Combined Ra-226 and Ra-228 concentration ≤ 5 pCi/L	0 pCi/L	1E-10 ^d pCi/L
	Uranium concentration ≤ 30 µg/L	0 µg/L	1E-10 ^d µg/L
	Sr-90 concentration ≤ 8 pCi/L ^e	NA	NA
	H-3 concentration ≤ 20,000 pCi/L	0 pCi/L	1E-10 ^d pCi/L

^a Compliance at 100 m downgradient of ERDF except for inadvertent intruder scenarios.

^b Not applicable for post-compliance time period.

^c Beta-gamma dose equivalent ≤ 4 mrem/yr (based on federal MCL) and calculated as $(C_{Peak}/MCL)^* 4$ mrem/yr. For Tc-99, which contributes almost the entire dose, $C_{Peak}=731$ pCi/L and $MCL=900$ pCi/L, so the equivalent dose is calculated to be 3.3 mrem/yr.

^d Concentrations less than 1E-10 pCi/L are essentially zero.

^e Not applicable; Sr-90 was screened out during evaluation of the groundwater pathway due to its relatively short half-life and its low mobility in the subsurface.

^f Peak dose based on assumed inadvertent intrusion at 100 years following loss of institutional control. Peak occurs at 100 years after closure.

EDE = effective dose equivalent
MCL = maximum contaminant level
NA = not applicable

The ERDF PA groundwater and air pathway results are used to develop waste acceptance criteria and estimate radionuclide inventory threshold levels. For the groundwater pathway, the total inventory thresholds are only provided for those radionuclides that arrive at the compliance location in groundwater within the 10,000-year time period. These radionuclides are technetium-99, niobium-94, molybdenum-93, chlorine-36, and iodine-129. For all other radionuclides emplaced in ERDF, no inventory threshold is imposed.

The groundwater pathway total inventory thresholds for the compliance time (2035 to 3035) and post-compliance time (>3035) for the ERDF are presented in Table ES-2. The thresholds are based on the predicted maximum groundwater pathway dose and predicted maximum concentrations in groundwater at the compliance location 100 m downgradient of ERDF. Since the groundwater concentrations are practically zero within the compliance time period, no inventory limits are imposed within the compliance time period.

Table ES-2. Groundwater Pathway Inventory Thresholds for the Environmental Restoration Disposal Facility.

Radionuclide	Inventory Thresholds (Ci) Based on Dose ^a		Concentration Threshold (pCi/L)		Inventory Thresholds (Ci) Based on Concentration ^d		
	Compliance	Post-Compliance	Based on EPA MCL ^b	Based on DOE Standard ^c	Compliance	Post-Compliance (EPA MCL)	Post-Compliance (DOE Standard)
Tc-99	NL	724	900	1650	NL	65	120
Nb-94	NL	349	300	670	NL	26	58
Mo-93	NL	811	600	480	NL	165	134
Cl-36	NL	342	700	1200	NL	50	86
I-129	NL	2.90E+05	1	12	NL	5.00E+03	6.00E+04

^a Inventory thresholds were calculated based on all-pathway effective dose equivalent limit of 25 mrem/yr based on peak dose.

^b MCL based on U.S. Environmental Protection Agency regulations.

^c Concentration threshold is based on DOE-STD-1196-2011 effective dose coefficients for ingestion as presented in Table 3-28 by assuming 2 L/day drinking water ingestion and 4 mrem annual effective dose equivalent to a reference person.

^d Peak concentrations for Tc-99, Nb-94, Mo-93, Cl-36, and I-129 occur, respectively, at 7225, 7155, 6740, 7230, and 1,0000 years (Chapter 4.0).

MCL = maximum contaminant level

NL = not limiting

For the air pathway, only radionuclides carbon-14, hydrogen-3, and iodine-129 are considered as they are the only volatile radionuclides considered for air-pathway dose calculations. Iodine-129 is the only radionuclide that is present in both the groundwater pathway and air-pathway inventory threshold calculations. However, the air-pathway inventory thresholds for iodine-129 are much lower than for the groundwater pathway inventory thresholds and thus are considered as the ultimate inventory threshold for iodine-129.

A summary of the calculated and recommended inventory thresholds for the radionuclides of concern is presented in Table ES-3 based on the evaluation of both groundwater and air-pathway inventory thresholds. The calculated inventory thresholds are based on the compliance time period (year 2035 to year 3035). Where inventory thresholds are indeterminate within the compliance time period they are recommended based on the post-compliance inventory threshold limits based on an all-pathway effective dose equivalent limit of 25 mrem/yr.

Table ES-3. Calculated and Recommended Inventory Thresholds for Radionuclides of Concern.

Radionuclide	Calculated Inventory Thresholds (Ci)	Recommended Inventory Thresholds (Ci)
Tc-99	Not limiting	724 ^a
Nb-94	Not limiting	349 ^a
Mo-93	Not limiting	811 ^a
Cl-36	Not limiting	342 ^a
I-129	4	4 ^b
C-14	2.43E+04	2.43E+04 ^b
H-3	1.15E+06	1.15E+06 ^b

^a Inventory thresholds based on all-pathway effective dose equivalent limit of 25 mrem/yr (Table ES-2).

^b Inventory thresholds based on air-pathway effective dose equivalent of 10 mrem/yr.

TABLE OF CONTENTS

1.0	INTRODUCTION.....	1-1
1.1	GENERAL APPROACH.....	1-2
1.2	GENERAL FACILITY DESCRIPTION.....	1-3
1.2.1	Waste Acceptance Criteria.....	1-5
1.2.2	General Land-Use Patterns.....	1-6
1.3	LOW-LEVEL WASTE DISPOSAL FACILITY LIFE CYCLE.....	1-6
1.4	RELATED DOCUMENTS.....	1-7
1.4.1	ERDF Relevant Documents.....	1-7
1.4.2	Other Relevant Documents.....	1-8
1.5	PERFORMANCE CRITERIA.....	1-10
1.5.1	Public Protection Performance Objective.....	1-12
1.5.2	Water Resource Impact Assessment.....	1-13
1.5.3	Intruder Analysis.....	1-13
1.5.4	ALARA Analysis.....	1-16
1.6	SUMMARY OF KEY ASSESSMENT ASSUMPTIONS.....	1-17
1.6.1	Engineered Barrier Degradation.....	1-17
1.6.2	Model Domain and Boundary Conditions.....	1-18
1.6.3	Representation of Geologic Units.....	1-18
1.6.4	Infiltration and Recharge.....	1-19
1.6.5	Geochemistry and Sorption.....	1-20
1.6.6	Vadose Zone and Saturated Zone Flow and Transport.....	1-21
1.6.7	Groundwater Concentration.....	1-21
1.6.8	Post-Closure Inventory and Source Term.....	1-22
1.6.9	State of ERDF at Closure.....	1-23
1.7	COMPARISON OF THE ERDF PERFORMANCE ASSESSMENT TO OTHER HANFORD SITE PERFORMANCE ASSESSMENTS.....	1-24
1.8	QUALITY ASSURANCE MEASURES.....	1-26
1.8.1	STOMP.....	1-27
1.8.2	GoldSim.....	1-27
1.8.3	Documentation and Records.....	1-28
2.0	DISPOSAL FACILITY CHARACTERISTICS.....	2-1
2.1	SITE CHARACTERISTICS.....	2-1
2.1.1	Geography and Demography.....	2-1

2.1.2	Meteorology and Climatology	2-6
2.1.3	Ecology	2-10
2.1.4	Geology, Seismology, and Volcanology	2-11
2.1.5	Hydrology	2-35
2.1.6	Geochemistry	2-48
2.1.7	Natural Resources	2-49
2.1.8	Natural Background Radiation	2-49
2.2	PRINCIPAL FACILITY DESIGN FEATURES	2-50
2.2.1	Water Infiltration	2-50
2.2.2	Disposal Unit Cover Integrity	2-58
2.2.3	Structural Stability	2-59
2.2.4	Inadvertent Intruder Barrier	2-60
2.3	WASTE CHARACTERISTICS	2-60
2.3.1	Current ERDF Inventory	2-72
2.3.2	Currently Forecasted ERDF Inventory	2-75
3.0	ANALYSIS OF PERFORMANCE	3-1
3.1	OVERVIEW OF ANALYSIS	3-1
3.2	CONCEPTUAL MODEL OF FACILITY PERFORMANCE	3-3
3.2.1	Source Term	3-7
3.2.2	Radionuclide Transport	3-9
3.2.3	Exposure Pathways and Scenarios	3-10
3.3	SOURCE TERM	3-11
3.4	ENVIRONMENTAL TRANSPORT OF RADIONUCLIDES	3-20
3.4.1	Groundwater Transport Pathway	3-20
3.4.2	Atmospheric Transport Pathway	3-51
3.5	RADON ANALYSIS	3-59
3.6	BIOTIC PATHWAY	3-59
3.7	DOSE ANALYSIS	3-63
3.7.1	Groundwater Pathway Dose Analysis	3-63
3.7.2	Air-Pathway Dose Analysis	3-75
3.8	ALARA ANALYSIS	3-79
3.9	SENSITIVITY AND UNCERTAINTY ANALYSES	3-80
3.9.1	Overview	3-80
3.9.2	Three-Dimensional Numerical Transport Analyses	3-81

3.9.3	Groundwater-Pathway Uncertainty Analyses.....	3-81
3.9.4	Sensitivity Analyses.....	3-82
3.9.5	One-Dimensional Abstraction Analyses Methodology	3-82
3.9.6	Sensitivity and Uncertainty Analyses Database	3-89
4.0	RESULTS OF ANALYSES	4-1
4.1	SOURCE TERM	4-1
4.2	ENVIRONMENTAL TRANSPORT OF RADIONUCLIDES	4-2
4.2.1	Result of Screening Analysis for Groundwater Pathway	4-3
4.2.2	Results of Compliance Case Evaluation for Groundwater Pathway	4-4
4.2.3	Results of Compliance Case Evaluation for Groundwater Pathway for the Post-Compliance Period.....	4-18
4.2.4	Results of Compliance Case Evaluation for the Air Pathway	4-20
4.3	RADON ANALYSIS	4-29
4.4	BIOTIC PATHWAYS.....	4-30
4.5	DOSE ANALYSIS	4-30
4.6	SENSITIVITY AND UNCERTAINTY ANALYSIS	4-35
4.6.1	Uncertainty Analysis	4-35
4.6.2	Sensitivity Analysis for the Groundwater Pathway	4-63
4.6.3	Sensitivity Analysis for the Air Pathway	4-89
4.6.4	Comparison with 1995 ERDF Performance Assessment Results	4-92
4.6.5	Peak Dose Calculation	4-94
5.0	INADVERTENT INTRUDER ANALYSIS.....	5-1
5.1	ACUTE EXPOSURE SCENARIOS	5-3
5.1.1	Well Driller Acute Scenario: Ingestion.....	5-5
5.1.2	Well Driller Acute Scenario: Inhalation.....	5-5
5.1.3	Well Driller Acute Scenario: External Exposure	5-6
5.2	CHRONIC SCENARIOS	5-6
5.2.1	Rural Pasture Chronic Scenario	5-7
5.2.2	Suburban Garden Chronic Scenario.....	5-11
5.2.3	Commercial Farm Chronic Scenario.....	5-15
5.3	INTRUDER ANALYSIS RESULTS.....	5-18
5.3.1	Acute Exposure Dose.....	5-19
5.3.2	Chronic Exposure Dose.....	5-20
5.4	INTRUDER SENSITIVITY/UNCERTAINTY ANALYSIS	5-22

6.0	INTERPRETATION OF RESULTS	6-1
6.1	ALL-PATHWAYS DOSE	6-1
6.2	RADON FLUX RESULTS	6-3
6.3	BIOTIC PATHWAY RESULTS	6-4
6.4	GROUNDWATER PROTECTION RESULTS.....	6-4
6.5	INADVERTENT INTRUDER ANALYSIS RESULTS.....	6-6
7.0	PERFORMANCE EVALUATION	7-1
7.1	COMPARISON OF RESULTS TO PERFORMANCE OBJECTIVES	7-1
7.2	USE OF PERFORMANCE ASSESSMENT RESULTS.....	7-1
	7.2.1 Inadvertent Intruder Waste Concentration Disposal Thresholds	7-3
	7.2.2 Air-Pathway Waste Acceptance Criteria	7-12
	7.2.3 Summary of Inventory Thresholds	7-13
7.3	ALARA ANALYSIS.....	7-14
7.4	FUTURE WORK	7-15
8.0	PREPARERS	8-1
9.0	REFERENCES.....	9-1

APPENDICES

A	TECHNICAL BASIS FOR THE GROUNDWATER PATHWAY CONCEPTUAL MODEL: FIELD DATA AND RELATED INVESTIGATIONS.....	A-i
B	DEVELOPMENT OF THE FATE AND TRANSPORT MODEL FOR THE ENVIRONMENTAL RESTORATION DISPOSAL FACILITY PERFORMANCE ASSESSMENT TO EVALUATE THE IMPACT OF THE GROUNDWATER PATHWAY	B-i
C	VALIDATION OF THE AIR-PATHWAY MODELING APPROACH	C-i
D	SURFACE BARRIER AND LINER PERFORMANCE AND WATER ACCUMULATION IN THE ERDF ENGINEERED STRUCTURE	D-i
E	RECOMMENDATIONS FOR WASTE ACCEPTANCE CRITERIA.....	E-i

FIGURES

1-1.	Location of the ERDF Facility on the Hanford Site.....	1-4
1-2.	August 2010 Aerial View of the ERDF Looking South.....	1-5
2-1.	Population Centers Within an 80-km (50-mi) Radius of the Hanford Site.	2-3
2-2.	Hanford Meteorological Monitoring Network Location Map.....	2-7

2-3.	Wind Roses at the 9.1-m (30-ft) Level of the Hanford Meteorological Station Network, Washington, 1982 Through 2006 (PNNL-6415).	2-8
2-4.	Geologic Elements of the Pasco Basin Portion of the Columbia Basin, Washington.	2-12
2-5.	Geologic Setting of the Columbia Basin and Pasco Basin.	2-13
2-6.	Conceptualization of Flood Water South of the Hanford Site, Washington, Between 18,000 to 13,000 Years Ago.	2-15
2-7.	Geologic Structures of the Pasco Basin and Vicinity.	2-16
2-8.	Generalized Stratigraphy of the Hanford Site Including the Central Plateau (PNNL-6415).	2-17
2-9.	Map of the Ice Age Flood Deposits (Hanford Formation).	2-20
2-10.	Comparison Between ERDF and Generalized Hanford Site Stratigraphy.	2-21
2-11.	Location of Boreholes Used to Generate the ERDF Hydrogeologic Conceptual Model.	2-23
2-12.	Hydrogeologic Cross Section L2-L2'.	2-24
2-13.	Hydrogeologic Cross Section L4-L4'.	2-25
2-14.	Cross-Section Running from the Rattlesnake Mountains Through the 200 Areas and Out to the Columbia River.	2-28
2-15.	Hydrogeologic Units Present at the Water Table in June 1998.	2-29
2-16.	Topography of the 200 Areas Central Plateau.	2-31
2-17.	Earthquake Activity in the Vicinity of the Hanford Site Between 1890 and 1970 (PNNL-6415).	2-32
2-18.	Earthquake Activity in the Vicinity of the Hanford Site Between 1970 and 2005 (PNNL-6415).	2-33
2-19.	Surface Water Features of the Hanford Site (Modified from PNNL-6415).	2-36
2-20.	Water Table Elevations in Meters for Year 2011 for the Unconfined Aquifer In the Central Plateau Portion of Hanford Site.	2-41
2-21.	Discharge History for the 216-T Pond and the 216-U Pond.	2-43
2-22.	Discharge History for the 216-B Pond and Gable Mountain Pond.	2-43
2-23.	Hindcast Water Table Map of the Hanford Site, January 1944.	2-44
2-24.	Existing Groundwater Contamination Plumes near ERDF.	2-47
2-25.	Aerial View of ERDF with Cells Used for Disposal.	2-51
2-26.	Plan View for Cells 7 and 8.	2-51
2-27.	Generic Cross-Sectional View for Cells 1 Through 8.	2-52
2-28.	Plan View of Super Cells 9 and 10.	2-52
2-29.	Cross-Sectional View of a Super Cell.	2-53
2-30.	Schematic Showing ERDF Sideslope and Floor Liners.	2-53
2-31.	Cross-Sectional View of Liners for Cells 7 and 8.	2-55
2-32.	Detailed Cross-Sectional View of Super Cell Single Sump Area.	2-55
2-33.	Schematic of ERDF Closure Surface Barrier Configuration.	2-56
2-34.	ERDF Generic Cover Design.	2-57
2-35.	Carbon-14 Inventory Summary.	2-62
2-36.	Cesium-137 Inventory Summary.	2-63
2-37.	Chlorine-36 Inventory Summary.	2-64
2-38.	Iodine-129 Inventory Summary.	2-65
2-39.	Nickel-63 Inventory Summary.	2-66
2-40.	Plutonium Total Inventory Summary.	2-67
2-41.	Strontium-90 Inventory Summary.	2-68
2-42.	Technetium-99 Inventory Summary.	2-69
2-43.	Tritium Inventory Summary.	2-70

3-1.	Overview of the Dose Calculations for Exposure Along the Groundwater Pathway and Air Pathway for the ERDF Performance Assessment.	3-2
3-2.	Schematic Conceptual Representation of the ERDF Site and Various Pathways.	3-3
3-3.	Conceptual Model of the ERDF Site Showing Stratigraphy.....	3-4
3-4.	Plan View of Three-Dimensional ERDF Model Domain Showing Surface Features and the Surrounding Area.....	3-5
3-5.	(a) West-East ERDF Stratigraphic Cross-Section.....	3-29
3-5.	(b) North-South Stratigraphic Cross-Section Through ERDF.....	3-30
3-6.	Clastic Dike Models and Infilled Material.....	3-34
3-7.	Location of Samples Used in Developing the ERDF Data Set of Soil Hydraulic Properties.....	3-38
3-8.	Fitted Moisture Retention and Hydraulic Conductivity Curves for Various Hydrostratigraphic Units.....	3-39
3-9.	Layout of ERDF Cells and Approximate Location of One-Dimensional Profiles Used in Screening Analysis.....	3-49
3-10.	Geologic Cross-Sections Through ERDF Cell Centerlines with One-Dimensional Profiles Used in Screening During Operation, Closure, and Post-Closure Periods Identified.....	3-50
3-11.	Three-Dimensional Conceptual Model for the Radon-222 Flux Analysis and the Corresponding One-Dimensional Abstraction Model for a Unit Surface Area (1 m ²) Above ERDF.....	3-53
3-12.	Comparison of Measured Tortuosity (i.e., Ratio of Diffusion Coefficient in Soil (D_{ef}) to that in Free Air (D_0)) with Fitted Tortuosity Models Given by Liu et al. (2006).....	3-57
3-13.	Burrow and Root Density with Depth in Various Northwestern Semiarid Sites (after Figure 2-3 of WMP-20570).....	3-62
3-14.	Three-Dimensional Model and One-Dimensional Abstraction Model for ERDF.....	3-83
3-15.	Top View of the Three-Dimensional Model Domain Used in STOMP with Twelve Representative Locations Used for One-Dimensional Model Flow Abstraction.....	3-84
3-16.	Geologic Cross Section Along the Representative Locations (a) On the North Side and (b) On the South Side.....	3-85
3-17.	One-Dimensional Model Abstraction Showing (a) Representative Column for One-Dimensional Model and (b) Grid Discretization of the One-Dimensional Model.....	3-86
4-1.	Cumulative Release of Carbon-14 (Ci) from the ERDF Source Term.....	4-2
4-2.	Extent of Transport of the Most Mobile Radionuclides Such as Technetium-99 ($K_d = 0$ mL/g) in the Vadose Zone at the End of the 1,000-year Compliance Period for 1 Ci Initial Inventory in ERDF.....	4-6
4-3.	Extent of Transport of Moderately Mobile Radionuclides Such as Iodine-129 ($K_d = 0.2$ mL/g for sand dominated units) in the Vadose Zone at the End of the 1,000-year Compliance Period for 1 Ci Initial Inventory in ERDF.....	4-8
4-4.	Extent of Transport of Moderately Mobile Radionuclides Such as Uranium-238 ($K_d = 0.8$ mL/g for Sand-Dominated Units) in the Vadose Zone at the End of the 1,000-year Compliance Period for 1 Ci Initial Inventory in ERDF.....	4-10
4-5.	Extent of Transport of the Most Mobile Radionuclides Such As Technetium-99 at the End of the 1,000-year Compliance Period for 1 Ci Initial Inventory Evaluated with the Maximum Recharge Values and Vadose Zone Hydraulic Parameters.....	4-12
4-6.	Extent of Transport of the Lesser Mobile Radionuclides Such as Iodine-129 at the End of the 1,000-year Compliance Period for 1 Ci Initial Inventory	

	Evaluated with the Maximum Recharge Values and Vadose Zone Hydraulic Parameters.....	4-14
4-7.	Moisture Content in the Vadose Zone at ERDF for Four Times of Interest: (a) ERDF Closure at Year 2035, (b) ERDF Composite Liner Failure at Year 2135, (c) End of Compliance Period at Year 3035, and (d) Approximate Reestablishment of Steady-State Flow Field.	4-16
4-8.	Darcy Flux in the Vadose Zone at ERDF for Four Times of Interest: (a) ERDF Closure at Year 2035, (b) ERDF Composite Liner Failure at Year 2135, (c) End of Compliance Period at Year 3035, and (d) Approximate Reestablishment of Steady-State Flow Field.	4-17
4-9.	Maximum Predicted Groundwater Concentration at 100 m Downgradient from ERDF Through the End of the Post-Closure Period.....	4-19
4-10.	Extent of Transport and Porewater Concentration of Technetium-99 in the Vadose Zone and Aquifer 4,000 years After Closure.	4-21
4-11.	Extent of Transport and Porewater Concentration of Technetium-99 in the Vadose Zone and Aquifer 7,000 years After Closure.	4-22
4-12.	Extent of Transport and Porewater Concentration of Technetium-99 in the Vadose Zone and Aquifer 10,000 years After Closure.	4-23
4-13.	Distribution and Volumetric Concentration of Technetium-99 in the Vadose Zone and Aquifer 4,000 years After Closure.	4-24
4-14.	Distribution and Volumetric Concentration of Technetium-99 in the Vadose Zone and Aquifer 7,000 years After Closure.	4-25
4-15.	Distribution and Volumetric Concentration of Technetium-99 in the Vadose Zone and Aquifer 10,000 years After Closure.	4-26
4-16.	Plan View Distribution of Technetium-99 in the Aquifer 3,000, 4,000, 5,000, and 6,000 years After Closure.	4-27
4-17.	Plan View Distribution of Technetium-99 in the Aquifer 7,000, 8,000, 9,000, and 10,000 years After Closure.	4-28
4-18.	Atmospheric Release (pCi/yr) per Unit Surface Area of ERDF.....	4-29
4-19.	Radon-222 Flux (pCi/s) per Unit Surface Area of ERDF.	4-30
4-20.	All-Pathway Receptor Dose for (a) Groundwater Pathway Only, (b) Atmospheric Pathway Only, and (c) Combined for Both Pathways.....	4-32
4-21.	Calculated Matric Potential for Various Hydrostratigraphic Units After 2,000 Years of Simulation.....	4-37
4-22.	Family of Unsaturated Hydraulic Conductivity Curves as a Function of Matric Potential for Various Hydrostratigraphic Units.....	4-38
4-23.	Example of Uncertainty in Volumetric Moisture Content and Vertical Darcy Velocity for Selected Grid Nodes in Hf2 and RFwie Hydrostratigraphic Units After Closure.	4-42
4-24.	Volumetric Moisture Content Profiles as a Function of Depth and Time (in Calendar Years) for Selected Spatial Locations.....	4-44
4-25.	Comparison of Technetium-99 Concentration at Selected Locations in the Vadose Zone Predicted by One-Dimensional Abstraction Model with the Three-Dimensional Model Results Using Compliance Parameter Values for 1 Ci Inventory Distributed Over ERDF Volume.	4-45
4-26.	Comparison of Technetium-99 Concentration in the Saturated Zone Predicted by the One-Dimensional Abstraction Model with the Three-Dimensional Transport Model at the Compliance Location 100 m Downgradient of ERDF Using Compliance Parameter Values for 1 Ci Inventory Distributed Over ERDF Volume.	4-48
4-27.	All-Pathway Dose Calculation Results Based on 500 Realizations Conducted Using a One-Dimensional Abstraction Model.....	4-50

4-28.	Uncertainty in the Groundwater-Pathway Dose Based on 500 Realizations.	4-51
4-29.	Selected Realizations for Groundwater Pathway Dose.	4-52
4-30.	Scatter Plots of Selected Uncertain Parameters Against Groundwater Pathway Dose at 10,000 years.	4-56
4-31.	Uncertainty in Atmospheric Pathway Dose Based on 500 Realizations.	4-58
4-32.	Scatter Plots of Selected Uncertain Parameters Against the Atmospheric Pathway Dose at Different Time Periods.	4-60
4-33.	Statistical Stability Analysis with Different Number of Realizations.	4-62
4-34.	Confidence Limits on the Mean Effective Dose Equivalent.	4-63
4-35.	Results and Regression Lines Associated with the Vadose Leachate Concentration and the Concentration in Groundwater for the Compliance Evaluation for Technetium-99 (Results Presented on a per Ci Source Basis).	4-67
4-36.	Results and Regression Lines Associated with the Vadose Leachate Concentration and the Concentration in Groundwater for the Hydrologic and Recharge Parameter Percentile Evaluations for Technetium-99 (Results Presented on a per Ci Source Basis).	4-69
4-37.	Results and Regression Lines Associated with the Vadose Radionuclide Flux and the Concentration in Groundwater for Hydrologic and Recharge Parameter Percentile Evaluations for Technetium-99 (Results Presented on a per Ci Source Basis).	4-70
4-38.	Results of the Longitudinal Saturated Dispersivity Sensitivity Evaluation Showing the Breakthrough of a Radionuclide with $K_d = 0$ mL/g (e.g., Technetium-99) to the Water Table for the Individual Hydrologic Parameter Percentile Sets (Results Presented on a per Ci Source Basis).	4-74
4-39.	Comparison of the One-Dimensional Transport Model Results to the Comparable Three-Dimensional Transport Model Results of the Breakthrough of a Radionuclide with $K_d = 0$ mL/g (e.g., Technetium-99) to the Water Table for the Individual Hydrologic Parameter Percentile Sets (Results Presented on a per Ci Source Basis).	4-79
4-40.	Cumulative Results for Radionuclides with $K_d = 0$ mL/g (e.g., Technetium-99) of the Individual Hydrologic Parameter Percentile Evaluations (Results Presented on a per Ci Source Basis).	4-80
4-41.	Results of the Individual Hydrologic Parameter Percentile Evaluations for Radionuclides with $K_d = 0$ mL/g (e.g., Technetium-99; Results Presented on a per Ci Source Basis).	4-82
4-42.	Sensitivity of Surface Barrier Thickness on Air-Pathway Dose.	4-90
4-43.	Sensitivity of Henry's Law Constants for Air-Water Partitioning of Carbon-14.	4-91
4-44.	Sensitivity Case Showing the Results of Peak Dose Calculations.	4-94
5-1.	Calculation of Target Field Concentrations.	5-3
5-2.	Exposure Pathways Considered in the Inadvertent Intruder Well Driller Acute Exposure Scenario.	5-4
5-3.	Exposure Pathways Considered in the Inadvertent Intruder Rural Pasture Chronic Exposure Scenario.	5-7
5-4.	Exposure Pathways Considered in the Inadvertent Intruder Suburban Garden Chronic Exposure Scenario.	5-12
5-5.	Exposure Pathways Considered in the Inadvertent Intruder Commercial Farm Chronic Exposure Scenario.	5-16
5-6.	Effective Dose for the Well Driller Acute Exposure Scenario.	5-19
5-7.	Effective Dose for the Rural Pasture Chronic Exposure Scenario.	5-20
5-8.	Effective Dose for the Suburban Garden Chronic Exposure Scenario.	5-21
5-9.	Effective Dose for the Commercial Farm Chronic Exposure Scenario.	5-22

5-10.	Sensitivity of Suburban Garden Scenario Dose with Modified Target Field and Well Area.....	5-24
7-1.	Concentration Threshold Based on Dose after 100 years of ERDF Closures for Different Scenarios.....	7-9

TABLES

1-1.	Performance Objectives and Measure for the ERDF Landfill Performance Assessment.....	1-11
2-1.	Lithostratigraphic Terminology for the Vadose Zone Beneath the ERDF.....	2-22
2-2.	Best Estimate of Current ERDF Inventory for Radionuclides with Half-Lives Greater than 6 Years and/or Inventories Greater than 1 Ci (Decayed to 2011).....	2-72
2-3.	Best Estimate of Current ERDF Inventory for Radionuclides with Half-Lives Less than 6 Years (Decayed to 2011).....	2-74
2-4.	Best Estimate of Current ERDF Inventory for Radionuclides with Half-Lives Less than 6 Years and Current Inventories Less than 1 Ci (Decayed to 2011).....	2-74
2-5.	Best Estimate of Currently Forecasted Inventory of Radionuclides with Half-Lives Greater than 6 Years and/or Present Inventories Greater than 1 Ci for Disposal at ERDF (Decayed to 2011).....	2-75
2-6.	Best Estimate of Currently Forecasted Inventory of Radionuclides with Half-Lives Less than 6 Years for Disposal at ERDF (Decayed to 2011).....	2-77
2-7.	Best Estimate of Currently Forecasted Inventory of Radionuclide with Half-Lives Greater than 6 Years and Current Inventories Less than 1 Ci (Decayed to 2011).....	2-77
3-1.	Best Estimate Inventory of Radionuclides at Closure for the ERDF Performance Assessment.....	3-8
3-2.	ERDF Inventory for Specific Radionuclides (WCH-479).....	3-13
3-3.	Fraction of Inventory by Waste Form Type.....	3-16
3-4.	Published Long-Term Fractional Leach Rates of Carbon-14.....	3-18
3-5.	Timeline Considered for Representing the Evolution of ERDF.....	3-22
3-6.	Estimates of Recharge Rate Available for Rupert Sand Without Vegetation.....	3-25
3-7.	Compliance Infiltration (Recharge) Estimates for Pre-Construction Period, Operational Period, and Following Emplacement of the ERDF Closure Barrier.....	3-27
3-8.	Composite van Genuchten-Mualem Parameters for Various Hydrostratigraphic Units (WCH-464).....	3-39
3-9.	Macroscopic Anisotropy Parameters for Various Hydrostratigraphic Units Based on the Polmann (1990) Model (WCH-464).....	3-41
3-10.	Effective Bulk Density (g/cm ³) Estimates for Various Hydrostratigraphic Units.....	3-42
3-11.	Macrodispersivity Estimates for Various Hydrostratigraphic Units (Based on Median Values of WCH-464 Data Set).....	3-43
3-12.	Average Percent Gravel Measured in Each Hydrostratigraphic Unit (According to WCH-464).....	3-45
3-13.	Aqueous/Solid Partitioning Ratio (K _d in mL/g) Estimates for Low-Organic/Low-Salt/Near-Neutral Waste Chemistry for Each Hydrostratigraphic Unit.....	3-45
3-14.	ERDF Unconfined Aquifer Flow and Transport Properties (WCH-515).....	3-47
3-15.	Saturated Longitudinal Macrodispersivity (α _L) Distribution.....	3-48
3-16.	Long-Term Recharge Rates Associated With the Different Modeling Periods Used in the Screening Phase.....	3-50
3-17.	Henry's Law Constants.....	3-55
3-18.	K _d (mL/g) Selected for ERDF Soils and Cover Material (WCH-515).....	3-56
3-19.	Diffusion Coefficients in Air at 20 °C and 1 Atm.....	3-56

3-20.	Atmospheric Pathway Modeling Parameters.	3-58
3-21.	Wind Speed Observed Above the Hanford Site (see Chapter 2.0) and Corresponding Pasquill Class for a Moderate Solar Radiation (Pasquill 1961).	3-59
3-22.	Estimates of Horizontal Dispersion Coefficient in Air (m) Obtained with CAP88 User's Guide Equation for Pasquill Class C (EPA 2007).	3-59
3-23.	Maximum Penetration Depths for Biota at the Hanford Site. (Source: WMP-20570, Table 2-1).....	3-61
3-24.	Scenario-Specific Parameters for the All-Pathways Farmer Scenario	3-69
3-25.	Parameters for Tritium Concentration Calculation in Crop.....	3-71
3-26.	Parameters for Tritium Concentration Calculation in Animal Products.	3-71
3-27.	Bioconcentration Factors Used in Calculations.....	3-72
3-28.	Dose Conversion Factors Used in Performance Assessment Calculations.....	3-73
3-29.	Dose-Specific Parameters for the Atmospheric Pathway.	3-78
3-30.	Discretization of ERDF One-Dimensional Abstraction Model Built Using GoldSim.	3-87
3-31.	Constraints on Data Useful to Select a Distribution Function Considering the Maximum Entropy Principle (Mishra 2002, According to Harr 1987).	3-89
3-32.	ERDF Performance Assessment Uncertainty and Sensitivity Analyses Database for Recharge (WCH-515).....	3-89
3-33.	ERDF Performance Assessment Uncertainty and Sensitivity Analyses Database for Vadose Zone Parameters (WCH-515).	3-90
3-34.	ERDF Performance Assessment Uncertainty and Sensitivity Analyses Database for Polmann Anisotropy Model Parameters (WCH-515).....	3-91
3-35.	ERDF Performance Assessment Uncertainty and Sensitivity Analyses Database for Saturated Zone Parameters (WCH-515).	3-91
3-36.	ERDF Performance Assessment Uncertainty and Sensitivity Analyses Database for Transport Parameters (WCH-515).....	3-91
3-37.	ERDF Performance Assessment Uncertainty and Sensitivity Analyses Database for K_d (mL/g) (WCH-515)	3-92
3-38.	ERDF Performance Assessment Uncertainty and Sensitivity Analyses Database for Contaminant Inventory (Curies or Metric Tons) Using Triangular Distribution (WCH-515).....	3-94
4-1.	First-Arrival Time (in Calendar Year) of Radionuclides for Various K_d Values Based on One-Dimensional Screening Analysis Using STOMP.....	4-3
4-2.	K_d Value Thresholds Developed on the Basis of First-Arrival Time Results of One-Dimensional Screening Analysis Using STOMP.....	4-4
4-3.	Maximum Groundwater Concentration at 100 m Downgradient from ERDF Over the Compliance and Post-Compliance Time Period.....	4-18
4-4.	Maximum All-Pathway Effective Dose Equivalent and Time to Maximum Dose for Compliance and Post-Compliance Time Periods at 100 m Downgradient of ERDF.	4-35
4-5.	Uncertainty in Recharge Rate Parameters.	4-36
4-6.	Values of van Genuchten-Mualem and Polmann Parameters at Selected Percentiles	4-39
4-7.	Sampled Parameter Values for Selected Realizations.	4-53
4-8.	Uncertain Parameters Important to Groundwater Pathway Dose.	4-55
4-9.	Uncertain Parameters Important to Atmospheric Pathway Dose at Various Times.	4-59
4-10.	Results of the Vadose Zone Hydrologic and Recharge Parameter Percentile Evaluations for Radionuclides with $K_d = 0$ mL/g (e.g., Technetium-99) Breakthrough to the Water Table (Results Presented on a per Ci Source Basis).....	4-65

4-11.	Results of the Vadose Zone Hydrologic and Recharge Parameter Percentile Evaluations for Radionuclides with $K_d = 0$ mL/g (e.g., Technetium-99) Breakthrough in the Aquifer at the Downgradient Point of Calculation (Results Presented on a per Ci Source Basis).....	4-66
4-12.	Results of the Aquifer Anisotropy Parameter Evaluations for Radionuclides with $K_d = 0$ mL/g (e.g., Technetium-99) (Results Presented on a per Ci Source Basis).....	4-71
4-13.	Results of the Radionuclide Mobility Evaluations for Radionuclides (e.g., Technetium-99 and Iodine-129) Breakthrough to the Water Table in the Aquifer at the Downgradient Point of Calculation (Results Presented on a per Ci Source Basis).....	4-72
4-14.	Results of the Aquifer Mixing Width Evaluations from the Outside Edges of the North and South Berms for Radionuclides with $K_d = 0$ mL/g (e.g., Technetium-99) (Results Presented on a per Ci Source Basis).....	4-73
4-15.	Results of the Percentile Recharge Evaluations for Radionuclides with $K_d = 0$ mL/g (e.g., Technetium-99; Results Presented on a per Ci Source Basis)	4-75
4-16.	Summary of Results of the What If Evaluations for Radionuclides with $K_d = 0$ mL/g (e.g., Technetium-99; Results Presented on a per Ci Source Basis)	4-85
4-17.	Comparison of the Peak Contaminant Concentration Results for the Past Performance Assessment (BHI-00169) and the Current Performance Assessment Analyses.	4-93
5-1.	Summary Description of the Inadvertent Intruder Scenarios Considered in the ERDF Performance Assessment.	5-2
5-2.	Parameters Common to Inadvertent Intruder Scenarios	5-2
5-3.	Parameters Considered in the Inadvertent Intruder Well Driller Acute Exposure Scenario.....	5-4
5-4.	Parameters Considered in the Inadvertent Intruder Rural Pasture Chronic Exposure Scenario	5-7
5-5.	Parameters Considered in the Inadvertent Intruder Suburban Garden Chronic Exposure Scenario	5-12
5-6.	Parameters Considered in the Inadvertent Intruder Commercial Farm Chronic Exposure Scenario	5-16
5-7.	Effective Dose Equivalent for the Inadvertent Intruder Scenarios at 100 Years and 500 Years Post-Closure Along with Major Dose-Contributing Radionuclides	5-18
5-8.	Relative Importance of Pathway Contributions to the Inadvertent Intruder Dose.....	5-23
5-9.	Sensitivity Analysis on Well and Garden Size Parameters.....	5-23
6-1.	Summary of All-Pathway Effective Dose Equivalent for the Compliance and Post-Compliance Periods 100 m Downgradient of ERDF.	6-2
6-2.	Summary of Air-Pathway Effective Dose Equivalent for the Compliance Period 100 m Downgradient of ERDF.	6-2
6-3.	Summary of Groundwater Pathway Effective Dose Equivalent for the Post-Compliance Period 100 m Downgradient of ERDF.	6-2
6-4.	Comparison of Peak Groundwater Concentration Results to Groundwater Protection Criteria.....	6-5
7-1.	Comparison of Performance Objectives and the ERDF Performance Assessment Results for the Compliance and Post-Compliance Periods.....	7-2
7-2.	Calculated Radionuclide Concentration Thresholds for Waste Disposal in ERDF for Acute and Chronic Inadvertent Intruder Scenarios Based on Dose after 100 years of ERDF Closure.....	7-5
7-3.	Groundwater Pathway Inventory Thresholds for ERDF.	7-12

7-4. Air-Pathway Inventory Thresholds for the ERDF for the Compliance
Time Period (Year 2035 to 3035).....7-13

REVISION HISTORY

Revision	Date	Reason for revision	Revision initiator
1	August 2013	Revised to incorporate comments from Low-Level Waste Disposal Facility Federal Review Group (LFRG) throughout the document.	S. Mehta
0	March 2013	Initial issuance	NA

ACRONYMS

ALARA	As Low As Reasonably Achievable
BET	Brunauer, Emmet, and Teller (method)
CERCLA	<i>Comprehensive, Environmental Response, Compensation, and Liability Act of 1980</i>
CHPRC	CH2M Hill Plateau Remediation Company
DAS	Disposal Authorization Statement
DNFSB	Defense Nuclear Facilities Safety Board
DOE	U.S. Department of Energy
EDE	effective dose equivalent
EIS	environmental impact statement
EMMA	Environmental Model Management Archive
EPA	U.S. Environmental Protection Agency
EPM	equivalent porous medium
ERDF	Environmental Restoration Disposal Facility
ESD	Explanation of Significant Difference
FEP	feature, event, and process
FFTF	Fast Flux Test Facility
FY	fiscal year
HDPE	high-density polyethylene
HFSUWG	Hanford Future Site Uses Working Group
HISI	Hanford Information Systems Inventory
HMS	Hanford Meteorological Station
ILAW	immobilized low-activity waste
LFRG	Low-Level Waste Disposal Facility Federal Review Group
LHS	Latin hypercube sampling
LLW	low-level waste
MCL	maximum contaminant level
NESHAP	National Emission Standards for Hazardous Air Pollutants
PA	performance assessment
PPE	personal protective equipment
RCCC	River Corridor Closure Contract
RCRA	<i>Resource Conservation and Recovery Act of 1976</i>
RI/FS	remedial investigation/feasibility study
ROD	record of decision
STOMP	Subsurface Transport Over Multiple Phases
TCE	trichloroethylene
TEDF	Treated Effluent Disposal Facility
WCH	Washington Closure Hanford
WMA	waste management area
WMIS	Waste Management Information System

1.0 INTRODUCTION

This document provides a performance assessment (PA) analysis for the Environmental Restoration Disposal Facility (ERDF), an analysis that is required for U.S. Department of Energy (DOE)-operated facilities that dispose of low-level radioactive waste generated by departmental activities. The fundamental objective of the ERDF is to support the timely removal and disposal of waste generated from remediation of waste sites within the Hanford Site.

The purpose of the PA analysis is to demonstrate that the facility is operated in a manner that ensures long-term environmental protection after facility closure. In 1999, DOE Order 435.1 (DOE O 435.1), *Radioactive Waste Management*, established quantitative post-closure environmental impacts limits and required a facility-specific PA analysis to demonstrate compliance with these limits. These limits are defined in terms of human health (e.g., dose limits) with respect to radioactive constituents in the waste. This analysis excludes the potential impacts of nonradiological hazardous constituents that may be present in the waste.

A preliminary ERDF PA analysis was completed in 1995 (BHI-00169, *Environmental Restoration Disposal Facility Performance Assessment*) prior to the receipt of waste. At that time DOE Order 5820.2A, *Radioactive Waste Management*, was in place. Because the ERDF was constructed for the express purpose of receiving and disposing of waste generated by the remediation of Hanford *Comprehensive Environmental Response, Compensation and Liability Act of 1980* (CERCLA) waste sites, a remedial investigation/feasibility study (RI/FS) (DOE/RL-93-99, *Remedial Investigation and Feasibility Study Report for the Environmental Restoration Disposal Facility*) was also completed, followed by the *Declaration of the Record of Decision for the Environmental Restoration Disposal Facility, Hanford Site, Benton County, Washington* (EPA/ROD/R10-95/100), hereby referred to as the ERDF ROD. A crosswalk between the ERDF ROD and the requirements of DOE Order 5820.2A was completed in 1996 (Dronen 1996) and adequately demonstrated compliance with the DOE order leading to the DOE permission for ERDF operations to begin. DOE Order 5820.2A was succeeded by DOE O 435.1 in 1999. Following the issuance of DOE O 435.1, a second crosswalk was completed between the ERDF ROD and requirements of DOE O 435.1 (Klein 2000) that confirmed that the ERDF operations meet the substantive requirements of the DOE order, which permitted continued operation of the ERDF.

Since the completion of the preliminary PA analysis and after 15 years of operation, two factors have led DOE and the U.S. Environmental Protection Agency (EPA) to the decision to update the PA analysis and complete the formal review process per DOE O 435.1, *Radioactive Waste Management*:

- The ERDF has accepted and will continue to accept additional radioactive waste at higher inventory levels than originally foreseen (although still within the limits provided in the preliminary PA analysis)
- New information has been developed at the Hanford Site that identifies large conservatisms in the initial analysis.

The updated PA analysis is intended to provide an improved technical basis for the evaluation of facility performance and to optimize the capability of the ERDF to complete its mission of disposing CERCLA remediation waste for the remainder of the Hanford Site cleanup activities.

Once completed, reviewed, and accepted, this analysis will support reissuance of a Disposal Authorization Statement (DAS) for continued ERDF operations.

1.1 GENERAL APPROACH

A PA is "an analysis of a radioactive waste disposal facility conducted to demonstrate there is a reasonable expectation that performance objectives established for the long-term protection of the public and the environment will not be exceeded following closure of the facility" (DOE O 435.1). The analyses goals and modeling approach differ depending on performance objective or measure and range in complexity from numeric modeling (e.g., the contaminant groundwater pathway for the all-pathways performance objective) to qualitative discussion (e.g., as low as reasonably achievable [ALARA]) as warranted. General characteristics of each type of analysis are as follows:

- **Performance Objective Analyses.** These analyses determine if characteristics of the closed ERDF that control radionuclide releases to the surrounding environment are sufficient to satisfy long-term (1,000 years post-closure) compliance objectives. Prescribed objectives include dose to humans from groundwater and air contamination (all-pathways 25 mrem/yr limit and a 10 mrem/yr atmospheric release limit) and a radon flux limit (20 pCi/m²/s). Of these the groundwater pathway is the most complex requiring numerical simulations for radionuclide release from the ERDF and transport to a downgradient aquifer well. In contrast, the atmospheric release and radon flux analyses can be completed with simpler numerical solutions or semi-analytic solutions, essentially as bounding calculations.
- **Performance Measures Analyses.** These analyses establish two kinds of waste acceptance criteria for the ERDF. First, radionuclide-specific concentration limits are quantified with respect to dose limit for inadvertent intruders that receive dose after exhuming waste. These analyses estimate dose from a set of algebraic equations that calculates the intensity and duration of exposure to the intruder. Second, radionuclide-specific inventory limits are calculated that prevent maximum concentrations at a 100-m downgradient well from exceeding EPA drinking water standards (e.g., maximum contaminant levels [MCLs]). This analysis presumes a cause-and-effect relationship between disposed inventory and groundwater contamination levels after release from the ERDF and employs the groundwater pathways analyses used for the all pathways analysis.
- **Other Analyses.** Other analyses include sensitivity/uncertainty, ALARA, and biota analyses. Sensitivity and uncertainty analyses are completed to determine plausible ranges of near-field environmental contamination caused by natural processes over time and are used most extensively to complete the groundwater pathways analyses. Both deterministic and probabilistic approaches are included that require numerical simulations. The ALARA analysis is a qualitative discussion about the value of using more environmentally protective disposal practices relative to current practices. The biota analysis is a calculation of dose to humans through contact with contaminated biota.

The ERDF PA presents a comprehensive, systematic analysis of the long-term impacts of the low-level waste (LLW) disposal in a semiarid, near-surface environment. Related assessment activities (e.g., safety assessments, risk assessments, engineering evaluations, and cost/design studies) have been evaluated in other documents related to the ERDF. Although occupational doses to workers are an important area of concern for facility operations, they are addressed by regulations and guidance different from those covering PAs. Additionally, this document

excludes the potential impacts of chemical toxicity of radiological constituents and nonradiological hazardous constituents that may be present in the waste.

1.2 GENERAL FACILITY DESCRIPTION

The ERDF was constructed to permanently dispose of all wastes generated by remediation of Hanford Site past-practice and CERCLA waste sites in an environmentally protective manner. Disposal of contaminated material at ERDF is the preferred remedy for much of the waste excavated from numerous Hanford waste sites. As of July 2013, approximately 13.6 million metric tons of waste has been disposed at ERDF since the facility started operations in July 1996 (an average of 800,000 metric tons/yr).

The ERDF was constructed on the Central Plateau portion of the Hanford Site between the 200 West and 200 East Areas (Figure 1-1). It is constructed in a modular fashion so that additional disposal space can be built as needed (Figure 1-2). The first eight disposal cells were built in pairs located at the west end of ERDF. Each cell is approximately 152 m by 152 m (500 ft by 500 ft) at the bottom, approximately 21 m (70 ft) deep, and has a 3:1 (horizontal to vertical ratio) side slope that extends 64 m (210 ft) horizontally from the base of the cells. The latest cell construction toward the east (supercells 9 and 10) combines the cell pairings into one larger cell, approximately the same size as each cell pair. Since the beginning of operations in July 1996, cells 1 through 4 have been filled; cells 5 through 8 are nearly filled; and supercells 9 and 10 are receiving waste. Using the lined, deep, single-trench configuration, the disturbed area needed for additional construction of ERDF (including the trench, container handling, material stockpile, and support facilities) will not exceed the maximum of 4.1 km² (1,024 ac) identified in the ERDF ROD.

Waste disposal at ERDF generally involves transport of high-volume slightly contaminated soils and debris by truck from remediation sites, followed by dumping and spreading in the ERDF cell and compaction to minimize void space and limit future waste volume subsidence. In a small number of cases, wastes are grouted to fill void space and/or sequester mobile radionuclides.

Characteristics of ERDF that strongly affect contaminant release and transport through the vadose zone and into the unconfined aquifer are its location, engineered features of the facility, and the nature of the disposed waste. The vadose zone (rock/soil zone above the water table) is approximately 80 to 100 m (262 to 328 ft) thick and provides the greatest possible distance to the water table compared to waste sites located elsewhere in the Hanford Site. In addition, because of its location in the middle of the Central Plateau it provides the largest contaminant migration distance possible to the Columbia River from the Hanford Site.

Figure 1-1. Location of the ERDF Facility on the Hanford Site.

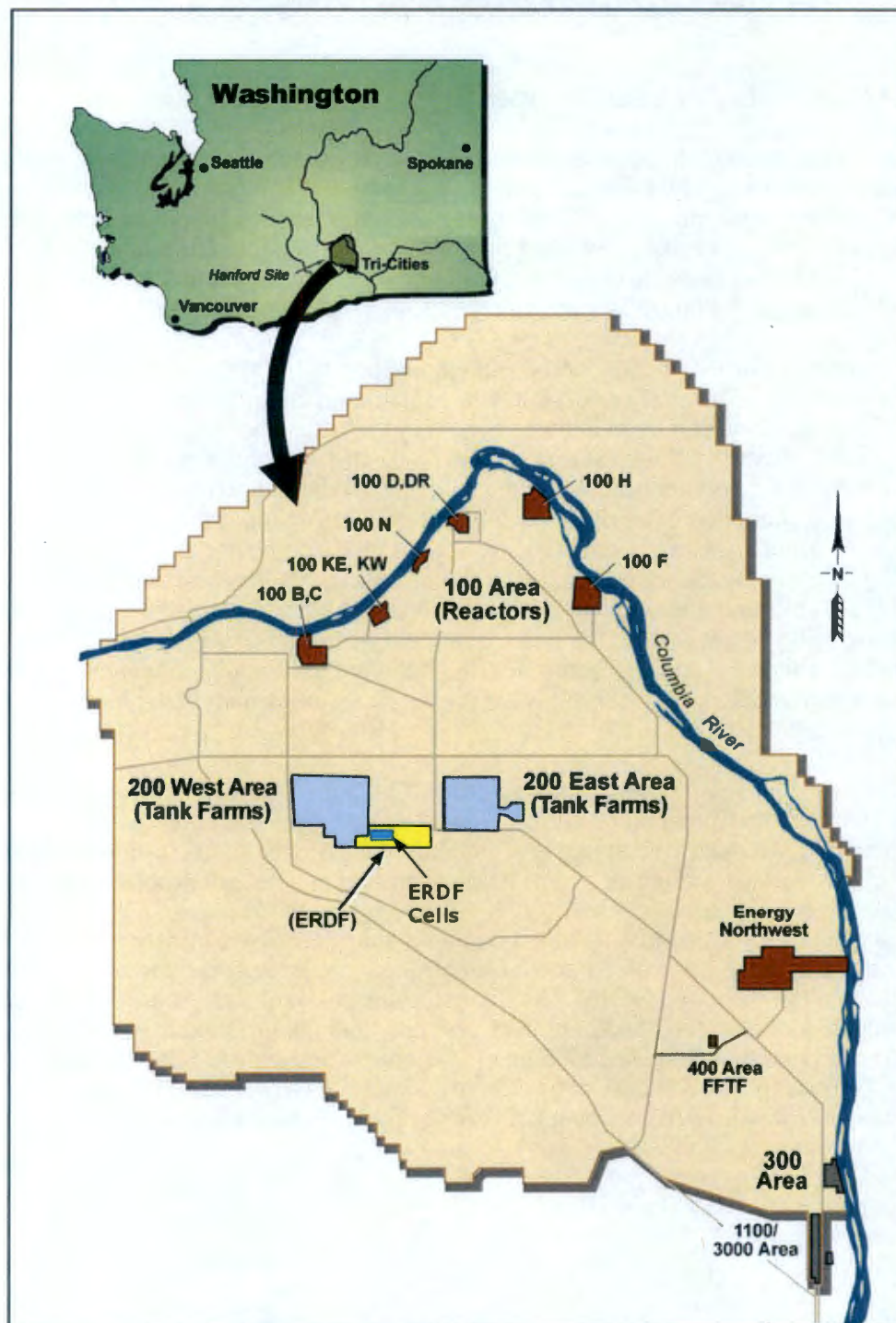


Figure 1-2. August 2010 Aerial View of the ERDF Looking South.



1.2.1 Waste Acceptance Criteria

Waste disposal criteria for the ERDF are outlined in WCH-191, *Environmental Restoration Disposal Facility Waste Acceptance Criteria*. The ERDF is authorized to accept waste from Hanford Site environmental restoration activities consistent with the ERDF ROD, the Explanation of Significant Difference (ESD), and ROD amendments (EPA/ROD/R10-95/100, EPA/ESD/R10-96/145, EPA/AMD/R10-97/101, EPA/AMD/R10-99/038, EPA/AMD/R10-02/030, 07-AMRC-0077, 09-AMRC-0179). Inactive treatment, storage, and disposal; RCRA past-practice; and decontamination and decommissioning waste may be placed in the ERDF through a remedial action ROD or removal action memorandum issued in accordance with CERCLA and the "Oil and Hazardous Substances Pollution National Contingency Plan" (40 CFR 300). On a case-by-case basis, other documents may be used to provide regulatory authority for disposal of waste at the ERDF. Waste that has not been subjected to the waste acceptance process defined in Section 3.0 of WCH-191 shall not be accepted for disposal at ERDF.

All waste received at ERDF is tracked using the Waste Management Information System (WMIS). Before waste is accepted into ERDF, a waste profile and a waste designation is developed and approved for each waste source in accordance with WMT-1, *Waste Management and Transportation*. Waste that is within the established profile, meets the *Supplemental Waste Acceptance Criteria for the Environmental Restoration Disposal Facility* (0000X-DC-W001), has been authorized for disposal by a regulator-approved CERCLA or RCRA past-practice decision document, and is accompanied by the appropriate documentation is disposed in accordance with the ERDF operation process.

The basis for acceptance criteria includes protection of human health and the environment, protection of the ERDF liner system, control of waste form, and compliance with environmental regulations. The ERDF users are responsible for characterization of waste submitted for acceptance into ERDF. The process for characterizing waste by the generator and acceptance by ERDF is described in WMT-1. Wastes that can be accepted at ERDF include wastes generated from Hanford Site CERCLA remedial and investigative activities and other agency-approved actions. These wastes typically include soils, drill cuttings, building demolition debris, boxed soils, and secondary CERCLA wastes such as personal protective equipment and secondary CERCLA wastes from waste processing and decontamination activities at ERDF.

1.2.2 General Land-Use Patterns

Land use at the Hanford Site is currently managed and operated by the DOE, Richland Operations Office, and its prime contractors for government-controlled industrial use. The primary use of Hanford Site land is to support facility and program operations dedicated to spent nuclear fuel management, hazardous and mixed waste management and minimization, cultural resources preservation, and environmental remediation. A security force is used to limit access to approved personnel and visitors. Restrictions limiting the use of groundwater beneath the Hanford Site by members of the public are in place. The distance from ERDF to the Hanford Site/City of Richland boundary is roughly 29 km (18 mi). DOE/EIS-0222F, *Final Hanford Comprehensive Land-Use Plan Environmental Impact Statement*; DOE/RL-2009-10, *Hanford Site Cleanup Completion Framework*; DOE/RL-2011-56, *Hanford Site Third CERCLA Five-Year Review Report*; and EPA/ROD/R10-100, *U.S. DOE Hanford Environmental Restoration Disposal Facility* describe the land use for the Hanford Site and ERDF in greater detail.

For nearer term land-use planning, the ROD (64 FR 61615) for DOE/EIS-0222-F prescribes the use in the 200 Areas as exclusively industrial (primarily waste management) with much of the surrounding land having the use of preservation or conservation. The Hanford Reach National Monument was established along the Columbia River corridor as well in lands at the northern and western edges of the site (65 FR 37253). As part of the efforts related to the end state vision, planning assumptions for land use within and adjacent to the Hanford Site indicate that much of the 200 Area of the Hanford Site, including ERDF, could remain under government control in perpetuity (DOE/RL-2009-10).

1.3 LOW-LEVEL WASTE DISPOSAL FACILITY LIFE CYCLE

The ERDF life cycle consists of three parts:

- **ERDF Operations (1996-2035).** The facility was constructed in the mid-1990s and began receiving waste in June 1996 in cells 1 and 2. Additional cells (3 through 10) have been constructed and have been completely or partially filled. The end of the operations period is uncertain because all CERCLA waste site remediation decisions have not been finalized and all remediation actions completed. For purposes of this analysis, a closure date of 2035 has been assumed as a best estimate.
- **ERDF Closure and Active Institutional Control (2035-2135).** Waste receipt ends by 2035 and the closure cap is installed with active site facility and environmental monitoring. Staff are present on site to prevent unauthorized public access, maintain facility structures (e.g., repair cover if, necessary) and conduct environmental monitoring.

- **Passive Institutional Control (2135-3035).** Staff are not present on site to service the facility or continue environmental monitoring. However, passive controls such as fences, historical records, and legal records are in place to deter human activity at the site.

1.4 RELATED DOCUMENTS

Authorization to operate the ERDF was granted by the EPA with the ROD (EPA/ROD/R10-95/100) and by the DOE with a DAS per DOE Order 5820.2A, *Radioactive Waste Management*. The primary technical analyses supporting approval to operate have been the RI/FS completed in 1994 (DOE/RL-93-99) for the ROD and a preliminary PA analysis (BHI-00169, *Environmental Restoration Disposal Facility Performance Assessment*) to address DOE Order 5820.2A requirements.

Below is a discussion of the most relevant ERDF documents and other environmental assessments.

1.4.1 ERDF Relevant Documents

BHI-00270, *Preoperational Baseline and Site Characterization Report for the Environmental Restoration Disposal Facility*, was completed in 1996. This site characterization report provided the results of the field data collection activities for ERDF site and assessment of the geology and the groundwater flow paths.

BHI-00169, *Environmental Restoration Disposal Facility Performance Assessment*, was written to support disposal of waste generated by the cleanup of the Hanford Site, but was not immediately issued. Instead, DOE/RL-93-99, *Remedial Investigation and Feasibility Study Report for the Environmental Restoration Facility*, was prepared. The ERDF is regulated under CERCLA. Most of the waste to be disposed of at ERDF is expected to be contaminated soil.

The Tri-Parties signed a CERCLA ROD (EPA/AMD/R10-99/038) in January 1995 authorizing the construction of ERDF to provide waste disposal capacity for cleanup of contaminated areas on the Hanford Site. The ERDF ROD provides the overall plan for construction of the facility and disposal of remediation waste from the Hanford Site. Subsequently, a crosswalk between the ERDF ROD and the requirements of DOE O 435.1 was performed and approved (DOE 2001), which confirmed that the ERDF Operations meet the substantive requirements of the DOE order and permitted continued operation of the ERDF. An ESD to the ERDF ROD was issued (EPA/ESD/R10-96/145) in July 1996. The ESD allows for the disposal of investigation-derived waste; decontamination and decommissioning waste; waste from RCRA past-practice operable units and closures; and non-RCRA waste from inactive treatment, storage, and disposal units. The ESD also authorized the conditional use of ERDF leachate for dust suppression and waste compaction.

The following ROD amendments have been issued for ERDF.

- **October 1997:** The first amendment was issued (EPA/AMD/R10-97/101) to authorize expansion of the facility by constructing two new disposal cells and to allow for limited waste treatment at ERDF.
- **March 1999:** The second amendment (EPA/AMD/R10-99/038) was issued authorizing the delisting of ERDF leachate. Delisting ERDF leachate was done to allow for implementation

of more cost-effective and appropriate leachate handling techniques. The basis for the delisting was leachate analytical results that showed no significant level of contaminants to be present.

- **January 31, 2002:** The third amendment (EPA/AMD/R10-02/030) was signed authorizing the second ERDF expansion to disposal cells 5 through 8, and allowed the staging of remediation waste at ERDF while awaiting treatment.
- **May 2007:** The fourth amendment authorized disposal of certain Hanford Site waste in storage and created a "plug-in" approach of Hanford-only generated waste in storage for ERDF disposal (07-AMRC-0077).
- **July 2009:** The fifth amendment (09-AMRC-0179) authorized supercells 9 and 10, including modification of the cell design to allow a single 'supercell' to be used in place of the double cell side-by-side configuration described in the initial ROD. The requirement that specified that an expansion will be authorized by ROD amendments was also changed to allow ERDF cells to be authorized for construction and operation upon EPA approval through issuance of a fact sheet by DOE.

The fifth ROD Amendment and ESD documents fundamental and significant changes to the remedy set forth in the 1995 ERDF ROD, as amended. The ERDF ROD states that the ERDF will be a single 21.3-m (70-ft)-deep trench consisting of a series of two side-by-side cells, each measuring 152 by 152 m (500 by 500 ft) at the base. The fifth ESD will allow a single "supercell" in place of the side-by-side configuration described in the ROD. A "supercell" is equivalent in size to what has been called two cells in the past. The supercells will continue to be equipped with a double liner and a leachate collection and recovery system that meets the requirements for hazardous waste landfills under RCRA (40 CFR 264, Subpart N), as required by the ERDF ROD. The fifth ESD also authorized the addition of future ERDF cells upon EPA approval through the issuance of a fact sheet by DOE that would be placed in the Administrative Record and Information Repositories, rather than the current ROD amendment process required by the original ERDF ROD. This change will allow additional ERDF cells to be constructed as needed without delay to support the disposal of Hanford Site remediation waste. The additional cells will be located entirely within the 4.1-km² (1,024-ac) area selected for ERDF, as defined in the ERDF ROD. The DOE and EPA will authorize the construction of additional disposal cells as required to support disposal of Hanford Site remediation waste.

1.4.2 Other Relevant Documents

1.4.2.1 Hanford Site Project-Specific Performance Assessments. This ERDF PA also builds on information gained from previous PAs prepared for the Hanford Site, in particular, the Hanford Immobilized Low-Activity Waste Performance Assessment: 2001 Version (DOE/ORP-2000-24, 2001), known as the immobilized low-activity waste (ILAW) PA, and the Initial Single-Shell Tank System Performance Assessment for the Hanford Site (DOE/ORP-2005-01, 2006), known as the SST-PA.

The ILAW PA addresses the disposal of packaged vitrified waste produced by the Hanford Waste Treatment and Immobilization Plant at a location 1.6 km (1 mi) southwest of Waste Management Area (WMA) C. The ILAW PA formed a preliminary basis for the disposal authorization of Waste Treatment Plant ILAW in an undesignated disposal site. Changes in treatment plans and identification of detailed disposal plans have prompted revision of the ILAW PA; that revision is planned in accordance with DOE M 435.1-1, *Radioactive Waste*

Management Manual, to support ILAW and bulk vitrified waste disposal, as well as secondary treatment waste disposal for high-level waste treatment processes. The Hanford Site presently has a disposal authorization statement that also covers disposal of wastes at the Solid Waste Burial Grounds and the ERDF.

The SST-PA (Single-Shell Tank PA) presents the analysis of the long-term impacts of radioactive and chemical contamination in the vadose zone and residual wastes assumed to remain after retrieval of tank wastes and closure of the SST farms. The SST-PA was the first comprehensive look at the closure of the single-shell tank system and builds upon prior field work and documents produced by the Tank Farm Vadose Zone Project.

The following PAs were developed under *Radioactive Waste Management* (DOE Order 5820.2A), a predecessor to DOE O 435.1:

- WHC-SD-WM-EE-004, *Performance Assessment of Grouted Double-Shell Tank Waste Disposal at Hanford* (1995), addresses the disposal of low-level liquid waste from the double-shell tanks. The waste was to be combined with cement, fly ash, and clay to form a grout that would cure and solidify in large subsurface vaults located to the east of the 200 East Area.
- WHC-EP-0645, *Performance Assessment for the Disposal of Low-Level Waste in the 200 West Area Burial Grounds* (1995), addresses the disposal of solid waste from operations at the Hanford Site and other DOE sites. These wastes are placed into trenches in the western part of the 200 West Area, and then covered with a surface cover.
- WHC-SD-WM-TI-730, *Performance Assessment for the Disposal of Low-Level Waste in the 200 East Area Waste Burial Grounds* (1996), addresses waste that is similar to that addressed in the 200 West Area PA (WHC-EP-0645, 1995). However, the disposal trenches for this waste are in the northern part of the 200 East Area.

1.4.2.2 General Hanford Site Environmental Assessments. Several environmental assessments have been prepared in the past at the Hanford Site related to tank waste remediation and solid waste disposal. The most recent, and perhaps the most comprehensive, environmental assessment, called the *Final Tank Closure and Waste Management Environmental Impact Statement for the Hanford Site, Richland, Washington (TC & WM EIS)* (DOE/EIS-0391), was published in November 2012. It combined the scope of the previously published "Solid Waste EIS" (DOE/EIS-0286F) and previously planned "Tank Closure EIS" to evaluate potential environmental impacts of (a) storing, retrieving, treating, and disposing of waste present in underground storage tanks at the Hanford Site; (b) ongoing solid waste management operations as well as proposed disposal of low-level and mixed low-level wastes; and (c) proposed activities to decommission the Fast Flux Test Facility (a nuclear test reactor) at the Hanford Site.

A selected number of environmental assessments prepared for Hanford Site activities are briefly described below. These assessments look at the Hanford Site as a whole or address environmental impacts in a more general manner.

PNNL-11800, *Composite Analysis for Low-Level Waste Disposal in the 200 Area Plateau of the Hanford Site*, was prepared in response to Recommendation 94-2 of the Defense Nuclear Facilities Safety Board (DNFSB) to the Secretary of Energy (DNFSB 1994).

The recommendation noted the need for a risk assessment that investigates the environmental impacts of all radioactive waste disposal actions or leaks at DOE sites. The LFRG conditionally approved the composite analysis in "Disposal Authorization Statement for the Hanford Site Low-Level Waste Disposal Facilities" (DOE 1999a), and provided further documentation in *Low-Level Waste Disposal Facility Federal Review Group Manual* (DOE 1999c). The schedule for updating the composite analysis is presented in DOE/RL-2000-29, *Maintenance Plan for the Composite Analysis of the Hanford Site, Southeast Washington*.

The *Final Hanford Comprehensive Land-Use Plan Environmental Impact Statement* (DOE/EIS-0222-F) analyzed the potential environmental impacts associated with implementing a comprehensive land-use plan for the Hanford Site. In the ROD for this EIS (64 FR 61615), DOE decided to adopt a comprehensive land-use plan for the Hanford Site. The purpose of this land-use plan and its implementing policies and procedures was to facilitate decision making about the site's use and facilities over at least the next 50 years. An Industrial-Exclusive and an Industrial land-use designation were selected for the 200 and 400 Areas, respectively.

The "Hanford defense waste EIS," *Final Environmental Impact Statement: Disposal of Hanford Defense High-Level Transuranic and Tank Wastes, Hanford Site, Richland, Washington*, (DOE/EIS-0113), was prepared to examine the potential impacts of processing transuranic waste and stored tank waste as well as future waste. Most LLW and waste associated with decommissioning of existing surplus or retired Hanford facilities were not considered.

The "Solid Waste EIS," *Final Hanford Site Solid (Radioactive and Hazardous) Waste Program Environmental Impact Statement, Richland, Washington* (DOE/EIS-0286F), addresses the disposal of non-CERCLA LLW at the Hanford Site. Such waste includes LLW generated at the Hanford Site, melters from the Waste Treatment and Immobilization Plant, ILAW, and LLW imported from other DOE sites. The ROD (69 FR 39449) selected the ILAW disposal site as the location of a new disposal facility named the Integrated Disposal Facility.

Pending issuance of a ROD for the *Final TC & WM EIS* (DOE/EIS-0391), the "Solid Waste EIS" remains in effect to support ongoing waste management activities at the Hanford Site.

1.4.2.3 Regulatory Agreements and Documents. The *Hanford Federal Facility Agreement and Consent Order* (Tri-Party Agreement) (Ecology et al. 1989) is an agreement between DOE, EPA, and the Washington State Department of Ecology (Ecology) concerning the cleanup of the Hanford Site. The Tri-Party Agreement contains legally enforceable milestones, many of which cover CERCLA; RCRA Corrective Action; and RCRA treatment, storage, and/or disposal closure activities. These milestones related to wastes that may be disposed of at ERDF are listed in M-015, M-016, and M-037.

1.5 PERFORMANCE CRITERIA

The ERDF landfill PA will estimate radiological exposure to future members of the public for at least a 1,000-year period after closure of the facility to demonstrate there is a reasonable expectation that performance criteria established for the long-term protection of the public and the environment will not be exceeded. Performance criteria consist of specific performance objectives identified in DOE M 435.1-1 and summarized in Table 1-1.

Table 1-1. Performance Objectives and Measure for the ERDF Landfill Performance Assessment.

Performance Objective/Measure	Dose or Concentration Limit	Receptor/Scenario
All-pathways (DOE O 435.1 Chg. 1)	25 mrem/yr effective dose equivalent (excluding dose from radon and progeny in air)	Hypothetical future member of the public exposed at least 100 m from ERDF at maximum dose location.
Atmospheric (40 CFR 61 Subpart H)	10 mrem/yr effective dose equivalent (excluding dose from radon and progeny in air)	Hypothetical future member of the public exposed at least 100 m from ERDF at maximum dose location.
Atmospheric (40 CFR 61 Subpart Q)	20 pCi m ⁻² s ⁻¹ radon flux (at surface of disposal facility)	Representative member of the public exposed at ERDF surface or boundary of facility.
Acute inadvertent intrusion (DOE O 435.1 Chg. 1)	500 mrem effective dose equivalent	Inadvertent intruder at the ERDF.
Chronic inadvertent intrusion (DOE O 435.1 Chg. 1)	100 mrem/yr effective dose equivalent	Inadvertent intruder at ERDF.
Groundwater Protection (40 CFR 141)	Beta-gamma dose equivalent ≤ 4 mrem/yr (based on federal MCL)	Hypothetical future member of the public exposed at least 100 m from ERDF at maximum dose location.
	Gross alpha activity concentration ≤ 15 pCi/L	
	Ra-226/Ra-228 concentration ≤ 5 pCi/L	
	Uranium concentration ≤ 30 µg/L	
	Sr-90 concentration ≤ 8 pCi/L	
	H-3 concentration ≤ 20,000 pCi/L	

CFR = Code of Federal Regulations
MCL = maximum contaminant level

As required by DOE M 435.1-1 IV.P.(2)(d), the dose analysis will use the currently approved DOE dose conversion factors for internal and external exposure of reference adults. The currently approved DOE dose conversion factors are obtained from DOE-STD-1196-2011, *Derived Concentration Technical Standard*, Table A.2 for Inhalation, Table A.1 for Ingestion, and Table A.3 for Air Immersion; and EPA-402-R-93-081, *Federal Guidance Report No. 12, External Exposure to Radionuclides in Air, Water, and Soil*, Table III.7 for external exposure. The effective dose coefficients of parent radionuclides for the external exposure and air immersion pathways are modified to include the dose effects from short-lived progeny by assuming secular equilibrium; effective dose coefficients for ingestion and inhalation already incorporate the dose effects from short-lived progeny.

The following sections describe each performance objective used to assess the long-term performance of the ERDF landfill.

1.5.1 Public Protection Performance Objective

The first applicable performance objective from DOE M 435.1-1 Chg 1 IV P.(I)(a) states:

“Dose to representative members of the public shall not exceed 25 mrem (0.25 mSv) in a year total effective dose equivalent from all exposure pathways, excluding the dose from radon and progeny in air.”

This performance objective is interpreted as requiring the performance analysis to provide a reasonable expectation that the “all-pathways” dose to a hypothetical future member of the public will not exceed 25 mrem effective dose equivalent (EDE), which includes the 50-year committed EDE from ingestion and inhalation of radionuclides, plus the external EDE received during the exposure period (1 year) from all exposure pathways, excluding doses from inhalation of radon and its short-lived progeny. “All-pathways” include any and all modes by which a receptor at the point of public access could be exposed, including the air pathway. The analysis will cover 1,000 years of compliance time period following closure of the disposal facility. Analysis beyond 1,000 years to calculate the maximum dose and the time of that dose shall be included as a means of increasing confidence in the outcome of the modeling. This extended time period will be restricted to 10,000 years following closure, as extrapolating such calculations over longer time frames can lead to excessive uncertainty in predicting the performance of the ERDF (EPA-SAB-RAC-ADV-99-006, 1999). It is expected that the 10,000-year time period will be sufficient to capture the peak dose from the more mobile long-lived radionuclides and will be sufficient to demonstrate the relationship of site suitability to the performance objective. This time period of analysis is also consistent with the recommendations by U.S. Nuclear Regulatory Commission (NUREG-1573, *A Performance Assessment Methodology for Low-Level Radioactive Waste Disposal Facilities: Recommendations of NRC’s Performance Assessment Working Group*). The point of compliance for this performance objective should normally be at the point of highest calculated dose beyond a 100-m buffer zone from the edge of the facility.

The second performance objective (DOE M 435.1-1 Chg 1 IV.P.(I)(b)) states:

“Dose to representative members of the public via the air pathway shall not exceed 10 mrem (0.10 mSv) in a year total effective dose equivalent, excluding the dose from radon and its progeny.”

Consistent with the National Emission Standards for Hazardous Air Pollutants (NESHAP) (40 CFR 61), radon-220, radon-222, and their progeny need not be included in the air-pathway analysis for comparison with the 10 mrem/yr EDE performance objective; separate controls for the emission of radon are discussed below. For the air-pathway dose analysis, the point of compliance should be the point of highest calculated dose beyond a 100-m buffer zone surrounding the waste. The 10 mrem/yr limit should be recognized to refer to all sources, not just the ERDF landfill. Therefore, if the PA assumes a point of compliance that corresponds to the future land-use boundary, a limit that is a fraction of the 10 mrem/yr dose limit should be used in recognition of the potential presence of other sources. Estimates of dose from current Hanford Site facilities are added to the ERDF landfill estimated dose and compared with the 10 mrem/yr dose limit.

The third performance objective (DOE M 435.1-1 Chg 1 IV.P.(l)(c)) states:

“Release of radon shall be less than an average flux of 20 pCi/m²/s (0.74 Bq/m²/s) at the surface of the disposal facility. Alternately, a limit of 0.5 pCi/l (0.0185 Bq/l) of air may be applied.”

The radon limit to be applied at the ERDF landfill is an average ground-surface emanation rate of 20 pCi/m²/s directly over the disposal unit.

1.5.2 Water Resource Impact Assessment

DOE M 435.1-1 Chg 1 does not contain a specific performance objective (e.g., dose or concentration standard) for water resource impacts; instead, DOE M 435.1-1 Chg 1, IV.P.(2)(g) states:

“For the purposes of establishing limits on radionuclides that may be disposed of near-surface, the performance assessment shall include an assessment of impacts to water resources.”

The closest water resource impacted by ERDF is the groundwater resources. The groundwater 100 m downgradient from the disposal site is analyzed to determine if it meets the drinking water standards as specified by 40 CFR 141.66 over the compliance period (see Table 1-1). The impact on groundwater resources will be evaluated by comparing the predicted groundwater concentrations against the drinking water standards.

The State of Washington has adopted the federal drinking water regulations (revised as of July 1, 2009) for MCLs for radionuclides in *Washington Administrative Code* Title 246, Chapter 246-290 (WAC 246-290-025 and WAC 246-290-310). As a result, no separate calculations are needed to satisfy the State of Washington drinking water standard.

1.5.3 Intruder Analysis

DOE M 435.1-1 Chg 1 IV.P.(2) states that the PA shall include an assessment of impacts calculated for a hypothetical person assumed to inadvertently intrude for a temporary period into the LLW disposal facility. For intruder analyses, institutional controls shall be assumed to be effective in deterring intrusion for at least 100 years following closure. It is also stated that the likelihood of inadvertent intruder scenarios may be considered in interpreting the results of the analyses and establishing radionuclide concentrations, if adequate justification is provided.

For the purpose of demonstrating compliance, potential dose to an inadvertent intruder is calculated by assuming intrusion occurs immediately following the loss of institutional controls at 100 years after closure. The peak dose results are compared to the performance measures for chronic and acute exposure scenarios, respectively, of 100 mrem/yr and 500 mrem total EDE (excluding radon in air). Credit is taken for effectiveness of active and passive institutional controls at the Hanford Site in deterring intrusion for at least 100 years following closure consistent with the institutional control assumption in DOE M 435.1-1 Chg 1 IV.P.(2).

Since the primary purpose of an inadvertent intruder scenario is to establish limits on concentrations of radionuclides for disposal, the likelihood of inadvertent intruder scenario needs to be considered. This is important because the concentration limits are affected by radionuclide decay and ingrowth. Establishing limits based on late intruder timing can allow

acceptance of higher radionuclide concentrations compared to earlier intruder timing. The likelihood of inadvertent intrusion at ERDF at 100 years following closure is deemed small because of access restrictions to the site due to following reasons:

1. Given that groundwater remediation in the 200 Area would be ongoing, DOE will be retaining control of the Central Plateau portion of the Hanford Site for a period beyond 100 years. The institutional control is required until the concentrations of hazardous substances in groundwater are at such levels to allow for unrestricted land use and exposure. The monitored natural attenuation remedy identified in the 200-UP-1 and 200-ZP-1 Groundwater Operable Units RODs (EPA/ROD/200UP1 and EPA/ROD/200ZP1, respectively) is estimated to require as long as 125 years.
2. Land use where ERDF is located is established as "Industrial Exclusive" in the NEPA *Record of Decision: Hanford Comprehensive Land-Use Plan Environmental Impact Statement* (64 FR 61615). The land resources used for waste management are considered to be a "permanent commitment" in the EIS (DOE/EIS-0222-F), with the land permanently designated as an area suitable and desirable for treatment, storage, and disposal of hazardous, dangerous, radioactive, and nonradioactive wastes. This land would remain under federal control for the next 150 years or longer (DOE/EIS-0222-F, 1999; DOE/EIS-0391).
3. The ROD for various operable units located in the 200 Area, specifically for the 200-CW-5, 200-PW-1, 200-PW-3, and 200-PW-6 Operable Units (EPA/ROD/200CW-PW), requires long-term institutional controls for waste sites where contamination is left in place and precludes an unrestricted land use. The ROD requires land-use controls to be maintained as long as the residual contamination (from isotopes of plutonium, americium, and cesium) remains at levels that do not allow for unrestricted use and unlimited exposure and shall not be removed without the prior authorization of EPA.

It should be noted that the ROD requirements related to institutional controls are binding, and DOE is responsible for implementing, maintaining, reporting on, and enforcing the institutional controls. Executive Order 12580: Superfund Implementation (EH-231-015/0593), signed by the President of the United States, delegates to a number of federal departments and agencies the authority and responsibility to implement certain provisions of CERCLA. This is the basis of DOE's authority to implement CERCLA at DOE facilities.

Based on the requirements of long-term access restrictions on the Central Plateau portion of the Hanford Site, the probability of having an inadvertent intruder within 100 to 150 years following ERDF closure is expected to be small. However, the likelihood of an inadvertent intruder increases with time. When estimating the likely timing of an inadvertent intruder, the location, accessibility to water resources, and other deterring features of ERDF need to be considered. These are discussed below.

1. Protection from inadvertent intruders involves providing active and passive deterrence to the intruder and disposing waste in a manner that provides some form of intruder barrier that is intended to prevent contact with the waste. To deter the inadvertent intrusion of humans into the waste, a marker system will be used to warn future generations of the dangers of the buried waste. Placement of permanent identification markers for disposal excavations is a requirement per DOE M 435.1-1 Chg 1 IV.P.(6). Permanent markers that identify the potential exposure hazards will be installed at boundaries of the landfill. If these measures should cease, other passive-type measures, such as recognizable warning markers, will

warn the inadvertent intruder from waste buried beneath the permanent cover barrier. Site information will be provided on an Internet website, U.S. Geological Survey maps, libraries, and other information repositories that would be readily available to the public.

2. The ERDF itself presents an obstacle to intrusion because of its size, shape, and recognizability. The ERDF landfill will clearly delineate the boundaries of the surface barrier by providing a distinct contrast with the surrounding terrain. The side slopes are engineered structures that will be obvious that the structure had been built by humans. These distinct side slopes in combination with warning signs are intended to minimize the risk of human intrusion. The facility is expected to maintain its shape and remain recognizable because the stability of the waste volume achieved by compaction is expected to minimize erosion and settlement.
3. The ERDF presents an unusual and distinctive surface feature that might serve to warn away potential intruders because of its height compared to the surrounding landscape. A driller would deliberately have to choose to drill atop ERDF because to do so would require scaling the side-slopes of the ERDF berm with the necessary drilling tools and machinery. Finally, the composition and compaction of the ERDF surface barrier and waste material could be considered an unusual material for which the intruder can be assumed to take reasonable, investigative actions upon discovery.
4. It seems unlikely that well drilling on the top of ERDF constitutes a reasonable inadvertent activity consistent with regional social customs or construction practices. There is no evidence or indication of prolonged human settlement in the 200 Areas prior to the United States government's occupation of the Hanford Site in 1943. The likelihood of community development necessitating a groundwater well on top of the ERDF seems remote. The land along the Columbia and Yakima Rivers, where prior settlement did occur, represents a far more desirable real estate, especially in regard to agriculture because of the abundance of irrigation water.

The above discussion does not consider the level of information or human knowledge that may exist about ERDF. This may be equally important, if not more, than the accessibility to ERDF because if the information exists in the society regarding the waste disposal area in the Central Plateau, it is more likely that humans will avoid that area altogether. After institutional control of the ERDF is lost, knowledge of the ERDF could endure for several hundreds of years because that knowledge may be retained by several different and disparate groups. The DOE, working with Tribal governments and federal, state, and local agencies, will develop several land-use alternatives for the Hanford Site. The cooperating agencies involved with developing these land-use alternatives will likely include the U.S. Department of the Interior (which includes the Bureau of Land Management, Bureau of Reclamation, and U.S. Fish and Wildlife Service); Benton, Franklin, and Grant Counties; and the City of Richland. The consulting Tribal governments will be the Nez Perce Tribe, Yakima Tribe, and the Confederated Tribes of the Umatilla Indian Reservation. With the knowledge of ERDF and its function distributed to so many different groups, it seems reasonable to expect that knowledge will be preserved for several centuries. This should be expected because Hanford Site is no ordinary location; it is now part of the Hanford Reach National Monument that is protected by Presidential proclamation. The national monument protects an irreplaceable natural and historic legacy.

EPA/ROD/R10-95/100 (ERDF ROD), along with its associated amendments, agreed to by the DOE, EPA, and Ecology (collectively referred to as Tri-Parties), authorizes the design, construction, and operation of the ERDF. Placement of waste in ERDF is assumed to represent

a permanent disposal action, involving an irreversible and irretrievable commitment of resources (EPA/ROD/R10-95/100). The commitment of the land used for waste disposal at ERDF was identified as "permanent waste disposal" in the *Siting Evaluation Report for the Environmental Restoration Disposal Facility* (WHC-SD-EN-EV-009, Rev. 2) that was used as a basis in the CERCLA decision-making process. Embedded in the ERDF ROD is the assumption that the protective measures included in the ERDF design such as active institutional controls, passive controls (e.g., markers and off-site records), and a minimum 4.6-m (15-ft)-thick surface barrier are sufficient to prevent inadvertent intrusion into the waste for at least 500 years.

Finally, it should be noted that decisions about the active and passive controls for ERDF cannot be made without considering other waste disposal areas located nearby within the Inner Area designated zone in the Central Plateau as described in DOE/RL-2009-10 (*Hanford Site Cleanup Framework*). Past decisions by the Tri-Parties have already established long-term waste management areas (such as low-level burial grounds and disposal facilities) within the Central Plateau Inner Area. The Tri-Parties have acknowledged that there will be a portion of the Central Plateau that will be dedicated to long-term waste management and containment of residual contamination. The Inner Area is anticipated to be approximately 26 km² (10 mi²), or less, and will remain under federal ownership and control as long as potential hazard exists. No time frame has been provided yet for the federal ownership of the Inner Area, but it is expected to be in the range of several hundred years.

Given that remediation activities will be ongoing and active and passive controls will be placed at and around ERDF, the possibility of having inadvertent intrusion is small at the end of assumed active institutional control period of 100 years. Furthermore, considering the wide distribution of knowledge of waste disposal at ERDF that could persist for considerable time, its elevation compared to the surrounding land posing difficulty in transporting drilling equipment up the berms, availability of plentiful water resources in areas away from the Central Plateau, and status of a National Monument, it is conjectured that inadvertent intruder-based drilling activity would be unlikely event with respect to the 100-year institutional control requirement of DOE M 435.1-1 Chg 1 IV.P.(2).

Even though the probability of intrusion after the loss of the institutional control period is small, it still cannot be fully excluded based on the currently existing state of information, decisions, policy, or regulations. For the purpose of establishing concentration limits for waste acceptance and disposal at ERDF, an inadvertent intrusion timing immediately following loss of institutional controls at 100 years after closure is assumed. This time is consistent with the intruder timing chosen for the peak dose evaluation for the compliance calculations.

1.5.4 ALARA Analysis

For the ERDF facility, the ALARA analysis will focus on comparing the long-term dose expected to a receptor located 100 m downgradient of ERDF to the dose from background radiation along with an evaluation of any potential enhancements in facility performance that could be achieved to further reduce the dose from ERDF. A short and qualitative discussion is expected because the practicality of using additional engineered barriers is limited and comparison of estimated performance with performance objectives in the previous PA indicated that the environmental impacts were minimal.

Engineered barriers to be considered are the double-liner leachate system, waste forms, and the engineered surface cover. Of these, long-term performance will be considered only for waste forms and the engineered cover.

1.6 SUMMARY OF KEY ASSESSMENT ASSUMPTIONS

The conceptual model framework for the ERDF PA can be divided into key conceptual model components, which include descriptions of the subsystems and associated features, events, and processes and assumptions that are important for description of the engineered and natural system. In addition to these assumptions, certain assumptions pertaining to closure activities and the status of ERDF at closure are necessary. The key conceptual model components include the following:

- Engineered barrier degradation
- Model domain and boundary conditions
- Geologic setting
- Infiltration and recharge
- Geochemistry and sorption
- Vadose zone and saturated zone flow and transport
- Groundwater concentration
- Post-closure inventory and source term
- State of ERDF at closure.

These conceptual model components are consistent with those identified in EPA guidelines for the evaluation of the protection of groundwater pathway (EPA 402-R-94-012, Luftig and Weinstock 1997, HNF-5294). Due to limited data and information pertaining to each model component, certain assumptions have to be made. These assumptions are discussed below for each model component.

1.6.1 Engineered Barrier Degradation

A cap or surface barrier is an important engineered barrier for post-closure conditions at ERDF. Once it is emplaced, the surface barrier performance directly impacts the amount of water percolating into the waste.

The surface barrier is designed to provide containment and long-term hydrologic protection for a period of at least 500 years (DOE/RL-93-33, Rev. 1). It is assumed that institutional controls prevent intrusion into the waste for at least 100 years and that passive controls prevent intrusion for 500 years. The design accounts for human and biointrusion control and includes a silt loam moisture storage unit, a capillary break between the silt loam and fill to enhance the storage capacity of the silt, and a geomembrane with a geocomposite drainage layer. Furthermore, it is assumed that because the waste is covered with at least 4.6 m (15 ft) of cover materials, intrusion into the waste due to excavation is precluded. It is also assumed that a surface barrier (RCRA barrier) will be degraded after 500 years so that the recharge through the barrier is similar to that through the undisturbed soil.

For time periods with extant liners under the ERDF cells, it was assumed that all leachate was retained by the high-density polyethylene liner and removed by the leachate collection system. The liners and leachate collection system are assumed to be extant during the entire operational period and for the first 100 years post-closure. The liner is assumed to fail after 100 years. The liner failure is assumed to be contiguous through its full areal extent.

1.6.2 Model Domain and Boundary Conditions

The model domain for the vadose zone and groundwater transport pathway includes the area occupied by current ERDF cells 1 through 10 (as shown in Figure 1-2) along with the berm and the surrounding disturbed and undisturbed area surrounding ERDF. The compliance point is located 100 m from the edge of the berm. The total length of the model domain is about 1.9 km. All of the radionuclide inventory is assumed to be uniformly distributed within cells 1 through 10. No additional cells are considered.

In the vadose zone and groundwater transport model approximation, the extent of the trench at the bottom is 915 m (3,000 ft) in the west-east direction and 305 m (1,000 ft) in the north-south direction. With 3:1 horizontal to vertical side slopes to the trench and a depth of 22 m (72 ft), the extent of the trench at ground surface is 1,050 m (3,440 ft) in the west-east direction and 440 m (1,430 ft) in the north-south direction. According to the exact solution for a trapezoidal prism, the ERDF disposal volume approximation is $8.04 \times 10^6 \text{ m}^3$ ($2.84 \times 10^8 \text{ ft}^3$). Interpolating the trapezoidal volume to the three-dimensional finite difference grid results in the following approximations of the dimensions. At the bottom of the trench, the dimensions are unchanged, but the surface dimensions in the west-east and north-south directions measure 1,035 m (3,400 ft) and 425 m (1,390 ft) in the numerical grid, respectively. Summing the volume of the numerical grid cells representing ERDF waste soil in the three-dimensional finite difference model grid produces a volume of $7.76 \times 10^6 \text{ m}^3$ ($10.2\text{E}+06 \text{ yd}^3$), which is within 4% of the exact solution.

The primary assumptions associated with the model boundary conditions are that the boundaries are chosen far enough away to avoid affecting the results in the area of interest. Boundary conditions applied at the top boundary approximate net infiltration and vary spatially and temporally depending on (1) site conditions, (2) location and physical dimensions of the ERDF, and (3) the timeline of operations. Boundary conditions at the sides of the model domain are assumed to be "no flow" in the vadose zone and "constant head" or prescribed flux in the saturated zone. The bottom boundary of the model in groundwater is defined as a vertical no-flow condition. Forecasted changes in Columbia River stage elevations are unlikely to affect the water table in the 200 West Area (where ERDF is located) due to large distances from the river and change in the hydrostratigraphic unit that forms the unconfined aquifer, moving from the 200 West Area to the 200 East Area.

Air emissions following ERDF closure are estimated using simple models that provide an upper bound on the possible doses from radionuclides in the air above the waste. A simple bounding approach was used to estimate the air release doses to avoid the task of precisely defining release mechanisms, surface barrier air flow properties, and rates of progress through the overlying barrier. The flux is inversely proportional to the distance between the waste and the ground (i.e., through the barrier). Even though the thickness of the surface barrier is not expected to decrease appreciably during its design life or even beyond that, the air-pathway calculation assumes a barrier thickness of 1 m for the purpose of providing an evident upper bound on the estimated radionuclide flux at ground surface.

1.6.3 Representation of Geologic Units

The primary assumption is that the stratigraphy can be adequately represented by the geometric approximation of the geologic units in the numerical grid, and as a porous media continuum. The geology has a large impact on the fate and transport of contaminants because the thickness and heterogeneity of the vadose zone sediment types affects the lateral spreading

and the rate at which contaminants are transported to the saturated zone. In addition, the geologic and hydrologic characteristics affect the sorption of dissolved and mobile contaminants. For the purpose of modeling flow and transport the geologic subunits are combined into hydrostratigraphic units and the hydraulic properties are developed based on the hydrostratigraphic units.

1.6.4 Infiltration and Recharge

The recharge conceptual model component typically has a large impact on the results, especially with respect to long-term recharge rates such as those associated with post-remediation conditions. The groundwater concentration depends on the mass flux of the contaminant into the groundwater, which depends on the recharge entering the aquifer. The primary assumptions associated with the use of recharge rate values concern those values associated with future post-remediation conditions. For all time periods, net infiltration through the ground surface is represented by an average recharge rate, which is dependent on surface conditions. The assumptions include the following:

- During the operation period, which started in 1996 and is assumed to last until 2035, the disturbed zone around the facility has no vegetation cover, but “mature shrub steppe” vegetation will reclaim the surface during the subsequent 100-year institutional control period.
- During the 500-year design life of the surface barrier, the average net infiltration rate is set at 0.5 mm/yr, and then it is doubled for the remainder of the simulation by assuming degraded capability of surface barrier. This is deemed to be a slightly conservative assumption because PNNL-14744, *Recharge Data Package for the 2005 Integrated Disposal Facility Performance Assessment*, indicates that the expected performance for such a barrier is on the order of 0.1 mm/yr for the life of the barrier. They also conclude that, with appropriate design considerations, the possibility of the most likely natural failure mechanisms (i.e., biointrusion of the silt loam layer, wind erosion, and accretion of windblown sand) to occur is quite low, and that the emplaced silt-loam soils is expected to perform as designed indefinitely. Additional details to justify these assumptions are presented in Section 4.2.1 of WCH-515, *Parameter Uncertainty for the ERDF Performance Assessment Uncertainty and Sensitivity Analysis*.
- Side slopes of the surface barrier are assumed to be compacted silty soil and therefore will have recharge similar to the undisturbed land. Additional details are presented in Section 4.2.1 of WCH-515.
- Long-term recharge estimates are primarily based on porewater chloride concentration data from boreholes located in the 200 Area (PNNL-14744). Chloride mass balance calculations factor in variations in past precipitation over long time periods (past several thousand years) and can be used to estimate the future recharge conditions.
- Revegetation of the surface barrier and land impacted by ERDF operations with native plants (e.g., sagebrush [*Artemisia tridentate*] and small bunchgrasses [*Elymus wawawaiensis* and *Poa secunda*]) is assumed to be successful. Revegetation of the land is specifically required by the ERDF ROD, along with other measures to mitigate the ecological impacts caused by construction and operation of the ERDF, including restoration of the site. According to the *Shrub-Steppe and Grassland Restoration Manual for the Columbia River*

Basin (Benson et al. 2011), restoration assists the recovery of an ecosystem that has been degraded, damaged, or destroyed, with the intent to return it to its historic condition. The manual includes the technical information necessary to successfully plan and execute habitat restoration projects for shrub-steppe habitat.

- The vegetation on the surface barrier and surrounding area is further assumed to remain shrub-steppe indefinitely after closure of the ERDF, and exert the same control on recharge that it has in the past. If the estimates of the mean annual precipitation during the past 75,000 years, which range from 25% to 50% below to 28% above modern levels (BHI-00007, *Prototype Hanford Surface Barrier: Design Basis Document*) are indicative and inclusive of future conditions, then the anticipated changes in precipitation rates and patterns resulting from changes in the local climate do not appear to be substantial enough to change the dominant shrub-steppe vegetation or its characteristic ability to control recharge.

Over the period of evaluation considered in this study (1,000 to 10,000 years post-closure), severe climatic change is not expected. The next glaciation period has been estimated to occur tens of thousands of years into the future. The wet and dry cycles that have occurred over the past 10,000 years will likely continue over the next 10,000 years (see Section 2.2.5 of DOE/ORP-2000-24). The variations in the recharge in the future (over next 10,000 years) are therefore expected to be about the same as that of the past. This all assumes that the human disturbances are minimal.

The Columbia Basin appears to be in an interglacial cooling period that began approximately 6,000 years ago and is expected to continue for the next 5,000 to 10,000 years (PNL-10788, *The Role of Plants and Animals in Isolation Barriers at Hanford, Washington*). While human activity may influence the change in climate, it cannot prevent the ultimate onset of the next ice age (PNL-10788). According to the analysis of the pollen record taken from bottom sediments of Carp Lake, located southwest of the Hanford Site, the mean annual precipitation has ranged from 25% to 50% below to 28% above modern levels during the past 75,000 years (BHI-00007). The annual precipitation at the Hanford Site (177 mm [6.98 in.]) is actually less than the lower end of the range usually associated with sagebrush-dominated ecosystems (200 to 500 mm/yr, U.S. Department of Agriculture, Natural Resources Conservation Service, Fact Sheets & Plant Guides, *Artemisia tridentata* ssp. *tridentata* http://plants.usda.gov/plantguide/pdf/pg_artrt.pdf). Therefore, a 28% increase in the annual precipitation only increases the annual amount to 227 mm/yr, which is still much closer to the low end of the range than to the middle of it. The water usage cycle of sagebrush, its ability to photosynthesize very early in the spring, mine water at depth, and curtail its photosynthetic activity and shed leaves to reduce moisture loss during the summer give it an adaptive advantage over sod-forming grasses. These characteristics also allow it to coexist with Pacific Northwest bunchgrasses that are ideally suited to take advantage of the secondary spring maxima, and then die back during the summer drought (PNL-10788).

1.6.5 Geochemistry and Sorption

The geochemical and sorption conceptual model primarily concerns the contaminant release mechanisms in ERDF, and the retardation of contaminants in the vadose zone. For the purpose of the PA analysis, the empirical equilibrium sorption-based approach is assumed to approximate contaminant sorption during transport. The focus of the modeling is on far-field transport, away from waste disposal location, as bulk of the residence time of contaminants is likely to be in the thick vadose zone and saturated zone. Concentration-dependent

sorption/desorption of radionuclides, development of reaction fronts from dissolution and precipitation of mineral phases, and variable soil vapor pressures, are possible at or very close to the source term. But away from the base of ERDF, the radionuclide concentrations are likely to be sufficiently low and given large sorption and buffering capacity in the thick vadose zone the leachate ionic strength and pH are expected to become similar to the ambient porewater within a short distance from the base of ERDF.

The use of the linear isotherm (constant K_d model) is assumed to be generally applicable when contaminants are present at low concentrations as would be expected away from the source, the geochemical environment being modeled is not affected by large spatial or temporal changes, and the amount of the contaminant of interest is not so large as to force the adsorption isotherm to become nonlinear. K_d values are chosen assuming low-salt, near-neutral waste chemistry. It is acknowledged that the K_d values used in fate and transport models are effective K_d values representing the effective combinations of processes contributing to the overall contaminant retardation and/or release behavior. The utility of the empirical linear adsorption model or K_d approach is that it is a simple, useful, and generally practical approach for modeling contaminant adsorption and transport in geologic systems.

1.6.6 Vadose Zone and Saturated Zone Flow and Transport

Averaged and upscaled parameter values for different soil types and geologic units are assumed to adequately represent the bulk flow and transport processes occurring in the vadose zone and saturated zone. Upscaling the parameters incorporates the effects of small-scale textural contrasts that introduce heterogeneity into the flow parameters sufficiently to approximate the bulk flow and transport of contaminants through the vadose zone and saturated zone. A thorough discussion of the upscaling approach and justification is presented in Appendix A.

The current water table is assumed to revert to levels comparable to those existing prior to the onset of Hanford Site operations. Changes in offsite land use (e.g., increased agriculture recharge or new reservoirs, or changes in river stage caused by dam breach, dam removal, or renegotiated treaties) are assumed to cause negligible changes to water levels or gradients in the vicinity of ERDF.

1.6.7 Groundwater Concentration

Contamination from the vadose zone that enters the aquifer is expected to be diluted with the groundwater by advective and dispersive processes. Concentrations calculated in the model for a specified depth, elevation, or interval in the aquifer are assumed to be comparable to concentrations that would be measured by sampling a well with a well screen at the same location. For purposes of calculation of groundwater concentration at the compliance location, a uniform well screen interval of approximately 5 m (16.4 ft) is assumed.

Groundwater in the vicinity of ERDF is located in the 200-UP-1 Operable Unit and has been impacted by Hanford Site operations. The 200-UP-1 ROD selected remedy addresses contaminated groundwater with the expectation of achieving cleanup levels for all contaminants of concern (COCs) in the 200-UP-1 OU, except iodine-129, within 125 years (EPA/ROD/200UP1). Because of the long travel times associated with radionuclide transport through the vadose zone, it is assumed that groundwater entering the upgradient boundary of the ERDF model domain will not contain any preexisting concentrations of radionuclides.

1.6.8 Post-Closure Inventory and Source Term

The groundwater concentration and risk results are often proportional to the contaminant inventory and the initial concentration/distribution in the vadose zone. Many assumptions are necessary for estimating contaminant inventory for developing the characteristics of the source term and are discussed in WCH-479, *Inventory Data Package for ERDF Waste Disposal*. Some of the key assumptions are as follows:

1. No transuranic waste will be disposed at ERDF. Transuranic waste is waste that meets the definition in subsection 180, Section 2 of the *Waste Isolation Pilot Plant Land Withdrawal Act*.
2. The majority of secondary waste generated from WTP operations and tank farm operations are assumed to be disposed at the Integrated Disposal Facility.
3. The mass of radionuclides is distributed evenly through the waste volume. Any local variation in concentration of radionuclides is ignored.
4. Average times are acceptable to estimate radionuclide quantities. Average times were used to decay inventories of the various sources (i.e., an average of 30 years was used to decay the waste in the 200 Area Low-Level Burial Ground [SW-2 Operable Unit]). A 40-year decay period was used for the tritium in the irradiated lithium target cores to provide a better estimate of the tritium inventory.
5. At least another two decades of waste receipt at ERDF is expected, but no offsite waste or tank waste (high-level waste) will be disposed at ERDF.
6. The cesium and strontium capsules along with German logs will not be disposed at ERDF.
7. Waste Greater-Than-Nuclear Regulatory Commission-Class C will not be disposed at ERDF.
8. Technetium-99 in uranium shipped offsite was obtained by difference (total technetium-99 produced in the reactors minus technetium-99 in waste onsite [except US Ecology waste]) is representative. It should be noted over 90% of Hanford uranium was recycled with technetium-99 already in it, and only a small technetium-99 fraction was removed from uranium in the offsite gaseous diffusion plants.

The radionuclides within the waste material (such as bulk soil) are assumed to be distributed homogeneously within the ERDF waste volume. The distribution of waste in ERDF is highly uncertain. While the chronology of waste site disposal at ERDF and the historical availability of the ERDF cells to receive the waste are known, ERDF operations make no effort to segregate waste received from the particular waste sites after disposal. When new cells have opened, waste from existing cells is often spread to the new cells to level the surface of the overall disposal area. Such mixing and redistribution of waste in the cells greatly diminishes the ability to approximate the spatial distribution of the radionuclides.

Groundwater pathway transport calculations are performed assuming a unit inventory source concentration and then scaling the results to the disposed inventory. The primary waste form is excavated soil with residual contamination that is generated from remedial actions taken at contaminated waste sites. Local equilibrium conditions are assumed in these soils from the contaminant release point of view because several pore volumes have likely been flushed

through these soils prior to remedial actions. In addition, because of thick vadose zone underneath ERDF, a large sorption capacity and chemical buffering capacity exists that would support assumption of linearity in sorption-desorption characteristics and transport behavior within a short distance from the base of ERDF.

1.6.9 State of ERDF at Closure

- Facility closure is assumed to occur in year 2035 for the purpose of analysis. The currently forecasted waste inventory at closure is estimated from waste sites where remediation decisions have been made (see Table 3-1). The waste inventory at closure is assumed to be no greater than the current ERDF inventory and forecast waste inventory identified in WCH-479.
- A modified RCRA-compliant surface barrier is assumed to be constructed at closure, which would provide containment and long-term hydrologic protection for a period of at least 500 years, after which the recharge through the barrier would become similar to that through the undisturbed soil as discussed in Section 3.4.1.3. The vegetation on the surface barrier and surrounding area is assumed to remain shrub-steppe after closure and exert the same control on recharge as a vegetated natural soil surface thereby maintaining an average recharge rate not exceeding 1 mm/yr underneath the surface barrier.
- The surface barrier will be designed to retain moisture and encourage evapotranspiration, maintaining the average recharge through the surface barrier to less than 0.5 mm/yr for 500 years under reasonably expected natural conditions. The upper surface of the soil cover will be composed of an admixture of silt and gravels to enhance resistance of the cover to burrowing animals and long-term wind erosion as per the design requirements mentioned in Section 2.2.2. Prior to cover construction, closure cover designs will be evaluated and the most appropriate closure cover design will be selected for construction. The design will, at a minimum, comply with applicable RCRA requirements found at 40 CFR 264, Subpart N.
- The surface barrier will be designed so that top of the waste is at least 4.6 m (15 ft) below the top of the surface barrier. Because of the large thickness the possibility for biotic intrusion into the waste from the surface is excluded (see Section 3.6 for details). Additional cover design details are presented in Sections 2.2.1 and 2.2.2.
- The compaction of waste in the ERDF must be sufficient to ensure that any long-term differential settlement under the load of surface barrier is within the design criteria of the surface barrier discussed in Section 2.2.3. The waste disposed in ERDF will be compacted to minimize settlement to meet the compaction acceptance criteria for ERDF discussed in Section 2.2.2.2.
- The double-leachate liners and collection and removal system are assumed to be extant during the entire operational period and for the first 100 years post-closure, but fail completely after 100 years. After the system fails, the inventory is assumed to become immediately available for release and transport through the composite liner material by advection and diffusion processes.
- The post-closure exposure scenarios assume that no residents live on top of the ERDF, and a resident groundwater receptor will have to be at least 100 m downgradient from the facility. It is assumed that institutional controls continue for at least 100 years after closure.

A combination of land-use restrictions, institutional controls, and active and passive barriers will be placed on and around the ERDF landfill and its adjacent buffer zone to deter inadvertent intrusion.

- For air-pathway modeling, a surface barrier thickness of 1 m is assumed to provide an upper-bound estimate of the radionuclide flux at ground surface from ERDF.

1.7 COMPARISON OF THE ERDF PERFORMANCE ASSESSMENT TO OTHER HANFORD SITE PERFORMANCE ASSESSMENTS

This section compares and contrasts the features and assumptions in three other Hanford Site PAs against those in the current ERDF PA. The ERDF PA as well as the other Hanford Site PAs provide reasonable assurance that the analysis, results, and conclusions of the PAs provide both a reasonable representation of the disposal facility's long-term performance, and a reasonable expectation that the disposal facility will remain in compliance with DOE O 435.1. The three other PAs are as follows:

- 200 West Area Solid Waste Burial Grounds Performance Assessment (WHC-EP-0645)
- 200 East Area Solid Waste Burial Grounds Performance Assessment (WHC-SD-WM-TI-730)
- Integrated Disposal Facility (IDF) Performance Assessment (RPP-15834).

The overall groundwater pathway, air pathway, and inadvertent intruder scenario for the preceding three PAs are consistent with those used in ERDF PA. Certain features and assumptions for ERDF PA are common to features and assumptions used in other Hanford Site PAs. Similar to ERDF PA groundwater pathway modeling, the compliance case (base case or reference case) analysis for the preceding three Hanford Site PAs utilize the following features and assumptions:

- A simulation period in excess of 1,000-year compliance period is used for evaluation due to the long time it may take for any discernible impacts to be observed in the environment.
- The burial ground PAs do not specify a facility closure date; the IDF PA estimates facility closure occurring in 2046, and the ERDF PA estimates facility closure occurring in 2035.
- For disposal facilities with significant radionuclide inventory, a surface barrier to infiltration is placed over the facility at closure and is assumed to perform at its design specifications for 500 years following closure, and then to perform in a degraded manner until the end of the simulation.
- For each PA, site-specific simulation information are developed including those for geology, contaminant inventory, and media properties.
- For the long-term simulations over tens of thousands of years, the infiltration rates are averaged on a yearly basis and the discrete episodic nature of the precipitation events are ignored.

- A range of distribution coefficient (K_d) values is used to represent sediment-contaminant chemical interaction. Single values and ranges of values are chosen that are radionuclide-specific. However, the same values are sometimes used for groups of radionuclides that show similar levels of chemical reactivity with Hanford Site soils and sediments.
- The overall long-term orientation of the unconfined aquifer flow follows the pre-Hanford condition, i.e., from west to east toward the Columbia River.

For ERDF PA as well as for other PAs, sensitivity and uncertainty analyses are conducted relative to the compliance case to provide insight into the impacts that selected assumptions and data choices have on the results. The inadvertent intruder pathway assumes intentional drilling through the disposal facility wastes and the subsequent spreading of the exhumed waste over the immediate area, ignoring both institutional and engineered controls left in place after closure. Other PAs assumed 500 years after closure as the likely time of inadvertent intrusion to calculate the radionuclide concentration thresholds. Similar to other PAs, modeling of the air migration pathway in the ERDF PA, in general, uses a bounding analysis because of the low impacts associated with the volatilization of radioactive gases.

With similarities notwithstanding, there are several important unique differences, as described below, between the current PA and other Hanford Site PA features and assumptions, especially relative to vadose zone flow and transport modeling:

- Unlike other PAs that use two-dimensional flow and transport, the ERDF PA uses a three-dimensional modeling domain.
- The ERDF PA recharge estimate for the closure surface barrier is based on the latest data and analysis of results for the 15-year continuous study of the Hanford Prototype Barrier in the 200 East Area (Appendix D). The large barrier performance data set and its analysis were nonexistent for earlier PAs.
- The ERDF PA modeling assumes that radionuclides are migrated with infiltrating moisture. For Hanford low-level solid waste burial grounds' PA, radionuclide release rates are modeled as advection-dominated, or diffusion-dominated, or solubility controlled release (WHC-EP-0645, WHC-SD-WM-TI-730). For the IDF PA, a specialized chemical weathering and transport code (STORM) is used to model release from vitrified glass waste form (RPP-15834).
- The ERDF PA vadose zone properties are based on the best available data set for the ERDF site as well as data from neighboring sites for similar lithostratigraphic units (WCH-464). Although the other three Hanford Site PAs use site-specific data to derive vadose properties, the available site-specific data were very limited and do not account for the additional knowledge and insight gained from neighboring borehole data.
- For the ERDF PA, using state-of-the-art stochastic upscaling techniques, each heterogeneous geologic unit is replaced by its homogeneous equivalent, and each geologic unit is assigned its upscaled or effective hydraulic properties (Chapter 3.0). No upscaling is considered in other PAs, and consequently the impact of media heterogeneities for the highly heterogeneous Hanford Site sediments is ignored.
- For the ERDF PA, the saturated media properties for the unconfined aquifer are based on large-scale slug tests and pumping. For the 200 East Area solid waste PA, the saturated hydraulic conductivity estimate for Ringold E is based on small-scale permeameter tests

(WHC-SD-WM-TI-730). The use of small-scale measurements for large-scale aquifer flow is not desirable.

Unlike other PAs, the ERDF PA features a discussion of alternate vadose zone conceptual models (Chapter 3.0 and Appendix A). This discussion includes results of independent testing of the vadose zone conceptual model used in current PAs as well as alternate conceptual models using the extensive data set of moisture content profiles at the neighboring Sisson and Lu field injection test site in the 200 East Area (Appendix A).

1.8 QUALITY ASSURANCE MEASURES

The work was completed according to the CH2M Hill Plateau Remediation Company (CHPRC) Environmental Quality Assurance Program Plan (CHPRC-00189). The intent of adhering to CHPRC environmental quality assurance requirements is to comply with Title 10, *Code of Federal Regulations* (CFR), Part 830, "Nuclear Safety Management," and Subpart A, "Quality Assurance" (10 CFR 830); DOE O 414.1D, *Quality Assurance*; and state and federal environmental regulations.

Quality assurance project planning for modeling follows the guidance in EPA/240/R-02/007, *Guide for Quality Assurance Project Plans for Modeling*. Model project planning includes documenting specific model development efforts and applications. It addresses as relevant and important all nine "Group A" elements presented in EPA/240/B-01/003, *EPA Requirements for Quality Assurance Project Plans*. The nine elements include problem definition and background, quality objectives and criteria for measurements and data acquisition leading to model inputs and outputs, data validation and usability, references, documentation and records management, special training requirements and certifications for modelers, and assessments and reports to management. The model documentation requirements identified during project planning align with DOE management expectations for compliance listed in EM-QA-001, Rev. 1, *EM Quality Assurance Program*, Attachment H, "Model Development, Use, and Validation."

All software used to implement the models was used in accordance with CHPRC procedure PRC-PRO-IRM-309, *Controlled Software Management*, to manage software, including configuration control, evaluation, implementation, verification and validation, and operation and maintenance. The software used to implement the models and perform calculations was approved under the requirements of, and use was compliant with, CHPRC-controlled software management procedures that align with DOE management expectations for compliance listed in EM-QA-001, Rev. 1, *EM Quality Assurance Program*, Attachment G – Software Quality Requirements.

The ERDF PA relies on two software packages to simulate the flow and transport in the subsurface, simulate source term releases, conduct inadvertent intruder calculations, and simulate air-pathway transport in order to calculate doses resulting from the disposal of waste at the ERDF. Both STOMP and GoldSim®⁴ Pro are qualified for controlled use by the CHPRC in accordance with their respective software management and testing plans and are registered in the Hanford Information Systems Inventory (HISI). HISI provides the platform for tracking all software in use at the Hanford Site, the approved versions, the authorized users, and instances

⁴ GoldSim® Pro is a registered trademark of GoldSim Technologies, Issaquah, Washington, in the United States and other countries.

of the software's usage. Software-specific descriptions and associated quality assurance documentation for each software package used in the PA are provided in more detail below.

1.8.1 STOMP

The vadose zone fate and transport calculations are performed using CHPRC Builds 2 and 3 of the STOMP software (PNNL-15782, *STOMP Subsurface Transport Over Multiple Phases: User's Guide Version 4.0*), registered in the HISI under identification number 2471. STOMP was developed at Pacific Northwest National Laboratory to meet NQA-1 -2000 software requirements, as well as the requirements specified under DOE Order 414.1D for Safety Software. STOMP use by the CHPRC for the ERDF PA is managed and controlled such that the computational needs filled by use of STOMP (and any associated utility codes) and the specific roles and responsibilities for management and the modeling staff and subcontractors have been identified and traced. These responsibilities include modeler training, source code installation and testing, preserving the software and verification test results, operation and maintenance of the original Fortran source code and executable files, validation and verification that the Pacific Northwest National Laboratory quality assurance documentation demonstrate that STOMP meets the CHPRC modeling needs and purposes, reporting and documenting any software errors (none encountered during the ERDF PA), management of the STOMP input files, and contingency and disaster recovery (not encountered during the ERDF PA). Acceptance and installation tests of the STOMP simulation software demonstrate that it is appropriate for its intended uses for the ERDF PA and that it has been successfully installed on CHPRC and CHPRC subcontractor computing systems.

STOMP was executed on the INTERA Richland GREEN Linux® cluster that is owned and managed by INTERA, Incorporated, a pre-selected subcontractor to the CHPRC. The computer property tag identifier for the front end node is #469 at INTERA's Richland, Washington office. This node is a DELL™ PowerEdge™ R510 with two 6-core Intel Xeon X5660 processors @ 2.80GHz and 48 GB of RAM.

DOE/RL-2011-50 contains a summary of the main model attributes and code selection criteria that serve as the basis for the demonstration of the adequacy of the STOMP code for use in vadose zone modeling at the Hanford Site. The results of the evaluation in DOE/RL-2011-50 show that the STOMP code is capable of meeting or exceeding the identified attributes and criteria.

1.8.2 GoldSim

Software development of Goldsim® Pro meets NQA-1 -2000 software requirements, as well as the requirements specified under DOE Order 414.1D for Safety Software. Goldsim® Pro use by the CHPRC for the ERDF PA is managed and controlled such that the computational needs filled by use of Goldsim® Pro (and any associated utility codes) and the specific roles and responsibilities for management and the modeling staff and subcontractors have been identified and traced. These responsibilities include modeler training, source code installation and testing, preserving the software and verification test results, validation and verification that the Goldsim® Pro quality assurance documentation demonstrate that Goldsim® Pro meets the CHPRC modeling needs and purposes, reporting and documenting any software errors (none encountered during the ERDF PA), management of the Goldsim® Pro input files, and

® Linux is the registered trademark of Linus Torvalds in the U.S. and other countries.
™ DELL and PowerEdge are trademarks of Dell Inc.

contingency and disaster recovery (not encountered during the ERDF PA). Acceptance and installation tests of the Goldsim® Pro simulation software demonstrate that it is appropriate for its intended uses for the ERDF PA and that it has been successfully installed on CHPRC and CHPRC subcontractor computing systems.

1.8.3 Documentation and Records

The three basic model components necessary to provide traceable, reproducible models, which are (a) the models themselves, (b) the basis for the model inputs, including data packages, and (c) the applications, are maintained in the Environmental Model Management Archive (EMMA). EMMA is identified in the Quality Assurance Project Plan (CHPRC-00189) as the approved means to maintain traceability and reproducibility for all model components by change control and version preservation of the model inputs, output, and identification of the software used. EMMA is essentially a disciplined file directory, but includes a software interface to enable identification of linkages between a specific basis, model, and the application components.

The model package reports provide the description and explanation of the modeling objectives, conceptualization, implementation, uncertainty and sensitivity evaluations, configuration control, and the limitations of the models. While the model package reports include information regarding the complete configuration managed version of the ERDF models, the environmental calculation includes the application of the STOMP and Goldsim® Pro models used to perform the calculations. The model package reports and environmental calculations prepared in support of the ERDF PA are archived on EMMA.

STOMP and GoldSim® Pro software configuration management utilizes MKS Integrity®⁵, which is the Hanford Site standard for preserving and managing source code and executable versions of software. MKS Integrity® provides a "checkpoint" feature that locks files at particular points, such as when an executable has passed quality assurance testing and is issued as ready for use.

⁵MKS Integrity, Integrity, and all other PTC product names and logos are trademarks or registered trademarks of Parametric Technology Corporation or its subsidiaries in the United States and in other countries.

2.0 DISPOSAL FACILITY CHARACTERISTICS

This section describes the Hanford Site, the environment, the ERDF landfill, and LLW characteristics. This information provides the basis for the PA conceptual model and an understanding of the method of analysis.

2.1 SITE CHARACTERISTICS

This section describes the geography and demography of the Hanford Site, including use of adjacent lands, the current population database, area socioeconomics, past and planned DOE activities, and the results of an investigation of future uses conducted for inclusion in the *Final Hanford Comprehensive Land-Use Plan Environmental Impact Statement* and associated ROD (DOE/EIS-0222-F, 64 FR 61615). Additional detailed information on the geography and demography of the site can be found in PNNL-6415, *Hanford Site National Environmental Policy Act (NEPA) Characterization*.

2.1.1 Geography and Demography

The Hanford Site encompasses approximately 1,517 km² (586 mi²) in Benton, Franklin, and Grant Counties, located in south-central Washington State within the semi-arid Pasco Basin of the Columbia Plateau. The Hanford Site stretches approximately 50 km (30 mi) north to south and about 40 km (24 mi) east to west, immediately north-northwest of the confluence of the Yakima and Columbia Rivers, the Cities of Kennewick, Pasco, and Richland (the Tri-Cities), and the City of West Richland. The Columbia River flows 80 km (50 mi) through the northern part of the Hanford Site and, turning south, forms part of the Site's eastern boundary. The Yakima River runs near the southern boundary of the Hanford Site, joining the Columbia River at the City of Richland. Rattlesnake Mountain, Yakima Ridge, and Umtanum Ridge form the southwestern and western boundaries of the Site, and Saddle Mountain forms its northern boundary. The plateau of the central portion of the Hanford Site is punctuated by two small east-west ridges, Gable Butte and Gable Mountain. Lands adjoining the Hanford Site to the west, north, and east are principally range and agricultural.

In June 2000, a Presidential proclamation (65 FR 37253) established the 78,917-ha (195,000-ac) Hanford Reach National Monument to protect the nation's only unimpounded stretch of the Columbia River above Bonneville Dam and the largest remnant of the shrub-steppe ecosystem that once blanketed the Columbia River Basin. In 2003, DOE and the U.S. Fish and Wildlife Service began management of the monument. The U.S. Fish and Wildlife Service administered three major management units of the monument totaling approximately 668 km² (258 mi²). These included (1) the Fitzner/Eberhardt Arid Lands Ecology Reserve Unit, a 311-km² (120-mi²) tract of land in the southwestern portion of the Hanford Site; (2) the Saddle Mountain Unit, a 129-km² (50-mi²) tract of land located north-northwest of the Columbia River and generally south and east of State Highway 24; and (3) the Wahluke Unit, a 225-km² (87-mi²) tract of land located north and east of both the Columbia River and the Saddle Mountain Unit.

The portion of the monument administered only by DOE included the McGee Ranch/Riverlands Unit (north and west of State Highway 24 and south of the Columbia River), the Columbia River islands in Benton County, the Columbia River corridor (one-quarter mile inland from the

shoreline) on the Benton County side of the Columbia River, and the sand dunes area located along the Hanford Site side of the Columbia River north of the Energy Northwest facilities.

2.1.1.1 Disposal Site Location. The ERDF site is located in an area of the Hanford Site Central Plateau between the 200 West Area and the 200 East Area (Figure 1-1). It is located near the southeastern boundary of the 200 West Area and just west of the disposal facility operated by US Ecology. Selection of this site resulted from an evaluation of criteria developed from applicable federal and state regulations, including CERCLA and criteria specified in the Washington State Dangerous Waste Regulations, DOE orders, and recommendations for future Hanford Site use from the Hanford Future Site Uses Working Group (HFSUWG). No other proposed location in the waste management area recommended by the HFSUWG met the size requirement. Final selection of this site occurred because of the following factors:

- The site is located in the waste management area delineated by the HFSUWG.
- The depth to groundwater is greater than any of the other proposed sites.
- The distance to the Columbia River is greater than any of the other proposed sites.
- The site has relatively flat topography, which reduces the complexity of design and construction.
- The site has the lowest development cost from among all of the proposed sites.

2.1.1.2 Disposal Site Description. Prior to construction of ERDF, the surface and shallow portion of the vadose zone were undisturbed because no Hanford operations occurred at the site. The elevation of the ERDF site before construction began ranged from 207 to 229 m (680 to 750 ft) above mean sea level (DOE/RL-93-99). The ERDF is constructed in a modular fashion so that added disposal space can be built on toward the east as needed. The first eight disposal cells were built in pairs located at the west end of ERDF. Each cell covers about 3 ha (8 ac), 152 m (500 ft) square at the bottom and 152 by 69 m (500 by 225 ft) side slope. The latest cell construction (supercells 9 and 10) combines the pairs into one larger cell approximately the same size as each pair of cells.

The east-west length of the ERDF will depend on the accrual volume of waste that is eventually disposed in the facility. The current plan is to construct short modules at the western end of the facility and add adjacent modules to the east as necessary.

2.1.1.3 Population Distribution. Demographic data are used in a PA to help set the scenarios for assessing risk and to select the dosimetry parameters. The major population centers within 80 km (50 mi) of the Hanford Site are identified in Figure 2-1, along with populations based on the 2010 Census (OFM 2011) estimates. This radius is centered on the Hanford Meteorological Station (HMS), located between the 200 East and 200 West Areas and approximately 1.6 km (1 mi) from ERDF. Portions of Benton, Franklin, Adams, Grant, Kittitas, Yakima, Klickitat, and Walla Walla Counties in Washington, and Morrow and Umatilla Counties in Oregon lie within the 80-km (50-mi) radius. Most of the people reside in Benton and Franklin Counties, which are two of the fastest growing counties in Washington with rates of growth during the 2000s of 23% and 58%, respectively.

mostly to the southwest and the southeast, live between 32 and 48 km (20 and 30 mi) from ERDF (PNNL-20631). The statewide 2010 population census results are available from the Washington State Office of Financial Management.

2.1.1.4 Uses of Adjacent Lands. This section describes the socioeconomics of the region, historical use of the land, and the expected future use of the land.

2.1.1.4.1 Socioeconomics. The major employers in the Tri-Cities area since 1970 have been DOE and the Hanford Site contractors; Energy Northwest (formerly the Washington Public Power Supply System), which operates a nuclear power plant north of Richland; agriculture; and a large food-processing industry; plus several smaller industrial operations. Other than DOE activities, agriculture and food processing are the dominant industries. The socioeconomics of the area surrounding the Hanford Site are more fully described in Section 4.7 of PNNL-6415.

The land use classification around the Hanford Site varies from urban to rural. Most of the land south of the Hanford Site is urban, including the Tri-Cities, while much of the land to the north and east is irrigated crop land. Most of the irrigation water comes from the Bureau of Reclamation Columbia Basin Project, which uses the water behind Grand Coulee Dam as the primary water source. The water is transported via canals to the areas north and east of the Columbia River. The land to the west of the Hanford Site is used for irrigated agriculture near the Yakima River and dry-land farming at the higher elevations. The Columbia River is used by the cities of Richland, Pasco, and Kennewick for drinking water. It is also used for recreation and hydroelectric power production for the western United States, and is a primary salmon spawning ground.

2.1.1.4.2 Past and Present DOE Activities at the Hanford Site. In 1943, the U.S. Army Corps of Engineers created the Hanford Site from small farming areas along the Columbia River to locate facilities used to produce nuclear weapon materials for World War II (WHC-MR-0293). Since then, the major activities on the Hanford Site have been controlled by DOE and its predecessors, the U.S. Atomic Energy Commission (1945 through 1975) and the Energy and Research Development Administration (1975 through 1976). Current major programs at the Hanford Site are dedicated to waste management, environmental restoration, long-term stewardship, and research and development.

DOE nuclear facilities occupy about 6% of the total available area of the site. The major operating areas, as shown in Figure 1-1, are identified by numbers: 100 Areas, 200 Areas, 300 Area, and 400 Area. The activities conducted in these areas are described in the following paragraphs.

100 Areas. The 100 Areas, directly bordering the Columbia River (Figure 1-1), contain nine graphite-moderated plutonium production reactors, eight of which were shut down by the early 1970s. The ninth is the N Reactor, the first dual-purpose reactor built in the United States. N Reactor began operating in 1963 and was shut down in 1986.

200 Areas. Fuel reprocessing, plutonium and uranium separation, plutonium finishing, and waste management, including treatment, storage, and disposal activities have been conducted in the 200 Areas. Waste from the research and development activities and fuel fabrication activities in the 300 Area, reactor operation programs conducted in the 100 Areas, and the Fast Flux Test Facility (FFTF) in the 400 Area is sent to the 200 Areas for storage and disposal. Waste management activities are scheduled to continue until the mid-21st century.

Waste management facilities are located in the 200 Areas, which are surrounded by security fencing. The following major facilities, many of which are inactive, are located in the 200 Areas.

- Burial trenches, burial grounds, and LLW burial grounds
- 18 underground storage tank farms (A, AN, AP, AW, AX, AY, AZ, B, BX, BY, C, S, SX, SY, T, TX, TY, and U tank farms)
- Very large fuel processing and recovery facilities (B, T, U, and Z Plants, and the Reduction-Oxidation [REDOX] and Plutonium Uranium Extraction [PUREX] facilities)
- Tank wastewater evaporator facilities (242-A, 242-S, and 242-T Evaporators)
- Office and warehouse buildings.

Between and just south of the 200 East and 200 West Areas is the ERDF (Figure 1-1). This facility is a trench system and will hold most of the contaminated soil and materials from facility decontamination and decommissioning and Hanford Site remediation.

Washington State leases a 3.9-km² (1.5-mi²) parcel located between the 200 West and 200 East Areas, which, in turn, subleases a portion of this land to US Ecology, Inc., a private company, for the disposal of commercially generated low-level radioactive waste.

400 Area. The FFTF is located in the 400 Area. This facility contains a liquid-metal cooled fast reactor previously used for testing breeder reactor fuels, materials, and components. The FFTF operated from 1982 until 1992. Energy Northwest leases a 4.4-km² (1.7-mi²) parcel northeast of the 400 Area for a commercial nuclear power reactor. The Columbia Generating Station, a boiling-water reactor, currently is the only operating nuclear reactor on the Hanford Site.

300 Area. Originally, the 300 Area was dedicated to fabricating fuel for Hanford Site reactors. Now, the 300 Area laboratories constructed over the last 30 years are used for research programs. Accelerated deactivation in the 300 Area focuses on several 300 Area buildings and structures that date back to 1943. It includes fuel supply facilities that were used to support the manufacturing of nuclear fuel for the Hanford Site reactors.

2.1.1.5 Future Hanford Land Use. In 1992, DOE, EPA, and Ecology gathered a group of stakeholders to study potential future uses for the Hanford Site land. This HFSUWG issued a summary (HFSUWG 1992a) and a detailed report (HFSUWG 1992b) of its findings. The Final Hanford Comprehensive Land- Use Plan Environmental Impact Statement (DOE/EIS-0222-F) is heavily based on the work of the HFSUWG. However, DOE land-use planning extends for only 50 years instead of the 100 years forecast by the HFSUWG.

HFSUWG (1992a) contains the following statement about near-term use of the 200 Areas, called the Central Plateau in the report:

“The presence of many different types of radionuclides and hazardous constituents in various forms and combinations throughout the site poses a key challenge to the Hanford cleanup. To facilitate cleanup of the rest of the site, wastes from throughout the Hanford Site should be concentrated in the Central Plateau. Waste storage, treatment, and disposal activities in the Central Plateau should be concentrated within this area as well, whenever feasible, to minimize the amount of land devoted

to, or contaminated by, waste management activities. This principle of minimizing land used for waste management should specifically be considered in imminent near-term decisions about utilizing additional uncontaminated Central Plateau lands for permanent disposal of grout.”

The report continues on the subject of future use options (HFSUWG 1992a):

“In general, the Working Group desires that the overall cleanup criteria for the Central Plateau should enable general usage of the land and groundwater for other than waste management activities in the horizon of 100 years from the decommissioning of waste management facilities and closure of waste disposal areas.”

Based on conversations of the HFSUWG, they could not agree on a definition of “general use.” For the “foreseeable future,” the HFSUWG developed options involving waste treatment, storage, and disposal of DOE low-level radioactive waste. The differences among the options are whether offsite waste (radioactive and/or hazardous) would be allowed to be disposed of on the Hanford Site. Finally, the report states (HFSUWG 1992a):

“The working group identified a single cleanup scenario for the Central Plateau. This scenario assumes that future uses of the surface, subsurface, and groundwater in and immediately surrounding the 200 West and 200 East Areas would be exclusive. Surrounding the exclusive area would be a temporary surface and subsurface exclusive buffer zone composed of at least the rest of the Central Plateau. As the risks from the waste management activities decrease, it is expected that the buffer zone would shrink commensurately.”

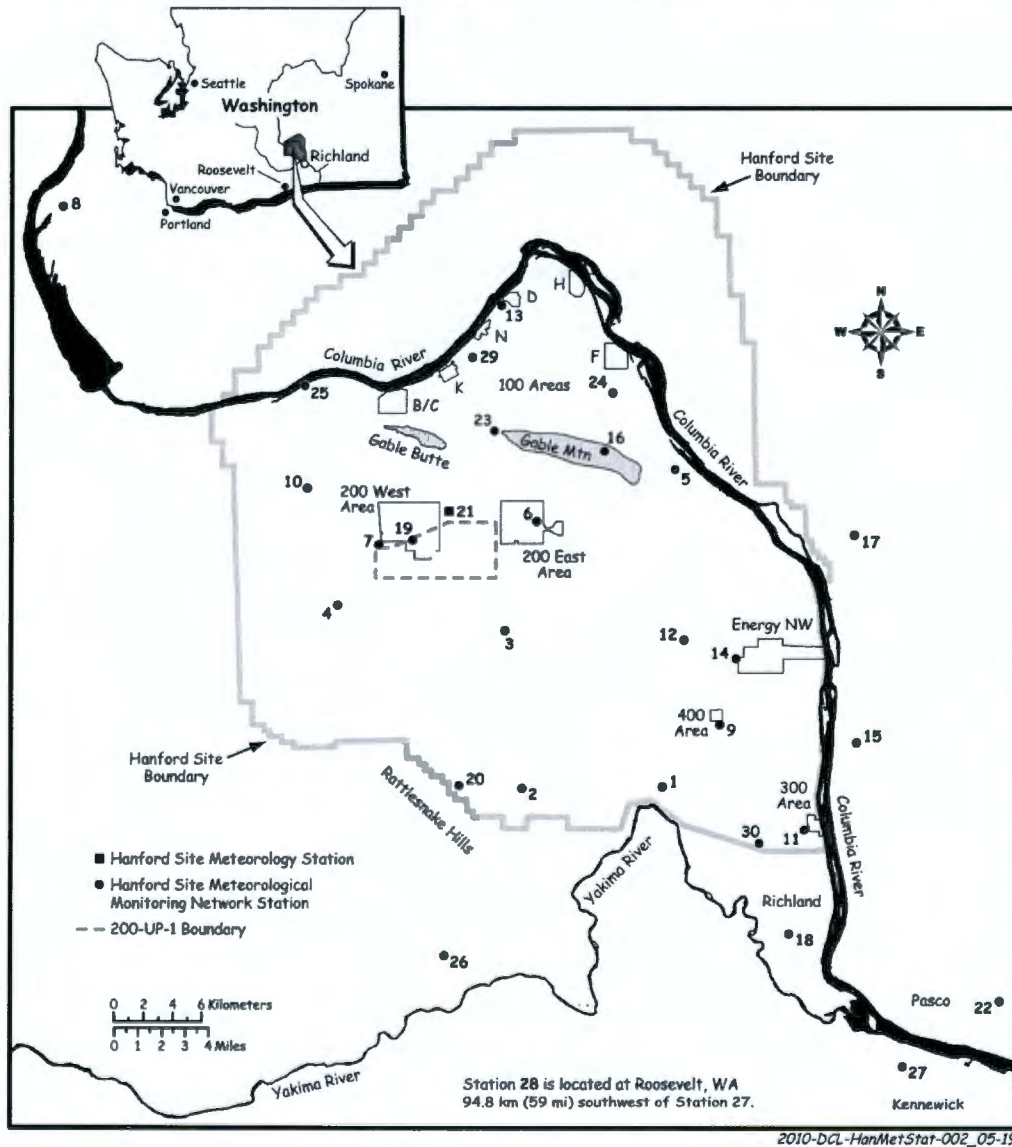
For nearer term land-use planning, the ROD (64 FR 61615) for DOE/EIS-0222-F, *Final Hanford Comprehensive Land-Use Plan Environmental Impact Statement*, identifies near-term land uses for the Hanford Site. The ROD prescribes the use in the 200 Areas as exclusively industrial (primarily waste management) with much of the surrounding land having the use of preservation or conservation. The Hanford Reach National Monument was established along the Columbia River corridor as well in lands at the northern and western edges of the site (65 FR 37253). For further discussion of Hanford land uses see DOE/EIS-0222-F and DOE/RL-2009-10, *Hanford Site Cleanup Completion Framework*.

2.1.2 Meteorology and Climatology

The Pacific Ocean moderates temperatures throughout the Pacific Northwest, and the Cascade Range (approximately 113 km [70 mi] west of the Hanford Site) generates a rain shadow that limits rain and snowfall in the eastern half of Washington State. The Cascade Range also serves as a source of cold air drainage, which has a considerable effect on the wind regime of the Site. The Rocky Mountains to the north and east of the region shield the area from the severe winter storms and frigid air masses that move southward across Canada.

Climatological data for the Hanford Site are compiled at the HMS, which is located on the Central Plateau, just outside the northeast corner of the 200 West Area and about 4 km (3 mi) west of the 200 East Area. To characterize meteorological differences accurately across the Hanford Site, the HMS operates a network that currently contains 30 monitoring stations (Figure 2-2).

Figure 2-2. Hanford Meteorological Monitoring Network Location Map.



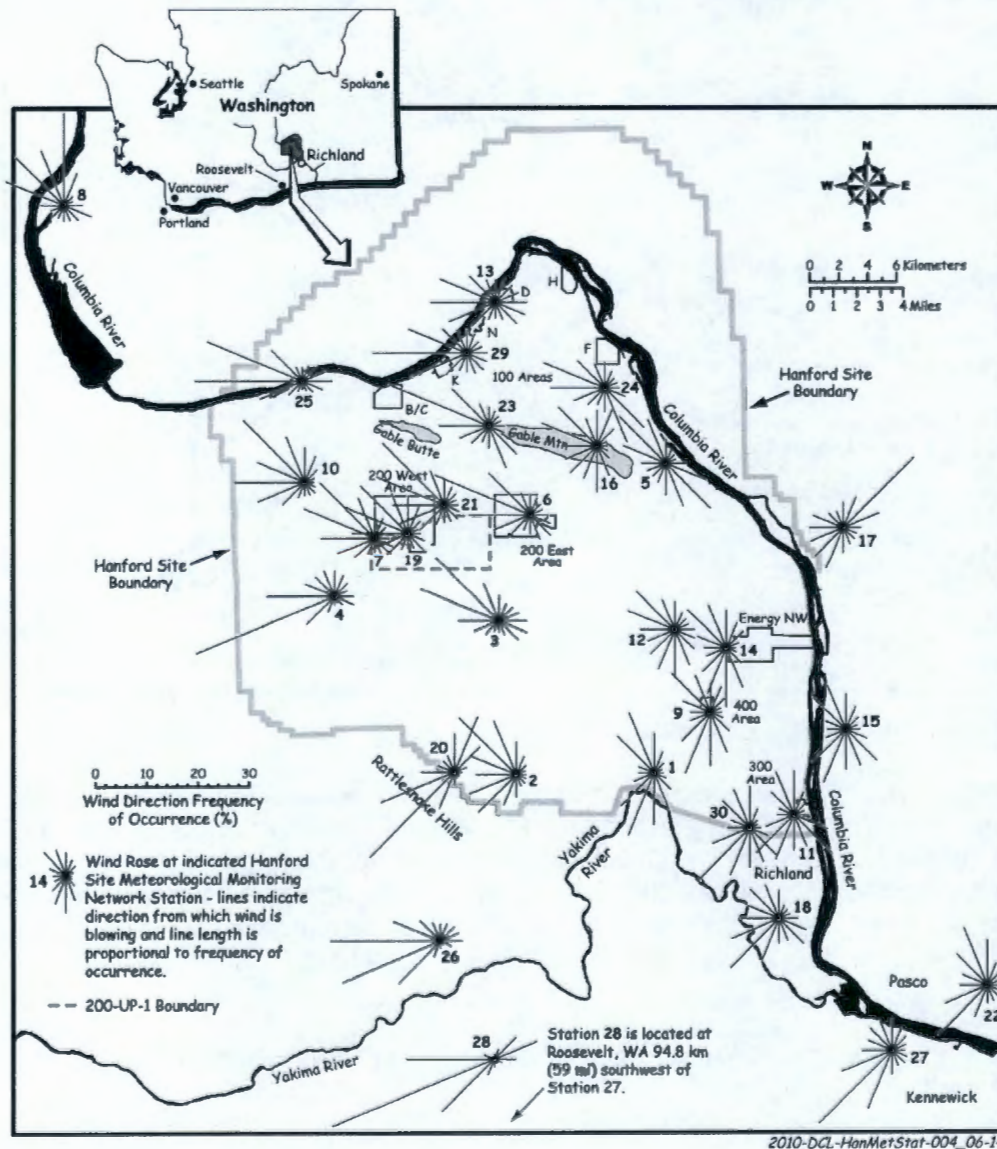
Data are collected and processed at each station, and information is transmitted to the HMS every 15 minutes. This monitoring network has been in full operation since the early 1980s. Data from the HMS capture the general climatic conditions for the region and describe the specific climate of the Central Plateau. Meteorological measurements have been made at the HMS since late 1944. Before the HMS was established, local meteorological observations were made at the old Hanford townsite (1912 through late 1943) and in Richland (1943 to 1944) (PNNL-6415).

Meteorological data collected at the HMS are considered to be representative of conditions in the ERDF landfill.

Over the period of evaluation considered in this study, severe climatic change is not expected as the next glaciation period has been estimated to occur tens of thousands of years into the future. The wet and dry cycles that have occurred over the past 10,000 years will likely continue over the next 10,000 years (see Section 2.2.5 of DOE/ORP-2000-24). The variations in the recharge in the future (over next 10,000 years) are therefore expected to be about the same as that of the past.

2.1.2.1 Wind. The prevailing surface winds on Hanford's Central Plateau are from the northwest, and occur most frequently during the winter and summer (PNNL-6415). Winds from the southwest are also common on the Central Plateau (Figure 2-3).

Figure 2-3. Wind Roses at the 9.1-m (30-ft) Level of the Hanford Meteorological Station Network, Washington, 1982 Through 2006 (PNNL-6415).



The Cascade Mountains have a considerable effect on the wind regime at the Hanford Site by serving as a source of cold (more dense) air drainage. This gravity drainage results in a northwest to west-northwest prevailing wind direction. Between 1945 and 2004, monthly average wind speeds 15.2 m (50 ft) above the ground were lower during the winter months, averaging 2.7 to 3.1 m/s (6 to 7 mi/hr), and faster during the spring and summer, averaging 3.6 to 4.0 m/s (8 to 9 mi/hr). The fastest wind speeds at the HMS are usually associated with flow from the southwest; however, the summertime drainage winds from the northwest frequently exceed speeds of 13 m/s (30 mi/hr). The maximum speed of the drainage winds (and their frequency of occurrence) tends to decrease moving toward the southeast across the Hanford Site. Surface features have less influence on winds aloft than on winds near the surface. During 2010, the average wind speed was 3.6 m/s (8.1 mi/hr), which was 0.2 m/s (0.5 mi/hr) above normal (PNNL-20548).

The monthly and annual prevailing wind directions, average speeds, and peak gusts are summarized in Tables 5.1 through 5.4 of PNNL-15160, *Hanford Site Climatological Summary 2004 with Historical Data*. The annual average wind speed for meteorological records kept from year 1945 to 2004 is calculated to be about 3.4 m/s (7.6 mi/hr) at 15.2 m (50 ft) above the ground.

2.1.2.2 Temperature and Humidity. Based on data collected from 1946 through 2010, the average monthly temperatures at the HMS range from a low of -0.2 °C (31.7 °F) in December to a high of 24.6 °C (76.3 °F) in July (PNNL-20548). Daily maximum temperatures at the HMS vary from an average of 2 °C (35 °F) in late December and early January to 36 °C (96 °F) in late July. On average, 52 days during the summer months have maximum temperatures greater than or equal to 32 °C (90 °F) and 12 days have maximum temperatures greater than or equal to 38 °C (100 °F). The largest number of consecutive days on record with maximum daily temperatures greater than or equal to 32 °C (90 °F) is 32 days. The record maximum temperature, 45°C (113 °F), was recorded at the HMS on July 23, 2006, July 13, 2002, and August 4, 1961.

From mid-November through early March, the average daily minimum temperature is below freezing; the daily minimum in late December and early January is -6 °C (21 °F). On average, the daily minimum temperature of less than or equal to -18 °C (approximately 0 °F) occurs only 3 days/yr; however, only about one winter in two experiences such low temperatures. The annual average relative humidity at the HMS is 55%; it is highest during the winter months, averaging about 76%, and lowest during the summer, averaging about 36%.

2.1.2.3 Precipitation. Average annual precipitation at the HMS is 17 cm (6.8 in.). Most precipitation occurs during the late autumn and winter, with more than half of the annual amount occurring from November through February. Average snowfall ranges from 0.25 cm (0.1 in.) during October to a maximum of 13.2 cm (5.2 in.) during December, decreasing to 1.3 cm (0.5 in.) during March. Snowfall accounts for about 38% of all precipitation from December through February. Precipitation during 2010 totaled 25.9 cm (10.2 in.), which is 146% of normal precipitation (17 cm (6.8 in.)). Snowfall for 2010 totaled 40.4 cm (15.9 in.), compared to normal snowfall of 39.1 cm (15.4 in.).

2.1.2.4 Severe Weather. Concerns about severe weather usually center on hurricanes, tornadoes, and thunderstorms. Fortunately, Washington does not experience hurricanes and tornadoes are infrequent and generally small in the northwestern portion of the United States. In the counties closest to the Site, only 24 tornadoes have been recorded from 1950 through November 2004. Of these, 17 tornadoes had maximum wind speeds estimated to be in the

range of 18 to 32 m/s (40 to 72 mi/hr), four had maximum wind speeds in the range of 33 to 50 m/s (73 to 112 mi/hr), and three had maximum wind speeds in the range of 51 to 71 m/s (113 to 157 mi/hr). No deaths or substantial property damage (in excess of \$50,000) were associated with any of these tornadoes. The estimated probability of a tornado striking a point on the Hanford Site is 9.6×10^{-6} /yr (NUREG/CR-4461).

The average occurrence of thunderstorms in the vicinity of the HMS is 10 per year. They are most frequent during the summer; however, they have occurred in every month. High-speed winds at the Site are more commonly associated with strong cold frontal passages. In rare cases, intense low-pressure systems can generate winds of near-hurricane force.

2.1.3 Ecology

This section summarizes the ecology of the Hanford Site, which consists of mostly undeveloped land, and emphasizes plant and animal activities that may affect exposure pathways. The information in this section is taken from Section 4.5 of PNNL-6415. The primary impact of ERDF on the environment would be through roots penetrating and animals burrowing through surface barriers into a disposal facility. However, the types of plants and animals and their density can affect net groundwater recharge, which is greatly influenced by surface vegetation and burrowing. PNNL-6415 details both the terrestrial and aquatic ecology of the Hanford Site and presents extensive listings of plant and animal species, but this section considers only terrestrial ecological effects because ERDF is not located near significant aquatic ecological systems.

The Hanford Site is characterized as a shrub-steppe ecosystem that is adapted to the region's mid-latitude semiarid climate (PNNL-6415). Such ecosystems are typically dominated by a shrub overstory with a grass understory. In the early 1800s, dominant plants in the area were big sagebrush (*Artemisia tridentata*) and an understory consisting of perennial Sandberg's bluegrass (*Poa sandbergii*) and bluebunch wheatgrass (*Pseudoregneria spicata*). Other species included threetip sagebrush, bitterbrush, gray rabbitbrush, spiny hopsage, needle-and-thread grass, Indian ricegrass, and prairie Junegrass. Of the 727 species of vascular plants recorded for the Hanford Site, approximately 25% are nonnative. The dominant non-native species, cheatgrass, is an aggressive colonizer and has become well established across the site. Over the past decade, several knapweed species also have become persistent invasive species in areas not dominated by shrubs.

With the advent of settlement, agriculture and livestock production were the primary subsistence activities at the turn of the century. Livestock grazing and agricultural production contributed to colonization by non-native vegetation species that currently dominate portions of the landscape. These activities ceased when the Hanford Site was designated in 1943. Most of the Hanford Site has not experienced tillage or agricultural grazing since the early 1940s when the government took control of the site. Chemical processing facilities, shutdown nuclear reactors, and supporting facilities occupy only about 6% of the site, so much of the Hanford Site remains undisturbed by human activity.

Approximately 300 species of terrestrial vertebrates have been observed on the Hanford Site, including approximately 42 species of mammals, 246 species of birds, 5 species of amphibians, and 12 species of reptiles. Terrestrial wildlife includes Rocky Mountain elk, mule deer, coyote, bobcat, badger, deer mice, harvest mice, grasshopper mice, ground squirrels, voles, and black-tailed jackrabbits. The most abundant mammal on the Hanford Site is the Great Basin pocket mouse. Bird species commonly found in the shrub-steppe habitats at the Hanford Site

include the western meadowlark, horned lark, long-billed curlew, vesper sparrow, sage sparrow, sage thrasher, loggerhead shrike, and burrowing owls.

Wildfires are frequent on the Hanford Site. Two large wildfires in the past two decades have burned over 15% of the site. Range fires that historically burned through the area during the dry summers eliminate fire-intolerant species (e.g., big sagebrush) and allow more opportunistic and fire-resistant species to establish.

The ERDF is actively managed to prevent vegetation, insects, and wildlife from using it as habitat. Herbicides and pesticides are used on a regular basis and fences are placed around the perimeter to keep larger animals out. Without a source of food within ERDF, smaller animals are less likely to enter.

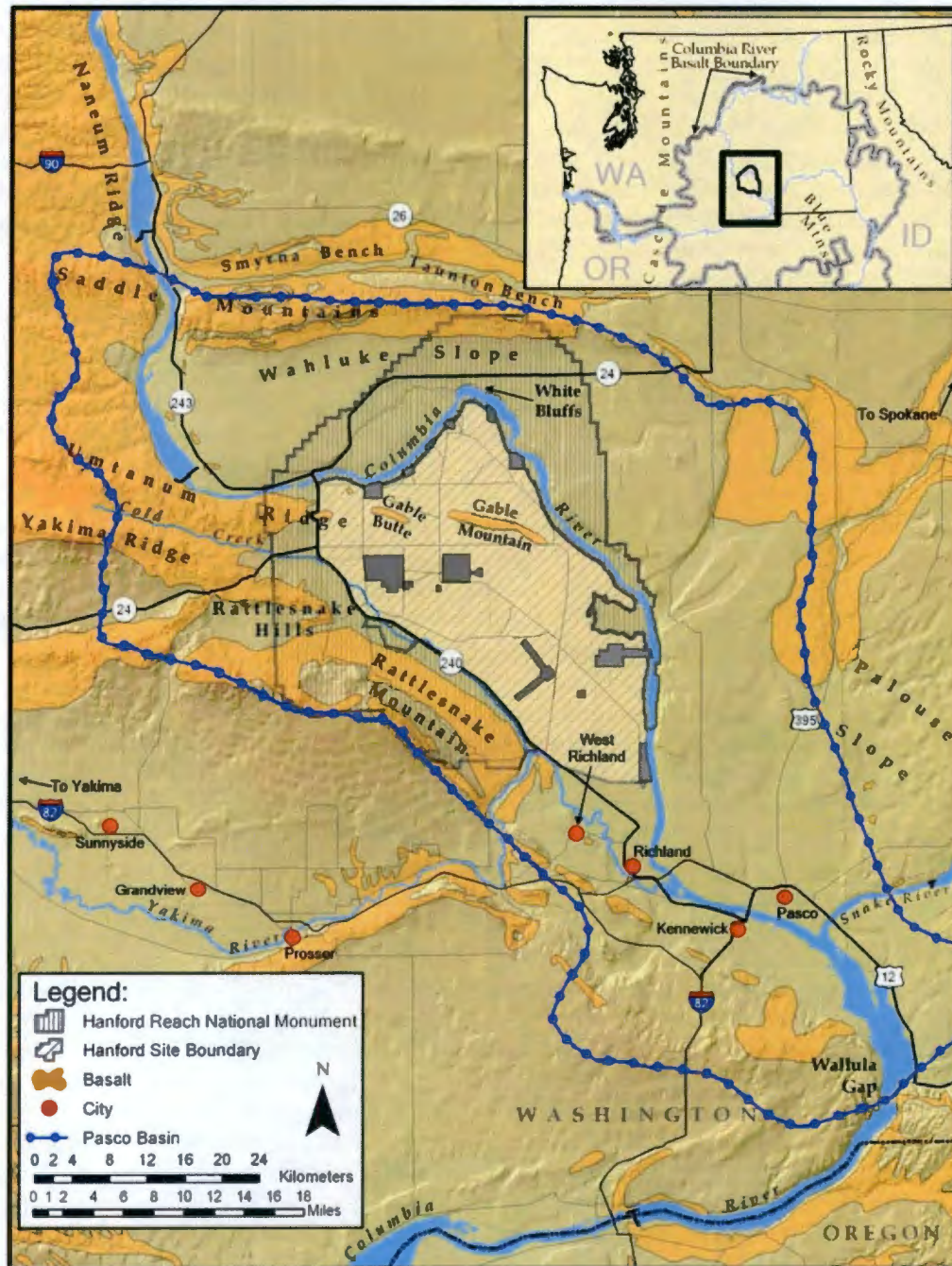
2.1.4 Geology, Seismology, and Volcanology

Since the Hanford Site started operating in the early 1940s, a large volume of information on the geology, seismology, and volcanology of the site has been collected and evaluated. WCH-463, *Hydrogeologic Model for the Environmental Restoration Disposal Facility, Hanford Site*, summarizes the geologic setting of the region and presents an updated hydrogeologic conceptual model for ERDF and surrounding area. Most of the data included in WCH-463 were collected by (or used by) several projects between about 1980 and the present. Those projects include the Basalt Waste Isolation Project; the Skagit Hanford Nuclear Project; the Washington Public Power Supply System safety analysis; several PAs; and numerous regulatory driven geologic and hydrologic characterizations, assessments, and monitoring projects.

The technical aspects of all of these projects, and thus the data, interpretations of the data, and conclusions, have been scrutinized by one or more regulatory agencies and stakeholder groups including the NRC, the National Academy of Science, the DNFSB, the EPA, the U.S. Geological Survey, the Washington State Departments of Ecology and Health, the Oregon Department of Energy, and the Yakama, Nez Perce, and Wanapum Indian Nations, and the Confederated Tribes of the Umatilla Reservation. The high level of oversight has helped ensure a rigorous understanding of bounding geologic, seismic, and volcanic risks.

2.1.4.1 Regional and Site-Specific Geology/Topography. The Hanford Site contains all the main geologic elements of the Columbia Basin (DOE/RW-0164, *Site Characterization Plan: Reference Repository Location, Hanford Site, Washington*). The Columbia Basin is the area bounded by the Cascade Range to the west, the Rocky Mountains to the northeast, and the Blue Mountains to the southeast (Figure 2-4). Four major geologic processes, occurring over millions of years, formed the soil, rocks, and geologic features (ridges and valleys) of the Columbia Basin and, therefore, the Hanford Site. The area was flooded with numerous basaltic lava flows between 17 and 6 million years ago, followed by tectonic forces that folded the basalt. In this landscape, the ancestral Columbia River meandered across the area leaving behind layers of sediment called the Ringold Formation. About 13,000 years ago, the area was inundated by a series of Ice Age floods (including the Missoula floods), which deposited more sediment in what is referred to informally as the Hanford formation.

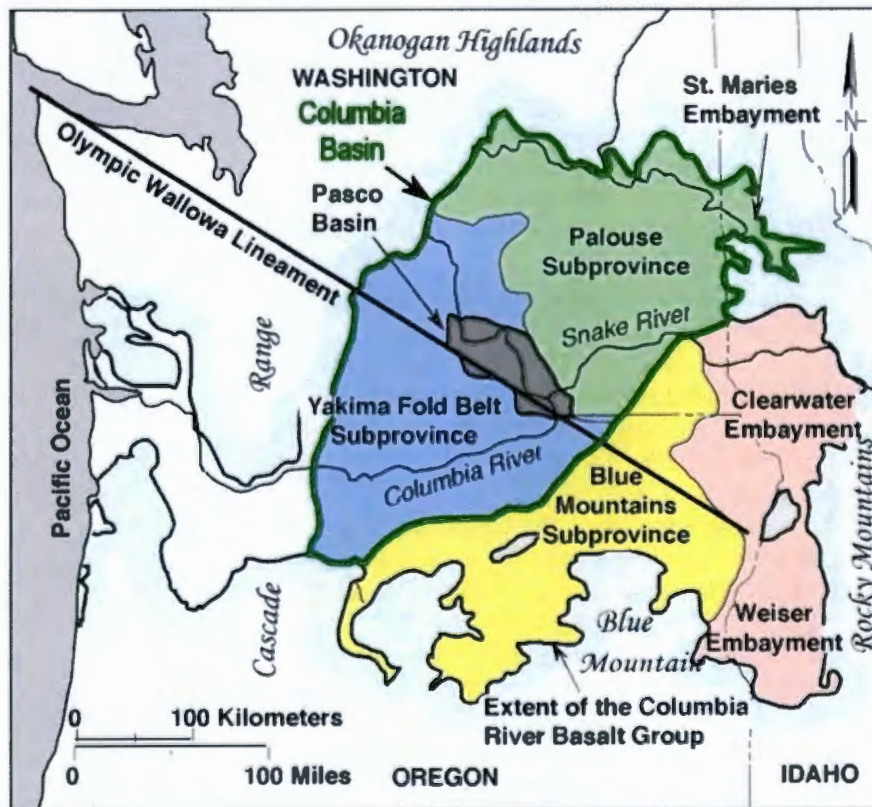
Figure 2-4. Geologic Elements of the Pasco Basin Portion of the Columbia Basin, Washington.



Source: DOE/ORP-2005-01, Rev. 0

2.1.4.1.1 Lava Flows. Lava flows erupted over a period of time from 17 to 6 million years ago. Under the Hanford Site, basaltic lava deposits (Columbia River Basalt Group) are over 4 km (13,000 ft) thick (Reidel and Hooper 1989), spreading over portions of Idaho, Oregon, and Washington. The Columbia Basin encloses the Columbia River Basalt Group. A depression in the lower part of the Columbia Basin is referred to as the Pasco Basin (Figure 2-5). The Pasco Basin is bounded by the Saddle Mountains to the north, Naneum Ridge to the west, Rattlesnake Hills to the south, and the Palouse Slope to the east, generally the area north of where the Snake River flows into the Columbia River. Geographically, the ridges surrounding the Hanford Site and vicinity define the Pasco Basin, which contains Ringold Formation sediment from the ancestral Columbia River and sediment deposited by the Ice Age floods.

Figure 2-5. Geologic Setting of the Columbia Basin and Pasco Basin.



Source: DOE/ORP-2005-01, Rev. 0

2.1.4.1.2 Crustal Folding. During and after the eruption of the lava flows, the Earth's tectonic forces buckled and folded the basalt in the western Columbia Basin into generally east-west trending, long, narrow ridges (anticlines), and intervening valleys (synclines). Collectively, this is identified as the Yakima Fold Belt.

2.1.4.1.3 Ancestral Columbia River Deposits. The ancestral Columbia River repeatedly changed its course over the past 15 million years, depositing gravel, sand, silt, and clay (RHO-BWI-ST-14; Fecht et al. 1987; DOE/RW-0164; Reidel et al. 1994; Lindsey 1996).

Uplifting basalt ridges diverted the course of the Columbia River from a southerly direction (toward Goldendale) to an easterly direction (toward Wallula Gap) and left behind the Ringold Formation (Fecht et al. 1987). Later regional uplift associated with the Cascade Mountains caused the river to cut through its own earlier deposits (the Ringold Formation) exposing the White Bluffs.

Within the Hanford Reach, the Columbia River continues to erode the White Bluffs. Groundwater seepage from irrigation along the bluffs makes them unstable. Consequently, the White Bluffs are landsliding and sloughing into the Columbia River along much of the shoreline (Fecht et al. 1987).

2.1.4.1.4 Ice Age Floods. The last major geological event was the Ice Age floods. The Ice Age floods began as early as 2.5 million years ago (Bjornstad et al. 2001) with the most recent occurring 18,000 to 13,000 years ago. During the freezes and thaws that occurred in the Ice Age, an ice dam across the Clark Fork River in Montana formed and failed many times, each time releasing a wall of water that surged southwest through the Columbia Basin, inundating the area that is now the Hanford Site. As the water moved across eastern Washington, it eroded the basalt, forming channels of barren rocky land referred to as the Channeled Scabland. At other localities, such as away from the main flood channels, the water deposited bars of gravel and sand. The waste management facilities in the 200 Areas of the Hanford Site are located on one prominent flood bar of sand and gravel, the Cold Creek bar (Bretz et al. 1956, DOE/RW-0164). Where the waters pooled behind obstacles such as Wallula Gap, they left behind deposits of sand and silt known as the Touchet Beds. Examples of Touchet Bed silt deposits are found in the Central Plateau of the Hanford Site at the US Ecology, Inc. site near the 200 Areas.

Figure 2-6 shows the southern Pasco Basin under water during the largest Ice Age flood. Ice Age floods became hydraulically dammed behind Wallula Gap, forming Lake Lewis. The largest and most frequent floods came from glacial Lake Missoula in northwestern Montana. Other floods may have escaped down-valley from the glacial lakes Clark and Columbia along the northern margin of the Columbia Basin (Waitt 1980, Baker and Bunker 1985) or down the Snake River from glacial Lake Bonneville (Malde 1968, O'Connor 1993) or from subglacial outbursts (Shaw et al. 1999).

2.1.4.1.5 Geologic Structure. This section briefly describes the geologic structure of the Columbia Basin; for additional information on the geologic structure see WCH-463. The Columbia Basin has two structural subdivisions or subprovinces: the Yakima Fold Belt and the Palouse Subprovince (Figure 2-5). The Yakima Fold Belt is a series of anticlinal ridges and synclinal valleys in the western part of the basin that has predominantly an east-west structural trend. The Palouse Subprovince is the eastern part of the basin and shows little deformation with only a few faults and low amplitude, long wavelength folds on an otherwise gently westward dipping paleoslope (DOE/RW-0164). The Hanford Site lies within the Pasco Basin, which is a smaller basin in the Yakima Fold Belt along the western margin of the Palouse Subprovince. The Saddle Mountains form the northern boundary of the Pasco Basin, Rattlesnake Mountain is the southern boundary, and the Hog Ranch-Naneum Ridge anticline forms the western boundary (Figure 2-7). The main Hanford Site WMAs, 200 East and 200 West Areas, lie in the Cold Creek syncline between Yakima Ridge and Umtanum Ridge in the southern portion of the Pasco Basin (Figure 2-7).

Figure 2-6. Conceptualization of Flood Water South of the Hanford Site, Washington, Between 18,000 to 13,000 Years Ago.



2.1.4.1.6 Stratigraphy. This section summarizes the strata and structure of the sediment and rocks that affect the Hanford Site/Pasco Basin. Figure 2-8 shows the various strata, their age, and epoch names for those geological periods of time. Additional information on the geology of the Pasco Basin, as well as more detailed descriptions of the stratigraphic units is given in WCH-463.

Columbia River Basalt Group. The bedrock of the Hanford Site is volcanic rock (basalt). Beneath the Hanford Site lay a minimum of 100 basalt flows with a maximum combined thickness of more than 4 km (almost 13,000 ft) (DOE/RW-0164), all part of the Columbia River Basalt Group.

To organize the many basalt deposits into a consistent nomenclature, geologists have named and grouped them based on their physical and chemical properties. The basalt deposit closest to the surface at the Hanford Site, and therefore most often referred to, is Saddle Mountains Basalt (Figure 2-8). Saddle Mountains Basalt consists of 10 distinct basaltic lava deposits (members). The most recent basalt flow underlying most of the Hanford Site is the Elephant Mountain Member of the Saddle Mountains Basalt. A younger basalt flow, the Ice Harbor Member, is found in the southern portion of the site near the 300 Area (DOE/RW-0164). This unit forms the base of the unconfined aquifer.

In addition to basalt, the Hanford Site has sedimentary formations. These are sediment (material that settles to the bottom of a liquid) that often has hardened into rock. Some of the sediment at the Hanford Site is found between the basaltic lavas and is called the Ellensburg Formation. The majority of the sediment is above the basalt with the Ringold Formation on the bottom, overlain by the Cold Creek unit, and topped with the Hanford formation (Figure 2-8). Understanding the formations, along with clastic dikes and the soil of the Hanford Site, contributes to understanding of how, for example, contaminants might travel through the vadose zone and unconfined aquifer in the 200 Areas.

Figure 2-7. Geologic Structures of the Pasco Basin and Vicinity.

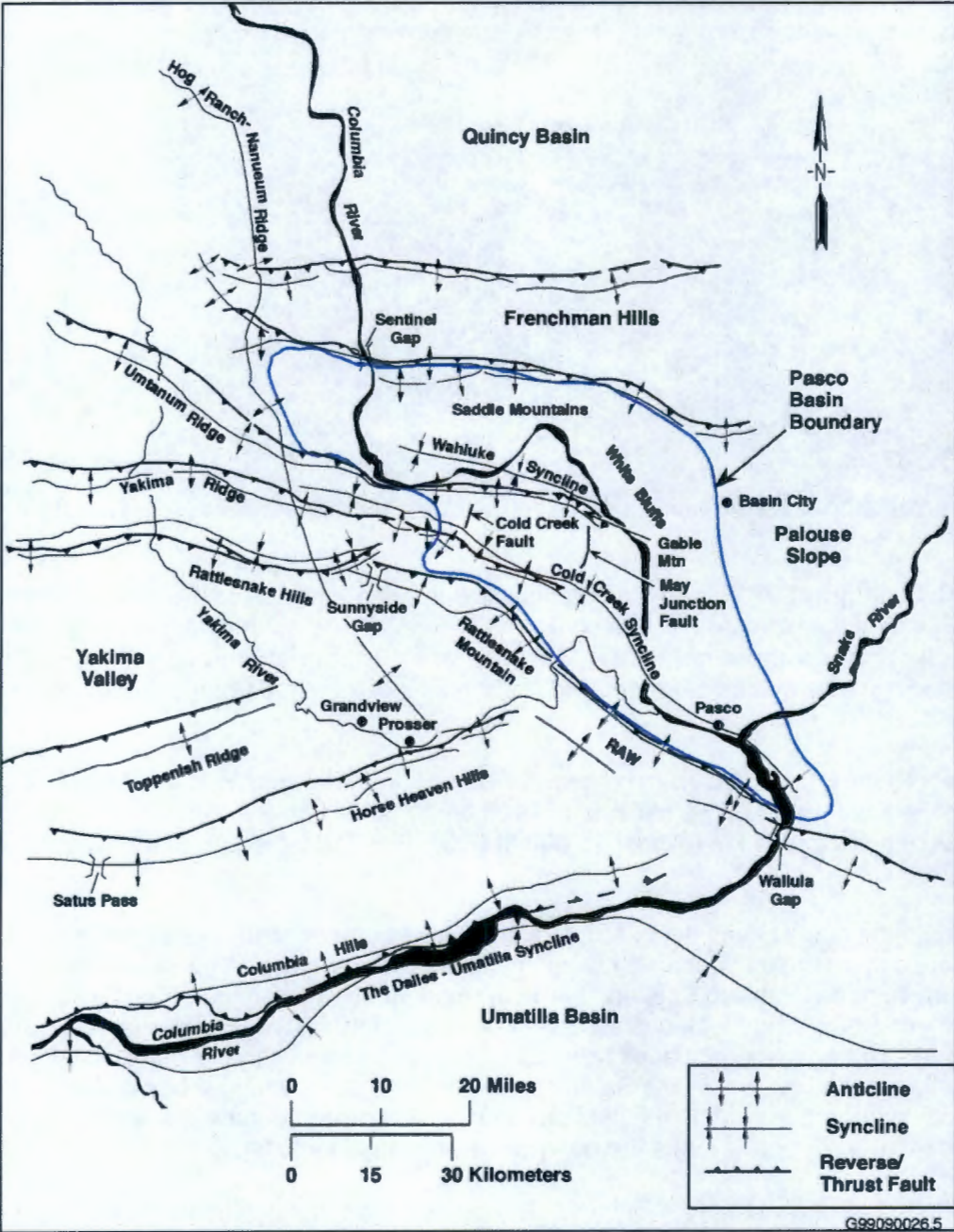
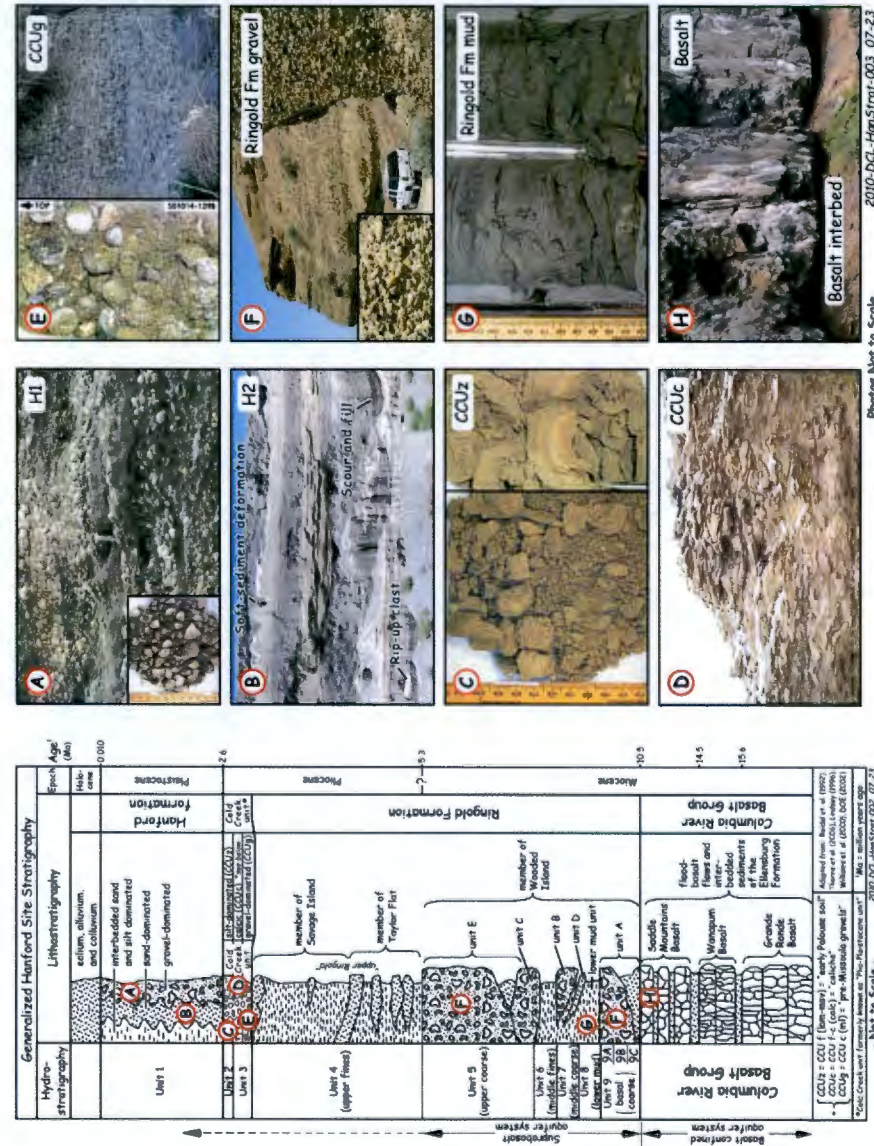


Figure 2-8. Generalized Stratigraphy of the Hanford Site Including the Central Plateau (PNNL-6415).



Photore Net to Scale 2010-DCL-HanfStrat-003_07-23

Ellensburg Formation. This is the sediment found interbedded with the Columbia River Basalt Group. The Ellensburg Formation formed as early as 15.6 million years ago, although the youngest portion on the Hanford Site may have formed as recently as 8 million years ago (DOE/RW-0164). The Ellensburg Formation was created when volcanic rock and sediment from uplands surrounding the Columbia Plateau interfingered with the basalt of the Columbia River Basalt Group (Swanson et al. 1979a, 1979b). The thickest accumulations of the Ellensburg Formation lie along the western margin of the Columbia Basin. While deposition along the western margin was primarily from volcanic debris flows and related stream and sheet floods, no volcanic debris flows have been identified at the Hanford Site (Reidel et al. 1994). Volcanic rock (formed from falling ash known as tuff) is the dominant material in the Hanford Site portion of the Ellensburg Formation. The Ellensburg Formation is commonly exposed along the ridges of the Yakima Fold Belt. The confined aquifer system underlying the Hanford Site is found in the basalt breccia or flow tops of this formation.

Ringold Formation, Cold Creek Unit, and Hanford Formation. Sediments overlying basalt in the Pasco Basin and Hanford Site, known as the suprabasalt, include the Ringold Formation, Cold Creek unit, and the Hanford formation. These formations are primarily exposed in the lower elevation areas around the Hanford Site, including White Bluffs.

Ringold Formation. The lower half of the Ringold Formation is the main unconfined aquifer under the Hanford Site and contains five separate stratigraphic intervals dominated by the fluvial gravels facies. These gravels, designated units A, B, C, D, and E (Figure 2-8), are separated by intervals containing deposits typical of the overbank and lacustrine facies (Lindsey 1991). The lowermost of the fine-grained sequences overlying, unit A, is designated the lower mud sequence. The uppermost gravel unit, unit E, grades upwards into interbedded fluvial sand and overbank deposits that are in turn overlain by lacustrine-dominated strata.

The upper part of the Ringold Formation, informally called the member of Taylor Flat (Lindsey 1995) consists of the sequence of fluvial sands, overbank deposits, and lacustrine sediments overlying unit E. This corresponds to the upper unit as originally defined by Newcomb (1958) along the White Bluffs in the eastern Pasco Basin. The fluvial sand facies is the principal facies of the upper part under the tank farms at the Hanford Site.

Cold Creek Unit. The Cold Creek unit (DOE/RL-2002-39) includes all material underlying the Hanford formation, overlying the Ringold Formation in the vicinity of the 200 West Area, and may extend over most of the central Pasco Basin. The Cold Creek unit distinguishes itself from the Hanford and Ringold formations because it was formed when the Ringold Formation was eroding and relatively little was being deposited at the Hanford Site. This subunit is found locally in the Cold Creek syncline in the subsurface. Distribution of the Cold Creek unit depends in part on erosion and weathering of the underlying Ringold Formation and post-depositional erosion by the Ice Age floods (Slate 1996). The thickness of the Cold Creek deposit ranges from 0 to 20 m. Locally the Cold Creek unit contains very hard rock that formed as precipitation evaporated and left behind minerals forming what geologists call caliche or hardpan. This layer can influence contaminant migration by slowing its rate of downward movement and potentially diverting contaminants laterally (Slate 1996). However, thin, fine-grained layers in the Hanford formation also cause lateral migration (PNNL-13757-1).

Hanford Formation. The Hanford formation is the informal name for the strata that lie on top of Cold Creek unit and Ringold Formation, and in a few locations, directly above the basalt. The Ice Age floods inundated the Hanford Site a number of times beginning as early as 1 to 2 million years ago (Bjornstad et al. 2001). The last major flood sequence occurred about

13,000 years ago. When the Ice Age floodwaters entered the Pasco Basin, they quickly became impounded behind Wallula Gap, which was too restrictive for the volume of water involved. Floodwaters formed temporary lakes with shorelines up to 381 m (1,250 ft) in elevation. The lakes lasted not more than a few days (O'Connor and Baker 1992). The deposits, known as the Hanford formation, that were left after the floodwater receded (Figure 2-9) blanket low-lying areas over most of the Hanford Site.

The Hanford formation is thickest in the vicinity of the 200 Areas where it is up to 100 m (300 ft) thick (DOE/RL-2002-39). Gravel, sand, and silt (Touchet Beds) dominate the Hanford formation (WHC-MR-0391). The different sediment types of the Hanford formation commonly interfinger laterally. The relative proportion of each sediment type at any given location is related to its distance from main high-energy flows at the time of deposition (DOE/RW-0164). Generally, gravel was deposited in the center of the Pasco Basin, while finer grained sand and silt were deposited along the margins of the basin.

ERDF-Specific Stratigraphy. In general, most stratigraphic units typically associated with the Hanford Site also occur beneath the ERDF site. Figure 2-10 compares the ERDF stratigraphic column with the generalized Hanford Site stratigraphic column. A total of 10 stratigraphic units are recognized in the ERDF area. Table 2-1 describes the stratigraphy from some of the identified units to aid in understanding the hydrogeologic conceptual model. Stratigraphic units recognized in the ERDF area include the following:

- Recent (Holocene) backfill material (Hdb)
- Hanford formation unit 1 – gravel-dominated sequence (Hf1 unit)
- Hanford formation unit 2 – sand-dominated sequence (Hf2 unit)
- Cold Creek unit silt – fine grained (CCu₂)
- Cold Creek unit calcic geosol – coarser grained (CCu_c)
- Ringold Formation member Taylor Flat – fine grained (RFtf)
- Ringold Formation unit E – silty, sandy gravel (RFwie)
- Ringold Formation lower mud unit – fine grained sequence (RFIm)
- Ringold Formation unit A – silty, sandy gravel (RFwia)
- Columbia River Basalt Group.

The cross section location lines (Figure 2-11) are depicted in Figures 2-12 and 2-13. Isopach (thickness of units) and structure contour maps (elevations of the tops of each unit) of the primary suprabasalt units are included in Appendix C of WCH-463. All interpreted hydrogeologic visualizations conform to the Hanford Site geologic graphics guidance documentation (PNNL-18819, *Hanford Site Guidelines for Preparation and Presentation of Geologic Information*).

Figure 2-9. Map of the Ice Age Flood Deposits (Hanford Formation).

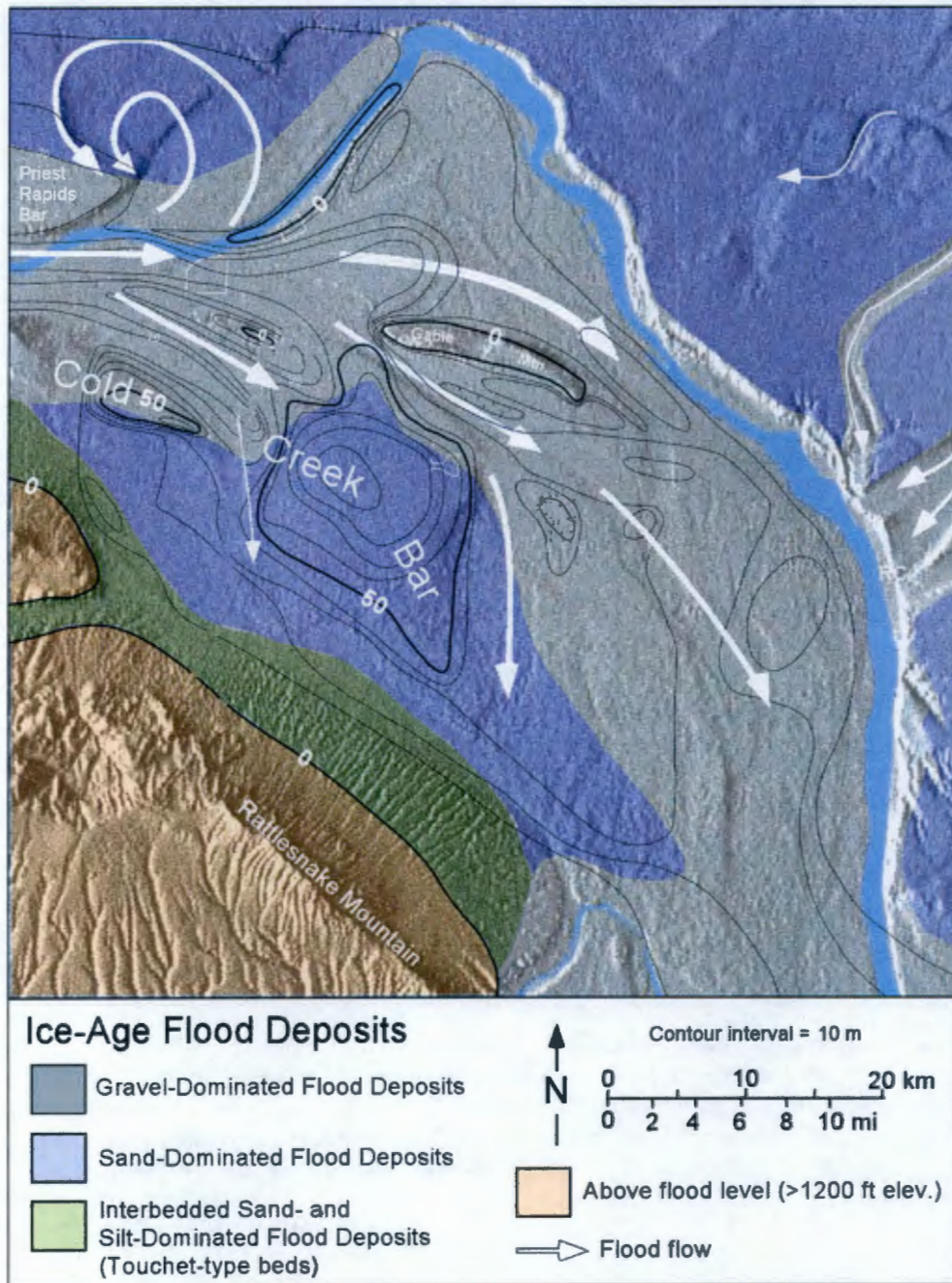
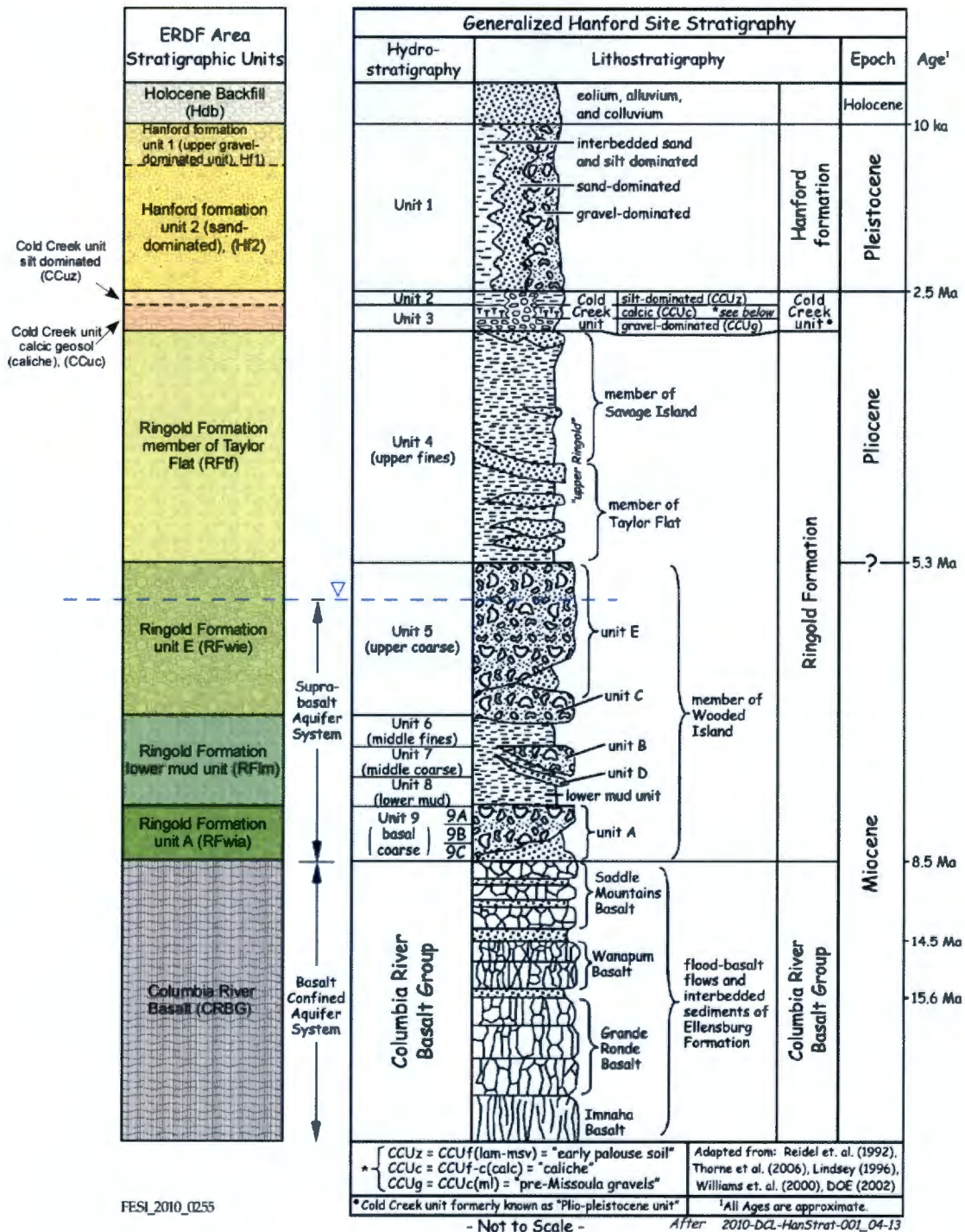


Figure 2-10. Comparison Between ERDF and Generalized Hanford Site Stratigraphy.



FESI_2010_0255

Table 2-1. Lithostratigraphic Terminology for the Vadose Zone Beneath the ERDF.

Stratigraphic Symbol	Lithostratigraphic Unit	Subunit	Description	Genesis
Holocene/Fill	Backfill	Hdb	Poorly sorted cobbles, pebbles, and coarse to medium sand with some silt derived from the Hanford formation ^a .	Anthropogenic
Hf1	Hanford formation	Hf1 unit	An upper gravelly sequence consisting of high-energy, gravel-dominated facies interbedded with lenticular and discontinuous layers of sand-dominated facies.	Cataclysmic flood deposits
Hf2		Hf2 unit	Sand sequence consisting predominantly of sand-dominated facies, with multiple graded beds of plane to foreset-bedded sand or gravelly sand, which sometimes grades upward to silty sand or silt.	
CCu _z	Cold Creek Unit	Silt	Silt sequence consisting of interstratified well sorted calcareous silt and fine sand.	Fluvial overbank and/or Eolian deposits (with some weakly developed paleosols)
CCu _c		Caliche	Caliche sequence consisting of interstratified caliche, sand, and gravel.	
RFtf	Ringold Formation	Member of Taylor Flat	Fine sand and silt sequence, consisting of interstratified silt and sand.	Ancestral Columbia River deposits
RFwie		Member of Wooded Island – unit E	Sand and gravel sequence consisting of poorly sorted sands and gravels.	

NOTE: Updated from HNF-5507, *Subsurface Conditions Description of the B-BX-BY Waste Management Area*, Rev. 0, CH2M HILL Hanford Group, Inc., Richland, Washington.

^a ARH-LD-137, 1976, *Geology of the 241-U Tank Farm*, Rockwell Hanford Operations, Richland, Washington.

CCu_z = Cold Creek unit silt

CCu_c = Cold Creek unit calcic geosol

ERDF = Environmental Restoration Disposal Facility

Hf1 = Hanford formation unit 1 – gravel-dominated sequence

Hf2 = Hanford formation unit 2 – sand-dominated sequence

RFtf = Ringold Formation Taylor Flat

RFwie = Ringold Formation Wooded Island – unit E

Figure 2-11. Location of Boreholes Used to Generate the ERDF Hydrogeologic Conceptual Model.

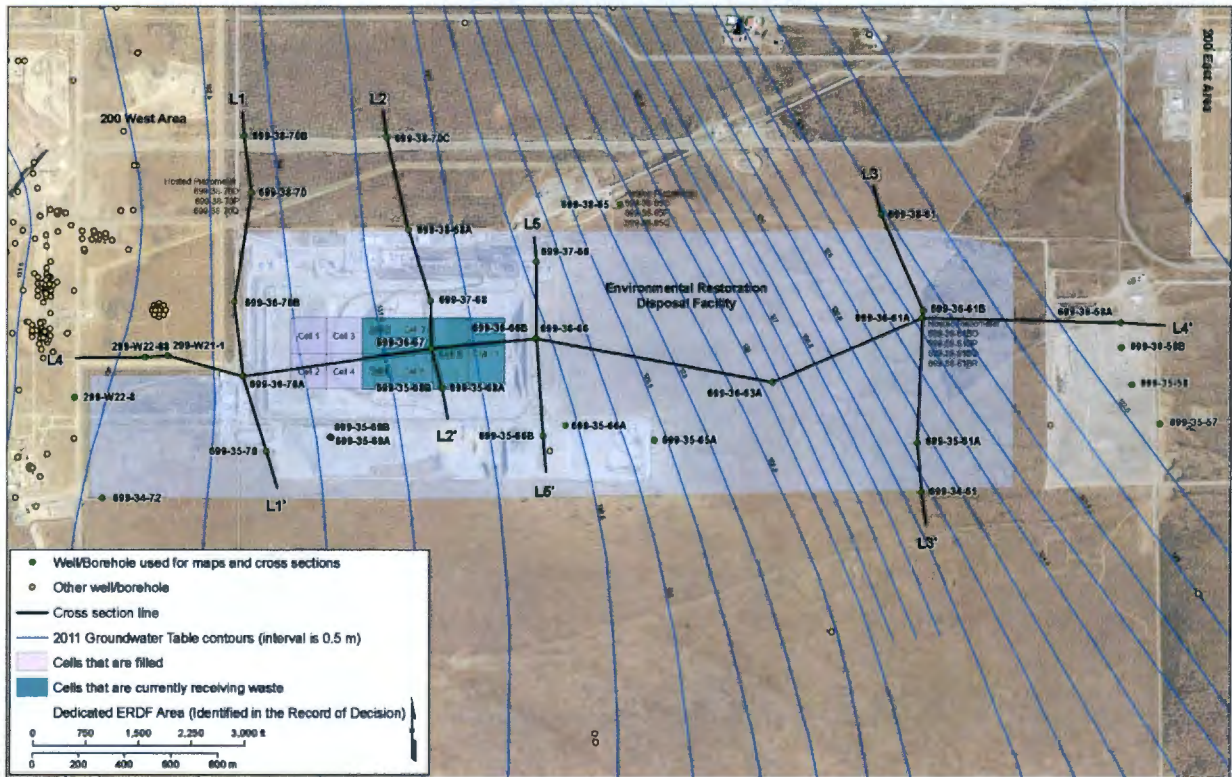


Figure 2-12. Hydrogeologic Cross Section L2-L2'.

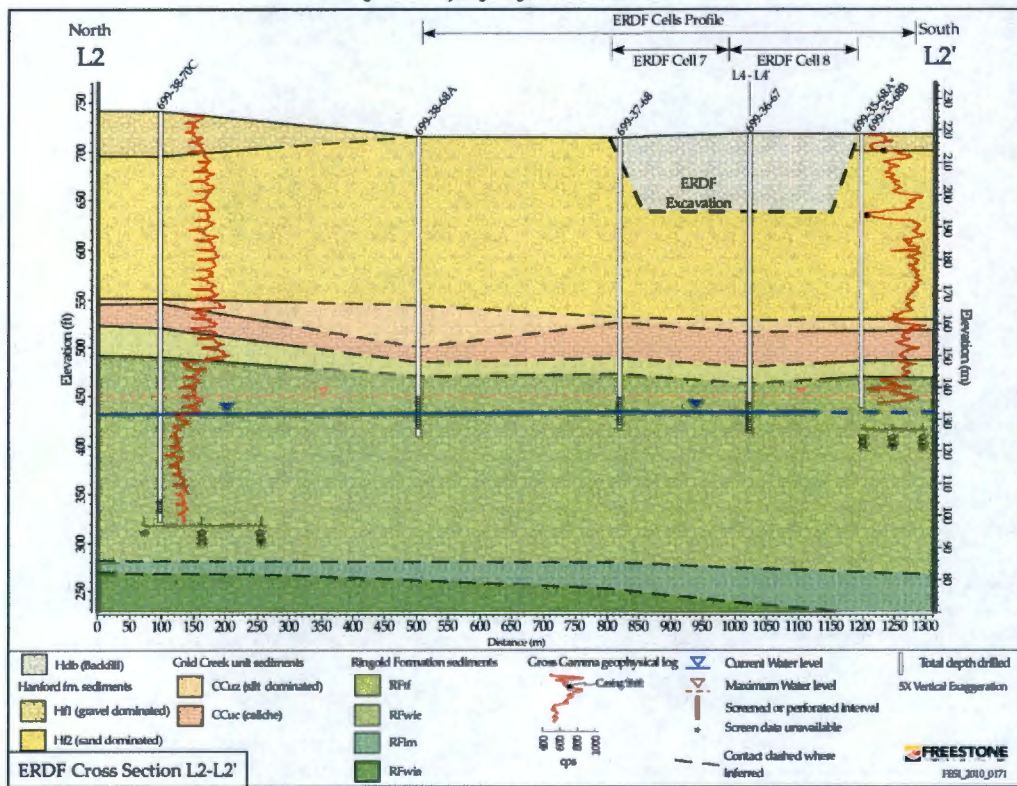
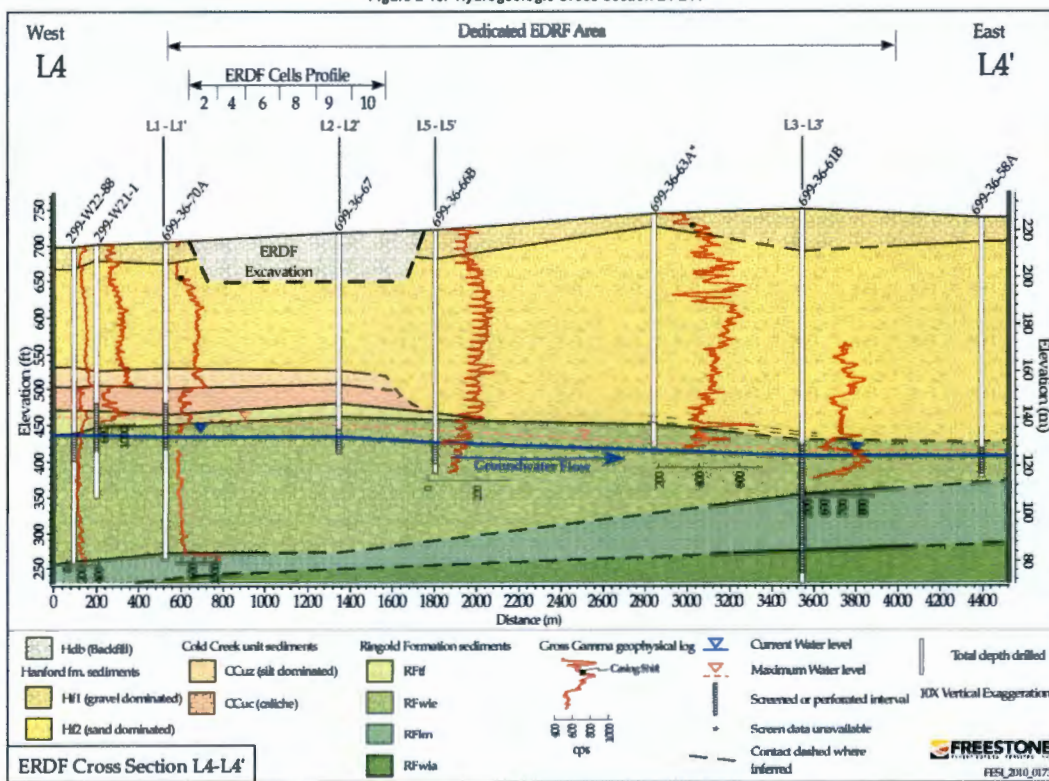


Figure 2-13. Hydrogeologic Cross Section L4-L4'.



The ERDF is underlain by 159 to 177 m (521.7 to 580.7 ft) of suprabasalt sediment that overlies the Elephant Mountain member of the Columbia River Basalt Group (bedrock). The vadose zone (interval above the water table) is approximately 80 to 100 m (262.4 to 328.1 ft) thick. The suprabasalt aquifer system ranges from 50 to 100 m (164.0 to 328.1 ft) thick. Groundwater generally flows to the east-northeast beneath the site (Figure 2-11) and is known to contain dissolved contaminants from past disposal facilities within the 200 West Area, located upgradient from ERDF. Perched groundwater has not been observed in the vicinity of ERDF.

The ERDF waste disposal cells are constructed in the near-surface sediments within the thick vadose zone consisting primarily of unconsolidated Pleistocene-aged Hanford formation and Cold Creek unit sediments. The ERDF disposal cell floors (bottom of cells) penetrate through the Hf1 unit and lie within the sand-dominated Hf2 unit. The Cold Creek unit lies directly beneath the Hanford formation and is subdivided into two subunits, the CCu_z and CCu_c. The CCu_z and CCu_c are laterally continuous throughout most of the 200 West Area, but are not present (truncated) to the east (within the ERDF) either because of paleo-flood erosion or by depositional thinning. East of this truncation, Hf2 sediment directly overlies Ringold Formation sediment. The deepest and oldest geologic units within the vadose zone consist of the Ringold Formation upper fine-grained unit (RFtf) and the upper portion of the fluvial-silty sandy gravel RFwie. A detailed description of the individual geologic units beneath ERDF can be found in WCH-463, *Hydrogeologic Model for the Environmental Restoration Disposal Facility*.

Clastic dikes have been found within the 200 Area of Hanford Site and towards the southern portion of 200 Area. Clastic dikes are fissures filled with sand, silt, clay, and minor coarser debris. They are commonly associated with, but not restricted to, Ice Age flood deposits in the Columbia Basin. Many dikes occur as sharp-walled, near-vertical tabular bodies filled with multiple layers of unconsolidated sediment. Thin clay/silt linings separate the margins of dikes and internal layers (BHI-01103, *Clastic Injection Dikes of the Pasco Basin and Vicinity – Geologic Atlas Series*). Dikes vary in width from less than 1 mm (0.039 in.) to greater than 2 m (6.5 ft). Vertical extents range from less than 1 m (3 ft) to greater than 50 m (164 ft) with a large number greater than 20 m (65 ft) (BHI-01103).

Clastic dikes are characteristic of unstable environments and tend to form when three conditions exist: (1) a state of horizontal tension, leading to cracking; (2) the presence of suitable source materials; and (3) excess pore-water pressure (Allen 1982). In glacial and subglacial environments, movement of a glacier or ice sheet over saturated, unconsolidated, fine-grained sediment could lead to such conditions. In warmer climates, such conditions could have resulted from the rapid dewatering of saturated, unconsolidated, fine-grained sediment in response to a triggering event. Both seismic events and hydraulic fracturing during flooding have been proposed as possible mechanisms for the injections (Lupher 1944, Alwin 1970; Obermeier 1996, Pogue 1998, BHI-01103). Newcomb (1962) suggested that clastic dikes in the Touchet Beds resulted from upward injections of groundwater, caused by bank-storage effluent when a large lowering of Lake Lewis created a pressure differential. Newcomb (1962) suggested the lowering could produce a hydraulic lift causing the injection of water into an equi-dimensional (polygonal) system of fractures. Later injections followed the established dike planes producing the many narrow beds of rock.

200 Areas Strata and Structure. At the end of Ringold time, western North America underwent regional uplift resulting in a change in the base level of the Columbia River system. Uplift caused a change from sediment deposition to regional incision and sediment removal. Regional incision is especially apparent in the Pasco Basin where nearly 100 m (328 ft) of

Ringold sediment has been removed from the Hanford area. The regional incision marks the beginning of Cold Creek time and the end of major deposition by the Columbia River. Regional incision and erosion during the Cold Creek time is most apparent in the surface elevation change of the Ringold Formation across the Hanford Site, shown in Figure 2-14, which is an east-west cross-section through the Hanford Site. The elevation of the surface of the Ringold Formation decreases toward the present day Columbia River channel. In the southwest part of the Pasco Basin near the 200 West Area, less incision of the Ringold Formation occurred than at the 200 East Area. The greatest amount of incision is near the present channel. This increasing incision into the Ringold Formation toward the present Columbia River channel occurred with time as the channel of the Columbia River moved eastward across the Hanford Site.

These events have caused the geology in the 200 West Area to be notably different from that in the 200 East Area even though they are separated by a distance of only 6 km (4 mi) (DOE/RW-0164) as shown in Figures 2-14 and 2-15. Figure 2-15 is a hydrogeologic map of the units present at the water table surface (for June 1998 to represent the water table before start of active remediation). The 200 West Area has sections containing all three formations including most of the Ringold Formation as well as the Cold Creek unit and the Hanford formation (DOE/RW-0164).

Figure 2-14. Cross-Section Running from the Rattlesnake Mountains Through the 200 Areas and Out to the Columbia River.

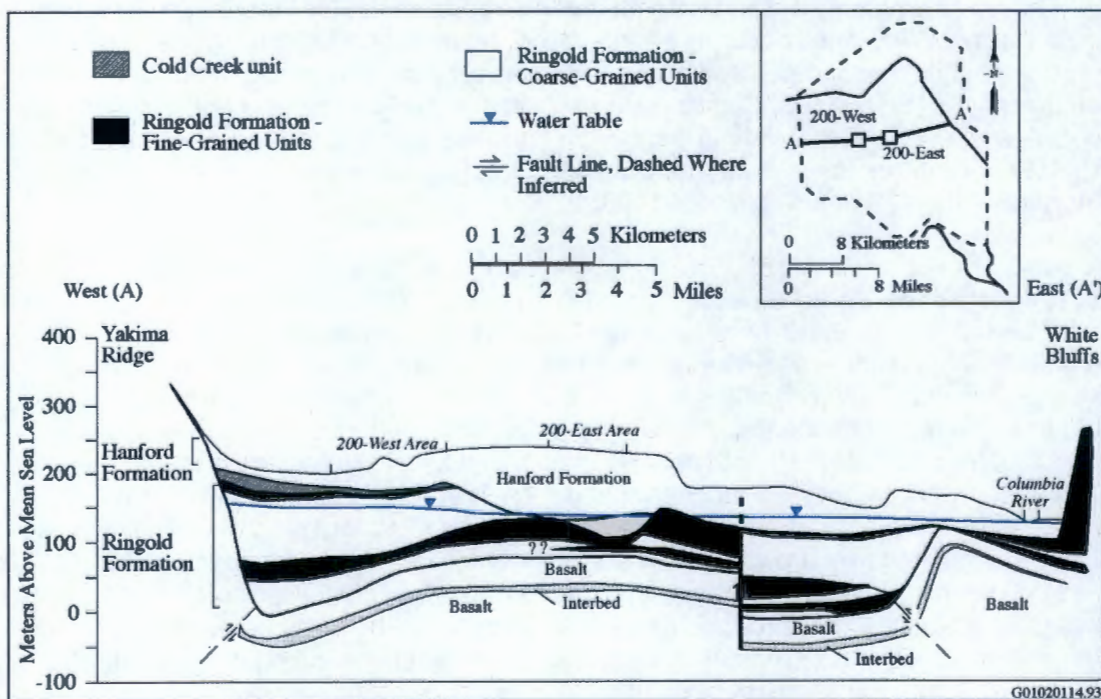
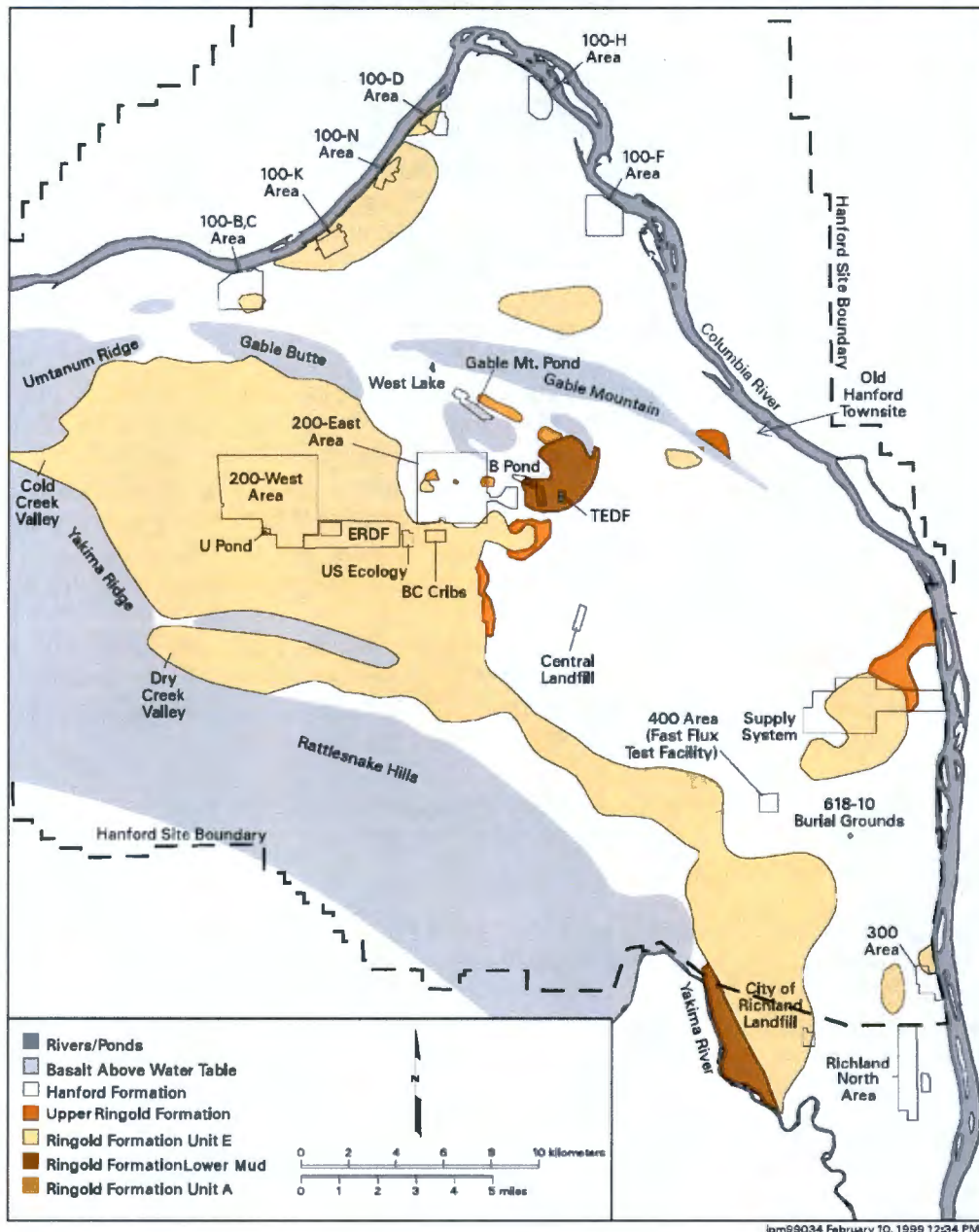


Figure 2-15. Hydrogeologic Units Present at the Water Table in June 1998.



In the 200 East Area, some of the Ringold Formation is present in the southern part but has been completely eroded in the northern part. On the north side of the 200 East Area, the Hanford formation rests directly on the basalt, and no Ringold sediment is present. Erosion by the ancestral Columbia River and Ice Age flooding are believed to have removed the Ringold Formation from this area. Material of questionable origin overlies basalt within WMA B-BX-BY (HNF-5507), located in the northern portion of the 200 East Area. This material may be equivalent or partially equivalent to the Cold Creek unit or it may represent the earliest

ice-age flood deposits overlain by a locally thick sequence of fine-grained non-flood deposits. This unit is referred to informally as Hanford-Cold Creek deposits.

Surface Soils. The Holocene deposits and exposed Hanford formation sediments have experienced soil development and evolved into identifiable soil types. BNWL-243, *Soil Survey: Hanford Project in Benton County*, describes 15 different surface soil types on the Hanford Site, varying from sand to silty and sandy loam. Various classifications, including land use, are also given in BNWL-243. These soil types control the flux of water reaching the water table (i.e., recharge) (PNNL-13033, *Recharge Data Package for the Immobilized Low Activity Waste 2001 Performance Assessment*). The soils found in the Central Plateau in and around the 200 Areas are Rupert sand (also known as Quincy sand), Burbank loamy sand, and Ephrata sandy loam. BNWL-243 described these types of soil as follows:

Rupert Sand (also known as Quincy Sand). This mapping unit represents one of the most extensive soils on the Hanford Site. The surface is a brown to grayish-brown, coarse sand, which grades to a dark grayish-brown sand at about 91 cm (36 in.). Rupert soils developed under grass, sagebrush, and hopsage in coarse sandy alluvial deposits, which were mantled by wind-blown sand. Relief characteristically consists of hummocky terraces and dune-like ridges. Active sand dunes are present. Some dune areas are separated; however, many small dunes, blow-outs, and associated small areas of Ephrata and Burbank soils are included.

Burbank Loamy Sand. This is a dark-colored (surface is very dark grayish-brown; subsoil is dark grayish-brown), coarse-textured soil that is underlain by gravel. The surface soil is usually about 41 cm (16 in.) thick but can be 76 cm.(30 in.) thick. The gravel content of the subsoil may range from 20 to 80 vol%.

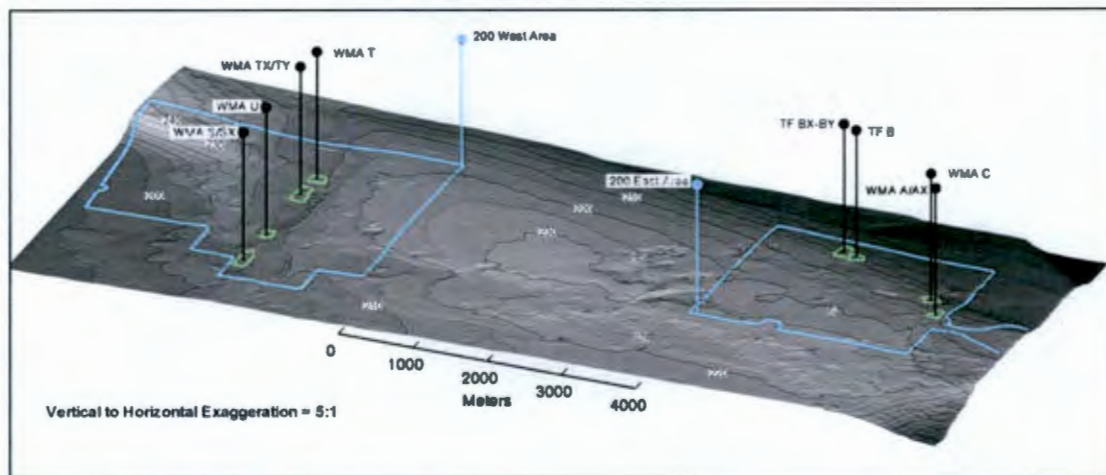
Ephrata Sandy Loam. The surface of this soil is dark colored with subsoil that is dark grayish-brown and medium-textured. It is underlain by gravelly material that may continue for many feet vertically downwards.

Esquatzel Silt Loam. This soil is not found within the 200 Areas Central Plateau, but rather to the south of the 200 West Area. It is considered a possible source for borrow material needed for the Modified RCRA Subtitle C Barrier (Petersen 2005). It is deep dark-brown soil formed in recent alluvium and is derived from loess and lake sediment. The subsoil grades to dark grayish-brown in many areas, but color and texture of the subsoil are variable because of the stratified nature of the alluvial deposits.

In addition to these soil types, the ERDF contains soil previously located near the surface in the 100 Areas. No soil has developed over the backfill and vegetation is controlled through herbicides.

200 Areas Topography. Figure 2-16 shows the 200 Areas in a perspective view (note that the vertical to horizontal exaggeration in this figure is 5:1). The 200 Areas Central Plateau contains a topographic high in between the 200 East and 200 West Areas with gently dipping sides, except in the northwest corner of the 200 West Area.

Figure 2-16. Topography of the 200 Areas Central Plateau.



2.1.4.2 Seismology. The general characteristics of seismic behavior at the Hanford Site are well understood after several decades of detailed measurements (a seismograph network was activated in 1969 for the Hanford Site and surrounding area) coupled with anecdotal information recorded as early as 1840 (PNNL-6415). Currently, measured seismic activity for the Hanford Site is reported quarterly and annually (e.g., PNNL-20302). Figures 2-17 and 2-18 provide summaries of known events at and around the Hanford Site between 1890 and 2005 (PNNL-6415).

The details of seismic behavior have been described in numerous previous documents dealing with environmental impacts from Hanford Site wastes (e.g., PNNL-6415).

The most frequent seismic occurrences at the Hanford Site are earthquake swarms that consist of multiple small energy events that fall within a small energy range and are constrained temporally (weeks to months) and spatially (5 to 10 km [3 to 6 mi] in length). Swarms tend to reoccur in particular locations, about 90% of individual earthquakes are at Richter scale magnitudes of 2 or less, and 70% to 80% of them occur at depths less than 4 km (2.5 mi) below ground surface. Larger isolated earthquakes also occur nearby (DOE/RW-0164). The largest single event earthquake recorded near the Hanford Site occurred in Milton-Freewater, Oregon, located about 80 km [50 mi] away in 1936 at a Richter magnitude of 5.75 and a maximum Modified Mercalli Intensity (MMI) of VII. The two next largest nearby earthquakes occurred north of the Hanford Site in 1917 and 1973 near Othello, Washington, about 49 km (30 mi) north of the 200 Areas with magnitudes above 4 on the Richter scale and MMI of V. The 1973 earthquake occurred about 1 km (0.6 mi) below ground surface. Since 1973, 80 small earthquakes (2.5 to 4.3 magnitudes) have been recorded within a radius of 90 km (56 mi) of the Hanford Site Central Plateau, the closest being a magnitude 3.3 event with the epicenter 8 km (5 mi) north of the 200 Areas. Earthquake depths vary for isolated events and have been estimated as deep as 30 km (~19 mi).

Figure 2-17. Earthquake Activity in the Vicinity of the Hanford Site Between 1890 and 1970 (PNNL-6415).

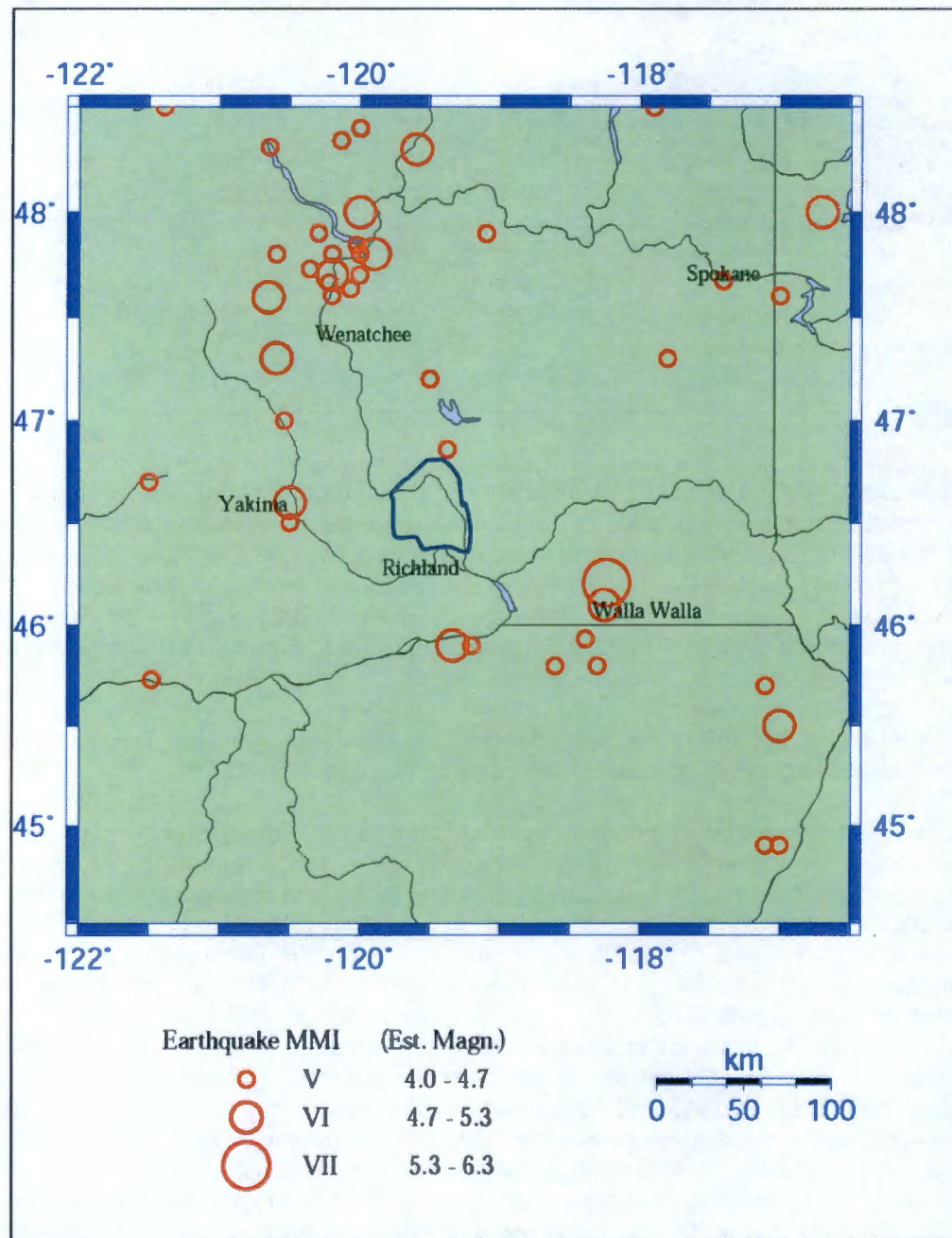
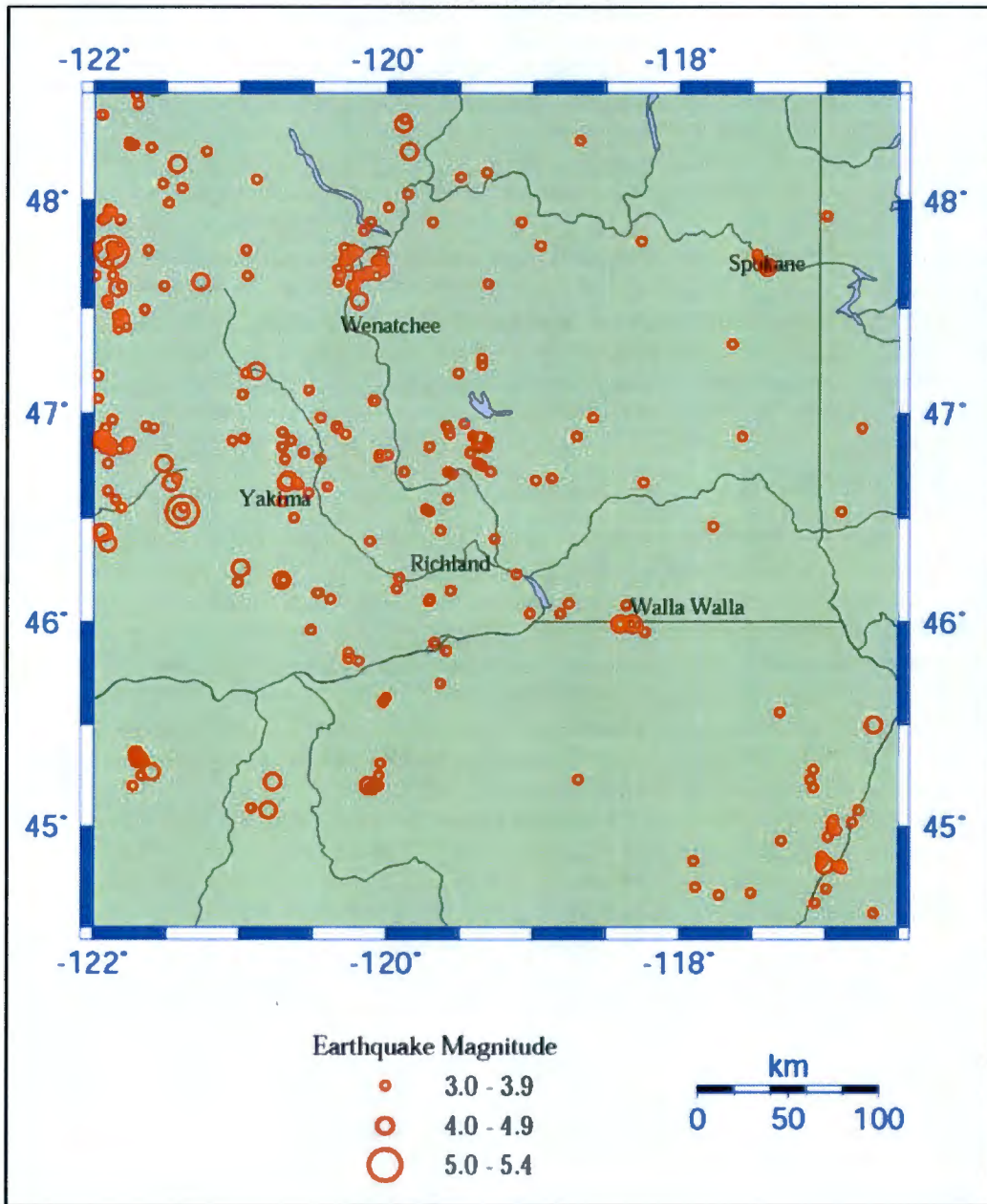


Figure 2-18. Earthquake Activity in the Vicinity of the Hanford Site Between 1970 and 2005 (PNNL-6415).



Greater magnitude earthquakes have been recorded at greater distances from Hanford Site at the edges of the Columbia Plateau, along the coastal subduction zones to the west and in the Rocky Mountains to the east. The Columbia Plateau, which is made up of thick and extensive sequences of flood basalt layers in the Columbia River Group, extends well beyond the Hanford Site covering parts of eastern Washington, eastern Oregon, and Idaho. Notable events in these areas are the 2001 "Nisqually earthquake" in the Puget Sound (6.8 magnitude), an approximate magnitude 6.8 to 7.4 earthquake in north-central Washington in 1872 near Lake Chelan, the 1959 Hebgen Lake earthquake (7.5 magnitude) in western Montana, and the 1983 Borah Peak earthquake in eastern Idaho (7.3 magnitude).

The gross pattern of seismic activity around the Hanford Site is consistent with our understanding of regional tectonic characteristics of the Northwest. That is, the flood basalts form a large and relatively competent block of rock that is surrounded by numerous complex zones of active faults where large scale stresses imposed primarily by the ongoing subduction of the Pacific and Juan de Fuca Plates underneath the North American Plate are mostly relieved. Consequently, relatively minimal stress relief occurs in the Columbia Plateau and earthquake energy is correspondingly small. This means that potential ground motion that accompanies these earthquakes is also relatively small.

Relative movement is commonly quantified as some fraction of gravitational acceleration (g) and has been generally correlated with earthquake magnitude. For the range of earthquake magnitudes suggested by data summarized above for the Hanford Site (<3 to 6), peak accelerations between <0.0017 and 0.18 g are proposed. The associated range of motion is generally imperceptible compared to clearly felt movement that can result in minimal building damage. A probabilistic seismic hazard analysis (WHC-SD-W236A-TI-002) estimated that a 0.1 g horizontal acceleration would occur every 500 years and a 0.2 g acceleration would occur every 2,500 years. With this information low-hazard facilities at the Hanford Site have typically been designed to withstand a horizontal acceleration of 0.12 g (WHC-SD-GN-DB-003). At the ERDF facility the operational concern was side slope stability. Because ERDF is considered a low-hazard facility, the side slope was designed to withstand this acceleration level. Notable physical disruption of the ERDF structures are expected to be essentially negligible over a several thousand year post-closure period.

2.1.4.3 Volcanology. Active and potentially active volcanoes are located in the Cascade Range that borders the western edge of the Columbia River flood basalts. The Cascade Range is oriented along a north-south axis parallel to the Washington coast line and extends southward into Oregon. The Cascade Range has formed because of active subduction of the Pacific and Juan de Fuca Plates beneath the North American Plate leading to orogenesis and magmatic eruptions. Orogenic activities began in the Miocene Age about 38 million years ago while currently active volcanoes were formed between 5 million years ago and the present (DOE/RW-0164).

The nearest volcano, Mount Adams, is about 160 km (100 mi) from the Hanford Site. The most recent major volcanic event was the Mount St. Helens eruption in 1980, which provided less than an inch of ash fall across the Hanford Site. Mount St. Helens is about 220 km (136 mi) west-southwest of the Hanford Site. Because of the distance of Cascade Range volcanoes from the Hanford Site, future impacts at the Hanford Site from volcanic events are expected to be similar to the Mount St. Helens event. Given the structural and tectonic characteristics of the region, volcanic activity will be limited to the Cascade Range over geologic time frames, and the occasional ash falls will have negligible impacts on facility performance.

2.1.5 Hydrology

The hydrology of the Hanford Site has been extensively study under CERCLA RI/FSs for various areas.

2.1.5.1 Surface Water. Naturally occurring surface water at the Hanford Site (Figure 2-19) includes the Columbia River, springs, and ponds. Intermittent surface streams, such as Cold Creek, may also contain water after large precipitation or snowmelt events. In addition, the Yakima River flows along a short section of the southern boundary of the Hanford Site and surface water associated with irrigation is located to the west, east, and north of the Site.

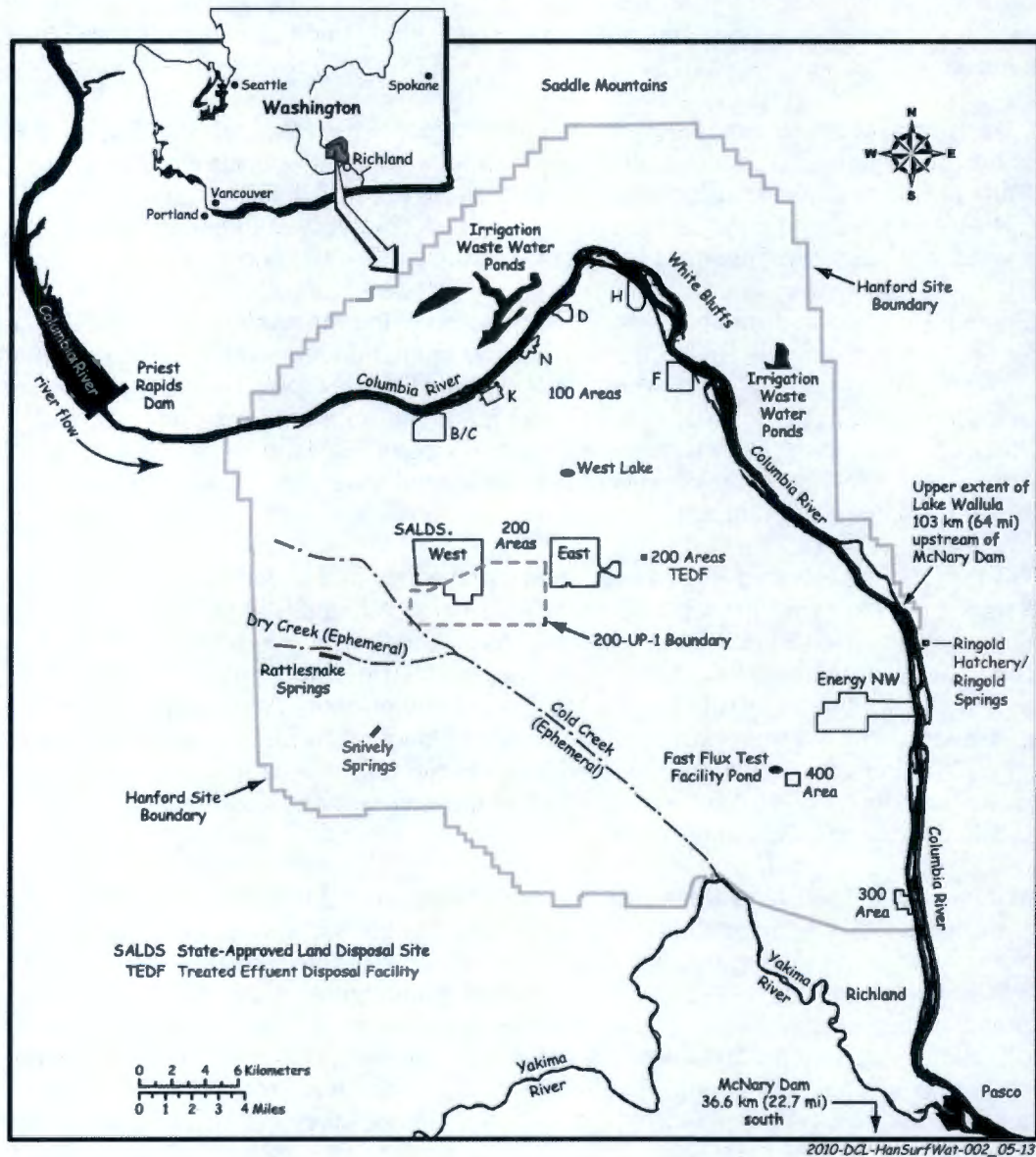
The Columbia River flows through the northern part and along the eastern border of the Hanford Site. Except for the Columbia River estuary, the only unimpounded stretch of the river in the United States is the Hanford Reach, which extends from Priest Rapids Dam (located upstream of the Site) downstream approximately 82 km (51 mi) to the northern upstream extent of Lake Wallula (formed by McNary Dam), which begins above Richland. The Hanford Reach of the Columbia River was recently incorporated into the land area established as the Hanford Reach National Monument.

River flow through the Hanford Reach fluctuates significantly and is controlled primarily by operations at upstream storage dams (Grand Coulee in the United States, and Mica and Keenleyside in Canada). Flows in the Hanford Reach are directly affected by releases from Priest Rapids Dam; however, Priest Rapids operates as a run-of-the-river dam rather than a storage dam. Flows are controlled to generate power and promote salmon egg and embryo survival. Several drains and intakes are also present along the Hanford Reach, including irrigation outfalls from the Columbia Basin Irrigation Project, Energy Northwest, and Hanford Site intakes for onsite water use. Much of the northern and eastern parts of the Hanford Site drain to the Columbia River.

The annual average flow of the Columbia River downstream of Priest Rapids Dam is estimated to be approximately 3,400 m³ (120,000 ft³) per second. In 2010, the Columbia River had below-normal flows; the average daily flow rate downstream of Priest Rapids Dam was 2,670 m³ (94,200 ft³) per second (PNNL-20548). As a result of fluctuation in discharges, the depth of the river varies significantly over time. The river stage (water-surface level) may change along the Hanford Reach by up to 3 m (10 ft) within a few hours. Seasonal changes of approximately the same magnitude are also observed. River-stage fluctuations measured at the 300 Area are approximately one-half the magnitude of those measured near the 100 Areas because of the effect of the pool behind McNary Dam (PNL-8580) and the relative distance of each area from Priest Rapids Dam. The width of the river varies from approximately 300 to 1,000 m (980 to 3,300 ft) as it passes through the Site.

Approximately one-third of the Hanford Site is drained by the Yakima River system. Cold Creek and its tributary, Dry Creek, are ephemeral streams on the Hanford Site that are within the Yakima River drainage system. Both streams drain areas along the western part of the Hanford Site and cross the southwestern part of the Site toward the Yakima River. Surface flow, which may occur during spring runoff or after heavier-than-normal precipitation, infiltrates and disappears into the surface sediments. Rattlesnake Springs, located on the western part of the Site, forms a small surface stream that flows for about 2.9 km (1.8 mi) before infiltrating into the ground.

Figure 2-19. Surface Water Features of the Hanford Site (Modified from PNNL-6415).



Mean annual runoff from the Pasco Basin is estimated to be less than $3.1 \times 10^7 \text{ m}^3/\text{yr}$ ($2.5 \times 10^4 \text{ acre-ft/yr}$), or approximately 3% of the total precipitation. The remaining precipitation is assumed to be lost through evapotranspiration with a small component (perhaps less than 1% recharging the groundwater system (DOE/RW-0164).

Historical Site activities discharged contaminated effluent to liquid waste sites, which caused the groundwater table to rise on the Central Plateau (DOE/RL-2001-54) creating artificial ponds and wetlands. In 1995, these management practices ceased, eliminating all man-made wetlands, with the exception of a small wetland identified in the 200 East Area during the 2001 Ecological Compliance Assessment Program survey.

Yakima River. The Yakima River follows a portion of the southwestern boundary of the Site and has much lower flows than the Columbia River (Figure 2-19). The average flow, based on 72 years of daily flow records (USGS 2007), is about $100 \text{ m}^3/\text{s}$ ($3,530 \text{ ft}^3/\text{s}$), with an average monthly maximum of $497 \text{ m}^3/\text{s}$ ($17,550 \text{ ft}^3/\text{s}$) and minimum of $4.6 \text{ m}^3/\text{s}$ ($165 \text{ ft}^3/\text{s}$). Average daily flow during 2006 was $100 \text{ m}^3/\text{s}$ ($3,530 \text{ ft}^3/\text{s}$) (USGS 2007).

The Yakima River System drains surface runoff from approximately one-third of the Site. Groundwater is expected to flow from the Yakima River into the aquifer underlying the Site rather than from the aquifer into the river because, based on well water level measurements, the elevation of the river surface is higher than the adjacent water table (PNL-10195). Therefore, groundwater contaminants from the Site do not reach the Yakima River.

Springs and Streams. Springs are found on the slopes of Rattlesnake Hills (Figure 2-19) along the western edge of the Site (DOE/RW-0164). An alkaline spring is located at the east end of Umtanum Ridge (TNC 1998). Rattlesnake and Snively Springs form small surface streams (Figure 3-6). Water discharged from Rattlesnake Springs flows in Dry Creek for about 3 km (1.6 mi) before disappearing into the ground. Cold Creek and its tributary, Dry Creek, are ephemeral streams within the Yakima River drainage system in the southwestern portion of the Site. These streams drain areas to the west of the Site and cross the southwestern part of the Site toward the Yakima River. When surface flow occurs, it infiltrates rapidly and disappears into the surface sediments in the western part of the Site. The quality of water in these springs and streams varies depending on the source; they are upgradient of Hanford waste sites and groundwater contamination plumes.

Columbia Riverbank Springs. During the early 1980s, researchers identified 115 springs along the Benton County shoreline of the Hanford Reach (PNL-5289). Seepage occurs both below the river surface and on the exposed riverbank, particularly at low-river stage. Riverbank springs flow intermittently, apparently influenced primarily by changes in river level. In many areas, water flows from the river into the aquifer at high river stage and then returns to the river at low river stage. This "bank storage" phenomenon has been modeled numerically for the 100-H Area (PNNL-13674). In areas of contaminated groundwater, riverbank springs are also generally contaminated. The concentrations in seeping water along the riverbank may be lower than groundwater, however, the mixing between river water and the contaminated aquifer contributed to the fluctuating bank storage phenomenon.

Contamination historically has been detected in near-shore samples downstream from riverbank springs (PNNL-20548). Riverbank springs are monitored for radionuclides at each of the 100 Areas, the Hanford townsite, and the 300 Area. Detected radionuclides include strontium-90, technetium-99, iodine-129, uranium-234, uranium-235, and uranium-238, and tritium, as well as arsenic, chromium, chloride, fluoride, nitrate, and sulfate.

Metals and anions (chloride, fluoride, nitrate, and sulfate) were detected in spring water from samples collected in 2005. Concentrations of volatile organic compounds were near or below their detection limits in all samples. Trichloroethylene (TCE) was detected ($1.4 \mu\text{g}/\text{L}$) in one sample from the 300 Area and was the only analyte detected at all shoreline spring sampling locations. TCE has been consistently detected at low concentrations in the 300 Area shoreline spring water (PNNL-20548).

Runoff and Net Infiltration. Total estimated precipitation over the Pasco Basin is about $9 \times 10^8 \text{ m}^3$ ($3.2 \times 10^{10} \text{ ft}^3$) annually (DOE/RW-0164). Precipitation varies both spatially and temporally with higher amounts generally falling at higher elevations. Mean annual runoff from

the Pasco Basin is estimated at $3.1 \times 10^7 \text{ m}^3/\text{yr}$ ($1.1 \times 10^9 \text{ ft}^3/\text{yr}$), or approximately 3% of the total precipitation (DOE/RW-0164). Most of the remaining precipitation is lost through evapotranspiration; however, a portion of the precipitation that infiltrates the soil eventually recharges the groundwater flow system. The amount of net infiltration varies spatially based primarily on soil texture and vegetation (Gee et al. 1992). Net infiltration also varies temporally with the majority occurring in the winter and spring. Some evidence exists that the most significant recharge events are associated with rapid melting of relatively large snowpacks, which may only occur a few times in a decade (PNNL-14744).

Flooding. Although large Columbia River floods have occurred in the past (DOE/EIS-0113), the likelihood of recurrence of large-scale flooding has been reduced significantly by the construction of several flood control/water storage dams upstream of the Hanford Site. Major floods on the Columbia River are typically the result of rapid melting of the winter snowpack over a wide area augmented by above-normal precipitation. The exceptionally high runoff during the spring of 1996 resulted in a maximum discharge of nearly $11,750 \text{ m}^3/\text{s}$ ($415,000 \text{ ft}^3/\text{s}$) (USGS 2007).

The probable maximum flood for the Columbia River downstream of Priest Rapids Dam has been calculated to be $40,000 \text{ m}^3/\text{s}$ (1.4 million ft^3/s) and is greater than the 500-year flood. This flood would inundate parts of the 100 Area adjacent to the Columbia River, but the central portion of the Hanford Site would remain unaffected (DOE/RW-0070). The U.S. Army Corps of Engineers has derived the Standard Project Flood with both regulated and unregulated peak discharges given for the Columbia River downstream of Priest Rapids Dam (U.S. Army Corps of Engineers 1989). The regulated Standard Project Flood for this part of the river is given as $15,200 \text{ m}^3/\text{s}$ ($54,000 \text{ ft}^3/\text{s}$) and the 100-year regulated flood as $12,400 \text{ m}^3/\text{s}$ ($440,000 \text{ ft}^3/\text{s}$). Impacts to the Hanford Site are negligible and would be less than the probable maximum flood.

The U.S. Army Corps of Engineers evaluated a number of scenarios on the effects of failures of Grand Coulee Dam, assuming flow conditions of $11,000 \text{ m}^3/\text{s}$ ($400,000 \text{ ft}^3/\text{s}$). The discharge or flood wave resulting from an instantaneous 50% breach at the outfall of the Grand Coulee Dam was determined to be $600,000 \text{ m}^3/\text{s}$ (21 million ft^3/s). In addition to the areas inundated by the probable maximum flood, the remainder of the 100 Area, the 300 Area, and nearly all of Richland would be flooded (DOE/RW-0070, RLO-76-4). The 50% scenario was believed to represent the largest realistically conceivable flow resulting from either a natural or human-induced breach (DOE/RW-0070). It was also assumed that a scenario such as the 50% breach would occur only as the result of direct explosive detonation, and not because of a natural event such as an earthquake, and that even a 50% breach under these conditions would indicate an emergency situation in which there might be other overriding major concerns.

Fewer than 20 major floods have occurred on the Yakima River since 1862 (DOE/RW-0070). The most severe occurred during November 1906, December 1933, May 1948, and February 1996; discharge magnitudes at Kiona, Washington, were $1,870 \text{ m}^3/\text{s}$ ($66,000 \text{ ft}^3/\text{s}$); $1,900 \text{ m}^3/\text{s}$ ($67,000 \text{ ft}^3/\text{s}$); $1,050 \text{ m}^3/\text{s}$ ($37,000 \text{ ft}^3/\text{s}$); and $1,300 \text{ m}^3/\text{s}$ ($45,900 \text{ ft}^3/\text{s}$); respectively. The average flow of the Yakima River is $104 \text{ m}^3/\text{s}$ ($3,665 \text{ ft}^3/\text{s}$), and the average monthly maximum is $490 \text{ m}^3/\text{s}$ ($17,500 \text{ ft}^3/\text{s}$). The recurrence intervals for the 1933 and 1948 floods are estimated at 170 and 33 years, respectively. The development of irrigation reservoirs within the Yakima River Basin has considerably reduced the flood potential of the river. The southern border of the Site could be susceptible to a 100-year flood on the Yakima River.

During 1980, a flood risk analysis of Cold Creek was conducted as part of the characterization of a basaltic geologic repository for high-level radioactive waste. In lieu of 100- and 500-year

floodplain studies, a probable maximum flood evaluation was performed based on a large rainfall or combined rainfall/snowmelt event in the Cold Creek and Dry Creek watershed (RHO-BWI-C-120/PNL-4219). The probable maximum flood discharge rate for the lower Cold Creek Valley was 2,265 m³/s (80,000 ft³/s) compared to 564 m³/s (19,900 ft³/s) for the 100-year flood. Modeling indicated that State Route 240, along the Hanford Site's southwestern and western areas would not be usable.

Nonriverine Surface Water. Active ponds on the Hanford Site include West Lake, the State-Approved Land Disposal Site, and the 200 Area Treated Effluent Disposal Facility (TEDF) disposal ponds (Figure 2-19). West Lake is north of the 200 East Area and is a natural feature recharged from groundwater (ARH-CD-775, PNL-7662). West Lake has not received direct effluent discharges from Site facilities; rather, its existence is caused by the intersection of the elevated water table with the land surface in the topographically low area. Water levels of West Lake fluctuate with water table elevation, which is influenced by wastewater discharge in the 200 Areas. The water level and size of the lake has been decreasing over the past several years because of reduced wastewater discharge.

The TEDF is east of the 200 East Area and consists of two disposal ponds. These ponds are each 0.02 km² (0.008 mi²) in size and receive industrial wastewater permitted in accordance with WAC 173-216. The wastewater evaporates into the air or percolates into the ground from the disposal ponds.

Several naturally occurring vernal ponds are located near Gable Mountain and Gable Butte (TNC 1998). The formation of these ponds in any particular year depends on the amount and temporal distribution of precipitation and snowmelt events. The vernal ponds range in size from about 6.1 m by 6.1 m to 45.73 m by 30.5 m (20 ft by 20 ft to 150 ft by 100 ft), and were found in three clusters. Approximately 10 were documented at the eastern end of Umtanum Ridge, 7 were observed in the central part of Gable Butte, and 3 were found at the eastern end of Gable Mountain.

2.1.5.2 Groundwater. This section describes the relevant characteristics of the groundwater hydrology, which has been studied and monitored in detail because of the waste disposal operations at the site. The hydrology characteristics of the Hanford Site are important to the definition of potential pathways for the ERDF contaminants to the public and impact the magnitudes of the estimated environmental impacts. Evaluating this pathway requires information about the types of aquifers present, depths to the water table, and regional flow paths toward surface water outlets. Surface water flow represents a pathway for carrying contaminants to the public. Because the uppermost unconfined aquifer is considered the primary pathway for possible contaminant transport from the ERDF, it is especially important in this PA.

The discussion focuses on the geohydrology of the 200 Areas but also includes information on the Hanford Site in general, highlighting those aspects that were important to the modeling of system performance. This information was summarized largely from material presented in PNNL-6415 and WCH-463 with additional information taken from DOE/RL-2011-118 and PNNL-20548:

- *Hanford Site Environmental Report for Calendar Year 2010* (PNNL-20548) provides the overview of the characterization and monitoring activities conducted at the Hanford Site during the calendar year. This document has been published annually since 1958.

- *Hanford Site Groundwater Monitoring for 2011* (DOE/RL-2011-118). This document describes the groundwater monitoring activities during the fiscal year.
- *Hanford Site National Environmental Policy Act (NEPA) Characterization* (PNNL-6415) provides a standardized description of the Hanford Site environment. This document has been published annually since 1988.

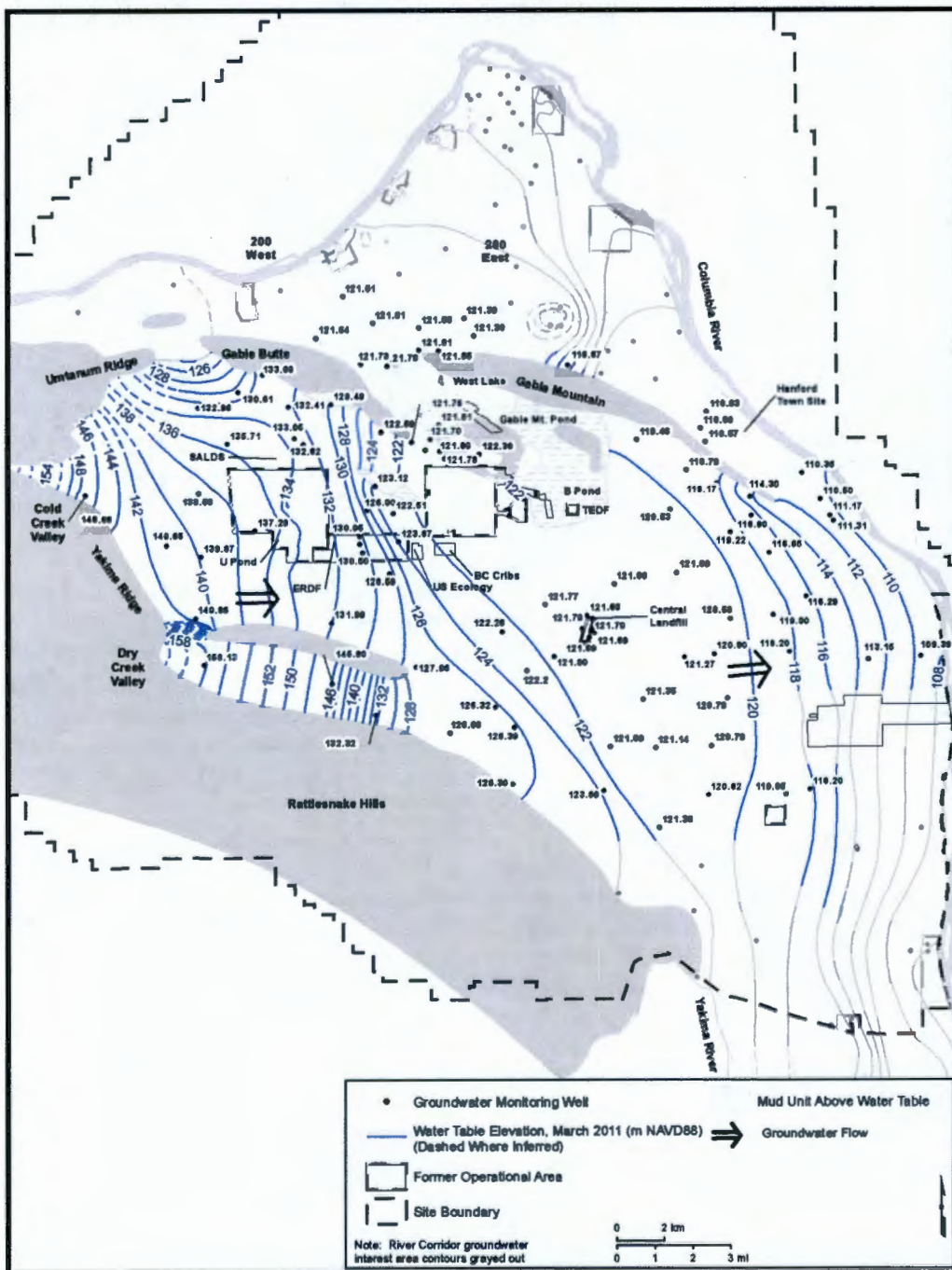
In addition to these overview documents, there have been site-specific documents that describe the groundwater hydrology at ERDF, including the site characterization report, the RI/FS, and ERDF PA from 1995.

The base of the uppermost aquifer system is defined as the top of the uppermost basalt flow. This aquifer system is bounded laterally by anticlinal basalt ridges and is about 152 m (500 ft) thick near the center of the Pasco Basin. Within the Hanford Site, this uppermost aquifer system lies at depths ranging from less than 0.3 m (1 ft) below the ground surface near West Lake and the Columbia and Yakima Rivers, to more than 107 m (350 ft) in the central portion of the Cold Creek syncline.

Unconfined Aquifer System. The unconfined aquifer system is composed primarily of the Ringold Formation and overlying Hanford formation (Figure 2-14). In some areas, the coarse-grained multilithic facies of the Cold Creek unit (pre-Missoula gravels) lie between these formations and below the water table. The other subunits of the Cold Creek unit are generally above the water table. Water table elevations (Figure 2-20) show that groundwater in the unconfined aquifer at the Hanford Site generally flows from recharge areas in the elevated region near the western boundary of the Hanford Site toward the Columbia River on the eastern and northern boundaries. The Columbia River is the primary discharge area for the unconfined aquifer. The Yakima River borders the Hanford Site on the southwest and is generally regarded as a source of recharge. Along the Columbia River shoreline, daily river level fluctuations may result in water table elevation changes of up to 3 m (10 ft). During the high river stage periods of 1996 and 1997, some wells near the Columbia River showed water level changes of more than 3 m (10 ft).

In the 200 West Area, the water table occurs almost entirely in the Ringold Unit E gravels, while in the 200 East Area, it occurs primarily in the Hanford formation and in the Ringold Unit A gravels (Figure 2-10). Along the southern edge of the 200 East Area, the water table is in the Ringold Unit E gravels. The upper Ringold facies were eroded in most of the 200 East Area by the ancestral Columbia River and, in some places, by the Missoula floods that subsequently deposited Hanford gravels and sands on what was left of the Ringold Formation (DOE/RL-2002-39). Because the Hanford formation and possibly the Cold Creek unit sand and gravel deposits are much more permeable than the Ringold gravels, the water table is relatively flat in the 200 East Area, but groundwater flow velocities are higher. On the north side of the 200 East Area, there is evidence of erosional channels that may allow interaquifer flow between the unconfined and uppermost basalt-confined aquifer (RHO-RE-ST-12P, PNL-6313).

Figure 2-20. Water Table Elevations in Meters for Year 2011 for the Unconfined Aquifer in the Central Plateau Portion of Hanford Site.



Horizontal hydraulic conductivities of sand and gravel facies within the Ringold Formation generally range from about 1 to 100 m/day, compared to 10 to 3,000 m/day for the Hanford formation and the coarse-grained multilithic facies of the Cold Creek unit (pre-Missoula gravels) (DOE/RW-0164, PNNL-13641, PNNL-14058). Because the Ringold Formation sediments are more consolidated and partially cemented, they are about 10 to 100 times less permeable than the sediments of the overlying Hanford formation. Before wastewater disposal operations at the Hanford Site, the uppermost aquifer was mainly within the Ringold Formation, and the water table extended into the Hanford formation at only a few locations (Newcomb et al. 1972). However, wastewater discharges raised the water table elevation across the site. The general increase in groundwater elevation caused the unconfined aquifer to extend upward into the Hanford formation over a larger area, particularly near the 200 East Area. This resulted in an increase in groundwater velocity because of both the greater volume of groundwater and the higher permeability of the newly saturated Hanford formation sediments.

The hydrology of the 200 Areas has been strongly influenced by the discharge of large quantities of wastewater to the ground. Between 1944 and the mid-1990s, an estimated 1.68×10^{12} L (4.44×10^{11} gal) of liquid was discharged to disposal ponds, trenches, and cribs. Wastewater discharge has decreased since 1984 and currently only contributes a volume of recharge in the same range as the estimated natural recharge from precipitation. The largest volumes of discharge in the 200 West Area were to the 216-T Pond system and the 216-U-10 Pond. Figure 2-21 shows the liquid discharge history for the two ponds. The 216-T Pond system is estimated to have received approximately 424 billion L of effluent (WHC-EP-0815) and the 216-U Pond to have received about 158 billion L of effluent (WHC-EP-007). The largest volumes of discharge around the 200 East Area were to the 216-B Pond system, the 216-A-25 (Gable Mountain) pond system, and several of the PUREX cribs in the southeast corner of 200 East Area. Figure 2-22 shows the liquid discharge history for the two ponds. The 216-B Pond system is estimated to have received approximately 293 billion L of effluent and the 216-B Pond to have received about 256 billion L of effluent.

Water levels in the uppermost and unconfined aquifer rose as much as 26 m and 9 m beneath the 200 West Area and 200 East Area, respectively, because of artificial recharge caused by liquid waste disposed from the mid-1940s to 1995. The volume of water that was discharged to the ground at the 200 West Area was actually less than that discharged at the 200 East Area. However, the lower hydraulic conductivity of the aquifer near the 200 West Area inhibited groundwater movement in this area, resulting in a higher groundwater mound. All nonpermitted discharges of liquid effluent to the ground were stopped in 1996.

A hindcast map showing water table elevations prior to the start of significant Hanford Site wastewater discharges is provided in Figure 2-23 (ERDA 1975). This water map includes the effects of limited irrigation near the former towns of White Bluff and Hanford, but not the effects of extensive irrigation now common in Cold and Dry Creeks. The 1944 water table contours suggest that groundwater flow is easterly toward the Columbia River with a relatively uniform hydraulic gradient (approximately 1.5 m/km [5 ft/mi]). Regional groundwater flow was generally toward the east-northeast, although flow north of Gable Mountain was more to the north.

Figure 2-21. Discharge History for the 216-T Pond and the 216-U Pond.

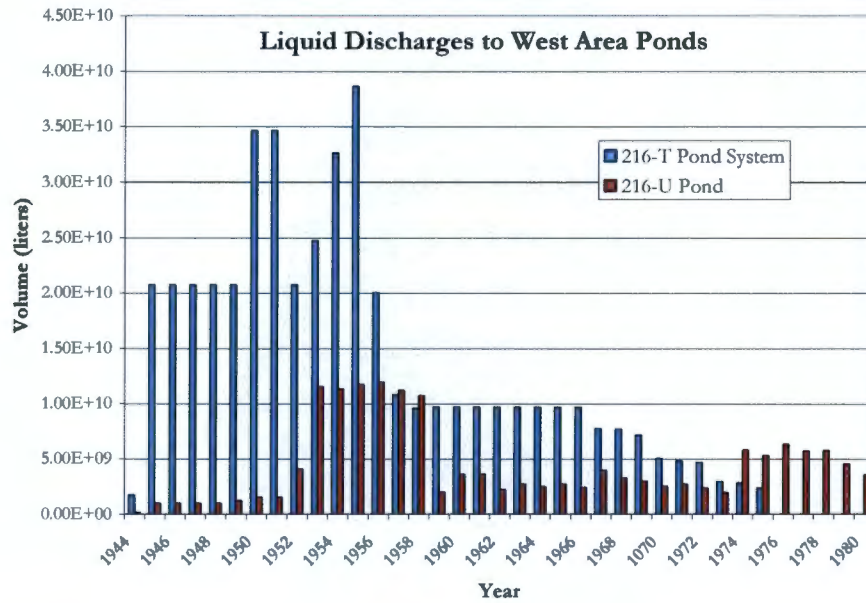


Figure 2-22. Discharge History for the 216-B Pond and Gable Mountain Pond.

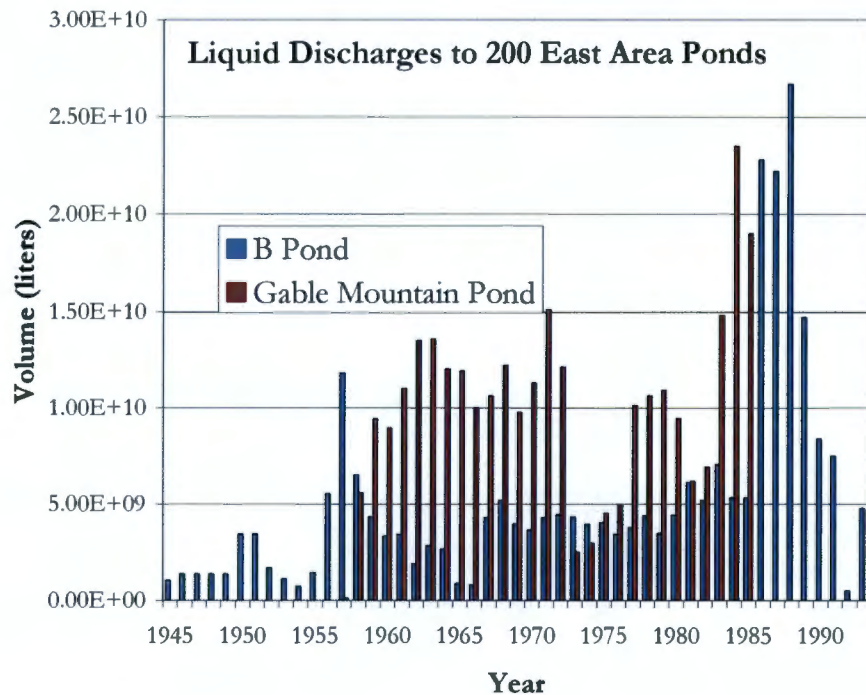
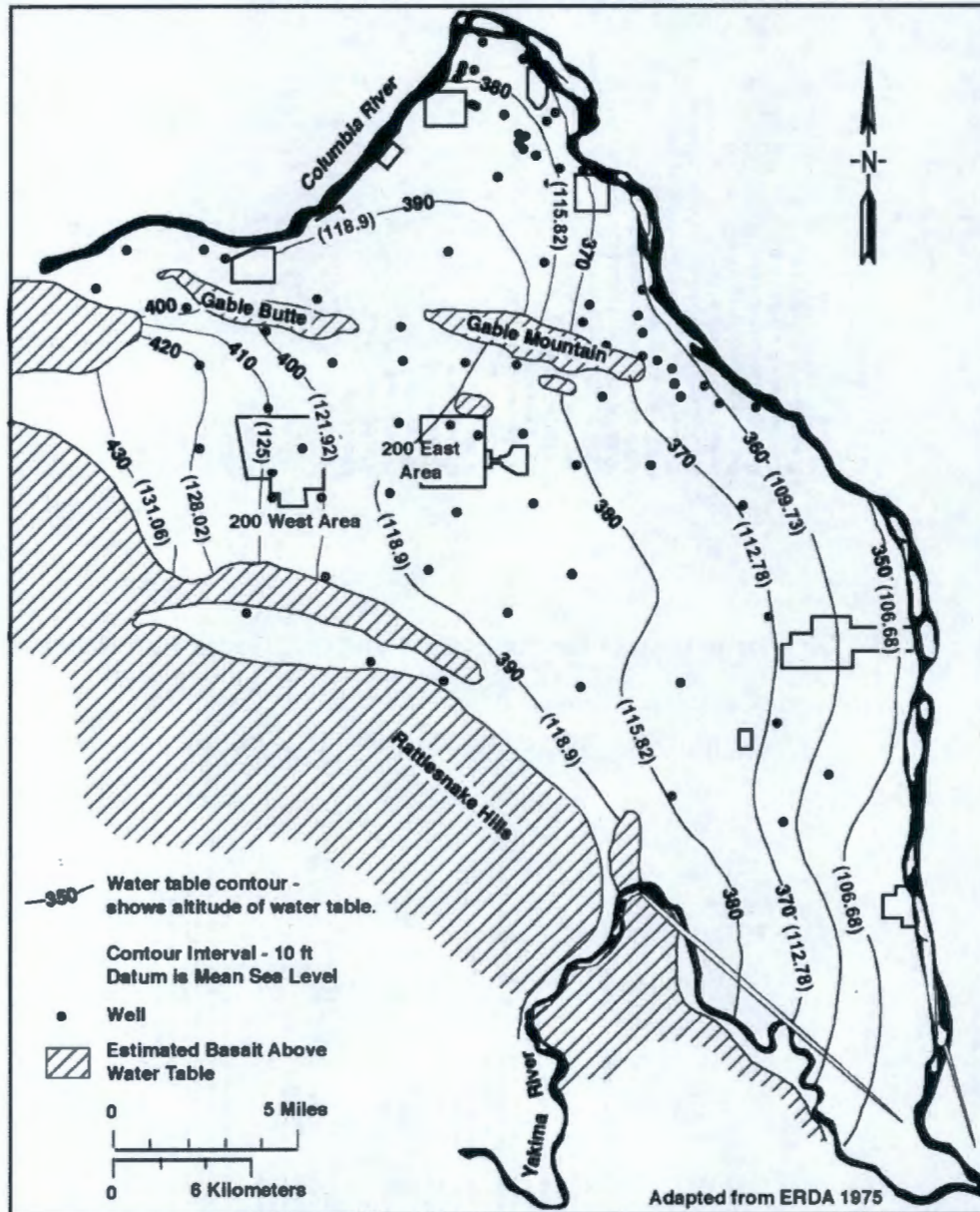


Figure 2-23. Hindcast Water Table Map of the Hanford Site, January 1944.



The pre-Manhattan Project water table in the 200 West Area and 200 East Area was approximately 123 m and 120 m above sea level, respectively (BNWL-B-360). In the 200 West Area, the water-table elevation increased rapidly from 1949 to 1956, but appeared to stabilize between the late 1960s and the late 1980s. Water levels began to decline in the late 1980s when wastewater discharges in the 200 West Area were reduced. In the 200 East Area, the water-table elevation increased rapidly from 1954 to 1963. The water table declined somewhat in the late 1960s and early 1970s, but then increased again in the early 1980s before beginning a final decline throughout the 1990s when wastewater discharges in the 200 East

Area were reduced. Although the reduction of wastewater discharges has caused water levels to drop significantly, a residual groundwater mound beneath the 200 West Area is still shown by the curved water table contours near this area, and small groundwater mounds exist near the 200 Area TEF and State-Approved Land Disposal Site wastewater disposal sites (Figure 2-20).

Comparing the approximate rate of water table decline in the 200 East Area with that in the 200 West Area shows that the rate of decline is three to four times faster in the 200 West Area. This is probably due, in part, to the greater increase in water level due to U Pond than to B Pond and that the 200 West Area tank farms are closer to the U Pond mound than are the 200 East Area tank farms to the B Pond mound. Also, the water table gradient is extremely flat in the 200 East Area, whereas the gradient is steeper beneath the 200 West Area. This means that a small increment of water table decline must be spread out over a much larger area in the 200 East Area than in the 200 West Area.

The groundwater mounds drastically changed the flow direction causing radial flow from the discharge areas, and, in some areas, resulted in a complete reversal of flow direction. Until about 1980, the edge of the mounds migrated outward from the sources. Groundwater levels have declined over most of the Hanford Site since 1984 because of decreased wastewater discharges (DOE/RL-2011-118), and since 1996, when all nonpermitted discharges to the ground ceased, groundwater flow has begun to return to pre-Hanford Site conditions.

A limited amount of hydraulic property data is available from testing of wells. Hydraulic test results from wells on the Hanford Site have been compiled for the Hanford Groundwater Monitoring Project and for environmental restoration efforts (BNWL-1709, WHC-SD-EN-TI-014, WHC-SD-EN-TI-019, PNL-8337, PNNL-14058, PNL-10835, PNNL-13342, PNNL-13378, PNNL-13514, PNNL-14113). Most hydraulic tests were conducted within the upper 15 m (49 ft) of the aquifer, and many were open to more than one geologic unit. In some cases, changes in water table elevation may have significantly changed the unconfined aquifer transmissivity at a well since the time of the hydraulic test.

Several past studies (e.g., PNNL-13641, PNNL-14398) have focused on evaluating the horizontal hydraulic conductivity of the Ringold E in the Central Plateau, which is the primary unconfined aquifer in the 200 West Area, where ERDF is located. According to pump test analysis and calibration results summarized in these studies, this parameter can range from 0.1 to more than 2,500 m/day. An updated review of Ringold E properties (DOE/RL-2007-28) indicated that this parameter more usually ranges from 1 to 100 m/day.

Recent slug tests conducted at multiple depths in the vicinity of ERDF that are presented in PNNL-19482, *Slug Test Characterization Results for Multi-Test/Depth Intervals Conducted During the Drilling of CERCLA Operable Unit OU UP-1 Wells 299-W19-48, 699-30-66, and 699-36-70B*, indicate that the horizontal hydraulic conductivity in Ringold E can vary from 0.3 to 10 m/day. Most recent estimate based on groundwater model calibration for the Central Plateau indicates a hydraulic conductivity for Ringold E to be near 5 m/day (CP-47631, *Model Package Report: Central Plateau Groundwater Model Version 3.3*).

2.1.5.3 Existing Groundwater Contamination Plumes near ERDF. Near the ERDF, technetium-99, uranium, tritium, iodine-129, nitrate, chromium (as hexavalent chromium), and carbon tetrachloride are the contaminants of greatest significance in groundwater, and form extensive plumes within the region. Groundwater plumes of tritium and iodine-129 that originated from 200 West Area ponds and cribs are dispersing naturally, whereas plumes

originating from the tank farms are generally growing in areal extent and exhibit increasing concentrations. The carbon tetrachloride plume has migrated into the 200-UP-1 Groundwater Operable Unit from the adjacent 200-ZP-1 Groundwater Operable Unit (Figure 2-24). The chromium plume east-southeast of ERDF originated primarily from effluent disposal to the S-SX cribs and ponds during the 1950s, although the REDOX Plant ponds and ditches to the south of the 200 West Area were also sources. Groundwater flow in the unconfined aquifer is primarily toward the east within the interest area. Below is a brief discussion of existing groundwater contamination for four radionuclides.

- Iodine-129
- Technetium-99
- Tritium
- Uranium.

Iodine-129

Iodine-129 plumes originate from both U Plant and REDOX Plant disposal facilities (Figure 2-24), although the most substantial releases occurred from the REDOX facilities. One plume originates from the 216-U-1/2 Cribs, and a second plume originates from the southern portion of the 200 West Area. At the current level of monitoring detail, these plumes merge downgradient and become indistinguishable. This combined plume (as defined by the 1 pCi/L contour) extends to the east a distance of ~3.5 km. The highest concentrations of iodine-129 within the operable unit, greater than 10 times the drinking water standard, occur in a region extending approximately 2 km east from the southeastern 200 West Area toward ERDF.

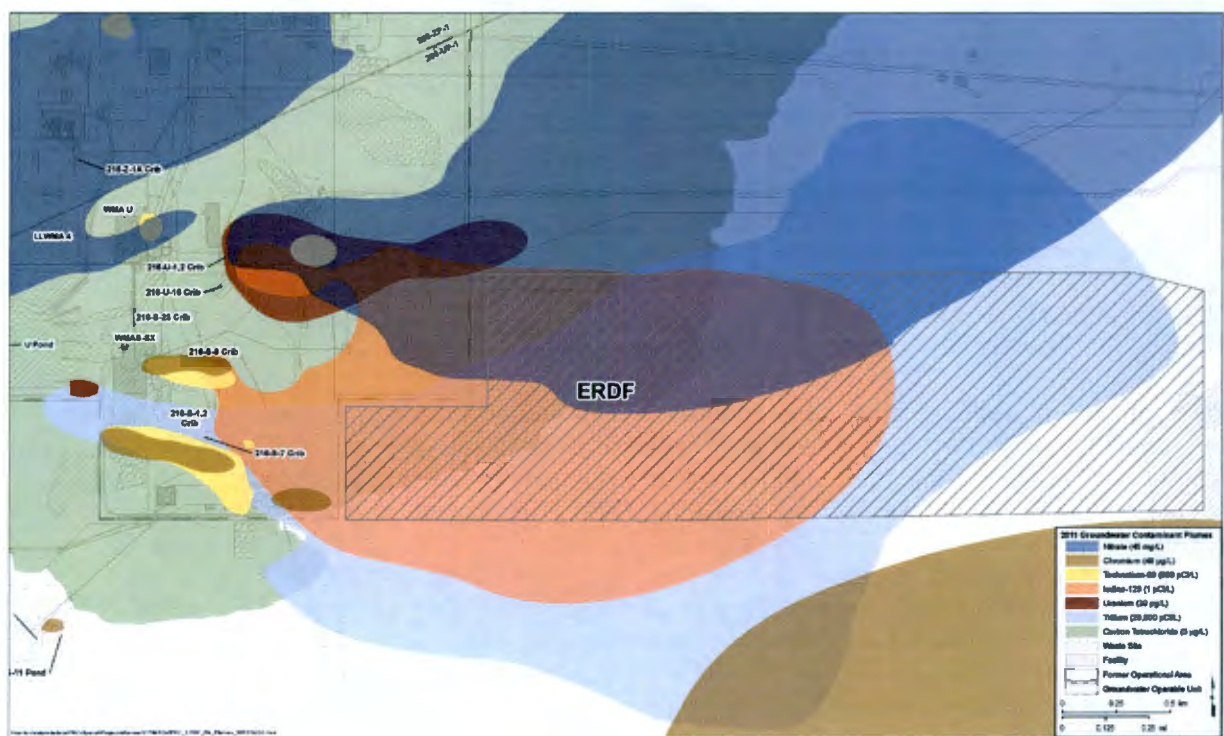
Technetium-99

In the vicinity of ERDF, technetium-99 concentrations occur above the drinking water standard of 900 pCi/L within two plumes in the vicinity of WMA S-SX (Figure 2-24). The highest technetium-99 concentrations occur in the southern plume at well 299-W23-19 (located inside the SX Tank Farm). During calendar year 2010, concentrations in this well fluctuated between 49,000 and 65,000 pCi/L. The southern plume from WMA S-SX is directly west of ERDF; this plume has increased in areal extent and concentrations are increasing in many of the downgradient wells.

Tritium

Disposal facilities associated with the REDOX Plant are the primary sources of tritium in the vicinity of ERDF. The REDOX Plant operated from 1952 until 1967, although effluent releases continued after that time. A large tritium plume from the REDOX Plant cribs originates from the southern portion of the 200 West Area and extends ~5 km toward the east (ERDF) and northeast at levels above the 20,000 pCi/L drinking water standard (Figure 2-24). The large extent of this plume is due to the large number of sources, the long time span since releases began, and the high mobility of tritium in the aquifer.

Figure 2-24. Existing Groundwater Contamination Plumes near ERDF.



Uranium

Uranium within the 200-UP-1 Groundwater Operable Unit primarily occurs in a plume downgradient from the 216-U-1/2 Cribs and is associated with the technetium-99 plume. The plume extends ~1.5 km to the east at levels above the 30 µg/L drinking water standard (Figure 2-24). The uranium originated from the 216-U-1/2 Cribs, which were active in the 1950s and 1960s. A small plume of uranium southwest of WMA S-SX is present that is interpreted to be leaching from the vadose zone beneath U Pond.

2.1.6 Geochemistry

Site characterization efforts show that soil mineralogy and groundwater chemistry are relatively constant on the Central Plateau of the Hanford Site. Soil-phase mineralogy is relatively consistent in the major stratigraphic units (largely quartz, feldspar, and minor but ubiquitous quantities of calcite, metal oxides/hydroxides, and clays), the notable exception being higher concentrations of calcite in the Cold Creek Unit caliche layer that could lead to different sorption characteristics due to variable reactivity with carbonate minerals. Similarly, the chemistry of undisturbed groundwater is stable. Typically, the pH is moderately alkaline and buffered by calcite; the dominant cations are calcium, sodium, magnesium, and potassium; and the dominant anions, other than bicarbonate and hydroxide, are sulfate and chloride. At subsurface wells around ERDF, average measured values are 7.75 for pH, ~50, 20, 16, and 6 mg/L for calcium, sodium, magnesium, and potassium, respectively, and ~32 and 22 mg/L for sulfate and chloride, respectively. In these wells, the range of cation and anion concentrations typically varies by 2 to 3 times their mean value.

No information is available for vadose zone porewater chemistry underneath ERDF, but some data have been collected for representative vadose zone soils from single-shell tank farm vadose zone characterization efforts just west of ERDF (RPP-7884, *Field Investigation Report for Waste Management Area S-SX*; RPP-23752, *Field Investigation Report for Waste Management Area T and TX-TY*). The soils were collected at various depths from three boreholes, 299-W22-48 and 299-W22-50 in the S-SX Tank Farms and 299-W10-27 at the T Tank Farm. At these locations the same major stratigraphic units are present as at ERDF. Because leaching tests were short term, completely stable water chemistry was probably not achieved. However, the test data show similar chemistry over depth and in comparison with groundwater chemistry. Average leaching values from the three-well data set resulted in pH of 7.5 and concentrations of 13, 16, 4, and 5 mg/L for calcium, sodium, magnesium, and potassium, respectively, and 13 and 2 mg/L for sulfate and chloride, respectively.

Once the ERDF leachate begins to percolate into the vadose zone, perturbation of natural geochemical conditions are not expected to be severe because the waste materials are largely composed of Hanford Site soils that should react with meteoric precipitation over the long term and modify water chemistry to resemble natural porewater. Currently, waste water leachate (collected by the leachate collection system) is moderately alkaline (pH ~7.6) with the same major dissolved species as groundwater. However, total concentrations are currently higher (5 to 15 times depending on the species) and relative concentrations between species are not quite the same as in groundwater (e.g., sodium concentrations are elevated). These observations are not unexpected given the handling of waste materials (which can expose fresh surfaces for leaching) and the disposal of materials other than soil. Over time, leachate concentrations will diminish with continued leaching. Regardless, total dissolved solids will diminish during transport through the vadose zone soil as the natural system responds to the influx of more concentrated fluids. These observations do not suggest a major perturbation of

the natural system or a significant change in the chemical reactivity of radionuclides with subsurface soils.

2.1.7 Natural Resources

The following section discusses the natural geologic and water resource on the Hanford Site. The Central Plateau of the Hanford Site has no important natural resources. No major mining operations exist in the Hanford Site area. Oil and gas exploration have occurred; however, no economically viable accumulations were found. Some local gravel processing is being done in the area.

2.1.7.1 Geologic Resources. Geologic resources at the Hanford Site are very limited. Hanford Site mineral resources include sand, gravel, silt, clay, and aggregate. Historically, these resources were extracted at several quarries or pits at the Hanford Site and used for road construction and maintenance, and waste burial activities. No major mining operations exist in the Hanford Site area. Oil and gas exploration have occurred; however, no economically viable accumulations were found.

2.1.7.2 Water Resources. The Columbia River is used as a source of both drinking water and industrial water for several Site facilities (PNNL-20548). The water systems of Richland, Pasco, and Kennewick withdrew a large portion of the 48.8 billion L (12.9 billion gal) used during 2006 from the Columbia River. Each city operates its own supply and treatment system, located downgradient and downriver of the Site. The Richland water supply system derives about 82% of its water directly from the Columbia River, while the remainder is split between a well field in North Richland (that is recharged from the river) and groundwater wells.

The City of Richland's total water usage during 2006 was 20.1 billion L (5.3 billion gal). The Kennewick system uses two wells and the Columbia River for its water supplies. These wells serve as the sole source of water between November and March and can provide approximately 40% of the total maximum supply of 94.6 billion L/day (25 million gal/day). Total 2006 usage in Kennewick was 13.4 billion L (3.5 billion gal). A significant number of Kennewick's residents (about 22,000 residential customers) draw irrigation water from the Kennewick Irrigation District, which has the Yakima River as its source. The City of Pasco system also draws from the Columbia River for its water needs. During 2006, Pasco consumed 15.3 billion L (4.1 billion gal). Energy Northwest operates the Columbia Generating Station northeast of the 400 Area. Energy Northwest uses Columbia River water for both potable and process/cooling water applications.

2.1.8 Natural Background Radiation

The Hanford Site has an extensive monitoring program. Studies have been directed at determining background levels of possible contaminants in the soil (DOE/RL-92-94, DOE/RL-95-55) and in the groundwater (WHC-EP-0595). Also, reports are issued annually covering general environmental conditions (PNNL-6415) and groundwater monitoring (DOE/RL-2011-118).

Low concentrations of some longer lived radionuclides such as isotopes of cesium, plutonium, potassium, strontium, and uranium are detectable that are associated with particulate matter that accumulated in riverbed sediments (PNNL-20548). The levels were similar to those measured in previous years. No discernible increase in concentration could be attributed to current Hanford Site operations. DOE/RL-91-45, *Hanford Site Risk Assessment Methodology*,

summarizes all the measurements taken to determine radionuclide background levels at the Hanford Site (see Appendix B, Section B.2.8).

Recent annual Hanford Site environmental reports (e.g., PNNL-20548) estimate that the total annual dose from Hanford Site operations in 2010 to a hypothetical maximally exposed individual at an offsite location was about 0.18 mrem. The air-pathway annual dose was 0.053 mrem (excluding radon) and 0.067 mrem (including radon). These radiation exposures are small compared to other natural and human produced sources that are estimated to contribute approximately 365 mrem annual dose to individuals living near the Hanford site (NCRP 1987).

2.2 PRINCIPAL FACILITY DESIGN FEATURES

The ERDF is designed to be a multi-celled landfill that can be expanded to meet the Hanford Site environmental restoration needs (Figure 2-25). The disposal cells located within the ERDF are approximately 21 m (70 ft) deep. Cells 1 through 8 are each approximately 152 m (500 ft) by 152 m (500 ft) at the base while “supercells” 9 and 10 are 152 m (500 ft) by 305 m (1,000 ft) at the base. In the current configuration, the base of ERDF covers an area of approximately 433,000 m² (107 acres) and the maximum waste holding capacity is approximately 19 million metric tons.

The first two cells, 1 and 2, came online in 1996. Additional pairs of cells were added in 1999 (cells 3 and 4), 2004 (cells 5 and 6), and 2009 (cells 7 and 8). Two “supercells,” 9 and 10, each the equivalent of a pair of preceding cells, were constructed in January 2011. The plan view of the cell pairings is shown in Figure 2-26 for cells 7 and 8, as an example. Figure 2-27 shows a cross section of the general layout, including the double-liner system and the two leach sumps. Figures 2-28 and 2-29 illustrate the respective plan and cross-sectional views of supercells 9 and 10.

The following subsections address the principal design features of the facility that contribute to the long-term isolation of disposed waste. These features serve to (1) minimize the infiltration of water through disposal units; (2) ensure integrity of disposal unit covers; (3) provide for the structural stability of backfill, waste, and covers; and (4) provide a barrier against intrusion.

2.2.1 Water Infiltration

Minimization of infiltration of water through the disposal units of the ERDF is accomplished by incorporation of a side slope and a bottom liner system as well as a surface cover. Information on the design features of the bottom liner and surface cover are provided in the following subsections.

2.2.1.1 ERDF Sideslope and Floor Liner. A schematic of the ERDF multi-layer liner system is shown in Figure 2-30. The ERDF sideslope liner comprises six layers: (1) a 0.9-m (3-ft) operations layer (sandy loam/silty sand) with an estimated saturated hydraulic conductivity of about 7.2×10^{-4} cm/s (WCH 2009), (2) a primary geocomposite drainage layer with a 3:1 (horizontal to vertical) drainage slope, (3) a primary 60-mil high-density polyethylene (HDPE) geomembrane liner, (4) a secondary geocomposite drainage layer with a 3:1 drainage slope, (5) a secondary 60-mil HDPE geomembrane liner, and (6) a 0.9-m (3-ft)-thick compacted admix layer with a minimum saturated hydraulic conductivity of 1×10^{-7} cm/s (WCH 2009).

Figure 2-25. Aerial View of ERDF with Cells Used for Disposal.



Figure 2-26. Plan View for Cells 7 and 8.

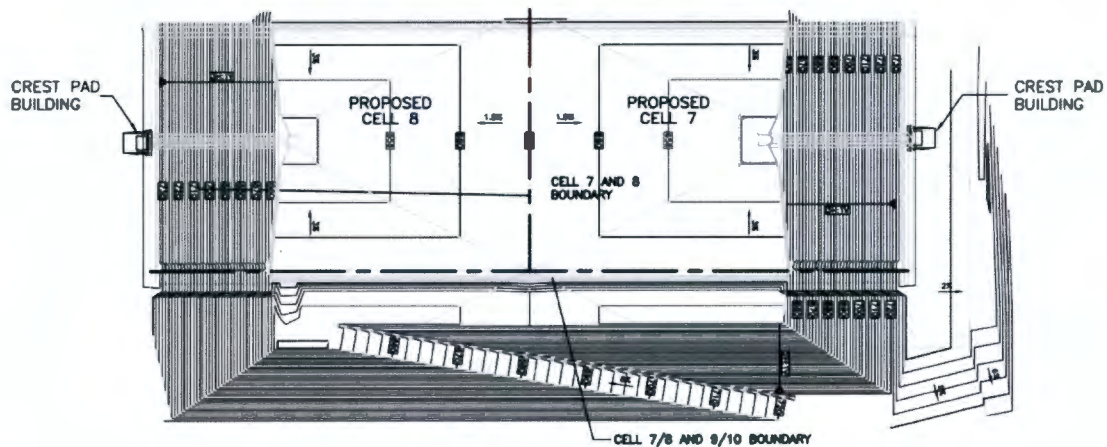


Figure 2-27. Generic Cross-Sectional View for Cells 1 Through 8.

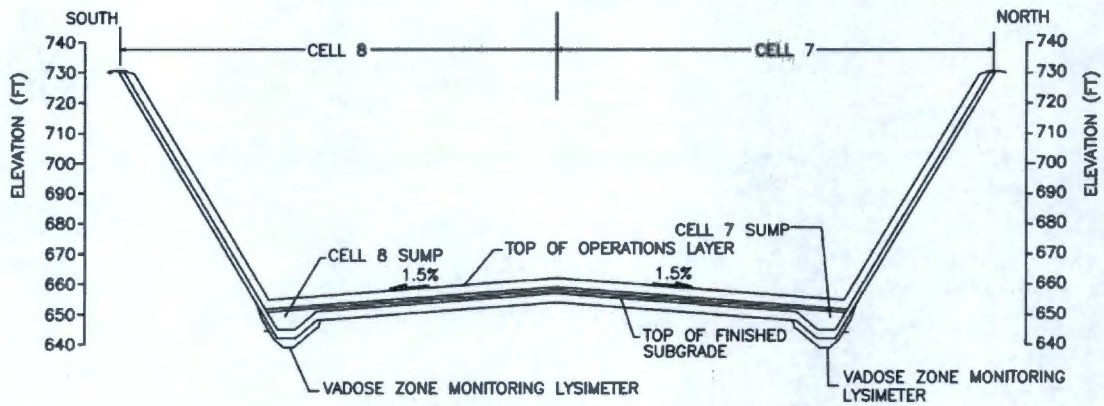


Figure 2-28. Plan View of Super Cells 9 and 10.

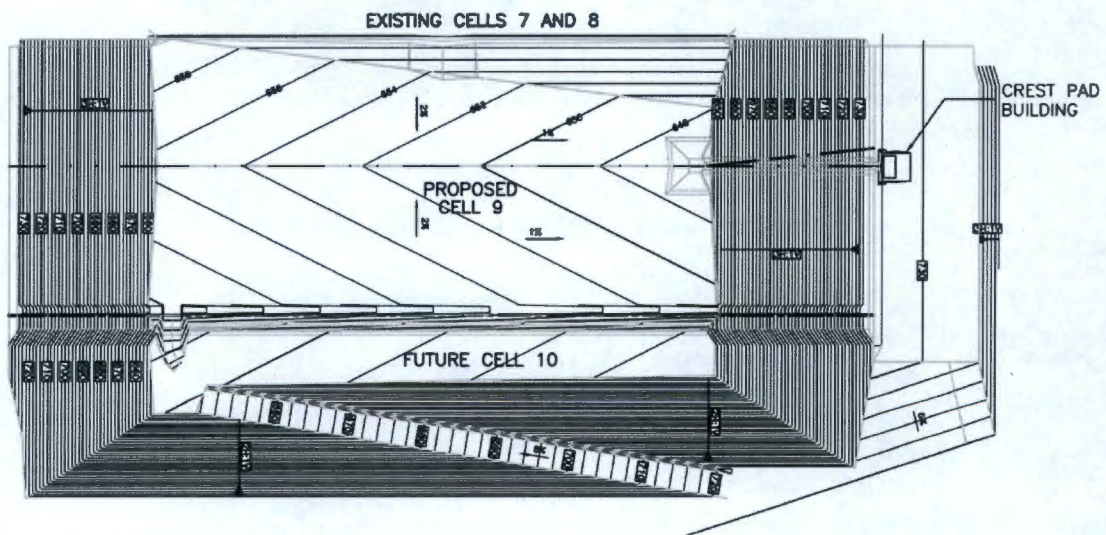


Figure 2-29. Cross-Sectional View of a Super Cell.

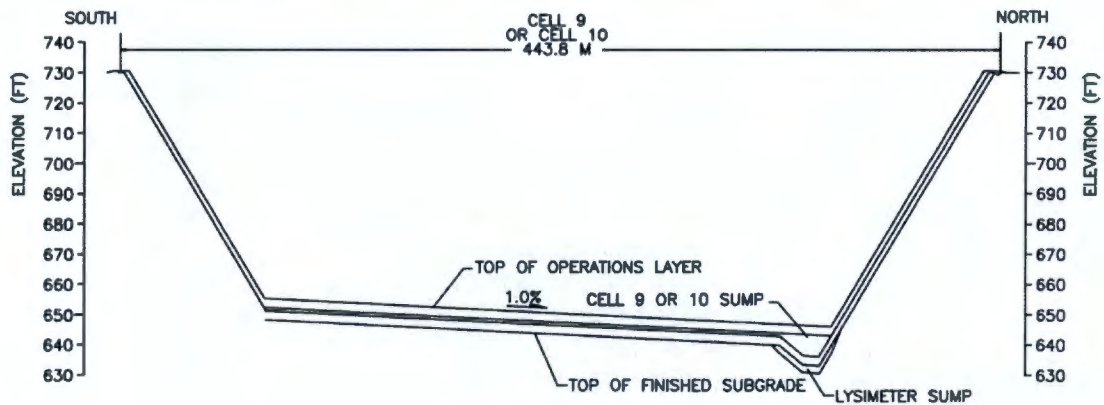
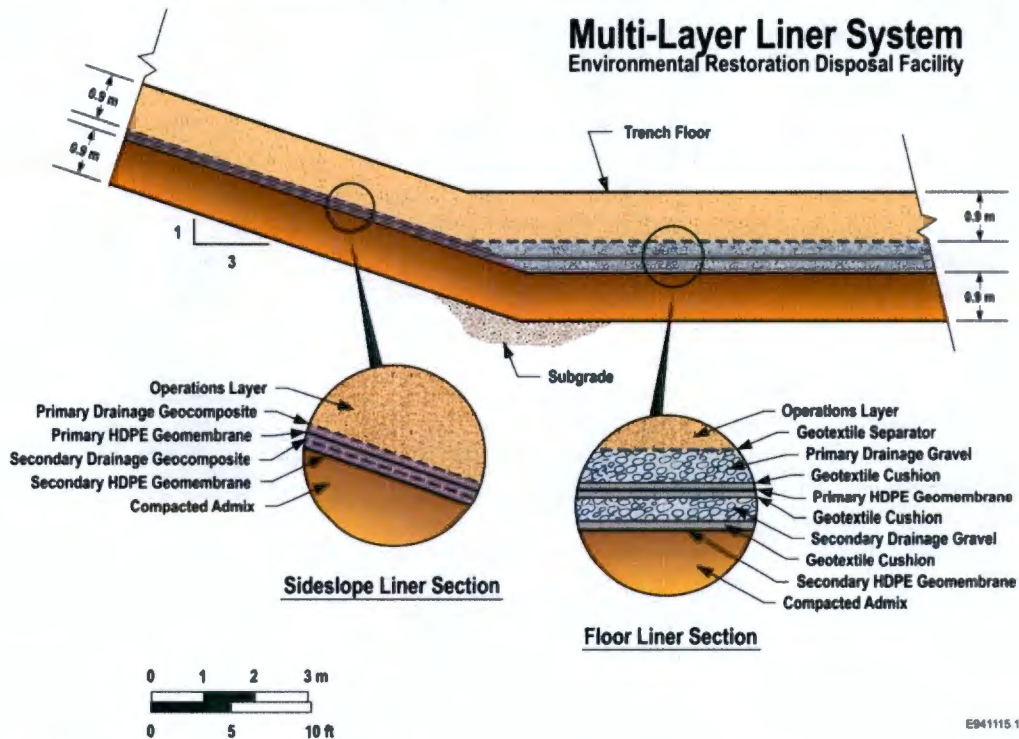


Figure 2-30. Schematic Showing ERDF Sideslope and Floor Liners.



The ERDF floor liner comprises 10 layers: (1) a 0.9-m (3-ft) operations layer (sandy loam/silty sand) having a saturated hydraulic conductivity of 7.2×10^{-4} cm/s, (2) a geotextile separator, (3) a primary gravel drainage layer with a designed 2.24% drainage slope and an estimated saturated hydraulic conductivity of 5×10^{-2} cm/s (WCH 2009), (4) a geotextile cushion, (5) a primary 60-mil HDPE geomembrane liner, (6) a geotextile cushion, (7) a secondary gravel drainage layer with a designed 2.24% drainage slope and an estimated saturated hydraulic

conductivity of 5×10^{-2} cm/s (WCH 2009), (8) a geotextile cushion, (9) a secondary 60-mil HDPE geomembrane liner, and (10) a 0.9-m (3-ft)-thick compacted admix layer with a minimum saturated hydraulic conductivity of 1×10^{-7} cm/s (WCH 2009).

The ERDF side slope and floor is lined with the double composite (i.e., primary geomembrane and secondary geomembrane) liner system for leak detection and to minimize the percolation of liquids into the subsurface. The primary liner is designed to keep leachate from leaking into the underlying primary leak detection recovery system. The secondary liner provides a means of identifying a leak from the primary system and provides an enhanced absorptive capacity for contaminants. The composite liner system thus provides an added protection from leaks. The lower liner at the composite will mitigate leaks from the upper layer, reducing flow through a hole or defect by keeping the hole or defect from becoming larger over time. For an added protection, below the secondary liner is the 0.9-m (3-ft)-thick compacted admix layer having a minimum saturated hydraulic conductivity of 1×10^{-7} cm/s (WCH 2009).

In general, as Figure 2-30 illustrates, the ERDF cells were constructed with a double-liner system for the purpose of collecting liquids, or leachate, that may travel through the waste materials stored at the disposal site. These liquids are typically generated from natural precipitation and the application of dust control water that percolates downward through the disposed waste materials and collects on the surface of the lining material. The primary (upper) and secondary (lower) liners each are designed to deliver leachate to sump areas. Sumps for the upper liners are independent from the sumps associated with the lower liners. The upper and lower sumps at each of the cells are routinely evacuated, and the leachate is stored in holding tanks prior to transfer to the Effluent Treatment Facility (WCH-399). The sump design used for cells 1 through 8 consist of two sump collection areas located at the north and south ends of the cell (Figure 2-27). This design was, in part, a function of the need to meet engineering parameters associated with the landfill's design and the ERDF ROD. One significant engineering parameter is that the design of the ERDF and, in general all engineered landfills, is based on the principle that the transfer of leachate should occur in an unconfined manner. To travel in an unconfined manner means that the leachate is to travel above the primary liner system of HDPE through a leachate collection system, without constraints (e.g., pressure from material above it). Typically, to achieve this, the leachate collection system is composed of conventional construction materials, such as sands or gravel aggregates. By allowing the liquid to travel through the drainage media in an unconfined manner, the liner's ability to transfer leachate through a liner system is reduced. The liner cross-section for cells 7 and 8 is presented in Figure 2-31.

Supercells 9 and 10 are designed to incorporate only a single sump. The purpose of moving toward a single sump design was to reduce the construction time involved in dual sump construction and reduce the required infrastructure for landfill expansion. Sump construction is typically one of the more challenging portions of landfill construction due to the steep slopes within a limited area. At the slope's crest for each sump is a crest pad building. The crest pad building is the term used for the buildings on the north and south ends of each 16,749-m² (16-ac) landfill portion. In the revised design, the south crest pad building was eliminated. These buildings contain the various mechanical and detection monitoring equipment necessary for the required environmental monitoring at the landfill. Figures 2-28 and 2-29 show the plan view and a cross-sectional view, respectively, of the single sump design. A more detailed cross section of the sump area can be found in Figure 2-32.

Figure 2-31. Cross-Sectional View of Liners for Cells 7 and 8.

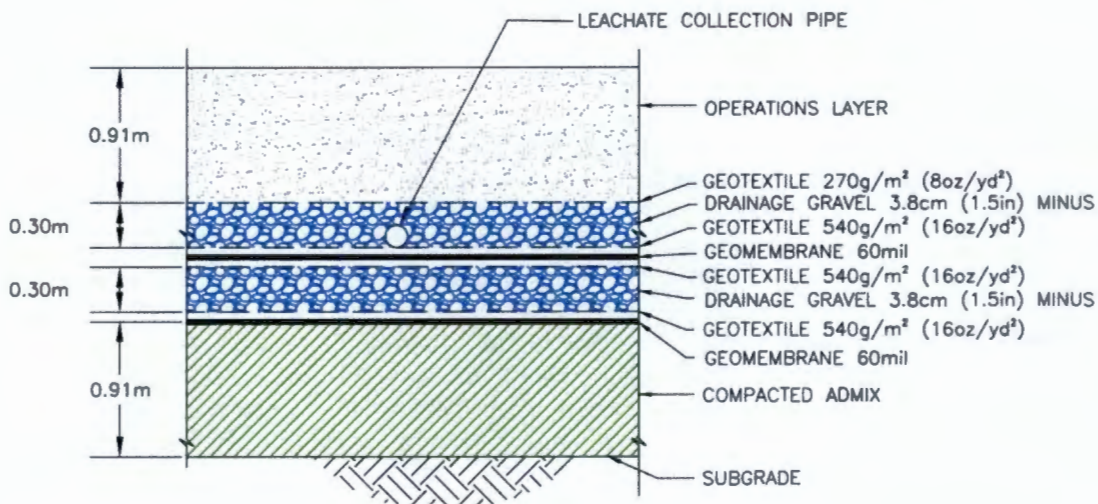
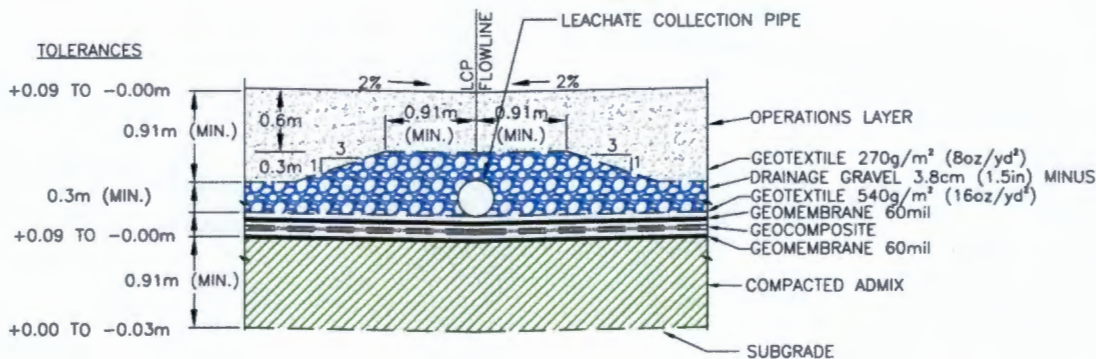


Figure 2-32. Detailed Cross-Sectional View of Super Cell Single Sump Area.



2.2.1.2 ERDF Surface Cover. The ERDF landfill will be closed by placing a modified RCRA-compliant closure cover over the waste as described by the ERDF ROD (EPA/ROD/R10-95/100). The surface cover does not currently exist but the cover will be designed to prevent direct exposure to the waste and include a vegetated surface layer of fine-grained soils to retain moisture and encourage evapotranspiration, thereby minimizing infiltration and vadose zone transport of contaminants to groundwater. The upper 50 cm (20 in.) of the soil cover system is composed of an admixture of silt and gravels. This layer is intended to both reduce infiltration through the cover and enhance the resistance of the cover to burrowing animals and long-term wind erosion. The RCRA-compliant cover generally consists of a layer of clay, geomembrane material, and sand and gravel. The RCRA-compliant cover will be modified by the addition of approximately 4.6 m (15 ft) of soil to provide shielding from radioactive material and to deter intrusion. It is anticipated that additional research into closure covers may result in site-specific enhancements to RCRA-compliant designs. Prior to cover construction, closure cover designs will be evaluated and the most appropriate closure cover design will be selected for construction. The design will, at a minimum, comply with applicable RCRA

requirements found at 40 CFR 264, Subpart N. Basalt from Hanford Site source areas will not be required for construction of the ERDF closure cover.

Figure 2-33 provides the schematic configuration of the surface barrier in relationship to the other engineered components, such as the double-liner system and the berm. The surface barrier tapers off on to the berm. Figure 2-34 provides a generic view of the modified RCRA-compliant design as well as types of materials for the surface barrier (DOE/RL-94-47, Rev. 1). This design configuration is used in building the fate and transport model.

For a degraded surface barrier, a range of potential recharge rates can be envisioned. PNNL-14744 investigated the possibility of the most likely natural failure mechanisms (i.e., bioturbation of the silt loam layer, wind erosion, and accretion of windblown sand). With appropriate design considerations, PNNL-14744 argue that the failure possibility of these natural systems is quite low, and the emplaced silt-loam soils will continue to perform for as long as they remain in place. Based on these arguments, PNNL-14744 concluded that the long-term effectiveness of the surface barrier would continue to limit recharge rates to less than 0.1 mm/yr for thousands of years.

Figure 2-33. Schematic of ERDF Closure Surface Barrier Configuration.

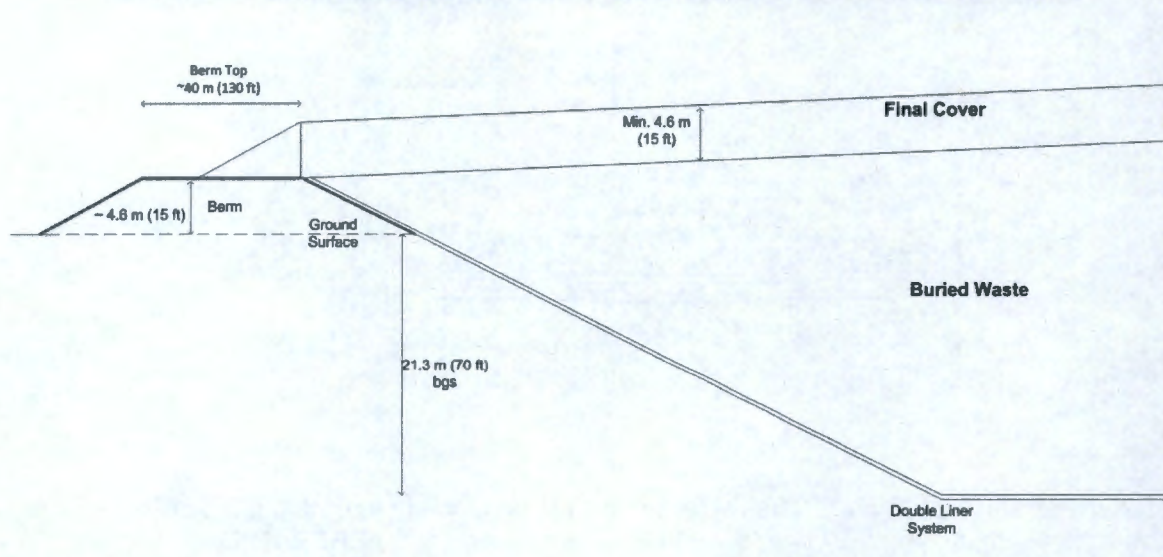
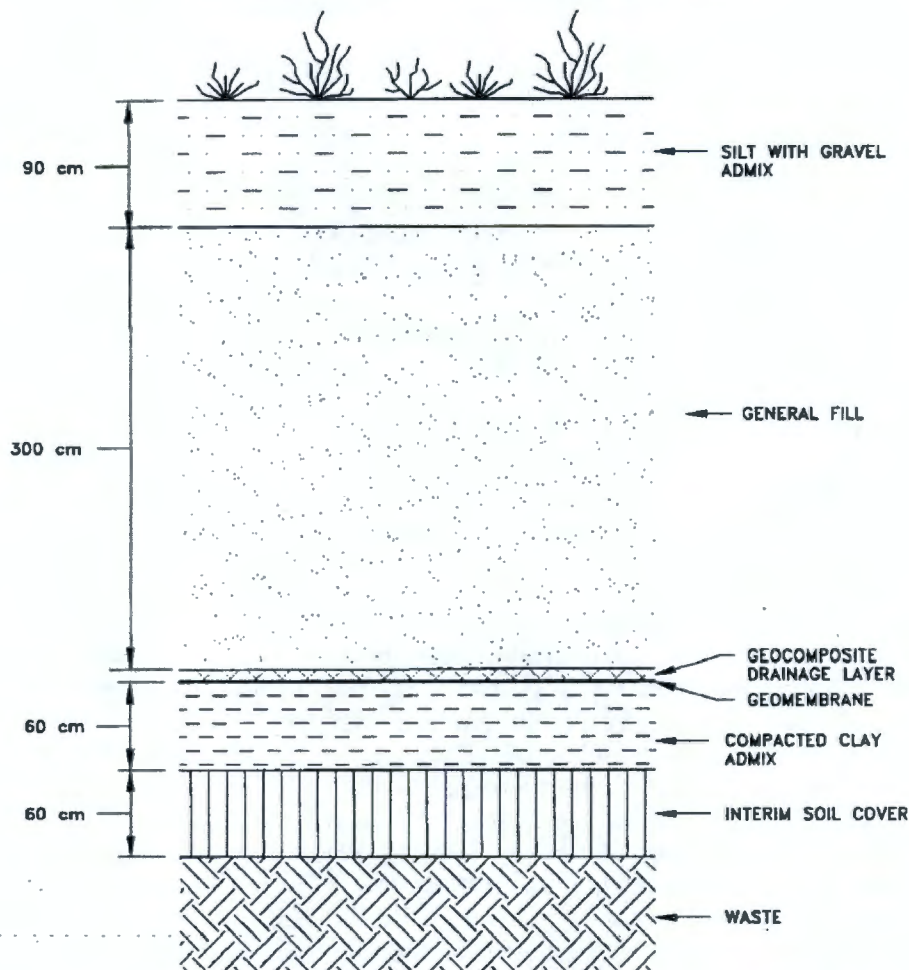


Figure 2-34. ERDF Generic Cover Design.



The modified RCRA-compliant closure cover being considered for ERDF will be designed to meet or exceed the regulatory requirements for applications at Category 1 and 3 LLW facilities. The cover design criteria are expected to be similar to that described in DOE/RL-93-33 for the Modified RCRA Subtitle C Barrier, which are summarized below:

- Minimize moisture infiltration through the cover.
- Design a multilayer cover of materials that are resistant to natural degradation processes.
- Design a durable cover that needs minimal maintenance during its design life.
- Design a cover with a functional life of 500 years.
- Prevent plants from accessing and mobilizing contamination (i.e., prevent root penetration into the waste zone).
- Prevent burrowing animals from accessing and mobilizing contamination.

- Ensure that the top of the waste is at least 5 m (16 ft) below final grade or include appropriate design provisions to limit inadvertent human intrusion.
- Facilitate drainage and minimize surface erosion by wind and water.
- Design the low-permeability layer of the cover to have a permeability less than or equal to any natural subsoils present.
- Design the cover to prevent the migration and accumulation of topsoil material within the lateral drainage layer (i.e., clogging of the lateral drainage layer).
- For frost protection, the lateral drainage layer and the low-permeability asphalt layer must be located at least 0.76 m (2.5 ft) below final grade.

2.2.2 Disposal Unit Cover Integrity

2.2.2.1 Erosion Protection. Water and wind erosion surface cover material can impact the integrity of a surface cover. The low precipitation, the low intensity of precipitation events, and the absence of surface run-on features at the Hanford Site all support the assumption that water erosion will not be a significant factor at ERDF. Wind erosion, however, has been observed at the Hanford Site, primarily in exposed sandy areas and in the sand dunes to the southeast of ERDF. The DOE (DOE/EIS-0222D) evaluated the potential for wind erosion for surface barriers. The DOE calculated that the worst-case potential erosion rate would be to lose 15 cm of silt loam in 500 years. The analysis method was derived for agricultural soils and did not consider the benefits of the pea gravel admix. Extensive wind tunnel studies performed at the Hanford Site show that a mixture of fine-grained soil and pea gravel significantly reduced erosion due to wind forces. Soil/pea gravel armoring can reduce erosion rates from 96.5% to more than 99% at wind speeds of 45, 56, and 67 mi/hr (PNL-8479, WHC-0673). With the lower reduction value (96%), the wind erosion potential would be 15 cm in 12,500 years. The experience at the Prototype Hanford Barrier (Wing and Gee 1994) suggests that wind erosion will be negligible within months after the barrier surface is vegetated (DOE/EIS-0222-F). Therefore, for all intents and purposes, wind erosion of the silt loam should be minor and is assumed to be so for the ERDF vegetated, closure surface barrier.

2.2.2.2 Subsidence Protection. The ERDF will contain contaminated bulk soil, debris (i.e., rubble, concrete, wood, drums, boxes, personal protective equipment [PPE], and metals), and treated waste that are generated at Hanford and meet the disposal requirements for ERDF. Total subsidence in the cover will be a cumulative of settlement amounts due to deformation in the landfill components listed below:

- Consolidation of the waste that is soil
- Consolidation of the waste due to degradation of waste debris
- Consolidation due to voids left in containerized waste
- Consolidation of the compacted clay liner and foundation soils
- Consolidation of the cover itself.

The consolidation estimates for different ERDF components are not available at this time. The majority of the waste in the landfill will be soil comprised of the sands and gravels found at the Site. The waste soils will be compacted to minimize settlement to meet the compaction acceptance criteria for ERDF detailed in WCH-178, *Environmental Restoration Disposal Facility*

Waste and Material Management Plan. The ratio of soil to debris is a minimum of one container of soil to one container of debris; however, large steel debris will require minimum of two containers of soil to one container of debris. Compaction with a landfill compactor and dozers will be performed on a daily basis. As mentioned in WCH-178, the compaction dozer shall have a ground pressure of at least 110 kPa (16 lb/in²) and a weight of at least 40,824 kg (90,000 lb). Each loose lift shall receive a minimum of five dozer passes. The dry density of material shall be a minimum of 90% of the maximum density.

As ERDF cells are being filled, care is taken to fill the voids. Since a large variety of waste types can be received and disposed, appropriate disposal methodologies are developed for different waste types. For example, concrete pieces will be broken into rubble and compacted to fill voids; drums will be crushed and compressed into the underlying soil layer to minimize voids; drums that should not be crushed due to nature of contents will be placed into structural vaults and grouted; miscellaneous debris such as glass, paper, pieces of metal, etc., will be combined with soil and placed in a manner to minimize voids; and waste wood that is received in significant quantities must be placed in a designed array following the principles established in WCH-382, *Washington Closure Hanford Evaluation of Wood Waste Settlement, ERDF Landfill, 200 West Area Hanford Site, Washington.*

The compaction of waste in the ERDF must be sufficient to ensure that settlement under the load of final landfill cap complies with the criteria of the conceptual cap design since the final cap has not been designed. WCH-273, *Washington Closure Hanford Report of Settlement Monitoring of ERDF Landfill*, describes the settlement monitoring tests that were conducted to determine the settlement behavior of waste emplaced within landfill from final closure loading. Results of the tests (of minimum 100 days duration) indicated that the expected combined immediate and long-term settlement of previously placed waste will be less than 15 cm (6 in.). The conceptual cap design assumed settlement within the waste matrix of about 0.64 m (2.1 ft) based on the load/deformation study prepared by the U.S. Army Corps of Engineers (1993). The estimated settlement is less than the settlement anticipated by the conceptual cap design, and therefore the conceptual cap design criteria will be met.

2.2.3 Structural Stability

The uppermost surface of the fill will be shaped to form a crown and will be covered with a nominal 0.6-m (2-ft)-thick layer of clean soil. Based on the settlement calculations and other design considerations (subsidence, erosion, and abrasion), a final grade of approximately 5% is chosen for the cover. This will ensure that a minimum slope is maintained even after any consolidation to promote surface water drainage off the cover system through its lifetime. The amount of consolidation or settling in the cover is expected to be very small as the granular nature of the matrix sands and gravels tend to make it ideal for bridging smaller voids through interlocking grains and preventing the formation of large voids. Another property of gravels conducive to limiting settlement is a relatively low-volume change resulting from densification. WCH (2011) calculation demonstrates that the underlying ERDF liner and leachate collection system will have sufficient strength to accommodate final cover of 5% slope and associated load from waste. A maximum differential settlement below the liner system was calculated to be approximately 5.3 cm (2.1 in.) for the supercell design, which is not expected to appreciably affect the liner system.

The landfill cover surface will be seeded and fertilized to promote plant growth. Vegetation will minimize erosion and accelerate removal of water from the water storage layer. Long-term considerations include periods of drought or fire so erosion and hydrologic modeling studies

have assumed a poor stand of vegetation. The vegetation will consist of local plant species based on vegetation studies performed for Hanford disturbed areas.

2.2.4 Inadvertent Intruder Barrier

To deter the inadvertent intrusion of humans into the waste, a marker system will be used to warn future generations of the dangers of the buried waste. Permanent markers that identify the potential exposure hazards will be installed at all corner boundaries of the landfill. The DOE is expected to maintain active control of the Hanford Site (using fences, patrols, alarms, and monitoring instruments). During the ERDF operational phase, it is expected that a woven mesh fence will be placed around the site to prevent animals and unauthorized persons from entering. If these measures should cease, other passive-type measures will warn the inadvertent intruder from waste buried beneath the permanent cover barrier. The measures may include recognizable warning markers and other physical features. Site information will be provided on an Internet website, U.S. Geological Survey maps, libraries, and other information repositories that would be readily available to the public. Land-use restrictions and institutional controls will be placed on the ERDF landfill and its adjacent buffer zone to permanently preclude development until unacceptable risk no longer remains at the site.

The ERDF landfill will clearly delineate the boundaries of the surface barrier by providing a distinct contrast with the surrounding terrain. The side slopes are engineered structures that will be obvious that the structure had been built by humans. These distinct side slopes in combination with warning signs are intended to minimize the risk of human intrusion.

As discussed above, the ERDF landfill cover also contains a biointrusion layer consisting of gravel. The function of this layer is to prevent small burrowing animals and rodents from penetrating the underlying cover components and the waste material. Barrier studies at Hanford have shown that a thin layer of gravel is effective in preventing animals and rodents from penetrating underlying waste materials (WHC-EP-0673). The biointrusion material will consist of gravel screened from the local available alluvium at the Hanford Site. The alluvium gravels at the Hanford Site are composed of granite, quartz, and other durable minerals that make it ideally suited for long-term applications.

2.3 WASTE CHARACTERISTICS

Since startup in July 1996, approximately 13.6 million metric tons of waste has been disposed at ERDF occupying approximately 6.5 million m³ of compacted volume (based on operational estimate of the compacted bulk density of 2,077 kg/m³). This waste has completely filled the first four ERDF cells, cells 5 through 8 are nearly filled, and supercell 9 started receiving waste in 2011.

The processes that generated Hanford Site remediation waste that can be disposed at ERDF, were the irradiation of uranium fuel in nine production reactors and chemical treatment of irradiated fuel to separate and purify plutonium and other important isotopes. These processes occurred during the Hanford operations period between the mid-1940s and mid-1980s, and caused a residual distribution of radionuclide inventory across many facilities and associated waste sites at Hanford.

The resulting waste sites and facilities are generally clustered in three geographic groups, the 100, 200, and 300/600 Areas. The 100 Area at the north end of the Hanford Site along the Columbia River contained the nine nuclear reactors that irradiated uranium fuel to produce plutonium. The 200 Area in the center of the Hanford Site on the Central Plateau contained the chemical processing facilities (T Plant, B Plant, U Plant, the Reduction-Oxidation [REDOX] facility, and the Plutonium/Uranium Extraction [PUREX] facility) used to extract plutonium and uranium from the irradiated fuel; tank farms to store separated fission product waste (e.g., cesium and strontium); facilities for purification, isolation, storage, and shipment of plutonium and uranium (231-Z, the Plutonium Finishing Plant and Uranium Trioxide Plant); cesium and strontium recovery, encapsulation, and storage facilities (B Plant and the Waste Encapsulation and Storage Facility [WESF]); storage of irradiated fuels (Canister Storage Building [CSB]); and support facilities (e.g., laboratories, evaporators). The 300/600 Areas contained facilities for fabricating fuel to be irradiated in the 100 Area reactors and support laboratories. At all three areas, numerous liquid waste discharge and solid waste facilities were developed.

Overall, facilities and waste discharge sites are the primary types of CERCLA sites being remediated along with some treatment of contamination plumes in groundwater underlying these areas. Waste materials typically disposed at ERDF include soils, facility rubble (e.g., concrete and wood), and metals (e.g., reactor parts). The ERDF is intended to continue operations until the remediation efforts are completed per the ERDF ROD. Because numerous CERCLA remediation decisions have not been finalized, a closure date has not been determined. However, at least another two decades of waste operation is expected.

Because some of the waste has already been disposed at ERDF while some is expected in the future, the inventory estimates are divided into two groups, namely, the current inventory and the currently forecasted inventory. The estimate of currently disposed and forecasted inventory is discussed separately. The ERDF is not permitted to receive offsite wastes.

Figures 2-35 through 2-44 provides charts that summarize the total amount (in curies or metric tons) of radionuclide generated during Hanford operations and their relative distribution among various waste sites and waste storage locations based on the mass balance information. These summary charts are only presented for the radionuclides that are deemed important contributors to the total dose. The pie chart in the upper right hand corner provides a relationship of the quantities by major source of a specific contaminant located at the Hanford Site as well as material shipped offsite. The pie chart in the lower right hand corner presents quantities of a specific radionuclide located at various sites that is a potential future source of waste for disposal at the ERDF. In this two subcategories are identified, one for the waste sites where some decision has been made for remediation and disposal to ERDF and other for the waste sites where no remediation decision has been made. The left hand side of the figure provides more details on the currently disposed inventory in ERDF along with major source (waste site) contributors. The type of waste form and associated radionuclide inventory currently disposed is also mentioned. For the majority of the radionuclides the inventory is associated with untreated waste (bulk soil).

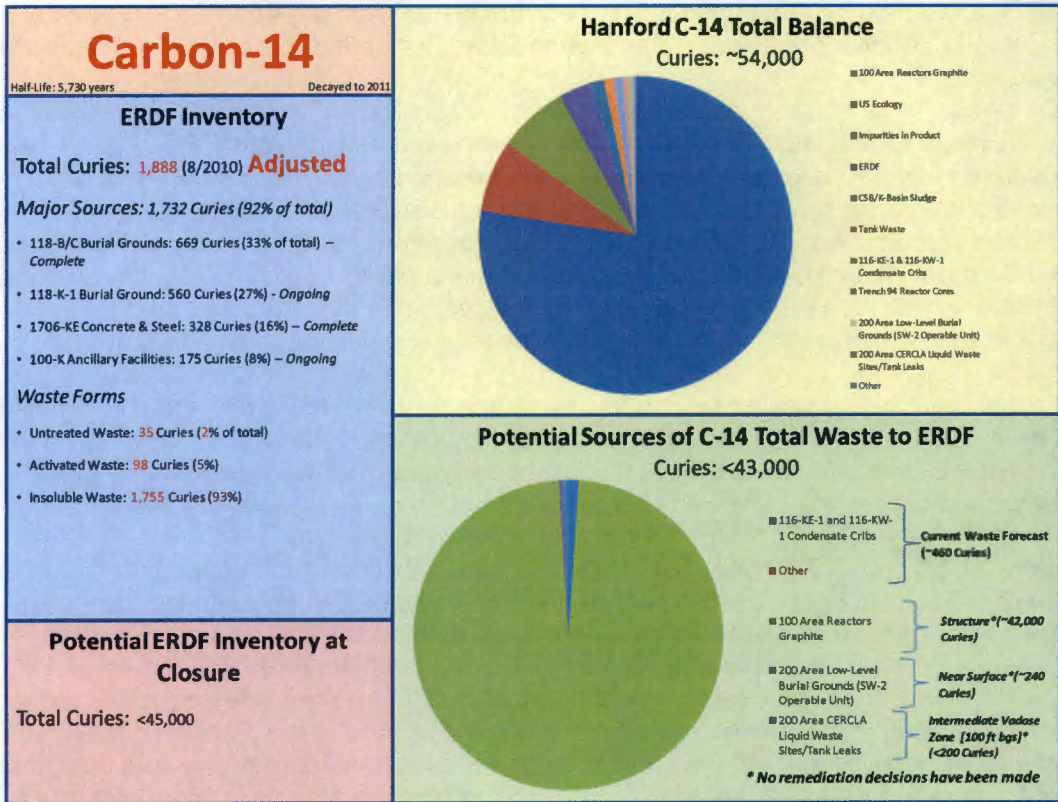


Figure 2-35. Carbon-14 Inventory Summary.

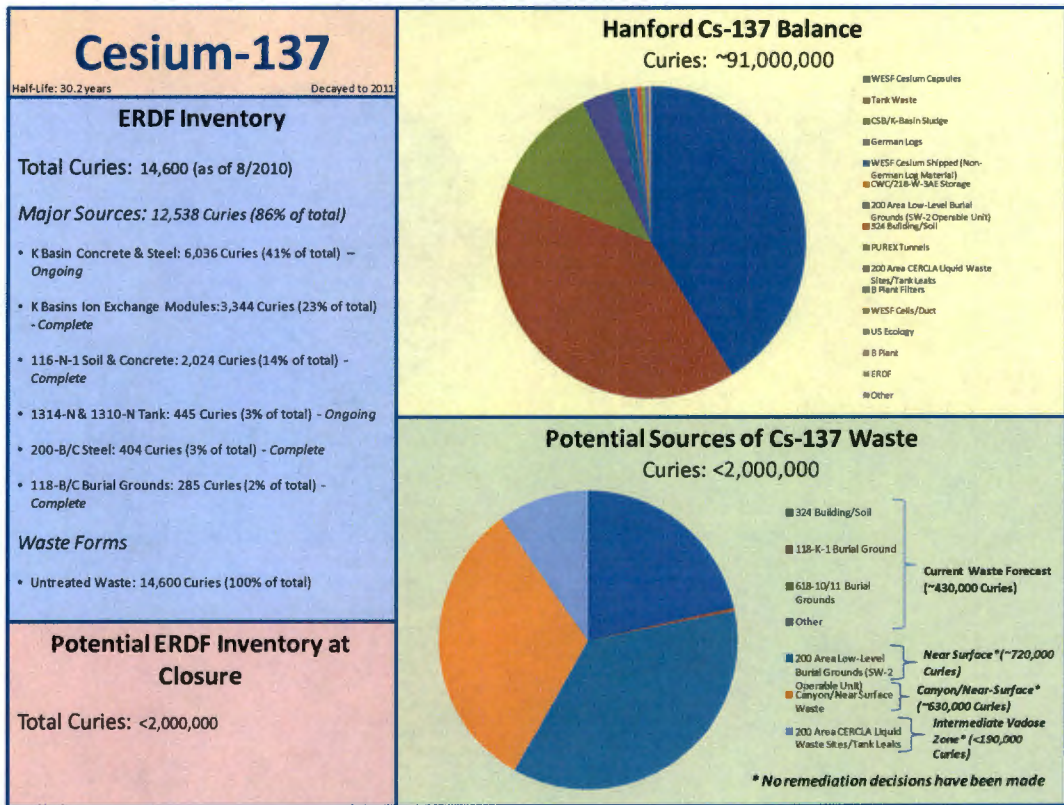


Figure 2-36. Cesium-137 Inventory Summary.

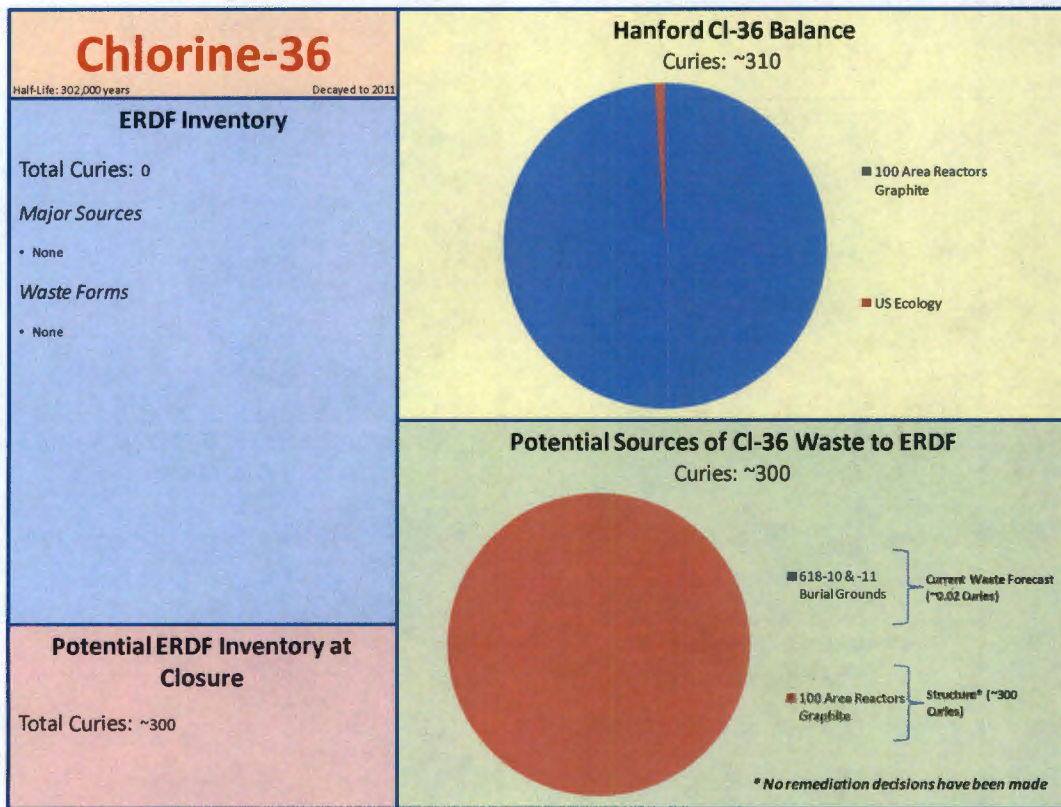


Figure 2-37. Chlorine-36 Inventory Summary.

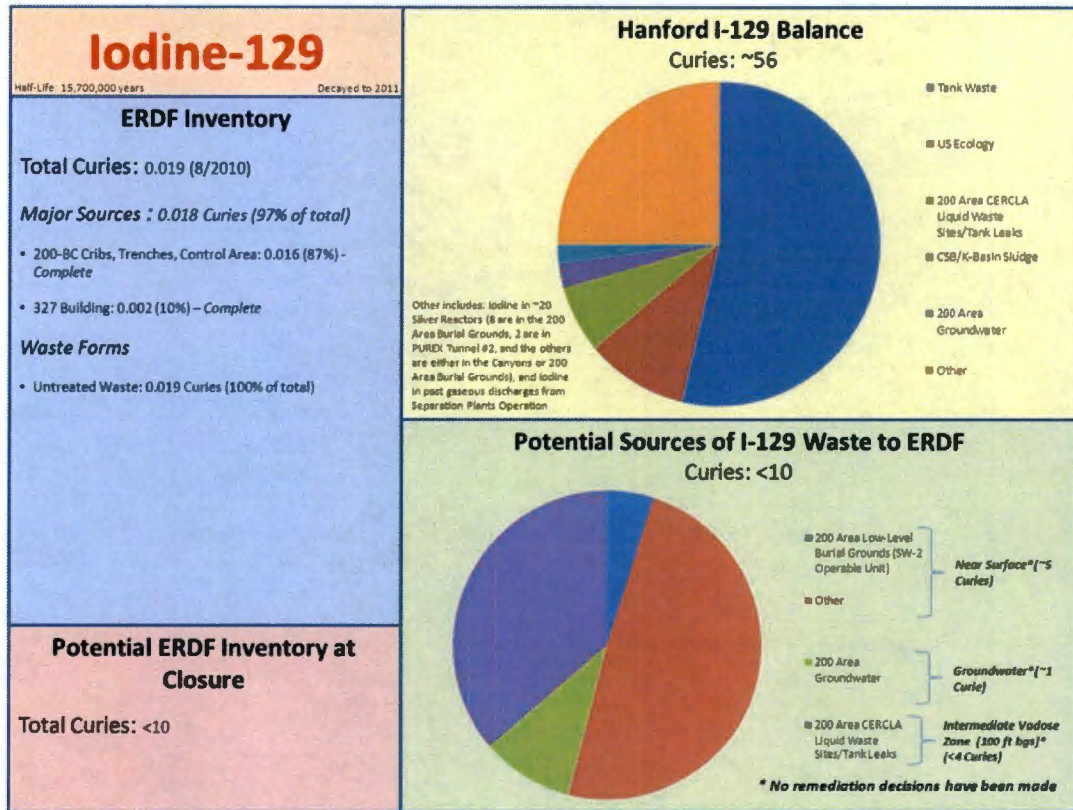


Figure 2-38. Iodine-129 Inventory Summary.

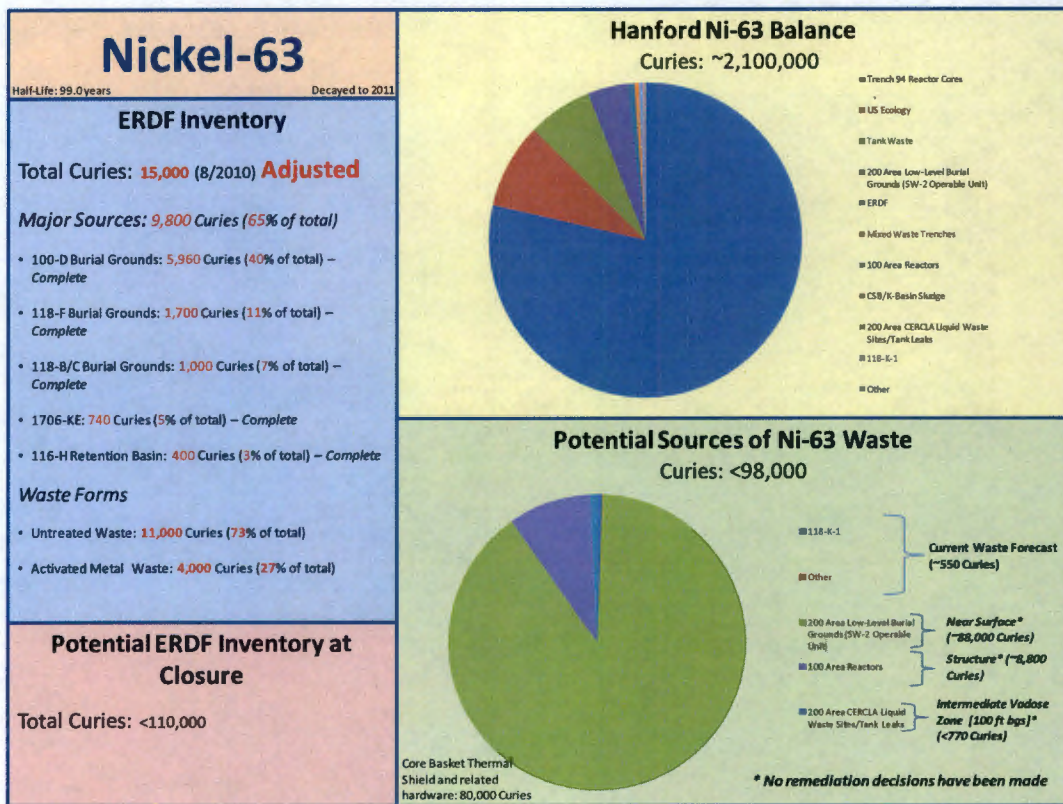


Figure 2-39. Nickel-63 Inventory Summary.

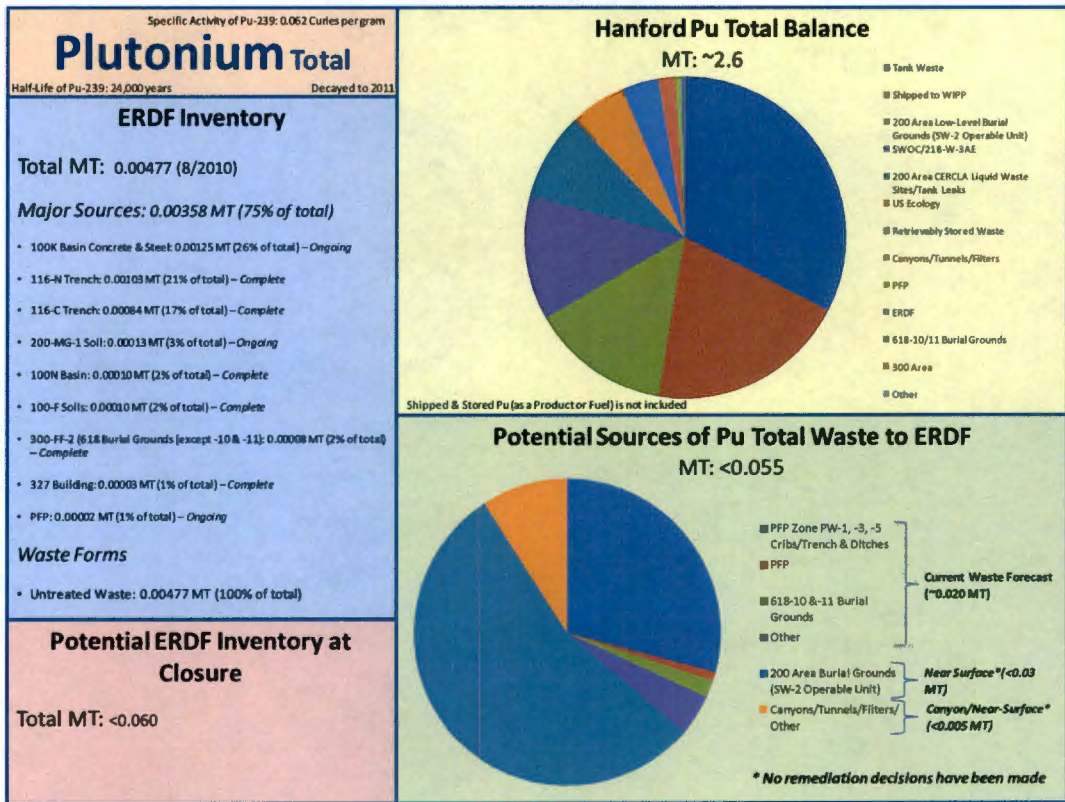


Figure 2-40. Plutonium Total Inventory Summary.

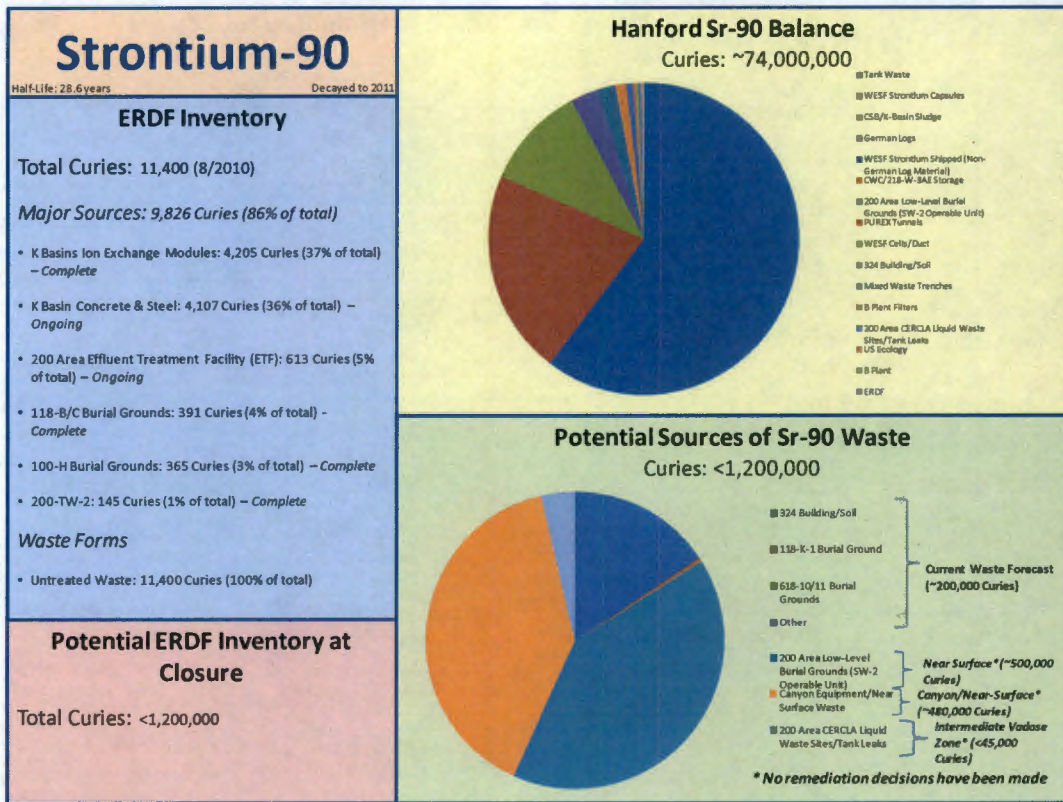


Figure 2-41. Strontium-90 Inventory Summary.

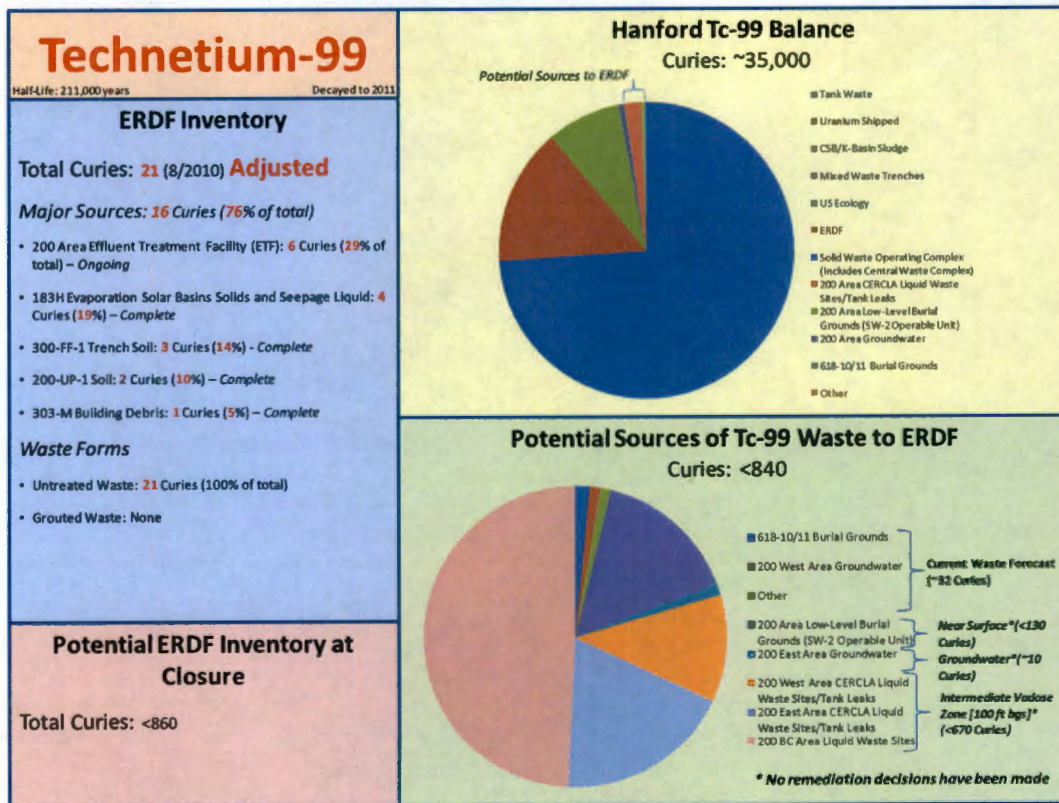


Figure 2-42. Technetium-99 Inventory Summary.

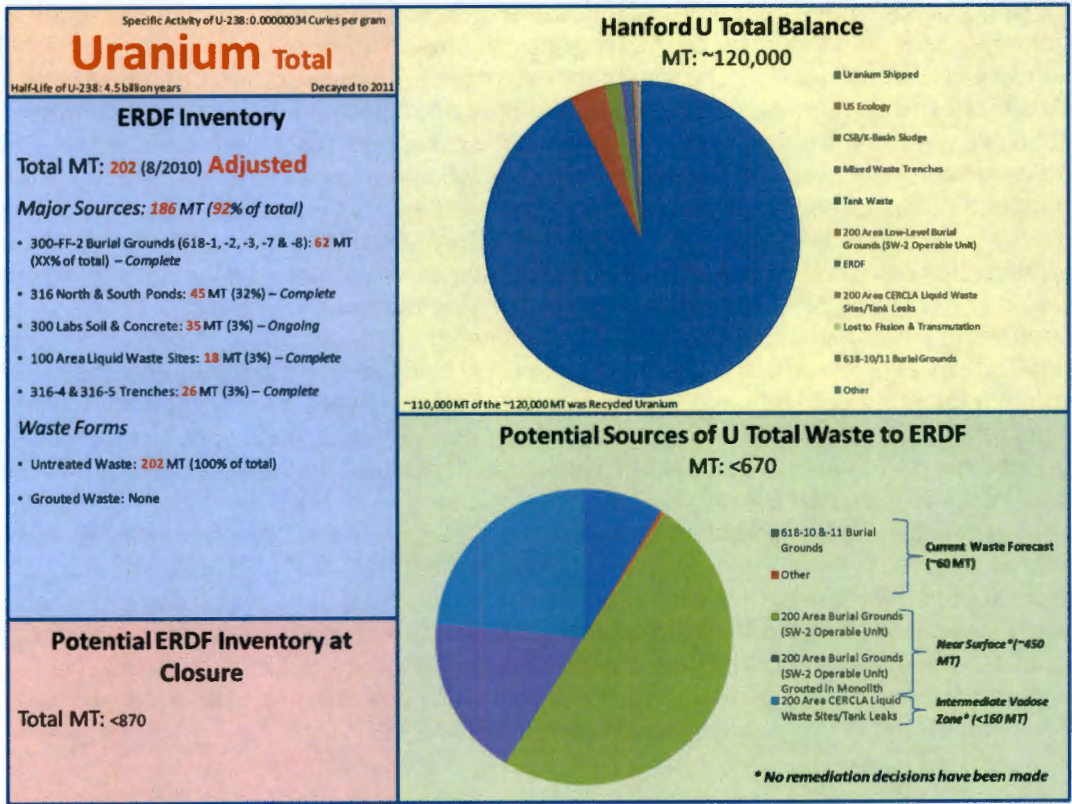


Figure 2-44. Uranium Total Inventory Summary.

2.3.1 Current ERDF Inventory

Quantitative estimates of specific radionuclide inventories (in curies or metric tons) are taken from an August 2010 ERDF WMIS summary. WMIS is an electronic database that stores inventory information that is estimated to be disposed at the ERDF. As further discussed in WCH-479, *Inventory Data Package for ERDF Waste Disposal*, a conservative or bounding bias is built into the inventory estimating process, generally resulting in larger than likely inventory estimates. To better understand this bias, additional reviews of waste sources were also conducted and alternative specific radionuclide estimates were developed where warranted. Field characterization data and historical records describing processes that generated these waste inventories provide the basis for these alternative estimates.

The radionuclides have been divided into three groups with inventory estimates listed in Tables 2-2, 2-3, and 2-4. The best estimates are presented here, although uncertainty in inventory is also estimated. The inventory estimates for those radionuclides that have been adjusted based on additional information and thus are different from information reported in WMIS are shown in **bolded text**. All radionuclide quantities have been decayed to year 2011, and an inventory of zero is assumed for all recorded inventories less than 10^{-6} Ci. The groupings reflect general differences in the expected inventory levels of radionuclides over the analysis time frame, approximately 1,000 to 10,000 years after closure. In the first group radionuclides have relatively long half-lives (greater than 6 years) and potentially non-negligible inventories at facility closure (greater than 1 Ci). Any radionuclides that are known to be important to PA analysis dose estimates are included in this group regardless of inventory (e.g., radium-226, which is the parent of radon-222 and iodine-129, a long-lived and mobile contaminant in the subsurface). Typically, more data are available that quantify inventory levels in this group compared to the other groups. The second two groups include radionuclides that are not expected to be present in large quantities at closure. In the second group radionuclides have half-lives less than 6 years and will have decayed to levels substantially below current levels at closure. Although not firmly established, facility closure is assumed to be year 2035 for analysis purposes. Given this closure date, approximately 5 half-lives will have happened for the longest half-life contaminant in this group, reducing expected inventories by more than an order of magnitude. In the third group, the radionuclide half-life is greater than 6 years and the expected inventory level is low (less than one curie) for one or more reasons. Typically, these radionuclides were not produced in large quantities by uranium fuel irradiation. Further discussion of ERDF inventories is presented in WCH-479.

Table 2-2. Best Estimate of Current ERDF Inventory for Radionuclides with Half-Lives Greater than 6 Years and/or Inventories Greater than 1 Ci (Decayed to 2011). (2 Pages)

Radionuclide	Waste Form	ERDF Inventory in Curies (Exceptions are in Metric Tons)
Silver-108m	Untreated	248
Americium-241	Untreated	545
Barium-133	Untreated	5.0
Carbon-14	Untreated	35
Carbon-14	Activated metal	98
Carbon-14	Insoluble	1755
Calcium-41	Untreated	0.3
Cadmium-113m	Untreated	3.0

Table 2-2. Best Estimate of Current ERDF Inventory for Radionuclides with Half-Lives Greater than 6 Years and/or Inventories Greater than 1 Ci (Decayed to 2011). (2 Pages)

Radionuclide	Waste Form	ERDF Inventory in Curies (Exceptions are in Metric Tons)
Chlorine-36	Untreated	0
Curium-244	Untreated	1.6
Cesium-137	Untreated	14,600
Europium-152	Untreated	4,840
Europium-154	Untreated	1,350
Tritium	Untreated	7,790
Iodine-129	Untreated	0.019
Potassium-40	Untreated	0
Molybdenum-93	Untreated	0.5
Niobium-93m	Untreated	4.8
Niobium-94	Untreated	0.2
Niobium-94	Activated metal	0.1
Nickel-59	Untreated	125
Nickel-59	Activated metal	65
Nickel-63	Untreated	10,600
Nickel-63	Activated metal	3,860
Neptunium-237	Untreated	0.4
Plutonium-238	Untreated	42
Plutonium-239	Untreated	260
Plutonium-240	Untreated	120
Plutonium-241	Untreated	5,100
Plutonium-242	Untreated	0.7
Plutonium total	Untreated	0.00477 MT
Radium-226	Untreated	0.9
Selenium-79	Untreated	0.1
Samarium-151	Untreated	259
Tin-121m	Untreated	17.0
Strontium-90	Untreated	11,400
Technetium-99	Untreated	21.0
Thorium-232	Untreated	1.1
Uranium-233	Untreated	14.6
Uranium-234	Untreated	13.5
Uranium-235	Untreated	7.6
Uranium-236	Untreated	0.4
Uranium-238	Untreated	67.5
Uranium Total	Untreated	202 MT
Zirconium-93	Untreated	16.0

NOTE: Adjusted inventories are shown in **bolded text**.
MT = metric tons

Table 2-3. Best Estimate of Current ERDF Inventory for Radionuclides with Half-Lives Less than 6 Years (Decayed to 2011).

Radionuclide	Waste Form	ERDF Inventory in Curies
Beryllium-7	Untreated	0
Cerium-144	Untreated	0.00006
Californium-252	Untreated	0
Cesium-134	Untreated	3.9
Cobalt-58	Untreated	0
Cobalt-60	Untreated	5,450
Curium-242	Untreated	0.0002
Europium-155	Untreated	120
Iron-55	Untreated	8.1
Iron-59	Untreated	0
Manganese-54	Untreated	0.001
Sodium-22	Untreated	0.000006
Promethium-147	Untreated	32.8
Radium-228	Untreated	0.2
Ruthenium-103	Untreated	0
Ruthenium-106	Untreated	0.001
Antimony-125	Untreated	14.8
Antimony-126	Untreated	0
Tin-113	Untreated	0
Thorium-228	Untreated	0.2
Thorium-234	Untreated	0
Zinc-65	Untreated	0.000001

Table 2-4. Best Estimate of Current ERDF Inventory for Radionuclides with Half-Lives Less than 6 Years and Current Inventories Less than 1 Ci (Decayed to 2011). (2 Pages)

Radionuclide	Waste Form	ERDF Inventory in Curies
Actinium-227	Untreated	0.000005
Americium-242m	Untreated	0.1
Americium-243	Untreated	0.6
Bismuth-207	Untreated	0
Californium-249	Untreated	0.0009
Cesium-135	Untreated	0.1
Curium-243	Untreated	0.1
Curium-245	Untreated	0
Curium-246	Untreated	0
Curium-247	Untreated	0
Curium-248	Untreated	0
Europium-150	Untreated	0.0002
Krypton-85	Untreated	0.4
Lead-210	Untreated	0.01

Table 2-4. Best Estimate of Current ERDF Inventory for Radionuclides with Half-Lives Less than 6 Years and Current Inventories Less than 1 Ci (Decayed to 2011). (2 Pages)

Radionuclide	Waste Form	ERDF Inventory in Curies
Proactinium-231	Untreated	0
Palladium-107	Untreated	0.02
Polonium-209	Untreated	0
Plutonium-244	Untreated	0
Rhenium-187	Untreated	0
Tin-126	Untreated	0.2
Titanium-44	Untreated	0.00002
Thorium-229	Untreated	0
Thorium-230	Untreated	0.02
Uranium-232	Untreated	0

2.3.2 Currently Forecasted ERDF Inventory

The currently forecasted waste inventories from waste sites where remediation decisions have been made or are expected are presented here. These sources have cleanup waste that is currently forecast to be complete from fiscal year (FY) 2011 through FY 2018, or is planned to be completed in the outyears. The radionuclides have been divided into three groups with inventory estimates listed in Tables 2-5 through 2-7, in a similar fashion as presented for the current inventory. The inventory estimates are not presented for waste sites where remediation decisions have not been made.

Waste remaining in the 100 Area are the reactor buildings and small-volume waste sites that include pipelines with associated soils, small solid waste sites, and building debris. The largest remaining solid waste site is the 118-K-1 Burial Ground, which was the main disposal facility for reactor waste in the 100-K Area. In the 300 Area, the remaining waste sites to be remediated are buildings that will provide debris. Two major solid waste sites, 618-10 and 618-11, remain and contain uranium metals, plutonium-contaminated metals, and research waste. The majority of the waste will be sent to ERDF for disposal from the waste sites located in the source operable units in the River Corridor.

Table 2-5. Best Estimate of Currently Forecasted Inventory of Radionuclides with Half-Lives Greater than 6 Years and/or Present Inventories Greater than 1 Ci for Disposal at ERDF (Decayed to 2011). (2 Pages)

Radionuclide	Currently Forecast Waste in Curies (Exceptions are in Metric Tons)
Silver-108m	0.8
Americium-241	330
Barium-133	0
Carbon-14	460
Calcium-41	0
Cadmium-113m	1.6

Table 2-5. Best Estimate of Currently Forecasted Inventory of Radionuclides with Half-Lives Greater than 6 Years and/or Present Inventories Greater than 1 Ci for Disposal at ERDF (Decayed to 2011). (2 Pages)

Radionuclide	Currently Forecast Waste in Curies (Exceptions are in Metric Tons)
Chlorine-36	0.02
Curium-244	28
Cesium-137	430,000
Europium-152	20
Europium-154	170
Tritium	23,000
Iodine-129	0
Potassium-40	0
Molybdenum-93	0.03
Niobium-93m	0.2
Niobium-94	0.08
Nickel-59	22
Nickel-63	550
Neptunium-237	0.03
Plutonium-238	50
Plutonium-239	1,200
Plutonium-240	300
Plutonium-241	800
Plutonium-242	0.02
Plutonium total	0.020 MT
Radium-226	0.8
Selenium-79	0.05
Samarium-151	62
Tin-121m	0.04
Strontium-90	200,000
Technetium-99	32
Thorium-232	0.2
Uranium-233	0.006
Uranium-234	4
Uranium-235	0.3
Uranium-236	0.1
Uranium-238	20
Uranium total	60 MT
Zirconium-93	2

MT = metric tons

Table 2-6. Best Estimate of Currently Forecasted Inventory of Radionuclides with Half-Lives Less than 6 Years for Disposal at ERDF (Decayed to 2011).

Radionuclide	Currently Forecast Waste in Curies (Exceptions are in Metric Tons)
Beryllium-7	0
Cerium-144	0
Californium-252	0
Cesium-134	4
Cobalt-58	0
Cobalt-60	30,000
Curium-242	0
Europium-155	72
Iron-55	18
Iron-59	0
Manganese-54	0.0001
Sodium-22	0
Promethium-147	62
Radium-228	0.2
Ruthenium-103	0
Ruthenium-106	0.01
Antimony-125	0.3
Antimony-126	0.01
Tin-113	0
Thorium-228	0.2
Thorium-234	20
Zinc-65	0

Table 2-7. Best Estimate of Currently Forecasted Inventory of Radionuclide with Half-Lives Greater than 6 Years and Current Inventories Less than 1 Ci (Decayed to 2011). (2 Pages)

Radionuclide	Currently Forecast Waste in Curies (Exceptions are in Metric Tons)
Actinium-227	0
Americium-242m	0.2
Americium-243	0.2
Bismuth-207	0
Californium-249	0
Cesium-135	0.03
Curium-243	0.8
Curium-245	0
Curium-246	0

Table 2-7. Best Estimate of Currently Forecasted Inventory of Radionuclide with Half-Lives Greater than 6 Years and Current Inventories Less than 1 Ci (Decayed to 2011). (2 Pages)

Radionuclide	Currently Forecast Waste in Curies (Exceptions are in Metric Tons)
Curium-247	0
Curium-248	0
Europium-150	0
Krypton-85	0
Proactinium-231	0
Lead-210	0
Palladium-107	0.009
Polonium-209	0
Plutonium-244	0
Radium-228	0.2
Rhenium-187	0
Tin-126	0.07
Titanium-44	0
Thorium-229	0
Thorium-230	0
Uranium-232	0

3.0 ANALYSIS OF PERFORMANCE

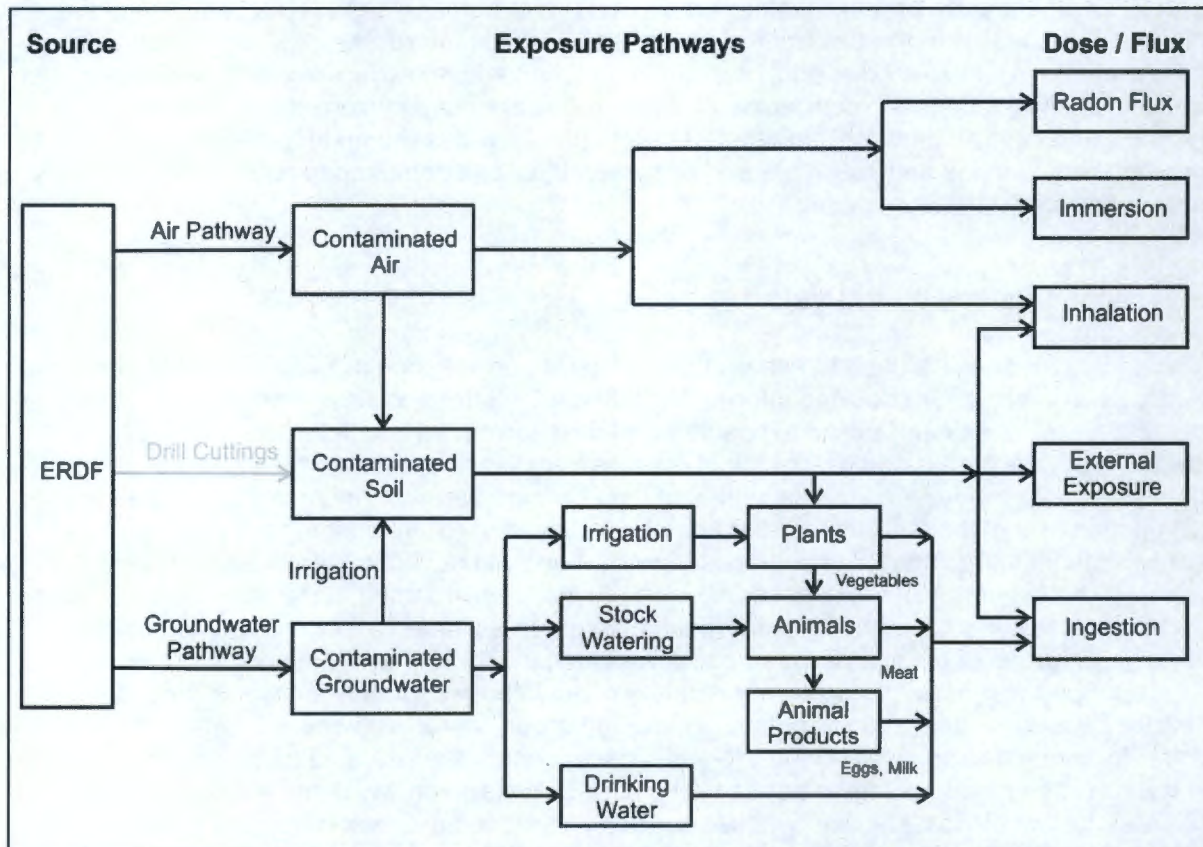
The ERDF PA provides an assessment of the long-term human health impacts following the closure of the facility in the Central Plateau portion of the Hanford Site. As part of that assessment, the postulated events (scenarios) that can lead to adverse human health impacts and the pathways by which contaminants within the final closed system can potentially reach humans in the future must be identified. This chapter provides the methodology developed to assess the scenarios and pathways and describes the approach used to estimate the impacts from the proposed closure action.

3.1 OVERVIEW OF ANALYSIS

The method of analysis used to assess the long-term performance of ERDF is briefly described in this section with more detailed information following in later sections. Performance is defined in terms of the onsite and offsite exposures and doses from radionuclides that may be inadvertently contacted and/or that might migrate from the disposal facility. Analysis of performance therefore requires estimates of the (1) source term of radionuclides in the facility, (2) release rate of these radionuclides from the facility, and (3) migration rates and concentrations of radionuclides released from the facility in environmental media (air, soil, water). The estimates of radionuclide concentrations in environmental media are then used to estimate doses to a hypothetical individual based on an assumed exposure scenario. The various pathways of possible exposure are illustrated in Figure 3-1. The most important exposure pathway for hydrologic transport is groundwater use for drinking water, irrigation, livestock watering, and biotic transport. Under the groundwater pathway, it is assumed that water from rain and snowfall enters the subsurface, contacts waste, and carries dissolved contaminants to the unconfined aquifer. The surface water pathway is not a possible exposure pathway for the disposal facility because surface water does not exist within the 100-m compliance distance from ERDF boundary. Atmospheric exposure scenarios are also limited because only a few radionuclides that can partition into the gas phase are present in the inventory. However, a conservative atmospheric pathway dose analysis is presented. Therefore, the main focus of this analysis of performance is on estimating the groundwater all-pathway dose to a hypothetical receptor that consumes contaminated groundwater, leafy vegetables and produce that were irrigated with contaminated groundwater, and milk and meat from animals that consume contaminated water and pasture grass irrigated with contaminated groundwater.

The strategy for the ERDF PA is to define and analyze both a compliance case and a suite of sensitivity and uncertainty cases. The compliance case is a deterministic calculation that includes the input values and assumptions that are most representative of the disposal system. The compliance case is developed using the best available information for the physical system and provides the "expected" estimate for how the system may perform given the information available. The approach used in the compliance case is not all inclusive; however, it does provide a reasonable estimate of the expected performance. Uncertainty and sensitivity cases were defined to explore the relative impact of uncertainties in the models and data (including assumptions) on the estimated health impacts. Uncertainty analyses are undertaken using an abstraction model so that a large number of analyses can be performed within a limited time.

Figure 3-1. Overview of the Dose Calculations for Exposure Along the Groundwater Pathway and Air Pathway for the ERDF Performance Assessment.



In an effort to establish credibility and confidence in the data, assumptions, and methods used in the analysis, the following aspects were recognized and addressed:

- Nearly all data, including those for contaminant inventory, geology, hydrology, and geochemistry, were based on site characterization, sampling, measurements, and supplemented by modeling.
- Field-scale processes that are characteristic of highly heterogeneous Hanford Site sediments (e.g., lateral flow and migration) were simulated in vadose zone flow and transport models.
- The groundwater pathway model-related studies were part of independent scientific and technical peer reviews (Appendix A).
- All computer codes used were benchmarked and verified.
- Sensitivity and uncertainty analyses were conducted to provide insight into the variability and robustness in the estimated impacts to selected assumptions and data choices made with respect to the calculations.

Results using the models and values are presented in Chapter 4.0 for the groundwater and air-pathway scenarios and in Chapter 5.0 for intruder scenarios. Chapter 6.0 also presents the comparison to performance objectives.

3.2 CONCEPTUAL MODEL OF FACILITY PERFORMANCE

The ERDF PA methodology uses conceptual models that are based on the physical system and expected contaminant migration pathways. Figure 3-2 provides a schematic representation of both the ERDF as it will exist at closure and the contaminant migration pathways evaluated in this PA. The ERDF is composed of manmade as well as natural components. The manmade components of the system that influence contaminant migration include a closure surface barrier, liner-leachate collection, the ERDF cells and infrastructure, and the distribution of waste in the subsurface. The natural components of the system that influence contaminant migration are a number of mostly horizontal stratigraphic layers within the vadose zone and an underlying stratigraphic layer that is part of the unconfined aquifer. Figure 3-3 illustrates the stratigraphy for the ERDF site that has a thick vadose zone and Cold Creek units that pinch out towards the east. The water table remains within the Ringold Formation Unit E with predominantly eastward flow.

Figure 3-2. Schematic Conceptual Representation of the ERDF Site and Various Pathways.

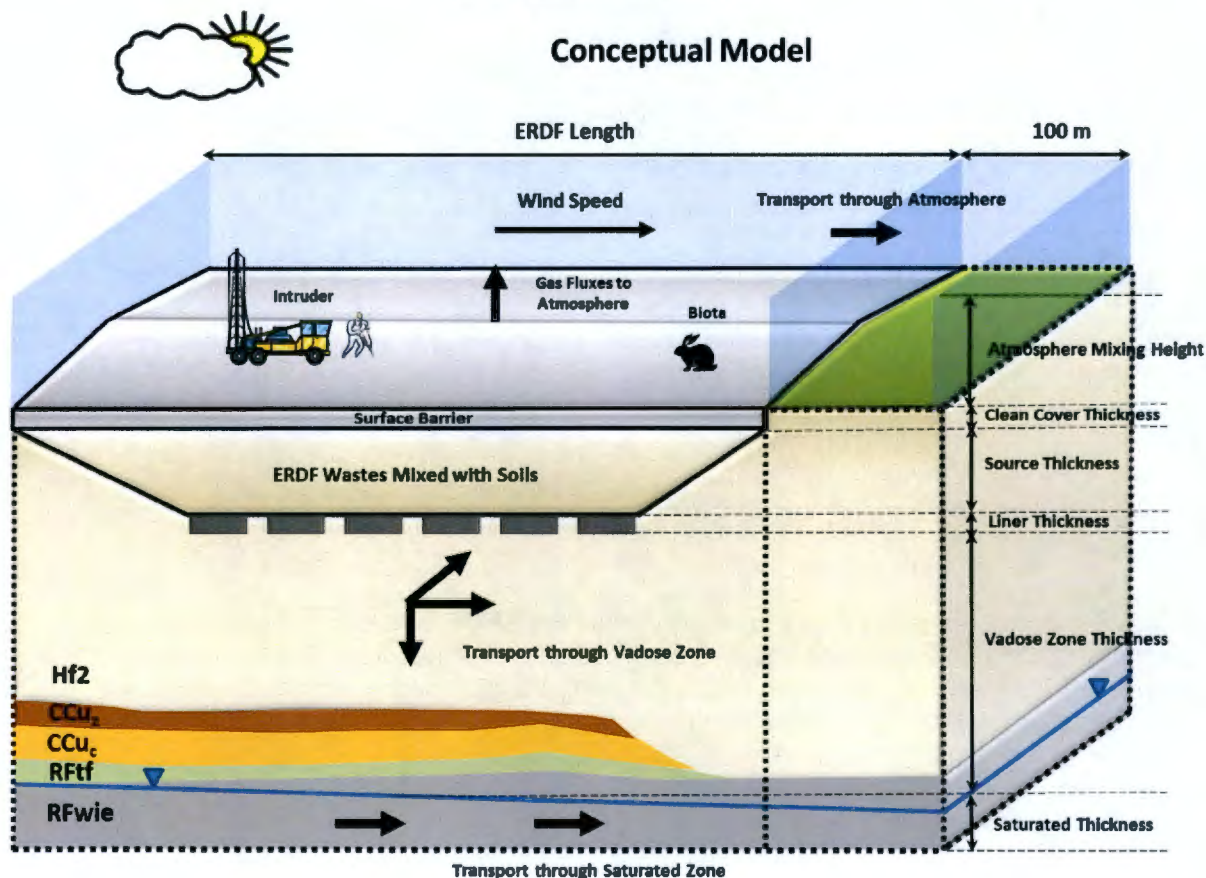


Figure 3-3. Conceptual Model of the ERDF Site Showing Stratigraphy.

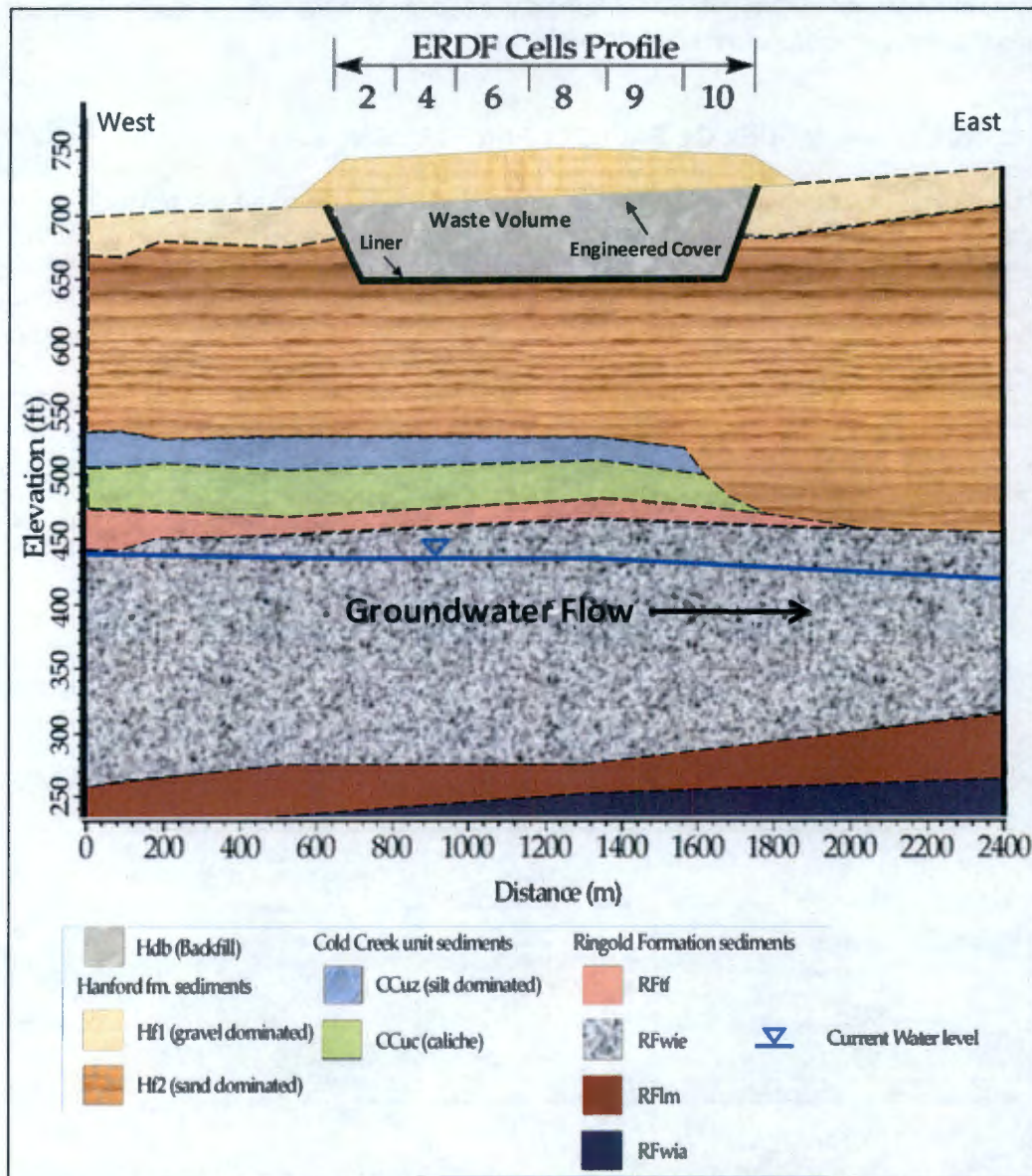
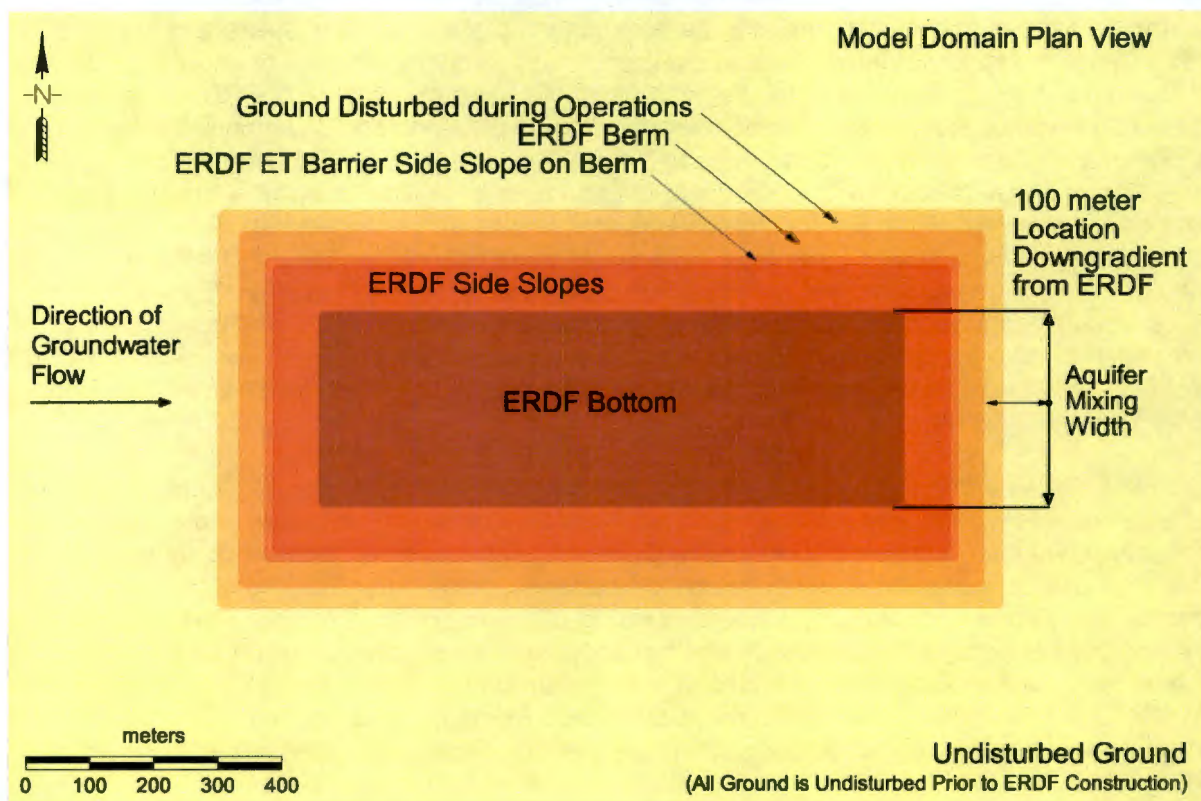


Figure 3-4 shows the plan view of the facility including ERDF side slopes, berm area, and surrounding disturbed and undisturbed area. Also shown is the location of the compliance boundary 100 m downgradient of ERDF berm, where a hypothetical well is assumed that supplies water for drinking and irrigation in the all-pathway dose scenario calculations.

Figure 3-4. Plan View of Three-Dimensional ERDF Model Domain Showing Surface Features and the Surrounding Area.



Several key features, events, and processes (FEPs) characterize conceptual models for release and transport of ERDF waste contaminants through the near-field environment. The relevant FEPs are discussed chronologically elsewhere (WCH-477, *Conceptual Models for Release and Transport of Environmental Restoration Disposal Facility Waste Contaminants through the Near Field Environment*) for a series of four time periods, including pre-operations and the initial ERDF construction, the ERDF operations, closure and monitored post-closure, and unmonitored post-closure. Specifically, from the perspective of FEPs, the time periods are as follows:

- Pre-operations and initial construction period (before 1996)
- Operations period (1996 to 2035)
- Closure and monitored post-closure period (2035 to 2135)
- Unmonitored post-closure period (2135 to 12135).

Overall, a 10,000-year post-closure period is considered in the ERDF PA. The FEPs identified (WCH-477) are compared against a general FEPs list adapted from international literature and developed for the Hanford Site and other radioactive waste disposal conditions (BHI-01573, *Groundwater/Vadose Zone Integration Project-The Application of FEP Methodology at the Hanford Site*; WMP-22922, *Prototype Hanford Features, Events, and Processes [HFEP] Graphical User Interface*).

Because the performance of a fully functioning engineered (manmade) component cannot be tested prior to it being built and monitored over a long period of time, an educated estimate of the lifetime of some of the engineered barriers to flow is considered along with the conceptualization of how and when the barriers might fail and how might they affect the recharge of meteoric water over time. To reduce the uncertainty from lack of knowledge on the failure times and mechanisms of failure, a conceptually stylized evolution of ERDF is considered that is purposely conservative, leading to early failure of the engineered components and, thereby, earlier transport of radionuclides to the natural system. Because the temporal evolution of ERDF is stylized, the timings for degradation and failure of barriers are fixed for the purpose of analysis. Four distinct time periods are considered from the point of view of flow and transport modeling and recharge rates: (1) a pre-operations time period (until 1996); (2) operations time period representing current conditions of disposal (1996-2035); (3) early post-closure time period representing intact surface barrier and intact geomembrane liner system followed by the end state of intact surface barrier but degraded geomembrane liner system; and (4) late post-closure time period representing degraded surface barrier conditions (in addition to the degraded liner system).

In the ERDF PA analysis, complete failure of the liner and surface barrier are assumed to occur at a given time. The recharge retaining capability of the double leachate liner is assumed to be fully degraded after 100 years from closure (coinciding with the time of loss of active institutional controls) and net infiltration is controlled by the surface barrier. After 500 years, the surface barrier is assumed to degrade resulting in doubling of the net infiltration rate. These assumptions appear to be conservative with respect to evaluating radionuclide transport through the vadose zone and consistent with those made in other analyses (e.g., in DOE/LX/07-0099&D2/R1, *Waste Disposal Alternatives Evaluation Remedial Investigation/Feasibility Study Work Plan at the Paducah Gaseous Diffusion Plant*, liner degradation is assumed to begin in 200 years).

Evaluation of prolonged liner performance with potential for water accumulation in ERDF is evaluated in Appendix D. Several water accumulation and release scenarios are evaluated including release by diffuse recharge or point source leaks from ERDF, once the liner is degraded. Results of the evaluation indicate that the effects would be negligible in terms of the transport of radionuclides through the vadose zone due to large water retention capacity within the vadose zone. Appendix D also presents water accumulation and retention data from the Hanford prototype barrier over a 15-year evaluation period. This data set derived at the field-scale indicates near zero infiltration through the top 2 m of the barrier thereby providing insight into the long-term recharge barrier capability that can be expected from a surface barrier emplaced at ERDF on closure. The effect of gradual surface barrier and liner degradation is also evaluated in Appendix D compared to the instantaneous degradation assumed for the compliance calculations. The base-case assumption of an instantaneous change in the recharge through the surface barrier upon its failure appears conservative, or negligibly different from the more gradual failure functions described in DOE/LX/07-0099&D2/R1, Appendix C (*Proposed Groundwater Modeling Methodology*). Appendix D also includes a comparison to the gradual failure functions evaluated in Appendix C of DOE/LX/07-0099&D2/R1 and indicates that the changes would be negligible.

Based on the conceptual models for different pathways, numerical models were developed to estimate the contaminant concentrations within water, air, or soil as a function of time for various scenarios discussed in Chapter 1.0. Functional numerical models cannot be devised to precisely calculate contaminant migration processes in a natural system; simplifying assumptions are required to approximate ubiquitous heterogeneities of the natural system.

Also, some aspects of future closure decisions that may affect contaminant migration estimates have not been finalized. Therefore, the numerical modeling approach must be sufficiently flexible to accommodate these uncertainties and to evaluate the effects of different closure decisions on contaminant migration estimates. Finally, contaminant concentration information is used to calculate estimated impacts with respect to the different exposure scenarios discussed in Chapter 1.0.

The groundwater pathway is expected to be the dominant pathway for transport of contaminants. For the groundwater pathway, it is conceptualized that the infiltration of moisture from precipitation eventually enters the facility, but most of the moisture is diverted around the ERDF during operations or around the surface barrier during closure. Following closure and once the double leachate liner fails, contaminants are released into the vadose zone by contact with recharge water. The infiltrating moisture, along with contaminants, travels through the vadose zone. The contaminants travel through the vadose zone until they reach the water table and the unconfined aquifer. In the final step of the model, the exposure scenario dose conversion factors are applied to the estimated groundwater concentrations at a 100-m downgradient location to determine total equivalent dose.

The ERDF PA vadose zone simulations are based on the equivalent porous medium (EPM) continuum modeling assumption. Such an assumption is supported by field data on moisture and contaminant plumes at various controlled and uncontrolled experiment sites as discussed in Appendix A. As discussed later in Section 3.4.1.6, we also consider and evaluate two types of alternative groundwater pathway conceptual models for the ERDF PA.

3.2.1 Source Term

The source term includes the inventory of radionuclides and processes associated with releases of radionuclides from the waste forms and containers into the natural environment. In this manner, the source term controls the rate at which radionuclides become available for transport through the groundwater and atmospheric pathways.

The inventory used in the source term model includes the currently disposed inventory (as of August 2010) and the forecasted inventory from FY 2011 to the closure time (year 2035) from waste sites where cleanup has been planned. The majority of the forecasted inventory is estimated from 100 Area reactor buildings (including pipelines with associated soil, solid waste, and building debris), remaining solid waste sites (such as the 118-K-1 Burial Ground), and the two solid waste sites in the 300 Area (618-10 and 618-11 Burial Grounds that contain uranium metals and research waste). A more detailed description of the waste sites from which inventory is estimated can be found in WCH-479, *Inventory Data Package for ERDF Waste Disposal*. Both the currently disposed and forecasted inventory is decay corrected until the assumed closure date of ERDF (year 2035) prior to implementation in the model. Uncertainty in the inventory estimate is also evaluated separately for the currently disposed and the forecasted inventory. The best estimate inventory of radionuclides is shown in Table 3-1.

Table 3-1. Best Estimate Inventory of Radionuclides at Closure for the ERDF Performance Assessment. (2 Pages)

Radionuclide ^a	Currently Disposed Activity (Ci) Decayed to 2035	Currently Forecast Activity (Ci) Decayed to 2035	Total Inventory (Ci) Decayed to 2035
^{108m} Ag	238.3	0.8	239.1
²⁴¹ Am	524	318	842
²⁴³ Am	0.6	0.2	0.8
¹⁴ C	1883	459	2341
^{113m} Cd	0.9	0.5	1.4
³⁶ Cl	0	0.02	0.02
²⁴³ Cm	0.06	0.46	0.52
²⁴⁴ Cm	0.6	11.2	11.8
⁶⁰ Co	236	1300	1536
¹³⁷ Cs	8416	247879	256295
¹⁵² Eu	1412	6	1417
¹⁵⁴ Eu	195	25	220
³ H	2014	5948	7962
¹²⁹ I	0.02	0	0.02
⁴⁰ K	0	0	0
⁹³ Mo	0.5	0.03	0.53
^{93m} Nb	1.71	0.07	1.78
⁹⁴ Nb	0.3	0.08	0.38
⁵⁹ Ni	190	110	300
⁶³ Ni	12223	465	12688
²³⁷ Np	0.4	0.03	0.43
²³⁸ Pu	35	41	76
²³⁹ Pu	260	1199	1459
²⁴⁰ Pu	120	299	419
²⁴¹ Pu	1606	252	1858
²⁴² Pu	0.7	0.02	0.72
²²⁶ Ra	0.9	0.8	1.7
⁷⁹ Se	0.1	0.05	0.15
¹⁵¹ Sm	215	52	267
^{121m} Sn	12.56	0.03	12.59
¹²⁶ Sn	0.2	0.07	0.27
⁹⁰ Sr	6372	111794	118166
⁹⁹ Tc	21	32	53
²³² Th	1.1	0.2	1.3
²³³ U	14.6	0.01	14.61
²³⁴ U	13.5	4	17.5

Table 3-1. Best Estimate Inventory of Radionuclides at Closure for the ERDF Performance Assessment. (2 Pages)

Radionuclide ^a	Currently Disposed Activity (Ci) Decayed to 2035	Currently Forecast Activity (Ci) Decayed to 2035	Total Inventory (Ci) Decayed to 2035
²³⁵ U	7.6	0.3	7.9
²³⁶ U	0.4	0.1	0.5
²³⁸ U	67.5	20	87.5
⁹³ Zr	16	2	18

^a Six additional radionuclides have been added during model implementation to allow ingrowth from decay of parent radionuclides. These are ²²⁷Ac, ²³¹Pa, ²³⁰Th, ²²⁹Th, ²²⁸Ra, and ²²²Rn.

The waste types received at ERDF include contaminated soil from the CERCLA waste site cleanup activities at the Hanford Site, debris generated from Hanford Site decontamination and decommissioning activities, and activated metal from solid waste burial grounds and other locations. Some waste emplaced at ERDF is grouted waste, but the fraction is very small and included as part of the untreated waste (contaminated soil) so that it is available for release when contacted with water. All waste material once received at ERDF is compacted at the time of disposal to minimize void space and potential subsidence in the future. For simplification, two categories of waste forms are considered (except for carbon-14), one associated with activated metal and the rest associated with untreated (bulk soil) waste. The inventory of carbon-14 associated with graphite blocks is considered separately as an insoluble waste form, and it constitutes the largest fraction of the total carbon-14 inventory.

The majority of activated metals comes from variety of waste types, such as steel and aluminum tubing, desiccant, zirconium cladding, lead cadmium poison pieces, and variety of scrap metal from past Hanford Site activities. The primary radionuclide contaminants of concern evaluated in activated metals are niobium-94, nickel-59, nickel-63, and carbon-14. For the purpose of waste form release calculations, the carbon-14 inventory from activated metals and the insoluble waste is combined and modeled using the graphite leach rates. For other radionuclides in the activated metals, a solubility control based on the solubility of iron oxy-hydroxide mineral is applied. This is because characterization information regarding the metal type, surface area, and dimensions is not well understood to apply the corrosion rates and fractional degradation rates.

The source term model predicts release of contaminants from waste buried in ERDF into the subsurface below the double liner. Input parameters include the radionuclide inventory associated with each waste form, recharge rates, leach rate for carbon-14, and solubility limits for the activated metals based on dissolution of iron oxy-hydroxide mineral phase.

3.2.2 Radionuclide Transport

Simplifications are used to model the actual process of radionuclide release for the solid and mixed wastes from ERDF. In the real system, radionuclides are distributed in a heterogeneous manner, and radionuclides would be released into solution at different rates because of the variability in waste material. Also, variable types and quantities of radionuclides are dissolved over time into the infiltrating moisture, depending on which waste material contacts a particular

fluid volume. To model the radionuclide release, averaging concepts are used to simplify the mathematical representation. The simplifications are, however, considered as being a conservative representation of the real system.

The following assumptions are made for the source-term release estimates.

- The radionuclide inventory is assumed to be homogeneously mixed in the entire volume of the ERDF.
- The release of contaminants is evaluated assuming that the recharge (infiltrating) water enters the facility, dissolves contaminants from the waste materials, and the release of contaminants occurs by infiltrating water migrating into and out of the facility. It is assumed that advection-dominated models describe release of contaminants from ERDF solid and mixed wastes. Radionuclides partition into a liquid and sorbed phase as described by the soil-water partitioning coefficient (K_d). The liquid phase is free-moving with the downward-moving infiltrating water, through the ERDF liner, and into the vadose zone. Diffusive transport is also modeled within the liquid phase and the gas phase to evaluate the transport of radionuclides in the air pathway and for radon flux calculation.
- For the untreated waste (contaminated soil), where majority of the inventory resides, it is assumed that the inventory will be immediately available for release and transport by advection and diffusion. No credit is taken for the grouted waste.
- Radionuclide releases from activated metal waste forms (niobium-94, nickel-59, nickel-63, and molybdenum-93) are modeled using the solubility of iron oxy-hydroxide mineral phase as these activated metals occur in trace quantities in the predominantly steel or aluminum matrix. Activated metal waste forms were assumed to be uniformly distributed throughout the ERDF disposal cell.
- Carbon-14 present in graphite (insoluble waste form) and activated metal is released based on the first-order fractional leach rates.
- Unit quantities are assumed in the modeling calculations for the untreated waste. Because dose estimates are directly proportional to initial inventory, the modeling runs with unit quantities can be scaled to calculate dose for any initial inventory values.

3.2.3 Exposure Pathways and Scenarios

The conceptual model for exposure pathways and scenarios includes several potential means for an exposure to occur. A summary of the exposure pathways is illustrated in Figure 3-1 for the all-pathway dose analysis. Exposure scenarios are the link between contaminated environmental media and the exposure of a hypothetical receptor. A receptor is assumed to reside 100 m downgradient from the ERDF boundary (taken to be the edge of the berm) at the end of institutional control. Details regarding the development of exposure scenarios are presented in the supporting data package WCH-478, *Exposure and Inadvertent Scenarios for the Environmental Restoration Disposal Facility*.

The important exposure pathway for hydrologic transport includes groundwater use for drinking water, irrigation, livestock watering, and biotic transport. The groundwater all-pathway scenario assumes a receptor consumes the following: (1) contaminated groundwater, (2) leafy vegetables and produce that were irrigated with contaminated groundwater, and (3) milk and

meat from animals that consume contaminated water and pasture grass irrigated with contaminated groundwater. Exposure from inhalation and ingestion of contaminated soil along with any external exposure to radiation is also considered. For evaluation of groundwater resource impacts, the receptor is assumed to consume 2 L of water per day for 365 days/yr.

Atmospheric transport of volatile radionuclides from ERDF is the only potential dose contributor through the air pathway. Based on the projected land use for ERDF and the assumption that the 5-m-thick closure cover precludes biotic intrusion of buried waste, nonvolatile radionuclides were not assessed. The air-pathway exposures include direct inhalation, air immersion, and external exposure from redeposition of contaminants on the land surface.

Groundwater resources impacts are also evaluated through comparison of predicted groundwater radionuclide concentrations with MCLs to meet the requirements of 40 CFR 141, "National Primary Drinking Water Regulations."

3.3 SOURCE TERM

As of July 2013, approximately 13.6 million metric tons of waste has been disposed at ERDF. This represents approximately 6.5 million m³ of compacted volume (based on operational estimate of the compacted bulk density of 2,077 kg/m³). Waste materials typically disposed at ERDF include soils, facility rubble (e.g., concrete and wood), and metals (e.g., reactor parts). The ERDF is intended to continue operations until the remediation efforts are completed per the ROD approved in 1995 (EPA/ROD/R10-95/100). Another two decades of waste receipt is expected from CERCLA waste site remediation efforts across the Hanford Site. No offsite waste is permitted.

A WMIS database (WCH-138, *Waste Management Information System [WMIS] User Guide*) is used to track the disposed mass of waste and inventory by each waste shipment from the waste generators. The WMIS database uses a combination of barcode scanning, handheld computers, and a radiofrequency identification tag system to track each waste shipment. The August 2010 WMIS inventory was used as the basis of estimating the currently disposed quantities of specific radionuclides. The general processes and information used to develop and track inventory estimates are provided in WCH-479, *Inventory Data Package for ERDF Waste Disposal*. To address the accuracy of the WMIS inventory, inventory estimates for specific radionuclides at specific waste sites were generated from pre-remediation waste site data (e.g., field data and historical records). These estimates were then compared with the WMIS information. Where warranted, adjustments to the current ERDF inventory were provided and the best estimate of the current inventory input for the PA analysis was developed. The rationale for these adjustments is provided in WCH-479.

Future waste inventory estimates are made for specific radionuclides using a three-step calculation that ultimately provides a bounding estimate of waste for potential disposal at ERDF. First, the total radionuclide-specific inventories generated on the Hanford Site for abundant or known environmental contaminants are estimated from historical documents, ongoing databases, and knowledge of Hanford Site operations (WCH-479, Section 3.0). The primary data in this step are Hanford Site production records that quantify the amount of fuel irradiated and fission products produced.

Second, waste inventories associated with each major waste management process at the Hanford Site area is estimated from the individual waste management process documentation.

In this exercise, the gross distributions of specific radionuclide inventories across the Hanford Site are recreated as fuel processing and waste generation evolve. For example, the largest fraction of the initial inventory is stored in underground tanks in the 200 Area. Tank wastes are solids and sludges generated by fuel dissolution and processing to extract plutonium and uranium. These wastes will be vitrified and disposed in the Integrated Disposal Facility or sent offsite to a high-level waste repository. Other wastes include cesium and strontium capsules that contain a portion of the initial tank waste and irradiated fuel elements that were not processed and are stored in the Canister Storage Building in the 200 Area. Inventories associated with these processes will not be going to the ERDF. By summing these inventories and comparing the sum with the total site estimate derived in step one, an "order of magnitude," or better estimate of inventory that is available for disposal at the ERDF can be calculated.

Third, and finally, the estimated available forecast inventory (from difference between step one and step two estimates) is broken down into two groups. The first group is the inventory present in waste from sites where well-established remediation decisions have been made or are imminent. Only this part of the forecast inventory has been considered in the ERDF PA. Some prominent waste sites include the following:

- 100 Area (i.e., 100-K)
- 200 Area (i.e., nontransuranic residual waste from the Plutonium Finishing Plant, contaminated soil from the 200-PW-1/3/6 liquid waste sites, liquid waste from the 200 Area Effluent Treatment Facility)
- 300 Area (e.g., 324 Facility waste and contaminated soils)
- 600 Area (solid waste in the 618-10 and 618-11 Burial Grounds).

The second group is the inventory in waste from sites where remediation decisions are not yet well established. These waste sites include the 100 Area (i.e., reactor cores) and 200 Area (i.e., solid waste in the 200-SW-2 Burial Grounds, residual waste in canyons and tunnels). Some quantity of waste will be generated by remediation of the 200 Area sites, but accurate projections of radionuclide inventories and waste volumes are highly uncertain because remediation decisions are not well formed. Consequently, these bounding estimates are not deemed reliable at this stage. The inventory in wastes for which no remediation decision has been made is therefore not considered in the ERDF PA.

In summary, the inventory estimates has been separated into the following two components:

- Currently disposed at the ERDF (as of August 2010)
- Currently forecast to be disposed at the ERDF (before its assumed closure in year 2035).

These two radionuclide inventory estimates are decay corrected to a common date corresponding to an assumed ERDF closure date of year 2035 and combined in order to develop the post-closure inventory for the PA calculations.

As a starting point, all radionuclides with half-lives greater than 6 years or inventories (currently disposed and forecast wastes decayed to 2011) greater than 1 Ci have been selected. Any radionuclides that are known to be important to PA analysis dose estimates are included in this

group regardless of inventory (e.g., radium-226, iodine-129). This list of radionuclides is further modified as follows:

- Six radionuclides are added to the list for which no current inventory is available but will in-grow from the decay of parent radionuclides. These are needed for the purpose of completing the decay chain and for calculating the dose. These are actinium-227, protactinium-231, thorium-230, thorium-229, radium-228, and radon-222. The currently disposed inventory is calculated from ingrowth due to radioactive decay of parent radionuclides over 25-year time period (year 2011 to 2035).
- Calcium-41 and barium-133 are excluded. Calcium-41 has a very low inventory (0.3 Ci decayed to 2011), is associated with impurities present in graphite and silica gel desiccant in trace quantities, and will not be available freely; and barium-133 will decay relatively quickly to a small activity due to its short half-life of 10.6 years (e.g., it will decay from 5 Ci in 2011 to 1 Ci in 2035 at assumed ERDF closure).
- Cobalt-60, tin-126, cesium-137, and americium-243 are included in the list of radionuclides for the ERDF PA due to relatively large initial inventory or because of decay to radionuclides that can impact the dose.

The final list of radionuclides of concern for the ERDF PA corresponds to 46 radionuclides. The inventory estimates for the currently disposed and forecasted waste are presented in Table 3-2 and have been decay corrected to a common date of year 2035 for PA calculations.

Table 3-2. ERDF Inventory for Specific Radionuclides (WCH-479). (2 Pages)

Number	Radionuclide	Currently Disposed Activity (Ci) Decayed to 2035 (WCH-479)	Currently forecast activity (Ci) decayed to 2035 (WCH-479)	Total Inventory (Ci) Decayed to 2035	Half-Life (yr) (Haynes and Lide 2011)
1	²²⁷ Ac ^a	0.0012	0	0.0012	2.18E+01
2	^{108m} Ag	238.3	0.8	239.1	4.18E+02
3	²⁴¹ Am	524	318	842	4.33E+02
4	²⁴³ Am	0.6	0.2	0.8	7.37E+03
5	¹⁴ C	1883	459	2341	5.72E+03
6	^{113m} Cd	0.9	0.5	1.4	1.41E+01
7	³⁶ Cl	0	0.02	0.02	3.01E+05
8	²⁴³ Cm	0.06	0.46	0.52	2.91E+01
9	²⁴⁴ Cm	0.6	11.2	11.8	1.81E+01
10	⁶⁰ Co	236	1300	1536	5.27E+00
11	¹³⁷ Cs	8416	247879	256295	3.02E+01
12	¹⁵² Eu	1412	6	1417	1.35E+01
13	¹⁵⁴ Eu	195	25	220	8.59E+00
14	³ H	2014	5948	7962	1.23E+01
15	¹²⁹ I	0.02	0	0.02	1.70E+07
16	⁴⁰ K	0	0	0	1.25E+09
17	⁹³ Mo	0.5	0.03	0.53	3.50E+03

Table 3-2. ERDF Inventory for Specific Radionuclides (WCH-479). (2 Pages)

Number	Radionuclide	Currently Disposed Activity (Ci) Decayed to 2035 (WCH-479)	Currently forecast activity (Ci) decayed to 2035 (WCH-479)	Total Inventory (Ci) Decayed to 2035	Half-Life (yr) (Haynes and Lide 2011)
18	^{93m} Nb	1.71	0.07	1.78	1.61E+01
19	⁹⁴ Nb	0.3	0.08	0.38	2.40E+04
20	⁵⁹ Ni	190	110	300	7.60E+04
21	⁶³ Ni	12223	465	12688	1.01E+02
22	²³⁷ Np	0.4	0.03	0.43	2.14E+06
23	²³¹ Pa ^a	0.004	0	0.004	3.25E+04
24	²³⁸ Pu	35	41	76	8.77E+01
25	²³⁹ Pu	260	1199	1459	2.41E+04
26	²⁴⁰ Pu	120	299	419	6.56E+03
27	²⁴¹ Pu	1606	252	1858	1.43E+01
28	²⁴² Pu	0.7	0.02	0.72	3.75E+05
29	²²⁶ Ra	0.9	0.8	1.7	1.60E+03
30	²²⁸ Ra ^a	1.04	0	1.04	5.76E+00
31	²²² Rn ^a	0	0	0	1.04E-02
32	⁷⁹ Se	0.1	0.05	0.15	3.30E+05
33	¹⁵¹ Sm	215	52	267	9.60E+01
34	^{121m} Sn	12.56	0.03	12.59	4.40E+01
35	¹²⁶ Sn	0.2	0.07	0.27	2.00E+05
36	⁹⁰ Sr	6372	111794	118166	2.89E+01
37	⁹⁹ Tc	21	32	53	2.13E+05
38	²²⁹ Th ^a	0.032	0	0.032	7.90E+03
39	²³⁰ Th ^a	0.0031	0	0.0031	7.56E+04
40	²³² Th	1.1	0.2	1.3	1.40E+10
41	²³³ U	14.6	0.01	14.61	1.59E+05
42	²³⁴ U	13.5	4	17.5	2.45E+05
43	²³⁵ U	7.6	0.3	7.9	7.03E+08
44	²³⁶ U	0.4	0.1	0.5	2.34E+07
45	²³⁸ U	67.5	20	87.5	4.47E+09
46	⁹³ Zr	16	2	18	1.50E+06

^a These radionuclides have been added during model implementation to track ingrowth from decay of parent radionuclides and for evaluating dose from progeny. Initial inventory is calculated from ingrowth due to decay of parent radionuclide.

The inventory of total uranium is estimated to be about 260 metric tons at the time of closure. The uncertainty is also estimated separately for the currently disposed and currently forecasted inventory.

Some of the key assumptions that were used in inventory estimation process are listed below:

- No transuranic waste will be disposed at ERDF.
- No offsite waste will be disposed at ERDF.
- No tank waste (high-level waste) will be disposed at ERDF.
- No spent fuel will be disposed at ERDF.
- The cesium and strontium capsules will not be disposed at ERDF.
- The German logs will not be disposed at ERDF.
- The 618-10 Burial Ground preliminary characterization data are representative (the final report has not been issued).
- Waste that will be disposed at ERDF from the 618-11 Burial Ground has the same radionuclide quantities as waste from the 618-10 Burial Ground (characterization of the 618-11 Burial Ground is not planned for a couple years).
- Technetium-99 in uranium shipped offsite was obtained by difference (total technetium-99 produced in the reactors minus technetium-99 in waste onsite [except US Ecology waste]) is representative. Note: The recorded technetium-99 in uranium shipped was much greater, but over 90% of Hanford Site uranium was recycled with technetium-99 already in it (only small technetium-99 was removed from uranium in the gaseous diffusion plants).
- An average of 0.25 Ci of iodine-129 per silver reactor is assumed.

Two categories of waste forms are considered at ERDF (except for carbon-14), one associated with untreated (bulk soil) waste and other as activated metal. The inventory of carbon-14 associated with graphite blocks is considered separately as insoluble waste form and it constitutes the largest fraction of the total carbon-14 inventory. The fraction of inventory associated with each waste form is estimated at the time of closure and is shown in Table 3-3.

For the untreated waste, where majority of the inventory resides, it is assumed that the inventory will be immediately available for release and transport by advection and diffusion when contacted with water. No credit is taken for the grouted waste.

The majority of activated metals come from variety of waste types, such as steel and aluminum tubing, desiccant, zirconium cladding, lead cadmium poison pieces, and a variety of scrap metal from past Hanford Site activities. The primary radionuclide contaminants of concern evaluated in activated metals are niobium-94, nickel-59, nickel-63, and carbon-14. Although molybdenum-93 is emplaced with untreated waste, it is most likely an activated metal and thus treated likewise in transport calculations.

Table 3-3. Fraction of Inventory by Waste Form Type. (2 Pages)

Radionuclide	Fraction Untreated (Bulk Soil)	Fraction Activated Metal	Fraction Insoluble Material
²²⁷ Ac	1	0	0
^{108m} Ag	1	0	0
²⁴¹ Am	1	0	0
²⁴³ Am	1	0	0
¹⁴ C (currently disposed)	0.02	0.05	0.93
¹⁴ C (currently forecasted)	0.07	0	0.93
^{113m} Cd	1	0	0
³⁶ Cl	1	0	0
²⁴³ Cm	1	0	0
²⁴⁴ Cm	1	0	0
⁶⁰ Co	1	0	0
¹³⁷ Cs	1	0	0
¹⁵² Eu	1	0	0
¹⁵⁴ Eu	1	0	0
³ H	1	0	0
¹²⁹ I	1	0	0
⁴⁰ K	1	0	0
⁹³ Mo ^a	1	0	0
^{93m} Nb	1	0	0
⁹⁴ Nb	0.67	0.33	0
⁵⁹ Ni	0.66	0.34	0
⁶³ Ni	0.73	0.27	0
²³⁷ Np	1	0	0
²³¹ Pa	1	0	0
²³⁸ Pu	1	0	0
²³⁹ Pu	1	0	0
²⁴⁰ Pu	1	0	0
²⁴¹ Pu	1	0	0
²⁴² Pu	1	0	0
²²⁶ Ra	1	0	0
²²⁸ Ra	1	0	0
²²² Rn	1	0	0
⁷⁹ Se	1	0	0
¹⁵¹ Sm	1	0	0
^{121m} Sn	1	0	0
¹²⁶ Sn	1	0	0
⁹⁰ Sr	1	0	0
⁹⁹ Tc	1	0	0
²²⁹ Th	1	0	0
²³⁰ Th	1	0	0
²³² Th	1	0	0
²³³ U	1	0	0

Table 3-3. Fraction of Inventory by Waste Form Type. (2 Pages)

Radionuclide	Fraction Untreated (Bulk Soil)	Fraction Activated Metal	Fraction Insoluble Material
²³⁴ U	1	0	0
²³⁵ U	1	0	0
²³⁶ U	1	0	0
²³⁸ U	1	0	0
⁹³ Zr	1	0	0

^a Inventory of molybdenum-93 is categorized in WMIS as untreated waste but is most likely an activated metal. For the purpose of modeling transport it is considered an activated metal.

WMIS = Waste Management Information System

For transport of activated metals, a solubility control based on the solubility limit of iron oxy-hydroxide mineral is applied. This is because characterization information regarding the metal type, surface area, and dimensions is not well understood to apply the corrosion rates and fractional degradation rates needed for waste form degradation and release of activated metals. It is expected that the majority of the activated metals are associated with steel components and are present as trace constituents. In order to bound the concentrations of these radionuclides, the solubility of hydrous ferric oxide (ferrihydrite) is applied by assuming congruent dissolution. A value of 10^{-6} mol/L is chosen over the pH range expected in the porewaters within ERDF (expected range from 6 to 9). Although other iron oxy-hydroxide mineral phases such as goethite and hematite may be thermodynamically favored under low-temperature conditions following the aging of iron oxides, using the solubility limit based on hydrous ferric oxide is conservative as it is over four orders of magnitude higher than goethite. This molar solubility limit is applied to niobium, nickel, and molybdenum (on an elemental basis).

A large inventory of uranium (about 260 metric tons) is forecasted to reside in ERDF from cleanup of waste sites (WCH-479, Appendix A). Based on available information from limited characterization studies, the uranium is precipitated in hexavalent valence state in the forms of silicate mineral phase (e.g., Na-boltwoodite, uranophane) and phosphates (metatorbernite). The mineral precipitates were found in restricted physical environments of sediments, suggesting specialized-formation conditions (PNNL-17031, *A Site-Wide Perspective on Uranium Geochemistry at the Hanford Site*). The dissolution of these uranium mineral phases under typical Hanford Site porewater and groundwater conditions leads to uranyl cation [UO_2^{2+}] that forms strong aqueous complexes with carbonate and hydroxide ions. Partial pressure of carbon dioxide in the subsurface plays an important role in determining the dissolution of uranium and degree of carbonate complexation with uranyl ion. Due to relatively little information on post-closure partial pressure of carbon dioxide expected within ERDF from degradation of various organic compounds and bacterial respiration considerable uncertainty exists on the solubility of uranium mineral phases. Elevated partial pressures of carbon dioxide can appreciably enhance the dissolution of uranium mineral phases and formation of uranyl-carbonate aqueous complexes. Due to uncertainty and variability in uranium solubility controlling mineral phase and the long-term partial pressure of carbon dioxide within ERDF, no solubility control is imposed on the uranium dissolution and its availability for transport. It is expected that due to moderate degree of sorption of uranium on the vadose zone sediments the breakthrough of uranium at the water table will not occur within the compliance and post-compliance time period, and thus the conservatism of imposing no mineral solubility control for uranium is defensible.

The primary source of carbon-14 in ERDF results from disposal of graphite and steel components irradiated in the 100 Area reactors (WCH-479). Various waste material types have been disposed at ERDF that contain carbon-14. These include the following:

- Graphite blocks in the reactors that housed the uranium fuel rods
- Dust/particles produced by the re-boring of the graphite cores
- Steel reactor parts containing trace amounts of carbon impurities that were activated during irradiation
- Desiccant used to remove moisture and other impurities from the reactor cover gas.

Table 3-3 provides the ratio of carbon-14 inventory for different waste forms based on WMIS records that are adjusted based on additional analyses (WCH-479). The majority of carbon-14 inventory (93%) is associated with insoluble waste (predominantly graphite blocks, chips, or powder), while a limited fraction is associated with activated metal (predominantly steel components) and untreated waste (bulk soil). The inventory associated with the untreated waste is derived from disposal of condensate waste streams or from miscellaneous wastes. It is likely that the graphite material is intermixed with soil and debris at ERDF.

For the purpose of modeling waste form degradation and release, the carbon-14 inventory from activated metals and the insoluble waste is combined and modeled using the graphite leach rates. A small fraction of carbon-14 associated with untreated waste (bulk soil) is considered to be available for transport when contacted with water.

Different graphite leachability studies have been published and are summarized in Table 3-4 based on information available in open literature. Among the studies cited in Table 3-4, only one (PNL-6769, *Leaching of ¹⁴C and ³⁶Cl from Hanford Reactor Graphite*) is focused on graphite samples originating from Hanford Site reactors. It provides Hanford Site-specific fractional leach rate estimates that are deemed the most reliable and representative of ERDF graphite waste leaching. The results are reported as fractional leach rates in units of 10⁻⁶/day.

Table 3-4. Published Long-Term Fractional Leach Rates of Carbon-14. (2 Pages)

Reference	Origin of Graphite	Type of Leachant	Leach Test Duration	Sample Type (Specific Surface Area, m ² /g)	Long-Term Fractional ¹⁴ C Leach Rate (10 ⁻⁶ d ⁻¹)
PNL-6769	Hanford Site (oxidized reactor core)	Deionized water at 20 °C	8 weeks	Block (5.2 m ² /g)	1.5
PNL-6769	Hanford Site (oxidized reactor core)	Deionized water at 50 °C	8 weeks	Block (5.2 m ² /g)	1.7
PNL-6769	Hanford Site (oxidized reactor core)	Deionized water at 90 °C	8 weeks	Block (5.2 m ² /g)	6.8

Table 3-4. Published Long-Term Fractional Leach Rates of Carbon-14. (2 Pages)

Reference	Origin of Graphite	Type of Leachant	Leach Test Duration	Sample Type (Specific Surface Area, m ² /g)	Long-Term Fractional ¹⁴ C Leach Rate (10 ⁻⁶ d ⁻¹)
PNL-6769	Hanford Site (oxidized reactor core)	Hanford Site groundwater at 20 °C	8 weeks	Block (5.2 m ² /g)	0.25
PNL-6769	Hanford Site (oxidized reactor core)	Hanford Site groundwater at 90 °C	8 weeks	Block (5.2 m ² /g)	2.4
PNL-6989	France	Deionized water at 20 °C	13 weeks	Block (0.3 m ² /g)	12 to 67
Takahashi et al. 2001	Japan	No information	102 weeks	Block (0.3 m ² /g)	0.01 to 0.09
CVP-2001-00002, App. D	Hanford Site (contaminated soil)	Deionized water	Quick centrifugation	Soil (not available)	No leaching observed

Static leach tests were performed on solid cylindrical samples of graphite prepared from a bar retrieved from a surplus Hanford Site production reactor (PNL-6769). The Hanford Site samples contained an average of 260 kBq/g of carbon-14. The dimensions of the specimens used in the experiment (3.05 cm long with 3.05-cm diameter) corresponded to a geometric surface area of 43.8 cm². However, the surface of the material in contact with water was much higher as water was able to penetrate pores and cracks of the samples that were entirely immersed during the tests. The BET method (i.e., Brunauer, Emmet, and Teller method), based on injecting nitrogen gas that penetrates all the nitrogen-accessible voids of the material, was used to determine the specific surface area of the samples. It was assumed that much of the BET surface area was accessible to water (even if H₂O molecules are bigger than nitrogen) so that this parameter was used in normalizing the leach rates obtained from the experiments. The method yielded an average specific surface area of 5.2 ± 0.2 m²/g. The BET-based surface area (190 m²) was 40,000 times greater than the geometric surface area (43.8 cm²). The oxidation of the graphite bar from which the samples were prepared was deemed responsible for this high BET area. It has been postulated that the ingress of air around the process tubes enriched the reactor atmosphere in nitrogen and resulted in fixation of nitrogen on the graphite surface, thus increasing the amount of carbon-14 within the graphite core (by nitrogen transmutation).

In the PNL-6769 leaching study, the leachates were entirely renewed and analyzed weekly in order to avoid saturating the solution with any of the leached constituents. Two types of leachates were tested: deionized water and Hanford Site groundwater, at temperatures of 20 °C to 90 °C for 8 weeks. Both leachants were first sparged with clean air to ensure air saturation. The objectives of this procedure were to investigate the leach rate temperature dependency, leachant dependency, and carbon-oxidation kinetics. The authors of PNL-6769 acknowledged that their estimations of the steady-state leach rates observed after 8 weeks could differ significantly from those that could be observed after several months or years, which are most likely lower. Differences between the carbon-14 leach rates in deionized water and

Hanford Site groundwater (Table 3-4) was postulated to be due to the initial bicarbonate content of the Hanford Site groundwater.

As no detailed information is available about the type of wastes (chips, block, or powder) disposed at ERDF and their specific surface areas, the carbon-14 fractional leach rate value of $1.5 \times 10^{-6} \text{ d}^{-1}$ obtained on block samples of Hanford Site graphite at 20 °C (PNL-6769) is used in the PA. This is a conservative estimate as the leach rate is expected to decline over time. To address uncertainty in this parameter a minimum value of $0.1 \times 10^{-6} \text{ d}^{-1}$ is considered that is calculated by rounding down the leaching rate of $0.25 \times 10^{-6} \text{ d}^{-1}$ determined using Hanford Site groundwater (PNL-6769).

3.4 ENVIRONMENTAL TRANSPORT OF RADIONUCLIDES

This section provides the method of analysis used for the transport of radionuclides for the groundwater and atmospheric pathways. The section also includes a discussion of the model selection and descriptions of the mathematical models.

3.4.1 Groundwater Transport Pathway

The groundwater pathway includes vertical transport through the thick vadose zone below ERDF to the water table and then laterally to a hypothetical well located 100 m downgradient. The vadose zone beneath ERDF can be viewed as a natural barrier. Once contaminants enter the vadose zone, the low recharge (infiltration rate) controlled by the surface cover, the thickness of the vadose zone between the facility bottom and the unconfined aquifer, and the soil-contaminant interaction prevent all but the least reactive contaminants from reaching the unconfined aquifer for thousands of years. Because the sensitivity-uncertainty analysis extends to 10,000 years, impacts to the performance of the vadose zone as a barrier caused by climate change are plausible. However, long-term climate studies indicate that for the last 10,000 years, precipitation ranged from 0% to 50% less than current levels, and from 75% to 128% of modern levels during the glacial period before the Holocene (PNNL-13033). The annual precipitation at the Hanford Site (6.98 in., 177 mm) is actually less than the lower end of the range usually associated with sagebrush-dominated ecosystems (200 to 500 mm/yr, U.S. Department of Agriculture, Natural Resources Conservation Service, Fact Sheets & Plant Guides, *Artemisia tridentata* ssp. *tridentata* http://plants.usda.gov/plantguide/pdf/pg_artrt.pdf). Thus, the sagebrush community appears capable of exploiting any increases in soil moisture caused by increases in the annual precipitation consistent with or even in excess of the previous glacial period. This indicates that climate change is not likely to affect the performance of the vadose zone as a barrier appreciably, and that the recharge rates applied to the design and post-design periods of the modeling are likely to remain unchanged even if the precipitation increases as a consequence of climate change.

This section provides an overview of major features that affect flow and transport within the vadose zone and saturated zone underlying ERDF. The transport of contaminants to the groundwater is a complicated process that depends on data and assumptions made for the following physical systems: (1) engineered features, and (2) the vadose zone beneath ERDF.

First, this section describes the disposal facility features important to the ERDF PA methodology. This is followed by a description of temporal evolution of ERDF and associated recharge rates, vadose zone stratigraphy, hydraulic properties, and geochemical effects that impact contaminant transport. Next, an overview is presented of the vadose zone flow and

transport numerical model used in the ERDF PA. Finally, a detailed justification is provided of important assumptions and simplifications of the vadose zone flow and transport model.

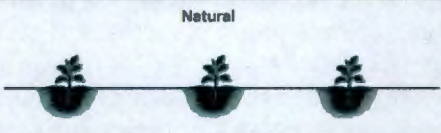
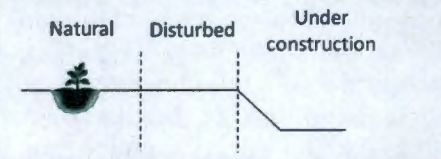
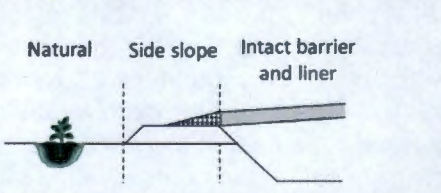
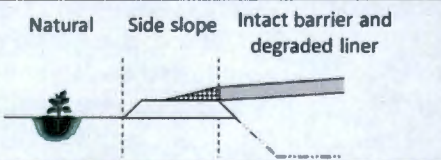
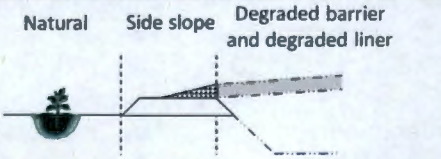
3.4.1.1 Disposal Facility Structures. Section 2.2.1 provides a description of the ERDF liner leachate collection systems and surface barrier. The physical system includes the closure barrier and the complex structures that make up the closed facility. The liner leachate collection systems keep the release of contaminants to a minimum. In addition, because of the built-in engineered capillary breaks, the closure barrier limits the flow of infiltrating moisture through the system. Moisture is one of the major transport mechanisms for moving contaminants from the closed system to the groundwater. Within the shallow subsurface of the ERDF trench, residual moisture fluxes are nonuniform, but low. In arid and semiarid regions with thick vadose zones, such as the Hanford Site, long-term factors such as climate change, changes in the annual precipitation rates, and changes in vegetation structure are required to influence the deep vertical water fluxes. In these regions large seasonal fluctuations in soil water potential are generally contained within the upper few meters of soil and the varying moisture fluxes even out within the deep subsurface above the water table. Simulation results representing the impact of a 20-year period of temporally varying precipitation on a surface barrier and a clean graveled surface indicate that the temporal variation in drainage can effectively be ignored and an average value can be used with little loss of accuracy (WHC-EP-0332, pp. 18-21, *Simulations of Infiltration of Meteoric Water and Contaminant Plume Movement in the Vadose Zone at Single-Shell Tank 241-T-106 at the Hanford Site*). Multiyear evaluations of soil moisture content data collected from vegetated desert soils throughout the United States indicate that water potentials remain very low and relatively invariant below depths of 2 to 5 m (Seyfried et al. 2005). In response to intermittent years of elevated precipitation, such as those caused by El Nino in the southwestern United States, the biomass usage of water by deep-rooted xeric vegetation increases, depleting the excess water, and no net increase in groundwater recharge occurs (Scanlon et al. 2006, Leary 1990). Net infiltration through the thick, heterogeneous vadose zone in the 200 Areas dampens the effect of discrete events; therefore, episodic precipitation events can be replaced by an average annual recharge rate.

For the conceptual model, the following simplifying assumptions were made:

- The impact of the closure barrier on moisture flow was approximated by an assumed recharge rate into the facility.
- The impact of the varying size and shapes of waste material within the disposal facility was ignored.
- Details associated with all waste material on moisture flow within the disposal facility were neglected.

3.4.1.2 Temporal Evolution of ERDF. With expected changes to the land cover over time due to growth of vegetation, several time periods have been conceptualized (Table 3-5) to represent the changes in recharge rates and hydrologic conditions at ERDF. Each of these time periods is characterized by a different recharge rate that will be discussed in Section 3.4.1.3.

Table 3-5. Timeline Considered for Representing the Evolution of ERDF.

Phase	Conditions	Duration	Conceptual Half Cross Section of the ERDF Area
Pre-operations	Before construction of ERDF	Until steady-state moisture conditions are achieved for the year.	
Operations	Current conditions	1996 to 2035	
Early Post-Closure	Transition to conditions of restricted recharge due to RCRA-compliant barrier and intact liner during the first 100 years of institutional control	2035 to 2135	
	Intact surface barrier and degraded liner after its assumed service life of 100 years	2135 to 2535	
Late Post-Closure	Degraded surface barrier conditions	Time needed to reach the groundwater table. At least 2535 to 3035 (possible extension to 12035)	

The hydrologic conditions prior to the facility construction (1996) control the initial moisture content and the matric potential in the vadose zone. To estimate the initial conditions, a pre-operations phase is considered, which will be used to produce initial moisture conditions for subsequent temporal changes conceptualized at ERDF. A vegetation cover representative of pre-ERDF construction is assumed over the whole domain during this period.

The operations period (current condition) is considered to represent the ERDF construction phase with a gradually extended liner over the ERDF area. This period starts in 1996 and is assumed to end in 2035 when a surface barrier is placed over the facility. A distinct recharge rate will be assigned to the following three different zones during this period:

- The undisturbed zone around the facility characterized by a vegetation cover representative of this area
- The disturbed zone around the facility, which has no vegetation cover
- The construction zone that corresponds to different cells under construction or equipped with a leachate collection liner but still not covered by vegetation.

At the end of the construction period, an early post-closure period is considered to represent the functioning of the RCRA-compliant barrier along with the underlying leachate collection liner. EPA/600/R-02/099, *Assessment and Recommendations for Improving the Performance of Waste Containment Systems*, states the life expectancy is likely to be about 160 years for a primary liner at 35 °C and greater than 600 years for a secondary geomembrane, provided the temperature is lower than 20 °C. According to the methodology suggested by the article "Long-Term Performance of Contaminant Barrier Systems" (Rowe 2005) to assess the long-term performance of contaminant barrier system, a 1.5-mm-thick HDPE liner has a life expectancy of 970 years for classical landfill conditions (aqueous anaerobic environment). The Proceedings from the Association of State Dam Safety Officials (Koerner and Husan 2003) report lifetime predictions of HDPE geomembranes at elevated field temperatures, which range from 109 years at 40 °C to 712 years at 20 °C. The longevity of a double HDPE geomembrane liner depends mainly on temperature and chemical aggressiveness of leachates (mainly driven by their oxygen content which controls HDPE oxidation). For the purpose of this PA, a conservative assumption is made about the life expectancy of the double liner. It is assumed that the double liner at ERDF will have a service life of 100 years corresponding to the institutional control period. This is a conservative assumption.

Because the expected design life of the RCRA-compliant surface barrier (500 years according to DOE/RL-93-33, *Focused Feasibility Study of Engineered Barriers for Waste Management Units in the 200 Areas*) is assumed to be longer than the double liner (100 years), the early post-closure period is split in the following two subperiods: (1) from year 2035 (assumed closure of ERDF) to year 2135 at the completion of the assumed 100-year service life of the double liner, and (2) from year 2135 to year 2535 to represent the end of the 500-year assumed life expectancy of the surface barrier.

For each of these two subperiods, a distinct recharge rate is assigned to three spatially distinct zones:

- The undisturbed zone, away from the surface barrier and the surrounding berm, characterized by a vegetation cover.
- The zone under the stabilizing side slopes of the surface barrier as it tapers on the berm (Table 3-5). The berm is built using silt derived from onsite soil and then 95% compacted. The recharge through this material is expected to be low.
- The zone beneath the extent of surface barrier that is designed to minimize infiltration of meteoric waters.

A late post-closure period is finally considered to represent the functioning of a degraded surface barrier with an underlying degraded liner. This period will start at the end of its assumed design life expectancy of the surface barrier (year 2535) and will continue through the rest of the simulated time period. A distinct recharge rate will be assigned to three different zones during this period:

- The undisturbed zone away from the barrier characterized by a vegetation cover representative of the area
- The side slopes of the barrier (compact silt)

- The degraded surface barrier fully covered with vegetation, which will have undergone soil and ecological processes.

3.4.1.3 Spatial and Temporal Recharge Rates at ERDF. Results from more than three decades of work are available on meteoric recharge estimates at the Hanford Site. Net infiltration (recharge) can vary greatly depending on factors such as climate, vegetation, surface condition, and soil texture. Studies conducted over the past two decades at the Hanford Site (Gee et al. 1992; PNNL-11367, *Hanford Prototype-Barrier Status Report: FY 1996*; Wing and Gee 1994; PNNL-10285, *Estimated Recharge Rates at the Hanford Site*; Fayer et al. 1996; PNNL-11463, *A Comprehensive Analysis of Contaminant Transport in the Vadose Zone Beneath Tank SX-109*; PNNL-13033) suggest that recharge rates can vary from less than 0.1 mm/yr (0.004 in./yr) on a variety of soil and vegetative combinations to greater than 130 mm/yr (5.1 in./yr) on bare basalt outcrops or bare, gravel-covered waste sites (Gee et al. 1992). Detailed experimental work has also been performed on net infiltration rates through surface barriers (PNNL-14744, *Recharge Data Package for the 2005 Integrated Disposal Facility Performance Assessment*).

Recharge is different than most other parameters because the values change in time and space and depend on certain assumptions about decisions made and conditions in the future. For the ERDF PA, the recharge rates can be divided into four distinct time periods (as noted above) representing different surface conditions consistent with the variable conditions expected for the facility as shown in Table 3-5. Further details on developing the recharge estimates are presented in WCH-515.

3.4.1.3.1 Recharge Estimates for Pre-Construction Condition (up to 1996). Recharge estimates for conditions prior to ERDF construction are based on correlations of soil types and infiltration characteristics of the native soils. Data supporting these recharge estimates for the 200 East and 200 West Areas soils are documented in PNNL-14725, *Geographic and Operational Site Parameters List (GOSPL) for the 2004 Composite Analysis*. Within the 200 East Area, recharge estimates range between 0.9 and 3.0 mm/yr for soils with established shrub-steppe vegetation. Similarly, within the 200 West Area, recharge estimates range between 3 and 4 mm/yr for soils with established shrub-steppe vegetation.

The compliance case ERDF infiltration rate representative of conditions prior to 1996 was assumed to be 1.7 mm/yr (0.067 in./yr). This was chosen based on Rupert sand as the predominant soil type with mature shrub-steppe vegetation cover. See WCH-515 for additional details.

3.4.1.3.2 Recharge During ERDF Operations (1996 to 2035). Three different recharge values are conceptualized during the ERDF operational period, which began in 1996 and is assumed to continue until 2035:

- The undisturbed zone characterized by a vegetative cover representative of the surrounding region
- The disturbed zone around the facility with no vegetative cover
- The region corresponding to different ERDF cells that are under construction or equipped with a leachate collection liner system but not covered by vegetation.

Undisturbed Region (1996 to 2035). As the undisturbed region is conceptualized to be under the influence of conditions similar to those observed (i.e., vegetated Rupert sand) prior to ERDF construction, the recharge estimate for the region will be same as the pre-operational period recharge. Therefore, for the ERDF undisturbed region, the compliance case infiltration rate for the period 1996 to 2035 was assumed to be 1.7 mm/yr (0.067 in./yr).

Disturbed Region (1996 to 2035). The ERDF disturbed region corresponds to disturbed Rupert sands without vegetation (i.e., bare soil). As indicated in Table 3-6, for Rupert sands, two recharge estimates are available in the literature corresponding to the case in which vegetation was removed and plants were prevented from reestablishing.

Table 3-6. Estimates of Recharge Rate Available for Rupert Sand Without Vegetation.

Recharge Estimate (mm/yr)	Method	Reference
44	Simulation estimate for the period 1957 to 1997	Reported by PNNL-14702 based on PNNL-13033
45	Simulation estimate for the period 1957 to 2006	PNNL-16688

In PNNL-16688, *Recharge Data Package for the Hanford Single-Shell Tank Waste Management Areas* (2007), the best estimate of 44 mm/yr given in PNNL-14702 was revised using a more extended weather record yielding a recharge estimate of 45 mm/yr (1.77 in./yr). Therefore, for the ERDF disturbed region, the compliance case infiltration rate for the period 1996 to 2035 was assumed to be 45 mm/yr (1.77 in./yr).

ERDF Region Under Construction (1996 to 2035). Because a double liner with leachate collection system is emplaced during the construction phase and gradually extended over the facility to collect any precipitation and dust-suppression water, the recharge rate estimate underneath the ERDF cells (construction area) is expected to be negligibly small. Water or recycled leachate is employed to minimize dust generation in ERDF during waste placement activities. For the compliance case, a recharge rate of zero is assumed for the ERDF area under construction for the period 1996 to 2035.

Since the pre-operational period is relatively short (only 39 years) in comparison to the simulation duration (at least 1,000 years and up to 10,000 years), this input parameter is not likely to have a significant impact on the ERDF PA flow and contaminant transport simulations.

3.4.1.3.3 Early Post-Closure and a Functioning Surface Barrier (2035 to 2535). Current plans are to use a modified RCRA-compliant closure cover for ERDF, which is expected to be at least 4.6 m (15 ft) thick. The current pre-conceptual design for the modified RCRA-compliant surface barrier is based on DOE/RL-94-47, Rev. 1, and includes cover vegetation, admixture of silt and gravels, geomembrane, and compacted clay admix over the grading fill layer (Figure 2-34). The silt with gravel admix layer provides for moisture storage and allows evapotranspiration to occur before deep percolation can occur. It also enhances the resistance to burrowing animals and wind erosion. The geomembrane and compacted clay admix layers impede moisture flow across their interfaces.

Extensive laboratory and modeling work and limited field testing of surface barriers have been performed; results are summarized in PNNL-14744 (2004). Lysimeter testing has been performed for different surface barrier concepts including a Modified RCRA Subtitle C Barrier with silt-loam layers having depths between 1 and 2 m. Lysimeter data from the prototype Hanford barrier (Wing and Gee 1994) have also been collected and analyzed. Finally, modeling has been performed to address potential climate change impacts and no vegetation impacts on surface barrier performance.

The lysimeter drainage data that have been collected since 1989 suggest that the recharge rate beneath surface barriers having at least 1 m of silt loam is zero under ambient precipitation conditions. Most of these lysimeters did not contain an asphalt layer. Simulation results reported in PNNL-14744 investigated the sensitivity of the lysimeter data to climate change, silt-loam hydraulic properties, vegetation changes, erosion, and dune formation above the surface barrier. Results indicated that the performance of these surface barriers was robust in that the estimated recharge rates remained below 0.1 mm/yr. For the cases investigated, only in the case of dune formation and no vegetation on the surface barrier were the simulated recharge rates above 0.1 mm/yr.

Based on a review of the results, PNNL-14744 recommend an expected recharge performance for a surface barrier with at least 1 m of silt loam above a gravel layer to be on the order of 0.1 mm/yr for the life of the barrier. This estimate did not take any credit for the asphalt layer that is part of the Modified RCRA Subtitle C Barrier design.

The final design for the surface barrier has not been developed; however, based on the extensive testing reported in PNNL-14744, surface barriers that will limit recharge rates are achievable. For the top portion of a fully functioning barrier for the early closure period (2035 to 2135), a compliance case recharge rate of zero is used in ERDF PA simulations; for the period 2135 to 2535, a compliance case recharge rate of 0.5 mm/yr (0.02 in./yr) is used for the top portion of the barrier. For the closure barrier undisturbed zone (Rupert sand with vegetation), the compliance case infiltration rate for the period 2035 to 2535 was assumed to be 1.7 mm/yr (0.067 in./yr) (i.e., the same value as in Section 3.4.1.3.1). The compliance value for the barrier side slopes (compacted silt) for the period 2035 to 2535 is based on the best estimate of 1.9 mm/yr (recommended by PNNL-16688) and rounded to 2 mm/yr (0.079 in./yr). See WCH-515 for additional details.

3.4.1.3.4 Late Post-Closure and a Degraded Surface Barrier (2535 to 3035 and Beyond).

For a degraded surface barrier, a range of potential recharge rates can be envisioned. PNNL-14744 investigated the possibility of the most likely natural failure mechanisms (i.e., bioturbation of the silt-loam layer, wind erosion, and accretion of windblown sand). With appropriate design considerations, PNNL-14744 presents an argument that the failure possibility of these natural systems is quite low, and the emplaced silt-loam soils will continue to perform for as long as they remain in place. Based on these arguments, in PNNL-14744 it is concluded that the long-term effectiveness of the surface barrier would continue to limit recharge rates to less than 0.1 mm/yr (0.004 in./yr) for thousands of years.

Since the final design for the surface barrier has not been developed and it is difficult to defend the continued performance of a surface barrier for long periods of time, the ERDF PA assumed that the closure barrier will maintain the recharge rate at or below 0.5 mm/yr (0.02 in./yr) for 500 years (i.e., the period 2135 to 2535), as discussed above in Section 3.4.1.3. At the end of 500 years, the top portion of the closure barrier is assumed to degrade to permit an infiltration rate of 1.0 mm/yr (0.039 in./yr) and maintain that infiltration rate for the remainder of the

simulation for the compliance case; the degraded side slopes with vegetation are assumed to maintain a compliance value of 2.0 mm/yr (0.078 in./yr) for the period 2535 to 3035 and beyond. For the closure barrier undisturbed zone (Rupert sand with vegetation), the compliance case infiltration rate for the period 2535 to 3035 and beyond was assumed to be 1.7 mm/yr (0.067 in./yr) (i.e., the same value as in Section 3.4.1.3.1). See WCH-515 for additional details.

PNNL-14744 suggested 0.9 mm/yr as an upper-bound recharge rate after the barrier design life. This value was chosen to be equivalent to the best estimate for recharge in undisturbed Rupert sand and Burbank loamy sand. The underlying assumption was that the upper-bound recharge from the degraded surface barrier would approach the expected (best estimate) recharge of undisturbed soil. In this PA, which utilizes the same logic, the upper range value is 2 mm/yr, which is comparable to the best estimate for undisturbed vegetated Rupert sand (1.7 mm/yr) and Burbank loamy sand (1.9 mm/yr) presented in PNNL-16688, which incorporates information from PNNL-14744 and other studies. The best estimate and upper-bounding values are considered sufficient to accommodate the increased uncertainty in the weather cycles and changes in the life cycle during the period after the design life of the barrier.

3.4.1.3.5 Compliance Case Recharge Estimates. Table 3-7 summarizes various timelines and the corresponding compliance case ERDF recharge estimates for a variety of surface conditions (e.g., undisturbed, disturbed, cells under construction, fully functional barrier, and degraded barrier).

Table 3-7. Compliance Infiltration (Recharge) Estimates for Pre-Construction Period, Operational Period, and Following Emplacement of the ERDF Closure Barrier.

Period	ERDF Region	Recharge Rate (mm/yr) Compliance Value
Pre-construction (before 1996)	Undisturbed region (Rupert sand with vegetation)	1.7
Operational period (1996-2035)	Undisturbed region (Rupert sand with vegetation)	1.7
	Disturbed region (Rupert sand without vegetation)	45
	Region under construction (ERDF cells)	0
Early post-closure (2035-2535)	Undisturbed region (Rupert sand with vegetation)	1.7
	Side slopes (compacted silt)	2
	Top portion of the barrier (2035-2135)	0
	Top portion of the barrier (2135-2535)	0.5
Late post-closure (2535-3035 and beyond)	Undisturbed region (Rupert sand with vegetation)	1.7
	Degraded side slopes with vegetation	2
	Degraded top portion of the barrier	1

3.4.1.4 Vadose Zone Stratigraphy Beneath ERDF. The vadose zone underlying ERDF consists of several heterogeneous layers of sedimentary units. The layers vary in thickness at different locations (Chapter 2.0) and for the purpose of simplification have been combined into hydrostratigraphic units. The hydraulic properties are defined by the hydrostratigraphic units. The western segment of ERDF (Figure 3-2) is distinguished from the eastern part primarily by the presence of a well-developed calcium carbonate-rich caliche unit (previously referred to as

the Plio-Pleistocene unit); the unit has been a relatively effective barrier to contaminant transport from past tank leaks, for example, in the vertical direction but is nonexistent beyond the ERDF in the 200 Area. Also, clastic dikes (anomalous, subvertical linear features composed of layers of differing particle size distributions), discussed later, can occur in the vadose zone that extend up to tens of meters in length and can cross cut the major layers. These features are typically less than 1 m wide.

The west-east and north-south geologic cross-sections (WCH-463) used in ERDF PA modeling are shown in Figures 3-5a and 3-5b, respectively. The hydrostratigraphic units overlying the basalt beneath the ERDF are, from top to bottom, as follows:

- Hanford formation unit 1 (Hf1) (gravel-dominated)
- Hanford formation unit 2 (Hf2) (sand-dominated)
- Cold Creek Unit silt-dominated (CCu_z)
- Cold Creek Unit caliche (CCu_c)
- Ringold Formation member Taylor Flat (RF_{tf}) (fine grained)
- Ringold Formation Unit E (RF_{we}) (silty sandy gravel).

3.4.1.5 Flow and Transport Model. The vadose zone hydrology of the 200 Areas, where ERDF is located, plays a key role on moisture movement and contaminant migration through the vadose zone to the water table. Numerous past studies of both controlled and uncontrolled (unplanned) flow and transport experiments in the 200 Areas have focused on understanding vadose zone flow and migration processes at the field scale. For numerical modeling of large flow domains such as ERDF, numerical techniques have been developed for upscaling small, core-scale measurements for application at the large, grid-block scale.

The flow and transport model developed for ERDF PA calculations are based on information synthesized from the past field experiments and modeling studies. A detailed discussion of the field and numerical modeling studies is presented in Appendix A, which also attempts to address such questions as the following:

- What field-scale processes are important for vadose zone moisture flow in the 200 Areas?
- What determines the rate of moisture flow and contaminant migration in relatively dry heterogeneous sediments?
- Why are subsurface media heterogeneities important?

As discussed in Appendix A, a two-staged approach is followed to address these questions. First, the results based on field observations are presented from existing "uncontrolled" (unplanned) releases as well as controlled field experiments conducted in the 200 Area (Sisson and Lu field injection site; also known as the Vadose Zone Test Facility). A summary of salient features and processes observed in the heterogeneous Hanford sediments is provided. Second, the information derived from field studies is discussed in the context of formulating a conceptual framework for the vadose zone modeling and testing (Appendix A).

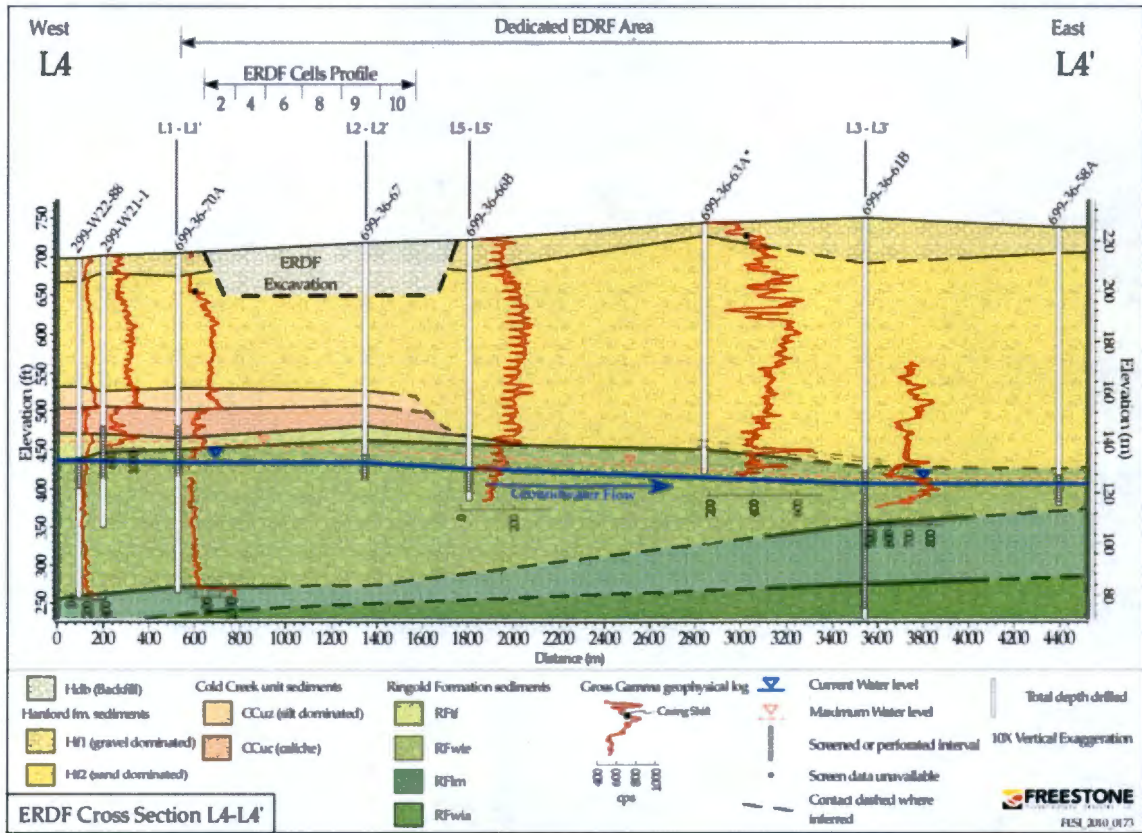
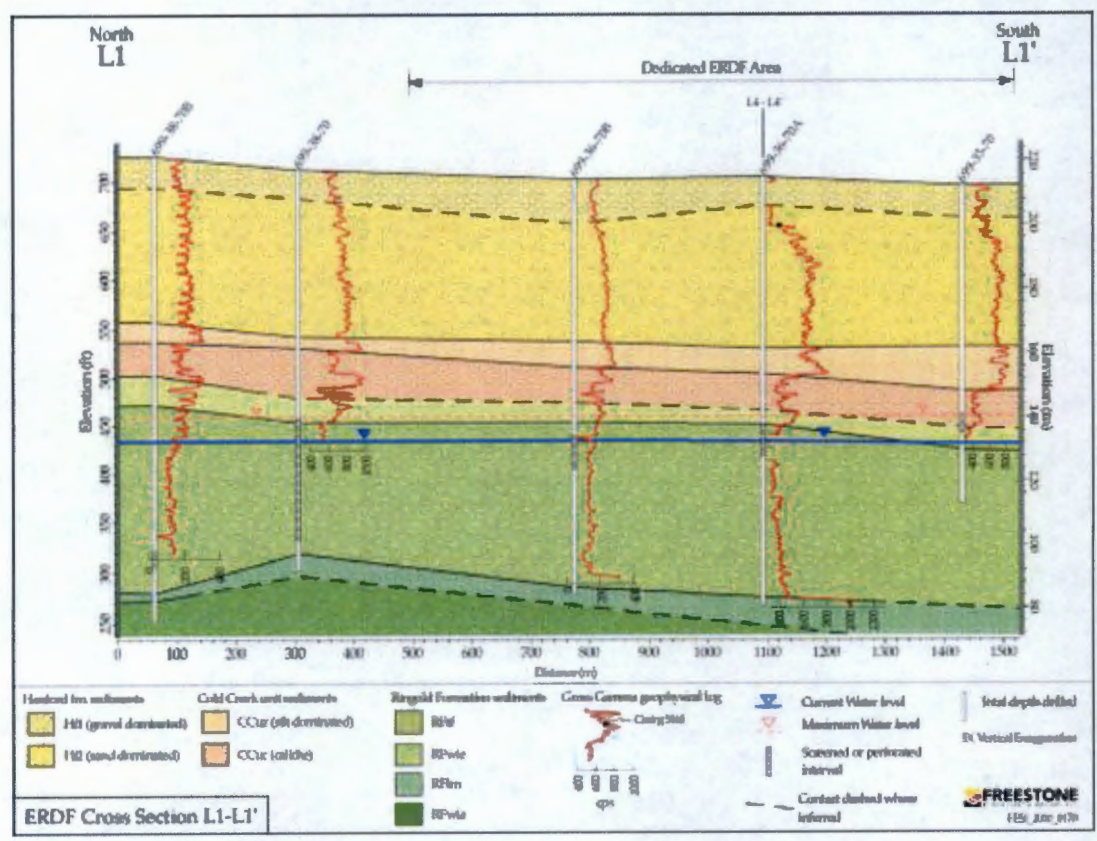


Figure 3-5. (a) West-East ERDF Stratigraphic Cross-Section.

Figure 3-5. (b) North-South Stratigraphic Cross-Section Through ERDF.



For ERDF PA modeling, a three-dimensional flow and transport numerical model is developed for the integrated vadose zone unconfined aquifer. An equivalent porous continuum model is assumed and the fluid flow within the vadose zone is described by Richards' equation (Jury and Horton 2004). The effective flow properties based on upscaling methods are applied to the model domain. The contaminant transport is described by the conventional advective-dispersive transport equation with an equilibrium linear sorption coefficient (K_d) formulation. No temperature effects are considered for the vadose zone model (i.e., the model used is isothermal).

Steady-state initial conditions (that represent pre-Hanford Site operations) were developed by simulating from a unit hydraulic gradient condition to a steady-state condition, dictated by the initial meteoric recharge at the surface, water table elevation, water table gradient, no flux vertical boundaries, and distribution of hydrologic properties. The transient simulations representing change in recharge rate over time and space are carried as outlined in Table 3-7. Transient conditions were conducted for the period from the time of ERDF construction to the year 2035, followed by a 10,000-year closure period (i.e., years 2035 to 12035) that involved changes in the flow fields in response to current conditions, placement of closure barrier, and effects of a degraded barrier. The details on building the three-dimensional model along with boundary conditions and modeling assumptions are presented in Appendix B. A summary of the model domain and boundary conditions setup is presented below.

3.4.1.5.1 Model Domain and Boundary Conditions. The model domain for flow and transport in the vadose zone is represented numerically as a three-dimensional, rectangular cube aligned in the general direction of groundwater flow. The numerical model adapts the physical elements of the conceptual model to a Cartesian grid and also assigns numerical values to the parameters used in algorithms to represent the physical and geochemical systems and processes.

The ERDF model domain is 1,880 m (6,168 ft) west to east, 1,415 m (4,642 ft) south to north, by approximately 121 m (397 ft), vertically, extending about 14.5 m to 17.5 m (48 ft to 57 ft) below the water table. Horizontal node spacing varied between 10 and 40 m (33 and 131 ft) throughout the model domain, becoming more refined in the area of the ERDF side slopes and berms and less refined elsewhere. The vertical spacing was 2 m except around the water table where the spacing increased to 2.25 and 3.0 m to keep the surface of the water table within one numerical layer. The total number of nodes equaled 493,240, although not all nodes were active because of unevenness in the ground surface and the void introduced by the construction of ERDF. During the pre-operational phase, the number of active nodes equals 443,434 (49,806 inactive); during the operational phase, the number of active nodes equals 425,319 (with 67,921 inactive), the increase in inactive nodes attributed to the inactivation of the nodes within the ERDF excavation; during the post-closure phases, the number of active nodes increases to 444,331 (with 48,909 inactive). Digitization of the geologic unit thickness and contact information presented in WCH-463 provided the basis for the development of the model domain. Further model building details are provided in Appendix B.

A specified-flux boundary condition was applied at the surface to simulate recharge. Recharge rates varied spatially and temporally along the upper boundary depending on site conditions, the location and physical dimensions of the ERDF, and the time of ERDF site operations and surface conditions simulated. Boundary conditions at the sides of the model domain were assumed to be no flow in the vadose zone. In the aquifer, the lengthwise boundary conditions are prescribed flux at the upgradient (west) boundary and prescribed head at the downgradient (east) boundary, and no-flow at the north and south boundaries. The bottom boundary of the

unsaturated (vadose) zone is the water table and the bottom of the model (aquifer) was defined as a vertical no flow boundary condition.

To describe the bulk (or mean) flow behavior, each heterogeneous formation (e.g., gravelly sand unit in Figure 3-5a,b) was replaced by its homogeneous equivalent, and effective or upscaled flow parameters were used to represent the homogeneous equivalent. Each formation unit was assigned different hydraulic properties. The laboratory-measured hydraulic properties were upscaled. Upscaling accounts for the fact that the numerical modeling applies to a scale that is much larger than the core scale at which laboratory measurements are available. As will be explained in Section 3.4.1.7, saturation-dependent anisotropy relationships (Polmann 1990) were invoked in recognition of field data from controlled and uncontrolled experiments that clearly show the dominant effect of lateral flow for the highly heterogeneous vadose sediments at the Hanford Site.

The flow modeling consisted of four stages. The first stage (pre-operational period) established steady-state hydraulic conditions within the model domain using boundary conditions consistent with conditions assumed to exist prior to the completed construction of the ERDF in 1996. The second stage represents transient hydraulic conditions during the period 1996 to 2035 (from the beginning time of ERDF operations to the planned closure of ERDF). During this second stage, the recharge boundary condition applied around ERDF was increased to reflect the altered surface conditions associated with operations and eliminated where the composite liner has been emplaced. The third stage (early post-closure) starts in 2035 and continues to 2135, at which point the composite liner is assumed to fail completely. The fourth stage (late post-closure) begins in 2135 and continues to the end of the simulation. Boundary conditions representing recharge for the changed surface conditions associated with the possible post-closure surface conditions commenced with the assumed dates of closure. Further modeling details are provided in Appendix B.

The contaminant mass is assumed to be uniformly distributed within the ERDF volume. The average thickness of ERDF is estimated to be 22 m (72 ft), while the total thickness of the vadose zone (including ERDF) in the model is approximately 90 m. The mass is released to the vadose zone nodes below ERDF following the failure of composite liner (after 2135). The contaminant transport through the vadose zone and resulting groundwater impacts are calculated after that time. The point of calculation of the groundwater concentration corresponds with the location 100 m downgradient from the edge of the facility (Figure 3-4).

The direction of groundwater flow around the ERDF near the 200 West Area is generally west to east. The water table elevation at steady-state conditions in the near future (within 100 years after closure) was estimated to be approximately 126.5 m (415 ft) and 123.5 m (405 ft) NAVD88 at the upgradient and downgradient boundaries, respectively (see Appendix B for additional details). The present-day groundwater table is expected to continue declining over the next few decades because the large discharges of operational liquid to the ground at the 216-U-10 Pond and other large discharge sites in the 200 West Area have ceased. For this modeling activity, a long-term average groundwater hydraulic gradient of 0.0015 is assumed for the future steady-state conditions (WCH-515, *Parameter Uncertainty for the ERDF Performance Assessment Uncertainty and Sensitivity Analysis*). The water table occurs within the Ringold Unit E. Within the model domain, the aquifer extends to a depth of approximately 14.5 m to 17.5 m (48 ft to 57 ft) below the water table, but the model evaluates concentrations in the approximate upper 5 m (16 ft) of the aquifer. The horizontal saturated hydraulic conductivity mean and compliance value for the aquifer is estimated to be 5 m/day (16 ft/day) (WCH-515)

3.4.1.6 Alternative Groundwater Pathway Conceptual Models. The ERDF PA vadose zone flow and transport simulations are based on the EPM continuum modeling assumption (Section 3.2). Such an assumption is supported by field data on moisture and contaminant plumes at various controlled and uncontrolled experiment sites as discussed in Appendix A. We now consider and evaluate two types of alternative groundwater pathway conceptual models for ERDF: (1) preferential pathways (Section 3.4.1.6.1), and (2) alternate EPM models using “soft” and “hard” data (Section 3.4.1.6.2).

3.4.1.6.1 Preferential Pathways. One preferential pathway or “fast flow” path in Hanford Site sediments can result from clastic dikes that often cross cut sedimentary units, especially in the Hanford formation (Figure 3-6). The dikes are sedimentary structures observed in some outcrops and trenches that expose the Hanford formation in the 200 Areas (BHI-01103). These are believed to represent dewatering structures that developed during compaction and settling of cataclysmic flood deposits during or soon after floodwaters drained from the Pasco Basin. The dikes are of particular interest because they occur as near-vertical tubular bodies filled with multiple layers of unconsolidated sediments. Generally, clastic dikes are composed of an outer skin of clay with relatively coarser infilling sediment made of sand, silt, clay, and gravel. There is very little evidence to indicate that they extend all the way from near the ground surface to the water table.

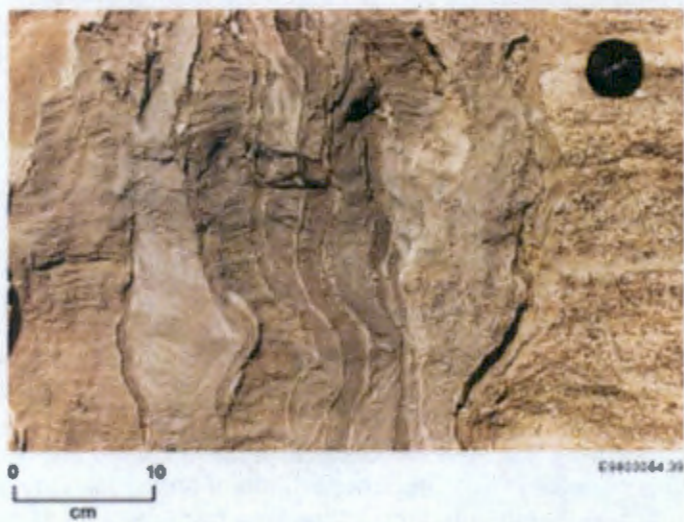
In general, the hydraulic properties of clastic dikes can be considered essentially as a subset of the porous matrix properties for the Hanford Site sediments. This is based on laboratory measurements of clastic dike samples. Under natural flow conditions, the infilled fine clastic dike sediments represent regions of lower permeability but higher moisture content compared to the surrounding matrix (PNNL-14224, *Influence of Clastic Dikes on Vertical Migration of Contaminants in the Vadose Zone at Hanford*). The implication for such a contrast in properties is illustrated, for example, by the setup shown in Figure 3-6. The middle portion of Figures 3-6a and 3-6b show the infilled (finer) sediments within a dike; the host (coarser) sediments are shown on the left and right edges of the two figures. Under unsaturated flow in a low-moisture regime, because of higher moisture-holding capacity of the infilled fine sediments, these dikes may in fact represent barrier to flow rather than fast flow channels (PNNL-14224). Thus, clastic dike sediments, representing fine sediment properties (e.g., fine sand, silt, and clay), often are regions of higher moisture content but not necessarily of fast transport under conditions of unsaturated flow and low fluxes (Murray et al. 2007).

Consider an alternate scenario whereby we have gravelly sediments as the clastic dike infilled media. The conceptual model schematic in Figure 3-6c illustrates this scenario, where the bulk of the fluid flow bypasses the media with large pore sizes (i.e., macropore) under unsaturated conditions. If the clastic dikes were filled with gravelly sediments, it is not feasible, for the following reasons, to have a scenario under unsaturated conditions where the bulk of the flow is through the dikes.

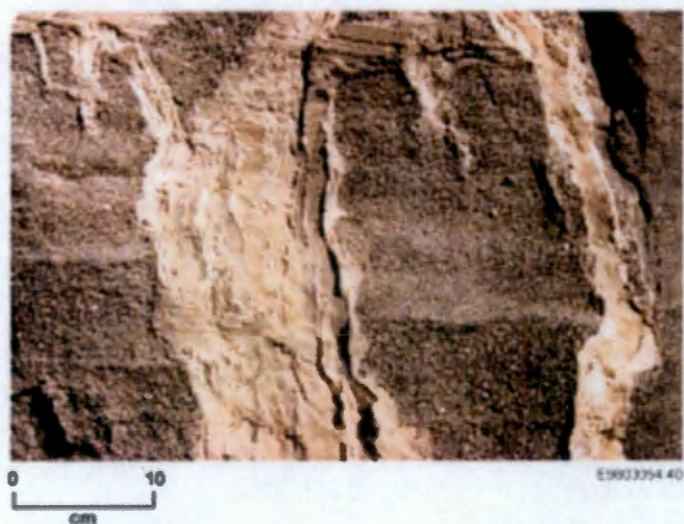
- The porous matrix has a much smaller average pore size than the gravelly media within the clastic dike.
- For the moisture regime under low recharge conditions, the gravelly sediments with a larger pore size than the surrounding porous matrix will have a limited ability to hold moisture, and the fluid will be attracted primarily to the porous matrix.

Figure 3-6. Clastic Dike Models and Infilled Material.

(a)



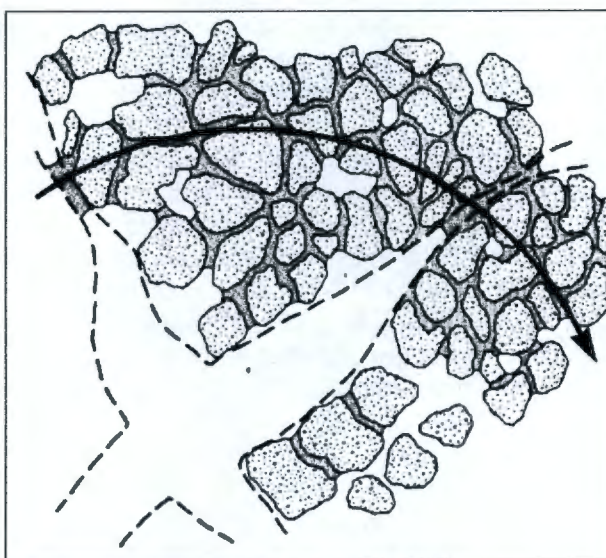
(b)



Source: BHI-01103, *Clastic Injection Dikes of the Pasco Basin and Vicinity – Geologic Atlas Series.*

Figure 3-6. (Continued)

(c)



After Wang and Narasimhan (1985)

The expanded vertical slice illustrates the fact that under unsaturated conditions and low recharge, the bulk flow bypasses the pathway formed by larger pore sizes and essentially follows the pathway formed by smaller pore size network. The large, open spaces in the figure mimic macropores such as those existing in a coarse-textured medium.

Thus, while clastic dikes do exist, the preceding two scenarios suggest that the presence of clastic dikes under conditions of unsaturated flow and low fluxes is unlikely to contribute much to contaminant transport and to long-term risk relative to higher peak concentrations for long-lived mobile radionuclides in groundwater. This is supported by the WMA S-SX Field Investigation Report simulation results (RPP-7884) and past Hanford Site performance assessment modeling results (WHC-EP-0645, WHC-SD-WM-TI-730). The numerical results are also supported by studies reported elsewhere. Literature studies suggest that, although preferential flow has been recognized and widely studied under saturated or near-saturated flow conditions (Nkedi-Kizza et al. 1983, De Smedt and Wierenga 1984), there is little evidence of it in arid and semiarid climates or under low water fluxes, particularly where soils are coarse textured, such as those beneath ERDF. Thus, under natural recharge conditions, precipitation at arid sites is usually too low (in relation to saturated hydraulic conductivity) to invoke preferential flow; much of the water in the dry soils is simply adsorbed onto the grain surfaces as film flow and cannot move along preferred pathways.

3.4.1.6.2 Alternate Equivalent Porous Medium (EPM) Models Using “Soft” and “Hard” Data. As mentioned earlier (Section 3.2), the ERDF PA vadose zone flow and transport simulations are based on the EPM porous continuum modeling assumption. The conventional EPM models often cannot reproduce the observed moisture plume variations, even though the first and second moments, based on simulations, compare well with the observed moments (Appendix A). To address this drawback, we considered alternate approaches (Deng et al. 2009, Ye and Khaleel 2008, Ye et al. 2007) based on an integration of “soft” data (data that can be easily obtained, for example, initial moisture content, bulk density, and soil texture) and “hard” data (data that are more difficult to obtain, e.g., soil hydraulic properties).

As part of testing of the vadose zone conceptual model, the moisture content data that were collected at the Sisson and Lu site (also known as the Vadose Zone Test Facility) in the 200 East Area were analyzed. The rich database at the Sisson and Lu site is an important resource in understanding large-scale moisture movement in imperfectly stratified heterogeneous media and a relatively dry moisture regime such as the ERDF site.

The data at the Sisson and Lu site are obtained from widely spaced boreholes; they provide relatively adequate information about heterogeneity in the vertical direction, but not necessarily in the horizontal direction. The use of hard as well as soft data allows us to characterize the spatial heterogeneity in the lateral direction by interpolating information between boreholes. In Appendix A, in addition to conventional EPM models, we present results for two alternate methods which use soft and hard data: the first uses an integration of cokriging and artificial neural network (Ye et al. 2007) and the second uses transition probability/Markov Chain (Ye and Khaleel 2008). Both methods are summarized in Appendix A; details on the methodology are described in the preceding two articles.

For the conventional as well as the alternate EPM-based upscaling methods, spatial moments (first and second moments) of the simulated plume based on the effective hydraulic conductivities were in good agreement with those for the observed plume at the Sisson and Lu site (Appendix A). Thus, while the use of both soft and hard data was valuable in producing the detailed moisture plume (i.e., the splitting of the moisture plume sandwiched within the coarse media between two fine layers), the observed and simulated spatial moments (first and second) were not significantly different from those using the conventional EPM medium-based upscaling. With the ERDF PA simulations being conducted over a large flow domain and over a long time frame, this is an important finding because, as the field data from controlled as well as uncontrolled experiments (Appendix A) suggest, the vadose zone heterogeneities are effective in smearing out the impact of small-scale heterogeneities over time and space.

3.4.1.7 Vadose Zone Flow and Transport Parameters. Details on vadose zone flow and transport parameters are provided in hydrology data package (WCH-464). As part of ERDF site characterization, data on soil physical and hydraulic properties were obtained in 1994. As part of other Hanford Site projects, particle-size distribution, saturated hydraulic conductivity, moisture retention, and unsaturated conductivity data are available for sediment samples in the vicinity of the ERDF site. Hydraulic properties data are lacking for the gravel-dominated sequence at the ERDF site. However, physical and hydraulic properties data are available for the sandy gravel sediments in 100 Area along the Columbia River. Because these samples compare well with the ERDF samples with respect to particle-size distribution, the 100 Area gravelly samples are used as surrogate to represent the hydraulic properties for the gravel-dominated sequence at the ERDF site.

The saturated as well as unsaturated hydraulic conductivities were measured in the laboratory on bulk split-spoon samples (including gravels). A variation of the unit gradient method was used to obtain unsaturated conductivity measurements (Klute and Dirksen 1986, Khaleel et al. 1995). The moisture retention measurements were made on much smaller core, non-gravelly samples. Unlike the hydraulic conductivity data, the retention measurements thus needed gravel correction (Khaleel and Relyea 1997). The moisture retention data for the laboratory samples for the drainage cycle of up to -1,000 cm of pressure head were measured using "Tempe" pressure cells; the rest of the drainage curve up to -15,000 cm was measured using the pressure plate extraction method (Klute 1986).

For each stratum defined by the stratigraphic cross-sectional model, the small-scale laboratory measurements were upscaled to obtain equivalent horizontal and vertical unsaturated hydraulic conductivities as a function of mean tension. In addition, to reflect field conditions, the laboratory-measured moisture retention data were corrected for the presence of any gravel fraction in the sediment samples. As with flow modeling, each stratum was modeled with different transport parameters (i.e., bulk density, diffusivity, and macrodispersivity).

The moisture retention data are described using an empirical relationship (van Genuchten 1980):

$$\theta(h) = \theta_r + (\theta_s - \theta_r) \left\{ 1 + [\alpha h]^n \right\}^{-m} \quad \text{Eq. 3.1}$$

where:

θ = volumetric moisture content (dimensionless)

h = matric potential or pressure head, which, for notational convenience, is considered as being positive (i.e., tension [cm])

θ_r = residual moisture content (dimensionless)

θ_s = saturated moisture content (dimensionless)

α = a fitting parameter (cm^{-1})

n = a fitting parameter (dimensionless)

$m = 1 - 1/n$.

Combining the van Genuchten model with Mualem's (1976) model for unsaturated conductivity:

$$K(h) = \frac{K_s \left\{ 1 - (\alpha h)^{mn} \left[1 + (\alpha h)^n \right]^{-m} \right\}^2}{\left[1 + (\alpha h)^n \right]^{m\ell}} \quad \text{Eq. 3.2}$$

where:

$K(h)$ = unsaturated hydraulic conductivity [cm/s]

K_s = saturated hydraulic conductivity [cm/s]

ℓ = pore-connectivity parameter [dimensionless], estimated by Mualem to be about 0.5 for many soils.

It is well recognized that the estimated unsaturated conductivities, based on saturated conductivity and the van Genuchten retention model, can differ by up to several orders of magnitude with measured conductivities at the dry end (e.g., Khaleel et al. 1995). Therefore, unlike the conventional approach, wherein the unsaturated conductivities are based on

predictions using the measured retention curve and the measured saturated conductivity, the ERDF soil hydraulic properties are based on a simultaneous fit of moisture retention and unsaturated conductivity data. All five unknown parameters θ_r , θ_s , α , n , and K_s , with $m=1-1/n$ (van Genuchten 1980) were fitted to the data via a code named RETention Curve (RETC) (EPA/600/2-91/065, *RETC Code for Quantifying the Hydraulic Functions of Unsaturated Soils*). Thus, in order to obtain a better agreement with experimental data for the region of interest (i.e., relatively dry moisture regime), K_s is treated as a fitted parameter during the curve-fitting process. This is considered appropriate because the ERDF PA predictions are needed for the relatively dry moisture regime observed in the field (see Appendix A field data for the nearby Sisson and Lu field injection site experiments), rather than for the saturated or near-saturated regime. The pore size distribution factor, ℓ (Mualem 1976) was kept fixed at 0.5 during the simultaneous fitting.

Figure 3-7 shows the location of sites that were used in deriving the ERDF data set of soil hydraulic properties. Figure 3-8 provides the corresponding fitted curves. As noted earlier, during the simultaneous fitting, the laboratory-measured K_s , for example, was allowed to float so as to obtain an acceptable fit for the modeled dry moisture regime. This resulted in composite fitted values for the α and K_s parameters for the CCuc and CCuz units, for example, being outside the bounds of the range of values for individual samples. Estimates for the equivalent horizontal and vertical hydraulic conductivities are presented in the following section.

Figure 3-7. Location of Samples Used in Developing the ERDF Data Set of Soil Hydraulic Properties.

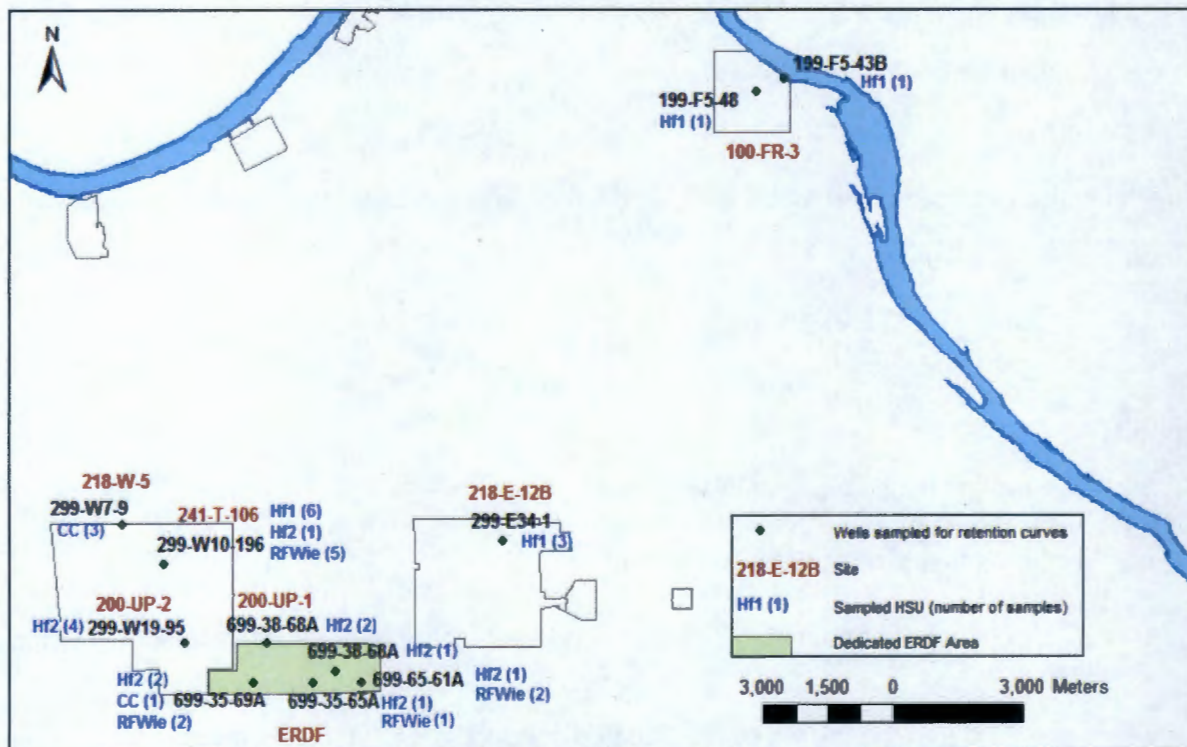


Figure 3-8. Fitted Moisture Retention and Hydraulic Conductivity Curves for Various Hydrostratigraphic Units.

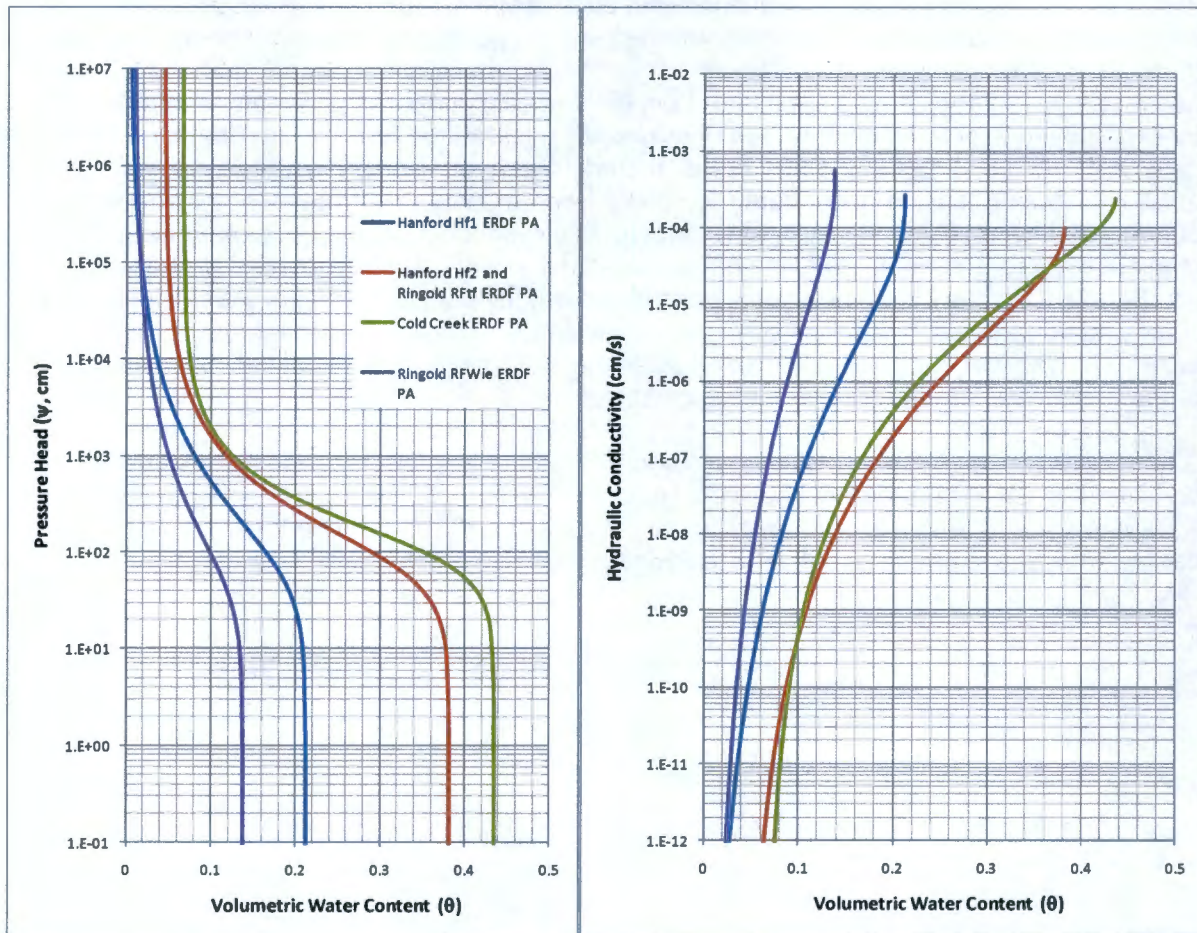


Table 3-8. Composite van Genuchten-Mualem Parameters for Various Hydrostratigraphic Units (WCH-464).

Strata	Number of Samples	θ_s	θ_r	α (1/cm)	n	ℓ	Fitted K_s (cm/s)
Hanford Hf1 (gravel-dominated)	11	0.2126	0.0032	0.0141	1.3730	0.5	2.62E-04
Hanford Hf2 (sand-dominated)	12	0.3819	0.0443	0.0117	1.6162	0.5	9.88E-05
Cold Creek CCu _z (silt-dominated) and CCu _c (caliche)	4	0.4349	0.0665	0.0085	1.8512	0.5	2.40E-04
Ringold RFtf	12	0.3819	0.0443	0.0117	1.6162	0.5	9.88E-05
Ringold RFWie	10	0.1380	0.0100	0.0210	1.374	0.5	5.60E-04

3.4.1.7.1 Moisture-Dependent Anisotropy. Vadose zone moisture-dependent anisotropy is used to account for the extensive lateral migration that is well documented for 200 East and 200 West Area sediments (Zhang and Khaleel 2010, Ye et al. 2005, Yeh et al. 2005). For saturated media, an averaging of the heterogeneities in geologic media at a smaller scale leads to an effective hydraulic conductivity value at the larger (macroscopic) scale, with the lateral hydraulic conductivity being much larger than the vertical conductivity. For unsaturated media, theoretical and experimental analyses of field-scale unsaturated flow indicate that for stratified sediments such as those in the 200 Areas, the effective hydraulic conductivity tensor is anisotropic with a tension-dependent (or moisture-dependent) anisotropy. The anisotropy ratio of horizontal hydraulic conductivity to vertical hydraulic conductivity increases with increasing tension or decreasing moisture content. Because the soil hydraulic properties are based on small-scale laboratory measurements, upscaling methods are used to apply them to the large-scale, heterogeneous vadose zone (Khaleel et al. 2002). Tension-dependent anisotropy provides a framework for upscaling small-scale measurements to the effective (upscaled) properties for the large-scale macroscopic vadose zone.

A stochastic model (Polmann 1990) was used to evaluate tension-dependent anisotropy for sediments at ERDF; results are shown in Table 3-9. Note that Polmann parameters (Table 3-9) were only used to assign anisotropy ratios for various strata within the vadose zone and are described by the following equation (Equation 3.3):

$$\begin{aligned}
 \langle \text{Ln}K \rangle &= \langle \text{Ln}K_s \rangle - A \langle h \rangle - \sigma_{\text{Ln}K_s}^2 \lambda [p - p^2 \langle h \rangle - \zeta^2 \langle h \rangle] / (1 + A\lambda) \\
 \sigma_{\text{Ln}K}^2 &= \sigma_{\text{Ln}K_s}^2 [(1 - p \langle h \rangle)^2 + \zeta^2 \langle h \rangle^2] / (1 + A\lambda) \\
 K_h^{eq} &= \exp[\langle \text{Ln}K \rangle + (\sigma_{\text{Ln}K}^2 / 2)] \\
 K_v^{eq} &= \exp[\langle \text{Ln}K \rangle - (\sigma_{\text{Ln}K}^2 / 2)]
 \end{aligned}
 \tag{Eq. 3.3}$$

where:

- $\sigma_{\text{Ln}K}^2$ = variance of log unsaturated conductivity (which depends on mean tension)
- $\langle h \rangle$ = mean tension (positive) = $|\psi|$
- ψ = matric potential (negative)
- $\sigma_{\text{Ln}K_s}^2$ = variance of $\text{Ln}K_s$
- $\langle \text{Ln}K_s \rangle$ = mean of $\text{Ln}K_s$
- p = slope of the β versus $\text{Ln}K_s$ regression line, where β is the slope of the unsaturated conductivity curve and approximated locally based on the Gardner's (1958) exponential model
- ζ = $\sigma_\delta / \sigma_{\text{Ln}K_s}$
- σ_δ = standard deviation of the residuals in the β versus $\text{Ln}K_s$ regression

- A = mean slope, β , for $\ln K$ vs. h
- λ = vertical correlation lengths for $\ln K_s$ (assumed to be same as that of β)
- K_h^{eq} = equivalent unsaturated horizontal conductivity
- K_v^{eq} = equivalent unsaturated vertical conductivity.

Table 3-9. Macroscopic Anisotropy Parameters for Various Hydrostratigraphic Units Based on the Polmann (1990) Model (WCH-464).

Strata	Number of Samples	$\langle \ln K_s \rangle$	$\sigma_{\ln K_s}^2$	p	ζ	λ (cm)	A
Hanford Hf1 (gravel-dominated)	11	-14.85	1.94	-2.6E-4	2.50E-4	30	0.00368
Hanford Hf2 (sand-dominated)	12	-14.6	1.50	-7.2E-4	6.55E-4	50	0.00620
Cold Creek CCu _z (silt-dominated) and CCu _c (caliche)	4	-10.43	1.01	2.4E-3	9.34E-4	50	0.0104
Ringold RFtf	12	-14.6	1.50	-7.2E-4	6.55E-4	50	0.00620
Ringold RFwie	10	-15.76	3.56	-1.1E-4	1.84E-4	30	0.00371

Note that in deriving the anisotropy parameters (Table 3-9), the Gardner (1958) exponential model was used to describe unsaturated hydraulic conductivity as a function of fitted K_s and tension h . Because of variability, a constant slope is however inadequate in describing the slope β for the Gardner model. The slope β is therefore approximated locally by straight lines over a fixed range of tension, and the $\ln K_s$ term in Table 3-9 is derived by extrapolating the local slopes back to zero tension. The mean and variance for anisotropy parameters, $\langle \ln K_s \rangle$ and $\sigma_{\ln K_s}^2$ are then based on the extrapolated $\ln K_s$ values.

As described in Appendix A, the parameterization process described herein was independently tested using the nearby Sisson and Lu field injection data. Through an integrated use of field data and numerical modeling, we demonstrated that the assumptions incorporated into the conceptual model are consistent with the available data, related investigations, and theory related to the conceptual model (Appendix A).

3.4.1.7.2 Bulk Density Estimates. Bulk density (ρ_b) estimates are needed to calculate retardation factors for different species. The average ρ_b , $E[\rho_b]$ (Table 3-10) estimates for various strata are based on WCH-464.

Table 3-10. Effective Bulk Density (g/cm³) Estimates for Various Hydrostratigraphic Units.

Strata/Material Type	E[ρ _b]
Sandy Hf2	1.76
Gravelly sand Hf1	2.07
Cold Creek Unit	1.65
Ringold RFtf/Ringold gravels RFwie	2.13

NOTE: These are based on median values of WCH-464 data set.

3.4.1.7.3 Effective Diffusion Coefficient. It was assumed that the effective, large-scale diffusion coefficients for all strata at ERDF are a function of volumetric moisture content, θ , and can be expressed using the Millington and Quirk (1961) empirical relation:

$$D_e(\theta) = D_0 \frac{\theta^{10/3}}{\theta_s^2} \quad \text{Eq. 3.4}$$

where:

$D_e(\theta)$ is the effective diffusion coefficient of an ionic species as a function of moisture content and D_0 is the molecular diffusion coefficient for the same species in free water. The molecular diffusion coefficient for all species in free water was assumed to be 2.5×10^{-5} cm²/s (WHC-SD-WM-EE-04, *Performance Assessment of Grouted Double-Shell Tank Waste Disposal at Hanford*).

3.4.1.7.4 Macrodispersivity Estimates for Nonreactive Species. The Gelhar and Axness equation (Gelhar 1993) is used to estimate asymptotic values of macrodispersivity. To account for the effects of unsaturated flow, a modified version is used:

$$A_L(\langle h \rangle) = \sigma_{\ln(K)}^2 \lambda_u \quad \text{Eq. 3.5}$$

where the longitudinal macrodispersivity depends on the mean tension $\langle h \rangle$ and the correlation length of the unsaturated hydraulic conductivity (λ_u).

To apply Equation 3.5, an estimate of the vertical correlation scale for unsaturated conductivity is needed. A correlation length of the order of about 50 cm was obtained for saturated hydraulic conductivity for sediments near the C tank farm in the 200 East Area (RPP-13310, *Modeling Data Package for an Initial Assessment of Closure of the C Tank Farm*). For unsaturated conditions, an increase in the variance of log unsaturated conductivity is expected to be compensated in part by a decrease in the correlation scale of log unsaturated conductivity. A correlation length of 30 cm is assumed for log unsaturated conductivity for all strata. Table 3-11 provides the log unsaturated conductivity variances and the estimated longitudinal (A_L) and transverse (A_T) macrodispersivities for various strata. The transverse dispersivities are estimated as one tenth of the longitudinal values (Gelhar et al. 1992).

Table 3-11. Macrodispersivity Estimates for Various Hydrostratigraphic Units (Based on Median Values of WCH-464 Data Set).

Strata	Correlation Length, λ_u cm	A_L cm	A_T cm
Sandy Hf2	30	~150	15
Gravelly Sand Hf1	30	~150	15
Cold Creek	30	~50	5
Ringold RFtf/Ringold Sandy Gravel RFwie	30	~150	15

3.4.1.7.5 Contaminant Distribution Coefficients. The choice of K_d values (and their uncertainty range) is guided by the chemistry of the leachate that could emanate from ERDF wastes. Six waste chemistry types were defined by PNNL-11800, *Composite Analysis for Low-Level Waste Disposal in the 200 Area Plateau of the Hanford Site*, in order to differentiate chemically distinct waste streams that impact the sorption of contaminants. PNNL-14702, *Vadose Zone Hydrogeology Data Package for Hanford Assessments*, reviewed this classification and defined semi-quantitative chemical concentrations for each waste stream category in order to provide a less ambiguous and more technically defensible approach for the assignment of K_d values. ERDF leachate samples were found to contain detectable concentrations of common metals, anions, and mobile radionuclides under near-neutral conditions (WCH-295, *Groundwater and Leachate Monitoring and Sampling at ERDF, CY 2007*; WCH-315, *Groundwater and Leachate Monitoring and Sampling at ERDF, CY 2008*). An average pH of 7.4 was measured over the period from June 2006 to December 2008 in leachate samples. Based on the categories defined in PNNL-14702, the ERDF leachate chemistry is judged to belong to category 4 (i.e., Low Salt/Near Neutral category).

The unconfined aquifer below the ERDF was also found to belong to this category because of near-neutral, low-salt, and low-organic conditions in the groundwater (WCH-295, WCH-315). Even if leachate chemistry were to evolve in the future as new ERDF cells are filled with other wastes, it is not expected to increase or decrease the pH or salt concentrations significantly in ERDF leachates, to the point of modifying the waste stream designation. Additionally, as no known Hanford Site operations period contamination has impacted the ERDF vadose zone prior to its construction, the "no impact" classification for the vadose zone sediments will be considered for selecting a K_d value for each radionuclide of concern.

As the majority of the K_d experiments currently available corresponds to measurements performed on fine-grained fraction of the sediments, extrapolation of these results to the ERDF-specific hydrostratigraphic units has required gravel correction, and changes in reactivity based on the carbonate or silt content. Consequently, the following four groups of ERDF hydrostratigraphic units having a specific K_d value have been distinguished:

- Sandy units that have negligible gravel content (Hf2 and RFtf)
- Gravelly units that have a significant gravel content (Hf1 and RFwie)
- Silt-dominated unit of Cold Creek (CCu_z)
- Carbonate-dominated unit corresponding to Cold Creek Caliche (CCu_c).

For units containing a significant amount of gravel (Hf1 and RFwie), K_d values are typically lower than those determined with <2-mm (0.8-in.) size material because the surface area and corresponding number of adsorption sites is much lower (PNNL-17154, *Geochemical Characterization Data Package for the Vadose Zone in the Single-Shell Tank Waste Management Areas at the Hanford Site*). Depending on the minimum K_d value, following equations as recommended by PNNL-17154, are used for gravel correction:

- For minimum $K_d \geq 10$ mL/g:

$$K_d(\text{gc}) = (1-0.77f) K_d(<2\text{mm}) \quad \text{Eq. 3.6}$$

- For minimum $K_d < 10$ mL/g:

$$K_d(\text{gc}) = (1-f) K_d(<2\text{mm}) \quad \text{Eq. 3.7}$$

where $K_d(\text{gc})$ is the gravel-corrected K_d value of K_d contaminants, f the weight fraction gravel, and $K_d(<2 \text{ mm [0.8 in.]})$ is the K_d determined for <2-mm (0.8-in.) size fraction of sediment material.

The average gravel fraction for each hydrostratigraphic unit is presented in Table 3-12. Based on the above equations for gravel correction, the best estimate K_d values are calculated and summarized in Table 3-13.

For carbon-14, the best estimate of 5 mL/g recommended by PNNL-17154 was lowered in order to be consistent with the multiphase transport results based on meso-scale unsaturated soil column experiment described in INEEL/EXT-04-01793 and Plummer et al. (2004). The results indicate that for silty and carbonated sediments the carbon-14 K_d value range from 0.8 to 2.4 mL/g. Note that the calcareous silt soil material used in the experiment is a more favorable substrate for carbon-14 sorption than the sand-dominated soil. Consequently, we chose a best estimate K_d value of 0.5 mL/g for sandy units (Hf2 and RFtf), which is a smaller value than the lower end of the derived range. This was then gravel corrected for the Hf1 and RFwie units. For the silt-dominated CCu_z unit a K_d value of 0.8 mL/g (lower end of the derived range) and for carbonate-dominated CCu_c unit a K_d value of 1.6 mL/g (middle of the derived range) was deemed as the best estimate value.

Table 3-12. Average Percent Gravel Measured in Each Hydrostratigraphic Unit (According to WCH-464).

Hydrostratigraphic Unit	Number of Samples	Percent Gravel (%)
Hf1 (gravel-dominated)	11	41.4
Hf2 (sand-dominated)	12	Rounded to 0
Cold Creek CCu _z (silt-dominated) and CCu _c (caliche)	4	Rounded to 0
Ringold RFtf	12	Rounded to 0
Ringold RFWie (Ringold E)	10	53.8

Hf1 = Hanford formation 1
Hf2 = Hanford formation 2
CCu_c = Cold Creek Caliche (carbonate-dominated unit)
CCu_z = Cold Creek silt-dominated unit
RFtf = Ringold Formation Taylor Flat Unit
RFWie = Ringold Formation Wooded Island Unit E

Table 3-13. Aqueous/Solid Partitioning Ratio (K_d in mL/g) Estimates for Low-Organic/Low-Salt/Near-Neutral Waste Chemistry for Each Hydrostratigraphic Unit. (2 Pages)

Analyte	Hf2 and RFtf (< 2 mm)		Hf1 (41.4% of Gravel)	RFWie (53.8% of Gravel)	CCu _z (silt-dominated)		CCu _c (carbonate-dominated)	
	Best Estimate	Ref ^a	Gravel corrected values	Gravel corrected values	Best Estimate	Ref*	Best Estimate	Ref*
²²⁷ Ac	300	4	300	4	300	1	300	1
³ H	0	1	0	0	0	1	0	1
³⁶ Cl	0	1	0	0	0	1	0	1
⁹⁹ Tc(VII)	0	1	0	0	0	1	0	1
¹²⁹ I	0.2	1	0.1	0.1	0.2	1	0.2	1
¹⁴ C	0.5	2	0.3	0.2	0.8	2	1.6	2
⁶⁰ Co(II,III)	10	1	5.9	4.6	10	1	15	1
U(VI), all isotopes	0.8	1	0.5	0.4	1.5	1	4	1
²³⁷ Np(V) (assumed same for ²³¹ Pa)	10	1	5.9	4.6	20	1	10	1
⁷⁹ Se(VI,IV)	5	1	2.9	2.3	5	1	5	1
²²⁶ Ra(II) and ²²⁸ Ra(II)	20	1	13.6	11.7	40	1	40	1
⁹⁰ Sr	20	1	13.6	11.7	40	1	40	1
¹²⁶ Sn(IV), all isotopes	50	1	34.1	29.3	100	1	50	1
⁶³ Ni, all isotopes	300	1	204.4	175.7	300	1	300	1
²⁴¹ Am, all isotopes	300	1	204.4	175.7	300	1	150	1
Eu(III), all	300	1	204.4	175.7	300	1	150	1

Table 3-13. Aqueous/Solid Partitioning Ratio (K_d in mL/g) Estimates for Low-Organic/Low-Salt/Near-Neutral Waste Chemistry for Each Hydrostratigraphic Unit. (2 Pages)

Analyte	Hf2 and Rf _{tf} (< 2 mm)		Hf1 (41.4% of Gravel)	RF _{wie} (53.8% of Gravel)	CCu _z (silt-dominated)		CCu _c (carbonate-dominated)	
	Best Estimate	Ref ^a	Gravel corrected values	Gravel corrected values	Best Estimate	Ref ^a	Best Estimate	Ref ^a
isotopes								
Pu, all isotopes	600	1	408.7	351.4	600	1	300	1
¹³⁷ Cs	2000	1	1362.4	1171.5	2000	1	2000	1
^{108m} Ag, all isotopes	400	3 Not specific for sand (soil/water values)	272.5	234.3	400	6	400	6
Nb, all isotopes	0	4	0	0	0	6	0	6
^{113m} Cd	300	5 Not specific for sand (soil/water value for 7<pH<8)	204.4	175.7	300	6	300	6
Th, all isotopes	1000	4	681.2	585.7	1000	6	1000	6
Cm, all isotopes	300	4	204.4	175.7	300	6	300	6
⁹³ Zr	1000	4	681.2	585.7	1000	6	1000	6
¹⁵¹ Sm	300	Assumed equivalent to Eu	204.4	175.7	300	6	300	6
⁹³ Mo	0	No relevant information	0	0	0	6	0	6
⁴⁰ K	0	No relevant information	0	0	0	6	0	6
²²² Rn	0	No relevant information	0	0	0	6	0	6

^a References:
 1: PNNL-17154
 2: INEEL/EXT-04-01793; Plummer et al. (2004)
 3: EPA/600/R-05/074
 4: PNNL-16663
 5: EPA-402-R-99-004B
 6: Same value as Hf2 (no relevant information)

3.4.1.8 Saturated Zone Flow and Transport Parameters. The flow and transport parameters needed for unconfined aquifer calculations are saturated hydraulic conductivity, specific storage, effective porosity, hydraulic gradient, depth to water table, and dispersivities. These parameters for the ERDF site are given in Table 3-14.

Table 3-14. ERDF Unconfined Aquifer Flow and Transport Properties (WCH-515).

Property	ERDF
Horizontal saturated hydraulic conductivity (m/day)	5
Ratio of vertical to horizontal saturated hydraulic conductivity	0.1
Specific storage (1/m)	1.32E-04
Effective porosity (dimensionless)	0.138 (Ringold)
Hydraulic gradient (m/m)	0.0015
Depth to water table (m)	90
Longitudinal macrodispersivity (m)	10.5
Longitudinal to transverse macrodispersivity ratio	10

Estimates of hydraulic properties are based on the Central Plateau groundwater model calibration reported in CP-47631, *Model Package Report: Central Plateau Groundwater Model Version 3.3*, and the work of Spang and Newcomer (PNNL-19491, *Slug Test Characterization Results for Multi-Test/Depth Intervals Conducted During the Drilling of CERCLA Operable Unit OU ZP-1 Wells 299-W11-43, 299-W15-50, and 299-W18-16*; PNNL-19482, *Slug Test Characterization Results for Multi-Test/Depth Intervals Conducted During the Drilling of CERCLA Operable Unit OU UP-1 Wells 299-W19-48, 699-30-66, and 699-36-70B*) that summarized results for a series of slug tests for wells located west and south of the ERDF site.

The hydraulic gradient estimate is based on the Central Plateau groundwater model (CP-47631, *Model Package Report: Central Plateau Groundwater Model Version 3.3*) estimates of future conditions at the Hanford Site. No appreciable change in hydraulic gradient is expected to occur after 100 years, once the remedial actions in the nearby operable units are completed and the water table is at or near steady state. It is expected that by the time the contaminants are released from ERDF and reach the water table, several hundred years would have passed and the water table would be at a steady-state condition. A single value of hydraulic gradient is chosen as the water table is expected to remain within Ringold Unit E. Anisotropy in saturated hydraulic conductivity, defined here as the ratio of vertical to horizontal hydraulic conductivity, for Ringold Unit E has been estimated from pumping tests, which indicate values ranging from 0.01 to 0.1 (PNNL-10886, *Development of a Three-Dimensional Ground-Water Model of the Hanford Site Unconfined Aquifer System: FY 1995 Status Report*) and 0.015 to 0.5 (DOE/RL-2007-28) for post-year 2000 testing. On the other hand, in the Central Plateau model, a vertical anisotropy of 0.1 was considered (CP-47631). This value was consistent with the previous modeling analyses (e.g., PNNL-14398, *Transient Inverse Calibration of the Site-Wide groundwater Flow Model (ACM-2): FY 2003 Progress Report*, and PNNL-14753, *Groundwater Data Package for Hanford Assessments*) prior to the development of the Central Plateau groundwater model.

The longitudinal and transverse macrodispersivity estimates in the saturated zone are based on the midpoint value (mean and median) of the uniform distribution assumed for the longitudinal dispersivity (WCH-515). The minimum and maximum values of the distribution, 1 m and 20 m, respectively, represent approximately 0.1% to 2% of the length of ERDF and the distance to the point of calculation (Table 3-15). The ratio of longitudinal to transverse macrodispersivity is assumed to be 10, which is common practice, e.g., (EPA/600/R-08/058, 2008; RPP-6296, *Modeling Data Package for S-SX Field Investigation Report (FIR)*; and Mallants et al. 2000, *Dispersivity Estimates from a Tracer Experiment in a Sandy Aquifer*).

Table 3-15. Saturated Longitudinal Macrodispersivity (α_L) Distribution.

	Minimum Value	Maximum Value	Mean/Median/ Compliance Case Value
Saturated longitudinal macrodispersivity	1	20	10.5

Source: WCH-515

3.4.1.9 Groundwater Pathway Screening Analysis. The three-dimensional fate and transport modeling used to evaluate impacts to groundwater included a preliminary one-dimensional screening phase to streamline the modeling by identifying those contaminants that are sufficiently mobile to impact groundwater during the compliance and sensitivity and uncertainty analysis timeframes. This reduced the computation time required to conduct the three-dimensional modeling considerably by limiting the number of radionuclides evaluated in the model. Several factors permit and support this phased approach to the modeling, including the graded approach identified for use at the Hanford Site (DOE/RL-2011-50, *Regulatory Basis and Implementation of a Graded Approach to Evaluation of Groundwater Protection*) and EPA guidance on soil screening for CERCLA applications (EPA/540/F-95/041, *Soil Screening Guidance: Fact Sheet*). EPA guidance for screening in CERCLA applications indicates that site-specific models prepared with simplifying but conservative assumptions are appropriate tools for screening.

The screening phase uses a set of one-dimensional models to determine the maximum K_d value of contaminants starting in the ERDF that reach the water table in 1,000 and 10,000 years. The one-dimensional models represented the center of the first eight ERDF cells and the northern and southern halves of supercells 9 and 10 (Figure 3-9). According to the facility performance requirements in DOE O 435.1, *Radioactive Waste Management*, performance objectives must be met for 1,000 years, and post-closure evaluations must extend out to 10,000 years to clarify long-term impacts. Previous analyses completed for the ERDF (BHI-00169,) and similar disposal facility configurations on the Central Plateau (e.g., DOE/ORP-2005-01, *Initial Single-Shell Tank System Performance Assessment for the Hanford Site*) have shown that the indigenous conditions impose long travel times on radionuclides between the facility bottom and the water table. These conditions include the combination of low infiltration and recharge rates imposed by the engineered system, a deep vadose zone underneath the facility, and chemical reactivity between radionuclides and sediments. The results of these analyses have shown that travel times well beyond 10,000 years are imposed for many radionuclides because of their reactivity with Hanford Site sediments.

Figure 3-9. Layout of ERDF Cells and Approximate Location of One-Dimensional Profiles Used in Screening Analysis.



The geologic profiles used in the screening represent the vadose zone near the centers of the first eight cells of ERDF and the centers of the northern and southern halves of supercells 9 and 10 (Figure 3-10). The one-dimensional model construction of the 12 representative geologic profiles only allows calculation of downward movement of water and contaminants and eliminates consideration of attenuation caused by lateral spreading and migration. The vadose zone properties associated with the maximum unsaturated vertical hydraulic conductivity for each geologic unit (Table A-2 in WCH-515, *Parameter Uncertainty for the ERDF Performance Assessment Uncertainty and Sensitivity Analysis*), and the maximum net infiltration rate present during the five different simulation periods (see Table 3-5 and Table 3-16) are used for the screening phase. Note that the maximum net infiltration rate is applied regardless of its location relative to the waste in ERDF. Additional water sources are not considered because long-term recharge after barrier and liner failure is the only source of water expected to result in any significant transport of contaminant from the facility to groundwater. ERDF does not accept liquid waste, and the construction and operation of ERDF is intended to prevent uncontrolled leachate from escaping the facility.

Figure 3-10. Geologic Cross-Sections Through ERDF Cell Centerlines with One-Dimensional Profiles Used in Screening During Operation, Closure, and Post-Closure Periods Identified.

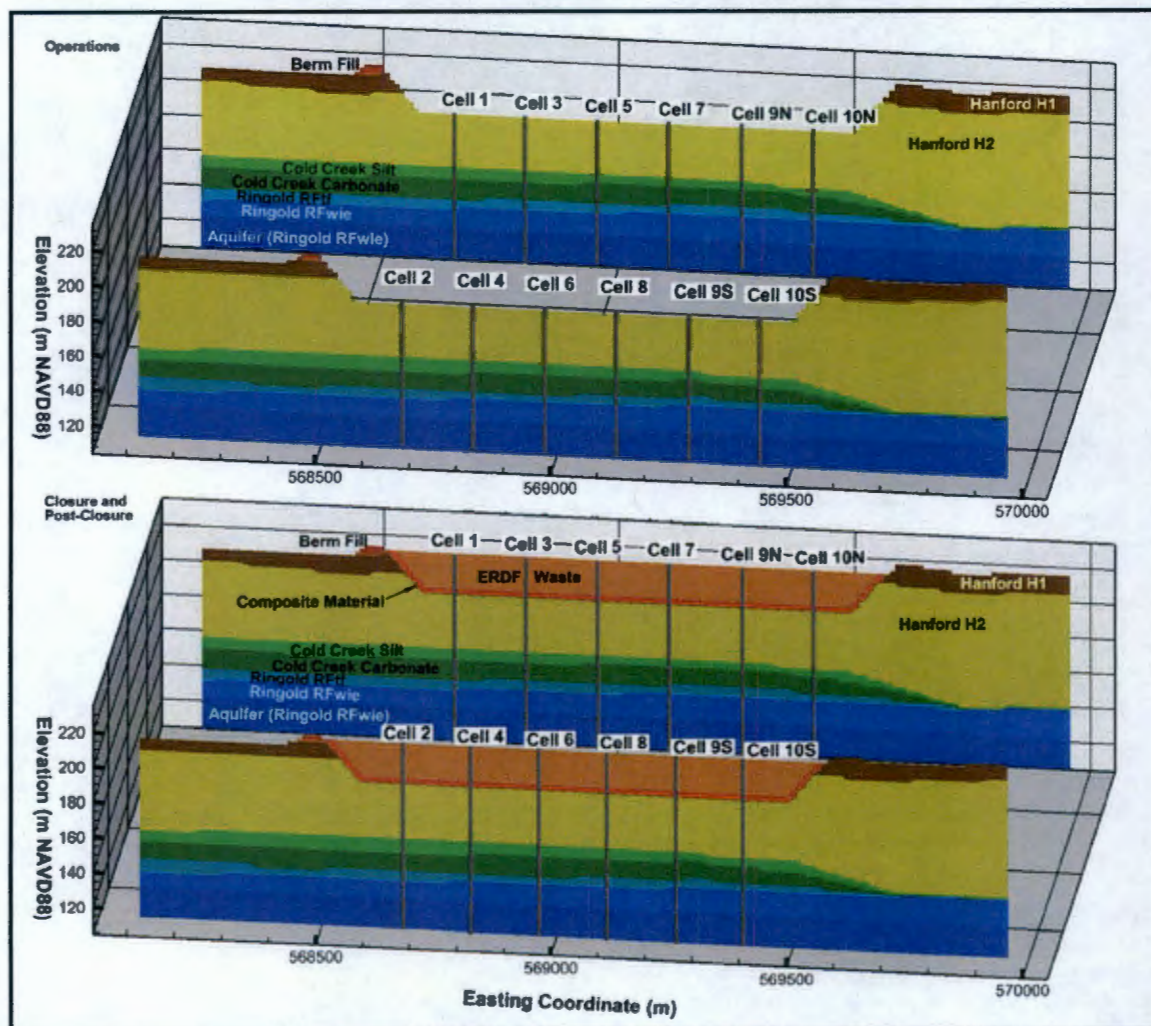


Table 3-16. Long-Term Recharge Rates Associated With the Different Modeling Periods Used in the Screening Phase.

Period	Duration	Surface Condition or Location of Maximum Recharge Rate	Screening Analysis Recharge Rate (mm/yr)
Pre-ERDF Construction	Steady state	Undisturbed natural conditions	4
ERDF Operational Period	1996 – 2035	Disturbed bare soil	90
Closure Period	2035 – 2135	Undisturbed natural conditions	4
Early Post-Closure Period	2135 – 2535	Undisturbed natural conditions	4
Late Post-Closure Period	2535 – 12035	Undisturbed natural conditions	4

The purpose of the initial screening analysis is to determine the threshold K_d value above which the three-dimensional fate and transport modeling calculations would show no impact to groundwater. The K_d threshold values are determined as a function of the modeled first non-zero concentration impact to groundwater for appropriate long-term recharge rates that can range from zero (0) mm/yr to values as large as 90 mm/yr (Table 3-16). The screening threshold is based on any non-zero impact to groundwater. This threshold represents the first indication of a groundwater impact, i.e., leading edge of a groundwater impact arrival time curve, rather than peak concentrations, which arrive later than the leading edge. The groundwater arrival time screening criteria are only focused on whether there was any non-zero impact to groundwater within the time frames considered and are applied regardless of subsequent peak concentrations.

For the purpose of the screening evaluation, the screening-phase model considers only the advective release of contaminants from the sediments. The release of contaminants is unlimited by any mechanisms that would restrain the release, such as solubility limits, metal precipitation, or contaminant sequestration from the advective flow path. All of the contamination in the source area is available for advective transport, and the release occurs according to the equilibrium K_d .

3.4.2 Atmospheric Transport Pathway

Gases and vapors could travel upward from the ERDF site through the surface barrier to the ground surface. As downward water flow also drives gases and vapors down, the air pathway is maximized while minimizing downward water movement from the ground surface through the surface barrier.

The principal mechanism by which nuclides migrate from the waste to the ground surface is gaseous diffusion. Both air pathway and radon flux calculations use a similar approach, but they are considered separately because their performance objectives differ.

The air emissions following closure are estimated using a simple model described below. Among the radionuclides contained in ERDF wastes at closure (WCH-479), four of them could potentially originate as gas from the buried wastes:

- Carbon-14 as CO_2 gas
- Hydrogen-3 as H_2 gas
- Iodine-129 as I_2 gas
- Radon-222 as radon gas (ERDF wastes are expected to contain 1.7 Ci of radium-226 and 87.5 Ci of uranium-238 that will produce radon-222 by radioactive decay).

As no information is currently available regarding their spatial distribution, it is assumed that they are uniformly distributed within the facility and mixed with soils so that gases could slowly emanate and diffuse through the porous medium. These releases are driven by the partitioning of the radionuclides among the solid fraction of the porous medium (sorbed fraction), aqueous dissolved fraction (soil/water partitioning), and the gaseous fraction (air/water partitioning) by considering the following equilibrium coefficients:

- K_d for soil/water partitioning
- Henry's law constant (K_h) for air/water partitioning.

The atmospheric transport pathway calculations are conducted in two steps (Figures 3-11 and 3-12):

1. First, gaseous fluxes emitted from a unit surface area (1 m^2) are calculated by assuming a zero concentration boundary above the surface barrier. This is conceptually equivalent to having a large enough wind speed above the ERDF such that the air parcel is renewed constantly thereby maximizing the diffusive gradient (Figure 3-11). The length of the diffusive pathway is considered to be the thickness of ERDF ($\sim 21 \text{ m}$) within which the radionuclide inventory is distributed and the 1-m thickness of clean cover (surface barrier). The thickness of the clean cover is conservatively assumed to be 1 m instead of $\sim 4.5 \text{ m}$ design thickness to maximize the diffusive flux.
2. Second, to estimate radionuclides mass flux in air along the length of ERDF, the gaseous fluxes emitted per square meter of ERDF are scaled up by the average length of ERDF (average of the length at top and bottom of ERDF) along a unit width to estimate radionuclides mass flux in air along the length of ERDF. The mass flux is uniformly distributed across the length of ERDF and then transported 100 m downgradient from ERDF (Figure 3-12) assuming advection and dispersion via wind movement to the receptor placed 100 m downwind. The air mixing height is assumed to be 2 m, which is the approximate average height of an adult. The calculated air concentrations are used for evaluating air-pathway dose and compared to the performance objective of 10 mrem/yr atmospheric release dose limit.

The gaseous forms emitted by considering equilibrium partitioning among solid, water, and air will diffuse through ERDF material into the overlying surface barrier. For simplification, the surface barrier is modeled as a porous medium having physical properties of Hf1 unit (gravel dominated). The radon-222 flux calculated during this step is compared with the performance objective of $20 \text{ pCi m}^{-2}\text{s}^{-1}$ atmospheric release flux limit.

Figure 3-11. Three-Dimensional Conceptual Model for the Radon-222 Flux Analysis and the Corresponding One-Dimensional Abstraction Model for a Unit Surface Area (1 m²) Above ERDF.

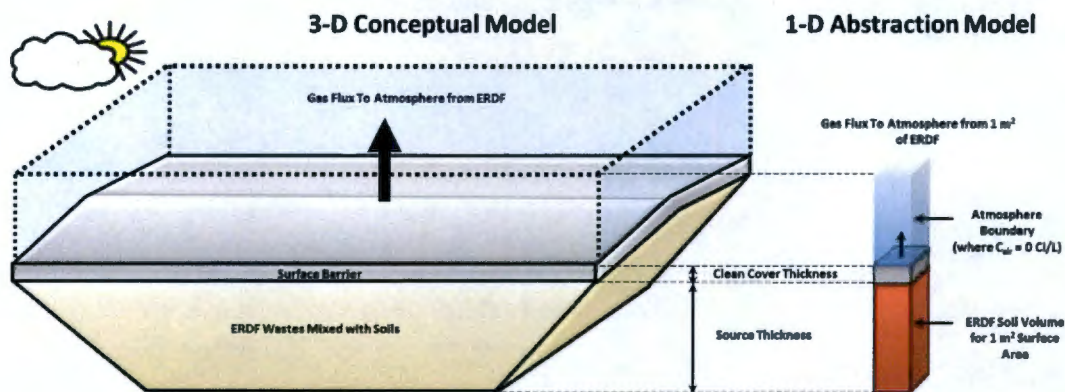
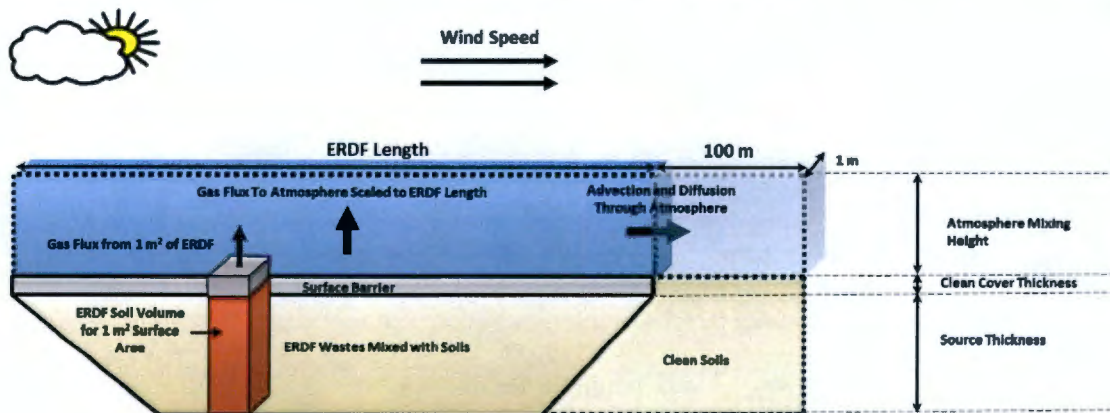


Figure 3-12. Conceptual Model for the Air-Pathway Analysis and Corresponding One-Dimensional Abstraction Model to Calculate Air Concentrations 100 m Downgradient from ERDF.



A one-dimensional model is developed to evaluate the diffusive release of gases at the ERDF surface and its subsequent transport downwind. To calculate the diffusive flux emanating at the surface of ERDF, a one-dimensional model (Figure 3-11) is developed using a finite difference network of batch-reactor cells. The verification and validation of this model is discussed in Appendix C. Following transport equation is numerically solved in order to compute the mass flux and concentration:

$$R_d \frac{\partial(\theta_a C)}{\partial t} = D_{ef} \frac{\partial^2 C}{\partial x^2} \quad \text{Eq. 3.8}$$

where:

$C(x,t)$ = the air concentration (kg/m^3) in the pore network of a given gas at the distance x (m) from the bottom of ERDF and time t (s) from ERDF closure (year 2035)

D_{ef} (m^2/s) = the effective diffusion coefficient of a given gas through the tortuous air pathway of the porous medium

R_d = the retardation coefficient of a given gas due to partitioning among different phases (air, water and solids) of the porous medium

θ_a (-) = the air content (or air-filled porosity) of the porous medium.

The diffusion coefficient for various gases of concern (CO_2 , H_2 , I_2 , and radon) through the tortuous air pathway of the porous medium is calculated as follows:

$$D_{ef} = D_0 \tau \quad \text{Eq. 3.9}$$

where:

D_{ef} (m^2/s) = the effective diffusion coefficient through the tortuous air pathway of the porous medium for a given gas

D_0 (m^2/s) = the binary diffusion coefficient of the gas of concern in the air

τ = the tortuosity of the porous medium for air pathway.

A zero concentration boundary condition is imposed above ERDF to maximize the diffusive flux of gases. This is conceptually equivalent to high wind conditions that sweep away any radionuclide mass diffusing from ERDF, thus maintaining an effectively zero concentration boundary condition. The diffusive flux from ERDF surface is calculated on a per unit area basis. A pipe pathway is conceptualized to extend along the length of ERDF (average length of 978 m is chosen based on an average of length at the top of 1,042 m and the length at the bottom of 914 m) over a unit surface area of ERDF. The diffusive fluxes are scaled by the length of ERDF and uniformly distributed in the volume of air that extends the length of ERDF with a mixing height of 2 m and width of 1 m in the first pipe pathway. A wind speed of 3.4 m/s is chosen for advective transport calculations based on the long-term annual average wind speed at the Hanford Site (see Section 2.1.2). A second pipe pathway is implemented to collect the mass flux from the first pipe and transport it 100 m downwind to the receptor location. The air

concentration calculated in the second pipe is used to evaluate ERDF performance in the air-pathway scenario. The second pipe pathway has the same cross-sectional geometry as the first pipe pathway (2 m high and 1 m wide).

Air dispersivity in each pipe pathway is calculated separately based on the length and wind conditions. In the first pipe pathway, the ERDF half-length is considered as an average transport distance, whereas for the second pipe pathway the entire 100-m distance is considered. The air dispersivity values are presented in Section 3.4.2.3.

The ai- pathway transport model is verified and validated by comparing the results to analytical solutions and other software-based model results. These are discussed in Appendix C.

3.4.2.1 Partition Coefficients. Sander (1999) and Plummer et al. (2004) provide estimates of the aqueous-to-gas partitioning Henry's law constant for the radionuclides of concern that are reported in Table 3-17. The aqueous-to-gas dimensioned values (mol atm⁻¹L⁻¹) have been converted to dimensionless gas-to-aqueous Henry's constant at 20 °C, which is the assumed temperature at ERDF, using the following equation:

$$K_h = \frac{1}{H \times R \times T} \quad \text{Eq. 3.10}$$

where:

- K_h = the gas-to-aqueous dimensionless Henry's constant at 20 °C
- H = the aqueous-to-gas Henry's constant (mol atm⁻¹L⁻¹)
- R = the ideal gas constant (0.082 atm L mol⁻¹ K⁻¹)
- T = the assumed temperature at ERDF (20 °C=293.15°K).

Table 3-17. Henry's Law Constants.

Radionuclide	Gas Form	Aqueous-to-Gas Henry's Constant	Reference	Calculated Gas-to-Aqueous Dimensionless Henry's Constant at 20 °C
C-14	CO ₂	4.5 (-)	Plummer et al. 2004	0.22
H-3	H ₂	7.80E-4 (mol atm ⁻¹ L ⁻¹)	Sander 1999	53.36
I-129	I ₂	3.10E+0 (mol atm ⁻¹ L ⁻¹)	Sander 1999	0.013
Rn-222	Rn	9.30E-3 (mol atm ⁻¹ L ⁻¹)	Sander 1999	4.47

Regarding the soil/water partition coefficient (K_d), the values assigned to the source zone (ERDF soils) and the overlying cover material (surface barrier) are those defined for the Hf1 gravely layer. These values are reported for conciseness in Table 3-18. The K_d value for radon-222 is set to zero due to lack of available information.

Table 3-18. K_d (mL/g) Selected for ERDF Soils and Cover Material (WCH-515).

Radionuclide	K_d of ERDF Soils and Clean Cover (mL/g)
^{14}C	0.3
^3H	0
^{129}I	0.1
^{222}Rn	0

NOTE: K_d of ERDF material including the surface barrier cover material is assumed to be the same as Hf1 (gravel-dominated lithology). Only compliance calculation values are presented here.

The Henry's constant for carbon-14 is derived from the meso-scale unsaturated soil column multiphase transport experiment discussed in INEEL/EXT-04-01793 and Plummer et al. (2004). As noted in Section 3.4.1.7.5, the carbon-14 K_d values for various units were based on these experimental results. In order to be consistent in deriving the parameter values for the gas-phase transport of carbon-14, the same experimental results are used. Based on matching the aqueous- and gas-phase carbon-14 profiles in the soil column an average aqueous-gas partitioning ratio is approximated to be 4.5, which translates to gas-aqueous dimensionless Henry's constant of 0.22. This value is somewhat smaller than the values reported elsewhere, for example, Sander (1999), where an equivalent gas-aqueous dimensionless Henry's constant is approximately 1.22 ($0.034 \text{ mol atm}^{-1} \text{ L}^{-1}$). Since carbon-14 in the buried waste is primarily contained in insoluble form (graphite) and would slowly leach out by the contacting water, it will first go in the dissolved phase (as bicarbonate ion) and then interact with the solid (porous medium) phase and gas phase. Because carbon-14 will be made available as a bicarbonate ion and because the multiphase transport experiments were conducted by injecting carbon-14 labeled bicarbonate solution in an unsaturated system consisting of mineral phases similar to the ERDF bulk soil, the gas-aqueous partitioning result from this study is considered the best estimate.

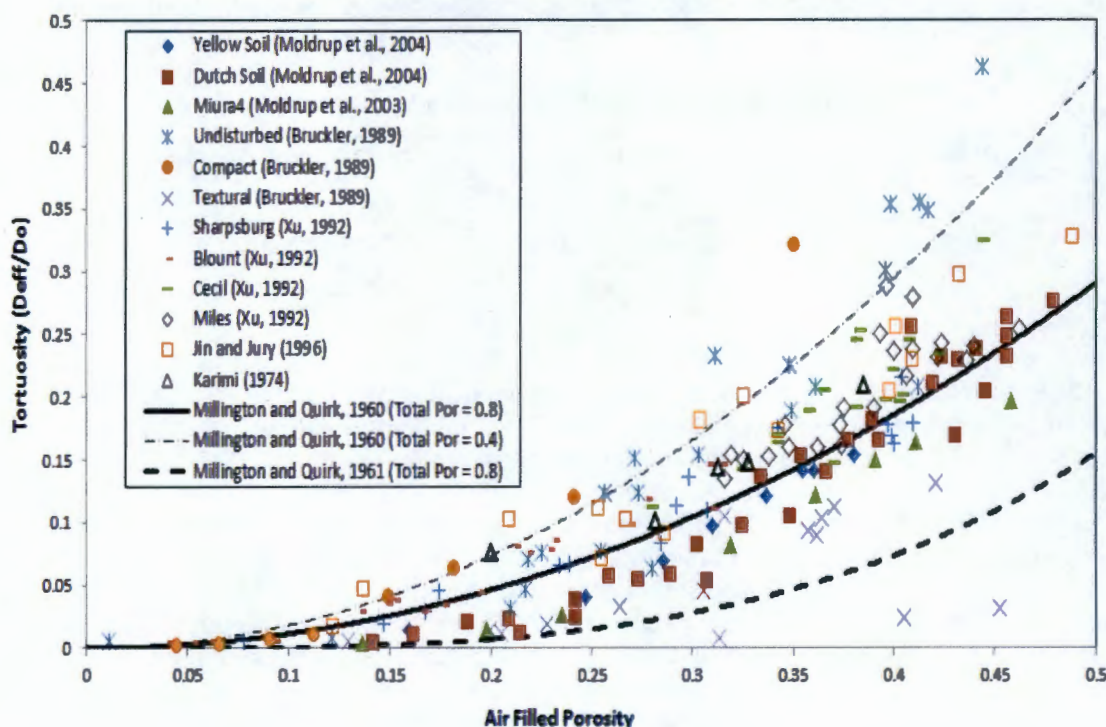
3.4.2.2 Diffusion Coefficients and Tortuosity. The binary diffusion coefficients of the different gases of concern in air have been calculated using the EPA methodology (EPA 2010) considering an atmospheric pressure of 1 atm and a temperature of 20 °C (assumed temperature for ERDF). The calculated diffusion coefficients are reported in Table 3-19 together with the gas boiling point estimates used in the calculations. For radon, another reference has been considered (*Radon and Its Decay Products in Indoor Air* [Nazaroff and Nero 1988]) as EPA (2010) did not consider diffusion coefficient calculation for this gas.

Table 3-19. Diffusion Coefficients in Air at 20 °C and 1 Atm.

Radionuclide	Gas Form	Diffusion Coefficient in Air (cm^2s^{-1})	Reference	Boiling Point (°C) Used in EPA Calculations (Haynes and Lide 2011)
^{14}C	CO_2	0.160	EPA 2010 (average method)	-78.55
^3H	H_2	0.819	EPA 2010 (average method)	-252.76
^{129}I	I_2	0.0897	EPA 2010 (FSG/LaBas method)	184.45
^{222}Rn	Rn	0.11	Nazaroff and Nero (1988) cited in Yu et al. (2001)	(-)

Liu et al. (2006) compiled data sets and presented the experimentally determined gas tortuosity (ratio of the effective diffusion coefficient in soil (D_{ef}) to that in free air (D_0)) as a function of the air-filled porosity (air content) for various soil types. They also provided the best fit lines and bounding estimates based on models presented by Millington and Quirk (1960, 1961). The results from Liu et al. (2006) are reproduced in Figure 3-12.

Figure 3-12. Comparison of Measured Tortuosity (i.e., Ratio of Diffusion Coefficient in Soil (D_{ef}) to that in Free Air (D_0)) with Fitted Tortuosity Models Given by Liu et al. (2006).



Using the Millington and Quirk (1960) gas tortuosity equation below (Eq. 3.11), Liu et al. (2006) found the best fit to the experimental data set by varying the value of the total porosity in the denominator and finally selecting a value of 0.8:

$$\tau = \frac{\theta_a^2}{\phi^{2/3}} = \frac{(\phi - \theta_w)^2}{\phi^{2/3}} \quad \text{Eq. 3.11}$$

where:

- τ = the tortuosity
- θ_a = the air content (or air-filled porosity) of the porous medium
- θ_w = the water content (or water-filled porosity) of the porous medium

- ϕ = the total porosity (measured)
 Φ = fitted total porosity; set equal to 0.8 for best fit (Liu et al. 2006).

Equation 3.11 is used for the ERDF compliance calculation for the air pathway. Note that Liu et al. (2006) made an error in referencing Millington and Quirk papers. They reversed the reference of a 1960 paper with a 1961 paper in the text and in the figure; the error is now corrected.

Parameters used in the calculations are summarized in Table 3-20. ERDF wastes mixed with soils have been assumed to have the same porosity as the Hf1 formation (Hanford gravelly layer). Note that the tortuosity varies as a function of time due to varying moisture content.

Table 3-20. Atmospheric Pathway Modeling Parameters.

Parameter	Value	Origin of the Value
ϕ	0.2126	Compliance value for Hf1
θ_w	Varies as a function of time	Model-calculated value
θ_a	Calculated	Calculated from θ_w and ϕ

3.4.2.3 Plume Dispersivity in Air. Horizontal dispersivities of the plume in air are required to calculate air concentrations downwind from ERDF in order to simulate the effect of dispersion due to wind flow over a horizontal one-dimensional pathway.

The CAP88 (Ver. 3.0) User Guide (EPA 2007) provides equations to calculate horizontal dispersion coefficients (σ_y) for dispersion calculations. In these equations, the dispersion coefficient is a function of the downwind distance x from a point source for different atmospheric turbulence classes under open-country conditions. These atmospheric turbulence classes are categorized according to the Pasquill classification (Pasquill 1961), which defines six stability classes named A, B, C, D, E, and F, with class A being the most turbulent and class F the most stable or least turbulent class. According to the wind speeds observed above the Hanford Site (Table 3-21), which usually ranges from 2.7 m/s during winter to 4 m/s during summer (monthly average), the most conservative Pasquill class for a moderate solar radiation above ERDF is Class C (i.e., "slightly unstable class"). The following equation is used to calculate the horizontal dispersion coefficient for Class C (EPA 2007):

$$\sigma_y = 0.11 x (1 + 0.0001x)^{-3/4} \quad \text{Eq. 3.12}$$

where σ_y is the horizontal dispersion coefficient (m) for Pasquill class C and x is the downwind distance (m) from the point source.

The dispersion coefficient estimates for air transport along the length of ERDF are calculated using the half length of ERDF (average distance of travel for gas emanating from ERDF and moving downwind) while for the transport 100 m downwind to the receptor the downwind distance is based on 100 m. The calculated values are reported in Table 3-22.

Table 3-21. Wind Speed Observed Above the Hanford Site (see Chapter 2.0) and Corresponding Pasquill Class for a Moderate Solar Radiation (Pasquill 1961).

Season	Wind Speed (monthly average from Chapter 2.0)	Pasquill Class for a Moderate Solar Radiation
Winter	2.7 to 3.1 m/s	B
Summer	3.6 to 4 m/s	B-C
Summertime drainage winds	13 m/s	D

Table 3-22. Estimates of Horizontal Dispersion Coefficient in Air (m) Obtained with CAP88 User's Guide Equation for Pasquill Class C (EPA 2007).

Dispersion Pathway	x	σ_y
Above ERDF, half the distance between ERDF edges	457 m	49.16 m
From ERDF edge to 100 m downwind	100 m	10.95 m

3.5 RADON ANALYSIS

The modeling approach for calculating radon flux is described in Section 3.4.2 and illustrated in Figure 3-11. A one-dimensional transport model is used to calculate diffusive flux of radon along with other volatile radionuclides. In order to maximize the upward diffusive flux from surface barrier to air no downward water flux from recharge is considered in the surface barrier (although water movement below the surface barrier is modeled).

The radon-222 emanation rate from the ground surface is estimated using the diffusion equation (Equation 3.8). This rate depends on the thickness of the waste, the depth of the soil cover, the assumed diffusivity of radon gas through the waste and soil cover, and the concentration of radium-226 in the waste. The radium-226 (half-life of 1,599 years) produces radon-222 (half-life of 3.82 days) by radioactive decay. The radium-226 is produced by the radioactive decay of, uranium-238 (half-life of 4.47E09 years), uranium-234 (half-life of 2.45E05 years), plutonium-238 (half-life of 87.7 years), and thorium-230 (half-life of 7.56E04 years). About 1.7 Ci of radium-226 is estimated in the initial inventory at the time of closure (Table 3-2), which is expected to contribute to almost all of the radon-222 flux at early times. Once the initial inventory of radium-226 is depleted, it will be generated slowly primarily from decay of uranium-238 and uranium-234.

3.6 BIOTIC PATHWAY

Construction and operations of the ERDF can potentially damage the natural environment at the facility proper and in an area around the facility. At closure, an engineered cover will be placed over the waste that is intended to mimic natural surface conditions to the extent possible. That is, natural vegetation will be planted on a soil layer intended to support growth of a stable ecology system that is the same as the surrounding conditions. The ambient ecological system is not totally pristine because colonization and agricultural practices have introduced additional

nonnative species that will likely remain at the Hanford Site. Ecological conditions at the Hanford Site have been studied extensively since the start of Hanford Site operations and numerous documents that describe and quantify local conditions have been completed. The most recent compilation (DOE/RL-2007-50, *Central Plateau Ecological Risk Assessment Data Package Report*) describes recent information and includes copies of significant previous summaries (e.g., DOE/RL-2001-54, *Ecological Evaluation of the Hanford 200 Areas-Phase 1: Compilation of Existing 200 Areas Ecological Data*). The descriptions provided below are taken from these documents and others.

The Hanford Site is a shrub-steppe ecosystem that is dominated by a shrub overstory with a grass understory. Because the climate is semi-arid, the dominant large shrub is big sagebrush (*Artemisia tridentata*) and the main grasses are Sandberg's bluegrass (*Poa Sandbergii*) and bluebunch wheatgrass (*Pseudoregneria spicata*). A ubiquitous nonnative species at the Hanford Site is cheatgrass, which often makes up a large fraction of the grasses. Less abundant plant species on the Central Plateau include threetip sagebrush, bitterbrush, gray rabbitbrush, spiny Hopsage, Indian ricegrass, and prairie June grass. Altogether, over 100 species of plants have been observed in the 200 Area on the Central Plateau. A survey of the ERDF site made prior to its construction showed the presence of big sagebrush and an understory of which approximately 90% was a mix of cheatgrass and Sandberg's bluegrass (PNNL-14233, *Biological Review of the Hanford Solid Waste EIS – Borrow Area C [600 Area], Stockpile and Conveyance Road Area [600 Area], Environmental Restoration Disposal Facility [ERDF] [600 Area], Central Waste Complex [CWC] Expansion [200 West], 218-W-5 Expansion Area [200 West], New Waste Processing Facility [200 West], Undeveloped Portion of 218-W-4C [200 West], Western Half & Northeastern Corner of 218-W-6 [200 West], Disposal Facility Near Plutonium-Uranium Extraction [PUREX] Facility [200 East], ECR #2002-600-012b*). The remaining 10% of the understory was a mix of cheatgrass and needle-and-thread grass.

Range fires can be expected to occur every few years. Observation has shown that regrowth vegetation is initially dominated by nonnative species, particularly cheatgrass and, to a lesser extent, Russian thistle. Native grasses and shrubs take longer to reestablish, particularly the big sagebrush which must regenerate from seed. However, repopulation with sagebrush and other smaller shrubs such as gray rabbitbrush, which reestablishes itself more easily than big sagebrush, eventually happens because these species are abundant in undisturbed areas that have been burned many times.

A wide variety of mammals (about 40 species), birds (about 100 species), reptiles (about 10 species), and insects (hundreds) have been observed on the Central Plateau. Large mammals include elk (*Cervus elaphus*) and mule deer (*Odocoileus hemionus*). Smaller species include badgers (*Taxidea taxus*), coyotes (*Canis latrans*), blacktail jackrabbits (*Lepus californicus*), Townsend ground squirrels (*Spermophilus townsendii*), pocket mice (*Perognathus parvus*), and deer mice (*Peromyscus maniculatus*). Of these the Great Basin pocket mice are the most abundant. The mammal most likely to burrow in the soil is the badger that can dig several feet down in search of food (e.g., mice and squirrels).

Birds commonly found on the Central Plateau include passerine varieties, raptors, game birds, and nesting birds. Common passerine birds are starlings (*Sturnus vulgaris*), meadowlarks (*Sturnella neglecta*), black-billed magpies (*Pica pica*), and ravens (*Corvus corax*). Common raptors are the American kestrels (*Falco sparverius*) and redtailed hawks (*Buteo jamaicensis*). Game birds include the mourning dove (*Zenaidura macroura*), California quail (*Callipepla californica*), and Chukar partridge (*Alectoris chukar*). Nesting birds include burrowing owls

(*Athene cunicularia*), sage sparrows (*Amphispiza belli*), loggerhead shrikes (*Lanius ludovicianus*), and long-billed curlews (*Numenius americanus*).

Abundant reptiles include gopher snakes (*Pituophis melanoleucus*) and sideblotched lizards (*Uta stansburiana*). Other less abundant species include sagebrush lizards (*Sceloporus graciosus*), horned toads (*Phrynosoma douglassii*), western spadefoot toads (*Scaphiopus intermontana*), yellow-bellied racers (*Coluber constrictor*), Pacific rattlesnakes (*Crotalus viridis*), and striped whipsnakes (*Masticophis taeniatus*). Amphibians are not expected at the ERDF location. Common groups of insects include several species of darkling beetles, grasshoppers, butterflies, bees, and ants. Of these, the harvester ants, darkling beetles, solitary bees, and pocket gophers burrow below ground surface (WMP-20570, *Central Plateau Terrestrial Ecological Risk Assessment Data Quality Objectives Summary Report-Phase I*).

The most likely means of plant and animal contact with buried waste is root penetration and burrowing habits. A summary of site-specific and generic data quantifying penetration depths for biota at the Hanford Site and similar semi-arid conditions is provided in WMP-20570. While most studies of biota at the Hanford Site catalogue biota populations, record surface expression of biota, and measure contaminant uptake, a few studies have been completed to quantify penetration depths (PNL-5247, *Rooting Depth and Distributions of Deep-Rooted Plants in the 200 Area Control Zone of the Hanford Site*; RHO-SA-211, "Invasion of Radioactive Waste Burial Sites by the Great Basin Pocket Mouse (*Perognathus parvus*)"; DOE/RL-2001-54). Measured maximum penetration depths at the Hanford Site are summarized in Table 3-23.

Table 3-23. Maximum Penetration Depths for Biota at the Hanford Site.
(Source: WMP-20570, Table 2-1).

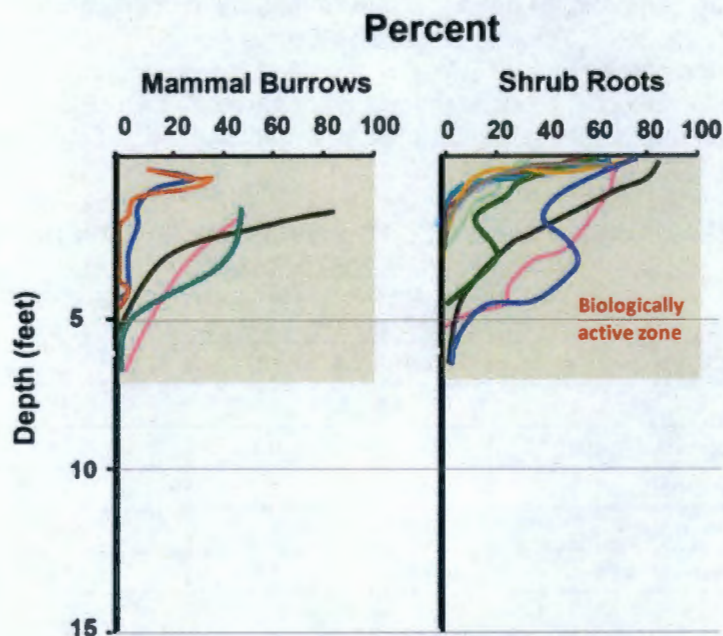
Species	Maximum Depth		Reference
	(cm)	(ft)	
Plants			
Antelope bitterbrush	300	9.8	PNL-5247
Big sagebrush	200	6.6	PNL-5247
Spiny hopsage	195	6.5	PNL-5247
Russian thistle	172	5.6	PNL-5247
Mammals			
Great Basin pocket mouse	200	6.6	RHO-SA-211
Soil Biota			
Harvester ants	270	8.8	PNL-2774

Two primary observations were made. First, the maximum likely depth is about 3 m (10 ft) below ground surface (bgs) for both plant and animal behavior. Second, the frequency of roots and burrow depths are heavily skewed towards the surface (<1.5 m [5 ft] bgs), with only a few percent of penetration events reaching maximum depth. Shallow soil sampling across Gable Mountain Pond and B Pond, two dried high-volume liquid discharge sites (DOE/RL-2001-54), yielded a large assortment of invertebrates, which with the exception of the harvester ant and solitary bees constructing burrows within a foot of the surface (several feet and 0.6 to 0.9 cm [2 to 3 ft], respectively). Among mammals, badger burrows have been observed on a

few occasions. One burrow in particular was found 1.2 m (4 ft) below a soil barrier (WHC-SA-1252-S, *Mammal Occurrence and Exclusion at the Hanford Site*). Offsite, badger burrows as deep as 3 m (10 ft) have been reported (*The Mammals of North America* [Hall 1981]).

Given the limited number of data collected at the Hanford Site, it is useful to compare these data with data collected at other semi-arid sites in the western United States. A collection of other site data is provided in INEEL/EXT-01-00273, *Biological Data to Support Operable Unit 7-13/14 Modeling of Plant and Animal Intrusion at Buried Waste Sites*, and WMP-20570 (Appendix F). Badgers, squirrels, and mice are found at several sites with burrow penetration depths similar to the Hanford Site (Figure 3-13). Plant data from other northern desert sites in Idaho and Wyoming include a common set of species (e.g., sagebrush and various grasses) with similar penetration depth profiles (Figure 3-13).

Figure 3-13. Burrow and Root Density with Depth in Various Northwestern Semiarid Sites (after Figure 2-3 of WMP-20570).



A modified RCRA-compliant closure cover will be placed above ERDF that would be about 4.5 m in thickness (Figure 2-34). This cover will be placed above the interim compacted soil cover of approximately 0.6 m. Thus, the minimum depth of intrusion needed to access the waste will be more than 5 m, which is most likely below the biologically active zone. The upper 0.9 m of the soil cover system is composed of an admixture of silt and gravels. This layer is intended to both reduce infiltration through the cover and enhance the resistance of the cover to burrowing animals and long-term wind erosion. In addition, a geocomposite drainage layer (with a HDPE geomembrane liner) and 0.6 m of compacted clay admix will be present at a depth of approximately 4 m, which will further enhance resistance to burrowing animals and plants. Given the features of the surface barrier above the ERDF, the likelihood of a biotic pathway to access the radionuclides from the waste is extremely small. As a result, the dose impact from this pathway is not considered in further analyses.

3.7 DOSE ANALYSIS

The method for estimating doses from the radionuclide transport calculations discussed in previous sections is provided. The dose calculation method for the all-pathway farmer scenario is discussed first where contaminated groundwater is the pathway of contamination. This is followed by the air-pathway dose calculation methodology. Additional details are presented in the supporting data package, WCH-478.

3.7.1 Groundwater Pathway Dose Analysis

For the all-pathways farmer scenario, the individual who receives dose is a single family farmer who resides near the disposal facility and draws contaminated water from a well downgradient of the ERDF. The exposed individual is an adult and is assumed to use the water to drink, irrigate crops, and water livestock. The DOE guidance for this exposed individual assumes that the waste facility is a newly developed disposal facility and no contamination is present outside the facility at closure. The exposed individual is assumed to receive dose by the following exposure pathways as shown in Figure 3-1:

- Ingestion of water
- Ingestion of garden vegetables grown on the farm
- Ingestion of beef raised on the farm
- Ingestion of milk from cows raised on fodder grown on the farm
- Ingestion of eggs from poultry fed with fodder grown on the farm
- Ingestion of poultry fed with fodder grown on the farm
- Ingestion of contaminated soil
- Inhalation of contaminated soil in the air
- External exposure to radiation.

Equations and calculations methodology for each pathway are given below. The input parameter values are summarized in Table 3-24. Note that unit conversion factors must be applied to these equations to make sure that the units are consistent. The bioconcentration factors (transfer coefficients) are provided on an element basis in Table 3-27, and the dose conversion factors on a radionuclide basis are provided in Table 3-28 (see WCH-478 for additional details).

Contamination of Soil Due to Irrigation with Contaminated Water:

When contaminated water is applied to soil, the contaminants are held in the soil by two mechanisms: sorption onto soil particles, and dissolved contaminants held in the water content in the soil. Concentration sorbed on the soil particles is given by

$$C_s = C_w \times K_d \quad \text{Eq. 3.13}$$

where:

- C_s = concentration in the soil (pCi/g)
- C_w = concentration in the applied water (pCi/L)
- K_d = soil-water partition coefficient for the given soil and radionuclide (mL/g).

Total radionuclide concentration in the soil (i.e., sorbed plus dissolved) is given by

$$C_{stot} = C_w \times \left(K_d + \frac{\theta_w + \theta_a \times H}{\rho_s} \right) \approx C_w \times \left(K_d + \frac{\theta_w}{\rho_s} \right) \quad \text{Eq. 3.14}$$

where:

- C_{stot} = total radionuclide concentration in soil (pCi/g)
- θ_w = soil volumetric water content [(mL water)/(cm³ soil)]
- θ_a = air-filled soil porosity [(mL air)/(cm³ soil)]
- H = Henry's Law constant (dimensionless)
- ρ_s = soil dry bulk density (g/cm³).

The volatile radionuclide inventory in the contaminated groundwater used for irrigation is likely to be negligibly small, so $\theta_a \times H$ can be ignored and the approximation is valid.

The above equations are used whenever C_s and C_{stot} are used in the remainder of this section.

Ingestion of Water:

The following equation is used to calculate dose due to ingestion of water.

$$D_w = C_w \times IR \times EF \times DCF_{ing} \quad \text{Eq. 3.15}$$

where:

- D_w = dose due to drinking contaminated water (mrem/yr)
- C_w = radionuclide concentration in water (pCi/L)
- IR = ingestion rate of water (L/day)
- EF = exposure frequency to drinking contaminated water (days/yr)
- DCF_{ing} = dose conversion factor for ingestion (mrem/pCi).

Ingestion of Garden Vegetables:

The following equations are used to calculate the dose due to ingestion of vegetables (including fruits).

Concentration in the crop ingested:

$$C_c = C_{stot} \times (B_v + B'_v) \quad \text{Eq. 3.16}$$

where:

$$\begin{aligned}
 C_c &= \text{radionuclide concentration in the crop (pCi/g)} \\
 C_{stot} &= \text{total radionuclide concentration in the surface soil layer (pCi/g)} \\
 B_v &= \text{crop-soil bioconcentration factor through uptake } \left(\frac{\frac{\text{pCi}}{\text{kg fresh weight of crop}}}{\frac{\text{pCi}}{\text{kg dry weight of soil}}} \right) \\
 B'_v &= \text{bioconcentration factor representing the resuspension/soil adhesion} \\
 &\quad \text{processes } \left(\left(\frac{\frac{\text{pCi}}{\text{kg fresh weight of crop}}}{\frac{\text{pCi}}{\text{kg dry weight of soil}}} \right) \right)
 \end{aligned}$$

Dose to the exposed individual:

$$D_c = C_c \times IR \times F_v \times DCF_{ing} \quad \text{Eq. 3.17}$$

where:

$$\begin{aligned}
 D_c &= \text{dose due to eating the vegetables (mrem/yr)} \\
 IR &= \text{ingestion rate of garden vegetables (kg/yr)} \\
 F_v &= \text{fraction of vegetables produced locally (dimensionless)} \\
 DCF_{ing} &= \text{dose conversion factor for ingestion (mrem/pCi)}.
 \end{aligned}$$

Ingestion of Beef:

Concentration in fodder (this equation applies to all of the following pathways that include fodder):

$$C_{fodder} = C_{stot} \times (B_p + B'_p \times d_f) \quad \text{Eq. 3.18}$$

where:

$$\begin{aligned}
 C_{fodder} &= \text{the radionuclide concentration in the feed } \left(\frac{\text{pCi}}{\text{g}} \right) \\
 C_{stot} &= \text{the total radionuclide concentration in the surface soil layer } \left(\frac{\text{pCi}}{\text{g}} \right) \\
 B_p &= \text{the crop-soil bioconcentration factor through uptake } \left(\frac{\frac{\text{pCi}}{\text{kg fresh weight of fodder}}}{\frac{\text{pCi}}{\text{kg dry weight of soil}}} \right) \\
 B'_p &= \text{the bioconcentration factor representing the resuspension - soil adhesion} \\
 &\quad \text{processes } \left(\left(\frac{\frac{\text{pCi}}{\text{kg dry weight of fodder}}}{\frac{\text{pCi}}{\text{kg dry weight of soil}}} \right) \right) \\
 d_f &= \text{dry-to-wet weight basis conversion factor for fodder } \left(\frac{\text{dry weight of fodder}}{\text{wet weight of fodder}} \right).
 \end{aligned}$$

Concentration in beef:

$$C_b = (C_w \times IR_w + C_{fodder} \times IR_{fodder} + C_{stoc} \times IR_s) \times BCF_{beef} \quad \text{Eq. 3.19}$$

where:

- C_b = radionuclide concentration in beef (pCi/kg)
- C_w = radionuclide concentration in water (pCi/L)
- IR_w = ingestion rate of water by the animal (L/day)
- IR_{fodder} = ingestion rate of fodder by the animal (kg/day)
- IR_s = ingestion rate of soil by the animal (kg/day)
- BCF_{beef} = bioconcentration factor of radionuclides in beef (day/L).

Dose due to ingestion of beef:

$$D_b = C_b \times IR \times F_a \times DCF_{ing} \quad \text{Eq. 3.20}$$

where:

- D_b = dose due to ingestion of beef (mrem/yr)
- IR = ingestion rate of beef (kg/yr)
- F_a = fraction of beef that is locally produced (dimensionless)
- DCF_{ing} = dose conversion factor for ingestion (mrem/pCi).

Ingestion of Milk:

Concentration in milk:

$$C_m = (C_w \times IR_w + C_{fodder} \times IR_{fodder} + C_{stoc} \times IR_s) \times BCF_{milk} \quad \text{Eq. 3.21}$$

where:

- C_b = radionuclide concentration in milk (pCi/L)
- C_w = radionuclide concentration in water (pCi/L)
- IR_w = ingestion rate of water by the animal (L/day)
- IR_{fodder} = ingestion rate of fodder by the animal (kg/day)
- IR_s = ingestion rate of soil by the animal (kg/day)
- BCF_{milk} = bioconcentration factor of radionuclides in milk (day/L).

Dose due to ingestion of milk:

$$D_m = C_m \times IR \times F_a \times DCF_{ing} \quad \text{Eq. 3.22}$$

where:

- D_m = dose due to drinking milk (mrem/yr)
 IR = milk ingestion rate for the exposed individual (L/yr)
 F_a = fraction of locally produced milk consumed (dimensionless)
 DCF_{ing} = dose conversion factor for ingestion (mrem/pCi).

Ingestion of Eggs:

Concentration in eggs:

$$C_e = (C_w \times IR_w + C_{fodder} \times IR_{fodder} + C_{stot} \times IR_s) \times BCF_{egg} \quad \text{Eq. 3.23}$$

where:

- C_e = concentration in eggs (pCi/kg)
 C_w = radionuclide concentration in water (pCi/L)
 IR_w = ingestion rate of water by the animal (L/day)
 IR_{fodder} = ingestion rate of fodder by the animal (kg/day)
 IR_s = ingestion rate of soil by the animal (kg/day)
 BCF_{egg} = bioconcentration factor of radionuclides in eggs (day/L).

Dose due to ingestion of eggs:

$$D_e = C_e \times IR \times F_a \times DCF_{ing} \quad \text{Eq. 3.24}$$

where:

- D_e = dose due to eating contaminated eggs (mrem/yr)
 IR = ingestion rate of eggs for the exposed individual (kg/yr)
 F_a = fraction of eggs consumed that are locally produced (dimensionless)
 DCF_{ing} = dose conversion factor for ingestion (mrem/pCi).

Ingestion of Poultry:

Concentration in poultry:

$$C_p = (C_w \times IR_w + C_{fodder} \times IR_{fodder} + C_{stot} \times IR_s) \times BCF_{poultry} \quad \text{Eq. 3.25}$$

where:

- C_p = concentration in poultry (pCi/kg)
 C_w = radionuclide concentration in water (pCi/L)
 IR_w = ingestion rate of water by the animal (L/day)
 IR_{fodder} = ingestion rate of fodder by the animal (kg/day)

IR_p = ingestion rate of soil by the animal (kg/day)
 $BCF_{poultry}$ = bioconcentration factor of radionuclides in poultry (day/L).

Dose due to ingestion of poultry:

$$D_p = C_p \times IR \times F_a \times DCF_{ing} \quad \text{Eq. 3.26}$$

where:

D_p = dose due to ingestion of poultry (mrem/yr)
 IR = ingestion rate of poultry (kg/yr)
 F_a = fraction of poultry eaten that is locally produced (dimensionless)
 DCF_{ing} = dose conversion factor for ingestion (mrem/pCi).

Ingestion of Soil:

Dose due to ingestion of soil:

$$D_s = C_s \times IR \times EF \times DCF_{ing} \quad \text{Eq. 3.27}$$

where:

D_s = dose due to ingestion of soil (mrem/yr)
 IR = ingestion rate of soil (mg/day)
 EF = exposure frequency of soil ingestion (days/yr)
 DCF_{ing} = dose conversion factor for ingestion (mrem/pCi).

Inhalation of Contaminated Soil in Air:

Dose due to inhalation of soil:

$$D_{inh} = C_s \times E_f (IR_{in} \times M_{in} \times t_{in} + IR_{out} \times M_{out} \times t_{out}) \times DCF_{inh} \quad \text{Eq. 3.28}$$

where:

D_{inh} = dose due to inhalation of soil (mrem/yr)
 E_f = enrichment factor (dimensionless)
 IR_{in} = inhalation rate of the exposed individual when indoors (m^3/yr)
 M_{in} = mass loading factor for indoor conditions (g/m^3)
 t_{in} = fraction of time spent indoors (dimensionless)
 IR_{out} = inhalation rate when outdoors (m^3/yr)
 M_{out} = mass loading factor for outdoor conditions (g/m^3)
 t_{out} = fraction of time spent outdoors (dimensionless)
 DCF_{inh} = dose conversion factor for inhalation (mrem/pCi).

External Exposure:

Dose due to external exposure to contaminated soil:

$$E_{ext} = C_{stot} \times (t_{in} \times \epsilon + t_{out}) \times DCF_{ext} \quad \text{Eq. 3.29}$$

where:

- E_{ext} = dose due to external exposure to soil (mrem/yr)
- C_{stot} = total radionuclide concentration in soil
- ϵ = transmission or shielding factor (dimensionless)
- DCF_{ext} = dose conversion factor for external exposure [(mrem/yr)/(p/Ci/g)].

Table 3-24. Scenario-Specific Parameters for the All-Pathways Farmer Scenario. (2 Pages)

Parameter	Notation	Value	Unit	Reference
Soil ingestion rate	IR	100	mg/day	EPA 2012; OSWER Directive 9285.6-03
Exposure frequency	EF	365	d/yr	Assumption
Water ingestion rate	IR	2	L/day	OSWER Directive 9285.6-03
Vegetable ingestion rate (including fruits)	IR	30.9	kg/yr	EPA 2012; EPA/600/P-95/002Fa; EPA 530-R-05-006
Beef ingestion rate	IR	50.2	kg/yr	EPA 2012; EPA/600/P-95/002Fa; EPA 530-R-05-006
Water ingestion rate for beef	$IR_{w,a}$	53	L/day	EPA 2012; EPA 1999
Soil ingestion rate for beef	$IR_{s,a}$	0.39	kg/day	EPA 2012; EPA 1999
Fodder ingestion rate for beef	$IR_{fodder,a}$	11.77	kg/day	EPA 2012; EPA 1999
Milk ingestion rate	IR	224.4	L/yr	EPA 2012; EPA/600/P-95/002Fa; EPA 530-R-05-006
Water ingestion rate for milk	$IR_{w,a}$	92	L/day	EPA 2012; EPA 1999
Soil ingestion rate for milk	$IR_{s,a}$	0.41	kg/day	EPA 2012; EPA 1999
Fodder ingestion rate for milk	$IR_{fodder,a}$	16.9	kg/day	EPA 2012; EPA 1999
Egg ingestion rate	IR	14.9	kg/yr	EPA 2012; EPA/600/P-95/002Fa
Poultry ingestion rate	IR	35.8	kg/yr	EPA 2012; EPA/600/P-95/002Fa
Water ingestion rate for egg/poultry	$IR_{w,a}$	0	L/day	EPA 530-R-05-006
Soil ingestion rate for egg/poultry	$IR_{s,a}$	0.022	kg/day	EPA 2012; EPA 530 R-05-006

Table 3-24. Scenario-Specific Parameters for the All-Pathways Farmer Scenario. (2 Pages)

Parameter	Notation	Value	Unit	Reference
Fodder ingestion rate for egg/poultry	$IR_{fodder,a}$	0.2	kg/day	EPA 2012; EPA 530-R-05-006
Inhalation rate when indoor	IR_{in}	8094	m ³ /yr	ICRP 1994
Mass loading factor for indoor conditions	M_{in}	6.66E-05	g/m ³	ICRP 1994
Fraction of time spent indoor	t_{in}	0.66	unitless	NUREG/CR-5512
Inhalation rate when outdoor	IR_{out}	8094	m ³ /yr	ICRP 1994
Mass loading factor for outdoor conditions	M_{out}	6.66E-05	g/m ³	ICRP 1994
Fraction of time spent outdoor	t_{out}	0.012	unitless	NUREG/CR-5512
Enrichment factor	E_f	0.7	(-)	NCRP 1999
Bioconcentration factor from resuspension/soil adhesion for vegetables	B'_v	0.004	(pCi/kg fresh wgt of crop)/(pCi/kg dry wgt of soil)	NCRP 1999
Bioconcentration factor from resuspension/soil adhesion for fodder	B'_p	0.1	(pCi/kg dry wgt of fodder)/(pCi/kg dry wgt of soil)	NCRP 1999
Fraction of vegetable produced locally	F_v	0.25	(-)	EPA/600/P-95/002Fa
Fraction of animal products produced locally	F_a	0.5	(-)	EPA/600/P-95/002Fa
Dry to wet conversion basis factor for fodder	d_f	0.25	(dry wgt of crop)/(wet wgt of crop)	NCRP 1999
Theta W	θ_w	0.2126	(-)	WCH-515 compliance value
Rho S	ρ_s	2.02	g/cm ³	WCH-515 compliance value

Tritium Concentration in Crop and Animal Products:

The tritium concentration in garden produce (e.g., vegetable and fruit) and fodder is calculated separately using an equilibrium model (see equation below). The garden produce and animal feeding material (e.g., silage) become contaminated by root uptake of radionuclides in the contaminated soil and groundwater.

$$C_c = \frac{C_w}{\rho_w} \times \frac{MW \text{ of } H_2O}{2 \times AW \text{ of } H} \times F_{H,c} \times \frac{I}{I+P} \times F_{c,i} \times CF \quad \text{Eq. 3.30}$$

The parameter descriptions and values are provided in Table 3-25. The first term in the equation expresses the water concentration in the unit of pCi/kg water. The second term is the ratio of the molecular weights of water and the atomic weight of hydrogen. It is used to convert the hydrogen fractions ($F_{H,c}$) in the produce to water fractions. Since the hydrogen fractions include organically bound hydrogen as well as water, the produce concentration is a bounding value. The third term, which contains the total precipitation amount (P) during the irrigation period, adjusts the calculated concentration for the presence of uncontaminated water in the growing environment. The time-integration factor, $F_{c,i}$, is the factor that results from the

time integral of the dose rate for tritium over the full year. For leafy vegetable, this factor value equals to 1. For conservativeness, it is assumed that $F_{C,I} = 1$ for all the produces. Using the parameter values given in Table 3-25, the tritium concentration in crop is calculated as:

$$C_c = 8.35 \times 10^{-4} \times C_w \quad \text{Eq. 3.31}$$

Table 3-25. Parameters for Tritium Concentration Calculation in Crop.

Parameter	Definition	Units	Input Value	Reference
C_c	Tritium concentration in crop	pCi/g fresh weight	Calculated	
C_w	Tritium concentration in the irrigation water	pCi/L	Calculated	
ρ_w	Density of water	kg/L	1	EPA/540/R-96/018
MW of H ₂ O	Molecular weight of water	g	18.016	
AW of H	Atomic weight of hydrogen	g	1.008	
$F_{H,C}$	Mass fraction of hydrogen in crops (vegetable and fruit) that are locally produced	unitless	0.1	NUREG/CR-5512
$F_{C,I}$	Factor from time integral of tritium dose rate	unitless	1	NUREG/CR-5512
I	Total irrigation water applied during the irrigation period	cm	82.3	HNF-SD-WM-TI-707
P	Total precipitation during the irrigation period	cm	5.766	HNF-SD-WM-TI-707
CF	Unit conversion factor	kg/g	1.00E-03	

Tritium concentration in animal products (C_a) is calculated using a similar equilibrium model:

$$C_a = \frac{C_w}{\rho_w} \times \frac{MW \text{ of } H_2O}{2 \times AW \text{ of } H} \times F_{H,A} \times \frac{MW,C}{MW,T} \times F_{A,I} \times CF \quad \text{Eq. 3.32}$$

The parameter descriptions and values are provided in Table 3-26 (for those parameters that are not discussed in Table 3-25). The tritium concentration in animal products is given as:

$$C_a = 9.83 \times 10^{-4} \times C_w \quad \text{Eq. 3.33}$$

Table 3-26. Parameters for Tritium Concentration Calculation in Animal Products.

Parameter	Definition	Units	Input Value	Reference
C _a	Radionuclide concentration in crop	pCi/g fresh weight	Calculated	
C _w	Radionuclide concentration in the irrigation water	pCi/L	Calculated	
F _{H,A}	Mass fraction of hydrogen in animal product that are locally produced	unitless	0.11	NUREG/CR-5512
F _{A,I}	Factor from time integral of tritium dose rate	unitless	1	NUREG/CR-5512
M _{W,C}	Mass of contaminated water ingested daily by the animal	kg/day	$\frac{M_{W,C}}{M_{W,T}} = 1$	Assumption
M _{W,T}	Total mass of contaminated water ingested daily by the animal	kg/day		
CF	Unit conversion factor	kg/g	1.00E-03	

Table 3-27. Bioconcentration Factors Used in Calculations. (2 Pages)

Element	Bioconcentration Factors (BCF)											
	Vegetables, Fruit, and Grain (B _v)		Fodder and Grass (B _p)		Milk (BCF _{milk})		Beef (BCF _{beef})		Poultry (BCF _{poultry})		Egg (BCF _{egg})	
	(pCi/kg fresh weight of crop)/(pCi/kg dry weight of soil)	Ref.	(pCi/kg fresh weight of crop)/(pCi/kg dry weight of soil)	Ref.	(day/L)	Ref.	(day/kg)	Ref.	(day/kg)	Ref.	(day/kg)	Ref.
Ac	1.00E-03	1	1.00E-03	1	2.00E-06	1	2.00E-05	1	4.00E-03	4	2.00E-03	4
Ag	4.00E-03	1	2.50E-02	1	6.00E-03	1	3.00E-03	1	2.00E+00	4	5.00E-01	4
Am	1.00E-03	1	1.00E-03	1	2.00E-06	1	5.00E-05	1	6.00E-03	4	3.00E-03	6
C	7.00E-01	2	1.75E-01	2	1.05E-02	2	4.89E-02	2	4.16E+00	2	3.12E+00	2
Cd	5.00E-01	1	2.50E-01	1	2.00E-03	1	1.00E-03	1	1.70E+00	6	1.00E-01	4
Cl	2.00E+01	1	2.50E+01	1	2.00E-02	1	4.00E-02	1	3.00E-02	4	2.00E+00	4
Cm	1.00E-03	1	1.00E-03	1	2.00E-06	1	2.00E-05	1	4.00E-03	4	2.00E-03	4
Co	8.00E-02	1	5.00E-01	1	2.00E-03	1	3.00E-02	1	9.70E-01	6	3.30E-02	6
Cs	4.00E-02	1	5.00E-02	1	1.00E-02	1	5.00E-02	1	2.70E+00	6	4.00E-01	6
Eu	2.00E-03	1	1.25E-02	1	6.00E-05	1	2.00E-03	1	4.00E-03	4	7.00E-03	4
H	8.35E-04	3	8.35E-04	3	9.83E-04	3	9.83E-04	3	9.83E-04	3	9.83E-04	3
I	2.00E-02	1	2.50E-02	1	1.00E-02	1	4.00E-02	1	8.70E-03	6	2.40E+00	6
K	3.00E-01	1	7.50E-01	1	7.00E-03	1	2.00E-02	1	4.00E-01	4	1.00E+00	5
Mo	1.00E-01	1	1.00E-01	1	2.00E-03	1	1.00E-03	1	1.80E-01	6	6.40E-01	6
Nb	1.00E-02	1	2.50E-02	1	2.00E-06	1	1.00E-06	1	3.00E-04	6	1.00E-03	6
Ni	5.00E-02	1	2.50E-01	1	2.00E-02	1	5.00E-03	1	1.00E-03	4	1.00E-01	4
Np	2.00E-02	1	2.50E-02	1	1.00E-05	1	1.00E-03	1	4.00E-03	4	2.00E-03	4

Table 3-27. Bioconcentration Factors Used in Calculations. (2 Pages)

Element	Bioconcentration Factors (BCF)											
	Vegetables, Fruit, and Grain (B _v)		Fodder and Grass (B _p)		Milk (BCF _{milk})		Beef (BCF _{beef})		Poultry (BCF _{poultry})		Egg (BCF _{egg})	
	(pCi/kg fresh weight of crop)/(pCi/kg dry weight of soil)	Ref.	(pCi/kg fresh weight of crop)/(pCi/kg dry weight of soil)	Ref.	(day/L)	Ref.	(day/kg)	Ref.	(day/kg)	Ref.	(day/kg)	Ref.
Pa	1.00E-02	1	1.25E-02	1	5.00E-06	1	5.00E-06	1	4.00E-03	4	2.00E-03	4
Pu	1.00E-03	1	2.50E-04	1	1.00E-06	1	1.00E-04	1	3.00E-03	4	1.20E-03	6
Ra	4.00E-02	1	5.00E-02	1	1.00E-03	1	1.00E-03	1	3.00E-02	4	2.00E-05	4
Rn	0.00E+00	NA	0.00E+00	NA	0.00E+00	NA	0.00E+00	NA	0.00E+00	NA	0.00E+00	NA
Se	1.00E-01	1	2.50E-02	1	1.00E-02	1	1.00E-01	1	9.70E+00	6	1.60E+01	6
Sm	2.00E-03	1	1.25E-02	1	6.00E-05	1	2.00E-03	1	4.00E-03	4	7.00E-03	4
Sn	3.00E-01	1	2.50E-01	1	1.00E-03	1	1.00E-02	1	2.00E-01	4	8.00E-01	4
Sr	3.00E-01	1	1.00E+00	1	2.00E-03	1	1.00E-02	1	2.00E-02	6	3.50E-01	6
Tc	5.00E+00	1	1.00E+01	1	1.00E-03	1	1.00E-04	1	3.00E-02	5	3.00E+00	5
Th	1.00E-03	1	2.50E-04	1	5.00E-06	1	1.00E-04	1	4.00E-03	4	2.00E-03	4
U	1.00E-03	1	2.50E-04	1	5.00E-06	1	1.00E-04	1	4.00E-03	4	2.00E-03	4
Zr	1.00E-03	1	1.25E-03	1	6.00E-07	1	1.00E-06	1	6.00E-05	6	2.00E-04	6

References:

1. NCRP, 1999 (No. 129, App. D)
 2. Equilibrium Model presented in HNF-SD-WM-TI-707, Rev. 5.
 3. Equilibrium Model for Tritium (Equations 3.31 and 3.33)
 4. NUREG/CR5512
 5. IAEA, 1994 (No. 364)
 6. IAEA, 2010 (No.472, Tables 34 & 35)
- NA = not applicable (gas)

Table 3-28. Dose Conversion Factors Used in Performance Assessment Calculations. (3 Pages)

Radionuclide	Inhalation (mrem/pCi) (DCF _{inh}) ^a	Ingestion (mrem/pCi) (DCF _{ing}) ^b	External Exposure (Groundwater Pathway) (mrem/yr)/(pCi/g) (DCF _{ext}) ^c	External Exposure (Air Pathway) (mrem/yr)/(pCi/m ³) (DCF _{ext} for air pathway) ^d	Air Immersion (mrem/yr)/(pCi/m ³) (DCF _{im}) ^e
²²⁷ Ac	2.78E-01	1.45E-03	1.59E+00	4.52E-05	3.68E-03
^{108m} Ag	3.07E-05	1.09E-05	7.64E+00	1.87E-04	8.46E-03
²⁴¹ Am	1.56E-01	8.81E-04	3.46E-02	3.21E-06	7.85E-05
²⁴³ Am	1.54E-01	8.73E-04	7.09E-01	2.53E-05	1.08E-03
¹⁴ C	8.21E-06	2.34E-06	1.07E-05	1.88E-09	3.04E-07
^{113m} Cd	2.05E-04	9.51E-05	5.13E-04	3.07E-08	1.08E-05
³⁶ Cl	2.98E-05	4.59E-06	1.89E-03	7.86E-08	1.94E-05
²⁴³ Cm	1.20E-01	6.66E-04	4.62E-01	1.46E-05	6.22E-04
²⁴⁴ Cm	1.01E-01	5.59E-04	9.97E-05	1.03E-07	4.67E-07

Table 3-28. Dose Conversion Factors Used in Performance Assessment Calculations. (3 Pages)

Radionuclide	Inhalation (mrem/pCi) (DCF _{inh}) ^a	Ingestion (mrem/pCi) (DCF _{ing}) ^b	External Exposure (Groundwater Pathway) (mrem/yr)/(pCi/g) (DCF _{ext}) ^c	External Exposure (Air Pathway) (mrem/yr)/(pCi/m ²) (DCF _{ext} for air pathway) ^d	Air Immersion (mrem/yr)/(pCi/m ³) (DCF _{im}) ^e
⁴⁰ K	5.74E-05	3.04E-05	8.24E-01	1.71E-05	9.27E-04
⁹³ Mo	2.24E-06	1.15E-05	5.50E-04	7.33E-07	2.34E-06
^{93m} Nb	2.26E-06	6.59E-07	8.24E-05	1.10E-07	3.55E-07
⁹⁴ Nb	4.37E-05	8.25E-06	7.66E+00	1.79E-04	8.33E-03
⁵⁹ Ni	5.48E-07	2.95E-07	0.00E+00	0.00E+00	8.08E-08
⁶³ Ni	2.01E-06	7.33E-07	0.00E+00	0.00E+00	0.00E+00
²³⁷ Np	8.51E-02	4.63E-04	8.70E-01	2.61E-05	1.18E-03
²³¹ Pa	3.52E-01	2.07E-03	1.74E+00	4.99E-05	3.84E-03
²³⁸ Pu	1.72E-01	9.73E-04	1.20E-04	9.79E-08	3.92E-07
²³⁹ Pu	1.86E-01	1.07E-03	2.34E-04	4.29E-08	4.40E-07
²⁴⁰ Pu	1.86E-01	1.07E-03	1.16E-04	9.38E-08	3.84E-07
²⁴¹ Pu	3.31E-03	1.93E-05	4.68E-06	2.25E-10	7.18E-09
²⁴² Pu	1.77E-01	1.01E-03	1.01E-04	7.79E-08	7.51E-07
²²⁶ Ra	1.41E-02	1.68E-03	8.87E+00	1.95E-04	9.80E-03
²²⁸ Ra	1.14E-02	5.92E-03	1.28E+01	2.73E-04	1.47E-02
⁷⁹ Se	1.05E-05	1.73E-05	1.47E-05	2.42E-09	3.56E-07
¹⁵¹ Sm	1.55E-05	5.00E-07	7.80E-07	5.88E-10	3.09E-09
^{121m} Sn	1.82E-05	1.96E-06	1.67E-03	5.81E-07	9.82E-06
¹²⁶ Sn	1.17E-04	2.36E-05	9.38E+00	2.29E-04	1.05E-02
⁹⁰ Sr	1.45E-04	1.33E-04	1.95E-02	6.55E-07	1.04E-04
⁹⁹ Tc	1.64E-05	3.33E-06	9.94E-05	9.11E-09	3.36E-06
²²⁹ Th	4.14E-01	2.25E-03	1.25E+00	3.68E-05	1.57E-03
²³⁰ Th	1.61E-01	9.36E-04	9.57E-04	8.76E-08	1.77E-06
²³² Th	1.73E-01	1.03E-03	1.28E+01	2.73E-04	1.47E-02
²³³ U	1.44E-02	2.23E-04	1.11E-03	8.36E-08	1.24E-06
²³⁴ U	1.41E-02	2.15E-04	3.18E-04	8.74E-08	7.17E-07
²³⁵ U	1.25E-02	2.03E-04	6.00E-01	1.94E-05	8.56E-04
²³⁶ U	1.29E-02	2.02E-04	1.70E-04	7.59E-08	4.41E-07
²³⁸ U	1.16E-02	1.94E-04	9.02E-02	2.82E-06	2.04E-04
⁹³ Zr	3.34E-05	3.70E-06	8.24E-05	7.97E-08	3.55E-07

Table 3-28. Dose Conversion Factors Used in Performance Assessment Calculations. (3 Pages)

Radionuclide	Inhalation (mrem/pCi) (DCF _{inh}) ^a	Ingestion (mrem/pCi) (DCF _{ing}) ^b	External Exposure (Groundwater Pathway) (mrem/yr)/(pCi/g) (DCF _{ext}) ^c	External Exposure (Air Pathway) (mrem/yr)/(pCi/m ²) (DCF _{ext} for air pathway) ^d	Air Immersion (mrem/yr)/(pCi/m ³) (DCF _{im}) ^e
²²² Rn	0.00E+00	0.00E+00	0.00E+00	0.00E+00	0.00E+00

^a DOE-STD-1196-2011, Table A.2.

^b DOE-STD-1196-2011, Table A.1.

^c EPA-402-R-93-081 (Federal Guidance Report No. 12), Table III.7.; Modified to include effects of progeny (WCH-478).

^d EPA-402-R-93-081 (Federal Guidance Report No. 12), Table III.3.; Modified to include effects of progeny (WCH-478).

^e DOE-STD-1196-2011, Table A-3.; Modified to include effects of progeny (WCH-478).

3.7.2 Air-Pathway Dose Analysis

Atmospheric pathway scenario is considered in which an individual is exposed to radionuclides that are diffused to the surface from the wastes disposed in ERDF and are transported 100 m downwind. Three exposure mechanisms are considered:

- Air immersion
- Inhalation
- External exposure to the contaminated ground surface.

External exposure results from a fraction of the wastes in the air that settles on the ground via dry and wet depositions as they are transported. The equilibrium concentration of radionuclides that accumulate on the ground surface is conservatively assumed to be less than 100 years.

The exposed individual is assumed to encounter the same exposure conditions as the commercial farmer (e.g., time spent outdoors). Inhalation of soil is not considered because redeposition of radionuclides to the soil and subsequent inhalation of dust from the soil results in much smaller exposure than already considered in the groundwater pathway dose analysis. The specific parameter values for this pathway are given in Table 3-29, and the dose conversion factors are summarized in Table 3-28.

Air Immersion Dose:

An individual in the contaminated volume of air will receive radiation exposure from each radionuclide in the surrounding air. The exposure is given by:

$$D_{im} = C_{air} \times ET \times EF \times \left(\frac{1}{24}\right) \times \left(\frac{1}{365}\right) \times GSF_o \times DCF_{im}$$

Eq. 3.34

where:

- D_{im} = dose via air immersion (mrem/yr)
 C_{air} = concentration of each radionuclide in the surrounding air (pCi/m³)
 EF = exposure frequency (day/yr)
 ET = exposure time (hr/day)
 GSF_o = outdoor gamma shielding factor (unitless)
 DCF_{im} = dose conversion factor for air immersion for each radionuclide $\left(\frac{(\text{mrem/year})}{(\text{pCi/m}^3)}\right)$.

Inhalation:

In addition to the radiation received from air immersion, the exposed individual will receive a dose from direct inhalation of gaseous radionuclides in the air. The dose is given by:

$$D_{inh} = C_{air} \times (IR_{in} \times t_{in} + IR_{out} \times t_{out}) \times DCF_{inh} \quad \text{Eq. 3.35}$$

where:

- D_{inh} = dose received from direct inhalation of radionuclides in air (mrem/yr)
 C_{air} = concentration in air of each radionuclide (pCi/m³)
 IR_{in} = inhalation rate while indoors (m³/yr)
 t_{in} = fraction of time spend indoors (unitless)
 IR_{out} = inhalation rate while outdoors (m³/yr)
 t_{out} = fraction of time spend outdoors (unitless)
 DCF_{inh} = dose conversion factor for inhalation for each radionuclide (mrem/pCi).

External Exposure:

The final exposure considered for the atmospheric scenario is direct exposure to radiation from radionuclides that have been redeposited on the ground. They are assumed to be uniformly distributed on the ground thickly enough that they approximate a plane that is infinitely thick and extends infinitely horizontally. The concentration accumulated on the ground surface is given by:

$$C_{grd} = TDep \times t_{accu} \quad \text{Eq. 3.36}$$

where:

- $TDep$ = total deposition rate [pCi/(m² · sec)]
 t_{accu} = time interval over which the deposition has occurred (sec).

Direct external exposure is given by:

$$D_{ext} = C_{grd} \times t_{out} \times DCF_{ext} \quad \text{Eq. 3.37}$$

where:

- D_{ext} = dose from the exposure to contaminated ground surface (mrem/yr)
 t_{out} = fraction of time spend outdoors (unitless)
 DCF_{ext} = dose conversion factor for external exposure to contaminated ground surface [(mrem/yr)/(pCi/m²)].

Contaminants in the air can be deposited on the ground both under dry conditions and wet conditions (rain or mist). The dry deposition rate is given by:

$$Dep_d = C_{air} \times V_d \quad \text{Eq. 3.38}$$

where:

- Dep_d = rate at which contaminants are deposited under dry conditions [pCi/(m² · sec)]
 C_{air} = concentration of the contaminant in the air (pCi/m³)
 V_d = velocity with which the dry deposition occurs (m/s).

The wet deposition rate is given by:

$$Dep_w = C_{air} \times RR \times SC \times H \quad \text{Eq. 3.39}$$

where:

- Dep_w = rate at which contaminants are deposited via wet deposition (e.g., rain, snow) mechanism [pCi/(m² · sec)]
 C_{air} = concentration of the contaminant in the air (pCi/m³)
 RR = rainfall rate (cm/yr)
 SC = scavenging coefficient (sec⁻¹)
 H = mixing layer height (m).

The total deposition rate [pCi/(m² · sec)] is given by:

$$TDep = Dep_d + Dep_w \quad \text{Eq. 3.40}$$

Table 3-29. Dose-Specific Parameters for the Atmospheric Pathway.

Parameter	Notation	Value	Unit	Reference
Dry deposition velocity for I-129	V_d	0.035	m/s	EPA-402-R-00-004
Dry deposition velocity for C-14 and H-3	V_d	0	m/s	EPA-402-R-00-004
Rainfall rate	RR	18.14	cm/yr	HMS 2012
Conversion factor for scavenging coefficient	CF	1.00E-07	yr/(cm s)	EPA-402-R-00-004
Mixing layer height	H	1500	m	HMS 2012
Exposure time	ET	8	hr/day	HNF-SD-WM-TI-707, Rev. 5
Exposure frequency	EF	180	d/yr	HNF-SD-WM-TI-707, Rev. 5
Gamma shielding factor	GSF_o	1	(-)	EPA 2012
Inhalation rate when indoor	IR_{in}	8103	m ³ /yr	HNF-SD-WM-TI-707, Rev. 5
Fraction of time spent indoor	t_{in}	0.66	(-)	NUREG/CR-5512
Inhalation rate when outdoors	IR_{out}	8103	m ³ /yr	HNF-SD-WM-TI-707, Rev. 5
Fraction of time spent outdoors	t_{out}	0.16	(-)	HNF-SD-WM-TI-707, Rev. 5
Accumulation time	t_{accu}	3.15E+09	s	Assumption

Consideration of Other Sources for Determining Air-Pathway Performance Objective:

The performance objective for the air-pathway dose to representative members of the public is 10 mrem/yr total EDE, excluding dose from radon and its progeny. The 10 mrem/yr limit at the 100-m compliance location is recognized to refer to not just the dose contribution from ERDF but includes all air-pathway sources upstream of ERDF that could contribute at the compliance location.

Both current and future upstream sources that can contribute via the air pathway to ERDF are evaluated. It is assumed that as remediation activities proceed on the Central Plateau portion of the Hanford Site, more and more waste sites would be cleaned up and by 100 years in the future (assumed institutional control period) all point and fugitive sources of air emissions, except those in the low-level burial grounds, would cease to exist.

The current point and non-point source contribution to the air-pathway dose is evaluated in DOE/RL-2012-19 Rev. 0 (*Radionuclide Air Emissions Report for the Hanford Site, Calendar Year 2011*). This report is prepared in compliance with the CFR Title 40, "Protection of the Environment," Part 61 "National Emission Standards for Hazardous Air Pollutants," Subpart H, "National Emission Standards for Emission of Radionuclides Other than Radon from Department of Energy Facilities." The dose to the nearest public receptor is evaluated from emissions from the 200 Areas (200 East and 200 West Areas combined). The EDE for the year is estimated to be about 3×10^{-4} mrem, which is essentially zero. The fugitive emissions from the 200 Areas are estimated to be small and a very conservatively calculated dose to the maximally exposed individual for year 2011 is approximately 1.8×10^{-2} mrem. These values are expected to reduce over time with cleanup of waste sites.

To estimate the future sources, past the institutional control time period of 100 years, the only likely air-pathway sources in the 200 Areas would be the low-level burial grounds located in the 200 East and 200 West Areas; other future disposal areas that are likely to be present nearby

is expected to have robust waste forms and therefore will have near zero air emissions of radionuclides. Estimates of air-pathway dose contributions from low-level burial grounds are provided in WHC-SD-WM-TI-730, Rev. 0 (*Performance Assessment for the Disposal of Low-Level Waste in the 200 East Area Burial Grounds*), and WHC-EP-0645, Rev. 0 (*Performance Assessment for the Disposal of Low-Level Waste in the 200 West Area Burial Grounds*). The estimated maximum annual air-pathway dose for the 200 East Area burial grounds is negligibly small, while that for 200 West Area burial grounds is about 1.2×10^{-2} mrem.

Based on the available information regarding current and future air emissions from waste sites located in the 200 East and 200 West Areas, the dose from air emissions is expected to remain negligibly small compared to the 10 mrem performance objective and can be neglected. Therefore, the air-pathway performance objective of 10 mrem/yr for ERDF is maintained without any modification.

3.8 ALARA ANALYSIS

The DOE's approach to radiation protection for ERDF disposal is based on two key components. One component is the performance objectives described in Chapter 1.0, which specify maximum doses for various pathways. The other component requires doses to be maintained ALARA.

The goal of the ALARA process is attainment of the lowest practical dose level after taking into account social, technical, economic, and public policy considerations. Therefore, in addition to providing a reasonable expectation that the performance objectives described in Chapter 1.0 will not be exceeded, the PA also needs to show that the ERDF disposal is being conducted in a manner that maintains releases of radionuclides to the environment ALARA. In keeping with this philosophy, an ALARA discussion for the ERDF will be included in Chapter 7.0, based on the approach outlined below.

The ERDF site is in a remote location, and the population is nonexistent or sparse in the region. No incorporated towns and/or residents of any kind are within miles of the facility. In addition to future institutional control, the substantial depth to the water table and lack of reliable water supplies make it difficult to establish a residence near ERDF in the future as well. However, consistent with the assumptions for the PA, for the purposes of the ALARA analysis, it is postulated that one or two families will establish residence 100 m downgradient of the facility. Given the typical family size in neighboring Benton and Yakima Counties, a conservative value will be assumed for the exposed population. The annual dose estimate will be then compared to the background radiation dose. It is expected that the estimated annual dose will be an insignificant fraction of background levels.

Other potential options that will be considered include a larger buffer zone, more robust engineered barriers, or other engineered measures; but, given the expected low collective dose and the incremental cost associated with any of these options, it is hard to imagine any of these options being cost-effective from the ALARA perspective.

3.9 SENSITIVITY AND UNCERTAINTY ANALYSES

The following sections provide a rationale for the selection of the uncertainty and sensitivity analysis case assumptions, methodology, and values.

3.9.1 Overview

A sensitivity and uncertainty analysis is required as part of the PA for ERDF. The guidance for completing the sensitivity and uncertainty analyses (DOE G 435.1, *Implementation Guide for Use with DOE M 435.1-1*) states that the dose rates have associated uncertainties and a discussion of uncertainties should be included in expressing the outcomes of any PA. The guidance further states that an estimate of the degree of uncertainty is needed for the analysis that includes the calculation of the maximum impact of the disposal facility beyond the 1,000-year compliance period.

Projections of environmental processes are inherently uncertain. Assessment of uncertainty in model results arising from assumptions and parameter values, for example, is necessary to support the determination that there is reasonable expectation of meeting the performance objectives. The objective of the uncertainty analysis is to estimate the plausible range of potential radionuclide contamination levels in the surrounding environment that results from selecting parameter values within their uncertainty ranges. When sufficient number of parameter combinations is evaluated over their plausible range, the predicted range of potential radionuclide dose can be used to quantify the uncertainty in the dose estimates and meet the requirements of DOE M 435.1-1.

The ERDF PA modeling will apply a graded approach that allows the activities and tools to be adapted to meet the level of rigor and confidence needed by the project (EPA/240/R-02/007). The groundwater pathway modeling analysis is the most complex and will be completed with different modeling approaches having different objectives. These include the following:

- Three-dimensional flow and transport analyses for compliance case (with the parameter values set at their expected values) and simple (one-off) sensitivity cases, and
- One-dimensional abstraction models for completing multiple-parameter sensitivity and uncertainty analyses.

The one-dimensional abstractions of the three-dimensional model are chosen to expedite the ERDF PA screening, sensitivity, and uncertainty analyses. These analyses can number in the hundreds and are not practical or feasible using a three-dimensional model. Because the intent of these analyses is to identify which assumptions and parameters have the greatest impact on the results, and to explain how the model assumptions and parameters affect the results, these analyses can be accomplished with one-dimensional approximations of the ERDF three-dimensional model. The results of these analyses provide the basis for the probabilistic analysis of identified key parameters, which requires a one-dimensional model abstraction to be feasible. The probabilistic analysis provides a means of quantifying the uncertainty by using multiple statistics and multiple probability distributions.

Expansive Sensitivity Analysis

(STOMP 1-D and 3-D Models)

- Complete set of high, median, low parameter sensitivity analyses
- Comprehensive simultaneous multiple parameter one-off sensitivities to identify parameter dependencies and correlations

Probabilistic Analysis (Goldsim 1-D abstraction from STOMP 3-D Model)

- Probability density functions of contaminant concentrations in groundwater within 10,000-year time frames
- Probabilistic analysis of key parameters identified in sensitivity analyses
 - Multiple distributions (normal, log-normal, exponential, triangular, uniform, etc.)
 - Multiple statistical parameters (median, variance, etc.)

3.9.2 Three-Dimensional Numerical Transport Analyses

For the analysis of post-closure performance and waste disposal limiting criteria calculations, further analysis of contaminants with K_d values less than the threshold screening value will proceed with a more detailed three-dimensional model. The three-dimensional simulations will provide results to evaluate the ERDF performance over the compliance period (1,000 years) and out to 10,000 years. The results will also provide a basis for establishing inventory limits as appropriate.

3.9.3 Groundwater-Pathway Uncertainty Analyses

One of the primary expectations of the PA modeling is to provide sufficient explanation of the uncertainty in the results. The intended ERDF PA sensitivity analysis includes complete sets of high-, median-, and low-parameter sensitivity analyses, and comprehensive multiple parameter one-off sensitivities to identify parameter dependencies and correlations. The uncertainty analysis intends to quantify, where possible, the uncertainty in the results associated with uncertainties in the conceptual model; assumptions about current or future events; and parameter estimates. The intent of these analyses is to improve understanding of what factors exert the greatest influence on the model output and results. For this purpose, simplified analyses capable of providing that understanding while expediting the execution and interpretation of results are highly beneficial.

Methods for addressing or quantifying uncertainty extend from those that employ deterministic bounding estimates (one-off evaluations) to those that utilize probabilistic modeling techniques of the full range of defensible and reasonable parameter distributions. The probabilistic component provides a way for quantifying uncertainty in the estimate of groundwater concentrations by exercising the model using various combinations of input parameter values over their uncertainty range.

3.9.4 Sensitivity Analyses

For the sensitivity cases performed using the one-dimensional and three-dimensional STOMP models, the primary assumptions remain unchanged from the three-dimensional compliance case, and parameter values are varied with respect to the compliance case values. Each sensitivity case typically involves a change in only one parameter value. On the basis of the range or distribution of the parameter values, the sensitivity analysis generally includes a compliance case value, a minimum value, and a maximum value. The parameters identified for the one-off evaluations include the following:

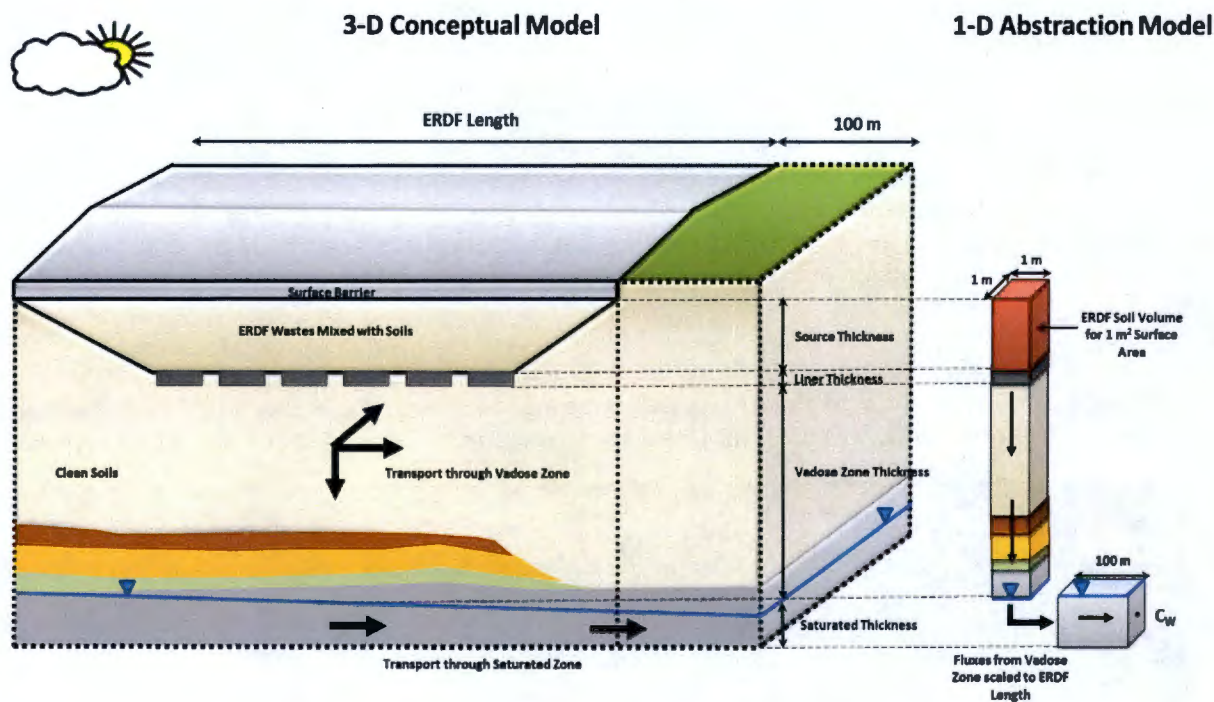
- Distribution coefficient (K_d)
- Recharge rate during pre-construction, closure and monitoring, post-closure with the barrier extant, and post-closure with the barrier degraded
- Hydraulic conductivity
- Saturated and residual moisture contents
- van Genuchten parameters α and n
- Macrodispersivity
- Macroscopic anisotropy.

“What if” cases represent assumptions or postulated conditions that are considered unlikely, but provide information about the ability of the closure system to perform under a variety of conceivable but unexpected conditions. The “what if” cases generally involve alteration of reference case assumptions or postulation that are represented by changes in input parameters. For ERDF, many of the “what if” cases involve changes in assumptions that pertain to recharge (e.g., “What if irrigation occurs immediately after the closure and monitoring period?”). To represent these changed conditions, the recharge rate representing irrigation is substituted for the post-closure barrier extant and barrier degraded periods. Other recharge “what if” cases evaluate changes to assumptions pertaining to barrier degradation. The “what if” cases do not, and are not intended to, lend credibility to the assumed or postulated event occurring. They are presented only to provide information about the protectiveness of the planned closure activities under a wide range of conditions.

3.9.5 One-Dimensional Abstraction Analyses Methodology

A one-dimensional flow and transport model is used as part of the abstraction towards undertaking uncertainty analyses. Figure 3-14 illustrates the transition from three-dimensional model to one-dimensional abstraction model for ERDF. The one-dimensional model is constructed in a manner such that it captures the main processes of the three-dimensional model and provides comparable results. A one-dimensional model abstraction is convenient and attractive as it reduces the run time and model file size leading to evaluation of multiple analyses where initial and boundary conditions can be varied.

Figure 3-14. Three-Dimensional Model and One-Dimensional Abstraction Model for ERDF.



To undertake an uncertainty analysis for ERDF PA, including evaluation of the coupled effects of uncertainty in source term, engineered system, and natural system, a PA abstraction model using GoldSim^{TM6} (GoldSim Technology Group 2009) was developed. GoldSim is a user-friendly, highly graphical, object-oriented program for carrying out dynamic, probabilistic simulations to support decision at a systems level. It is designed to simulate the release, transport, and fate of contaminants within complex engineered and/or natural environmental systems.

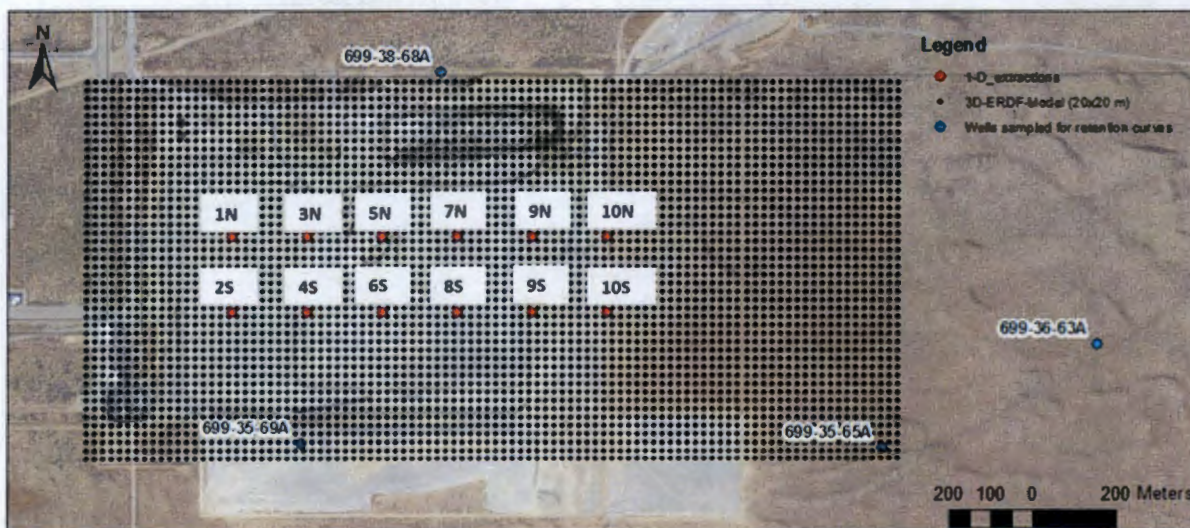
A one-dimensional model was developed using the GoldSim Cell pathway capability for modeling contaminant transport. The cell pathway in GoldSim is equivalent to a mixing cell (a batch-reactor) and can explicitly represent processes such as species dependent partition coefficient, solubility constraints, mass transport (advection and diffusion by liquid phase or suspended particles), and any radioactive decay and ingrowth. When multiple cells are linked together, the behavior of the cell network is mathematically identical to a network of finite difference nodes describing a coupled system of differential equations. Both vadose zone and saturated zone transport can be modeled using this capability. A specialized GoldSim element called a source is used to model the release rate of contaminants (through waste matrix) and evaluate uncertainty in the source term. The cell pathways require user inputs for the advective flow, as the flow equation is not solved by GoldSim. As a result, the flow rates and moisture content are abstracted from the STOMP three-dimensional calculation. Uncertainty in flow conditions is incorporated by abstracting the results from various STOMP models run under varying recharge boundary conditions and hydraulic parameters.

⁶ GoldSim is a trademark of and distributed by GoldSim Technology Group LLC, Redmond, Washington, Copyright 2006. All rights reserved.

One-Dimensional Abstraction Model Grid and Flow-Field Discretization:

The flow field generated from the three-dimensional STOMP model was evaluated prior to abstraction of the results. Since GoldSim relies on the user to provide the moisture content, saturation, and Darcy velocity as state variables in order to solve the advection-dispersion equation for contaminant transport, these parameter values were extracted from the output of the three-dimensional STOMP model. An abstraction process was undertaken by selecting 12 representative locations on the surface of the three-dimensional model grid that generally correspond to the center of each of the ERDF disposal cells (Figure 3-15). Note that the disposal cells 9 and 10 are supercells, and thus two locations are selected in each of these supercells. These locations are chosen so that they line up with the rest of the geographic locations.

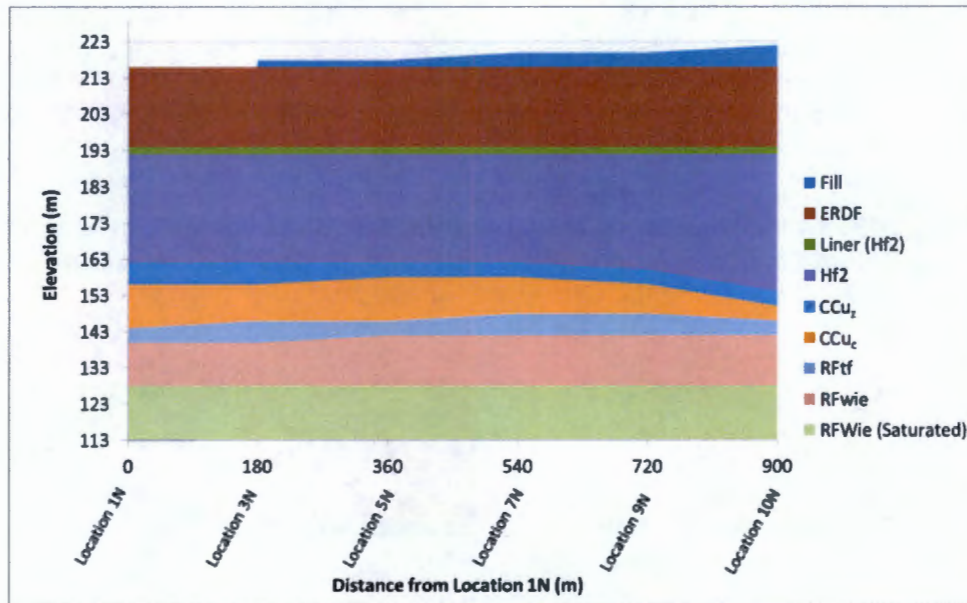
Figure 3-15. Top View of the Three-Dimensional Model Domain Used in STOMP with Twelve Representative Locations Used for One-Dimensional Model Flow Abstraction.



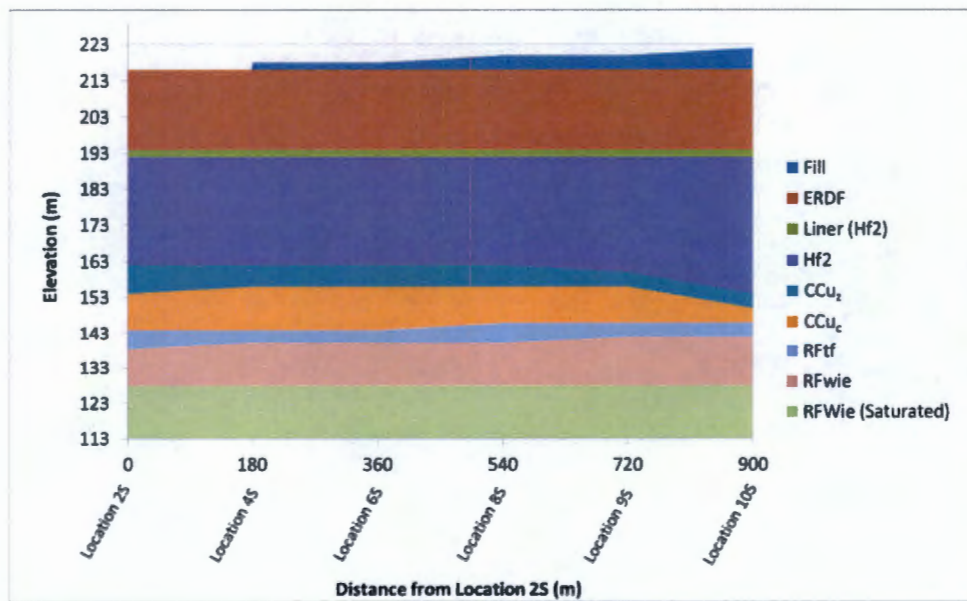
These 12 locations are deemed sufficient as they capture the spatial variability in the hydrostratigraphic unit contacts and thereby the flow properties. Two geologic cross-sections, one along the representative locations located on the north side and one along the south side, are presented in Figure 3-16. As can be seen there is little difference between the two cross-sections indicating limited variability in the north-south direction. The spatial variability is mostly in the east-west direction with thickening of Hf2 unit towards east and thinning of CCu₂ and CCu₁ units.

At each of the 12 representative locations, the moisture content and vertical Darcy velocity is extracted from the three-dimensional STOMP model output for all of the nodes located vertically from the surface down to the water table. The outputs are saved at selected times with finer time discretization adopted near the time of liner failure to capture any transient effects and coarser time discretization beyond 1,000 years of simulation when steady-state conditions are largely established through most of the model domain.

Figure 3-16. Geologic Cross Section Along the Representative Locations (a) On the North Side and (b) On the South Side.



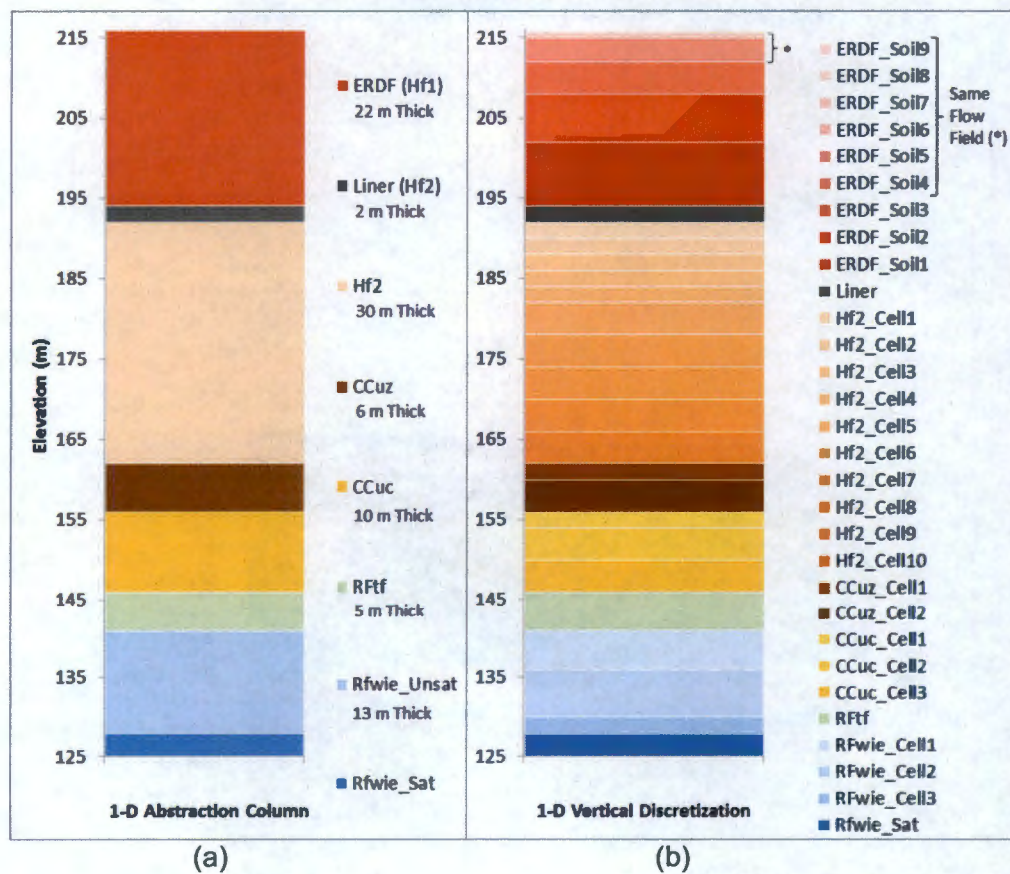
(a)



(b)

A representative one-dimensional grid is developed after evaluation of the depth of hydrostratigraphic unit contacts at all 12 locations. Because of the variable thickness of some hydrostratigraphic units, primarily in the east-west direction, the hydrostratigraphic unit thicknesses under all 12 locations are assembled and then a median value is taken in order to derive a representative thickness for the one-dimensional model. Figure 3-17a presents the representative thickness of hydrostratigraphic units along with their contact elevations. Figure 3-17b provides the grid discretization considered in the one-dimensional abstraction model.

Figure 3-17. One-Dimensional Model Abstraction Showing (a) Representative Column for One-Dimensional Model and (b) Grid Discretization of the One-Dimensional Model.



The thickness of ERDF is taken to be 22 m followed by 2-m-thick liner at the bottom of the facility. Finer discretization is applied to the top 1 m of ERDF for the purpose of radon flux calculation and other atmospheric releases. In the Hf2, CCu_c, and CCu_z hydrostratigraphic units located below ERDF, finer discretization is applied near the top of the hydrostratigraphic unit with gradually coarser discretization away to capture changes in contaminant transport near the hydrostratigraphic unit boundaries from changes in transport properties and hydraulic properties. A total of 29 grid cells of varying thicknesses are applied to represent thickness of 88 m from the top of ERDF to the water table. The details of the grid discretization are given in Table 3-30. The saturated zone is modeled as a one-dimensional stream tube running along the full length of ERDF using the pipe pathway capability of GoldSim. The volumetric flow rate through the stream tube is calculated based on the hydraulic gradient under steady-state conditions and saturated hydraulic conductivity of Ringold unit E.

Table 3-30. Discretization of ERDF One-Dimensional Abstraction Model Built Using GoldSim.

Unit	Thickness (m)	Physical Properties	Number of Grid Block Cells	Cell Discretization	Flow Field Discretization (Moisture Content and Vertical Darcy Flux)
ERDF wastes mixed with soils	22	Same as Hf1	9	5 at 0.2 m, 1 at 3 m, 1 at 4 m, 1 at 6 m, 1 at 8 m	One flow field for the first 4 m (first six cells). One flow field for each remaining cell (leading to three flow fields over last 18 m)
Liner	2	Same as Hf2	1	2 m	One flow field
Sand-dominated Hanford (Hf2)	30	Hf2	10	5 at 2 m, 5 at 4 m.	One flow field per cell
Silt-dominated Cold Creek (CCu _z)	6	Undifferentiated CC	2	1 at 2 m, 1 at 4 m	One flow field per cell
Carbonate-dominated Cold Creek Caliche (CCu _c)	10	Undifferentiated CC	3	1 at 2 m, 2 at 4 m	One flow field per cell
Ringold Formation Taylor Flat (RFtf)	5	Same as Hf2	1	1 at 5 m	One flow field per cell
Unsaturated Ringold Formation Wooded Island Unit E (RFwie)	13	RFwie	3	1 at 5 m, 1 at 6 m, 1 at 2 m	One flow field per cell
Saturated Ringold Formation Wooded Island Unit E (RFwie_Sat)		RFwie		Stream tube	One flow field

NOTE: Grid cells representing surface barrier of 1 m thickness are placed above ERDF for the air-pathway dose calculation and for radon flux calculation.

The volumetric moisture content and the vertical Darcy velocity information is extracted from the three-dimensional STOMP model grid nodes for each of the 12 locations. Based on the node elevations, these grid blocks are mapped to the grid blocks used in the one-dimensional model abstraction-based discretization. The volumetric moisture content and vertical Darcy velocity values are averaged when multiple three-dimensional STOMP model grid nodes fall within the coarse discretization employed in the one-dimensional model. Table 3-30 presents the details regarding the flow-field discretization. In the end, a spatially averaged time varying moisture content and vertical Darcy velocity profile is created for each discretized grid block in the one-dimensional abstraction model.

The uncertainties in parameters are explicitly represented by creating probability distributions and then running the model in a probabilistic mode using Monte Carlo sampling methodology. Results from multiple realizations lead to a range of estimates in the dose representing uncertainty. Statistical techniques such as step-wise regression and partial-rank correlations, among others, are used to evaluate and identify the stochastic parameters that lead to most uncertainty in the overall system results.

Although it is more desirable to generate probability distributions for uncertain parameters on the basis of observed and/or simulated data, distributions are often inferred on the basis of only a limited amount of information and are also subject to rather ad-hoc assumptions. In that case, "Assigning Probability Distributions to Input Parameters of Performance Assessment Models" (Mishra 2002) recommends considering the principle of maximum entropy that states that a distribution function has to be chosen for maximizing the entropy of the modeled system (i.e., for preserving the maximum uncertainty about the data). The ERDF PA uses the maximum entropy approach for assigning the distribution functions. Details are given in WCH-515.

From a practical perspective, the use of the maximum entropy principle in assigning a distribution function implies the following considerations:

- If all the samples are equally likely because no constraint on the plausible parameter values is available, the maximum entropy is reached and corresponds to the uniform distribution.
- On the other hand, if some information is available, uncertainty is reduced as much as possible by using all information (i.e., by satisfying all constraints), but no further by unnecessary assumptions. This ensures that ignorance is acknowledged and forces the analyst to retain maximum uncertainty in the distribution developed from the data. In that case, the distribution function will have a concentration of probability away from the extreme values, leading to a reduction of uncertainty and hence a reduction of entropy in comparison to the uniform distribution.

The constraints that can be used for selecting a distribution function in accordance with the maximum entropy principle are summarized in Table 3-31.

Table 3-31. Constraints on Data Useful to Select a Distribution Function Considering the Maximum Entropy Principle (Mishra 2002, According to Harr 1987).

Constraint	Distribution
Upper bound, lower bound	Uniform
Minimum, maximum, mode	Triangular
Mean, standard deviation	Normal
Range, mean, standard deviation	Beta
Mean occurrence rate	Poisson

3.9.6 Sensitivity and Uncertainty Analyses Database

The sensitivity and uncertainty analyses database is developed in WCH-515 along with the rationale for the parameter distribution type and statistical metrics for the parameter (e.g., mean, minimum, maximum, and mode). The following tables summarize the database for the individual parameters considered as part of the ERDF PA sensitivity and uncertainty analyses:

- Table 3-32 for recharge
- Table 3-33 for vadose zone parameters
- Table 3-34 for Polmann anisotropy model parameters
- Table 3-35 for saturated zone parameters
- Table 3-36 for transport parameters
- Table 3-37 for K_d estimates for contaminants
- Table 3-38 for contaminant inventory.

Note that, for bounding the uncertainty in radionuclide inventory at ERDF, the recommended uncertainty ranges for specific radionuclides provided in WCH-479 are used. For other radionuclides, uncertainties of 30% less for minimum and 50% more for maximum from the best estimate value are assumed.

Table 3-32. ERDF Performance Assessment Uncertainty and Sensitivity Analyses Database for Recharge (WCH-515). (2 Pages)

Period	Zone	Distribution Type	Value (mm/yr)
Pre-operation (before 1996)	Undisturbed zone (Rupert Sand with vegetation)	Triangular	Mean: 1.7 Min: 0.26 Max: 4 Mode: 0.9
Operation (1996-2035)	Undisturbed zone (Rupert Sand with vegetation)	Triangular	Mean: 1.7 Min: 0.26 Max: 4 Mode: 0.9
	Disturbed zone (Rupert Sand without vegetation)	Triangular	Mean: 45 Min: 22.5 Max: 90 Mode: 22.5
	Under construction zone (ERDF cells)	Fixed value	Best estimate: 0

Table 3-32. ERDF Performance Assessment Uncertainty and Sensitivity Analyses Database for Recharge (WCH-515). (2 Pages)

Period	Zone	Distribution Type	Value (mm/yr)
Early Post-Closure (2035-2535)	Undisturbed zone (Rupert Sand with vegetation)	Triangular	Mean: 1.7 Min: 0.26 Max: 4 Mode: 0.9
	Degraded Side slopes with vegetation	Fixed value	Best estimate: 2
	Top portion of the barrier from 2035 to 2135	Fixed value	Best estimate: 0
	Top portion of the barrier from 2135 to 2535	Triangular	Mean: 0.5 Min: 0.05 Max: 1 Mode: 0.5
Late Post-Closure (past 2535)	Undisturbed zone (Rupert Sand with vegetation)	Triangular	Mean: 1.7 Min: 0.26 Max: 4 Mode: 0.9
	Degraded side slopes with vegetation	Fixed value	Best estimate: 2
	Degraded top portion of the barrier	Triangular	Mean: 1 Min: 0.1 Max: 2 Mode: 1

Table 3-33. ERDF Performance Assessment Uncertainty and Sensitivity Analyses Database for Vadose Zone Parameters (WCH-515).

Hydrostratigraphic Unit	Number of Samples	θ_s		θ_r		$\alpha(1/cm)$		n		Fitted K_s (cm/s)	
		Uniform Distribution		Uniform Distribution		Uniform Distribution		Uniform Distribution		Log-Uniform Distribution	
		Min	Max	Min	Max	Min	Max	Min	Max	Min	Max
Hanford Hf1 (gravel-dominated)	11	0.175	0.28	0	0.029	0.0025	0.0438	1.3253	1.7674	2.38E-5	2.43E-3
Hanford Hf2 (sand-dominated)	12	0.29	0.5026	0	0.1301	0.0054	0.0293	1.4342	2.2565	1.55E-5	1.23E-3
Cold Creek CCu _z (silt-dominated) and CCu _c (caliche)	4	0.352	0.489	0	0.0608	0.0037	0.0066	1.6486	2.3247	2.81E-5	2.30E-4
Ringold RFtf	12	0.29	0.5026	0	0.1301	0.0054	0.0293	1.4342	2.2565	1.55E-5	1.23E-3
Ringold RFWie	10	0.1	0.236	0	0.0177	0.0025	0.03	1.3079	1.6577	1.06E-6	3.42E-4

NOTE: Diffusive porosity (used in STOMP) is equivalent to the saturated water content, and the identical uncertainty range is applied.

Table 3-34. ERDF Performance Assessment Uncertainty and Sensitivity Analyses Database for Polmann Anisotropy Model Parameters (WCH-515).

Hydrostratigraphic Unit	Number of Samples	$\langle \text{Ln}K_s \rangle$	$\sigma_{\text{Ln}K_s}^2$	p	ζ	λ (cm)	A	Mean Tension Range (cm)
Hanford Hf1 (gravel-dominated)	11	-14.85	1.94	-2.6E-4	2.50E-4	30	0.00368	700 – 1000
Hanford Hf2 (sand-dominated)	12	-14.6	1.50	-7.2E-4	6.55E-4	50	0.00620	500 – 700
Cold Creek CCu _z (silt-dominated) and CCu _c (caliche)	4	-10.43	1.01	2.4E-3	9.34E-4	50	0.0104	300 – 400
Ringold RFtf	12	-14.6	1.50	-7.2E-4	6.55E-4	50	0.00620	500 – 700
Ringold RFWie	10	-15.76	3.56	-1.1E-4	1.84E-4	30	0.00371	700 – 1000

Table 3-35. ERDF Performance Assessment Uncertainty and Sensitivity Analyses Database for Saturated Zone Parameters (WCH-515).

Parameter	Distribution Type	Distribution Features
Ringold E saturated horizontal hydraulic conductivity	Log-Uniform	Min: 0.1 m/day Max: 10 m/day
Saturated vertical anisotropy	Triangular	Min: 0.01 Max: 0.5 Mode: 0.1 (Mean: 0.2)
Specific storage	Fixed value	1.32E-4 m ⁻¹
Hydraulic gradient	Fixed value	0.0015

Min= Minimum; Max = Maximum

Table 3-36. ERDF Performance Assessment Uncertainty and Sensitivity Analyses Database for Transport Parameters (WCH-515).

Parameter		Distribution	Hf1	Hf2	CCu _z	CCu _c	RFtf	RFWie
Bulk density (g/cm ³)	Min	Uniform	1.85	1.60	1.60	1.60	1.60	1.93
	Max		2.19	1.98	1.72	1.72	1.98	2.32
Effective diffusion coefficient (cm ² /s)	Best	Fixed value	2.5E-5					
Vadose zone longitudinal macrodispersivity (cm)	Best	Fixed value	150	150	50	50	150	150
Vadose zone transverse macrodispersivity (cm)	Best	Fixed value	15	15	5	5	15	15
Saturated zone longitudinal macrodispersivity (m)	Min	Uniform	NA	NA	NA	NA	NA	1
	Max							20
Ratio longitudinal/transverse macrodispersivity (-)	Min	Uniform	NA	NA	NA	NA	NA	5
	Max							10

NA = not applicable

Table 3-37. ERDF Performance Assessment Uncertainty and Sensitivity Analyses Database for K_d (mL/g) (WCH-515). (2 Pages)

K_d (mL/g)		Distribution	Hf1	Hf2	CCu _z	CCu _c	RFff	RFwie
³ H	Best	Fixed value	0	0	0	0	0	0
³⁶ Cl	Best	Fixed value	0	0	0	0	0	0
⁹⁹ Tc(VII)	Mode	Triangular	0	0	0	0	0	0
	Min		0	0	0	0	0	0
	Max		0.1	0.1	0.2	2	0.1	0
¹²⁹ I	Mode	Triangular	0.1	0.2	0.2	0.2	0.2	0.1
	Min		0	0	0	0	0	0
	Max		1.2	2	5	2	2	0.9
¹⁴ C	Mode	Triangular (or uniform for CCuc)	0.3	0.5	0.8		0.5	0.2
	Min		0	0	0.8	0.8	0	0
	Max		1.4	2.4	2.4	2.4	2.4	1.1
⁶⁰ Co(II,III)	Mode	Triangular	5.9	10	10	15	10	4.6
	Min		0	0	0	3	0	0
	Max		1172	2000	2000	2000	2000	924
U(VI), all isotopes	Mode	Triangular	0.5	0.8	1.5	4	0.8	0.4
	Min		0.1	0.2	0.2	3	0.2	0.1
	Max		2.3	4	20	20	4	1.8
²³⁷ Np(V)	Mode	Triangular	5.9	10	20	10	10	4.6
	Min		1.4	2	5	2	2	1.2
	Max		17.6	30	60	30	30	13.9
⁷⁹ Se(VI,IV)	Mode	Triangular	2.9	5	5	5	5	2.3
	Min		2	3	3	3	3	1.8
	Max		5.9	10	30	30	10	4.6
²²⁶ Ra(II)	Mode	Triangular	13.6	20	40	40	20	11.7
	Min		6.8	10	20	20	10	5.9
	Max		34.1	50	200	200	50	29.3
⁹⁰ Sr	Mode	Triangular	13.6	20	40	40	20	11.7
	Min		6.8	10	20	20	10	5.9
	Max		34.1	50	200	200	50	29.3
¹²⁶ Sn(IV), all isotopes	Mode	Triangular	34.1	50	100	50	50	29.3
	Min		34.1	50	50	50	50	29.3
	Max		170.3	250	250	250	250	146.4
⁶³ Ni, all isotopes	Mode	Triangular	204.4	300	300	300	300	175.7
	Min		34.1	50	50	50	50	29.3
	Max		1703.1	2500	2500	2500	2500	1464.4
²⁴¹ Am, all isotopes	Mode	Triangular	204.4	300	300	150	300	175.7
	Min		409	60	200	60	60	35.5
	Max		1362.4	2000	4000	2000	2000	1171.5
Eu(III), all isotopes	Mode	Triangular	204.4	300	300	150	300	175.7
	Min		409	60	200	60	60	35.5
	Max		1362.4	2000	4000	2000	2000	1171.5

Table 3-37. ERDF Performance Assessment Uncertainty and Sensitivity Analyses Database for K_d (mL/g) (WCH-515). (2 Pages)

K_d (mL/g)		Distribution	Hf1	Hf2	CCu _z	CCu _c	RF _{tf}	RF _{wie}
Pu, all isotopes	Mode	Triangular	408.7	600	600	300	600	351.4
	Min		136.2	200	200	200	200	117.1
	Max		1362.4	2000	4000	2000	2000	1171.5
¹³⁷ Cs	Mode	Triangular	1362.4	2000	2000	2000	2000	1171.5
	Min		136.2	200	600	200	200	117.1
	Max		6812.2	1000	10000	10000	1000	5857.4
^{108m} Ag, all isotopes	Mode	Triangular	272.5	400	400	400	400	243.3
	Min		6.8	10	10	10	10	5.9
	Max		20436	30000	30000	30000	30000	17572
Nb, all isotopes	Mode	Triangular	0	0	0	0	0	0
	Min		0	0	0	0	0	0
	Max		0.1	0.1	0.1	0.1	0.1	0
^{113m} Cd	Mode	Triangular	204.4	300	300	300	300	175.7
	Min		54.5	80	80	80	80	46.9
	Max		681.2	1000	1000	1000	1000	585.7
²³² Th	Mode	Triangular	681.2	1000	1000	1000	1000	585.7
	Min		27.2	40	40	40	40	23.4
	Max		1703	2500	2500	2500	2500	1464.4
Cm, all isotopes	Mode	Triangular	204.4	300	300	300	300	175.7
	Min		40.9	60	60	60	60	35.1
	Max		885.6	1300	1300	1300	1300	761.5
⁹³ Zr	Mode	Triangular	681.2	1000	1000	1000	1000	585.7
	Min		27.2	40	40	40	40	23.4
	Max		1703	2500	2500	2500	2500	1464.4
¹⁵¹ Sm	Mode	Triangular	204.4	300	300	300	300	175.7
	Min		40.9	60	60	60	60	35.1
	Max		1362.4	2000	2000	2000	2000	1171.5
⁹³ Mo	Best	Fixed value	0	0	0	0	0	0
⁴⁰ K	Best	Fixed value	0	0	0	0	0	0

Table 3-38. ERDF Performance Assessment Uncertainty and Sensitivity Analyses Database for Contaminant Inventory (Curies or Metric Tons) Using Triangular Distribution (WCH-515). (2 Pages)

Radionuclides	Activity (Ci) Currently Disposed Decayed to 2035			Activity (Ci) Currently Forecast Decayed to 2035		
	Best	Min	Max	Best	Min	Max
^{108m} Ag	238.32	166.83	357.49	0.77	0.54	1.15
²⁴¹ Am	524.45	367.12	786.68	317.56	222.29	476.34
¹⁴ C	1882.53	1495.65	2492.75	458.67	458.67	917.33
^{113m} Cd	0.89	0.62	1.34	0.48	0.33	0.71
³⁶ Cl	0.00	0.00	0.00	0.02	0.01	0.04
²⁴⁴ Cm	0.64	0.45	0.96	11.17	7.82	16.75
¹³⁷ Cs	8416.35	6917.55	10952.78	247878.76	178703.29	299760.36
¹⁵² Eu	1411.50	988.05	2117.25	5.83	4.08	8.75
¹⁵⁴ Eu	195.10	136.57	292.65	24.57	17.20	36.85
³ H	2014.47	1603.30	2585.98	5947.74	4137.56	9050.91
¹²⁹ I	0.02	0.01	0.03	0.00	0.00	0.01
⁴⁰ K	0	0	1	0.00	0.00	0.00
⁹³ Mo	0.50	0.35	0.75	0.03	0.02	0.04
^{93m} Nb	1.71	1.20	2.56	0.07	0.05	0.11
⁹⁴ Nb	0.30	0.21	0.45	0.08	0.06	0.12
⁵⁹ Ni	189.96	132.97	284.94	109.98	76.98	164.96
⁶³ Ni	12223.38	8556.37	18335.07	464.93	329.68	929.86
²³⁷ Np	0.40	0.28	0.60	0.03	0.02	0.04
²³⁸ Pu	34.74	27.79	45.17	41.36	33.09	62.04
²³⁹ Pu	259.82	207.86	337.77	1199.17	959.34	1798.76
²⁴⁰ Pu	119.70	95.76	155.61	299.24	239.39	448.86
²⁴¹ Pu	1606.40	1285.12	2088.32	251.98	201.59	377.98
²⁴² Pu	0.70	0.56	0.91	0.02	0.02	0.03
²²⁶ Ra	0.89	0.62	1.34	0.79	0.55	1.19
⁷⁹ Se	0.10	0.07	0.15	0.05	0.03	0.07
¹⁵¹ Sm	215.29	150.70	322.94	51.54	36.08	77.31
^{121m} Sn	12.56	8.79	18.84	0.03	0.02	0.04
⁹⁰ Sr	6372.24	5030.72	8384.53	111793.72	55896.86	134152.47
⁹⁹ Tc	21.00	17.00	32.00	32.00	22.00	63.99
²³² Th	1.10	0.77	1.65	0.20	0.14	0.30
²³³ U	14.60	11.68	18.98	0.01	0.00	0.01
²³⁴ U	13.50	10.80	17.55	4.00	2.80	8.00
²³⁵ U	7.60	6.08	9.88	0.30	0.21	0.60
²³⁶ U	0.40	0.32	0.52	0.10	0.07	0.20
²³⁸ U	67.50	54.00	87.75	20.00	14.00	40.00
⁹³ Zr	16.00	11.20	24.00	2.00	1.40	3.00
⁶⁰ Co	236.18	165.33	354.27	1300.07	910.05	1950.10

Table 3-38. ERDF Performance Assessment Uncertainty and Sensitivity Analyses Database for Contaminant Inventory (Curies or Metric Tons) Using Triangular Distribution (WCH-515). (2 Pages)

Radionuclides	Activity (Ci) Currently Disposed Decayed to 2035			Activity (Ci) Currently Forecast Decayed to 2035		
	Best	Min	Max	Best	Min	Max
¹²⁶ Sn	0.20	0.14	0.30	0.07	0.05	0.10
²⁴³ Cm	0.06	0.04	0.09	0.46	0.32	0.69
²⁴³ Am	0.60	0.42	0.90	0.20	0.14	0.30

3.9.6.1 Intruder Pathway, Air Pathway, and Radon Flux Sensitivity and Uncertainty.

Sensitivity analyses for the intruder pathway were focused on a range of human activities (e.g., scenarios) that cause variable levels of exposure to contaminants. Four exposure scenarios, one acute and three chronic, are described in Chapter 5.0, and parameter changes affecting the assumed amounts of exhumed waste and degree of mixing with soil are summarized in Chapter 5.0.

The uncertainty in the air-pathway analysis is evaluated with respect to uncertainty in tortuosity (besides the uncertainty in inventory). Uncertainty in calculated tortuosity is considered using two other curves given by Liu et al. (2006) as shown in Figure 3-12:

- The minimum envelope curve obtained with the model of Millington and Quirk (1961) with Φ , fitted total porosity = 0.8

$$\tau = \frac{\theta_a^{10/3}}{\Phi^2} = \frac{(\Phi - \theta_w)^{10/3}}{\Phi^2} \tag{Eq. 3.41}$$

- The maximum envelope curve obtained with the model of Millington and Quirk (1960) with Φ , fitted total porosity = 0.4.

$$\tau = \frac{\theta_a^2}{\Phi^{2/3}} = \frac{(\Phi - \theta_w)^2}{\Phi^{2/3}} \tag{Eq. 3.42}$$

4.0 RESULTS OF ANALYSES

This chapter presents the results of the analyses described in Chapter 3.0 and discusses the (1) release of radionuclides from the source term (Section 4.1), (2) environmental transport of radionuclides via the groundwater pathway (Section 4.2), (3) radon analysis (Section 4.3), (4) biotic pathways (Section 4.4), (5) groundwater pathway dose analysis and assessment of groundwater protection (Section 4.5), and (6) uncertainty and sensitivity analysis (Section 4.6). The results of the analyses conducted for each part of the modeling effort are summarized independently, leading to the discussion of the all-pathways dose calculations presented in Section 4.5. Intermediate results are presented to illustrate the influence of each analysis step on the overall result. Results are provided for two time periods: compliance period (1,000 years) (2035 to 3035), and post-compliance period (up to 10,000 years from closure). Results are provided for the receptor located 100 m downgradient from ERDF. Intermediate results and doses are projected out 10,000 years to identify peaks for some radionuclides that migrate slowly through the environment. These results are given for completeness, but these are not part of the compliance determination.

4.1 SOURCE TERM

Three source terms are considered for the purpose of analysis (Section 3.3):

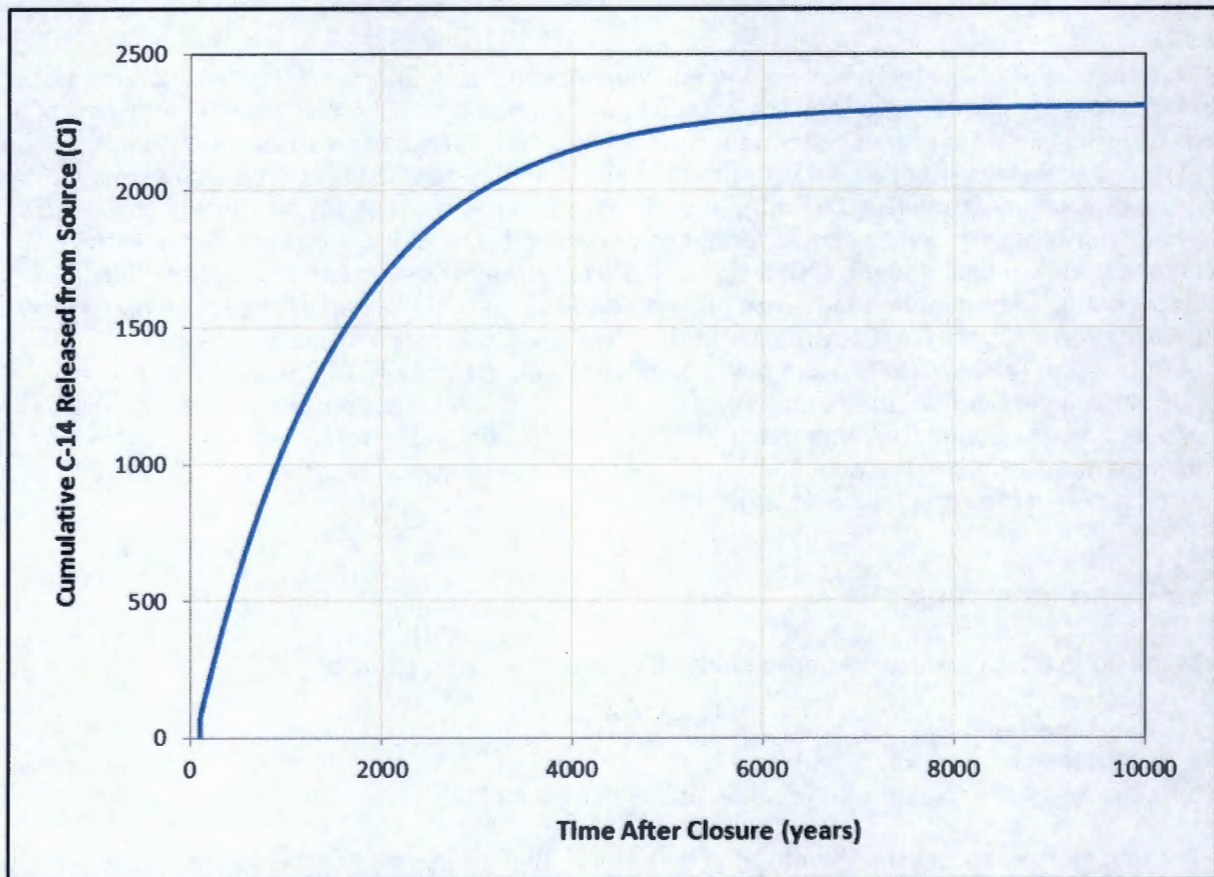
1. Untreated bulk soil
2. Activated metals (except carbon-14)
3. Carbon-14 associated with graphite and activated metals.

The inventory associated with untreated bulk soil is all available for release to the subsurface once the composite liner fails (Section 3.2.1). The mass release is primarily a function of advection and depends on the recharge rate. As indicated in Table 3-3, almost the entire radionuclide inventory (except for carbon-14) is associated with bulk soil.

The majority of activated metals come from variety of waste types, such as steel and aluminum tubing, desiccant, zirconium cladding, lead cadmium poison pieces, and variety of scrap metal from past Hanford Site activities. The primary radionuclide contaminants of concern evaluated in activated metals are niobium-94, nickel-59, nickel-63, and carbon-14. Although molybdenum-93 is emplaced with untreated waste in the initial inventory, it is most likely an activated metal, and thus treated likewise in transport calculations. To model the release of radionuclides from activated metals a solubility limit of 10^{-6} mol/L is imposed that is based on the solubility of hydrous ferric oxide (Section 3.3). Evaluation of transport results indicate that the highest concentrations for these radionuclides remain well below the solubility limit (by at least three to four orders of magnitude) due to very small inventory and thus are not affected by the solubility limit.

The release of carbon-14 inventory associated with graphite and activated metals is based on the graphite leaching rate. A fractional leach rate of $1.5 \times 10^{-6} \text{ d}^{-1}$ obtained on block samples of Hanford Site graphite at 20 °C is applied. The cumulative release of carbon-14 from the source term is shown in Figure 4-1. The release starts once the composite liner fails at 100 years.

Figure 4-1. Cumulative Release of Carbon-14 (Ci) from the ERDF Source Term.



The small initial increase is due to release of unbounded carbon-14 inventory associated with bulk soil that forms a minor fraction (<0.07 fraction) of the total carbon-14 inventory. The remaining portion of the cumulative release is controlled by the leach rate. By about 8,000 years, almost all of the carbon-14 is released and is available for transport in the vadose zone.

4.2 ENVIRONMENTAL TRANSPORT OF RADIONUCLIDES

As discussed in Chapter 3.0, the screening evaluation helps in reducing the number of radionuclides to be evaluated using three-dimensional modeling analysis. The groundwater pathway screening analysis results are discussed first followed by a discussion of results of radionuclide transport within the vadose zone and saturated media. The air-pathway modeling results are discussed next.

4.2.1 Result of Screening Analysis for Groundwater Pathway

The results of the screening analysis, described in Section 3.4.1.8, indicate that even when using conservative parameter values, radionuclides with a $K_d > 0.1$ mL/g do not reach groundwater within the 1,000-year compliance time frame, and radionuclides with a $K_d > 0.9$ mL/g do not reach groundwater within the 10,000-year post-compliance period (Table 4-1). The screening evaluation helps in reducing the number of radionuclides to be evaluated using three-dimensional modeling analysis.

Table 4-1. First-Arrival Time (in Calendar Year) of Radionuclides for Various K_d Values Based on One-Dimensional Screening Analysis Using STOMP.

ERDF Cell Locations	K_d (mL/g)												
	0	0.1	0.2	0.3	0.4	0.5	0.6	0.7	0.8	0.9	1.0	1.5	2.0
1	2161	3285	4548	5831	6964	8214	9484	10759	DNA	DNA	DNA	DNA	DNA
2	2161	3285	4548	5831	6964	8214	9484	10759	DNA	DNA	DNA	DNA	DNA
3	2160	3252	4498	5756	6874	8099	9339	10594	11864	DNA	DNA	DNA	DNA
4	2160	3256	4501	5758	6874	8099	9339	10594	11859	DNA	DNA	DNA	DNA
5	2160	3252	4498	5756	6874	8099	9339	10594	11864	DNA	DNA	DNA	DNA
6	2160	3256	4501	5758	6874	8099	9339	10594	11859	DNA	DNA	DNA	DNA
7	2158	3220	4448	5681	6784	7979	9199	10429	11674	DNA	DNA	DNA	DNA
8	2160	3252	4498	5756	6874	8099	9339	10594	11864	DNA	DNA	DNA	DNA
9N	2158	3220	4448	5681	6784	7979	9199	10429	11674	DNA	DNA	DNA	DNA
9S	2159	3223	4451	5683	6784	7979	9194	10429	11669	DNA	DNA	DNA	DNA
10N	2158	3221	4451	5683	6784	7979	9199	10434	11674	DNA	DNA	DNA	DNA
10S	2158	3221	4451	5683	6784	7979	9199	10434	11674	DNA	DNA	DNA	DNA

ERDF closure occurs at 2035. 1,000-year compliance period ends 3035, and 10,000-year sensitivity and uncertainty evaluation period ends 12035.

DNA = did not arrive

ERDF cell locations are shown in Figure 3-9.

Under the screening analysis, the first-arrival time of radionuclides with $K_d = 0$ mL/g is within the 1,000-year compliance time frame, but the first-arrival time of radionuclides with a $K_d > 0$ is about 200 years past the compliance time frame. For the 10,000-year post-compliance time frame chosen for evaluating sensitivity and uncertainty analysis (up to calendar year 12035), the first arrival of radionuclides with $K_d > 0.9$ mL/g does not occur within this time frame. The first arrival times for each of the 12 representative geologic columns used in one-dimensional calculations using STOMP (Section 3.4.1.8) are summarized in Table 4-2. On the basis of Table 4-2 results, radionuclides with $K_d > 0.1$ mL/g are not considered in the groundwater pathway compliance evaluation, and those with $K_d > 0.9$ mL/g are not considered in the groundwater pathway post-compliance evaluation.

Table 4-2. K_d Value Thresholds Developed on the Basis of First-Arrival Time Results of One-Dimensional Screening Analysis Using STOMP.

ERDF Cell Locations	Maximum Contaminant K_d Value (mL/g) with Arrival Time Less Than the Indicated Time Frames	
	Compliance Time Frame (1,000 years)	Sensitivity and Uncertainty Analysis Time Frame (10,000 years)
1	0.1	0.8
2	0.1	0.8
3	0.1	0.9
4	0.1	0.9
5	0.1	0.9
6	0.1	0.9
7	0.1	0.9
8	0.1	0.9
9N	0.1	0.9
9S	0.1	0.9
10N	0.1	0.9
10S	0.1	0.9

ERDF locations are shown in Figure 3-9.

Of the list of radionuclides in the ERDF inventory and on the basis of the results of the screening phase, only hydrogen-3, chlorine-36, technetium-99, niobium-94, niobium-93m, molybdenum-93, and potassium-40 are sufficiently mobile to impact groundwater during the compliance period. Additionally, during the sensitivity and uncertainty analysis time frame, iodine-129, carbon-14, and the uranium isotopes are sufficiently mobile to impact groundwater. The other radionuclides in the ERDF inventory are excluded from further groundwater impact analysis because they do not reach the water table within the evaluation time frames.

It is important to note that the screening K_d value thresholds are based on any non-zero impact to groundwater, obtained by using vadose zone properties associated with the maximum transport rates for each geologic unit and the maximum net infiltration rate present during the five different simulation periods, regardless of its location relative to the waste in ERDF. The application of these parameter values is a conservatism accepted for the screening, per the EPA guidance to use simple methods and conservative or simplified assumptions (EPA/540/F-95/041).

4.2.2 Results of Compliance Case Evaluation for Groundwater Pathway

The results of the compliance case modeling, developed on the basis of unit curie inventories, indicate that no radionuclides from ERDF reach groundwater within the compliance period (1,000 years). The earliest first arrival of any radionuclide at the point of calculation is year 4420, which is 2,385 years after closure. Hydrogen-3 and niobium-93m do not exist anywhere in the model domain in significant quantities after 1,000 years and decay to insignificant quantities (less than $1E-14$ Ci per Ci source) before reaching the water table. The extent of transport in the vadose zone at the end of the compliance period of the most

mobile radionuclides (e.g., technetium-99, $K_d = 0$ mL/g) appear as deep as the top of the Cold Creek silt (CCu_z) unit, approximately 30 m above the water table (Figure 4-2). The extent of transport of the lesser mobile radionuclides (e.g., iodine-129 and uranium-238) appears contained within the Hanford Hf2 sand unit ($K_d = 0.2$ mL/g for iodine-129 and $K_d = 0.8$ mL/g for uranium-238), approximately 48 and 57 m above the water table, respectively (Figures 4-3 and 4-4).

The moisture content in the vadose zone underneath ERDF changes slightly in response to changes in the recharge regime imposed by the surface conditions and composite liner system (Figure 4-7). The moisture content in the ERDF waste material decreases slightly from the time the composite liner is assumed to fail in year 2135 (100 years post-closure) until steady-state conditions are reestablished in approximately 2,000 years (year 4135, compare Figure 4-7(b) and (d)). The movement of moisture from the ERDF waste material to the Hanford Hf2 sand causes a slight increase in moisture content directly beneath the ERDF composite liner, where the presence of the ERDF composite liner initially prevented moisture from moving into the sand (compare Figure 4-7(b) and (c)). Overall, the changes in the moisture content throughout the profile are small.

The changes in the vertical Darcy flux (the bulk flow rate of moisture in the vadose zone) are more apparent than the changes in moisture content (Figure 4-8). The function of the ERDF composite liner is visible in Figure 4-8(a) where the trend approaches zero directly beneath the ERDF composite liner, but is approximately equal to the pre-ERDF undisturbed surface condition recharge rate of 1.7 mm/yr throughout the remainder of the vadose zone. By the time the liner is assumed to fail in 2135, the Darcy flux appears to have been impacted throughout the Hanford H2 sand (Figure 4-8 (b)), although the flux appears to remain unchanged in the units below the sand. At the end of the compliance period in 3035 and when the near-steady-state conditions are reestablished (Figure 4-8 (c) and (d)), the profile approaches an almost vertical orientation, indicating relatively uniform downward flow at a rate approximately equal to the recharge rate for evapotranspiration barrier past the 500-year design life (i.e., 1 mm/yr).

Within the range of parameters evaluated, only the combination of the maximum vadose zone properties values (that maximize the unsaturated vertical hydraulic conductivity) and the maximum recharge values (that maximize the Darcy flux) produces breakthrough of the most mobile radionuclides at the point of calculation within the 1,000-year compliance time frame, with first arrival occurring approximately 840 years after closure (Figure 4-5). With this set of parameters values (as used in the screening analysis described in Section 3.4.1.8), the extent of transport of the lesser mobile radionuclides (e.g., iodine-129; K_d of 0.1 to 0.2 mL/g) appears contained within the Hanford Hf2 sand unit, approximately 43 m above the water table (Figure 4-6).

Figure 4-2. Extent of Transport of the Most Mobile Radionuclides Such as Technetium-99 ($K_d = 0$ mL/g) in the Vadose Zone at the End of the 1,000-year Compliance Period for 1 Ci Initial Inventory in ERDF.

a) Cross-section view along northern line of ERDF cells, (b) Cross-section view along southern line of ERDF cells.

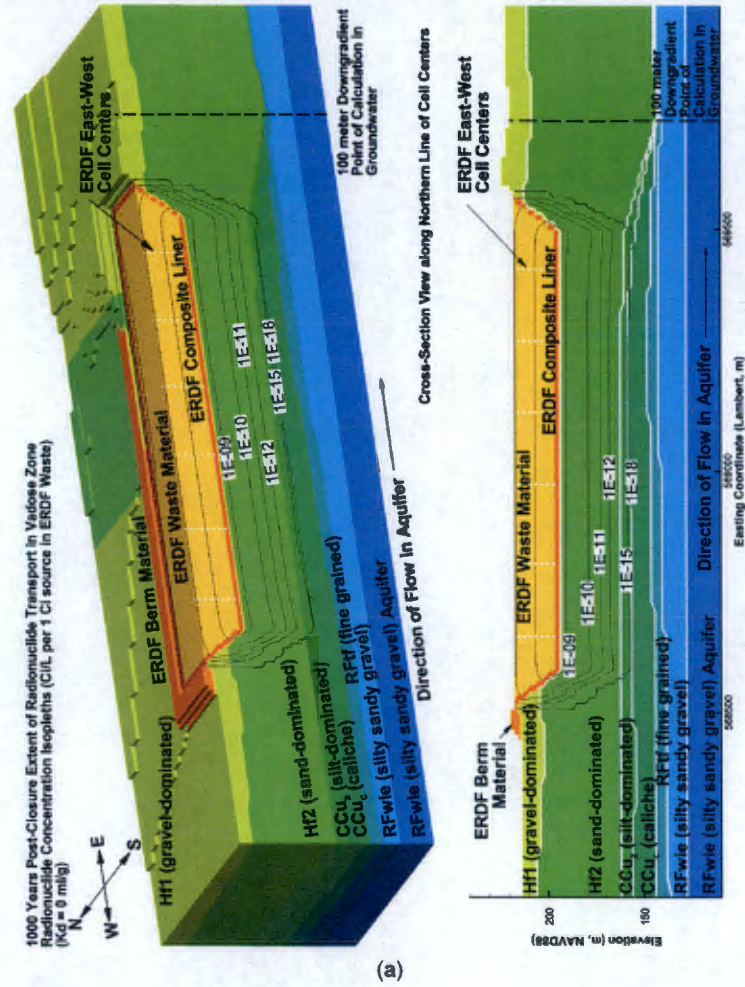


Figure 4-2. (Continued)

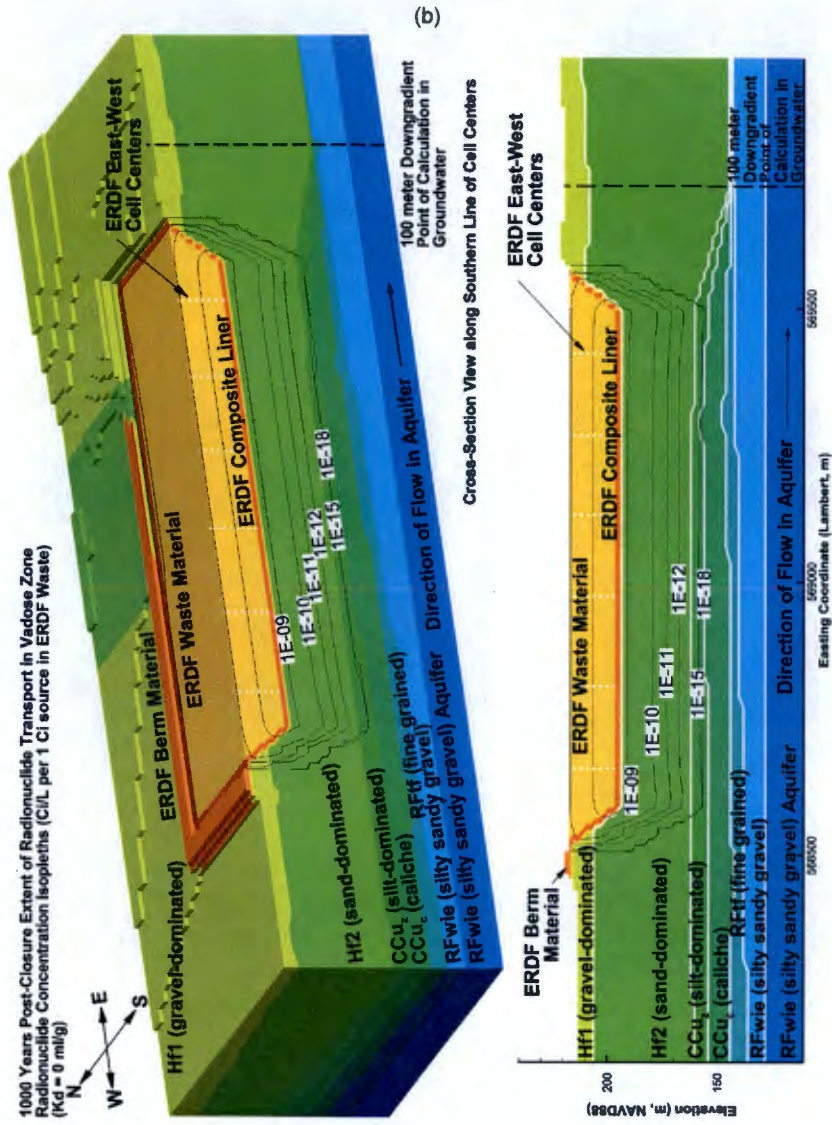


Figure 4-3. Extent of Transport of Moderately Mobile Radionuclides Such as Iodine-129 ($K_d = 0.2$ mL/g for sand dominated units) in the Vadose Zone at the End of the 1,000-year Compliance Period for 1 Ci Initial Inventory in ERDF:

(a) Cross-section view along northern line of ERDF cells, (b) cross-section view along southern line of ERDF cells.

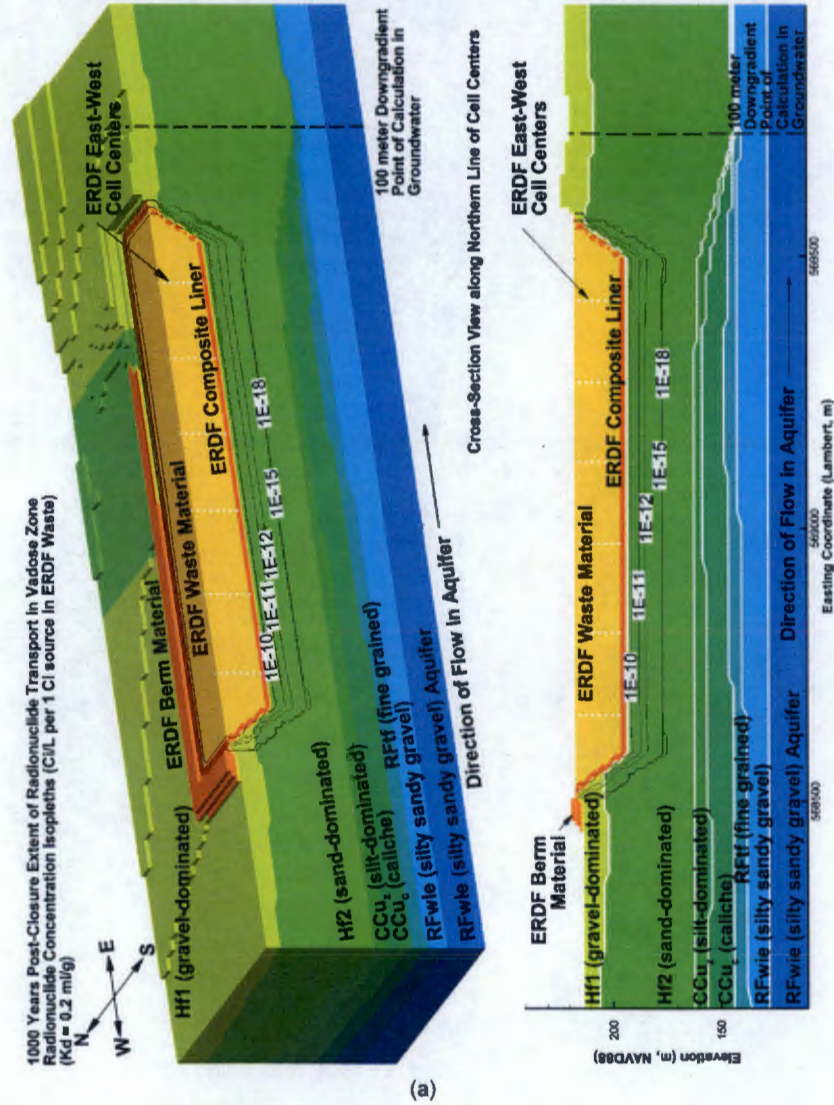


Figure 4-4. Extent of Transport of Moderately Mobile Radionuclides Such as Uranium-238 ($K_d = 0.8$ mL/g for Sand-Dominated Units) in the Vadose Zone at the End of the 1,000-year Compliance Period for 1 Ci Initial Inventory in ERDF:

(a) Cross-section view along northern line of ERDF cells, (b) cross-section view along southern line of ERDF cells.

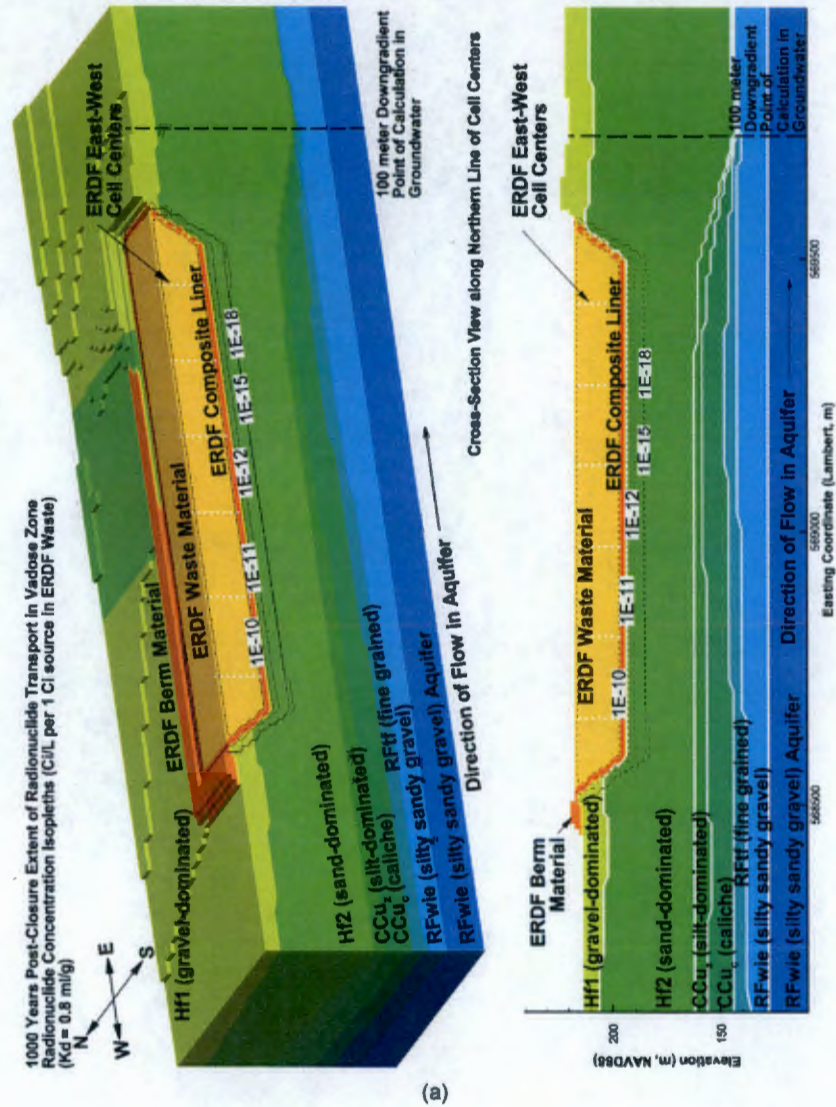
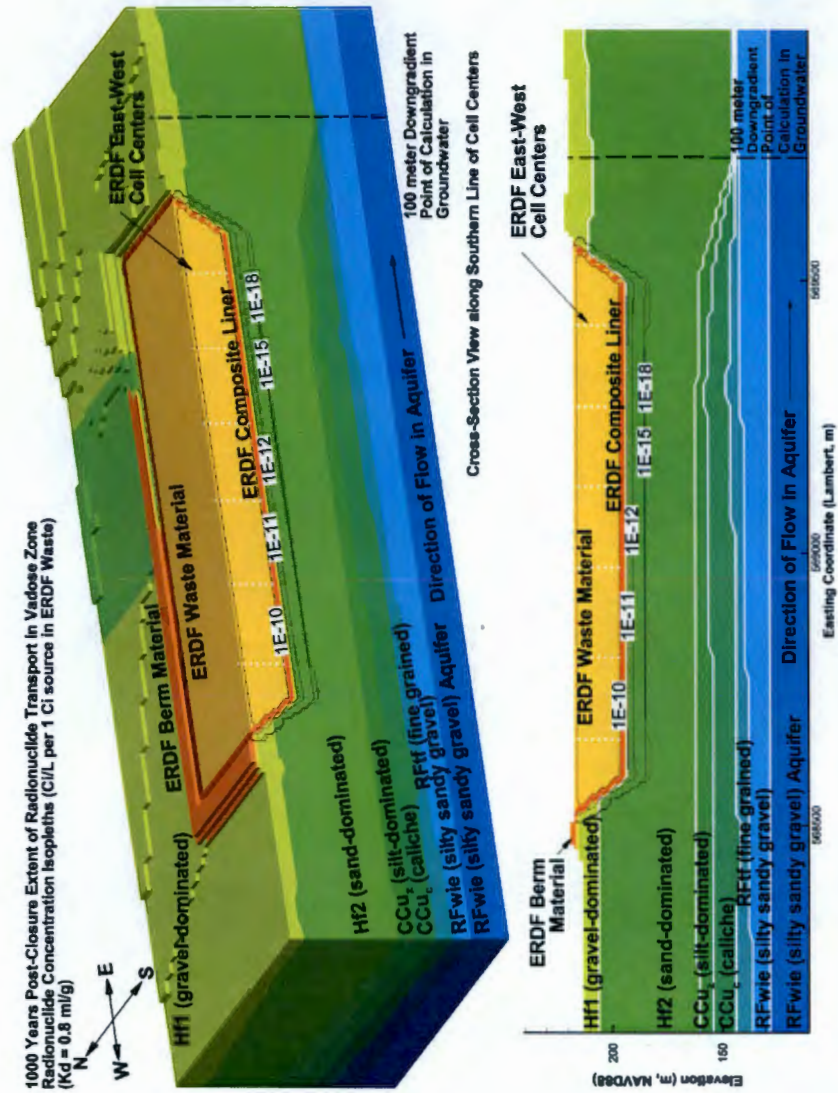


Figure 4-4. (Continued)



(b)

Figure 4-5. Extent of Transport of the Most Mobile Radionuclides Such As Technetium-99 at the End of the 1,000-year Compliance Period for 1 Ci Initial Inventory Evaluated with the Maximum Recharge Values and Vadose Zone Hydraulic Parameters:

(a) Cross-section view along northern line of ERDF cells, (b) cross-section view along southern line of ERDF cells.

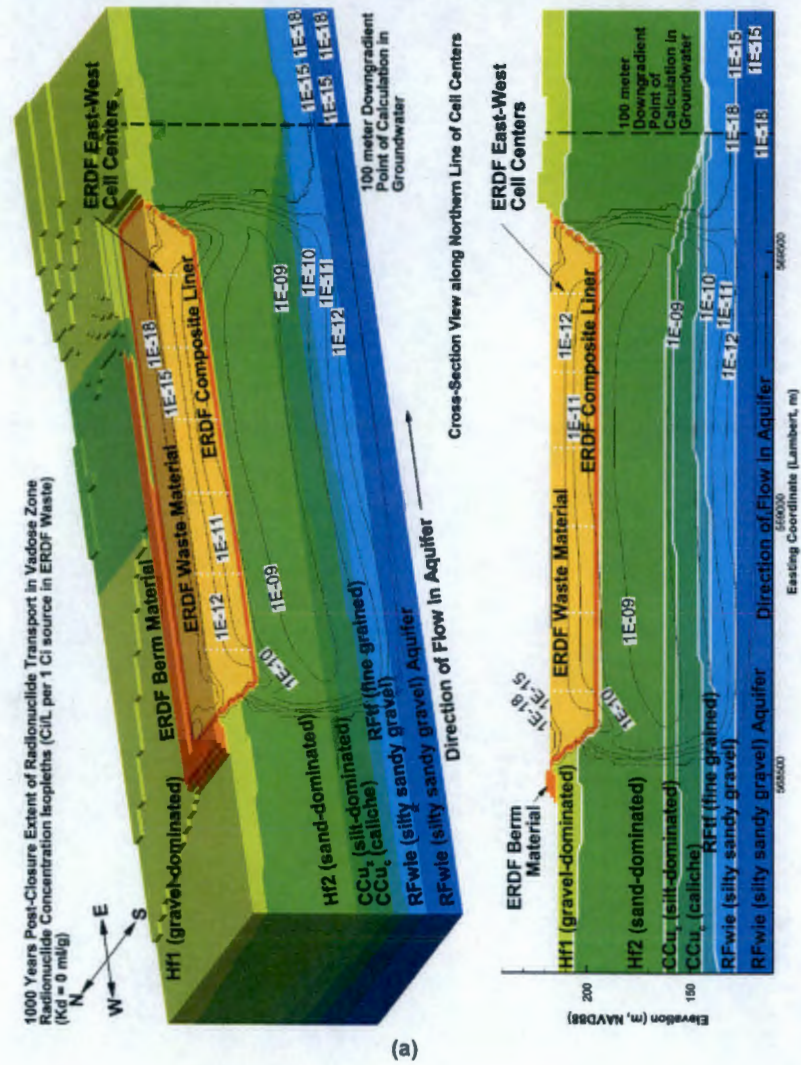
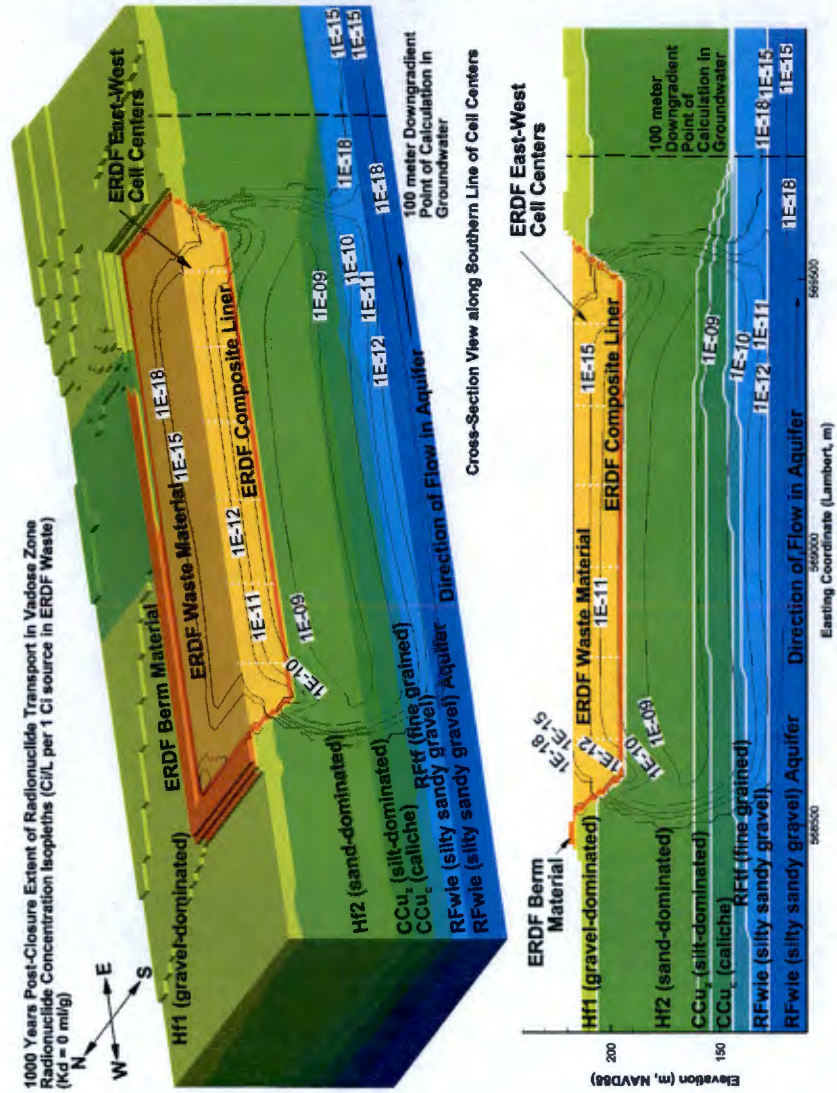


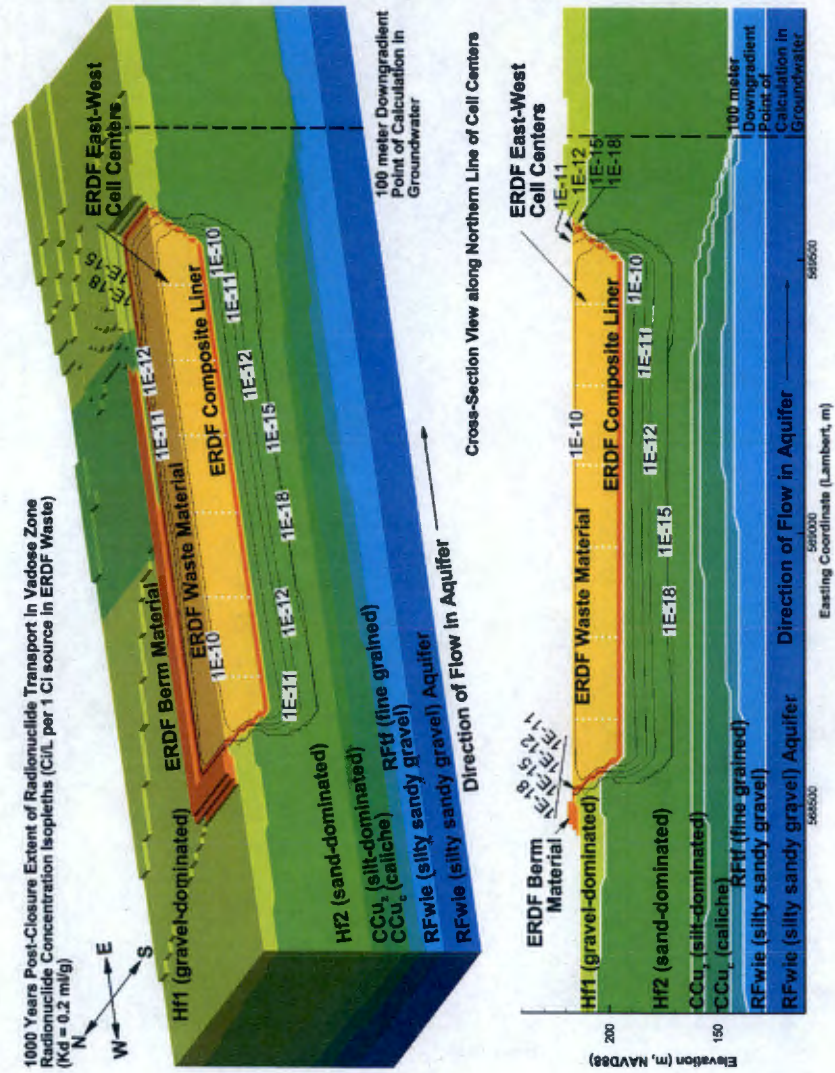
Figure 4-5. (Continued)



(b)

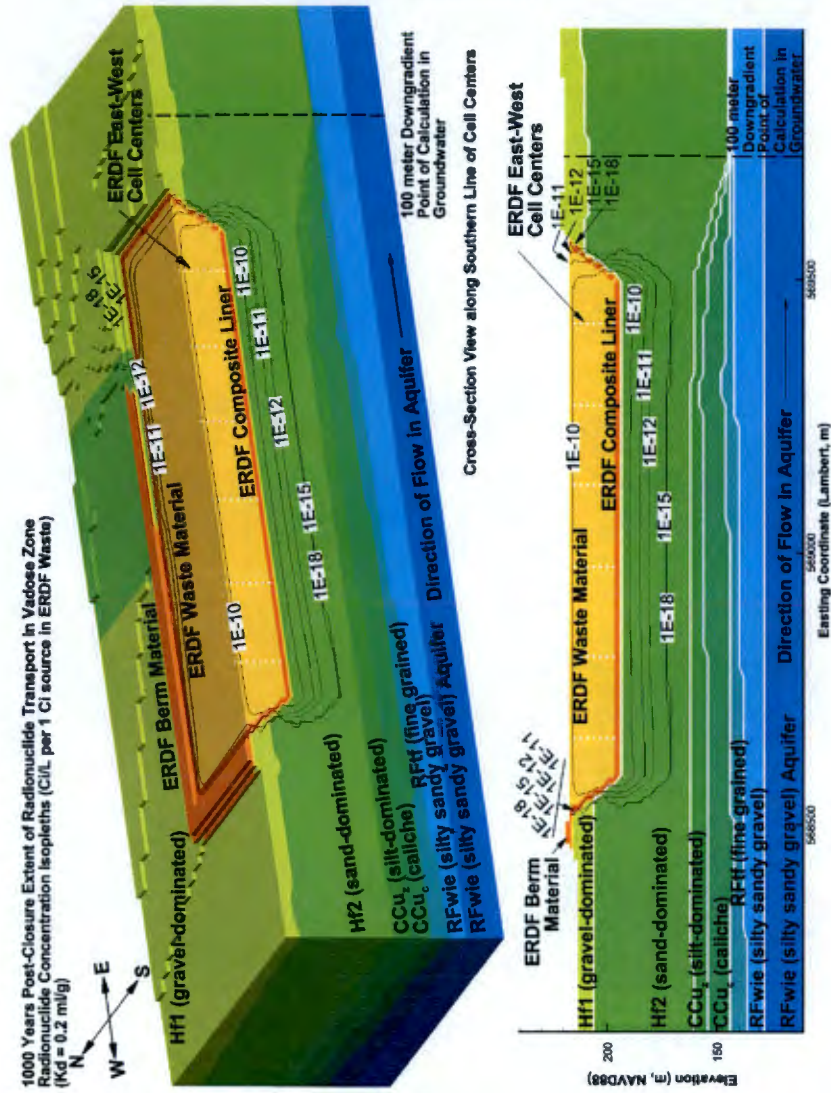
Figure 4-6. Extent of Transport of the Lesser Mobile Radionuclides Such as Iodine-129 at the End of the 1,000-year Compliance Period for 1 Ci Initial Inventory Evaluated with the Maximum Recharge Values and Vadose Zone Hydraulic Parameters:

(a) Cross-section view along northern line of ERDF cells, (b) cross-section view along southern line of ERDF cells.



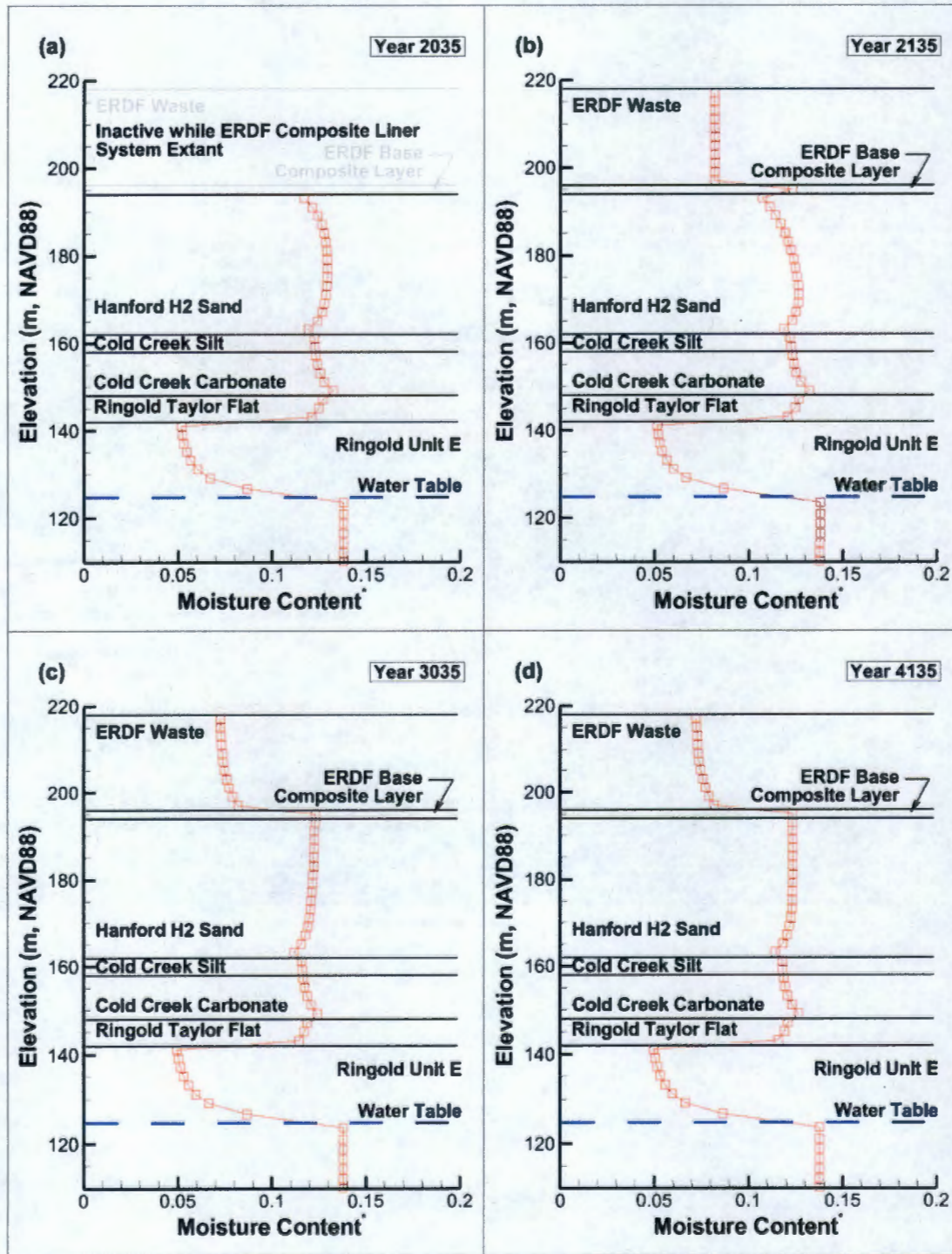
(a)

Figure 4-6. (Continued)



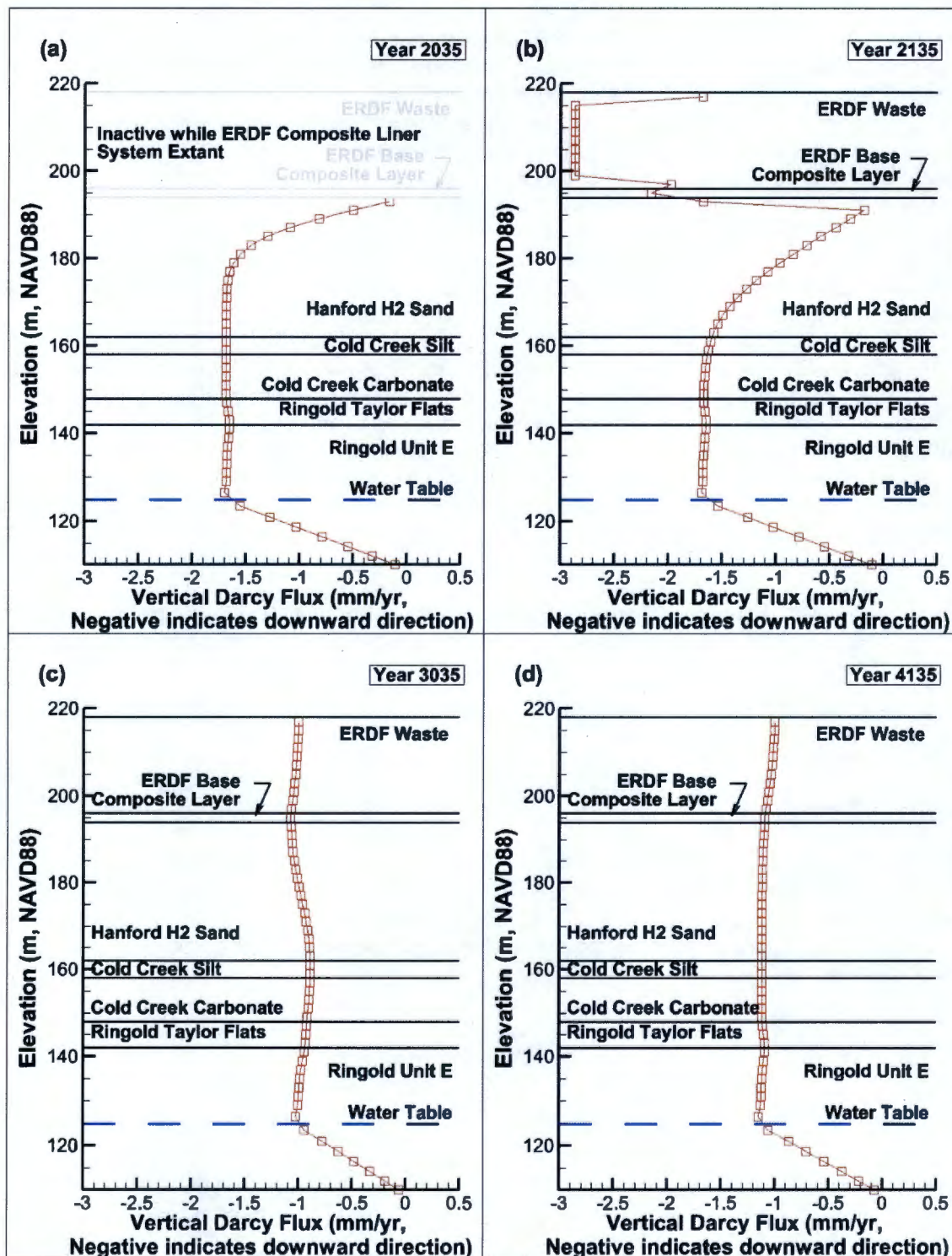
(b)

Figure 4-7. Moisture Content in the Vadose Zone at ERDF for Four Times of Interest:
 (a) ERDF Closure at Year 2035, (b) ERDF Composite Liner Failure at Year 2135,
 (c) End of Compliance Period at Year 3035, and (d) Approximate
 Reestablishment of Steady-State Flow Field.



The moisture content below the water table is equal to the porosity.

Figure 4-8. Darcy Flux in the Vadose Zone at ERDF for Four Times of Interest: (a) ERDF Closure at Year 2035, (b) ERDF Composite Liner Failure at Year 2135, (c) End of Compliance Period at Year 3035, and (d) Approximate Reestablishment of Steady-State Flow Field.



4.2.3 Results of Compliance Case Evaluation for Groundwater Pathway for the Post-Compliance Period

During the post-compliance period 1,000 to 10,000 years after closure, chlorine-36, technetium-99, niobium-94, molybdenum-93, and iodine-129 breakthrough at the point of compliance (100 m downgradient of the ERDF) as shown in Figure 4-9. Iodine-129 is the only radionuclide with a K_d value greater than zero to do so. The breakthrough curves for radionuclides (except iodine-129) reach peak values during and are decreasing at the end of the post-compliance period, whereas the iodine-129 concentration has just begun to rise and is increasing at the end of the post-compliance period. Technetium-99 has the largest peak concentration (731 pCi/L) and compliance case inventory (53 Ci) compared to any of these radionuclides. The other radionuclides all have inventories less than 1 Ci. Although the results of the different radionuclides vary because of differing radioactive decay rates, the results indicate that for long-lived nonsorbing radionuclides approximately 1 Ci of inventory translates to a maximum concentration of approximately 14 pCi/L in groundwater at the downgradient point of calculation.

Radionuclides with shorter half-lives reach peak concentrations sooner than those with longer half-lives, but the peaks are greatly reduced because of the decay. This is apparent in the results for niobium-94 and molybdenum-93, which have half-lives of $24,000^7$ years and 3,500 years, respectively. The molybdenum-93 reaches its peak concentration approximately 400 years before the niobium-94, but the peak concentration of niobium-94 is about 2.5 times greater even though the inventories are approximately the same. Table 4-3 presents a summary of the peak arrival times and maximum concentration values of the radionuclides.

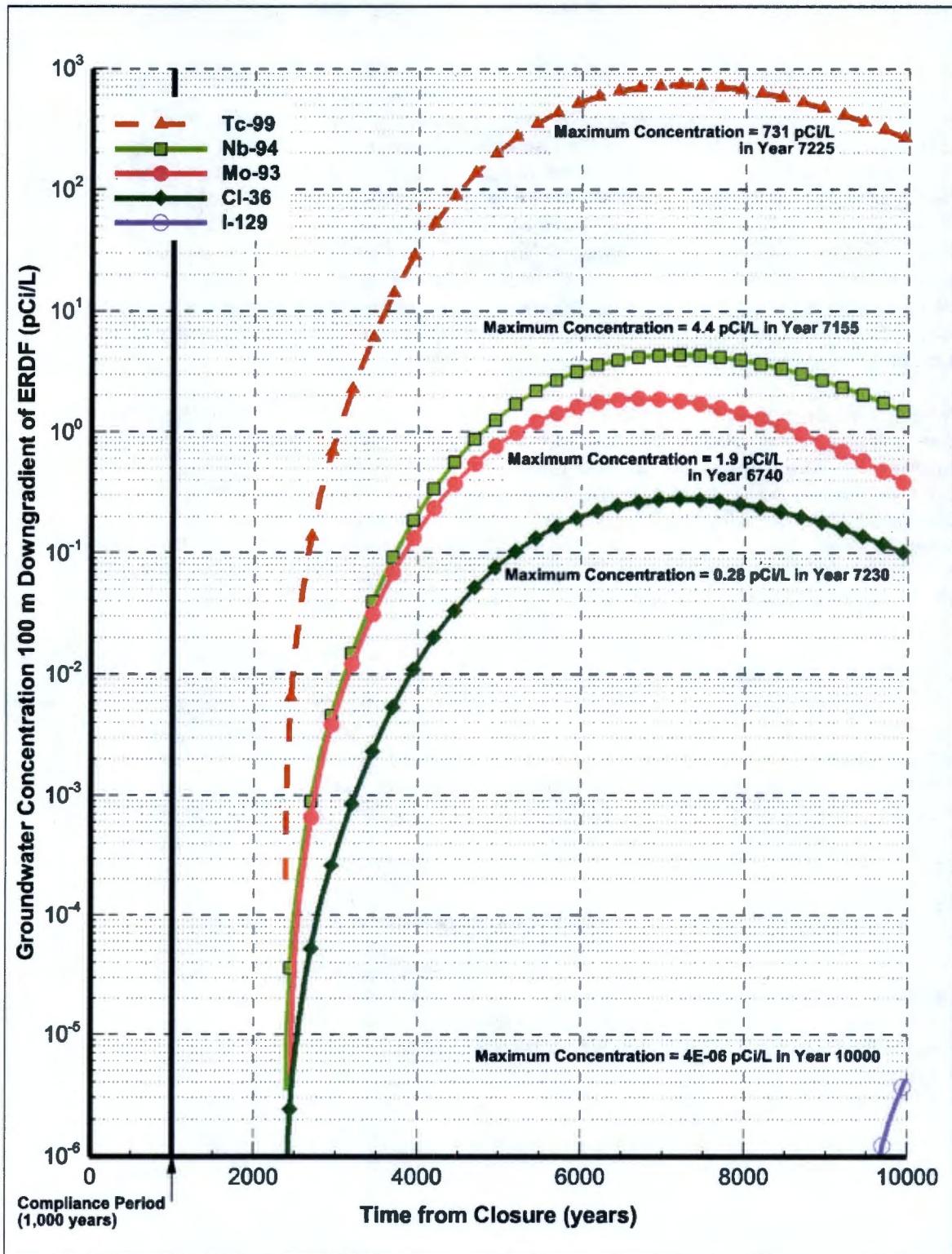
Table 4-3. Maximum Groundwater Concentration at 100 m Downgradient from ERDF Over the Compliance and Post-Compliance Time Period.

Radionuclide	Maximum Concentration (pCi/L)	Post-Closure Time to Maximum Concentration (Rounded)	Initial Inventory (Ci)
Tc-99	731	7200	53
Nb-94	4.4	7200	0.38
Mo-93	1.9	6740	0.53
Cl-36	0.28	7200	0.02
I-129	4.0E-6	10000	0.02

NOTE: Time is given as simulated time for post-closure (from calendar year 2035) and all values are rounded to no more than 2 significant digits.

⁷ Haynes and Lide, 2011, *CRC Handbook of Chemistry and Physics*, 92nd Edition (2011-2012), page 11-42, indicates that the half-life of ⁹⁴Nb is 2.4×10^4 years. Audi et al. (2003) and the National Nuclear Data Center "NuDat 2.1" database indicate that the half-life is 20,300 years. The value used in this evaluation is 24,000 years. The impact of the difference in half-life values is considered negligible on the results.

Figure 4-9. Maximum Predicted Groundwater Concentration at 100 m Downgradient from ERDF Through the End of the Post-Closure Period.



Figures 4-10 through 4-12 show the progress of technetium-99 in the porewater moving in the vadose zone and aquifer at 4,000, 7,000, and 10,000 years post-closure. These times correspond to early arrival of technetium-99 at the downgradient point of calculation, the approximate time of the peak concentration, and the conclusion of the 10,000-year simulation period. At 4,000 years after closure, the center of the plume is located primarily in the Hanford Hf2 sand unit and Cold Creek silt (CCu_z) unit. Concentrations greater than 1.0E-10 Ci/L (100 pCi/L) extend from the base of ERDF into the Ringold Taylor Flat (RFtf) unit, with some intrusion into the Ringold Unit E (RFWie) near the eastern edge of the ERDF trench. After 7,000 years, when the peak concentration occurs at the point of calculation located 100 m downgradient of ERDF, the center of the plume in the vadose zone is located primarily in Cold Creek carbonate (CCu_c) and Ringold Taylor Flat (RFtf) units, with concentrations greater than 100 pCi/L extending from approximately 22 m below the base of ERDF all the way to the water table. After 10,000 years, no porewater concentration exceeds 5.0E-10 Ci/L (500 pCi/L) and the area with concentrations greater than 100 pCi/L extends from the top of the Ringold Taylor Flat (RFtf) unit to the water table. The concentration in the aquifer at the point of calculation is has decreased from the peak value to approximately 300 pCi/L.

Figures 4-13 through 4-15 show the volumetric concentration of technetium-99 in the vadose zone and aquifer at 4,000, 7,000, and 10,000 years post-closure. While the aqueous concentration indicates the progress of the radionuclides in the porewater, the volumetric concentration provides an indication of the amount of technetium-99 contained in the different hydrogeologic units. After 4,000 years, most of the technetium-99 mass is located in the Hanford Hf2 sand unit. After 7,000 years, most of the mass has moved from the Hanford Hf2 unit into the Cold Creek (CCu_z and CCu_c) and Ringold Taylor Flat (RFtf) units, with most occurring in the RFtf unit. After 10,000 years, most of the mass occurs in the RFWie.

Figures 4-16 and 4-17 show the movement of the technetium-99 plume through the aquifer and to the point of compliance. The first arrival approximately 4,000 years into the future occurs near the northeast corner of the facility. In general, the vadose zone flux producing the highest concentration in groundwater appears to arrive at the water table near the eastern edge of ERDF. Although increasing in magnitude from 5,000 to 7,000 years into the future and decreasing in magnitude thereafter, the concentration in groundwater appears to remain relatively uniform between the eastern edge of ERDF and the eastern boundary of the model during the period 5,000 years to 9,000 years into the future. The width of the plume in groundwater does not ever appear to exceed the width of the ERDF side slopes.

4.2.4 Results of Compliance Case Evaluation for the Air Pathway

The atmospheric release is modeled for only those radionuclides that can partition into the gas phase from the dissolved phase (in water). These radionuclides are carbon-14, hydrogen-3 (tritium), iodine-129, and radon-222. The atmospheric release calculation methodology is described in Section 3.4.2. The results of the calculation are presented in Figure 4-18 in terms of diffusive mass flux per unit surface area of ERDF. The radon-222 flux is not presented as it is discussed separately in Section 4.3.

Figure 4-10. Extent of Transport and Porewater Concentration of Technetium-99 in the Vadose Zone and Aquifer 4,000 Years After Closure.

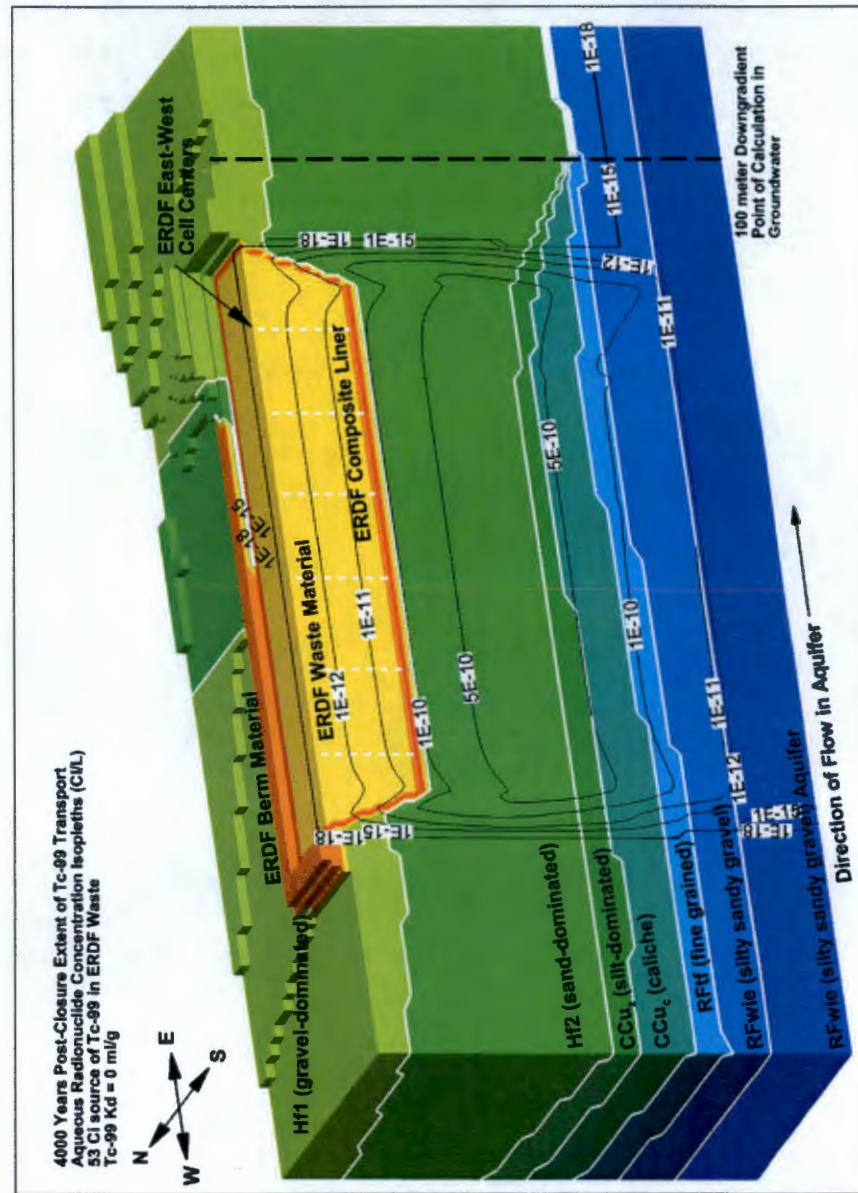


Figure 4-11. Extent of Transport and Porewater Concentration of Technetium-99 in the Vadose Zone and Aquifer 7,000 Years After Closure.

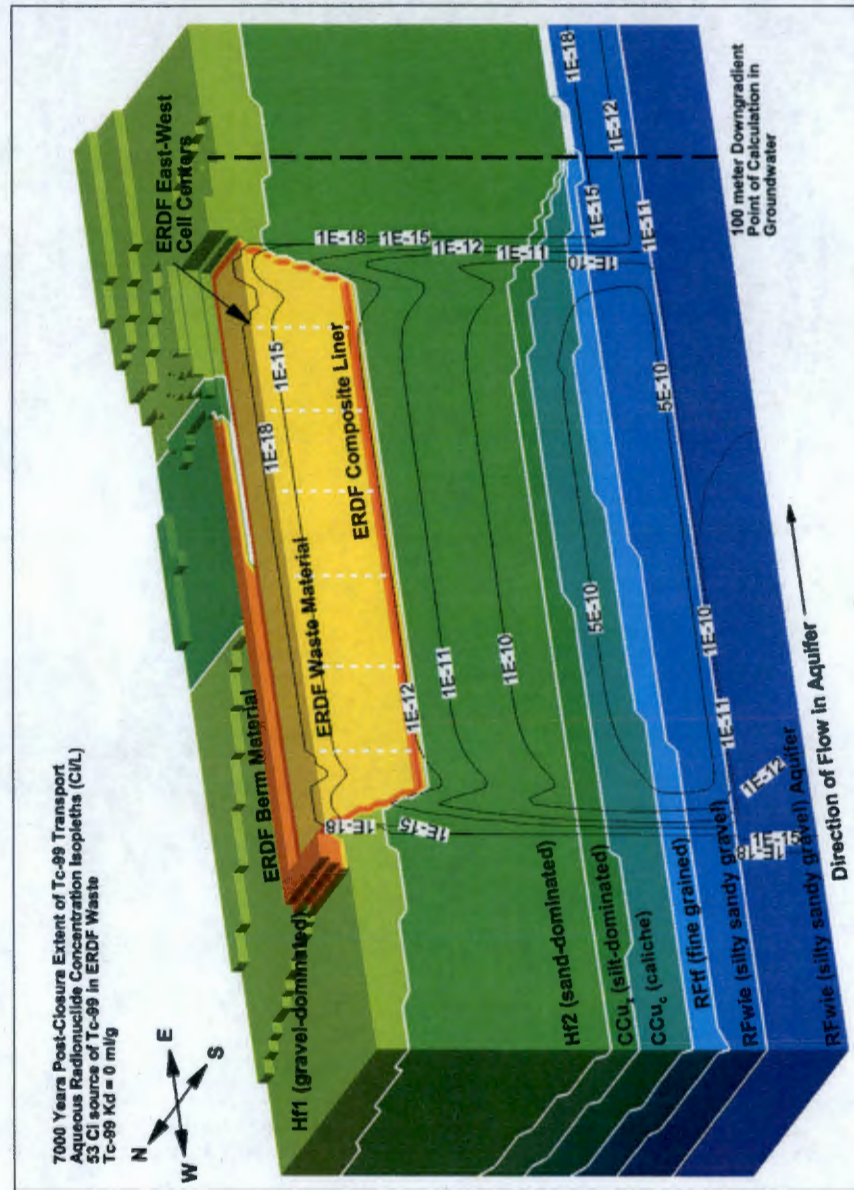


Figure 4-12. Extent of Transport and Porewater Concentration of Technetium-99 in the Vadose Zone and Aquifer 10,000 Years After Closure.

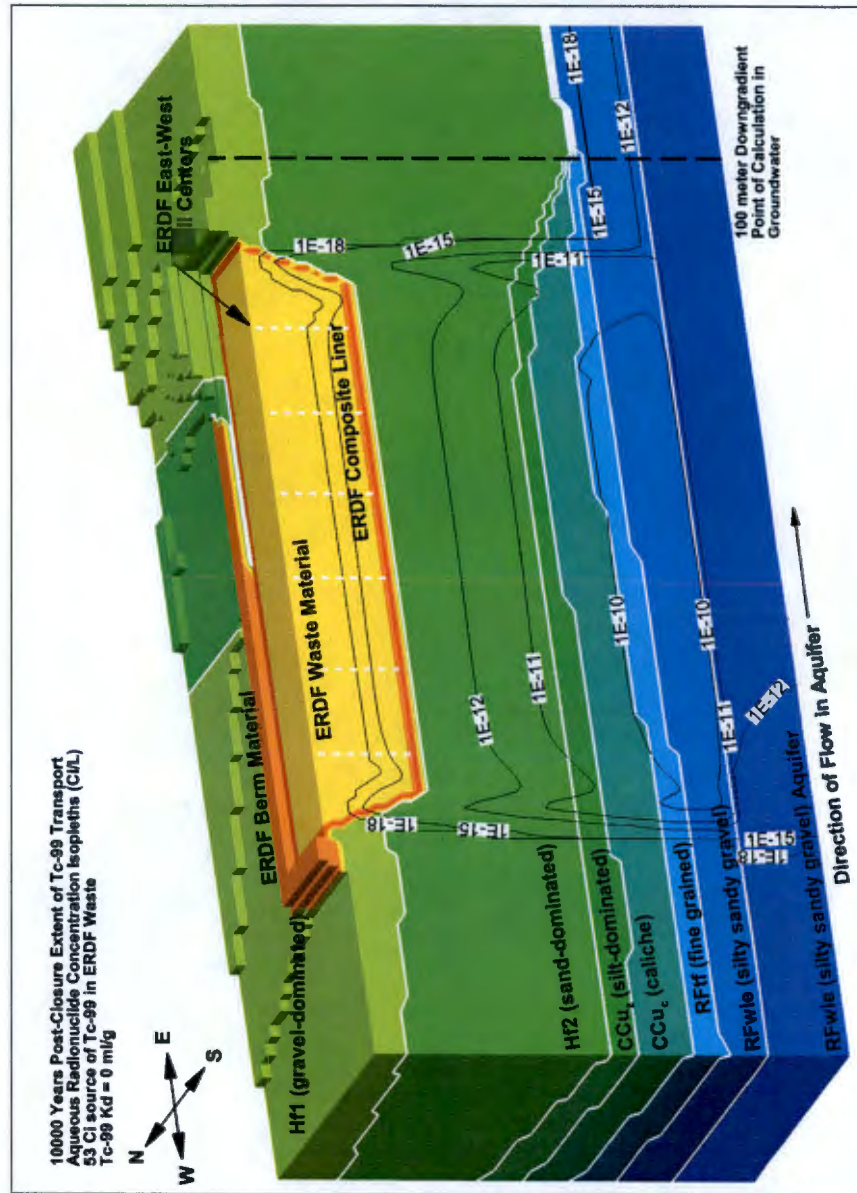


Figure 4-13. Distribution and Volumetric Concentration of Technetium-99 in the Vadose Zone and Aquifer 4,000 Years After Closure.

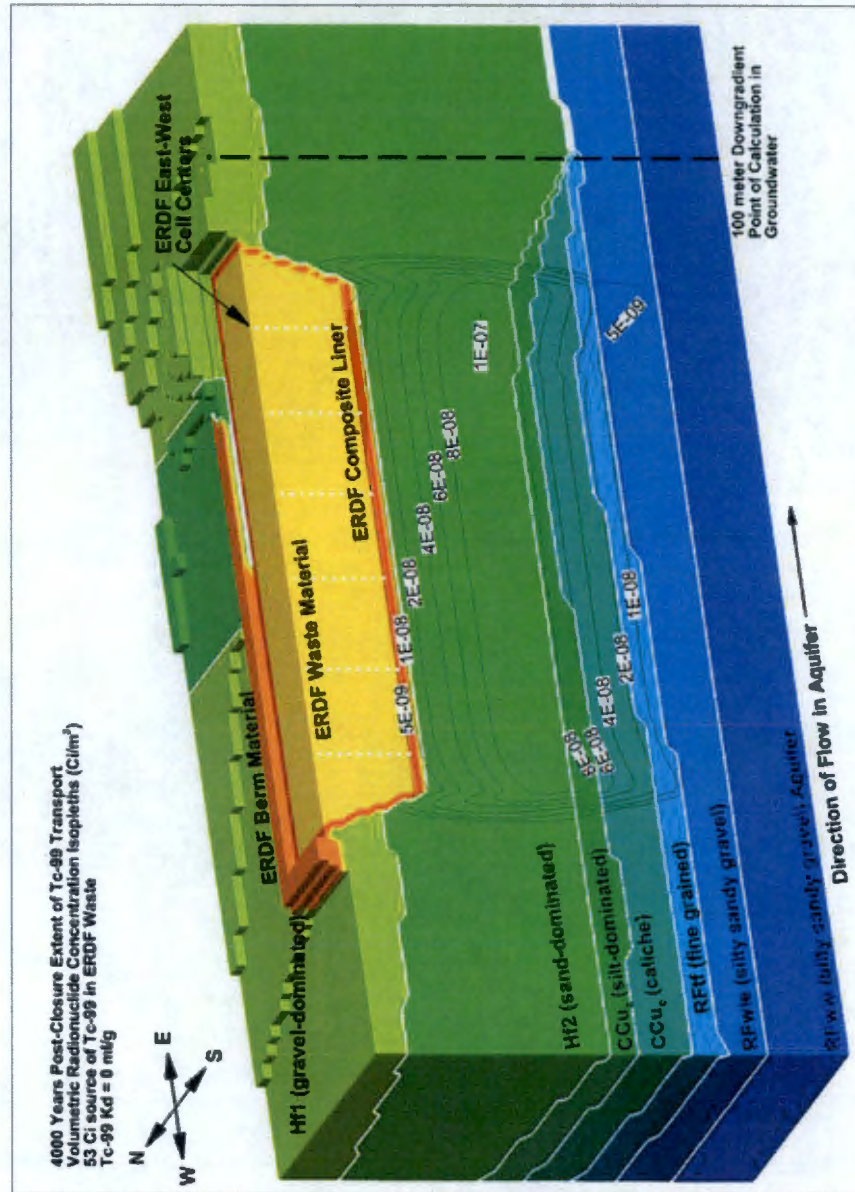


Figure 4-14. Distribution and Volumetric Concentration of Technetium-99 in the Vadose Zone and Aquifer 7,000 Years After Closure.

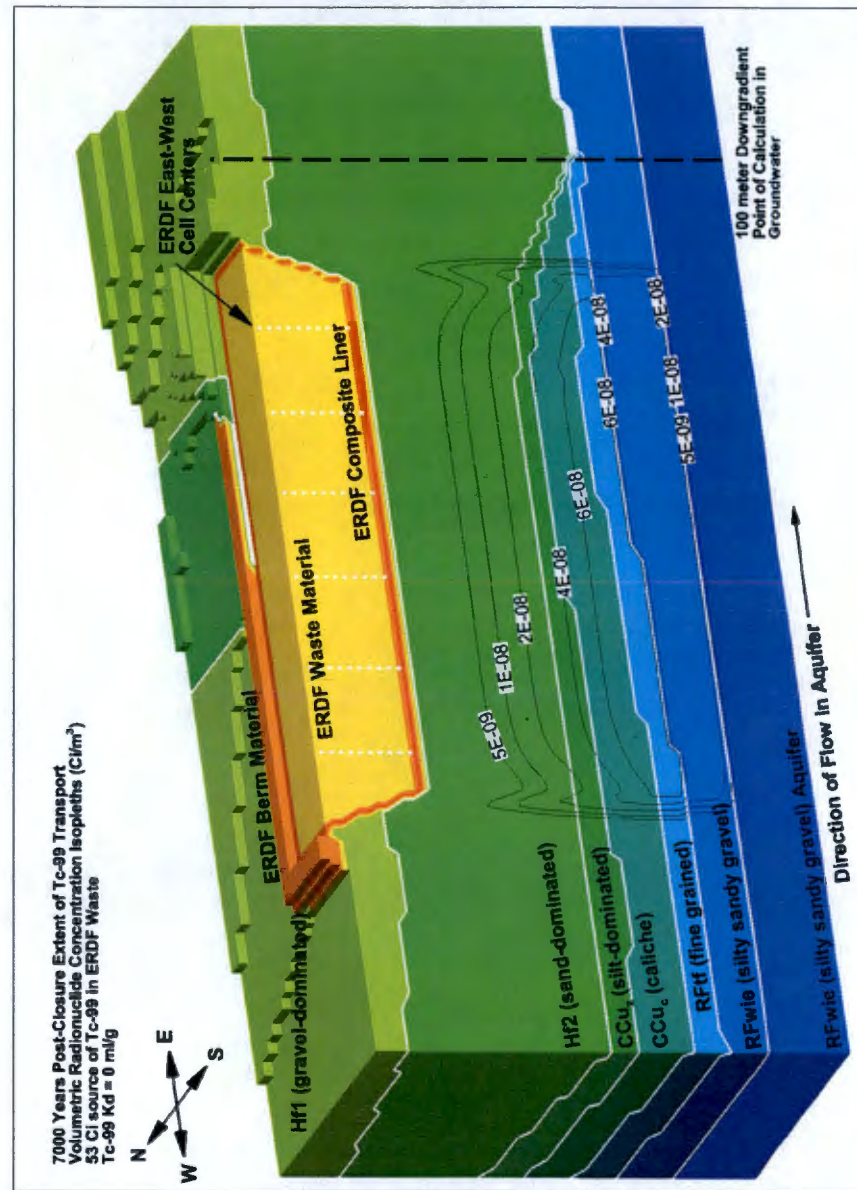


Figure 4-16. Plan View Distribution of Technetium-99 in the Aquifer 3,000, 4,000, 5,000, and 6,000 years After Closure.

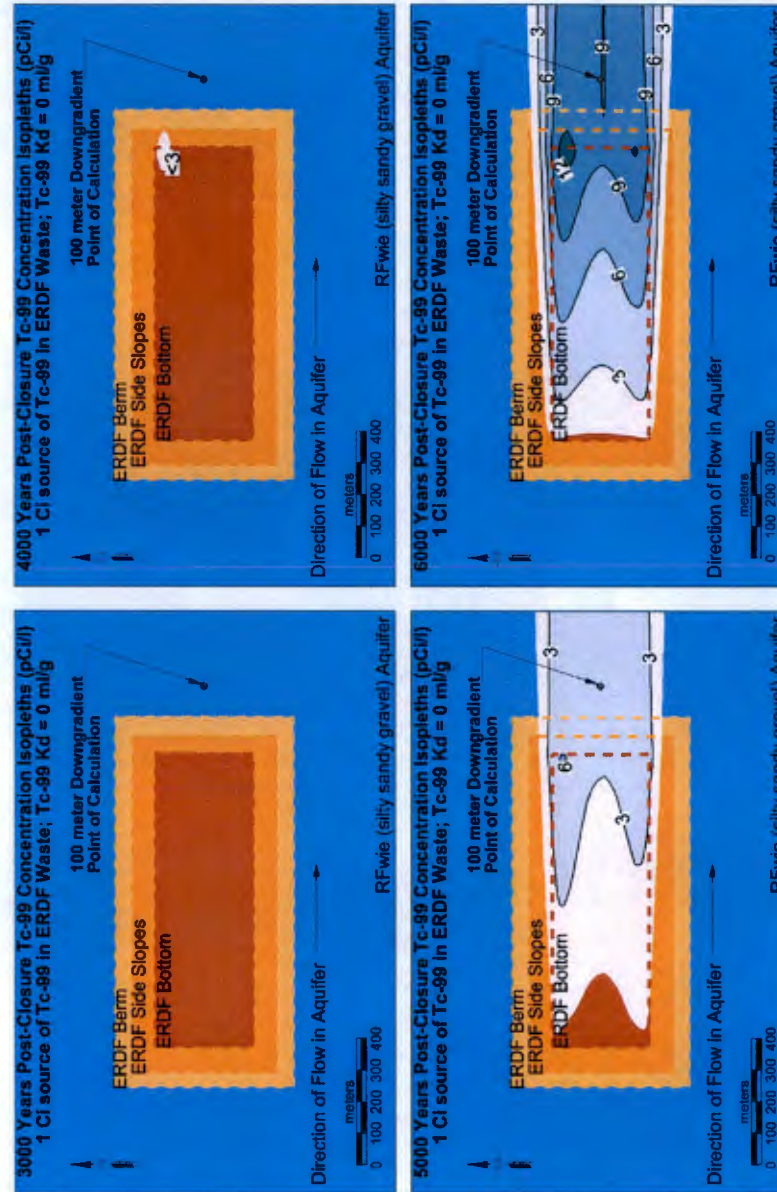


Figure 4-17. Plan View Distribution of Technetium-99 in the Aquifer 7,000, 8,000, 9,000, and 10,000 Years After Closure.

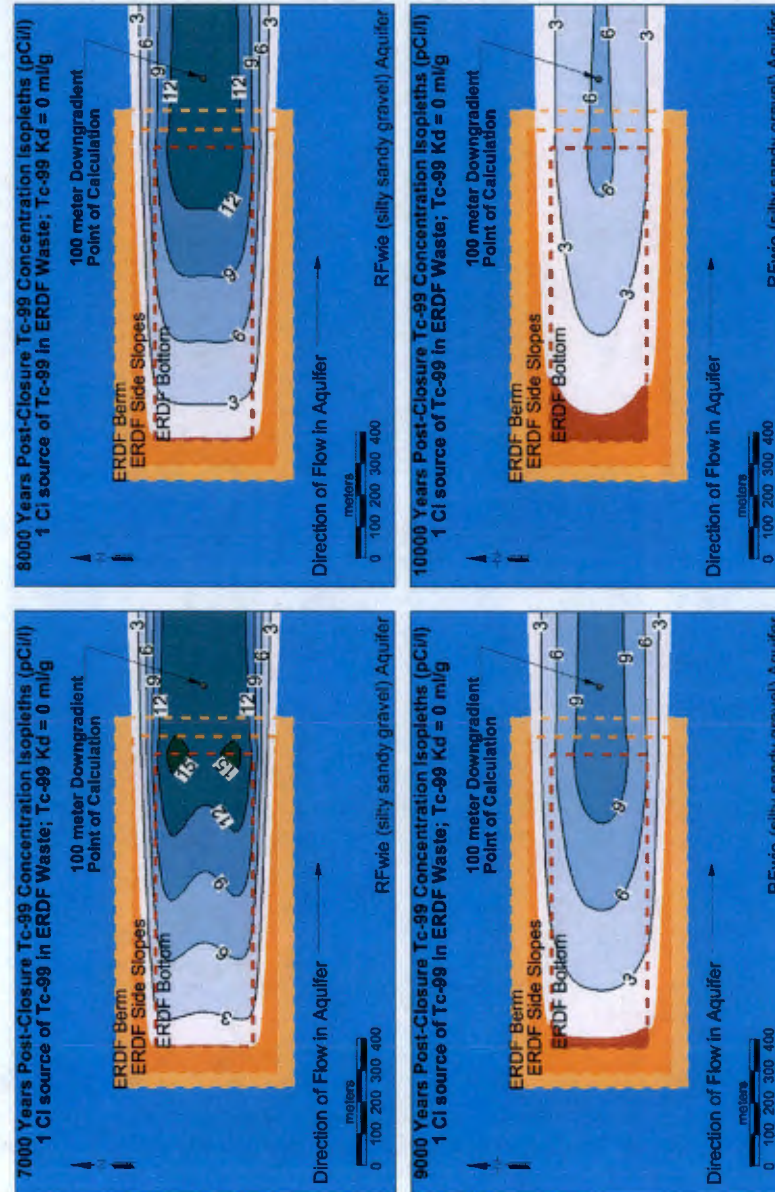
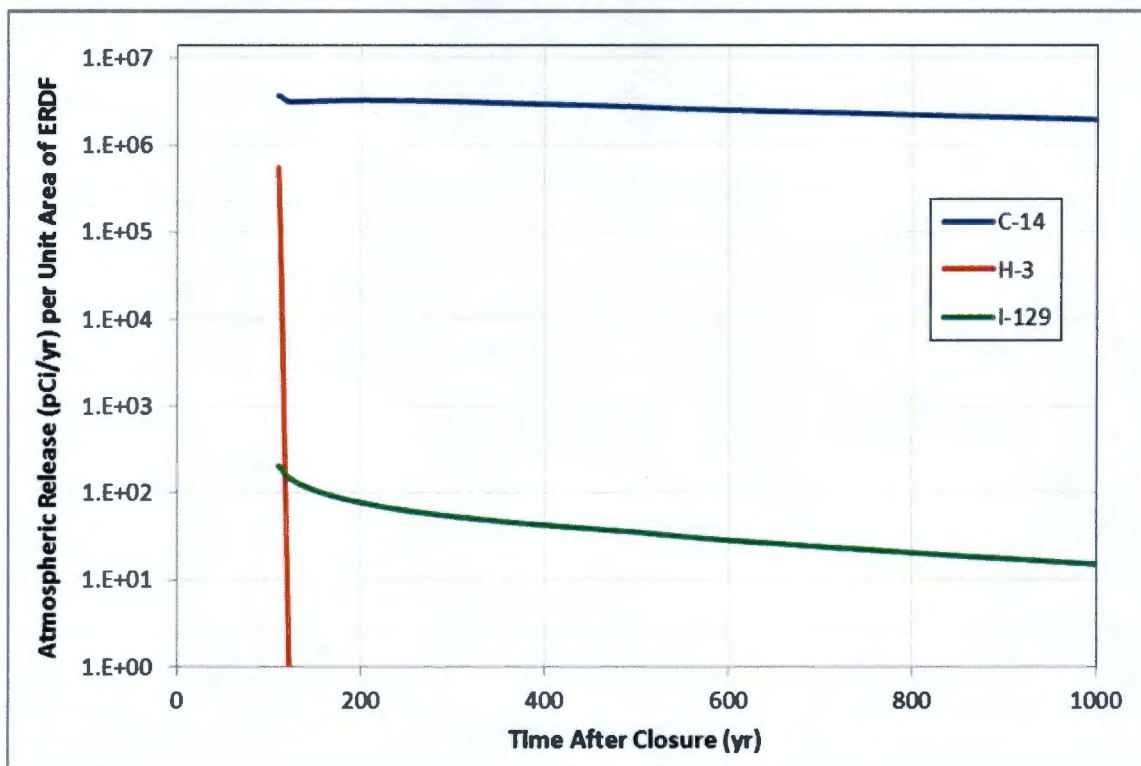


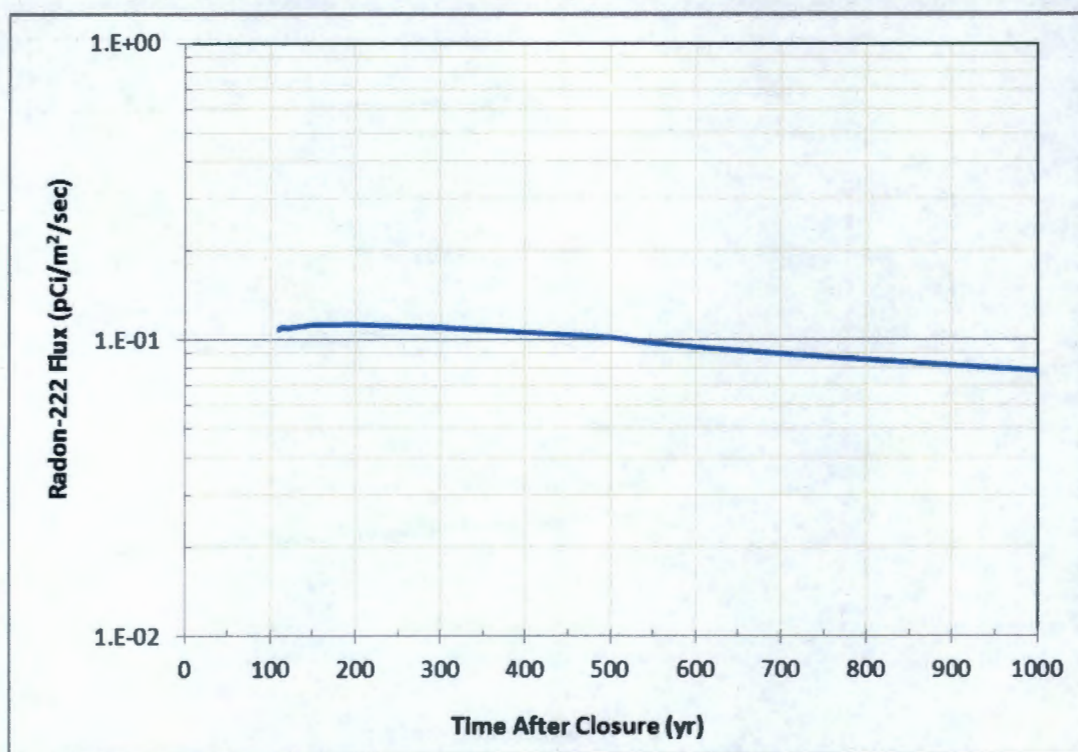
Figure 4-18. Atmospheric Release (pCi/yr) per Unit Surface Area of ERDF.

The results indicate that the atmospheric carbon-14 release is the dominant release in comparison to other radionuclides. It is sustained by a slow continuous release from the source term as a function of the graphite leaching rate. The hydrogen-3 mass flux declines sharply because the entire inventory is immediately available for release and gets transported either in the gas phase or in the dissolved phase without retardation. In addition, the hydrogen-3 mass flux declines quickly due to short half-life. The iodine-129 inventory persists due to retardation from sorption in the vadose zone and due to long half-life. Due to the small initial inventory and small gas-to-aqueous partitioning coefficient, the iodine-129 mass flux remains small throughout the simulation.

4.3 RADON ANALYSIS

As described in Section 3.5, the projected waste inventory is not a significant radon source. The initial inventory of radium-226 is estimated to be about 1.7 Ci and is expected to contribute to almost all of the radon-222 flux at early times. The computed outward diffusive flux at the ERDF surface is presented in Figure 4-19.

The peak radon flux for the 1,000-year compliance period is estimated to be about 0.11 pCi/m²/s. The flux declines as the radium-226 inventory is depleted, while the ingrowth from decay of uranium-238 and uranium-234 remains negligibly small.

Figure 4-19. Radon-222 Flux (pCi/s) per Unit Surface Area of ERDF.

4.4 BIOTIC PATHWAYS

Biointrusion into the waste from plant and animal activity is not expected due to placement of a 4.5-m-thick RCRA-compliant closure cover over ERDF. This cover will be placed above the interim compacted soil cover of approximately 0.6 m, leading to a minimum depth of intrusion of over 5 m needed to access the waste. The upper 0.9 m of the soil cover is composed of an admixture of silt and gravels that is intended to enhance the resistance to burrowing animals and long-term wind erosion. Given the features of the surface barrier (as discussed in Section 3.6), it is unlikely to become a viable biotic pathway. The release of radionuclides from this pathway is therefore not modeled.

4.5 DOSE ANALYSIS

Results of all-pathway EDE (referred in this section as dose) for the groundwater pathway is shown first followed by the air pathway and then the combined dose for both pathways using the compliance case parameter values (Sections 3.3 and 3.4). For the groundwater pathway no radionuclide arrival is predicted at the 100-m downgradient location within the compliance time period of 1,000 years (Figure 4-20a). The first arrival of radionuclides occurs past 2,000 years. The radionuclides for which a non-zero dose is calculated within the 10,000 year post-compliance time period are technetium-99, niobium-94, molybdenum-93, chlorine-36, and iodine-129. All these are long-lived radionuclides and except for iodine-129 all are transported

unretarded in the vadose and saturated zone using the compliance case parameter values. The iodine-129 breakthrough occurs just before the end of the 10,000-year simulation time.

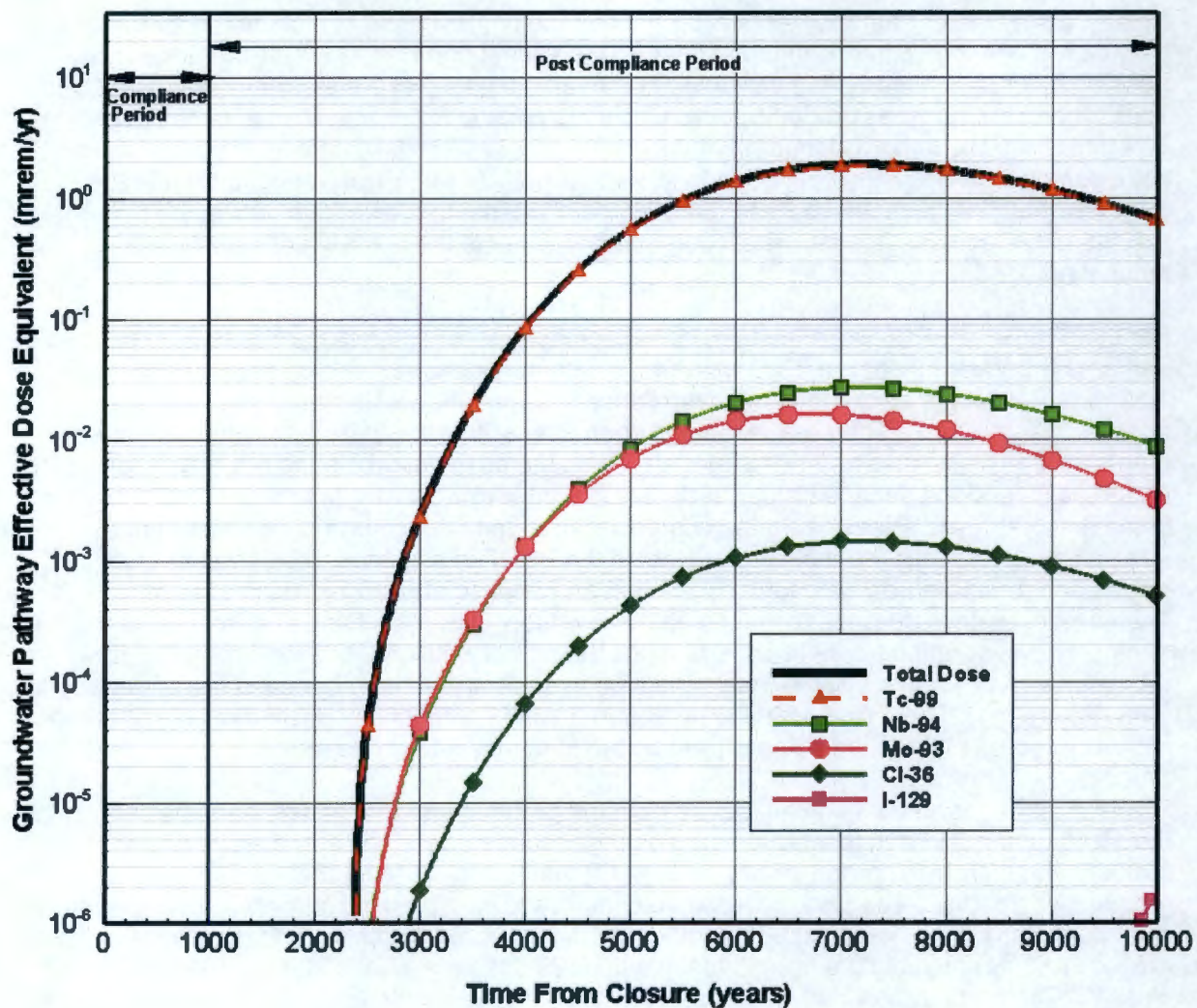
For the groundwater pathway, technetium-99 has the highest dose contribution over the entire time period and thus controls the total dose. The contribution to total groundwater pathway dose by other radionuclides is negligible. The peak total dose of 1.88 mrem/yr occurs around 7,200 years and declines gradually, which includes peak technetium-99 dose of 1.83 mrem/yr. The niobium-94 and molybdenum-93 dose curves are very similar, but the molybdenum-93 dose contribution declines earlier due to its shorter half-life (3,500 years) compared to the relatively long half-life of niobium-94 (24,000 years⁸). Among the various pathways, the dose resulting from drinking (ingestion) of contaminated water is the primary pathway for the technetium-99 dose.

For the atmospheric pathway, the total dose is predominantly a function of dose from release of carbon-14 to the atmosphere (Figure 4-20(b)). The atmospheric pathway peak total dose of 1.02 mrem/yr occurs early within the compliance time period, which includes peak carbon-14 dose of 0.96 mrem/yr. The dose is highest soon after 100 years of closure, when the release through the ERDF surface barrier is modeled, with the assumption that no release occurs prior to 100 years and the surface barrier thickness is conservatively assumed to be 1 m. Note that in the first 100 years after closure the composite liner and surface barrier are assumed to remain intact, and thus the moisture content in the ERDF is assumed to be near residual values and therefore no waste form dissolution and release of radionuclide is assumed. The carbon-14 dose declines over time as the inventory is depleted and undergoes radioactive decay. However, the carbon-14 dose remains the primary dose for the atmospheric pathway as the carbon-14 is made available from continued release of inventory bound in graphite waste form (Figure 4-1). The iodine-129 and hydrogen-3 dose contributions decline rapidly after the initial release as most of the mass is transported in the dissolved phase.

Figure 4-20(c) shows the combined dose from the groundwater and atmospheric pathway over the 10,000 years. Within the 1,000-year compliance time period the only dose is due to atmospheric pathway (predominantly carbon-14) that is controlled by the release from a graphite waste form. The peak dose within compliance time period is approximately 1 mrem/yr (with peak carbon-14 dose of 0.96 mrem/yr). Within the post-compliance time period the peak dose of 1.88 mrem/yr occurs from the technetium-99 dose that peaks at about 7,200 years after closure. The groundwater pathway dose becomes larger than the atmospheric pathway dose after about 4,000 years due to increasing dose contribution from technetium-99. The dose contribution from iodine-129 in the atmospheric pathway and groundwater pathway can be seen together in Figure 4-20(c). Table 4-4 summarizes the maximum dose and time to maximum dose over the compliance and post-compliance time periods for the receptor located 100 m downgradient of ERDF.

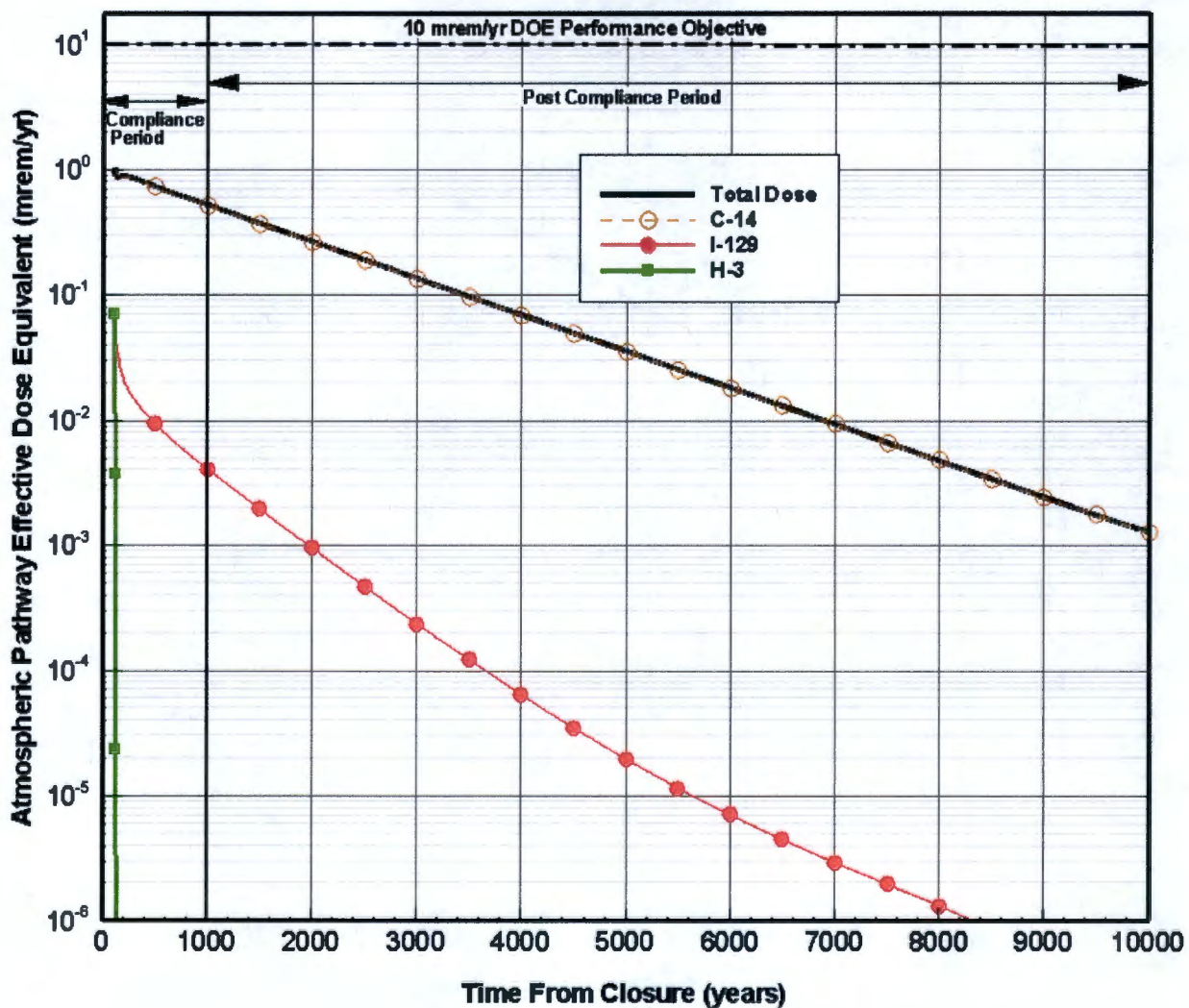
⁸ Haynes and Lide, 2011, *CRC Handbook of Chemistry and Physics*, 92nd Edition (2011-2012), page 11-42, indicates that the half-life of ⁹⁴Nb is 2.4×10^4 years. Audi et al. (2003) and the National Nuclear Data Center "NuDat 2.1" database indicate that the half-life is 20,300 years. The value used in this evaluation is 24,000 years. The impact of the difference in half-life values is considered negligible on the results.

Figure 4-20. All-Pathway Receptor Dose for (a) Groundwater Pathway Only, (b) Atmospheric Pathway Only, and (c) Combined for Both Pathways.



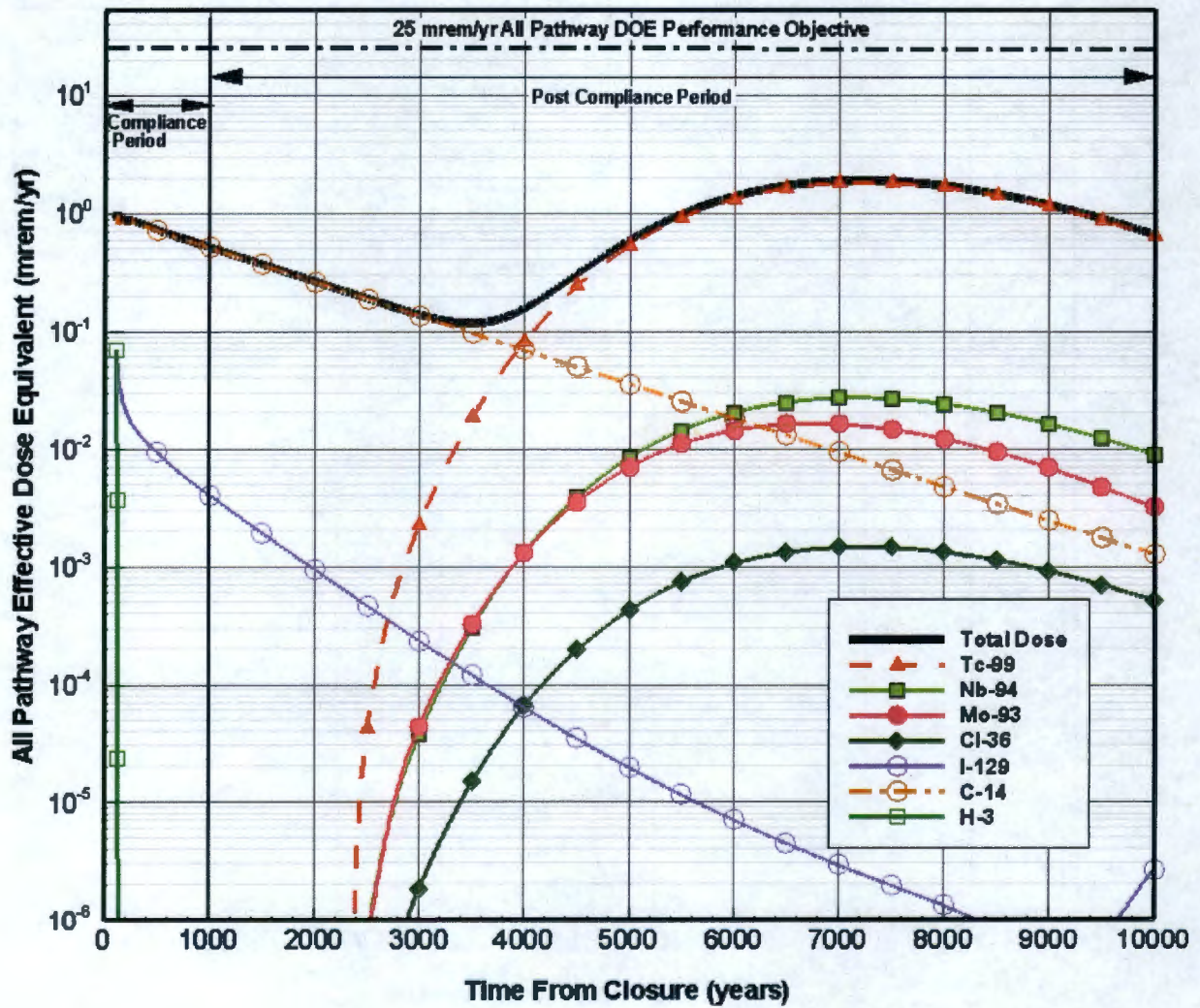
(a)

Figure 4-20. (Continued)



(b)

Figure 4-20. (Continued)



(c)

Table 4-4. Maximum All-Pathway Effective Dose Equivalent and Time to Maximum Dose for Compliance and Post-Compliance Time Periods at 100 m Downgradient of ERDF.

Radionuclide	Compliance Period ($\leq 1,000$ yr)		Post-Compliance Period ($> 1,000$ yr)	
	Maximum Dose (mrem/yr)	Time To Maximum Dose (years)	Maximum Dose (mrem/yr)	Time To Maximum Dose (years)
C-14	9.65E-01	120	5.10E-01	1010
Cl-36	0.00E+00	NA	1.46E-03	7200
H-3	6.93E-02	110	0.00E+00	NA
I-129	5.34E-02	120	3.39E-03	1010
Mo-93	0.00E+00	NA	1.63E-02	6740
Nb-94	0.00E+00	NA	2.72E-02	7200
Tc-99	0.00E+00	NA	1.83E+00	7200

NOTE: Time is given as simulated time from post-closure (calendar year 2035) and has been rounded.
NA = not applicable due to no release

4.6 SENSITIVITY AND UNCERTAINTY ANALYSIS

4.6.1 Uncertainty Analysis

The uncertainty analysis is undertaken by sampling the uncertain parameters in a probabilistic manner using Monte-Carlo based Latin hypercube sampling (LHS) methodology. The approach for the uncertainty analysis is summarized in Section 3.9 including the parameter uncertainty and probability distribution assignments. The parameter uncertainty selection details and methodology can be found in WCH-515. The probabilistic uncertainty analysis is conducted using the one-dimensional abstraction of the three-dimensional flow and transport model for ERDF, as described in Section 3.9.5.

The flow-field uncertainty is developed first by evaluating the STOMP three-dimensional flow modeling results. As discussed in Section 3.9.5, the volumetric moisture content and vertical Darcy velocity from grid blocks under 12 representative locations is averaged to derive the inputs for the one-dimensional model. The three-dimensional flow modeling was initially conducted for five combinations of uncertainties in recharge rates and vadose zone hydraulic properties, as described below.

First, the uncertainty in recharge rates was derived from sampling the probability distributions listed in Table 3-32 for parameters that vary spatially and temporally. To cover the parameter range the values were selected at five different percentiles from each probability distribution function: 0th percentile (minimum), 25th percentile (lower quartile), 50th percentile (median), 75th percentile (upper quartile), and 100th percentile (maximum). The five sampled values were judged adequate in order to balance the computational burden without sacrificing the full range of uncertainty. Table 4-5 presents the selected recharge parameter values for the uncertainty analysis along with the value chosen for the compliance case for the purpose of comparison. It is important to note that the percentiles refer to sets of parameter values and not to the individual parameters.

Table 4-5. Uncertainty in Recharge Rate Parameters.

Recharge Zone	Unit	Distribution	Min	25th Percentile	Median	75th Percentile	Max	Compliance Value
Undisturbed zone/ natural conditions	mm/yr	Triangular	0.26	1.05	1.59	2.30	4	1.7
Disturbed zone; revegetated to natural conditions	mm/yr	Fixed value	2	2	2	2	2	2
Disturbed zone (bare soil) from 1996 to 2035	mm/yr	Triangular	22.5	31.54	42.27	56.25	90	45
Below side slopes and berm (for all times)	mm/yr	Fixed value	2	2	2	2	2	2
Below intact liner (construction area) from 2035 to 2135	mm/yr	Fixed value	0	0	0	0	0	0
Below the top portion of the surface barrier from 2135 to 2535 (degraded liner)	mm/yr	Triangular	0.05	0.38	0.51	0.66	1	0.5
Below the degraded top portion of the surface barrier after 2535 (degraded liner)	mm/yr	Triangular	0.1	0.75	1.03	1.31	2	1

Second, the uncertainty in the vadose zone hydraulic parameter was considered by evaluating the combination of parameter values that lead to uncertainty in unsaturated hydraulic conductivity as a function of soil matric potential (the component of water potential due to capillary and imbibitional forces). As discussed in WCH-515 a family of 200 unsaturated hydraulic conductivity curves as a function of soil matric potential (water tension) is generated based on sampling the uncertainty in van Genuchten-Mualem parameters listed in Table 3-33 for each hydrostratigraphic unit. The uncertainty in unsaturated hydraulic conductivity curves is evaluated over-representative soil matric potential between -600 cm and -1,000 cm, which is typical of vadose zone sediments under ERDF (Figure 4-21). An empirical cumulative distribution function is calculated and the hydraulic parameter set corresponding to the 0th (minimum), 25th (lower quartile), 50th (median), 75th (upper quartile), and 100th percentile (maximum) unsaturated hydraulic conductivity curves within the soil matric potential range of -600 cm and -1,000 cm are selected (typically at -700 cm for simplification). Results for various hydrostratigraphic units are presented in Figure 4-22 showing the 200 family of curves and the selected curves for the purpose of propagating uncertainty. Table 4-6 provides the selected hydraulic parameter values for the uncertainty analyses along with the value chosen for the compliance case for the purpose of comparison. Also included is the sampled uncertainty in Polmann parameters (Table 3-34) that provide moisture-dependent anisotropy in flow for different hydrostratigraphic units. Further details on this parameter are presented in WCH-515.

Figure 4-21. Calculated Matric Potential for Various Hydrostratigraphic Units After 2,000 Years of Simulation.

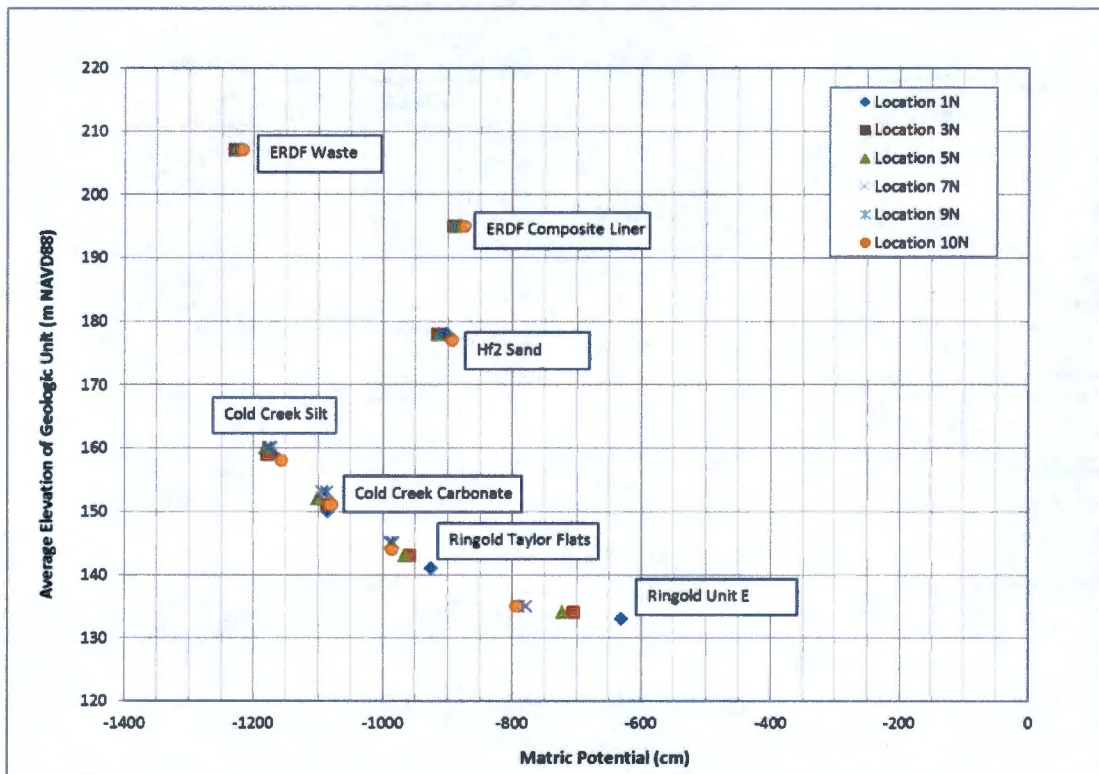


Figure 4-22. Family of Unsaturated Hydraulic Conductivity Curves as a Function of Matric Potential for Various Hydrostratigraphic Units.

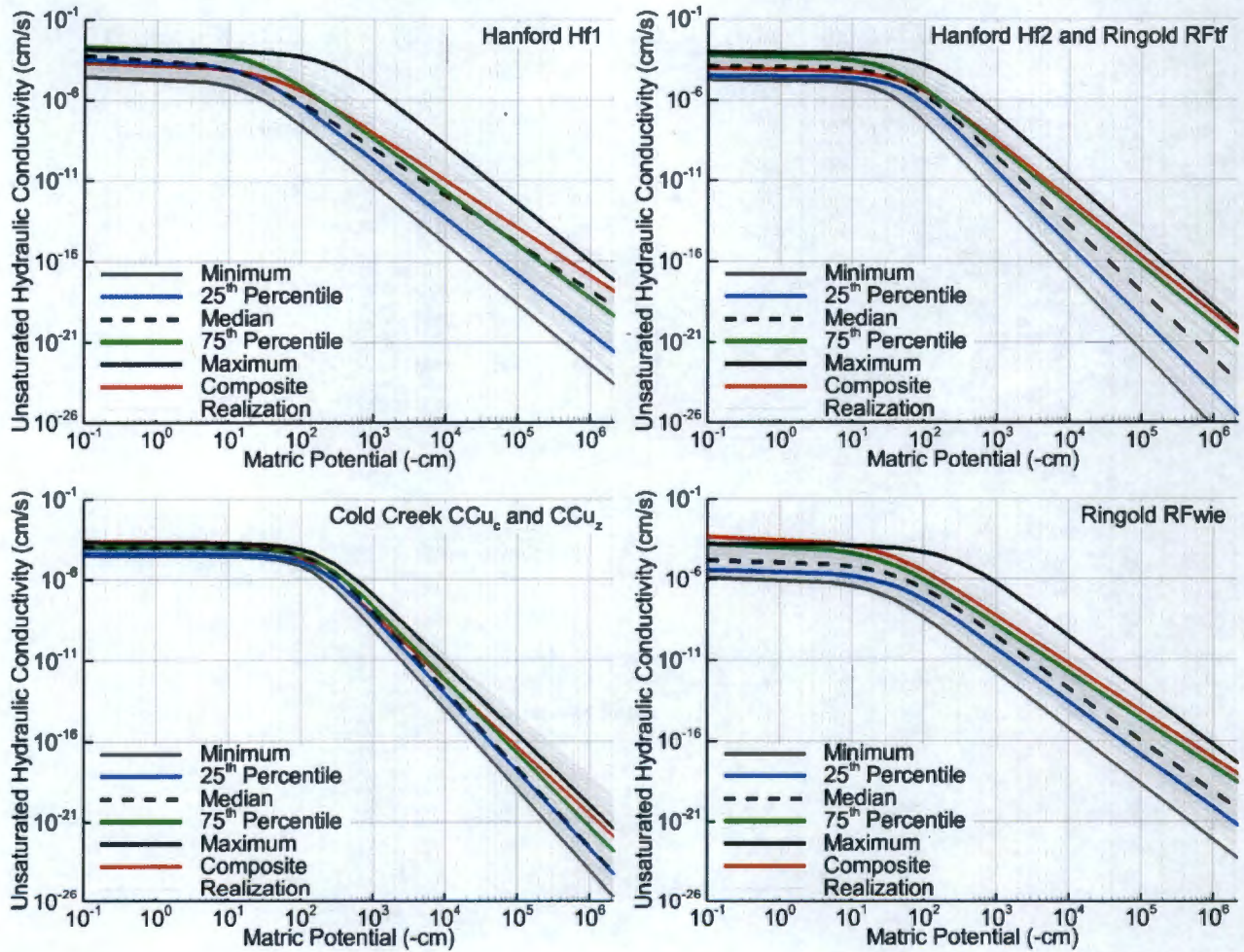


Table 4-6. Values of van Genuchten-Mualem and Polmann Parameters at Selected Percentiles. (2 Pages)

Parameter ^a	Hydrostratigraphic Unit	Unit	Type	Minimum	25th	Median	75th	Maximum	Compliance Value
van Genuchten α	Hf1	cm ⁻¹	Selected	3.98E-02	3.88E-02	2.86E-02	1.11E-02	2.70E-03	1.41E-02
	Hf2 and RFtf	cm ⁻¹	Selected	2.70E-02	1.49E-02	1.22E-02	8.33E-03	6.17E-03	1.17E-02
	CCu ₂ and CCu _c	cm ⁻¹	Selected	6.32E-03	6.00E-03	5.04E-03	4.50E-03	3.79E-03	8.50E-03
	Rfwie	cm ⁻¹	Selected	2.74E-02	1.86E-02	1.31E-02	1.51E-02	2.63E-03	2.10E-02
van Genuchten n	Hf1	(-)	Selected	1.68E+00	1.75E+00	1.71E+00	1.58E+00	1.64E+00	1.37E+00
	Hf2 and RFtf	(-)	Selected	2.09E+00	2.03E+00	1.93E+00	2.00E+00	1.79E+00	1.62E+00
	CCu ₂ and CCu _c	(-)	Selected	2.19E+00	2.09E+00	2.14E+00	2.03E+00	1.94E+00	1.85E+00
	Rfwie	(-)	Selected	1.59E+00	1.58E+00	1.33E+00	1.48E+00	1.56E+00	1.37E+00
van Genuchten-Mualem saturated water content (θ_s)	Hf1	(-)	Selected	2.33E-01	2.73E-01	2.02E-01	2.08E-01	2.03E-01	2.13E-01
	Hf2 and RFtf	(-)	Selected	4.08E-01	3.31E-01	3.68E-01	3.53E-01	3.52E-01	3.82E-01
	CCu ₂ and CCu _c	(-)	Selected	4.28E-01	3.60E-01	4.36E-01	3.84E-01	3.92E-01	4.35E-01
	Rfwie	(-)	Selected	1.76E-01	1.26E-01	2.06E-01	1.17E-01	1.37E-01	1.38E-01
van Genuchten-Mualem residual water content (θ_r)	Hf1	(-)	Selected	2.24E-02	5.51E-03	1.07E-02	2.17E-02	4.87E-03	3.20E-03
	Hf2 and RFtf	(-)	Selected	1.00E-01	9.56E-02	1.29E-01	1.03E-01	2.38E-02	4.43E-02
	CCu ₂ and CCu _c	(-)	Selected	4.69E-02	2.33E-02	2.81E-02	1.14E-02	1.11E-02	6.65E-02
	Rfwie	(-)	Selected	1.37E-02	6.88E-03	1.30E-02	2.17E-03	2.97E-03	1.00E-02
van Genuchten-Mualem fitted saturated hydraulic conductivity (K_s)	Hf1	cm/s	Selected	2.89E-05	1.05E-03	1.20E-03	1.15E-04	1.42E-03	2.62E-04
	Hf2 and RFtf	cm/s	Selected	1.86E-05	2.85E-05	5.00E-05	6.19E-05	9.14E-04	9.88E-05
	CCu ₂ and CCu _c	cm/s	Selected	3.07E-05	9.09E-05	1.02E-04	9.27E-05	1.99E-04	2.40E-04
	Rfwie	cm/s	Selected	1.35E-06	8.52E-06	8.59E-06	8.43E-05	1.74E-04	5.60E-04
van Genuchten-Mualem parameter ℓ	All units	(-)	Fixed	5.00E-01	5.00E-01	5.00E-01	5.00E-01	5.00E-01	5.00E-01
Polmann Mean of $\ln K_s$	Hf1	cm/s	Fixed	1.49E+01	1.49E+01	1.49E+01	-1.49E+01	1.49E+01	-1.49E+01
	Hf2 and RFtf	cm/s	Fixed	1.46E+01	1.46E+01	1.46E+01	-1.46E+01	1.46E+01	-1.46E+01
	CCu ₂ and CCu _c	cm/s	Fixed	1.04E+01	1.04E+01	1.04E+01	-1.04E+01	1.04E+01	-1.04E+01
	Rfwie	cm/s	Fixed	1.58E+01	1.58E+01	1.58E+01	-1.58E+01	1.58E+01	-1.58E+01
Polmann Variance of $\ln K_s$	Hf1	cm ² /s ²	Fixed	1.94E+00	1.94E+00	1.94E+00	1.94E+00	1.94E+00	1.94E+00
	Hf2 and RFtf	cm ² /s ²	Fixed	1.50E+00	1.50E+00	1.50E+00	1.50E+00	1.50E+00	1.50E+00
	CCu ₂ and CCu _c	cm ² /s ²	Fixed	1.01E+00	1.01E+00	1.01E+00	1.01E+00	1.01E+00	1.01E+00
	Rfwie	cm ² /s ²	Fixed	3.56E+00	3.56E+00	3.56E+00	3.56E+00	3.56E+00	3.56E+00

Table 4-6. Values of van Genuchten-Mualem and Polmann Parameters at Selected Percentiles. (2 Pages)

Parameter ^a	Hydrostratigraphic Unit	Unit	Type	Minimum	25th	Median	75th	Maximum	Compliance Value
Polmann ρ	Hf1	cm ⁻¹	Fixed	-2.60E-04	-2.60E-04	-2.60E-04	-2.60E-04	-2.60E-04	-2.60E-04
	Hf2 and RFtf	cm ⁻¹	Fixed	-7.20E-04	-7.20E-04	-7.20E-04	-7.20E-04	-7.20E-04	-7.20E-04
	CCu _c and CCu _z	cm ⁻¹	Fixed	2.40E-03	2.40E-03	2.40E-03	2.40E-03	2.40E-03	2.40E-03
	Rfwie	cm ⁻¹	Fixed	-1.10E-04	-1.10E-04	-1.10E-04	-1.10E-04	-1.10E-04	-1.10E-04
Polmann zeta (ζ)	Hf1	cm ⁻¹	Fixed	2.50E-04	2.50E-04	2.50E-04	2.50E-04	2.50E-04	2.50E-04
	Hf2 and RFtf	cm ⁻¹	Fixed	6.55E-04	6.55E-04	6.55E-04	6.55E-04	6.55E-04	6.55E-04
	CCu _c and CCu _z	cm ⁻¹	Fixed	9.34E-04	9.34E-04	9.34E-04	9.34E-04	9.34E-04	9.34E-04
	Rfwie	cm ⁻¹	Fixed	1.84E-04	1.84E-04	1.84E-04	1.84E-04	1.84E-04	1.84E-04
Polmann lambda (λ)	Hf1	cm	Fixed	3.00E+01	3.00E+01	3.00E+01	3.00E+01	3.00E+01	3.00E+01
	Hf2 and RFtf	cm	Fixed	5.00E+01	5.00E+01	5.00E+01	5.00E+01	5.00E+01	5.00E+01
	CCu _c and CCu _z	cm	Fixed	5.00E+01	5.00E+01	5.00E+01	5.00E+01	5.00E+01	5.00E+01
	Rfwie	cm	Fixed	3.00E+01	3.00E+01	3.00E+01	3.00E+01	3.00E+01	3.00E+01
Polmann A	Hf1	s ⁻¹	Fixed	3.68E-03	3.68E-03	3.68E-03	3.68E-03	3.68E-03	3.68E-03
	Hf2 and RFtf	s ⁻¹	Fixed	6.20E-03	6.20E-03	6.20E-03	6.20E-03	6.20E-03	6.20E-03
	CCu _c and CCu _z	s ⁻¹	Fixed	1.04E-02	1.04E-02	1.04E-02	1.04E-02	1.04E-02	1.04E-02
	Rfwie	s ⁻¹	Fixed	3.71E-03	3.71E-03	3.71E-03	3.71E-03	3.71E-03	3.71E-03
Polmann minimum of VZ anisotropy ratio (K _v /K _w)	Hf1	(-)	Calculated	1.21E+01	1.21E+01	1.21E+01	1.21E+01	1.21E+01	1.21E+01
	Hf2 and RFtf	(-)	Calculated	9.40E+00	9.40E+00	9.40E+00	9.40E+00	9.40E+00	9.40E+00
	CCu _c and CCu _z	(-)	Calculated	1.10E+00	1.10E+00	1.10E+00	1.10E+00	1.10E+00	1.1
	Rfwie	(-)	Calculated	4.33E+01	4.33E+01	4.33E+01	4.33E+01	4.33E+01	43.3
Polmann maximum of VZ anisotropy ratio (K _v /K _w)	Hf1	(-)	Calculated	1.79E+01	1.79E+01	1.79E+01	1.79E+01	1.79E+01	17.9
	Hf2 and RFtf	(-)	Calculated	1.70E+01	1.70E+01	1.70E+01	1.70E+01	1.70E+01	16.96
	CCu _c and CCu _z	(-)	Calculated	1.10E+00	1.10E+00	1.10E+00	1.10E+00	1.10E+00	1.1
	Rfwie	(-)	Calculated	5.77E+01	5.77E+01	5.77E+01	5.77E+01	5.77E+01	57.7

^a The parameters are defined in Section 3.4.1.7 along with the equations that they are used in.

Note that the parameter sets presented in Table 4-6 correspond to the percentile curves selected from the unsaturated hydraulic conductivity-matric potential relationships shown in Figure 4-22. For example, in Table 4-6, the parameter set associated with the "maximum" case implies the parameter combination that leads to the maximum unsaturated hydraulic conductivity curve shown in Figure 4-22. It does not imply that the individual parameters are set to the maximum value of their range.

Third, in order to derive the uncertainty in flow field, the recharge rates sampled for the given percentile were combined with the vadose zone hydraulic parameters for the corresponding percentile. For example, the 75th^h percentile recharge rate values from Table 4-5 and 75th percentile vadose zone hydraulic parameter values from Table 4-6 are used as input to the three-dimensional STOMP flow model. As a result five flow fields are generated for the purpose of evaluating uncertainty. The results are extracted from grid blocks under 12 representative locations (Figure 3-15) and then averaged for use in the one-dimensional abstraction model using GoldSim. As noted in Table 3-30, each flow field result is vertically discretized into 15 spatial zones based on the hydrostratigraphic unit type and distance from the base of ERDF. As an example, Figure 4-23 presents the uncertainty in volumetric moisture content and vertical Darcy velocity for a representative grid cell within Hf2 and RFWie (Ringold Unit E) units (see Figure 3-17 for location of the grid cells in the vertical profile). Figure 4-24 shows the volumetric moisture content profiles for selected spatial locations as a function of depth and time. The profiles do not show appreciable variation spatially indicating that averaging the results spatially can provide representative flow-field conditions.

The uncertainty in flow field is combined with uncertainty in transport parameters. The transport parameters are sampled within GoldSim based on a one-dimensional abstraction model from probability distributions specified in Tables 3-36 through 3-38. The uncertainty in saturated zone flow hydraulic conductivity is implemented based on the probability distribution specified in Table 3-35. GoldSim can solve the mass transport equations, and its batch reactor cell-pathway capability is used for this purpose. The GoldSim cell pathway is equivalent to a mixing cell (a batch-reactor) and can explicitly represent processes such as species-dependent partition coefficient, solubility constraints, mass transport (advection and diffusion by liquid phase or suspended particles), and any radioactive decay and ingrowth. When multiple cells are linked together, the behavior of the cell network is mathematically identical to a network of finite difference nodes describing a coupled system of differential equations. Both vadose zone and saturated zone transport can be modeled using this capability. A specialized GoldSim element called a source element is used to model the release rate of contaminants (including slow leaching of carbon-14 from graphite) and to evaluate uncertainty in the source term. The cell pathways require time-dependent inputs for advective flow and water content, which are provided by the flow-field discretization in the vertical direction.

The adequacy of the one-dimensional transport model is tested by comparing the results to the three-dimensional STOMP-based transport model. Figure 4-25 shows the vadose zone transport results based on the compliance flow-field and transport parameter values assuming 1 Ci inventory of technetium-99 within the ERDF volume. Due to coarser vertical discretization in the one-dimensional abstraction, the results from those nodes that are closest to the three-dimensional model grid nodes are compared. The results indicate good comparison between the one-dimensional abstraction model and the three-dimensional model in the vadose zone. The differences in peak concentrations are less than 15%.

Figure 4-23. Example of Uncertainty in Volumetric Moisture Content and Vertical Darcy Velocity for Selected Grid Nodes in Hf2 and RFwie Hydrostratigraphic Units After Closure.

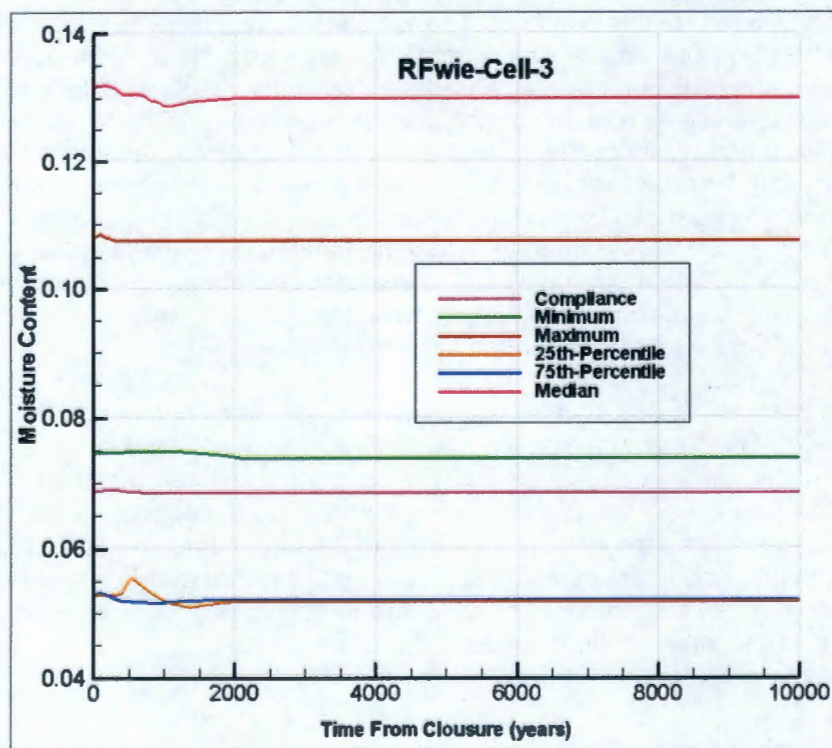
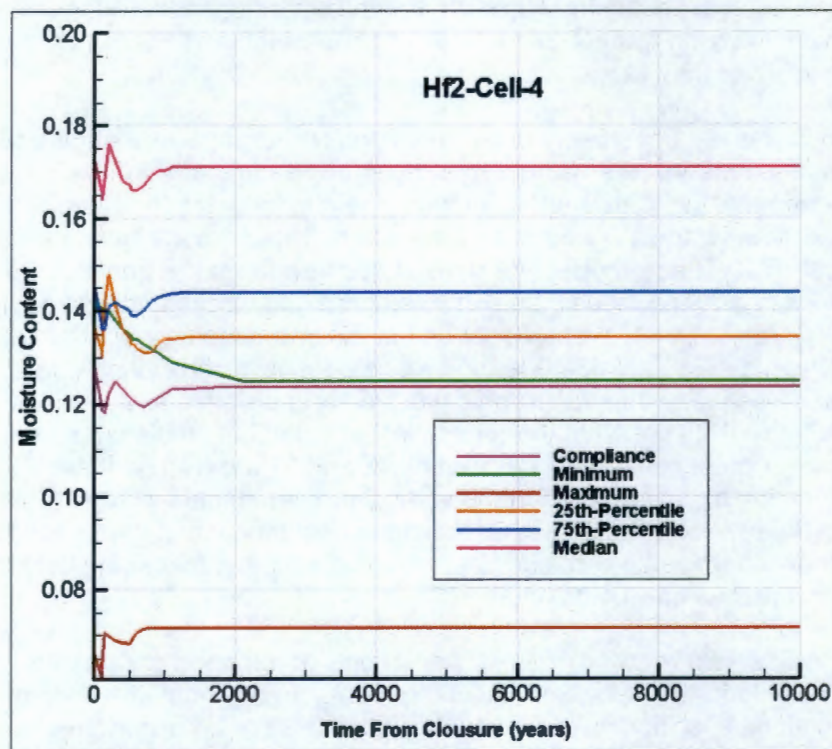


Figure 4-23. (Continued)

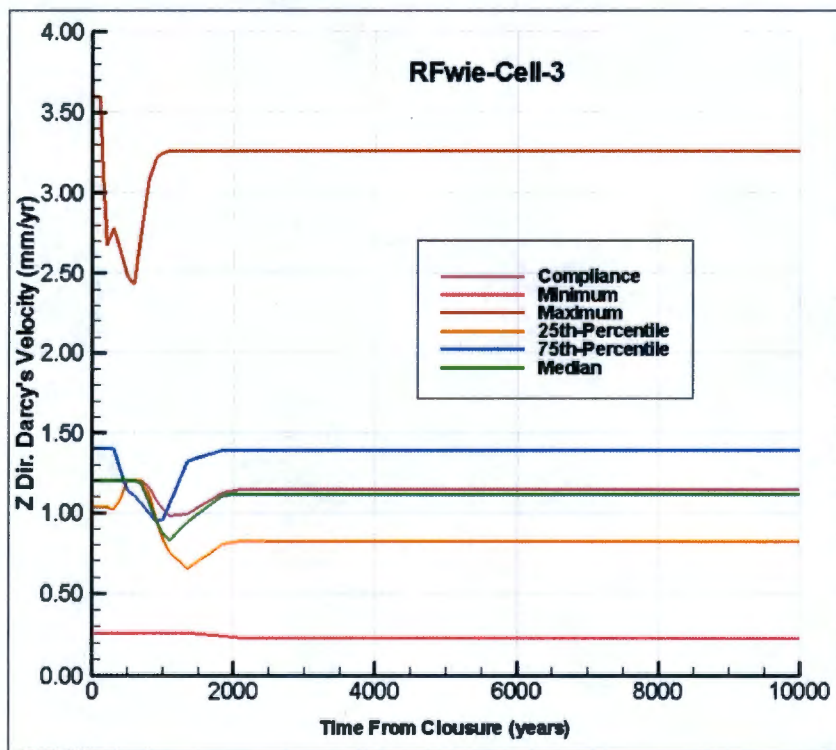
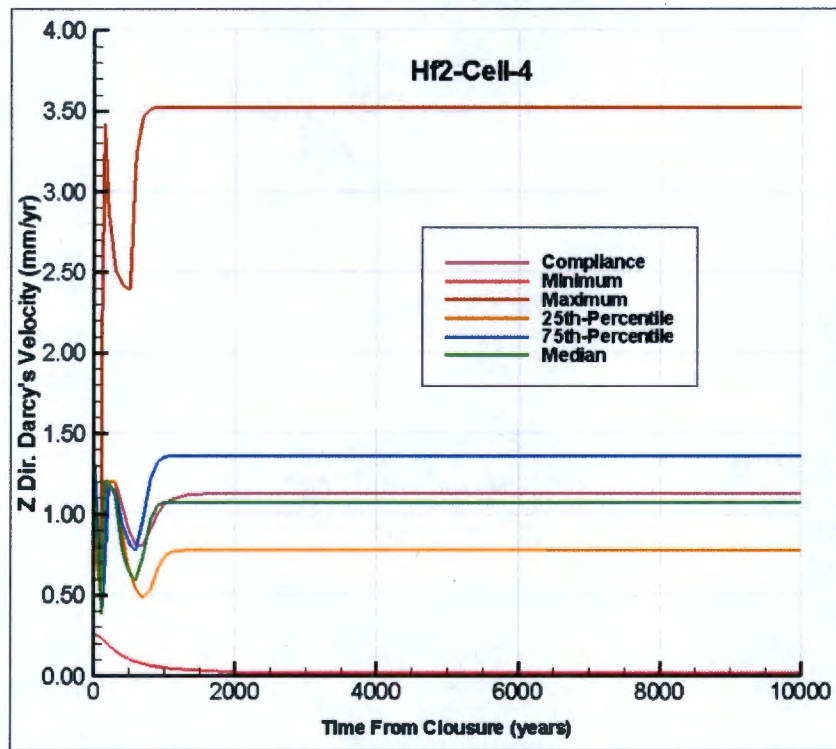


Figure 4-24. Volumetric Moisture Content Profiles as a Function of Depth and Time (in Calendar Years) for Selected Spatial Locations.

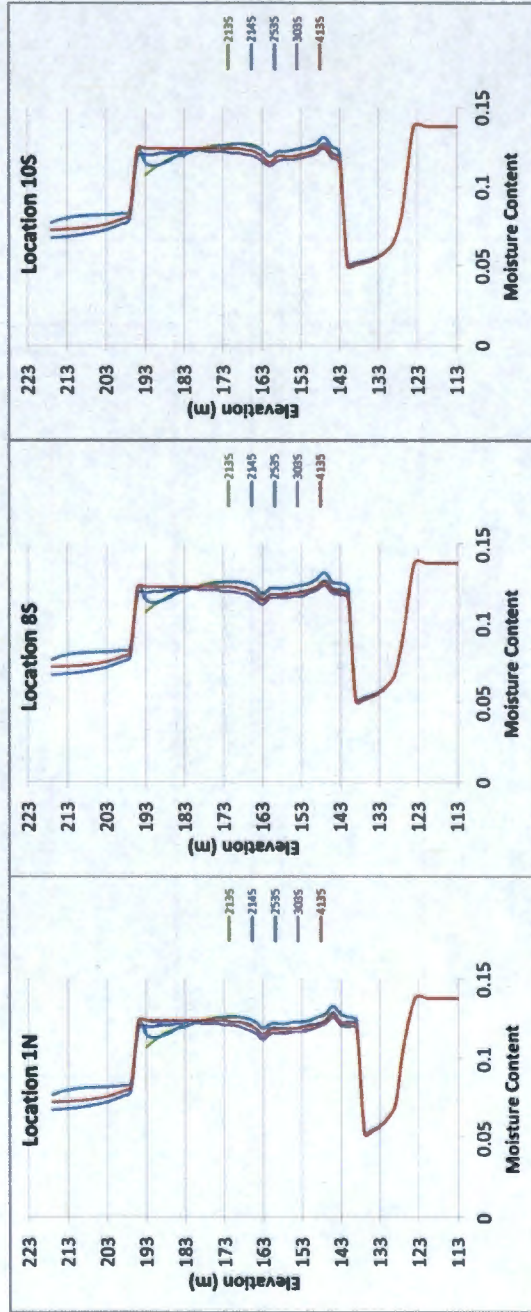


Figure 4-25. Comparison of Technetium-99 Concentration at Selected Locations in the Vadose Zone Predicted by One-Dimensional Abstraction Model with the Three-Dimensional Model Results Using Compliance Parameter Values for 1 Ci Inventory Distributed Over ERDF Volume.

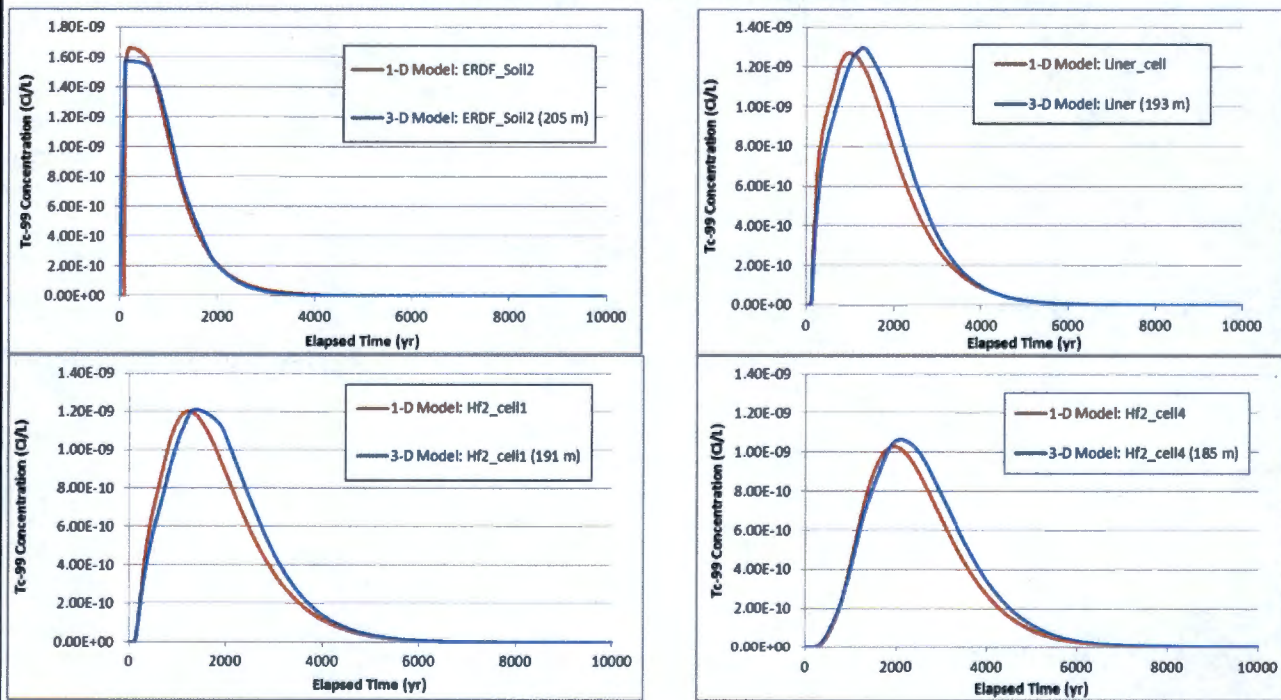


Figure 4-25. (Continued)

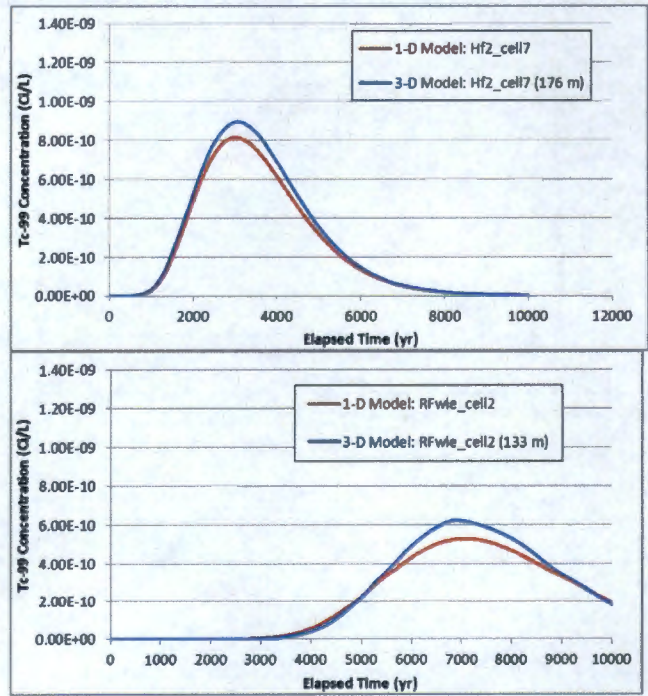
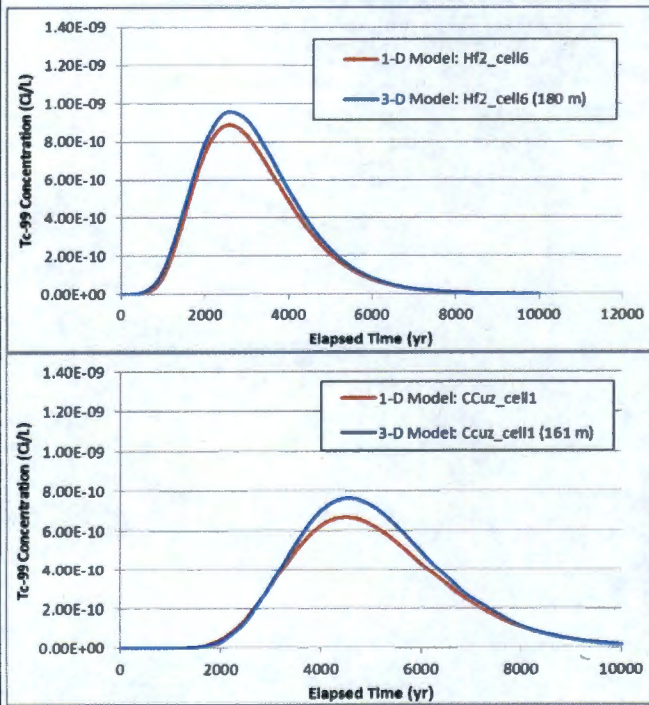


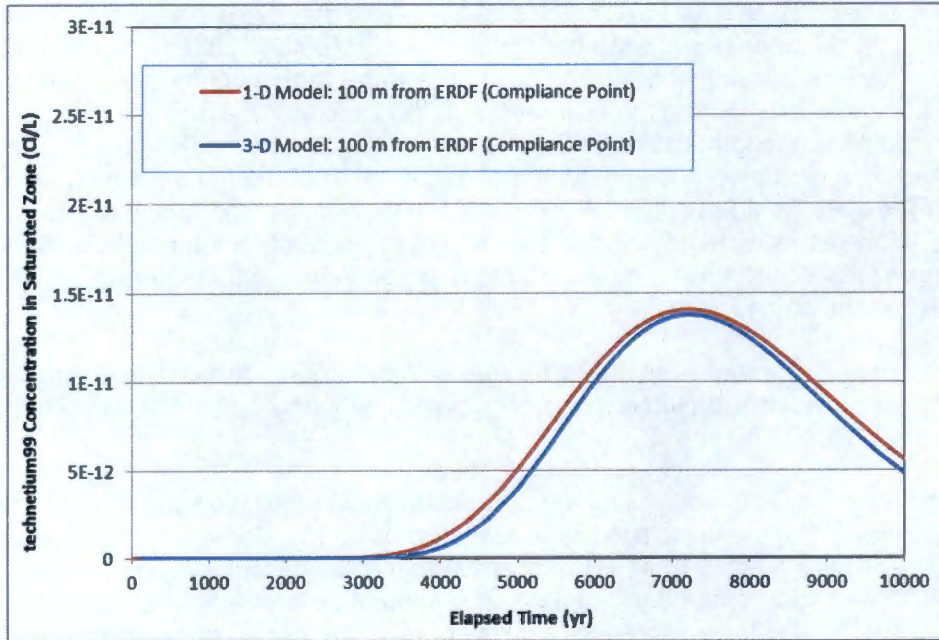
Figure 4-26 presents the comparison results in the saturated zone at compliance location 100 m downgradient of ERDF. The saturated zone is conceptualized as a one-dimensional stream tube and modeled using the pipe pathway capability of GoldSim. The pipe pathway element in the GoldSim contaminant transport module is used to calculate rates of contaminant transport along pathways that behave as stream tubes or fluid conduits. Pipe pathways use a Laplace transform approach to provide analytical solutions to a broad range of advection-dominated mass transport systems involving one-dimensional advection, longitudinal dispersion, retardation, decay and ingrowth, and exchanges with immobile storage zones. The geometry of the pathway is defined by specifying length, a cross-sectional area, and a perimeter. Mass enters over specified length of pipe (equivalent to ERDF length) and is transported through with advection, dispersion, sorption, and diffusion within the mobile zone of the pipe, and then exits at the other end.

The one-dimensional abstraction model parameters for the saturated zone transport are adjusted to match the results of the three-dimensional model in order to account for dispersion in the vertical direction over the transport length and nonuniform mass flux from the vadose zone to the saturated zone over the length of ERDF. Note that in the one-dimensional transport model the grid block dimensions in the horizontal direction (both X- and Y-directions) are held at a unit length, thereby calculating the mass flux to the water table over the unit area of ERDF in the vertical (Z-) direction. During the calibration (a) the vadose zone mass flux to the saturated zone calculated over a length of 1 m (in the X-direction, parallel to the flow direction) is scaled to 800 m instead of approximately 900 m length of ERDF (at the base) to account for nonuniform mass flux at the water table over the full length of ERDF, and (b) the vertical dimension of the stream tube (pipe pathway) is adjusted to about 13 m to account for dilution from vertical and lateral mixing as the solute travels over a 500-m average length in the saturated zone with considerable residence time.

The results of the one-dimensional model for the verification case are deemed satisfactory and provide confidence that the implementation is done properly and the model can be used for uncertainty analysis.

A full uncertainty analysis is undertaken by performing multi-realization simulations in the probabilistic mode. The uncertainties are propagated using the Monte Carlo sampling methodology and utilizing the inbuilt LHS scheme. In the Monte Carlo simulation, the entire system is simulated a large number of times; each simulation is equally likely and is referred to as a *realization* of the system. For each realization, all of the uncertain parameters are sampled and the system is simulated through time (with the given set of input parameters) such that the performance of the system can be computed. At the start of each realization, each stochastic element generates a new random seed that forms the basis for sampling the element during the realization. The LHS scheme allows for efficient sampling of the probability space so that full uncertainty can be represented without doing too many realizations. In this scheme each stochastic element's probability distribution (0 to 1) is divided into equally likely strata or slices equal to the number of realizations. The strata are then "shuffled" into a random sequence, and a random value is picked from each stratum in turn. This approach ensures that uniform spanning sampling is achieved. Note that each element has an independent sequence of shuffled strata that are a function of the element's random number seed and the number of realizations in the simulation. The LHS appears to have a significant benefit for problems involving a few independent stochastic parameters, and with moderate number of realizations.

Figure 4-26. Comparison of Technetium-99 Concentration in the Saturated Zone Predicted by the One-Dimensional Abstraction Model with the Three-Dimensional Transport Model at the Compliance Location 100 m Downgradient of ERDF Using Compliance Parameter Values for 1 Ci Inventory Distributed Over ERDF Volume.



For the purpose of performing the uncertainty calculations, the five flow fields generated need to be sampled. Applying equal probability to each flow field would not be accurate for propagating uncertainty as the minimum and maximum flow fields should intuitively be less likely to occur while the median flow field should be more likely to occur as the underlying recharge rates have a triangular distribution (Table 3-32). Since the long-term vertical flow velocities are most influenced by the late post-closure recharge rate below the ERDF, the triangular probability distribution for this recharge rate is used to develop the probability distribution of the flow field. As a result, the minimum and maximum flow fields are each given 5% probability weight, the 25th and 75th percentile flow fields are each given 20% probability weight, and the median flow field is given 50% probability weight. The flow field is indexed from 1 to 5, with 1 = Minimum, 2 = 25th percentile, 3 = Median, 4 = 75th percentile, and 5 = Maximum.

The probability distribution of flow and transport related properties used in the uncertainty analysis are shown in Tables 3-32 through 3-38. The uncertainty in the carbon-14 fractional leach rate is propagated by sampling a uniform distribution with a minimum value of $0.1 \times 10^{-6} \text{ d}^{-1}$ and a maximum value of $1.5 \times 10^{-6} \text{ d}^{-1}$ (Section 3.3)

The one-dimensional abstraction model is exercised by running 500 realizations. The results are presented in Figure 4-27 in terms of mean of total dose (from all radionuclides) along with the mean dose contribution of individual radionuclides. The early dose (from 100 to 1,000 years) primarily results from the release of carbon-14 from the air pathway, and the late dose (past 1,000 years) results primarily from the technetium-99 release from the groundwater pathway. In the groundwater pathway, the second highest dose results from potassium-40, whose inventory is set to 0 Ci for the compliance calculation (best estimate) but because of the use of the right triangular distribution to represent uncertainty (with minimum and mode set to 0 Ci and the maximum set to 1 Ci), the mean is calculated as 0.33 Ci. Because of its long half-life and being unretarded, potassium-40 persists throughout the simulated time period. The breakthrough of potassium-40 is slightly earlier than technetium-99 because the K_d of potassium-40 is zero in all hydrostratigraphic units while there is a small non-zero K_d for technetium-99 applied at the upper bound of the triangular distribution for most hydrostratigraphic units (Table 3-37).

The other radionuclides of interest are molybdenum-93, niobium-94, and chlorine-36, which are mobile (with no or very small retardation) and have long half-lives. Iodine-129 and hydrogen-3 have early dose contribution from the air pathway, but their contribution declines quickly. The uncertainty in groundwater and air pathways is discussed separately.

4.6.1.1 Groundwater Pathway. Figure 4-28 shows the uncertainty in the groundwater pathway dose for all 500 realizations along with the mean, median, 5th, and 95th percentile values. For all realizations, technetium-99 dose is the primary dose contributor, and thus the uncertainty in groundwater-pathway dose (representing contribution of all radionuclides) is almost all due to uncertainty in technetium-99 dose.

Figure 4-27. All-Pathway Dose Calculation Results Based on 500 Realizations Conducted Using a One-Dimensional Abstraction Model.

Results present the Mean of Total Dose and Mean Dose from Individual Radionuclides

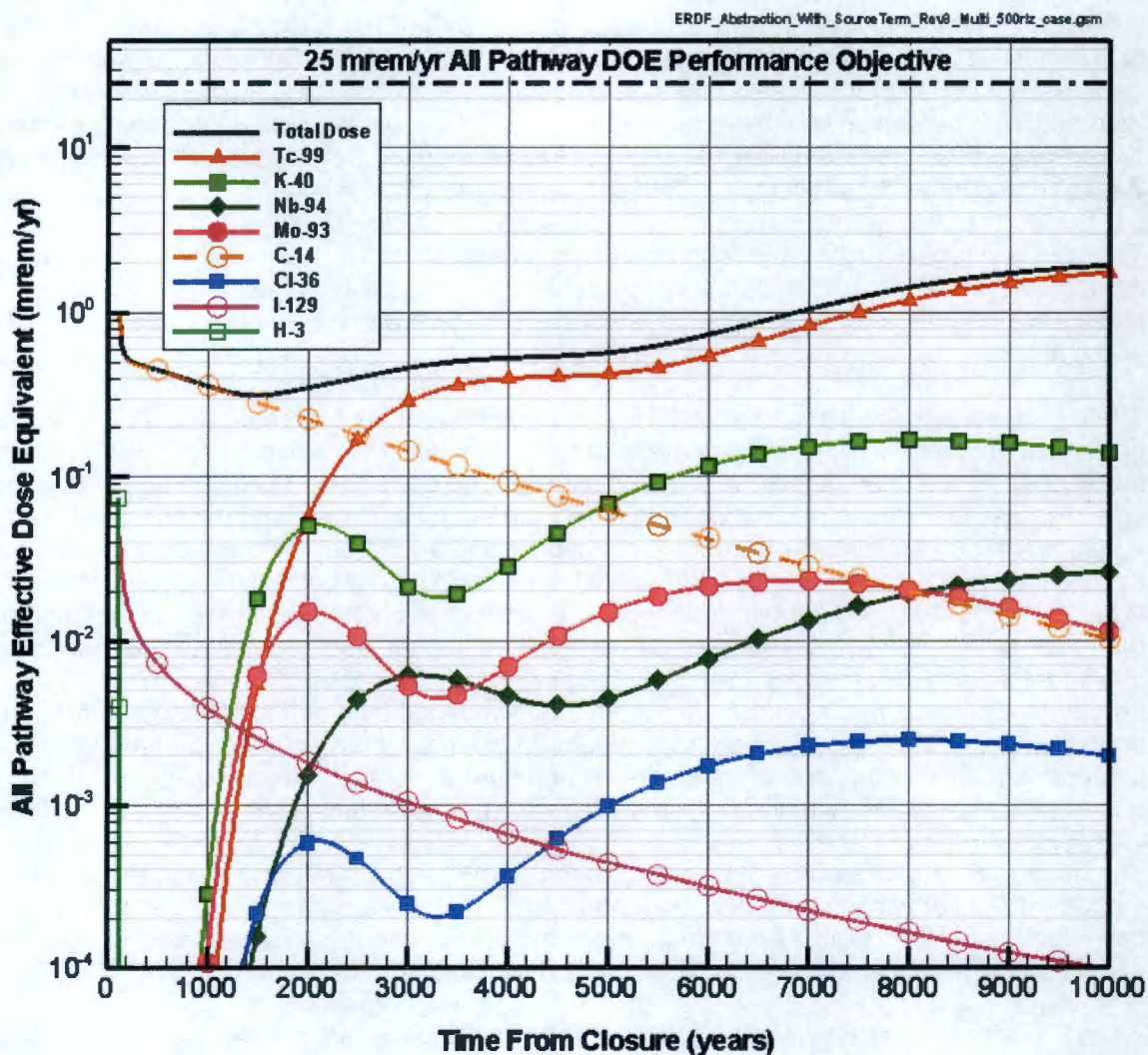
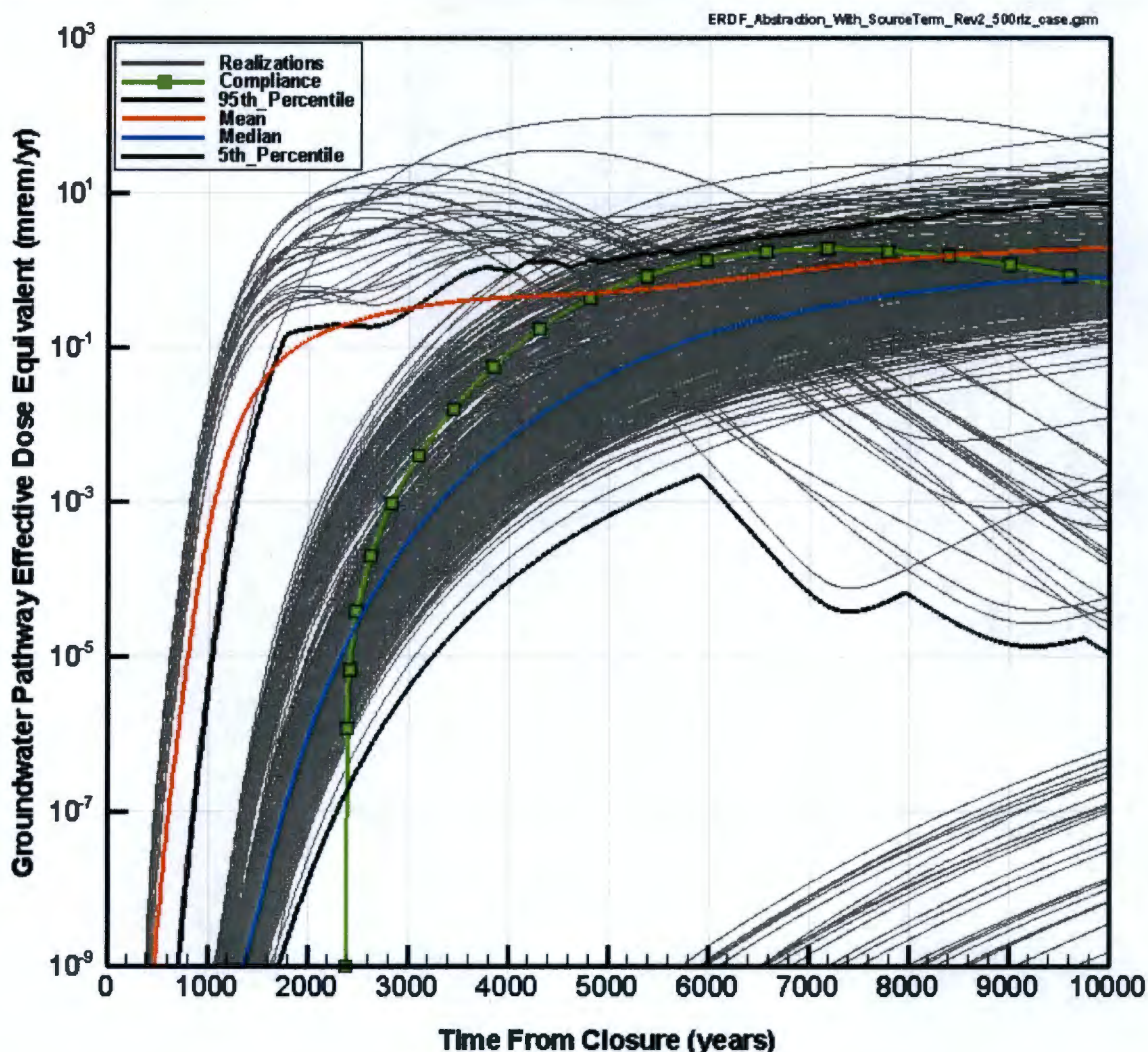


Figure 4-28. Uncertainty in the Groundwater-Pathway Dose Based on 500 Realizations.



Out of 500 realizations, 25 realizations show earlier breakthrough (<1,500 years) and have significant dose (>0.1 mrem) at early times (<2,000 years) compared to rest of the realizations. This is primarily due to selection of a maximum flow field having an assigned probability weighting of 5%. Due to maximum flow field selection, the advective transport in the vadose zone is fast (from combination of maximum recharge rates and vadose zone hydraulic properties that provide maximum vertical hydraulic conductivity and flow velocities). For the 25 realizations the realization with the highest peak dose (Rlz# 47), as shown in Figure 4-29, results from a combination of sampling saturated zone hydraulic conductivity (0.11 m/day) at the low end of the uncertainty distribution and a relatively higher inventory of technetium-99 for the maximum flow field condition (Table 4-7). As a result the mass flux from the vadose zone is higher and the dilution in the saturated zone is relatively lower resulting in a higher peak concentration. Selected uncertain parameter values for two other early peaking realizations (Rlz# 213 and 325), displayed in Figure 4-29, are presented in Table 4-7. Rlz# 213 has the second highest peak in the early times but relatively lower than Rlz# 47. It results from a combination of maximum flow field, a relatively low saturated zone hydraulic conductivity (0.6 m/day), and a relatively high K_d in

the Hf2 unit of 0.09 mL/g (sampled at 99 percentile of the distribution) leading to an early but lower peak. The earlier breakthrough of Rlz# 213 and 325 at the 100-m downgradient location, compared to Rlz# 47, is due to relatively higher saturated zone hydraulic conductivity.

Figure 4-29. Selected Realizations for Groundwater Pathway Dose.

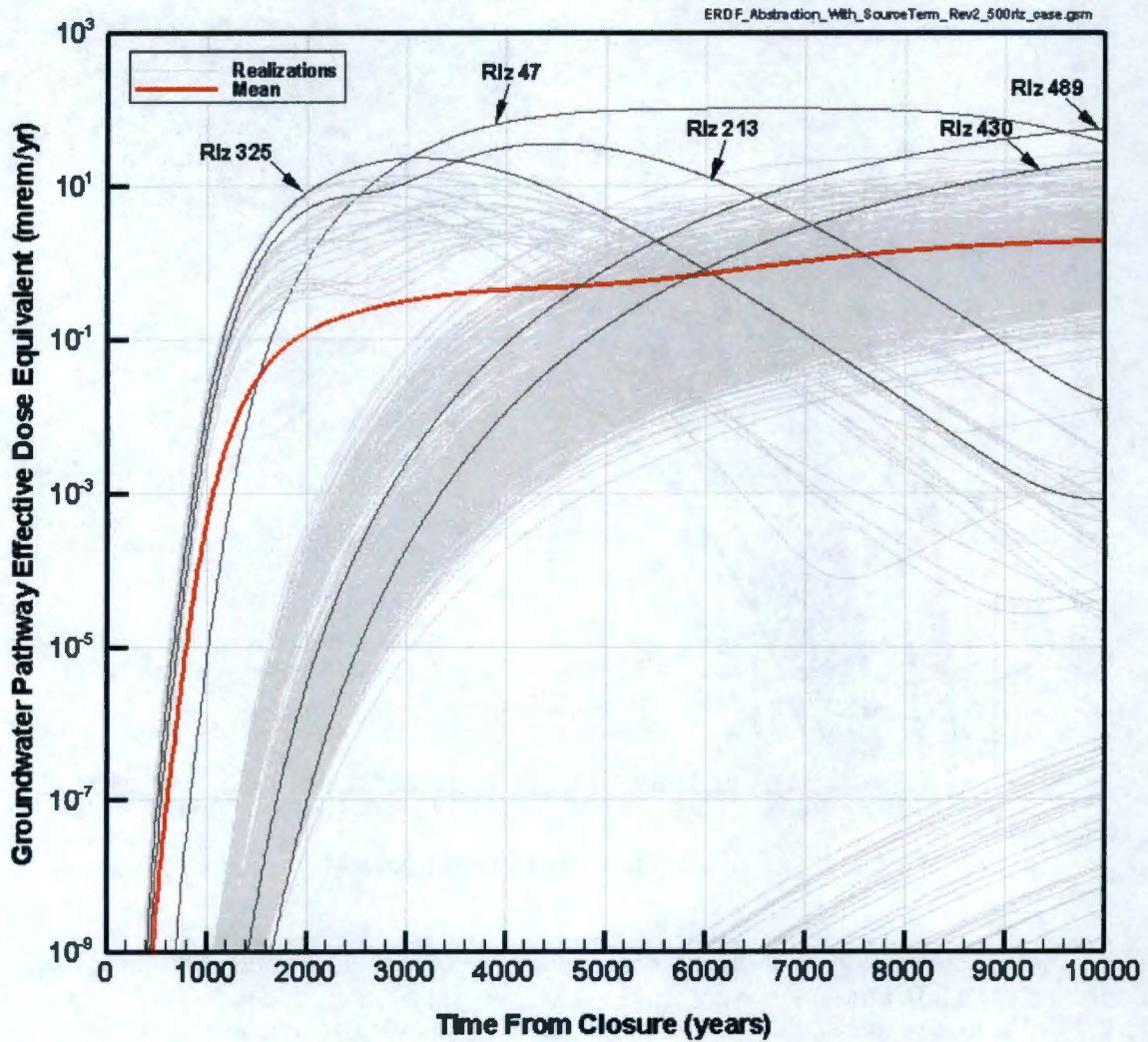


Table 4-7. Sampled Parameter Values for Selected Realizations.

Realization	Flow Field Index	Late Post-Closure Recharge Rate Below ERDF (mm/yr)	Saturated Hydraulic Conductivity (m/day)	Inventory of Tc-99 (Ci)	K _d of Tc-99 (mL/g) for Hf2 (Hanford Sand-Dominated) Unit
47	5	1.87	0.11	77.6	0.013
213	5	1.72	0.59	63.7	0.093
325	5	1.98	0.94	51.9	0.025
430	3	1.12	0.21	79.5	0.015
489	4	1.60	0.12	73.5	0.018

The set of realizations that show delayed breakthrough (beyond 5,000 years) and are below the 5th percentile curve are due to selection of minimum flow field.

In the rest of the realizations where the peak occurs late (past 6,000 years), the realization with the highest dose within the simulation period (Rlz # 489, as shown in Figure 4-29) results from a combination of relatively higher velocities in the vadose zone (sampling the 75th percentile flow field), relatively lower saturated hydraulic conductivity (0.12 m/day) that leads to lower dilution and delayed breakthrough at the compliance location, and a technetium-99 inventory of 74 Ci that is above the median value. Selected uncertain parameter values for this and another realization (Rlz #430; see Figure 4-29) are presented in Table 4-7. The dose estimate from Rlz #430 is lower due to selection of median flow field.

In some of the early peaking realizations, following a decline in dose, a late rise (past 7,000 years) is observed. This is due to increasing iodine-129 dose contribution, which is slightly more retarded than technetium-99 and thus has delayed breakthrough. A multivariate analysis is conducted to evaluate the importance of uncertain parameters on the groundwater pathway dose calculations (on total dose as opposed to the dose of individual radionuclides). The analysis is conducted at the time of peak mean dose, which occurs at 10,000 years. The analysis is based on the ranks (rather than values) of the uncertain parameters. Two types of analyses are primarily conducted: (a) the rank (Spearman) correlation coefficient and (b) the Importance Measure. Standardized rank regression coefficients and partial rank correlation coefficients are also computed as part of the analysis but are not discussed in detail as they do not seem to provide any more insight than the correlation coefficient and importance measure regarding the parameter influence on the dose. The total number of uncertain parameters that are used directly in the one-dimensional abstraction model is 286. The uncertain parameters related to most recharge rates that are used in the three-dimensional flow model to generate flow fields but are not directly used in the abstraction model are excluded from the analysis.

The rank correlation coefficient expresses the extent to which there is a linear relationship between the selected result and an input variable. The coefficients range between -1 and 1 with extreme values indicating strong negative or positive correlations. The calculation is performed using the following equation:

$$C_{rp,rank} = \frac{\sum_{i=1}^n (Rp_i - m_{Rp})(Rr_i - m_{Rr})}{\sqrt{\sum_{i=1}^n (Rp_i - m_{Rp})^2 \sum_{i=1}^n (Rr_i - m_{Rr})^2}} \quad \text{Eq. 4-1}$$

where

- $C_{rp,rank}$ = the rank correlation coefficient
- n = the number of selected data points (realizations)
- Rp_i = the rank (from 1 to n) of output p for realization I
- m_{Rp} = mean value of the rank of output p
- m_{Rr} = mean value of the rank of output r.

The standardized rank regression coefficients and partial rank correlation coefficients also vary between -1 and 1. These calculations are based on the variable ranks rather than on the actual values of the variables. The standardized rank regression coefficients provide a normalized measure of the linear relationship between variables and the result (dose). They are regression coefficients found when all of the variables and the result are transformed and expressed in terms of the number of standard deviations away from the mean. The partial correlation coefficients reflect the extent of the linear relationship between the selected result and an input variable, after removing the effects of any linear relationships between the other input variables and both the results and the input variable in question. Both formulations are based on NUREG/CR-4122, *A FORTRAN Program and User's Guide for the Calculations of Partial Correlation and Standardized Regression Coefficients*.

The importance measure (as calculated using GoldSim) expresses the nonlinear, non-monotonic relationship between an input variable and the result, which the conventional correlation coefficient may not reveal. This measure varies between 0 and 1, and represents the fraction of the result's variance that is explained by the variable. The importance measure presented here is a normalized version of a measure discussed in Saltelli and Tarantola (2002), and is calculated as:

$$M_{y,i} = 1 - \frac{E[v_y(Y|X_i)]}{v_y} \quad \text{Eq. 4-2}$$

where

- $M_{y,i}$ = the importance measure for the sensitivity of the result (Y) to input variable X_i
- v_y = the current variance in the result Y
- $E[v_y(Y|X_i)]$ = the expected value of v_y if the input variable X_i was perfectly known.

Thus, the Importance Measure $M_{y,i}$ represents the fraction of the result variance that is explained by X_i . For additional computational details refer to Appendix B of the GoldSim User's Guide (GoldSim Technology Goup 2009b).

The uncertainty analysis results of the 500 realization case for the groundwater pathway are presented in Table 4-8. Only the most important stochastic parameters are presented that contribute significantly to the uncertainty in total dose for the groundwater pathway. The results are sorted by the uncertain parameters from highest to lower numbers in terms of Importance Measure for those parameters that have correlation coefficients greater than about 0.2 (in absolute value). Other uncertainty analysis measures (such as correlation coefficients, etc.) generally follow the same trend. The uncertainty analysis for the groundwater pathway is conducted by evaluating the dose from all realizations at time 10,000 years since the dose is the highest at this time. Therefore, the results of the multivariate analysis presented are only applicable to that time.

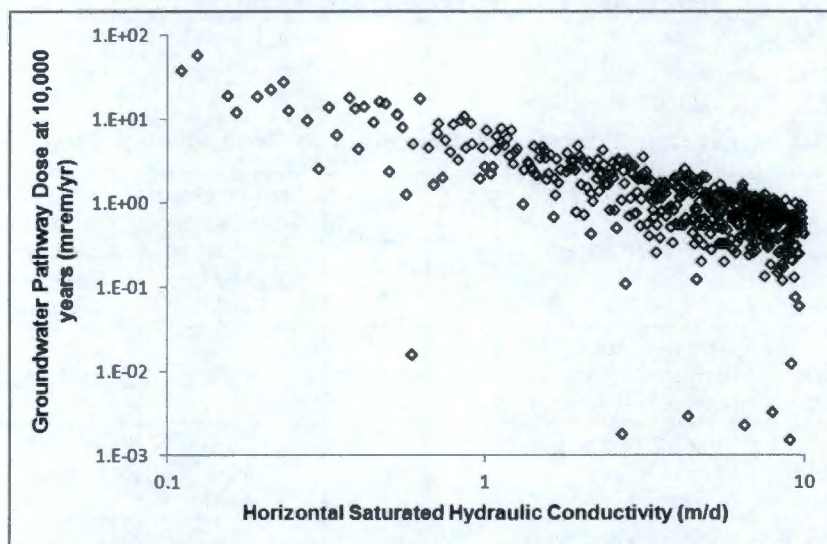
Table 4-8. Uncertain Parameters Important to Groundwater Pathway Dose.

Stochastic Parameter ID	Description	Correlation Coefficient Based on Ranks	Standardized Regression Coefficient Based on Ranks	Partial Correlation Coefficient Based on Ranks	Importance Measures Based on Ranks
Sat_Kh_stochastic	Saturated zone horizontal hydraulic conductivity (m/day)	-0.62	-0.62	-0.71	0.41
Flow_Field_Selector	Selector of flow field used in a given realization	0.30	0.20	0.12	0.26
Rch_TopLate	Long-term recharge rate at ERDF after degradation of surface barrier	0.28	0.09	0.06	0.23
Kd_Hf2[Tc]	K_d of Tc-99 in the Hf2 hydrostratigraphic unit	-0.23	-0.25	-0.37	0.05
Kd_Hf1[Tc]	K_d of Tc-99 in Hf1 hydrostratigraphic unit (used for ERDF soil)	-0.17	-0.13	-0.21	0.04

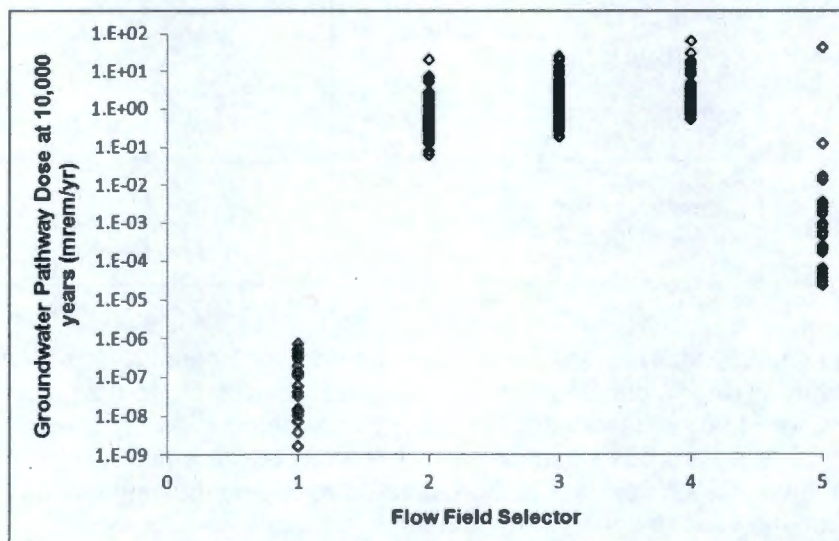
Based on the uncertainty analysis, the most important uncertain parameter is found to be horizontal saturated hydraulic conductivity. It is negatively correlated to the groundwater pathway dose. Given that no uncertainty is explicitly considered in the hydraulic gradient in the saturated zone (fixed at 1.5E-03), the uncertainty in horizontal saturated hydraulic conductivity linearly affects the volumetric flow rate in the saturated zone and thus influences the dilution of the mass flux from the vadose zone. Thus, the larger the saturated zone hydraulic conductivity the more the dilution will be and the smaller the radionuclide concentration will be in the saturated zone and hence smaller the dose. This is indicated in the scatter plot shown in Figure 4-30a. The second most important uncertain parameter is the flow-field selector. It has a

positive correlation to the groundwater pathway dose (see the scatter plot in Figure 4-30b). The higher the flow field, the more the advective flux through the vadose zone will be (as almost all of the radionuclide mass is available for transport following the liner failure), which would lead to greater mass flux to the saturated zone and larger concentration in the groundwater. The dose contributions from flow-fields 1 (minimum) and 5 (maximum) at 10,000 years are relatively small compared to other flow fields because for the minimum flow field the peak dose would occur later than the simulated time while for the maximum flow field the peak occurred much earlier than 10,000 years and by 10,000 years the dose is very small and declining.

Figure 4-30. Scatter Plots of Selected Uncertain Parameters Against Groundwater Pathway Dose at 10,000 years.



(a)



(b)

The long-term recharge rate through the ERDF after degradation of the ERDF surface barrier is used by the flow-field selector to select the flow-field type based on the sampling of the long-term recharge rate (and therefore internally correlated). However, long-term recharge rate also influences the dose through the vadose zone velocity and saturation field that is computed using the three-dimensional model using STOMP and then abstracted in the one-dimensional model. The K_d for technetium-99 in Hf2 and Hf1 (used for ERDF soil) indicate small influence on the long-term dose magnitude. This is expected as technetium-99 would be slightly retarded but because of long half-life and relatively high mobility, the magnitude of dose would not change much.

The coefficient of determination based on linear regression for uncertain parameters shown in Table 4-8 taken together is approximately 0.55. This indicates that these parameters represent about a 0.55 fraction of the total variance in the dose result (at 10,000-year assessment time). The horizontal saturated hydraulic conductivity alone accounts for about a 0.39 fraction of the total variance in the dose.

4.6.1.2 Atmospheric Pathway. Figure 4-31 presents the uncertainty in the atmospheric pathway dose for all 500 realizations along with the mean, median, 5th, and 95th percentile values. In all realizations, carbon-14 dose is the primary dose contributor (as shown by the mean dose value in Figure 4-27), and thus the uncertainty in atmospheric pathway dose (representing contribution of all radionuclides) is almost all due to uncertainty in carbon-14 dose throughout the simulated time frame. An early sharp decline in carbon-14 dose (in the mean and median curves) within the first 200 years is noticeable followed by a steady decline. The early sharp decline is due to availability of carbon-14 from the small fraction in the untreated bulk soil that is immediately available for release. After approximately 200 years the slow decline in dose is controlled by slow release from graphite (insoluble material fraction in Table 3-3).

The uncertainty analysis results of the 500 realization case for the atmospheric pathway are presented in Table 4-9 based on dose results at three different time periods: (a) early time period (at 200 years); (b) intermediate time period (at 1,000 years); and (c) post-compliance time period (at 10,000 years). Only the most important stochastic parameters are presented that contribute significantly to the uncertainty in total dose for the atmospheric pathway. The results are sorted by the uncertain parameters from highest to lower numbers in terms of Importance Measure for those parameters that have correlation coefficients ≥ 0.2 .

Figure 4-31. Uncertainty in Atmospheric Pathway Dose Based on 500 Realizations.

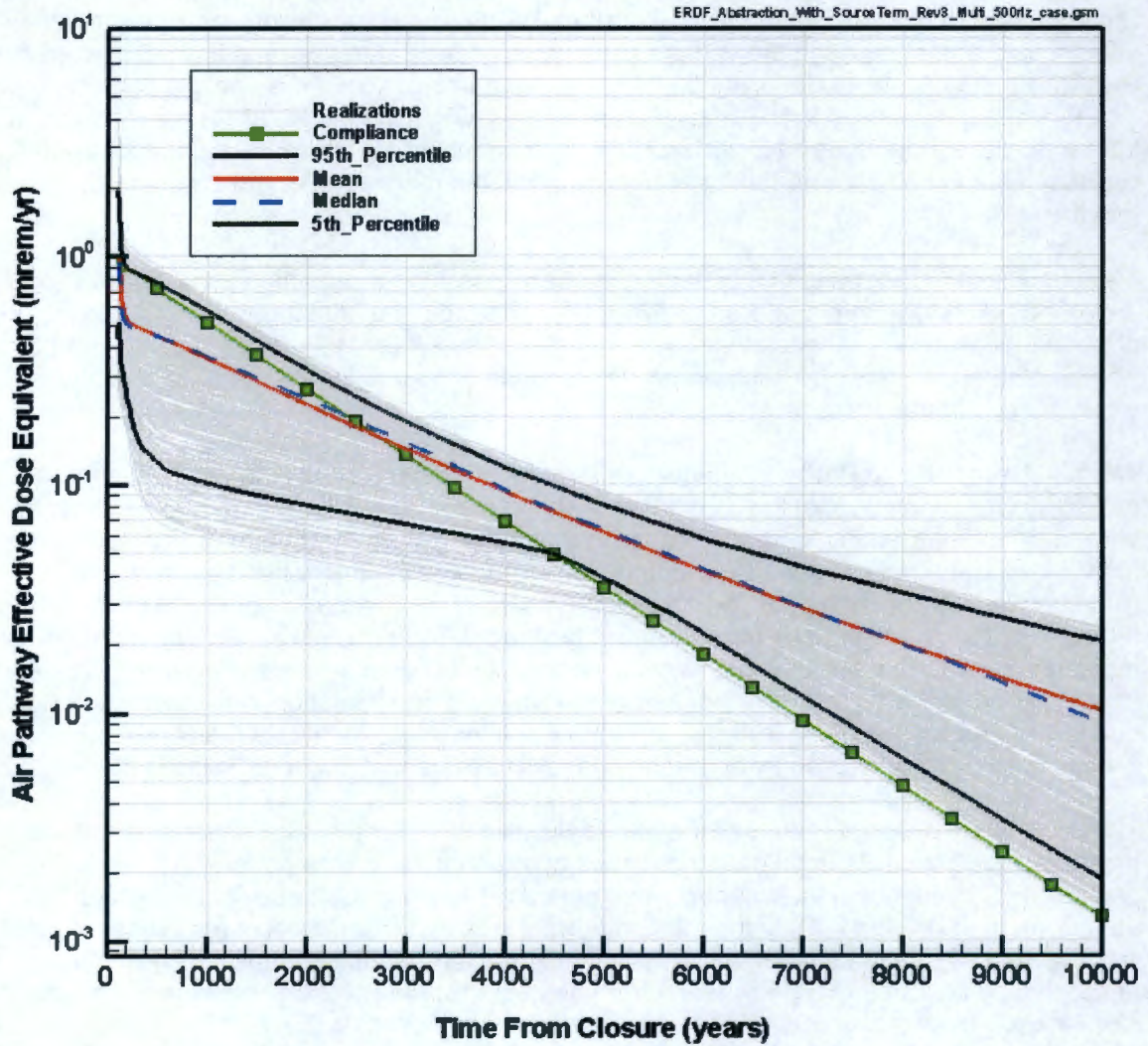


Table 4-9. Uncertain Parameters Important to Atmospheric Pathway Dose at Various Times.

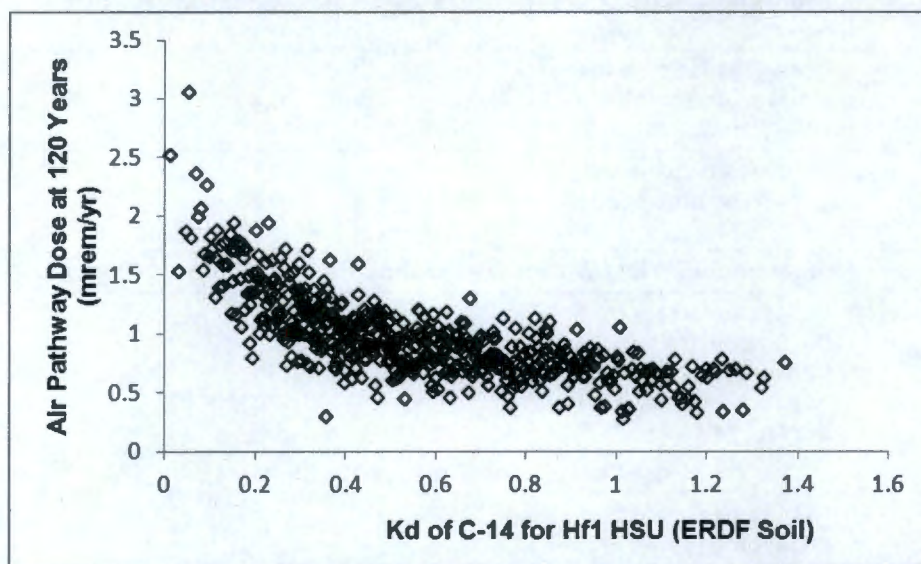
Stochastic Parameter ID	Description	Correlation Coefficient Based on Ranks	Standardized Regression Coefficient Based on Ranks	Partial Correlation Coefficient Based on Ranks	Importance Measures Based on Ranks
At Early Time (Before 200 years)					
Kd_Hf1[C]	K _d of C-14 for Hf1 hydrostratigraphic unit (used for ERDF soil)	-0.75	-0.74	-0.94	0.56
ERDF4to9_Tortuos_Air_Stoch	Tortuosity factor in the air pathway for the ERDF soils	0.46	0.43	0.84	0.24
Forecast_2035_stochastic[C14]	Forecasted inventory of C-14 to be emplaced by year 2035	0.28	0.23	0.65	0.1
At Intermediate Time Within Compliance Period (200 to 1,000 years)					
C14_LeachRate_Stoch	C-14 release rate from the source term due to fractional leaching of graphite and activated metal	0.96	0.95	0.99	0.91
Post-Compliance Time (at 10,000 years)					
C14_LeachRate_Stoch	C-14 release rate from the source term due to fractional leaching of graphite and activated metal	-0.97	-0.97	-0.97	0.94

In the early time period (200 years), because the initial inventory of carbon-14 from bulk soil is all available for release, the primary uncertain parameter that affects the concentration in air is the K_d of carbon-14 for the Hf1 hydrostratigraphic unit which is used to represent in ERDF soil. It is negatively correlating as increasing the K_d would reduce the amount available in dissolved phase and therefore less would partition into the gas phase. The scatter plot in Figure 4-32a indicates the relationship between this parameter and the atmospheric dose at 120 years. The other two stochastic parameters presented in Table 4-9 at early times show positive correlation. This is expected as the tortuosity term is a multiplier to convert the free-air diffusion coefficient to effective diffusion coefficient of radionuclides in air due to tortuous pathway. Increasing this would increase the effective diffusion coefficient. The fraction of inventory of carbon-14 available in the bulk soil (untreated fraction) is larger in the forecasted inventory compared to the currently disposed inventory (Table 3-3) and thus shows a greater correlation to dose.

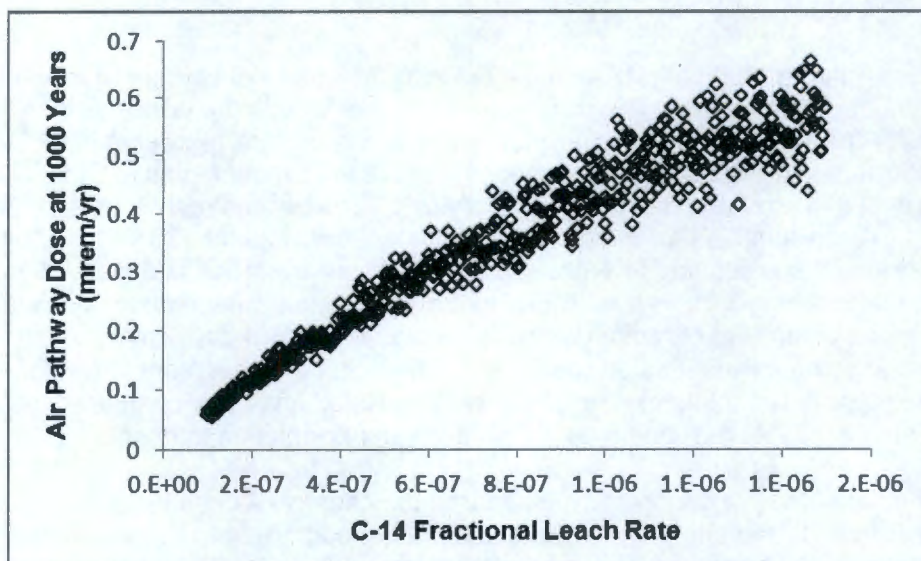
In the intermediate time period (up to 1,000 years), the carbon-14 dose in the atmospheric pathway is controlled predominantly by the availability of carbon-14 from leaching of insoluble material (graphite). A strong positive correlation is indicated and shown in the scatter plot in Figure 4-32b. The higher the fractional leach rate the larger the carbon-14 amount available for release.

At the late time period (at 10,000 years), the atmospheric pathway dose is still controlled by the fractional leach rate (Table 4-9), but the scatter plot in Figure 4-32c shows a negative correlation beyond very small leach rates. This is because the larger the fractional leach rate the more mass will be made available early on and very little will remain available by 10,000 years for diffusive release into the air.

Figure 4-32. Scatter Plots of Selected Uncertain Parameters Against the Atmospheric Pathway Dose at Different Time Periods.

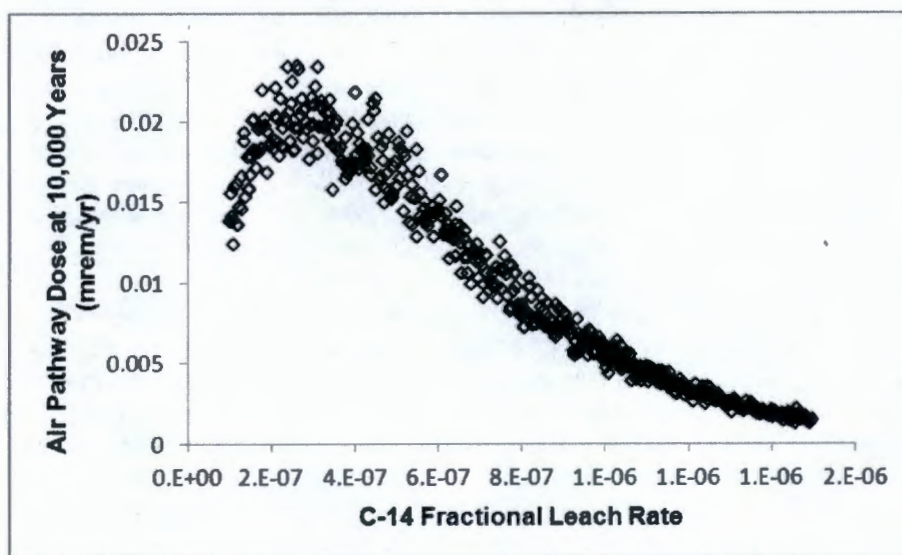


(a)



(b)

Figure 4-32. (Continued)



(c)

4.6.1.3 Statistical Stability. A stability analysis is conducted to determine whether a sufficient number of realizations have been obtained to ensure that the results of the calculations are statistically stable. The one-dimensional abstraction model is statistically stable if the mean annual dose computed by the model is stable. Demonstrating stability of the mean annual dose requires evaluation of the sufficiency of sample size of uncertain parameters so that possible parameter combinations are adequately represented in the system analyzed. Performing uncertainty analysis with an inadequate number of realizations can result in erroneous interpretation of important uncertain parameters. Statistical stability is generally determined by demonstrating that the estimate of the mean annual dose does not depend on the sample size.

The total mean annual dose, $\bar{D}(\tau)$, for a multi-realization case is estimated at time τ by numerically evaluating

$$\bar{D}(\tau) = \int_{\mathbf{E}} D(\tau|\mathbf{e}) d_{\mathbf{E}}(\mathbf{e})d\mathbf{E} \quad \text{Eq. 4-3}$$

where, \mathbf{E} is a probability space comprising the epistemic uncertain parameters and $D(\tau|\mathbf{e})$ computes the annual dose at time τ for a given element \mathbf{e} (a vector of all uncertain parameters evaluated per realization) in \mathbf{E} . The evaluation of the function $D(\tau|\mathbf{e})$ is performed by numerically solving a complex, coupled system of differential equations such as describing radionuclide decay, mass transport, flow, and other physical processes. The numerical integration is performed by the Monte Carlo technique and employing LHS of epistemic uncertain parameters.

For stability analysis, the mean annual dose and uncertainty in underlying distribution is evaluated by performing calculations with different number of realizations (i.e., by varying the sample size) for the all pathway exposure scenario (includes groundwater and air pathway). Four cases are performed with an increasing number of realizations: (a) 100 realizations;

(2) 200 realizations; (3) 300 realizations; and (4) 500 realizations. The dose statistics (mean, median, and 95th percentile) derived from different cases are compared in Figure 4-33. The results indicate that past 6,000 years the uncertainty in the respective statistics narrows considerably. The variance in the median and 95th percentile values among different cases is small, and the peak mean dose is within a factor of two for all cases. Between 2,000 and 6,000 years, because only few realizations have breakthrough at the 100-m downgradient location, the dose results are not stable due to small sample size. However, the peak dose occurs past 6,000 years, and it can be concluded that 500 realizations are adequate for the purpose of performing uncertainty analysis.

Figure 4-34 provides the upper and lower confidence limits on the grand mean (mean of the means) based on five different cases (including a 50 realization case) at a 97.5 confidence level (significance level, $\alpha = 0.025$). The range between the confidence bounds widens between 2,000 and 6,000 years but narrows past 6,000 years indicating a narrow band of uncertainty over which the mean dose is likely to vary. The grand mean (the mean of the means) is shown in a thick black line. Near the end of the simulation, where the peak mean dose occurs, the mean of the 500 realization case virtually overlaps with the grand mean indicating sufficiency of using 500 realizations for uncertainty analysis.

Figure 4-33. Statistical Stability Analysis with Different Number of Realizations.

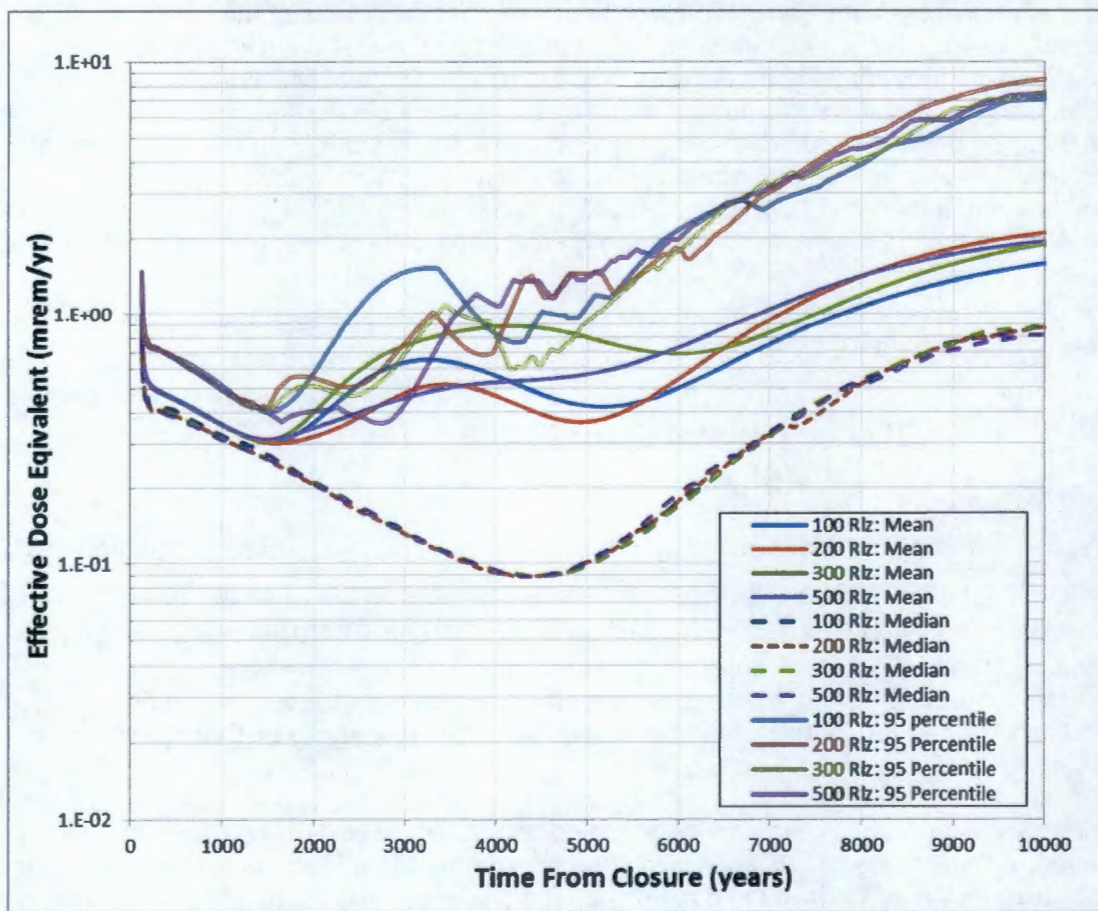
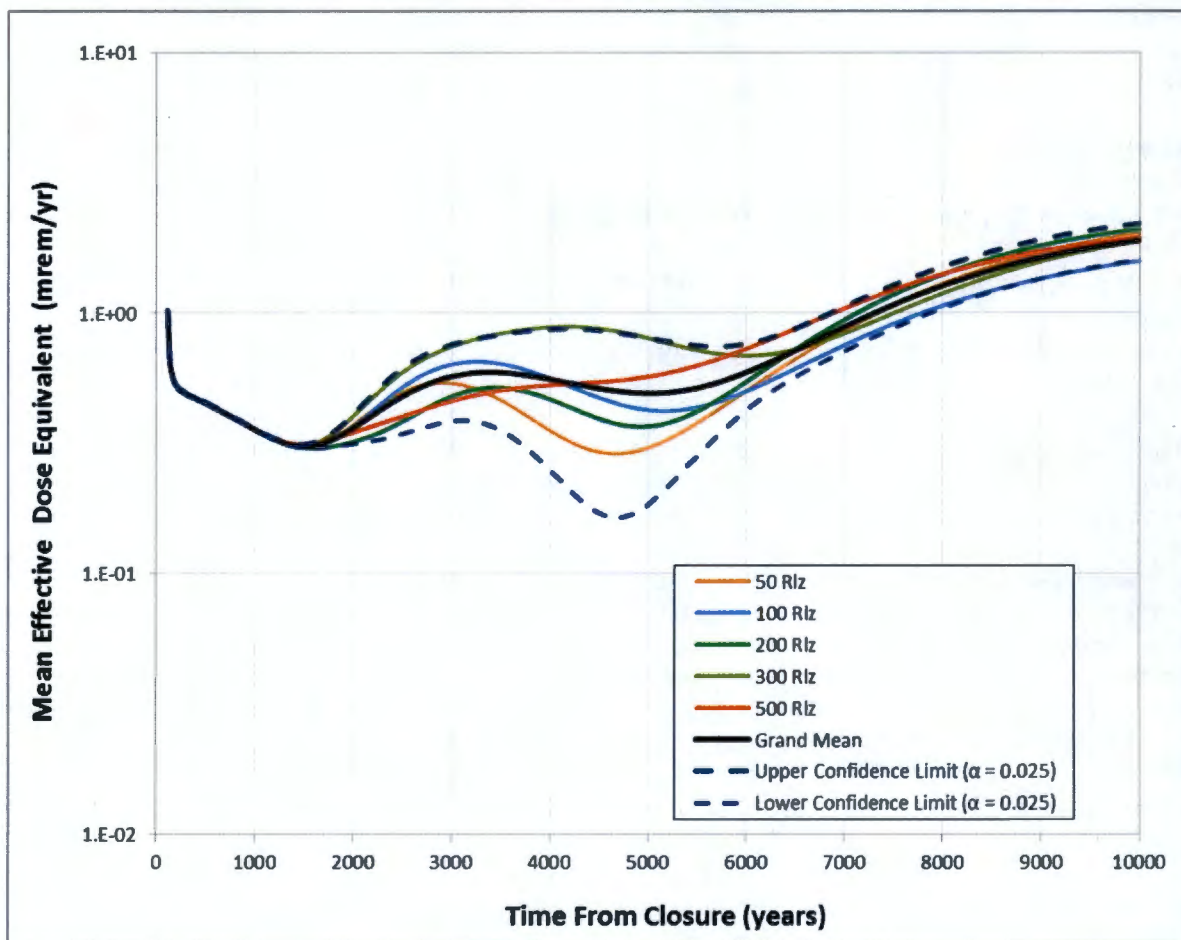


Figure 4-34. Confidence Limits on the Mean Effective Dose Equivalent.



4.6.2 Sensitivity Analysis for the Groundwater Pathway

Sensitivity analyses evaluate changes in estimated groundwater impacts that result from changes in modeling input parameter estimates, either individually or cumulatively. Parameter value ranges used in these analyses were selected to reflect the inherent variability of site-specific conditions. In general, sensitivity analyses refer to changes in parameter estimates to address the inherent variability (also termed aleatory uncertainty) that exists in certain model parameters. The sensitivity analyses evaluate the effects modifying particular parameters have on the groundwater concentrations at the point of calculation. The results of these analyses indicate what changes in parameters may cause the largest variability in the results, and how much changes in certain parameters, which are variable by their nature or dependent on future events, may cause the results to vary.

Primary sources of variability in parameter values are natural system heterogeneities, long-term engineered surface barrier performance, and human actions. Unlike classic uncertainty analyses, these variability analyses estimate a range of future impacts without assigning a likelihood of occurrence to a particular result other than a qualitative expectation that the actual outcome should tend toward the compliance case estimate. This approach to variability was selected for several reasons:

- Most performance objectives are deterministic.
- In general, there is a sufficient understanding of "how the system works."
- Existing databases support and provide a reasonable quantification of the range of parameter values.

The sensitivity analyses quantify the ranges of plausible estimated groundwater contamination outcomes due to single or multiple parameter site-specific variability, and determine the relative importance between parameters. With respect to the defense-in-depth concept, the analyses quantify the impacts that parameter variability associated with the natural and engineered barriers have on groundwater contamination estimates to evaluate the total system performance. Ranges of plausible future groundwater contamination levels can be estimated that are derived from disposal system (natural and engineered components) variability. These estimates can provide a reliable determination of system performance adequacy with regard to performance criteria involving the use of contaminated groundwater. These analysis results are an effective tool for making waste acceptance and closure action decisions for ERDF.

From these analyses, several key observations and conclusions were drawn:

- For mobile contaminants ($K_d = 0$ mL/g), the most significant parameter is recharge rate after the design life of the surface barrier (assumed 500 years after closure).
- Within the range of parameter values estimated to reflect plausible variability in the geologic features and engineered system components, the estimated maximum concentration values at the point of calculation increased or decreased by factors less than 10.

The following sections present the sensitivity case results in three categories: (1) changes in aquifer properties, (2) changes in recharge, and (3) changes in vadose zone hydrologic parameters. The sensitivity analysis for the aquifer parameters examines the impacts associated with radionuclide transport and mixing in the aquifer between the ERDF and the point of calculation 100 m downgradient of the facility. The recharge sensitivity simulation cases examine the impacts of changes in recharge rate estimates during both pre- and post-design life performance periods of the surface barrier. The recharge category addresses elements associated with the surface barrier function. The hydrologic cases examine the impacts of changes in the hydrologic parameters and address those elements of the defense in depth associated with the vadose zone function. Because the screening analysis and compliance case results indicate that only the most mobile radionuclides break through to a peak concentration in groundwater within the 10,000-year sensitivity-uncertainty evaluation time frame, comparative results are presented for radionuclides with K_d values equal to zero, in particular, technetium-99.

Included in the sensitivity analysis is a collection of results for the "what if" scenarios. The results of these scenarios provide information about the ability of the closure system to perform under a

variety of conceivable but unexpected conditions arising in the future. The "what if" cases generally involve alteration of compliance case assumptions or postulations pertaining to surface barrier or liner degradation.

4.6.2.1 Percentile Evaluations. Tables 4-5 and 4-6 identify minimum, maximum, median, 25th, and 75th percentile values for several flow and transport parameters. These sets of parameters were evaluated in the three-dimensional model to provide additional benchmarking results for the development of the GoldSim uncertainty analysis. The results also provide insight into the overall working of the hydraulics of the system. In particular, the results indicate that the vadose zone and aquifer components of the transport appear to function independently of one another, and that the dilution and attenuation caused by transport in the aquifer may be approximated using a simple linear formula applied to the radionuclide flux or leachate concentration at the water table.

The results included in Table 4-10 show that the water flux into the aquifer beneath the bottom of the ERDF is very close to the surface barrier post-design life recharge rate, but the water flux can be affected by the vadose zone properties. At the maximum surface barrier post-design life recharge rate and with the maximum vadose zone properties, the water flux exceeds the post-design life recharge rate by more than 50%. The comparison of the compliance case to the median percentile results shows that the compliance case flux exceeds the median percentile case flux even though the post-design life recharge rate in the compliance case is slightly less than that in the median percentile case. In the compliance and maximum percentile cases, the recharge rates applied to the areas outside ERDF affect the moisture content and transport in the vadose zone beneath ERDF. However, in the other percentile simulations, the contaminant flux into the aquifer is almost exclusively a function of the surface barrier post-design life recharge rate, and the recharge rates applied to the areas outside ERDF do not appear to have as much effect on the results.

Table 4-10. Results of the Vadose Zone Hydrologic and Recharge Parameter Percentile Evaluations for Radionuclides with $K_d = 0$ mL/g (e.g., Technetium-99) Breakthrough to the Water Table (Results Presented on a per Ci Source Basis).

Flow and Transport Parameter Percentile Values	Arrival Time of Maximum Radionuclide Flux at Water Table (Years Post-Closure)	Maximum Radionuclide Flux at Water Table (Ci/yr)	Water Flux at Water Table (mm/yr)	Surface Barrier Post-Design Life Recharge Rate (mm/yr)	Pre-ERDF Construction Recharge Rate (mm/yr)
Minimum	N/A	0.00E+00	0.11	0.10	0.26
25 th Percentile	8210	1.37E-04	0.82	0.75	1.05
Median	8015	1.41E-04	1.11	1.03	1.59
Compliance	7180	2.01E-04	1.16	1.00	1.70
75 th Percentile	5705	2.30E-04	1.39	1.31	2.30
Maximum	1825	8.80E-04	3.33	2.00	4.00

The results included in Table 4-11 show that the concentration at the point of calculation 100 m downgradient from the outside base of the ERDF berm appears to be indeterminate on the basis of the radionuclide flux at the water table or the aquifer hydraulic conductivity individually. However, the transformation factor between the radionuclide flux at the water table and the downgradient aquifer concentration appears to be inversely proportional to the aquifer hydraulic conductivity, regardless of the radionuclide flux.

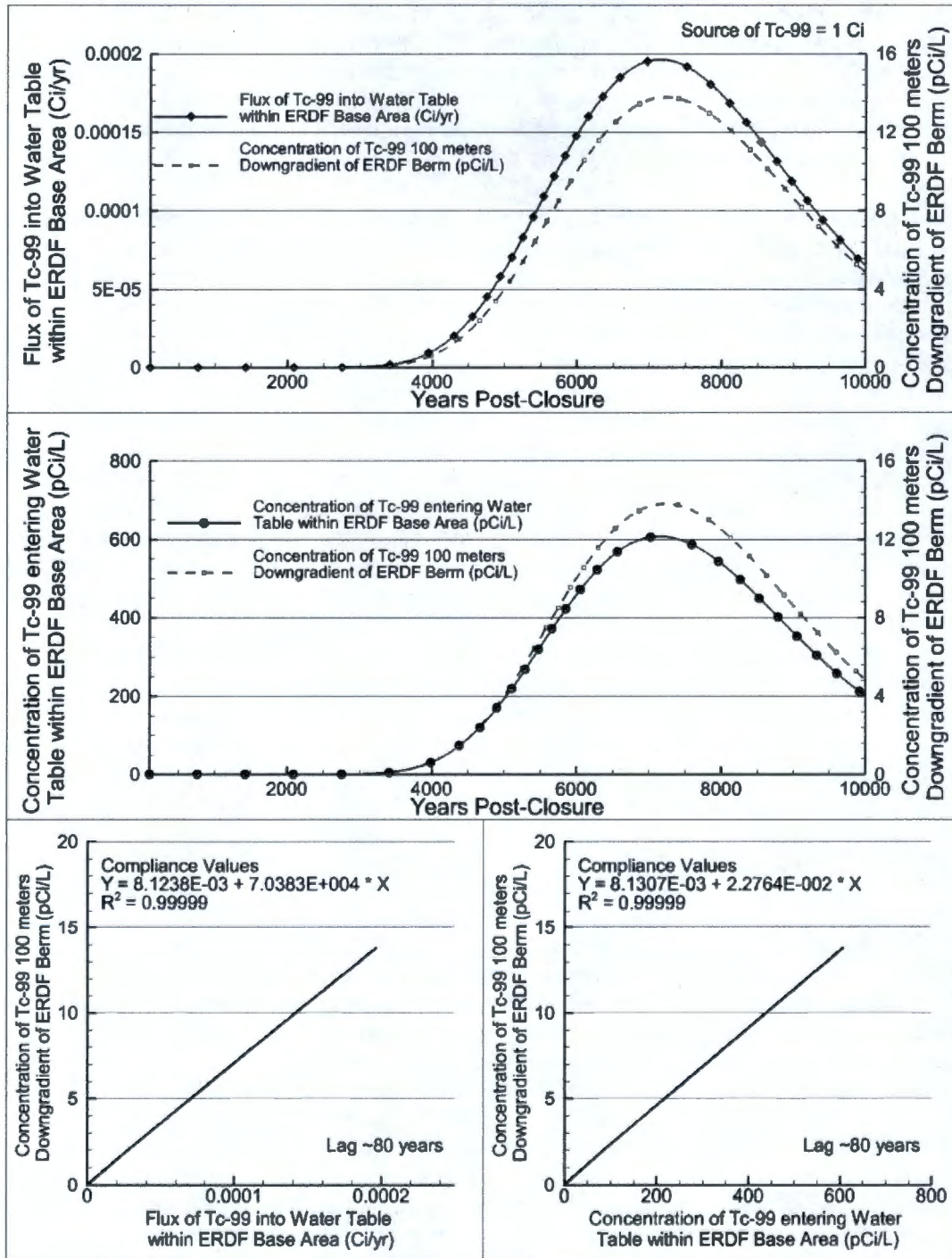
Table 4-11. Results of the Vadose Zone Hydrologic and Recharge Parameter Percentile Evaluations for Radionuclides with $K_d = 0$ mL/g (e.g., Technetium-99) Breakthrough in the Aquifer at the Downgradient Point of Calculation (Results Presented on a per Ci Source Basis).

Flow and Transport Parameter Percentile Values	Maximum Radionuclide Flux at Water Table (Ci/yr)	Arrival Time of Maximum Concentration at 100-m Downgradient Point of Calculation (Years Post-Closure)	Maximum Concentration at 100-m Downgradient Point of Calculation (pCi/L)	Transformation Factor Between Maximum Radionuclide Flux at Water Table and Maximum Concentration at 100-m Downgradient Point of Calculation (pCi/L per Ci/yr)	Aquifer Hydraulic Conductivity (m/day)
Minimum	0 ^a	10000	1.7E-05 ^a	N/A	0.1
25 th Percentile	1.37E-04	8380	19	137,600	2.575
Median	1.41E-04	8185	9.8	69,700	5
Compliance	2.01E-04	7220	14	70,300	5
75 th Percentile	2.30E-04	5795	11	46,400	7.525
Maximum	8.80E-04	1860	31	35,400	10

^a No radionuclide mass entered the aquifer within the area projected at the water table by the base of ERDF, but some mass entered the aquifer outside of this area because of dispersive movement and the relatively higher recharge rates applied to the area outside of ERDF.

The results of the compliance and percentile evaluations also illustrate the linear relationship between the radionuclide flux and leachate concentration entering the water table and the concentration at the point of calculation in the groundwater. Figure 4-35 shows for the compliance case the coincident breakthrough curves of the technetium-99 entering the water table (Ci/yr per Ci source) and the leachate concentration (pCi/L per Ci source) entering the water table with the resulting concentration in groundwater 100 m downgradient of ERDF berm (pCi/L per Ci source). As seen in the figure, the curves overlay one another fairly closely, indicating that the downgradient concentration in groundwater is likely correlated to the flux of technetium-99 and concentration of the leachate entering the aquifer. The relationship between the flow rate and leachate concentration of technetium-99 and the resulting groundwater concentration provides an indication of the extent to which the correlation is linear.

Figure 4-35. Results and Regression Lines Associated with the Vadose Leachate Concentration and the Concentration in Groundwater for the Compliance Evaluation for Technetium-99 (Results Presented on a per Ci Source Basis).



The coefficient of determination for both regression lines is essentially equal to 1, which means the lines fit the values almost perfectly. Thus, the downgradient concentration in groundwater of technetium-99 can be estimated by either the flux or concentration of technetium-99 in the leachate entering the aquifer and a linear scalar. In the case of the technetium-99 flux, the scalar needs only to account for the aquifer flow rate. In the case of the leachate concentration, the scalar needs to account for the flow rates of the leachate and the aquifer. For the compliance case evaluation for technetium-99, the inverse of the slope of the regression line between the groundwater and leachate concentration indicates that the leachate concentration is reduced by a factor of 44 in the aquifer, i.e., $1 / 0.022764$.

Regression lines fitted to the relationship between vadose zone leachate concentration and groundwater concentration for the four percentile cases that produced peak concentrations in groundwater during the 10,000-year sensitivity-compliance time frame provide an approximate dilution-attenuation factor for the different percentiles of the aquifer properties (Figure 4-36). The slope values range between 0.018 and 0.033 (pCi/L in groundwater per pCi/L in leachate). The magnitude of the dilution-attenuation factor ranges between 30 and 60 and appears to be approximately 44 to 45 for the compliance and median cases, although no pattern appears to emerge from this correlation. The dilution-attenuation factor needs to account for the water fluxes of the leachate and the aquifer, and the ratio between the leachate and aquifer fluxes is not constant or prescribed in the different percentile case parameters or results. The dilution-attenuation factor for the maximum percentile case is the lowest of those evaluated because the ratio between the leachate flux and the aquifer water flux is the highest value. The dilution-attenuation factors for the compliance and median cases are essentially equal because the water fluxes into the aquifer and the aquifer parameters for these two cases are essentially the same.

A definite pattern does emerge from the relationship between the radionuclide flux and the downgradient groundwater concentration. Figure 4-37 shows the results of the four percentile cases with the regression lines fitted to the relationship between vadose radionuclide flux and the groundwater concentration. The inverse of these slope values, when plotted as a function of the aquifer hydraulic conductivity, also exhibit a linear relationship. Thus, the factor for transforming the radionuclide flux to groundwater concentration for any aquifer hydraulic conductivity value can be estimated using this regression line. The peak concentration in groundwater can then be estimated using the peak radionuclide flux at the water table and the transforming factor estimated from the regression line.

4.6.2.2 Aquifer Anisotropy Evaluations. The aquifer hydraulic conductivity and dispersivity anisotropy ratios were evaluated in every combination of their minimum, median, and maximum values to evaluate the sensitivity of the results to the aquifer transport anisotropy parameters. In this analysis, the hydraulic conductivity anisotropy is defined as the ratio of the vertical to the horizontal hydraulic conductivity. The dispersivity anisotropy is defined as the ratio of the longitudinal to the transverse dispersivity. Because of the necessary multidimensional component of this analysis, it was conducted using the three-dimensional model. For this analysis, the recharge values, vadose zone hydraulic properties, and aquifer horizontal hydraulic conductivity remained unchanged from their median values. The results of the analysis (Table 4-12) show that the variability in these parameters introduces negligible variability in the groundwater concentration of technetium-99 at the point of calculation, indicating that the transport occurring laterally to the primary direction of flow in the aquifer is fairly constant regardless of the anisotropy parameters.

Figure 4-36. Results and Regression Lines Associated with the Vadose Leachate Concentration and the Concentration in Groundwater for the Hydrologic and Recharge Parameter Percentile Evaluations for Technetium-99 (Results Presented on a per Ci Source Basis).

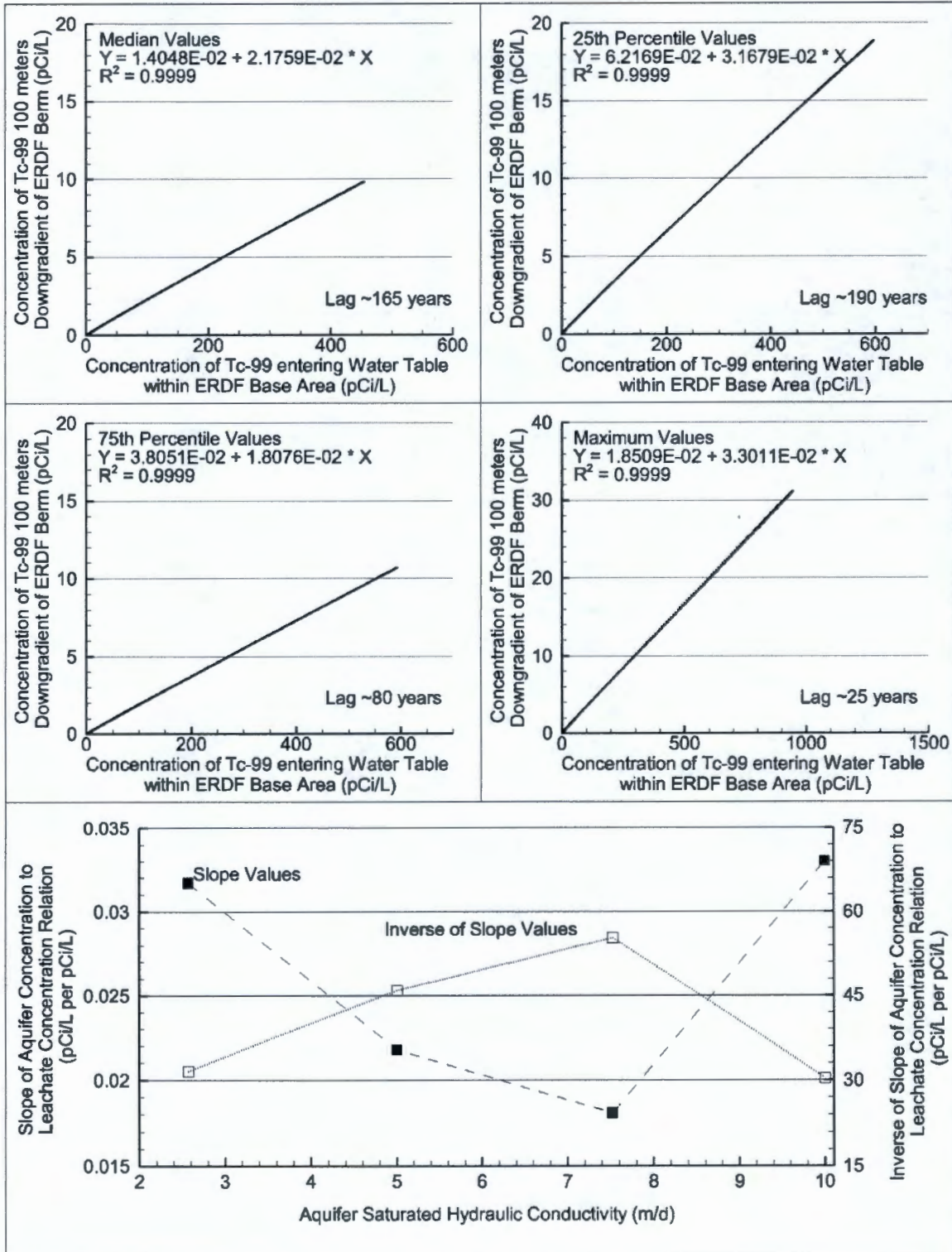


Figure 4-37. Results and Regression Lines Associated with the Vadose Radionuclide Flux and the Concentration in Groundwater for Hydrologic and Recharge Parameter Percentile Evaluations for Technetium-99 (Results Presented on a per Ci Source Basis).

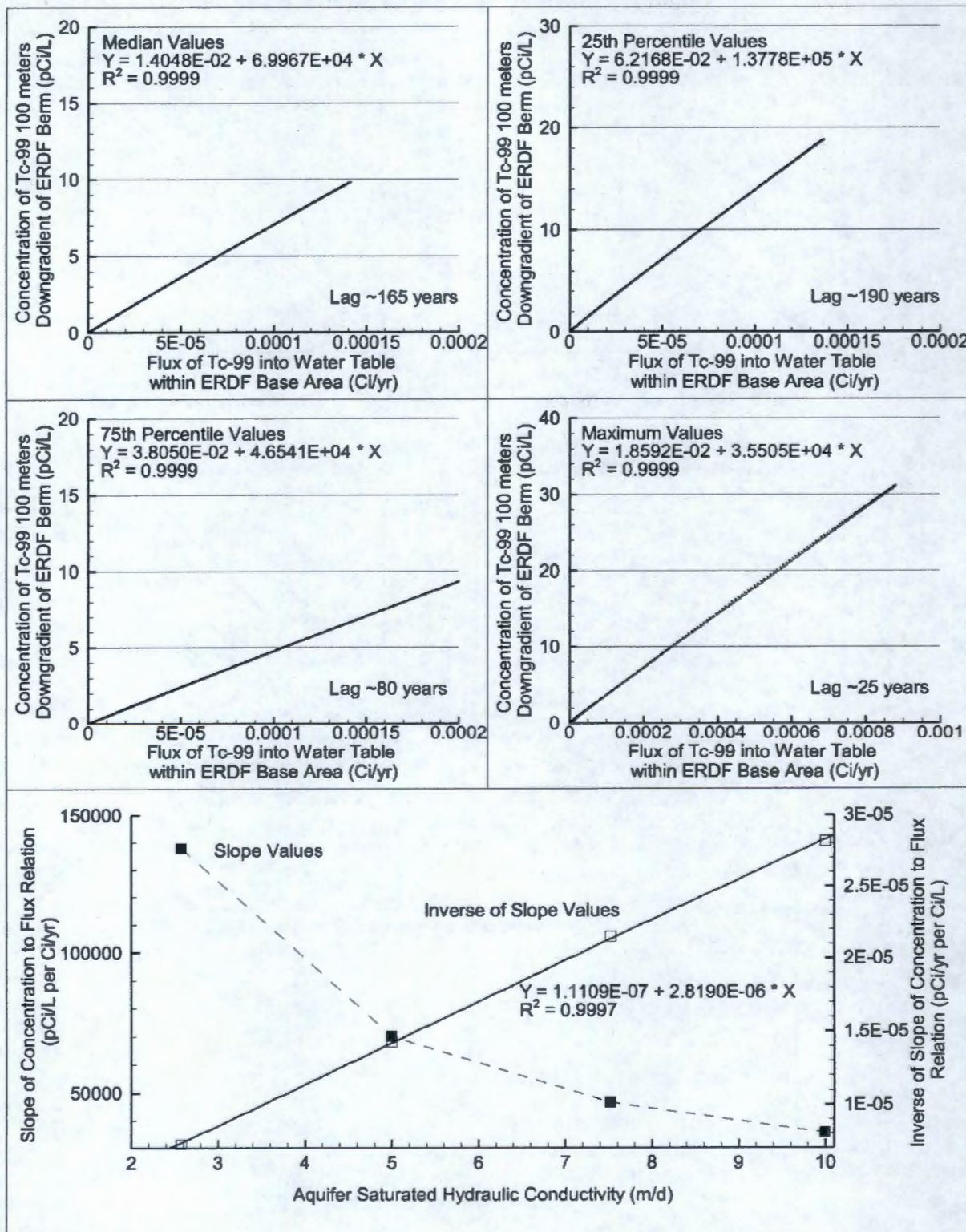


Table 4-12. Results of the Aquifer Anisotropy Parameter Evaluations for Radionuclides with $K_d = 0$ mL/g (e.g., Technetium-99) (Results Presented on a per Ci Source Basis).

Ratio of Vertical to Horizontal Aquifer Hydraulic Conductivity Minimum = 0.01 Median = 0.187 Maximum = 0.5	Aquifer Dispersivity Anisotropy (Longitudinal to Transverse Ratio) Minimum = 5 Median = 7.5 Maximum = 10	Arrival of Peak Concentration (Years Post-Closure)	Maximum Concentration at 100 m Downgradient Point of Calculation (pCi/L)	Percent Deviation from Median Value Results
Minimum	Minimum	8185	9.6	-2.4%
Median	Minimum	8190	9.6	-2.4%
Maximum	Minimum	8190	9.6	-2.4%
Minimum	Median	8180	9.8	0.0%
Median	Median	8180	9.8	0.0%
Maximum	Median	8180	9.8	0.0%
Minimum	Maximum	8175	10	1.4%
Median	Maximum	8175	10	1.4%
Maximum	Maximum	8175	10	1.4%

4.6.2.3 Radionuclide Mobility Evaluations. Radionuclide mobility is described by each radionuclide's distribution or partitioning coefficient (K_d), which is the ratio of the concentration of the radionuclide on the soil solid phase to the concentration of the radionuclide in the liquid phase. Because of the long travel times through the vadose zone at ERDF, the threshold K_d value for determining whether radionuclides are sufficiently mobile to impact groundwater appears to be close to 0.2 mL/g in the three-dimensional models. The results of the radionuclide mobility sensitivity tests presented in Table 4-13 show the impact that the K_d value has on the results. The difference in peak groundwater concentration results between radionuclides with a K_d value of 0 mL/g and 0.1 mL/g for the fate and transport percentile results is one to two orders of magnitude. The difference in the peak concentration results for radionuclides with a K_d value of 0.1 mL/g and 0.2 mL/g is three orders of magnitude, with the exception of the maximum percentile case, for which the difference is a factor of 2. With the exception of iodine-129, the K_d for all of the radionuclides that have an impact to groundwater within the sensitivity-uncertainty time frame is zero. Because the inventory of iodine-129 is small and the arrival of it at the groundwater point of calculation is limited to delayed breakthrough near the end of the simulated time frame, sensitivity in the K_d values is not expected to have a major effect on the results.

The radionuclide mobility evaluation also considered estimating the impact that the distribution of the radionuclide inventory in ERDF has on the results. The ERDF radionuclide inventory was limited to the eastern half of the facility with all parameters unchanged from the compliance case. The actual distribution of waste in the ERDF is not well documented and subject to change with continued operations, but limiting the inventory to the eastern half of ERDF seems like an acceptable bound to the unevenness of the distribution for the purpose of this evaluation. The results of this evaluation indicate that the initial distribution of inventory within ERDF is not consequential to the impacts to groundwater, especially for the mobile radionuclides.

Table 4-13. Results of the Radionuclide Mobility Evaluations for Radionuclides (e.g., Technetium-99 and Iodine-129) Breakthrough to the Water Table in the Aquifer at the Downgradient Point of Calculation (Results Presented on a per Ci Source Basis).

Flow and Transport Parameter Percentile Values	Radionuclide K_d Value (ml/g)	Arrival Time of Maximum Radionuclide Flux at Water Table (Years Post-Closure)	Maximum Radionuclide Flux at Water Table (Ci/yr)	Arrival Time of Maximum Concentration at 100 m Downgradient Point of Calculation (Years Post-Closure)	Maximum Concentration at 100 m Downgradient Point of Calculation (pCi/L)
Minimum	0	N/A	0	10000	1.7E-05 ^a
	0.1	N/A	0	10000	0
	0.2	N/A	0	10000	0
25 th Percentile	0	8210	1.37E-04	8400	19
	0.1	10000	1.29E-06	10000	0.12
	0.2	10000	1.09E-09	10000	9.9E-06
Median	0	8015	1.41E-04	8180	9.8
	0.1	10000	5.69E-06	10000	0.30
	0.2	10000	2.44E-08	10000	9.2E-04
75 th Percentile	0	5705	2.30E-04	5785	11
	0.1	10000	1.72E-05	10000	0.64
	0.2	10000	3.03E-08	10000	5.8E-04
Maximum	0	1825	8.80E-04	1850	31
	0.1	6660	2.56E-04	6645	7.8
	0.2	10000	1.22E-04	10000	3.7
Initial Distribution of Radionuclides Limited to Eastern Half of ERDF					
Compliance	0	7025	1.97E-04	7080	14
	0.1	10000	7.20E-06	10000	0.47
	0.2	10000	1.66E-08	10000	8.2E-04

^a No radionuclide mass entered the aquifer within the area projected at the water table by the base of ERDF, but some mass entered the aquifer outside of this area because of dispersive movement and the relatively higher recharge rates applied to the area outside of ERDF.

The maximum concentrations calculated at the downgradient point of calculation for technetium-99 for the compliance case (assuming uniform distribution) and the eastern half distribution sensitivity are 13.8 and 14.1 pCi/L, respectively, and for iodine-129 the maximum concentrations calculated are 1.3E-04 and 8.2E-04 pCi/L for the respective cases. While the relative difference between the maximum concentration values of iodine-129 is large, the magnitude of the numbers is very small. Therefore, while the assumption that the radionuclides are uniformly distributed throughout the ERDF waste volume is not likely to be accurate, the actual distribution of radionuclides in the ERDF does not appear to be consequential to the calculation of the impacts to groundwater.

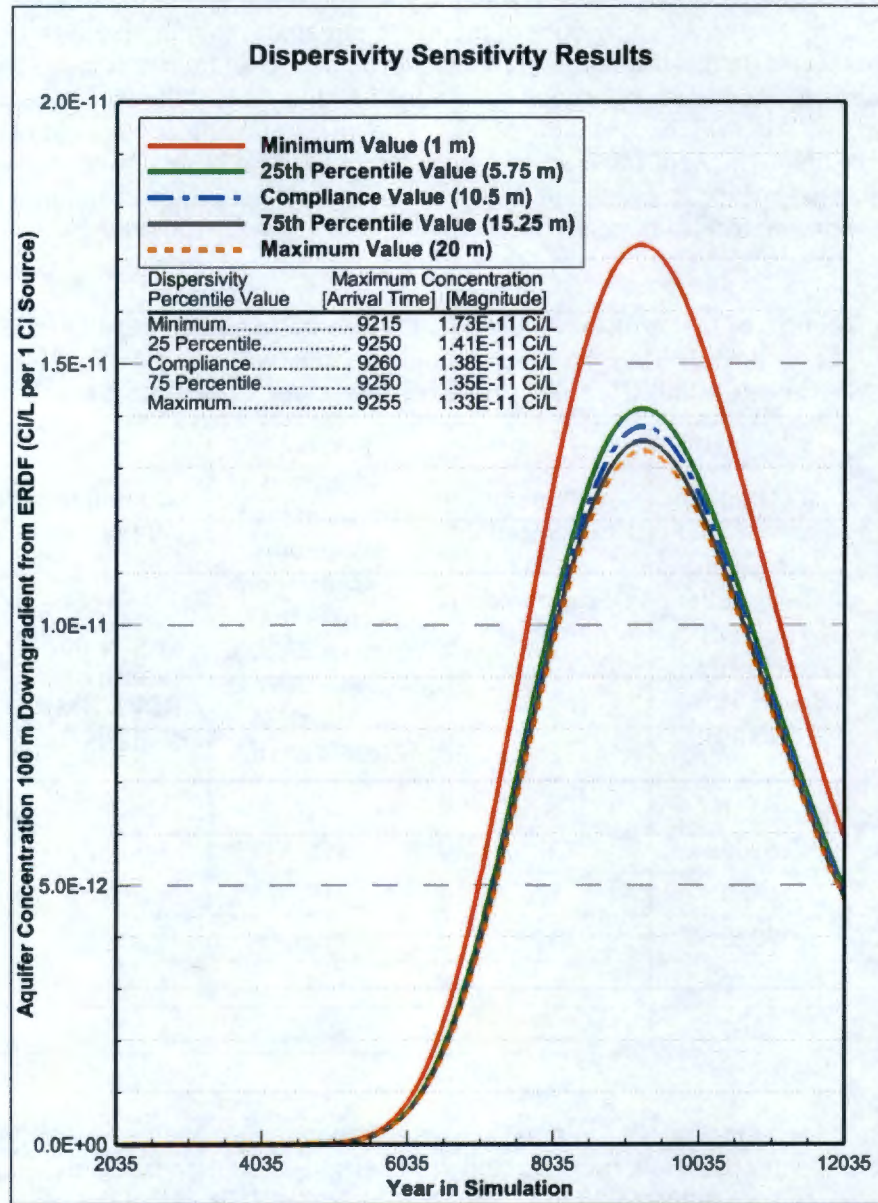
4.6.2.4 Aquifer Mixing Width and Dispersivity Evaluations. The compliance evaluation considered the average concentration in the upper 5 m of the aquifer across the base width of the ERDF. If the width is extended to the entire width of the ERDF, from the outside edges of the north and south berms, the concentration is reduced by approximately one third for the percentile sets of parameters (Table 4-14). The width at the base of ERDF is 305 m, and the width across the berms is 555 m. Approximately 80% of the mass remains within the base width of ERDF compared to the width across the berms. The reduction in concentration in the results is therefore consistent with the simple scalar determined by the ratio of the widths and ratio of the mass flux, i.e., $1 - ((305 \text{ m})/(555 \text{ m}))/0.80 = 31\%$. The incongruously large percent difference between the maximum concentration across the width of ERDF's base and across the width of ERDF's berms in the minimum percentile case results is a consequence of the maximum concentrations not reaching their peak values during the sensitivity-uncertainty time frame.

Table 4-14. Results of the Aquifer Mixing Width Evaluations from the Outside Edges of the North and South Berms for Radionuclides with $K_d = 0 \text{ mL/g}$ (e.g., Technetium-99) (Results Presented on a per Ci Source Basis).

Flow and Transport Parameter Percentile Values	Arrival Time of Maximum Concentration at 100 m Downgradient Point of Calculation (Years Post-Closure)	Maximum Concentration at 100 m Downgradient Point of Calculation (pCi/L)	Percent Difference Between the Maximum Concentration Across the Width of ERDF's Base and Across the Width of ERDF's Berm	Cumulative Mass Flux in Upper 5 m of the Aquifer	
				Across the Width of ERDF's Base (Ci)	Across the Width of ERDF's Berms (Ci)
Minimum	10000	1.2E-03	7232%	1.57E-10	2.24E-07
25 th Percentile	8380	12	35%	1.06E-01	1.25E-01
Median	8185	6.5	34%	1.01E-01	1.23E-01
Compliance	7220	9.2	35%	1.16E-01	1.38E-01
75 th Percentile	5795	7.2	32%	1.06E-01	1.31E-01
Maximum	1860	20	36%	1.15E-01	1.36E-01

The evaluation of the sensitivity of the aquifer concentration results to the variability in aquifer dispersivity includes the plausible range for longitudinal saturated macrodispersivities below the ERDF, which ranges between 1 to 20 m (3.2 to 65.6 ft) (WCH-515). All of the other parameter values used in the evaluation were held at their compliance case values, including the anisotropy ratio between longitudinal and transverse macrodispersivity. It was held constant at 10 because the results of the aquifer anisotropy parameter evaluations indicated that variability in the anisotropy parameters introduces essentially negligible variability into the results (refer to Table 4-12). Because of the multidimensional component of dispersivity and its potential impact on the results, the simulations involved the three-dimensional model. The results follow an expected pattern with the maximum concentration at the 100-m downgradient point of calculation inversely related to the magnitude of the longitudinal macrodispersivity (Figure 4-38).

Figure 4-38. Results of the Longitudinal Saturated Dispersivity Sensitivity Evaluation Showing the Breakthrough of a Radionuclide with $K_d = 0$ mL/g (e.g., Technetium-99) to the Water Table for the Individual Hydrologic Parameter Percentile Sets (Results Presented on a per Ci Source Basis).



The results show little variability from the compliance case value results, with the exception of the minimum dispersivity value results (~25% greater), when the longitudinal macrodispersivity is a factor of 10 less than the compliance case value. Excluding that case, the breakthrough curves at the point of calculation almost overlay one another (Figure 4-38) and the time of arrival of the maximum concentration is within 10 years in the simulations. Overall, the results indicate that with the exception of the extreme lower value of dispersivity, the maximum concentration in

the aquifer at the downgradient point of calculation is not affected by the variability in dispersivity, and it is not a large source of uncertainty in the model results.

4.6.2.5 Recharge Evaluations. The spatially varying recharge parameters were varied to determine the impact that the recharge rates applied to the different areas representing the ground surface have on the results. Because of the spatial component of this analysis, it was conducted using the three-dimensional model. For this analysis, the vadose zone and aquifer hydraulic properties remained unchanged from their median values. Only the median and maximum surface barrier post-design life recharge rates were evaluated because the results of the minimum value percentile evaluation indicated that the groundwater concentration at the point of calculation did not reach a peak within the sensitivity-uncertainty time frame of 10,000 years. The results of the analysis show that the variability in the results caused by the variability in the recharge rates applied to the areas outside the ERDF and to the surface barrier during its design life is minor when the vadose zone properties are assigned median values.

The peak groundwater concentration ranges between 9.5 and 10.1 pCi/L (per 1 Ci source) for all of the cases with post-design life recharge rates set to the median value, and this range brackets the result of the median percentile evaluation (9.8 pCi/L) (Table 4-15). This includes cases in which the recharge rates applied to the areas outside of ERDF, representing both undisturbed and disturbed ground, and to the surface barrier during its design life, were set to the minimum and maximum values of their respective ranges. For the two cases with the post-design life recharge rate set to the maximum value, the peak groundwater concentration is essentially the same. Thus, for the range of recharge rates included in this evaluation, the only parameter variability that appears capable of introducing appreciable variability into the peak groundwater concentration results is the surface barrier post-design life recharge rate.

Table 4-15. Results of the Percentile Recharge Evaluations for Radionuclides with $K_d = 0$ mL/g (e.g., Technetium-99; Results Presented on a per Ci Source Basis). (2 Pages)

Pre-ERDF and Undisturbed Ground Recharge Rate Percentile (Value)	Recharge Rate of Disturbed Ground During Operations Percentile (Value)	Intact Surface Barrier and Degraded Liner Recharge Rate Percentile (Value)	Post-Design Life Surface Barrier Recharge Rate Percentile (Value)	Maximum Concentration at Down-gradient Point of Calculation (pCi/L)	Maximum Radio-nuclide Flux at Water Table (Ci/yr)	Water Flux into Aquifer beneath ERDF at Time of Maximum Radio-nuclide Flux (mm/yr)
Median Percentile Vadose Zone and Aquifer Parameters						
Maximum (4 mm/yr)	Median (42.3 mm/yr)	Median (0.5 mm/yr)	Median (1.0 mm/yr)	9.5	1.42E-04	1.12
Median (1.6 mm/yr)	Maximum (90 mm/yr)	Median	Median	9.8	1.41E-04	1.11
Median	Median	Maximum (1.0 mm/yr)	Maximum (2.0 mm/yr)	18	2.70E-04	2.11

Table 4-15. Results of the Percentile Recharge Evaluations for Radionuclides with $K_d = 0$ mL/g (e.g., Technetium-99; Results Presented on a per Ci Source Basis). (2 Pages)

Pre-ERDF and Undisturbed Ground Recharge Rate Percentile (Value)	Recharge Rate of Disturbed Ground During Operations Percentile (Value)	Intact Surface Barrier and Degraded Liner Recharge Rate Percentile (Value)	Post-Design Life Surface Barrier Recharge Rate Percentile (Value)	Maximum Concentration at Down-gradient Point of Calculation (pCi/L)	Maximum Radio-nuclide Flux at Water Table (Ci/yr)	Water Flux into Aquifer beneath ERDF at Time of Maximum Radio-nuclide Flux (mm/yr)
Median	Median	Maximum	Median	9.8	1.41E-04	1.11
Median	Median	Minimum	Maximum	18	2.71E-04	2.11
Median	Median	Minimum	Median	9.9	1.42E-04	1.11
Median	Minimum (22.5 mm/yr)	Median	Median	9.8	1.41E-04	1.11
Minimum (0.26 mm/yr)	Median	Median	Median	10	1.41E-04	1.11
Median	Median	Median	Median	9.8	1.41E-04	1.11
Median	Median	Minimum (0.05 mm/yr)	Minimum (0.1 mm/yr)	0.007	8.20E-08	0.21
Maximum Percentile Vadose Zone and Aquifer Parameters						
Maximum	Maximum	Maximum	Maximum	31	8.80E-04	3.33
Compliance (1.7 mm/yr)	Compliance (45 mm/yr)	Compliance (0.5 mm/yr)	Compliance (1.0 mm/yr)	19	5.08E-04	1.96
Median	Median	Median	Median	19	5.10E-04	1.95
Compliance Vadose Zone and Aquifer Parameters						
Compliance	Compliance	Compliance	Compliance	14	2.01E-04	1.16
Maximum	Maximum	Maximum	Maximum	23	3.51E-04	2.11

Although the variability in the recharge rates applied to the areas outside the ERDF and to the surface barrier during its design life does not appear to introduce variability into the maximum groundwater concentration results when the vadose zone properties are assigned median values, variability in these recharge rates does introduce variability into the results when the vadose zone properties are assigned maximum values. The maximum radionuclide flux at water table for the maximum percentile evaluation (both recharge and vadose zone properties assigned their maximum values) is 8.8E-04 Ci/yr, which is more than 3 times greater than the maximum flow rate for either evaluation of the maximum value post-design life recharge rate with the median soil hydraulic properties (2.7E-04 Ci/yr). The water flux at the water table at the time of arrival of the maximum radionuclide flux is greater for the maximum vadose zone and aquifer parameter percentile case than either of the maximum value post-design life recharge rate cases with median vadose zone and aquifer parameters (3.33 mm/yr compared to 2.11 mm/yr). This indicates that the vadose zone properties, when set to their maximum values instead of the

median values, increase the calculated amount of lateral flow moving from outside ERDF, where the recharge rates are higher, toward the vadose zone beneath ERDF and downward to the water table. However, the radionuclide flux is 3 times greater but the water flux is only 1.5 times greater than the median percentile case results. The increase in the radionuclide flux appears to be more a consequence of the change in the vadose zone properties than the increased recharge rate. Additionally, comparing the maximum contaminant flux at the water table of the median and compliance case evaluations, in which the surface barrier recharge rates are essentially equal (1.11 compared to 1.16 mm/yr), shows that the compliance case radionuclide fluxes are approximately 40% greater than the median case results (2.01E-4 compared to 1.14E-04 Ci/yr). This difference is not caused by lateral flow because the water fluxes at the water table are essentially equal for the two cases. The difference appears to be caused by differences in the vadose zone properties causing differences in the contaminant velocity through the vadose zone.

4.6.2.6 Vadose Zone Hydraulic Properties Evaluations. The vadose zone hydraulic properties were varied to determine the impact that the inherent variability in these parameters has on the results. Four vadose zone parameters were varied: van Genuchten α and n (coupled), saturated moisture content (θ_s), residual moisture content (θ_r), and fitted saturated hydraulic conductivity (K_s). The parameters were varied individually and independently, although the van Genuchten moisture retention α and n parameters are assumed to be coupled, and were varied in unison for the different geologic soil units. For example, for the evaluations using the 25th percentile value for hydraulic conductivity, all of the geologic soil units were assigned their 25th percentile value for hydraulic conductivity. It is important to note that the percentiles refer to sets of parameter values and not to the properties individually (as discussed in Section 4.6.1 and WCH-515). Thus, the maximum van Genuchten residual saturation parameter does not necessarily represent the largest value of θ_r , but the value associated with the maximum unsaturated hydraulic conductivity curve (Figure 4-22) and the corresponding set of the parameters identified in Table 4-6. The values of four vadose zone parameters, van Genuchten α and n (coupled), θ_s , θ_r , and fitted saturated hydraulic conductivity (K_s) varied over the six cases (five percentile cases and one compliance case) produced 1296 combinations of vadose zone hydraulic properties. These evaluations used the median recharge values, which are essentially equivalent to the compliance case values.

Because the results of the recharge analysis indicated that the recharge rates apart from surface barrier post-design life rate do not appear to affect the results appreciably, and that the groundwater concentration appears to be the product of a simple scalar and the contaminant mass flux into the aquifer, this analysis was conducted using a one-dimensional abstraction of the three-dimensional model. Thus, the variability in the flux of radionuclides into the aquifer is equivalent to the variability in the groundwater concentrations. The vadose zone template representing the northern half of ERDF cell 9 location was selected for this evaluation (see Figure 1-2).

The applicability of the one-dimensional transport models to evaluate the sensitivity of the results to the individual hydraulic properties is indicated by comparing the percentile results of the one-dimensional transport models to the comparable three-dimensional transport model results. Figure 4-39 shows the breakthrough of technetium-99 with an assumed 1 Ci inventory within the ERDF volume from the vadose zone to the aquifer for the percentile flow and transport parameter values. The results indicate good comparison between the one-dimensional abstraction model and the three-dimensional model results for the minimum, 25th percentile, median, and 75th percentile parameter sets. The relative difference between the one-dimensional and the three-dimensional model results is somewhat larger for the compliance and maximum parameter sets, which appears to be a consequence of using the cell 9 location vadose zone template and the anisotropic lateral flow that is calculated in the three-dimensional model when the compliance and maximum parameter sets are used.

In the screening analysis, the arrival time associated with transport from the northern half of ERDF cell 9 location to the water table was one of the fastest values. It is consistent with these results that the comparison of the one-dimensional and the three-dimensional model results for the compliance case parameter set indicates that the breakthrough of technetium-99 occurs sooner in the one-dimensional model than the three-dimensional model. The recharge rates are similar for the two parameter sets, especially the post-design life surface barrier recharge rates. For these parameter sets, the difference in flow caused by vadose zone anisotropy is minimal.

The results contained in Table 4-10 indicate that the water flux into the aquifer at the time of the peak contaminant breakthrough is only slightly higher for the compliance case parameter set (1.16 mm/yr) than the median case parameter set (1.11 mm/yr), even though the post-design life recharge rate is slightly higher in the median case parameter set (1.03 mm/yr versus 1.00 mm/yr). This indicates that although more net infiltration originating from outside the ERDF surface barrier area, where the recharge rate is higher, is calculated to affect transport within the ERDF surface barrier area for the compliance case parameter set than the median case parameter set, the difference is almost negligible.

In the case of the maximum parameter sets, the breakthrough of technetium-99 occurs later in the one-dimensional model than the three-dimensional model. The water flux into the aquifer at the time of the peak contaminant breakthrough in the three-dimensional model (3.33 mm/yr) is definitely higher than the post-design life recharge rate (2.00 mm/yr). This indicates that substantial net infiltration originating from outside the ERDF surface barrier area, where the recharge rate is higher, is calculated to affect transport within the ERDF surface barrier area for maximum parameter set in the three-dimensional model.

Overall, vadose zone parameter values that tend to increase the time of the maximum radionuclide flux into water table tend to decrease the magnitude of the maximum radionuclide flux into the aquifer (Figure 4-40). The highest maximum flux values are all associated with arrival times less than 5,000 years, and no maximum flux value associated with an arrival time greater than 7,000 years exceeds the compliance case result. Thus, those vadose zone parameters with the greatest impact on the velocity of the radionuclides moving downward through the vadose zone are likely to have the greatest impact on the maximum radionuclide flux value.

Figure 4-39. Comparison of the One-Dimensional Transport Model Results to the Comparable Three-Dimensional Transport Model Results of the Breakthrough of a Radionuclide with $K_d = 0$ mL/g (e.g., Technetium-99) to the Water Table for the Individual Hydrologic Parameter Percentile Sets (Results Presented on a per Ci Source Basis).

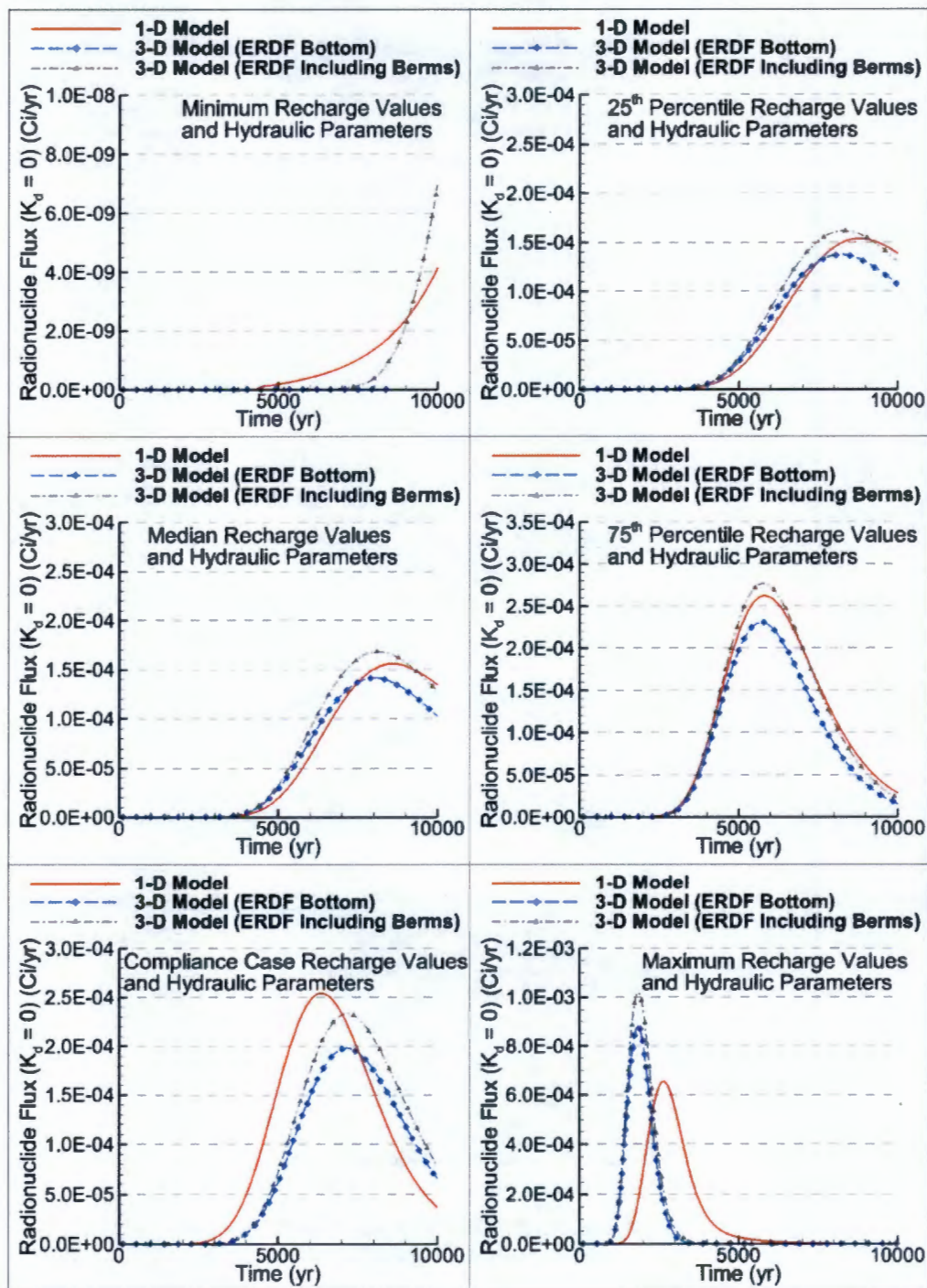
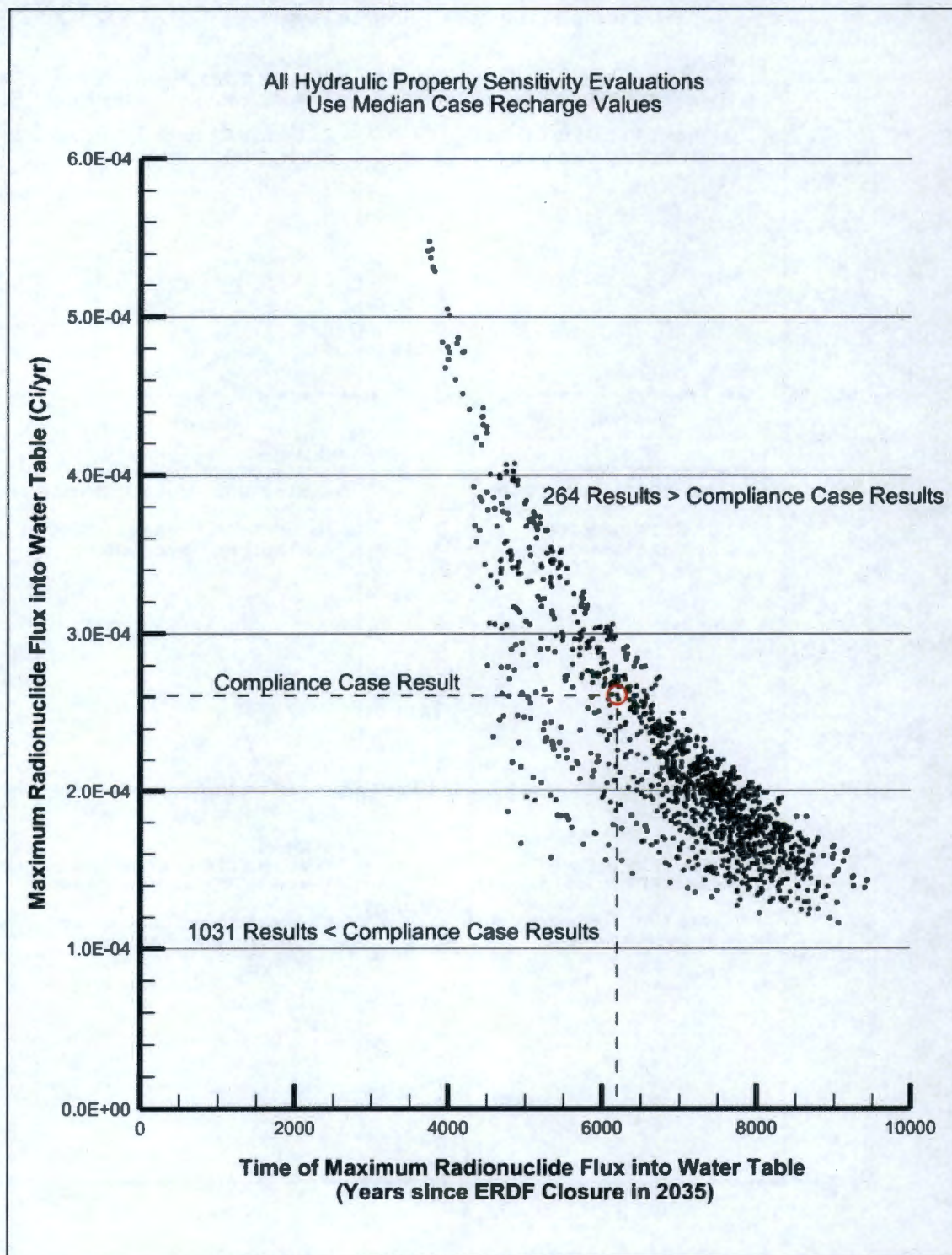


Figure 4-40. Cumulative Results for Radionuclides with $K_d = 0$ mL/g (e.g., Technetium-99) of the Individual Hydrologic Parameter Percentile Evaluations (Results Presented on a per Ci Source Basis).



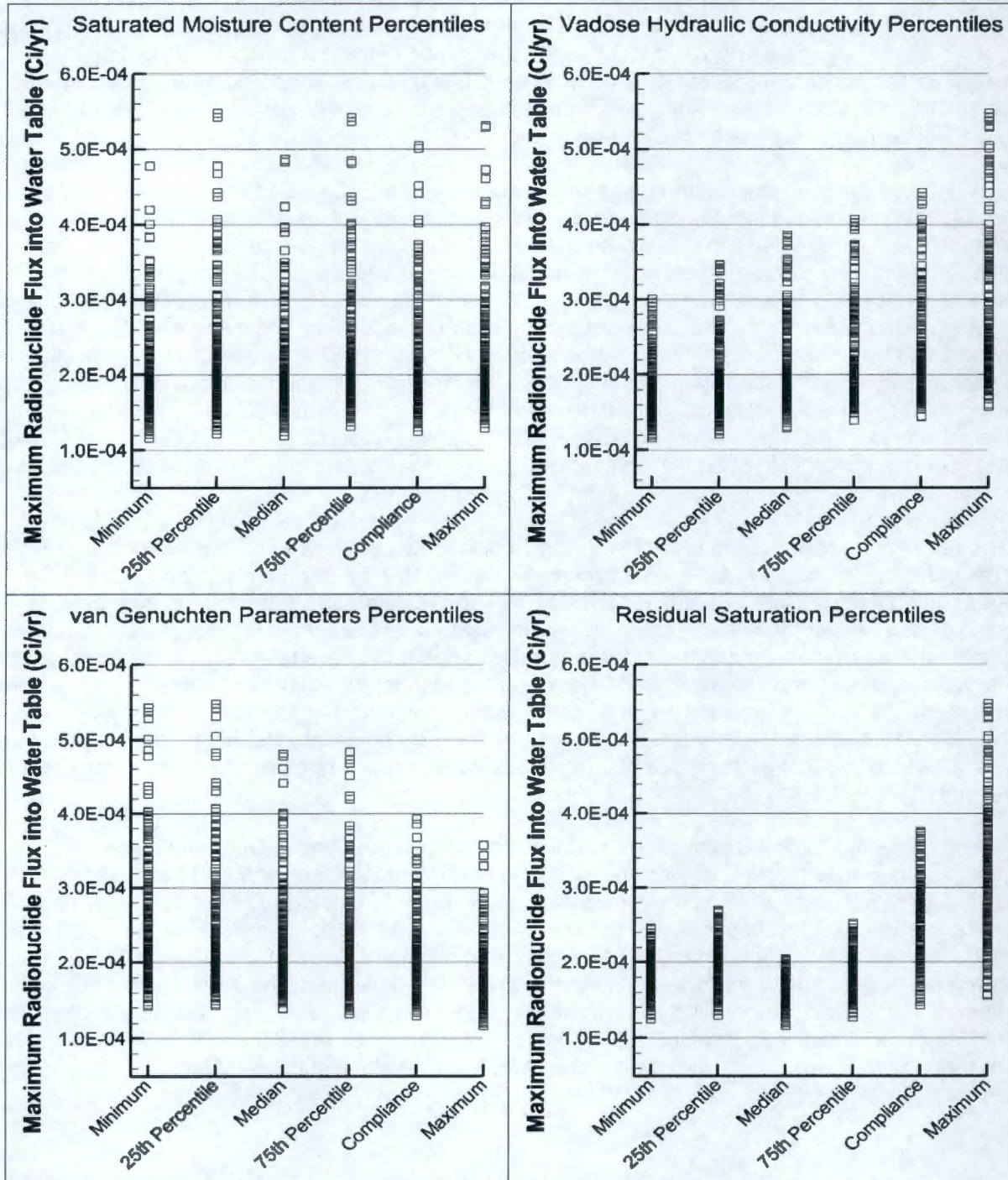
To determine the impact and control that the different vadose zone parameters have on the results, the results of the evaluation are organized in Figure 4-41 by each parameter and each percentile value. The columns represent all of the results associated with the identified percentile value of the indicated vadose zone parameter. As noted earlier, the percentile categories refer to the sets of parameter values that produce the percentile unsaturated hydraulic curves identified in Figure 4-22, and not to the magnitude of the parameters individually. For example, the maximum percentile value of the van Genuchten-Mualem residual water content (θ_r) for the Hanford Hf2 and Ringold Rf2f units is 0.0238 (Table 4-6), which is less than any of the other percentile values for those units.

The compliance case results appear to be bounded between $\sim 1.4\text{E-}04$ Ci/yr and $\sim 4.0\text{E-}04$ Ci/yr by the coupled van Genuchten-Mualem α and n and the residual water content (θ_r) parameters (Figure 4-41). The scatter in these two parameters' compliance case results is less than the scatter in the other two parameters' compliance case results. The results also provide an indication as to which parameter values or combination of parameter values produce the largest radionuclide fluxes. The results organized by hydraulic conductivity show that only the results associated with maximum percentile value exceed $\sim 4.6\text{E-}04$ Ci/yr. Likewise, only the results organized by residual saturation and associated with maximum percentile value exceed $4.0\text{E-}04$ Ci/yr. Thus, the results shown on the other plots exceeding $4.0\text{E-}04$ Ci/yr must involve the maximum percentile residual saturation value, and any exceeding $4.6\text{E-}04$ Ci/yr must involve the maximum percentile hydraulic conductivity and the maximum percentile residual saturation value.

The range and scatter of the results in a single column indicate how much variability exists in the results for the indicated vadose zone parameter value. The greater the range and scatter, the less control that particular parameter value has on the results. The individual parameter analyses show that the results organized by the residual saturation percentiles appear to have the least scatter, indicating that residual saturation appears to have relatively greater control on the results. There is comparatively little range in the results, especially those associated with the minimum, 25th percentile, median, and 75th percentile values. The range in the results associated with the residual saturation maximum value is comparable to the overall range in the results, indicating that at this value, the residual saturation does not have as much control on the results.

The results associated with the range of unsaturated hydraulic conductivity values appear to be positively correlated, which is consistent with the method of using unsaturated hydraulic conductivity within the expected soil matric potential range to establish the combinations of percentile values. The upper bound of the results increases as the magnitude of the parameter value, as described by its percentile, increases from minimum to maximum. The results of the analysis show that the variability in the other parameters, particularly the saturated moisture content, introduces comparatively little variability into the results. The range and distribution of maximum radionuclide flux values exhibit only minor differences for all the percentile case results for these parameters, which include the compliance case values in this evaluation.

Figure 4-41. Results of the Individual Hydrologic Parameter Percentile Evaluations for Radionuclides with $K_d = 0$ mL/g (e.g., Technetium-99); Results Presented on a per Ci Source Basis).



The relatively small variability in the residual saturation results for the minimum, 25th percentile, median, and 75th percentile values, compared to the corresponding ranges of results for any of the other properties, indicates that the residual saturation is the strongest controlling vadose zone hydraulic parameter. None of the results of the four previously mentioned percentile values exceeds $3.0\text{E-}04$ Ci/yr, and the only maximum flux results greater than $4.0\text{E-}04$ Ci/yr occur with the maximum percentile value for residual saturation. Residual saturation is the dominant parameter because the magnitude of the maximum radionuclide flux into the aquifer appears to be inversely related to the time of the maximum radionuclide flux into water table (Figure 4-41), and the vadose zone moisture content dictates the pore-water velocity of vadose zone when the recharge is constant (as it is in these sensitivity evaluations). In conditions where the soil is very dry, such as it is in the vicinity of ERDF, the moisture content approaches its residual value. Thus, the residual moisture content is the dominant indicator of vadose zone moisture content, which is the dominant indicator of pore-water velocity, and is therefore the primary determinant of arrival time and maximum radionuclide flux.

Overall, the results range between $1.2\text{E-}04$ Ci/yr and 5.5 Ci/yr. The compliance case results in this evaluation ($2.6\text{E-}04$ Ci/yr) appear biased high; they exceeded 1,031 of 1,296 results of the individual parameter evaluations. The results of the evaluations with all parameters set to their minimum, 25th percentile, median, 75th percentile, compliance, and maximum percentile values indicate that the maximum radionuclide fluxes were $1.6\text{E-}04$ Ci/yr, $2.1\text{E-}04$ Ci/yr, $1.6\text{E-}04$ Ci/yr, $2.1\text{E-}04$ Ci/yr, $2.6\text{E-}04$ Ci/yr, and $3.4\text{E-}04$ Ci/yr, respectively. Thus, the range of results appears to be within an approximate factor of 2 between the compliance case results ($2.6\text{E-}04$ Ci/yr) and the results of the evaluations with all parameters set to their minimum ($1.2\text{E-}04$ Ci/yr) and maximum ($5.5\text{E-}04$ Ci/yr) values.

4.6.2.7 "What If" Analysis. The "what if" analysis included alterations to the assumptions regarding the time of liner failure, including performance capable of producing the bathtub effect, the inclusion of irrigation after periods of institutional control, and unexpectedly poor performance of the surface barrier. The results of these analyses are intended only for relative comparison purposes, and not for quantifying absolutely the consequences of the assumed or postulated event occurring. They are conducted using the one-dimensional model abstraction of the ERDF cell 9 location and median percentile vadose zone parameter set.

The bathtub effect refers to conditions in which the sub-grade liner remains intact and the facility fills with water that infiltrates through the surface barrier. The concern regarding the bathtub effect is having the facility fill with leachate that eventually breaches the liner and/or possibly overflows, resulting in focused infiltration and rapid vadose zone transit times. The bathtub effect was not evaluated quantitatively for ERDF because the arid environment of the Hanford Site and the likely performance of the surface barrier and subgrade liner system are not conducive to this type of situation arising. The bottom liner design satisfies the requirements of 40 CFR 264.310 for hazardous waste landfills, and the surface barrier is identified as a modified RCRA-compliant cover (EPA/ROD/R10-95/100) for which EPA has issued design guidance to prevent the bathtub effect from occurring (EPA 542-F-11-001).

The composite material comprising the subgrade liner includes a 0.9-m (3-ft)-thick layer of a compacted admix (bentonite-soil mixture) with a hydraulic conductivity of 1×10^{-07} cm/s ($2.8\text{E-}04$ ft/day or 32 mm/yr) and a 0.9-m (3-ft)-thick operations layer of clean fill material (Figure 2-30). The admix and fill material provide both storage thickness and counteract any settling and other geological stresses. Between these two layers are two gravel drainage layers and two synthetic HDPE geomembranes that protect the clay against desiccation. The geotextile cushions that overlie the HDPE geomembranes minimize damage to the geomembranes during

placement of the drainage layers. With these safeguards, it seems highly unlikely that leachate in the waste could breach the liner system instead of having to percolate through it. If water does collect atop the bentonite-soil mixture, the hydraulic conductivity of it is more than 10 times greater than the maximum estimate for the post-closure surface barrier recharge rate, which would preclude ponding and allow the leachate to percolate based on the saturated vertical hydraulic conductivity of the admix layer.

Any bathtub effect is unlikely to occur because of the arid environment at the Hanford Site and small volumes of water associated with natural processes. Assuming that the liner remains intact for 500 years instead of 100 years, and the surface barrier only limits net infiltration to 1 mm/yr, then the amount of water entering the ERDF waste volume is 500 mm (1.6 ft or 0.5 m). For the range of porosity values considered for ERDF waste material (0.20 to 0.27), this quantity of water translates to a hydraulic head of approximately 1.9 to 2.5 m (6.2 to 8.2 ft), which is well below the depth of the ERDF trench. In addition, the bentonite-soil mixture and operations layer may retain or restrain the downward movement of much of the water because of their moisture retention capacity. Only assuming worst-case circumstances produces a hydraulic head approximately equal to the depth of the ERDF trench, e.g., the liner remaining intact for 1,000 years and the surface barrier only limiting the net infiltration to the maximum rate representing natural undisturbed ground surface (4 mm/yr [0.16 in.]). However, this amount of time is equal to the compliance time frame. If the liner remained intact for 1,000 years, then no radionuclides from the waste could impact groundwater during the compliance time frame.

In addition to the hydrologic considerations and drainage layers, relief of contained water through defects in the HDPE geomembrane liner and into the composite layer is likely to attenuate any bathtub effect. Following liner construction, which likely introduced at least a few defects into the liner (Giroud 1997, Giroud et al. 1997), additional defects (e.g., enlarging of installation-related defects and/or environmental stress cracking-induced defects) could also be generated in the HDPE liner due to internal polymer degradation (deterioration) and stress effects. These post-construction defects could develop within the 500-year post-closure period (Environment Agency 2004). These types of defects further limit the possibility of the bathtub effect occurring in ERDF.

Overall, the results appear to be mostly dependent on the post-design life surface barrier recharge rate, although the cases evaluating the minimum recharge value for this later period do exhibit some variability depending on the pre-ERDF and undisturbed ground and intact surface barrier and degraded liner recharge rates. There is essentially no impact to the peak flux of mobile radionuclide to the water table caused by changes in the timing of the postulated liner failure, except for the cases with the minimum post-design surface barrier recharge rate (Table 4-16). Changing the time of liner failure causes changes in the timing of radionuclide breakthrough, but not changes in the radionuclide peak concentration. In the case of the minimum post-design recharge rate, the maximum concentration occurs at the end of the sensitivity-uncertainty time frame of 10,000 years. The maximum concentration does not actually represent a peak, but a value on the rising limb of the breakthrough curve. Thus, the apparent change in the maximum concentration caused by changes in the timing of liner failure is caused by the change where the end of the sensitivity-uncertainty time frame intersects the radionuclide breakthrough curve. The recharge rates applied to the periods of undisturbed ground prior to construction of ERDF and during the design life of the surface barrier have no apparent effect on the results.

Table 4-16. Summary of Results of the What If Evaluations for Radionuclides with $K_d = 0$ mL/g (e.g., Technetium-99; Results Presented on a per Ci Source Basis). (4 Pages)

Pre-ERDF and Undisturbed Ground Recharge Rate (Percentile)	Intact Surface Barrier and Degraded Liner Recharge Rate (Percentile or Value)	Post-Design Life Surface Barrier Recharge Rate (Percentile or Value)	Arrival Time of Maximum Radionuclide Flux at Water Table (Years Post-Closure)	Water Flux into Aquifer Beneath ERDF (mm/yr)	Maximum Radionuclide Flux at Water Table (Ci/yr)	Decrease in Arrival Time of Maximum Radionuclide Flux at Water Table from Comparable Baseline Comparison Case (Years) ^a	Ratio of Maximum Radionuclide Flux at Water Table to Comparable Baseline Comparison Case Results
All What If Evaluations: Median Percentile Vadose Zone and Aquifer Parameters							
What If Baseline Comparison Cases ^b							
Maximum (4 mm/yr)	Maximum (1 mm/yr)	Maximum (2 mm/yr)	4895	2.00	3.11E-04	-----	-----
Median (1.6 mm/yr)	Median (0.5 mm/yr)	Median (1 mm/yr)	8590	1.03	1.56E-04	-----	-----
Minimum (0.26 mm/yr)	Minimum (0.05 mm/yr)	Minimum (0.1 mm/yr)	10000	0.10	1.94E-09	-----	-----
Liner Fails at Closure in Year 2035							
Maximum	Maximum	Maximum	4840	2.00	3.11E-04	55	1.00
Maximum	Maximum	Median	8315	1.03	1.56E-04	100	1.00
Maximum	Maximum	Minimum	10000	0.10	1.95E-08	0	1.59
Maximum	Median	Maximum	4960	2.00	3.11E-04	30	1.00
Maximum	Median	Median	8540	1.03	1.56E-04	50	1.00
Maximum	Median	Minimum	10000	0.10	7.11E-09	0	1.37
Maximum	Minimum	Maximum	5075	2.00	3.11E-04	5	1.00
Maximum	Minimum	Median	8755	1.03	1.56E-04	10	1.00
Maximum	Minimum	Minimum	10000	0.10	2.35E-09	0	1.13
Median	Maximum	Maximum	4840	2.00	3.11E-04	55	1.00
Median	Maximum	Median	8315	1.03	1.56E-04	100	1.00

Table 4-16. Summary of Results of the What If Evaluations for Radionuclides with $K_d = 0$ mL/g (e.g., Technetium-99; Results Presented on a per Ci Source Basis). (4 Pages)

Pre-ERDF and Undisturbed Ground Recharge Rate (Percentile)	Intact Surface Barrier and Degraded Liner Recharge Rate (Percentile or Value)	Post-Design Life Surface Barrier Recharge Rate (Percentile or Value)	Arrival Time of Maximum Radionuclide Flux at Water Table (Years Post-Closure)	Water Flux into Aquifer Beneath ERDF (mm/yr)	Maximum Radionuclide Flux at Water Table (Ci/yr)	Decrease in Arrival Time of Maximum Radionuclide Flux at Water Table from Comparable Baseline Comparison Case (Years) ^a	Ratio of Maximum Radionuclide Flux at Water Table to Comparable Baseline Comparison Case Results
Median	Maximum	Minimum	10000	0.10	1.92E-08	0	1.58
Median	Median	Maximum	4960	2.00	3.11E-04	30	1.00
Median	Median	Median	8540	1.03	1.56E-04	50	1.00
Median	Median	Minimum	10000	0.10	6.96E-09	0	1.35
Median	Minimum	Maximum	5075	2.00	3.11E-04	5	1.00
Median	Minimum	Median	8755	1.03	1.56E-04	10	1.00
Median	Minimum	Minimum	10000	0.10	2.29E-09	0	1.11
Minimum	Maximum	Maximum	4845	2.00	3.11E-04	50	1.00
Minimum	Maximum	Median	8320	1.03	1.56E-04	95	1.00
Minimum	Maximum	Minimum	10000	0.10	1.82E-08	0	1.55
Minimum	Median	Maximum	4960	2.00	3.11E-04	30	1.00
Minimum	Median	Median	8540	1.03	1.56E-04	55	1.00
Minimum	Median	Minimum	10000	0.10	6.48E-09	0	1.32
Minimum	Minimum	Maximum	5075	2.00	3.11E-04	10	1.00
Minimum	Minimum	Median	8755	1.03	1.56E-04	10	1.00
Minimum	Minimum	Minimum	10000	0.10	2.08E-09	0	1.07
Liner Fails after 500 years in Year 2535							
Maximum	0 mm/yr	Maximum	5105	2.00	3.11E-04	-115	1.00
Maximum	0 mm/yr	Median	8805	1.03	1.56E-04	-215	1.00

Table 4-16. Summary of Results of the What If Evaluations for Radionuclides with $K_d = 0$ mL/g (e.g., Technetium-99; Results Presented on a per Ci Source Basis). (4 Pages)

Pre-ERDF and Undisturbed Ground Recharge Rate (Percentile)	Intact Surface Barrier and Degraded Liner Recharge Rate (Percentile or Value)	Post-Design Life Surface Barrier Recharge Rate (Percentile or Value)	Arrival Time of Maximum Radionuclide Flux at Water Table (Years Post-Closure)	Water Flux into Aquifer Beneath ERDF (mm/yr)	Maximum Radionuclide Flux at Water Table (Ci/yr)	Decrease in Arrival Time of Maximum Radionuclide Flux at Water Table from Comparable Baseline Comparison Case (Years) ^a	Ratio of Maximum Radionuclide Flux at Water Table to Comparable Baseline Comparison Case Results
Maximum	0 mm/yr	Minimum	10000	0.10	1.43E-09	0	0.28
Median	0 mm/yr	Maximum	5105	2.00	3.11E-04	-115	1.00
Median	0 mm/yr	Median	8805	1.03	1.56E-04	-215	1.00
Median	0 mm/yr	Minimum	10000	0.10	1.42E-09	0	0.28
Minimum	0 mm/yr	Maximum	5105	2.00	3.11E-04	-115	1.00
Minimum	0 mm/yr	Median	8805	1.03	1.56E-04	-210	1.00
Minimum	0 mm/yr	Minimum	10000	0.10	1.39E-09	0	0.28
Irrigation begins after 100 years in Year 2135							
Maximum	69 mm/yr	69 mm/yr	297.5	69.00	8.18E-03	8292.5	52.55
Median	69 mm/yr	69 mm/yr	297.5	69.00	8.19E-03	8292.5	52.56
Minimum	69 mm/yr	69 mm/yr	297.5	69.00	8.19E-03	8297.5	52.59
Irrigation begins after 500 years in Year 2535							
Maximum	Maximum	69 mm/yr	692.5	69.00	8.31E-03	7722.5	53.35
Maximum	Median	69 mm/yr	695	69.00	8.29E-03	7895	53.21
Maximum	Minimum	69 mm/yr	697.5	69.00	8.27E-03	8067.5	53.10
Median	Maximum	69 mm/yr	692.5	69.00	8.31E-03	7722.5	53.35
Median	Median	69 mm/yr	695	69.00	8.29E-03	7895	53.21
Median	Minimum	69 mm/yr	697.5	69.00	8.27E-03	8067.5	53.10
Minimum	Maximum	69 mm/yr	692.5	69.00	8.31E-03	7722.5	53.35

Table 4-16. Summary of Results of the What If Evaluations for Radionuclides with $K_d = 0$ mL/g (e.g., Technetium-99; Results Presented on a per Ci Source Basis). (4 Pages)

Pre-ERDF and Undisturbed Ground Recharge Rate (Percentile)	Intact Surface Barrier and Degraded Liner Recharge Rate (Percentile or Value)	Post-Design Life Surface Barrier Recharge Rate (Percentile or Value)	Arrival Time of Maximum Radionuclide Flux at Water Table (Years Post-Closure)	Water Flux into Aquifer Beneath ERDF (mm/yr)	Maximum Radionuclide Flux at Water Table (Ci/yr)	Decrease in Arrival Time of Maximum Radionuclide Flux at Water Table from Comparable Baseline Comparison Case (Years) ^a	Ratio of Maximum Radionuclide Flux at Water Table to Comparable Baseline Comparison Case Results
Minimum	Median	69 mm/yr	695	69.00	8.29E-03	7900	53.20
Minimum	Minimum	69 mm/yr	697.5	69.00	8.27E-03	8067.5	53.10
Surface barrier limits recharge only to 4 mm/yr							
Maximum	4 mm/yr	4 mm/yr	2570	4.00	6.22E-04	6020	4.00
Median	4 mm/yr	4 mm/yr	2570	4.00	6.22E-04	6020	4.00
Minimum	4 mm/yr	4 mm/yr	2570	4.00	6.22E-04	6025	4.00

^a Negative values indicate that the arrival time occurred earlier than in the comparable median parameter set results.

^b There are a total of 27 "What If" baseline comparison cases: maximum, median, and minimum values for the three different recharge rate periods. The results contain little variability so only the results of the baseline cases with equal recharge rates for the three periods are shown. The maximum radionuclide flux at the water table is the same respective value for all baseline cases with the maximum and median post-design life surface barrier recharge rate. The maximum radionuclide flux at the water table ranges between 1.94E-09 to 1.22E-08 Ci/yr for the baseline cases with the minimum post-design life surface barrier recharge rate. The arrival time of the maximum radionuclide flux at the water table ranges between 4895 and 5085 years for the baseline cases with the maximum post-design life surface barrier recharge rate, between 8415 and 8765 years for the baseline case with the median post-design life recharge rate, and is 10,000 years for all baseline cases with the minimum post-design life recharge rate.

The irrigation scenarios involve the condition that active irrigation-based farming occurs on ERDF. Two possible times of surface barrier removal are considered: at the end of the institutional control period 100 years after closure, and after 500 years, the design life of the surface barrier. Recharge from irrigated farming is assumed to average 69 mm/yr on the basis of the assumptions and methodology presented in DOE/RL-96-17 (*Remedial Design Report/Remedial Action Work Plan for the 100 Area*, Rev. 6). The irrigation scenarios impact the results in an expected manner. The magnitude of radionuclide flux is increased by approximately a factor of 50, regardless of whether the irrigation begins immediately after the 100-year institutional control period or after the design life of the surface barrier. In either case, the peak arrives during the 1,000-year compliance period. The disproportionality between the relative increase in the recharge rate (69 mm/yr versus 1 mm/yr) and the peak flux into the aquifer (approximately 50) is caused by the increased dispersion resulting from the increase in the flow velocity in the irrigation scenario.

In the event the surface barrier performs poorly and only limits recharge to 4 mm/yr, the arrival time of the peak concentration is much earlier compared to that in the median percentile evaluation. The peak does not occur during the 1,000-year compliance time frame, although first arrival of the radionuclide at the water table does (approximately 680 years). The change in radionuclide flux is directly proportional to the change in recharge: a factor of 4 greater than the median baseline comparison cases and a factor of 2 greater than the maximum baseline comparison cases, indicating that the increase in the flow velocity in the "what if" case is not sufficient to increase the dispersion appreciably.

4.6.3 Sensitivity Analysis for the Air Pathway

A sensitivity analysis is conducted to evaluate the impact of surface barrier (cover) thickness on the atmospheric dose calculation. For the compliance calculations a conservative thickness of 1 m was chosen for the surface barrier through which the transport of volatile radionuclides was modeled. The thickness of surface barrier is doubled (to 2 m) and then increased to the designed cover thickness of approximately 4.5 m. The results are presented in Figure 4-42. As expected the magnitude of the peak release reduces with increasing thickness. The initial increase is primarily due to carbon-14 present in the bulk soil. Past 200 years the release is controlled by the leaching rate of carbon-14 from graphite. However, because of increasing thickness of the surface barrier, the diffusive flux is smaller initially as the effective zero concentration boundary at the ERDF-air interface is placed farther away. After some time the effects of the changed boundary distance diminish.

The gas-to-aqueous phase partitioning of carbon-14 for air-pathway calculations is implemented using the dimensionless Henry's law constant of 0.22 and assuming carbon dioxide as the gas form that is in equilibrium with the bicarbonate ion in the solution (Section 3.4.2.1). However, a value of approximately 1.22 has been reported in the literature for carbon dioxide gas (Sander 1999). A sensitivity analysis is conducted where the dimensionless Henry's constant is increased from 0.22 to 1.22. The results are presented in Figure 4-43 in terms of air concentration of carbon-14 at the receptor location. Increasing the partitioning ratio increases the air concentration at an early time by about a factor of two. After the initial peak the concentration profiles are fairly similar in both cases. The initial increase is primarily due to carbon-14 present in the bulk soil and thus available for transport, while the later concentrations are controlled by the leaching of graphite and release of carbon-14. The early initial increase is an artifact of the conservative assumption of not transporting any carbon-14 present in the bulk soil prior to the 100-year institutional control period, even though it is likely to diffusive throughout the waste emplacement time period.

Figure 4-42. Sensitivity of Surface Barrier Thickness on Air-Pathway Dose.

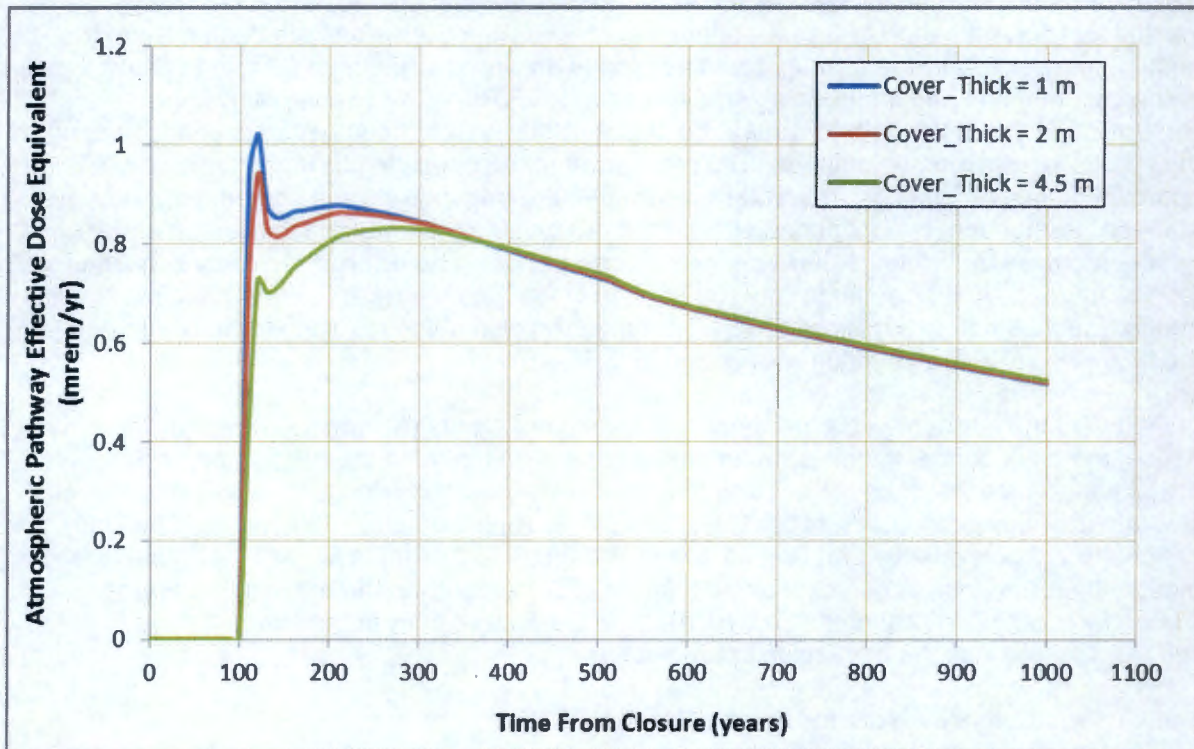
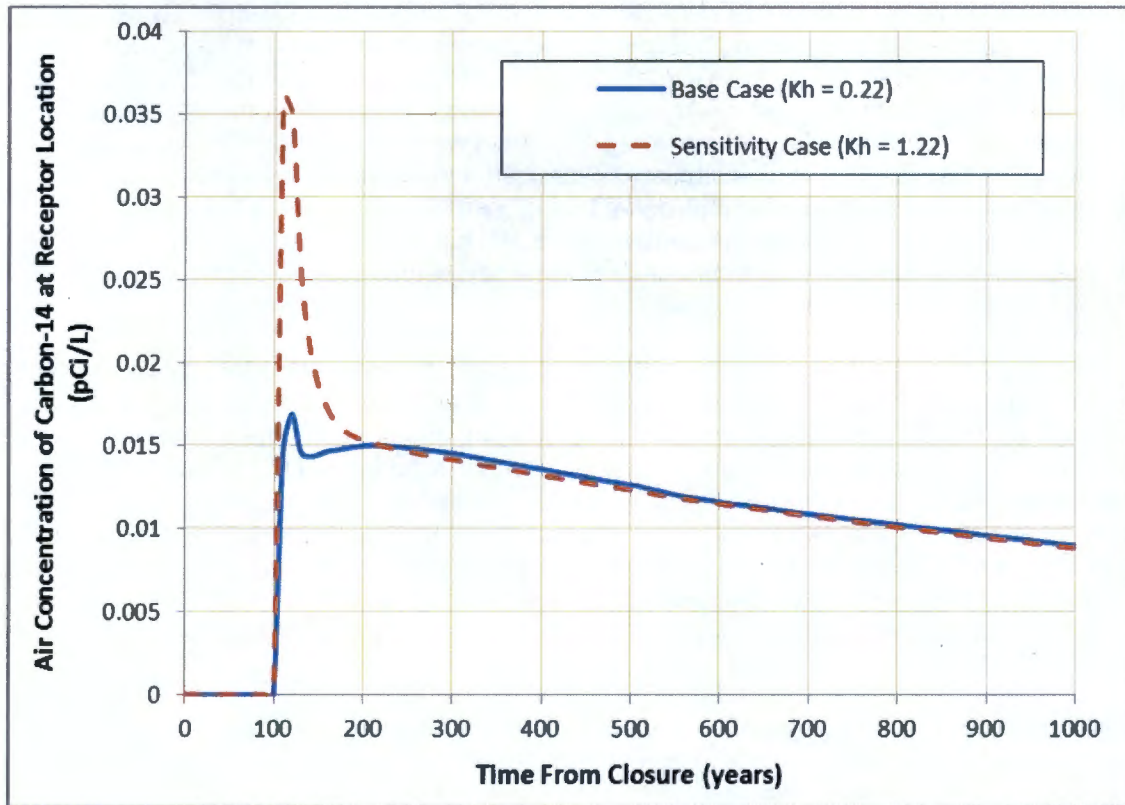


Figure 4-43. Sensitivity of Henry's Law Constants for Air-Water Partitioning of Carbon-14.



4.6.4 Comparison with 1995 ERDF Performance Assessment Results

The analysis described in the ERDF PA conducted in 1995 (BHI-00169) applied a two-dimensional cross-section modeling approach to accommodate a variety of facility sizes because of the uncertainty about the actual size of the final facility and limitations imposed by the computing capability circa 1995. At the time, the immediate ERDF construction plans included only four cells, but the plans allowed for further expansion to the east as additional disposal space became needed. It was acknowledged that the final east-west length of the facility would depend on the amount of waste that is generated by CERCLA remediation actions. To simplify the analysis, the conceptual model consisted of approximately half of the length of the four cell trench design and utilized symmetry arguments to allow extrapolation of the results to the entire length of the trench.

The model length was oriented parallel to the general direction of groundwater flow (west-east), and the width was assumed to be 1 m wide in the direction perpendicular to flow (north-south). The ERDF cells were assumed to be 19 m deep and 300 m long along the bottom in the east-west direction and, with the side walls sloping up at a 3 to 1 horizontal to vertical ratio, 426 m (~1,400 ft) along the top. For the conceptual model, the trench slope geometry nearest the downstream well was simply approximated as orthogonal and not inclined. The numerical model geometry included the half of the trench closest to the downstream well, with a length of 210 m (-690 ft). The west-east dimension of the entire model domain was 310 m (-1,000 ft) to include the 100-m downgradient point of calculation, with an overall thickness (or height) of 115 m (-380 ft).

The source term consisted of a unit inventory (1 Ci) that was assumed to be emplaced homogeneously within the simulated ERDF volume (3,990 m³). Key parameters that differ between the 1995 PA base case and the current PA compliance case analyses include the closure barrier long-term recharge rate (5 mm/yr), and the unconfined aquifer hydraulic conductivity (5.5 m/day) and hydraulic gradient (0.00305) estimates. Also, the vadose zone properties used in the 1995 PA differ from those used in the current PA and did not account for upscaling. The 1995 PA sensitivity analysis included 1 mm/yr (0.04 in./yr) in the evaluation of the closure barrier long-term recharge rate, which is comparable to the current PA compliance case value for recharge after the design-life of the surface barrier. The current PA uses the STOMP code; the 1995 PA simulations were performed using the VAM3D-CG finite element code (Huyakorn and Panday 1989).

Table 4-17 provides a summary of simulated peak contaminant concentration results for the past and current PA analyses. As indicated, following parameter revisions and normalization for inventory, recharge, geometry, and aquifer hydraulic gradient values, the simulated peak concentrations for technetium-99 for the two PAs compare well, i.e., 7.42E-06 Ci/m³ for the 1995 PA versus 5.21E-06 Ci/m³ for the current PA. The updated methodology and parameter estimates in the current PA analysis result in a decrease in peak concentration of approximately 30% from the past PA analysis.

Table 4-17. Comparison of the Peak Contaminant Concentration Results for the Past Performance Assessment (BHI-00169) and the Current Performance Assessment Analyses.

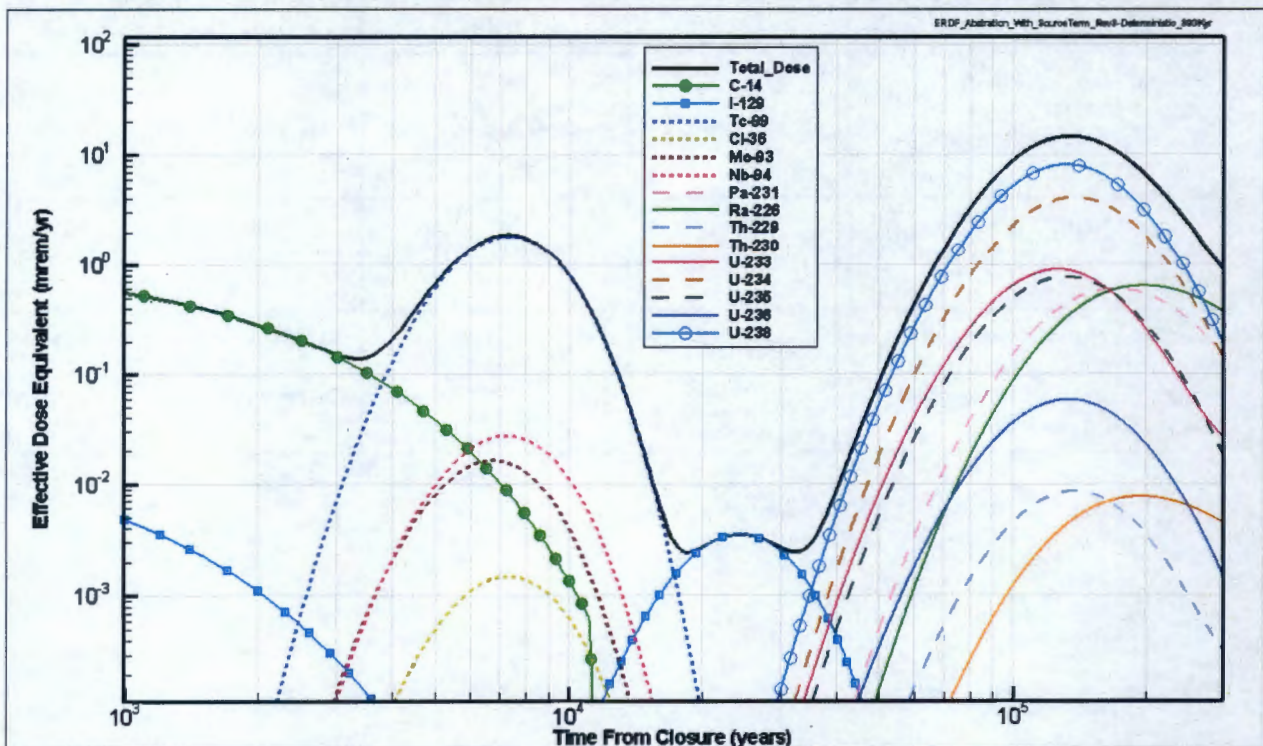
Comparison Criteria	Past PA (BHI-00169)	Current PA	Comments
Long-Term Recharge Rate	1 mm/yr (sensitivity case)	1 mm/yr (compliance case)	Past PA: recharge is time invariant Current PA: recharge is 0.5 mm/yr for the first 500 years followed by 1 mm/yr indefinitely
Width of ERDF (m)	1	370	Past PA: 2-D cross-section model Current PA: 3-D model using average width of the ERDF trapezoidal volume geometry)
Inventory of Tc-99 (Ci)	1	53	Past PA: 1 Ci in 3,990 m ³ Current PA: 53 Ci in 7.78E+06 m ³
Inventory per unit width (Ci/m)	1	0.14	
Peak concentration in groundwater 100 m downgradient of the ERDF (Ci/m ³)	3.71E-06	7.30E-07	Based on modeling results
Peak concentration (Ci/m ³) per unit inventory per unit width	3.71E-06	5.21E-06	Peak concentration normalized to inventory per unit width
Peak concentration (Ci/m ³) per unit inventory per unit width normalized to revised hydraulic gradient estimate	7.42E-06	5.21E-06	Past PA gradient estimate: 0.00305 Current PA gradient: 0.0015 estimate

4.6.5 Peak Dose Calculation

A sensitivity case was run using a GoldSim-based one-dimensional abstraction model that was originally developed for the uncertainty analysis and for the air-pathway analysis for the 10,000-year time period to evaluate the peak dose that occurred beyond the 10,000-year time frame. For this purpose the compliance case flow-field that was developed for the 10,000-year time period was extended such that assumptions of constant recharge rate were maintained and all the processes that were applicable over the 10,000-year time frame were assumed to be applicable for the extended duration. The calculations were run for a period of 300,000 years and the results are presented in Figure 4-44 in terms of EDE that includes dose from both the groundwater and air the pathway. Beyond 10,000 years the dose is contributed by the groundwater pathway.

The peak dose occurs around 135,000 years and the magnitude is about 14.6 mrem/yr. It is controlled by the arrival of uranium isotopes at the compliance location (100 m downgradient) along the groundwater pathway. The primary dose drivers are uranium-238 and uranium-234, with relatively minor contributions from other radionuclides with long half-lives. It is also interesting to note that iodine-129 is the peak dose driver between 20,000 and 30,000 years, the time period when technetium-99 dose has declined sufficiently and prior to increase in dose from uranium-238 and uranium-234.

Figure 4-44. Sensitivity Case Showing the Results of Peak Dose Calculations.



5.0 INADVERTENT INTRUDER ANALYSIS

This section presents the analysis of the doses to a hypothetical individual who inadvertently intrudes into the ERDF site. The analyses were performed in accordance with DOE O 435.1 and DOE M 435.1 requirements. Guidance for the intruder analysis comes from DOE G 435.1-1, which states the following:

“Although DOE is committed to retaining control of land containing residual radioactive material, such as disposed low-level waste, it is nonetheless appropriate to consider the impacts of potential inadvertent intrusion. Intrusion should be considered as an accident scenario which could occur during lapses of institutional controls. It is a hypothetical situation assumed simply to provide a basis for determining the acceptability of waste for near-surface disposal and may be used for establishing concentrations of radioactive material in a near-surface disposal facility.”

DOE G 435.1-1 states that the development of inadvertent intruder scenarios needs to be consistent with best management practices and other current industry standards such as those issued by the National Council for Radiation Protection, International Council for Radiation Protection, and others. In developing these scenarios (DOE 1999b), a supplemental document to DOE G 435.1-1 provides the following guidance on the groundwater pathway for use in the inadvertent intruder analysis:

“The purpose of the inadvertent intruder analysis is to provide a surrogate for the determination of LLW that is acceptable for near-surface disposal. The inadvertent intruder analysis does not have the purpose of protecting future members of the public. As a result, the ingestion of contaminated water need not be considered as part of the inadvertent intruder analysis, because the protection of water resources is considered explicitly as one of the performance criteria for the performance assessment.”

Two types of exposure scenarios are considered in order to estimate dose to the hypothetical intruder: (1) acute scenarios, and (2) chronic scenarios. Acute scenarios evaluate a relatively large dose received over a short fixed period of time from well drilling activity and exposure to waste in the drill cuttings, while chronic scenarios consider continuing exposure to radiation over time from spreading of drill cuttings over a land area and living and/or working in that area. One acute exposure scenario and three chronic exposure scenarios are considered in this analysis and are summarized in Table 5-1. The calculation methodology and parameters are presented in the following sections, but for additional details the reader is referred to WCH-478, *Exposure and Inadvertent Scenarios for the Environmental Restoration Disposal Facility*. The dose conversion factors and bioconcentration factors are taken from Tables 3-28 and 3-27, respectively.

Table 5-1. Summary Description of the Inadvertent Intruder Scenarios Considered in the ERDF Performance Assessment.

Scenario	Description
Acute Exposure: Well Driller	Dose is a result of drilling through the disposal facility. Exposure pathways are external exposure, soil inhalation, and soil ingestion. Exposure takes place during the drilling operation. Exposure does not depend on the borehole diameter.
Chronic Exposure: Rural Pasture	The well is drilled to serve a rural pasture. Contaminated drill cuttings are mixed with the soil over the pasture area. Exposure pathways are soil ingestion, milk ingestion, soil inhalation, and external exposure.
Chronic Exposure: Suburban Garden	The well is drilled to serve a suburban garden. Contaminated drill cuttings are mixed with the soil over an area where a residential house and a garden are constructed. Exposure pathways are vegetable ingestion, soil ingestion, soil inhalation, and external exposure.
Chronic Exposure: Commercial Farm	The well is drilled to serve a commercial farm. Contaminated drill cuttings are mixed with the soil over the commercial farm area. Exposure pathways are soil ingestion, soil inhalation, and external exposure.

NOTE: For additional details refer to WCH-478, *Exposure and Inadvertent Scenarios for the Environmental Restoration Disposal Facility*.

Inadvertent intruder doses are calculated for two times after closure: 100 years and 500 years. The 100-year calculations are presented to demonstrate compliance under the assumption of inadvertent intrusion occurring immediately after the loss of institutional controls (see Section 1.5.3 for additional discussion). DOE O 435.1 allows institutional controls to be effective in deterring intrusion for at least 100 years following closure. The 500-year calculation is included as additional information to quantify the decline in dose with time, since the peak dose occurs at 100 years.

The inadvertent intruder scenarios are summarized in Table 5-1, and the parameters that are common to all inadvertent intruder scenarios are presented in Table 5-2. For all inadvertent intruder scenarios, the dose calculations are based on the emplaced radionuclide inventory in the ERDF (considering radioactive decay and ingrowth), but conservatively ignoring any depletion due to transport of radionuclides from the disposal facility. The emplaced wastes are assumed to be distributed uniformly throughout the volume of ERDF. All exposures are assumed to occur 100 years after facility closure. For each of the four scenarios, the cuttings are assumed to be brought to the land surface and spread over a target field, as illustrated in Figure 5-1.

Table 5-2. Parameters Common to Inadvertent Intruder Scenarios. (2 Pages)

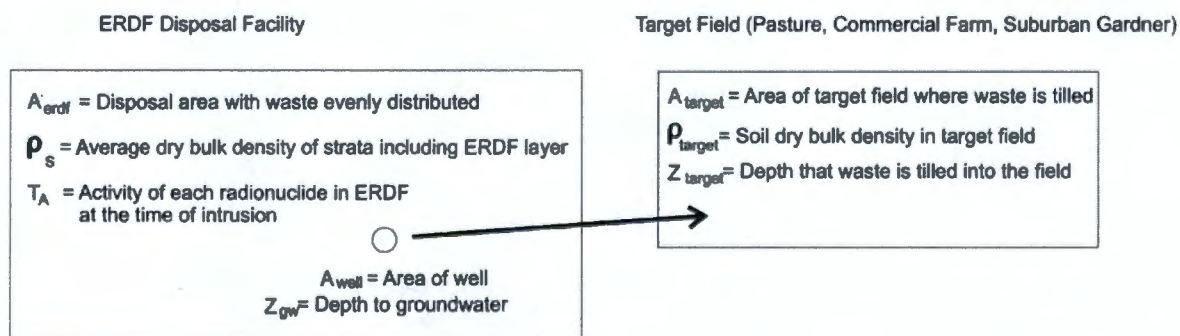
Parameter	Value	Unit	Notation	Reference
Time of intrusion	100 and 500 years after closure	yr	T_{in}	DOE M 435.1-1; 10 CFR 61
Thickness of wastes intercepted by the borehole	2.1E+03	cm	Z_{ws}	Chapter 2.0 (approximate thickness of ERDF)
Soil dry bulk density (for soil layers below ERDF)	1.83	g/cm ³	ρ_{sl}	Calculated (density weighted by average thickness of soil layers below ERDF)

Table 5-2. Parameters Common to Inadvertent Intruder Scenarios. (2 Pages)

Parameter	Value	Unit	Notation	Reference
Disposed waste bulk density	2.08	g/cm ³	ρ_{ws}	Chapter 2.0 (ERDF operational density)
Depth to groundwater	9.0E+03	cm	Z_{gw}	Chapter 2.0 (approximate depth from ERDF surface)
Area over which the waste is evenly distributed	2.79E+09	cm ²	A_{erdf}	Calculated based on ERDF dimensions
Soil dry bulk density in target field	2.02	g/cm ³	ρ_g	WCH-515; same as for Hf1 unit (surface soil layer)
Soil dry bulk density in drilling cuttings	1.89	g/cm ³	ρ_s	Calculated (weighted by average thickness of soil layers below ERDF + inside ERDF)

Figure 5-1. Calculation of Target Field Concentrations.

Source Term for Inadvertent Intruder Chronic Scenarios



5.1 ACUTE EXPOSURE SCENARIOS

The acute exposure scenario for the ERDF PA evaluates the exposure to a well driller who drills a well to the water table for the supply of water. As a well is drilled through the ERDF-emplaced waste, the driller will be exposed to the radiation dose from the cuttings. The drilling time period is considered to be 5 days with exposure time period of 40 hours (8 hr/day). The dose is calculated assuming that the cuttings are spread evenly across the drill pad, and the pad is small enough that concentrations are not diluted by mixing with uncontaminated soil.

The borehole diameter is not a factor in determining dose for this case because the radionuclide concentrations in the drill cuttings are independent of the size, and because the cuttings are assumed to be distributed over the drill pad with limited mixing with uncontaminated soil. For the purpose of calculating the external exposure, the thickness and lateral extent of the

contaminated layer is conservatively assumed to be effectively infinite. Exposure pathways considered under this scenario are soil ingestion, soil inhalation, and direct exposure and are illustrated in Figure 5-2. Parameters specific to the well driller scenario are provided in Table 5-3 along with the underlying references.

Figure 5-2. Exposure Pathways Considered in the Inadvertent Intruder Well Driller Acute Exposure Scenario.

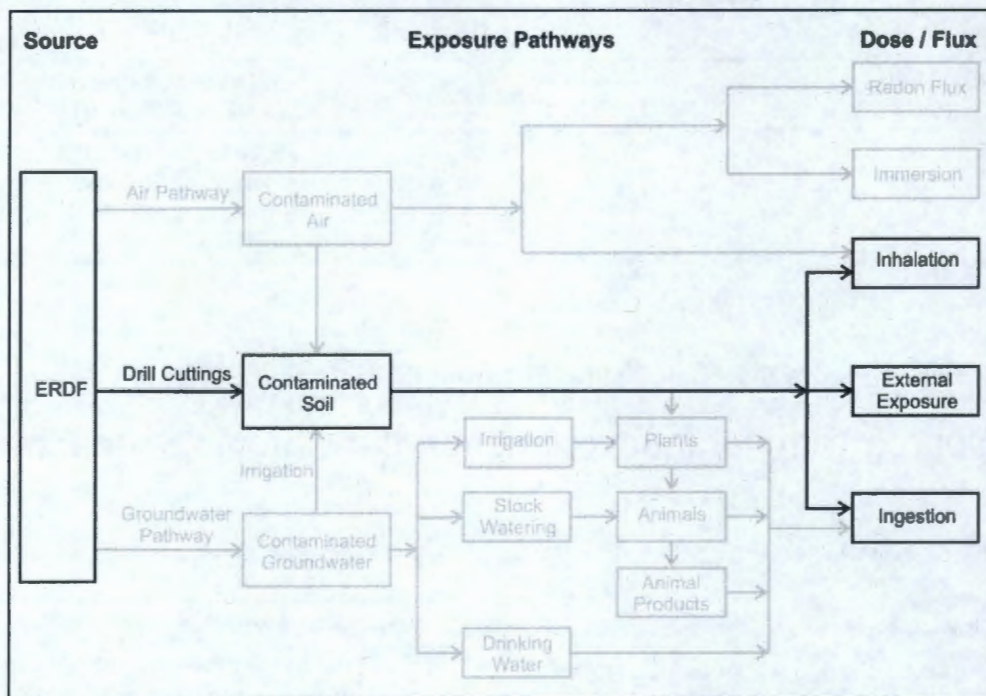


Table 5-3. Parameters Considered in the Inadvertent Intruder Well Driller Acute Exposure Scenario.

Parameter	Value	Units	Notation	Reference
Area of the well	1379.51	cm ²	A _{well}	HNF-SD-WM-TI-707, Rev. 5
Diameter of the well	41.91	cm	D _{well}	HNF-SD-WM-TI-707, Rev. 5
Soil ingestion rate	100	mg/day	IR	OSWER Directive 9285.6-03
Exposure frequency	5	d/yr	EF	HNF-SD-WM-TI-707, Rev. 5
Enrichment factor	0.7	Unitless	E _f	NCRP 1999
Inhalation rate when outdoor	48.4	m ³ /yr	IR _{out}	HNF-SD-WM-TI-707, Rev. 5
Mass loading factor for outdoor conditions	6.66E-05	g/m ³	M _{out}	ICRP 1994
Fraction of time spent outdoor	4.56E-3	Unitless	T _{out}	HNF-SD-WM-TI-707, Rev. 5 (40 hours in a year)

The radionuclide concentrations in the cuttings are calculated using Equation 5-1.

$$C_{ds} = \frac{C_{ws} \times Z_{ws} \times \rho_{ws}}{Z_{ws} \times \rho_{ws} + (Z_{gw} - Z_{ws}) \times \rho_{sl}} \quad \text{Eq. 5-1}$$

where

- C_{ds} = the concentration in the cuttings (pCi/g)
- C_{ws} = the concentration in the emplaced wastes at the time of intrusion (pCi/g)
- Z_{ws} = the thickness of the emplaced waste stratum (m)
- ρ_{ws} = the disposed waste bulk density (g/cm^3)
- Z_{gw} = the depth to groundwater (m)
- ρ_{sl} = the soil dry bulk density for strata below the emplaced waste (g/cm^3).

The following sections provide the calculation methodology used to evaluate dose for this scenario.

5.1.1 Well Driller Acute Scenario: Ingestion

Dose, D_s in mrem/yr, to the well driller due to ingestion of drill cuttings is calculated as:

$$D_s = C_{ds} \times IR \times EF \times DCF_{ing} \quad \text{Eq. 5.2}$$

where

- C_{ds} = the concentration in the cuttings (pCi/g)
- IR = the soil ingestion rate (mg/day)
- EF = the frequency of cuttings exposure experienced by the driller ($days/yr$)
- DCF_{ing} = the dose conversion factor for ingestion ($mrem/pCi$).

5.1.2 Well Driller Acute Scenario: Inhalation

Dose, D_{inh} in mrem/yr, to the driller due to inhalation of cuttings is calculated as:

$$D_{inh} = C_{ds} \times E_f \times IR_{out} \times M_{out} \times t_{out} \times DCF_{inh} \quad \text{Eq. 5-3}$$

where

C_{ds}	=	the concentration in the cuttings (pCi/g)
E_f	=	the enrichment factor (<i>dimensionless</i>)
IR_{out}	=	the inhalation rate of the driller while outdoors (m^3/yr)
M_{out}	=	the mass loading factor for outdoor conditions (g/m^3)
t_{out}	=	the fraction of time the driller spends outdoors (<i>dimensionless</i>)
DCF_{inh}	=	the dose conversion factor for inhalation ($mrem/pCi$).

5.1.3 Well Driller Acute Scenario: External Exposure

Dose, D_{ext} in mrem/yr, to the driller due to external exposure is calculated as:

$$D_{ext} = C_{ds} \times t_{out} \times DCF_{ext} \quad \text{Eq. 5-4}$$

where

C_{ds}	=	the concentration in the cuttings (pCi/g)
t_{out}	=	the fraction of time the driller spends outdoors (<i>dimensionless</i>)
DCF_{ext}	=	the dose conversion factor for external exposure ($mrem/yr$)/(pCi/g).

5.2 CHRONIC SCENARIOS

Three chronic exposure scenarios are considered assuming that the well has been drilled and the cuttings have been spread: rural pasture, suburban garden, and commercial farm. For each of the three scenarios, radionuclides in the drill cuttings are assumed to be spread over a "target field" and tilled into the soil. The contaminant concentrations in the target field are controlled by the diameter of the well that is drilled to support the scenario, the area of the target field over which the drill cuttings are spread, and the depth to which the drill cuttings are tilled into the soil. In the chronic scenarios the exposed individual does not drill or add the cuttings to the soil but simply lives or works on the land where the cuttings have been tilled into the soil.

Based on the well log data from the State of Washington from 1960 to 2003, the diameter of the borehole could range from 2.5 cm (1 in.) up to 76 cm (30 in.), with about 70% of the domestic water wells having about a 16.5-cm (6.5-in.) diameter (HNF-SD-WM-TI-707, Rev. 5). Although a 16.5-cm (6.5-in.) diameter may be common, it may not be representative for the target field considered in a given scenario. For example, although irrigation of the rural pasture is a small-scale operation it typically requires a larger pump than normal domestic service. Similarly, a commercial irrigator typically uses a larger diameter well to extract water at a higher flow rate. For each of the scenarios, common sizes for the target field and well vary over a broad range. In selecting these parameters, characteristics specific to the Hanford Site as well as parameters selected for previous analyses were considered. Sensitivity analyses provide confidence that the calculated performance parameters are robust enough to support sound decisions.

Other parameters used in the dose calculations were selected from DOE and EPA documents, and from national and international standards such as the NCRP and ICRP, as appropriate. The exposure pathways are determined by the land use.

5.2.1 Rural Pasture Chronic Scenario

The rural pasture scenario evaluates the doses that might result if the target field was a pasture used for milk production from cows. In this scenario, a 26.67-cm (10.5-in.)-diameter well is assumed and drill cuttings are spread over the pasture and hay area totaling 5,000 m². The exposed individual is a worker who tends to the cows that eat fodder from the pasture and drinks their milk. In addition to exposure from ingesting milk, the worker is exposed by ingestion of pasture soil, inhalation of the soil, and external exposure to the soil. Figure 5-3 shows the exposure pathways. The sizes of the pasture and well were selected from previous Hanford Site documents. Parameters specific to the rural pasture scenario are given in Table 5-4.

Figure 5-3. Exposure Pathways Considered in the Inadvertent Intruder Rural Pasture Chronic Exposure Scenario.

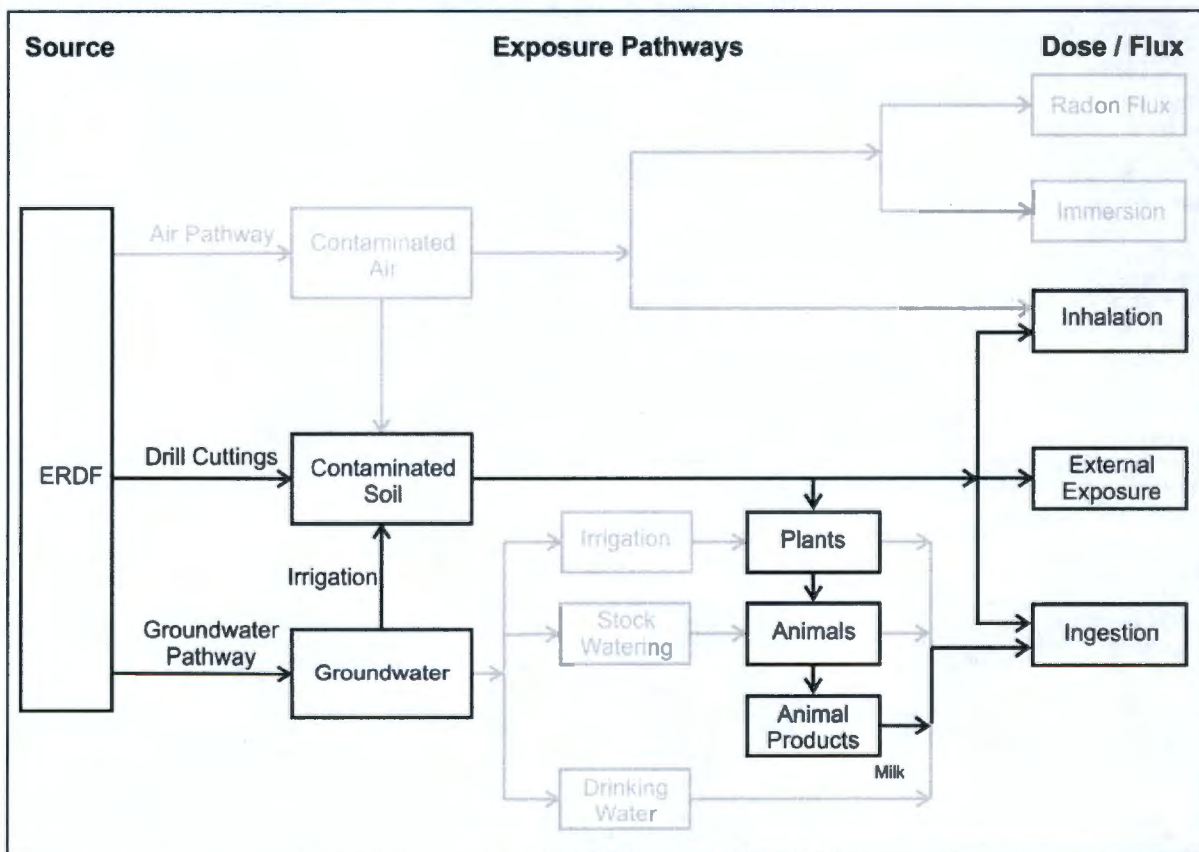


Table 5-4. Parameters Considered in the Inadvertent Intruder Rural Pasture Chronic Exposure Scenario. (2 Pages)

Parameter	Value	Units	Notation	Reference
Area of pasture	5E+07	cm ²	A _p	HNF-SD-WM-TI-707, Rev. 5
Area of the well	558.6	cm ²	A _{well}	HNF-SD-WM-TI-707, Rev. 5
Diameter of the well	26.67	cm	D _{well}	HNF-SD-WM-TI-707, Rev. 5

Table 5-4. Parameters Considered in the Inadvertent Intruder Rural Pasture Chronic Exposure Scenario. (2 Pages)

Parameter	Value	Units	Notation	Reference
Soil ingestion rate	100	mg/day	IR _s	OSWER Directive 9285.6-03
Exposure frequency	180	d/yr	EF	HNF-SD-WM-TI-707, Rev. 5
Tilled depth of target field	15	cm	Z _p	HNF-SD-WM-TI-707, Rev. 5
Milk ingestion rate	116	L/yr	IR _m	HNF-SD-WM-TI-707, Rev. 5
Fraction of locally produced animal products	1	Unitless	F _a	HNF-SD-WM-TI-707, Rev. 5
Ingestion rate of water by the animal	92	L/day	IR _{wa}	EPA 1999
Ingestion rate of soil by the animal	0.41	kg/day	IR _{sa}	EPA 1999
Ingestion rate of fodder by the animal	16.9	kg/day	IR _{fodder}	EPA 1999
Crop-soil bioconcentration factor resuspension fodder	0.1	(pCi/kg dry wgt of crop)/(pCi/kg dry wgt of soil)	B _p	NCRP 1999
Dry-to-wet conversion basis factor for fodder	0.25	dry wgt of fodder/wet wgt of fodder	d _f	NCRP 1999
Enrichment factor	0.7	Unitless	E _f	NCRP 1999
Inhalation rate when outdoors	8103	m ³ /yr	IR _{out}	HNF-SD-WM-TI-707, Rev. 5
Mass loading factor for outdoor conditions	6.6E-05	g/m ³	M _{out}	ICRP 1994
Fraction of time spent outdoors	0.08219	Unitless	T _{out}	HNF-SD-WM-TI-707, Rev. 5
Inhalation rate when indoors	8103	m ³ /yr	IR _{in}	HNF-SD-WM-TI-707, Rev. 5
Mass loading factor for indoor conditions	6.6E-05	g/m ³	M _{in}	ICRP 1994
Fraction of time spent indoors	0.66	Unitless	T _{in}	NUREG/CR-5512

The concentration in pasture soil resulting from the drill cuttings is calculated by first calculating the inventory of each radionuclide in the drill cuttings and then calculating the concentration in the pasture soil. The same calculation must be made for each chronic scenario, the differences among the scenarios being the diameter of the well and the depth to which the cuttings are tilled into the soil of the target field (rural pasture, suburban garden, or commercial farm).

The total inventory of radionuclides, in pCi, in the drill cuttings, S_A is given by:

$$S_A = T_A \times \left(\frac{A_{well}}{A_{stdf}} \right) \quad \text{Eq. 5-5}$$

where

- T_A = the total emplaced waste activity of each radionuclide at time of intrusion (*pCi*)
 A_{well} = the cross-sectional area of the drilled well (*cm²*)
 A_{erdf} = the total area over which the wastes are emplaced (*cm²*).

Concentration in the pasture soil, C_{ps} in pCi/g, is given by:

$$C_{ps} = \frac{S_A}{A_p \times Z_p \times \rho_p + A_{well} \times Z_{gw} \times \rho_s} \quad \text{Eq. 5-6}$$

where

- S_A = the inventory of each radionuclide in the drill cuttings (*pCi*)
 A_p = the area of the pasture (*cm²*)
 Z_p = the depth to which the cuttings are tilled into the pasture (*cm*)
 ρ_p = the soil dry bulk density in the pasture (*g/cm³*)
 A_{well} = the area of the well (*cm²*)
 Z_{gw} = the depth to groundwater (*cm*)
 ρ_s = the dry bulk density of the drill cuttings (*g/cm³*).

5.2.1.1 Ingestion of Pasture Soil. Dose, D_s in mrem/yr, due to ingestion of pasture soil is given by:

$$D_s = C_{ps} \times IR_s \times EF \times DCF_{ing} \quad \text{Eq. 5-7}$$

where

- IR_s = the ingestion rate of soil by exposed individuals (*mg/day*)
 EF = the exposed individual exposure frequency (*days/yr*)
 DCF_{ing} = the dose conversion factor for ingestion (*mrem/pCi*).

5.2.1.2 Ingestion of Contaminated Milk. This pathway includes exposure from drinking contaminated milk from cows that consumed the contaminated pasture. Plants (used as fodder) would uptake water and radionuclides in the contaminated soil and then pass the contamination on to cows that ate the fodder. Some of that contamination would then be present in milk from the cows through the bioconcentration process. The equations needed to calculate the uptake of radionuclides in fodder, the resulting milk contamination, and the ultimate human dose are given below.

Concentration in fodder, C_{fodder} in pCi/g, is given by:

$$C_{fodder} = C_{ps} \times (B_v + B'_v \times d_f) \quad \text{Eq. 5-8}$$

where

- C_{ps} = the total radionuclide concentration in the pasture soil surface layer (pCi/g)
- B_v = the crop-soil bioconcentration factor through uptake $\left(\frac{\left(\frac{pCi}{kg \text{ dry weight of soil}} \right)}{\left(\frac{kg \text{ fresh weight of crop}}{pCi} \right)} \right)$
- B'_v = the bioconcentration factor with resuspension processes $\left(\frac{\left(\frac{pCi}{kg \text{ dry weight of soil}} \right)}{\left(\frac{kg \text{ dry weight of crop}}{pCi} \right)} \right)$
- d_f = the dry-to-wet weight basis conversion factor for fodder $\left(\frac{\text{dry weight of fodder}}{\text{wet weight of fodder}} \right)$.

Concentration in milk, C_m in pCi/L , is given by:

$$C_m = (C_{fodder} \times IR_{fodder} + C_{ps} \times IR_{ps}) \times BCF_{milk} \quad \text{Eq. 5-9}$$

where

- IR_{fodder} = the cow's ingestion rate of fodder (kg/day)
- IR_{ps} = the cow's ingestion rate of soil (kg/day)
- BCF_{milk} = the bio-concentration factor for milk (day/L).

Dose, D_m in $mrem/yr$, due to ingestion of milk is given by:

$$D_m = C_m \times IR_m \times F_a \times DCF_{ing} \quad \text{Eq. 5-10}$$

where

- C_m = radionuclide concentration in milk (pCi/L)
- IR_m = the exposed individual's rate of milk consumption (L/yr)
- F_a = the fraction of milk consumed that is produced from the pasture (*dimensionless*)
- DCF_{ing} = the dose conversion factor for ingestion ($mrem/pCi$).

5.2.1.3 Inhalation of Pasture Soil. Dose, D_{inh} in $mrem/yr$, from inhalation of contaminated pasture soil is calculated as follows:

$$D_{inh} = C_{ps} \times E_f \times (IR_{in} \times M_{in} \times t_{in} + IR_{out} \times M_{out} \times t_{out}) \times DCF_{inh} \quad \text{Eq. 5-11}$$

where

- C_{ps} = the total radionuclide concentration in the pasture soil surface layer (pCi/g)
- E_f = the enrichment factor (*dimensionless*)
- IR_{in} = the inhalation rate of the pasture worker while outdoors (m^3/yr)
- M_{in} = the mass loading factor for indoor conditions (g/m^3)
- t_{in} = the fraction of time the pasture worker spends outdoors (*dimensionless*)

- IR_{out} = the inhalation rate while outdoors (m^3/yr)
 M_{out} = the mass loading factor for outdoor conditions (g/m^3)
 t_{out} = the fraction of time outdoors (*dimensionless*)
 DCF_{inh} = the dose conversion factor for inhalation ($mrem/pCi$).

5.2.1.4 External Exposure. External dose from direct radiation, D_{ext} in mrem/yr, from the contaminated pasture soil is calculated as:

$$D_{ext} = C_{ps} \times t_{out} \times DCF_{ext} \quad \text{Eq. 5-12}$$

where

- C_{ps} = the total radionuclide concentration in the pasture soil surface layer (pCi/g)
 t_{out} = the fraction of time the pasture worker spends outdoors (*dimensionless*)
 DCF_{ext} = the dose conversion factor for external exposure ($mrem/yr$)/(pCi/g).

5.2.2 Suburban Garden Chronic Scenario

The suburban garden scenario evaluates the doses that might result if the target field was a home construction lot with a garden and a well was drilled prior to the construction of the house and garden. A 2,500- m^2 lot size and 30-cm (12-in.) diameter of the well was assumed based on the choice made in the past Hanford Site PA documents (e.g., WHC-SD-WM-EE-004 and BHI-00169). The size of the home garden was chosen to be 100 m^2 based on the discussions presented in HNF-SD-WM-TI-707, Rev. 5, where this size of the garden was deemed reasonable to provide 25% of the daily vegetable diet for a family of four living in the home. The major food types assumed to come from the garden include leafy vegetables and fruit but no grains.

In this scenario, the drill cuttings are assumed to be spread over the 2,500- m^2 lot size and tilled over a 15-cm depth. The exposed individual is a resident who is exposed by ingestion of the vegetables from the garden, soil ingestion, soil inhalation, and external exposure. Figure 5-4 shows the exposure pathways. Parameters specific to the suburban garden scenario are given in Table 5-5.

Figure 5-4. Exposure Pathways Considered in the Inadvertent Intruder Suburban Garden Chronic Exposure Scenario.

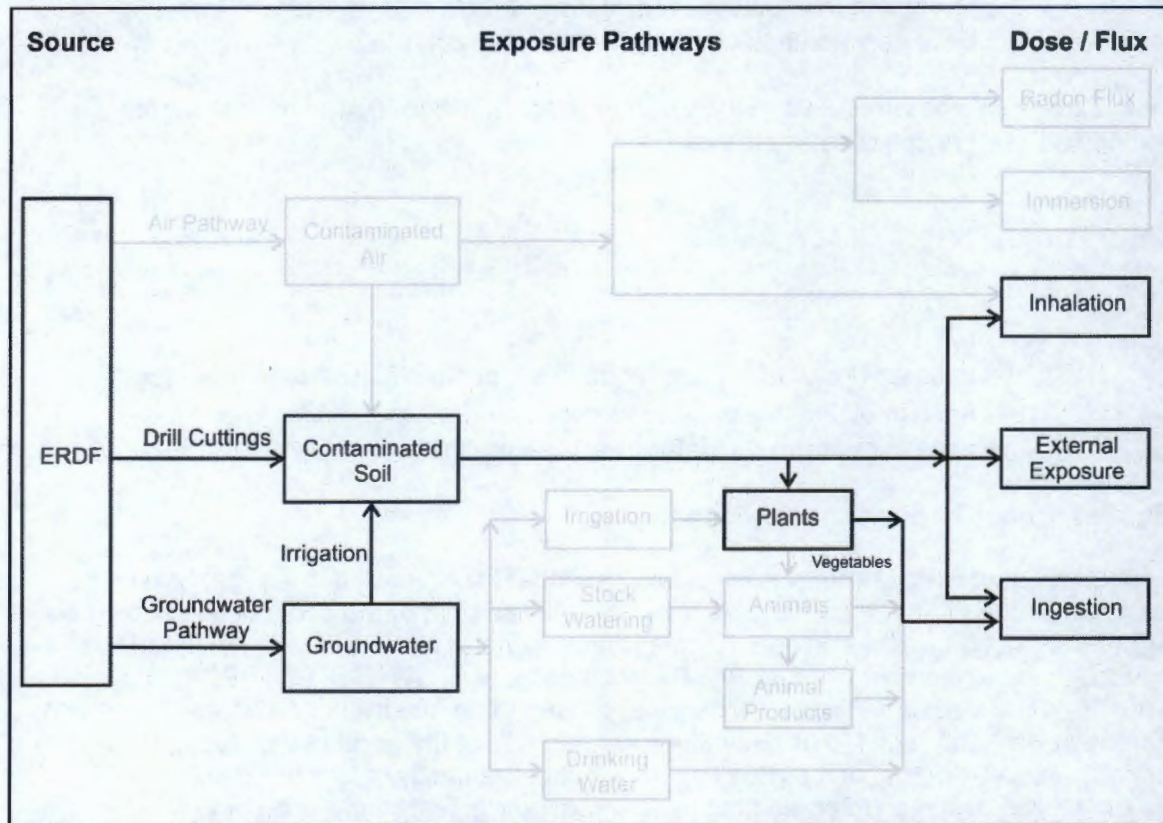


Table 5-5. Parameters Considered in the Inadvertent Intruder Suburban Garden Chronic Exposure Scenario. (2 Pages)

Parameter	Value	Units	Notation	Reference
Area of suburban garden	1E+06	cm ²	A_{sg}	HNF-SD-WM-TI-707, Rev. 5
Area of the home construction lot (target field)	2.5E+07	cm ²	A_{tf}	BHI-00169, WHC-SD-WM-EE-004
Area of the well	706.86	cm ²	A_{well}	BHI-00169, WHC-SD-WM-EE-004
Diameter of the well	30	cm	D_{well}	BHI-00169, WHC-SD-WM-EE-004
Soil ingestion rate	100	mg/day	IR_s	OSWER Directive 9285.6-03
Exposure frequency	180	day/yr	EF	HNF-SD-WM-TI-707, Rev. 5
Tilled depth of target field	15	cm	Z_f	HNF-SD-WM-TI-707, Rev. 5
Crop (vegetable and fruit) ingestion rate	47.5	kg/yr	IR_c	HNF-SD-WM-TI-707, Rev. 5

Table 5-5. Parameters Considered in the Inadvertent Intruder Suburban Garden Chronic Exposure Scenario. (2 Pages)

Parameter	Value	Units	Notation	Reference
Crop-soil bioconcentration factor resuspension (vegetable)	0.004	(pCi/kg fresh wgt of crop)/(pCi/kg dry wgt of soil)	B'_p	NCRP 1999
Fraction of crops (vegetable and fruit) that are locally produced	1	Unitless	F_p	HNF-SD-WM-TI-707, Rev. 5
Enrichment factor	0.7	Unitless	E_f	NCRP 1999
Inhalation rate when outdoors	8103	m ³ /yr	IR_{out}	HNF-SD-WM-TI-707, Rev. 5
Mass loading factor for outdoor conditions	6.66E-05	g/m ³	M_{out}	ICRP 1994
Fraction of time spent outdoors	0.041	Unitless	t_{out}	HNF-SD-WM-TI-707, Rev. 5
Inhalation rate when indoors	8103	m ³ /yr	IR_{in}	HNF-SD-WM-TI-707, Rev. 5
Mass loading factor for indoor conditions	6.66E-05	g/m ³	M_{in}	ICRP 1994
Fraction of time spent indoors	0.66	Unitless	t_{in}	NUREG/CR-5512

Concentration in Garden Soil:

Radionuclide concentration in the garden soil (C_{gs}) is calculated using the same equations and parameters as in the rural pasture scenario (Equation 5-6) except for the following:

- The diameter of the borehole is a different size
- The area of the target field is a different size than that of the pasture. The target field is the home construction lot area.

5.2.2.1 Ingestion of Garden Soil. Dose, D_s in mrem/yr, due to ingestion of garden soil is given by:

$$D_s = C_{gs} \times IR_s \times EF \times DCF_{ing} \quad \text{Eq. 5-13}$$

where

- C_{gs} = the total radionuclide concentration in the garden soil surface layer (pCi/g)
 IR_s = the ingestion rate of soil by exposed individuals (mg/day)

EF = the exposed individual exposure frequency (*days/yr*)
 DCF_{ing} = the dose conversion factor for ingestion (*mrem/pCi*).

5.2.2.2 Ingestion of Garden Vegetables. This exposure pathway assesses the dose received by residents eating vegetables grown in the garden. It is necessary to first evaluate the radionuclide concentrations in the vegetables, and then the concentration in people eating the vegetables.

Concentration in Crop:

Radionuclide concentration in the crop, C_c in pCi/g, is calculated using the following equation:

$$C_c = C_{gs} \times (B_v + B'_v) \quad \text{Eq. 5-14}$$

where

C_{gs} = the total radionuclide concentration in the garden soil surface layer (*pCi/g*)

B_v = the crop-soil bioconcentration factor through uptake $\left(\frac{\left(\frac{\text{pCi}}{\text{kg fresh weight of crop}} \right)}{\left(\frac{\text{pCi}}{\text{kg dry weight of soil}} \right)} \right)$

B'_v = the bioconcentration factor with resuspension processes $\left(\frac{\left(\frac{\text{pCi}}{\text{kg dry weight of crop}} \right)}{\left(\frac{\text{pCi}}{\text{kg dry weight of soil}} \right)} \right)$.

Dose, D_c in mrem/yr, due to ingestion of the vegetables is calculated using the following equation:

$$D_c = C_c \times IR \times F_v \times DCF_{ing} \quad \text{Eq. 5-15}$$

where

C_c = the radionuclide concentration in the crop (*pCi/g*)

IR = the ingestion rate of garden vegetables (*kg/yr*)

F_v = the fraction of vegetables produced locally (*dimensionless*)

DCF_{ing} = the dose conversion factor for ingestion (*mrem/pCi*).

5.2.2.3 Inhalation of Garden Soil. Dose, D_{inh} in mrem/yr, due to inhalation of garden soil is calculated by the following equation:

$$D_{inh} = C_{gs} \times E_f \times (IR_{in} \times M_{in} \times t_{in} + IR_{out} \times M_{out} \times t_{out}) \times DCF_{inh} \quad \text{Eq. 5-16}$$

where

C_{gs}	=	the total radionuclide concentration in the garden soil surface layer (pCi/g)
E_f	=	the enrichment factor (<i>dimensionless</i>)
IR_{in}	=	the inhalation rate while indoors (m^3/yr)
M_{in}	=	the mass loading factor for indoor conditions (g/m^3)
t_{in}	=	the fraction of time the gardener spends indoors (<i>dimensionless</i>)
IR_{out}	=	the inhalation rate while outdoors (m^3/yr)
M_{out}	=	the mass loading factor for outdoor conditions (g/m^3)
t_{out}	=	the fraction of time the gardener spends outdoors (<i>dimensionless</i>)
DCF_{inh}	=	the dose conversion factor for inhalation ($mrem/pCi$).

5.2.2.4 External Exposure. Dose, D_{ext} in mrem/yr, from direct radiation from the soil is calculated by:

$$D_{ext} = C_{gs} \times t_{out} \times DCF_{ext} \quad \text{Eq. 5-17}$$

where

C_{gs}	=	the total radionuclide concentration in the garden soil surface layer (pCi/g)
t_{out}	=	the fraction of time the gardener spends outdoors (<i>dimensionless</i>)
DCF_{ext}	=	the dose conversion factor for external exposure ($mrem/yr$)/(pCi/g)

5.2.3 Commercial Farm Chronic Scenario

The commercial farm scenario evaluates the doses that might result if the target field was used as a commercial farm and the well was sized to irrigate the farm. In this scenario a 41.91-cm (16.5-in.)-diameter well is assumed as a representative diameter and the drill cuttings are spread in a field $6.47E+04 \text{ m}^2$ (160 acres) for growing food crops. The exposed individual is a farm worker who grows and tends to the crops but does not consume them. The farm worker is exposed by ingestion and inhalation of soil, and by external exposure. Figure 5-5 illustrates the exposure pathways. Parameters specific to the commercial farm scenario are given in Table 5-6.

Figure 5-5. Exposure Pathways Considered in the Inadvertent Intruder Commercial Farm Chronic Exposure Scenario.

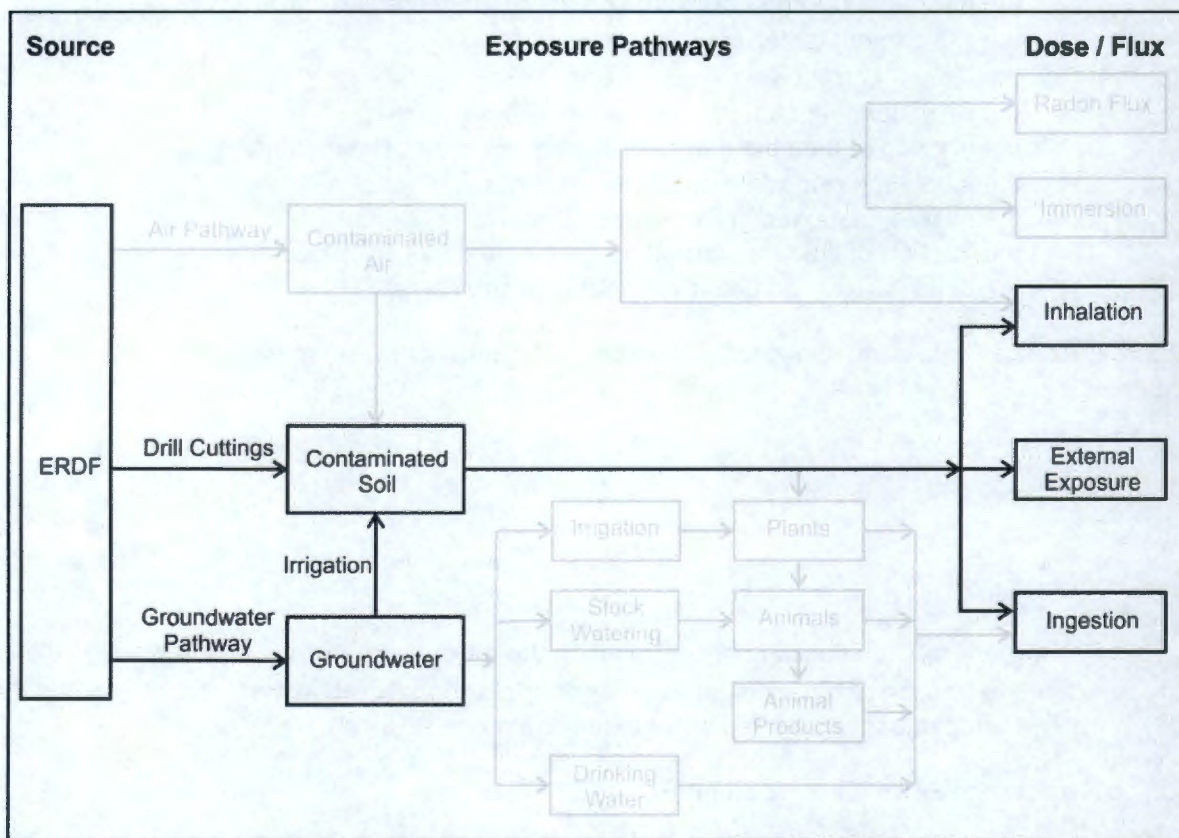


Table 5-6. Parameters Considered in the Inadvertent Intruder Commercial Farm Chronic Exposure Scenario. (2 Pages)

Parameter	Value	Units	Notation	Reference
Area of commercial farm	6.47E+09	cm ²	A_{cf}	HNF-SD-WM-TI-707, Rev. 5
Area of the well	1379.51	cm ²	A_{well}	HNF-SD-WM-TI-707, Rev. 5
Diameter of the well	41.91	cm	D_{well}	HNF-SD-WM-TI-707, Rev. 5
Soil ingestion rate	100	mg/day	IR_s	OSWER Directive 9285.6-03
Exposure frequency	180	d/yr	EF	HNF-SD-WM-TI-707, Rev. 5
Tilled depth of target field	15	cm	Z_f	HNF-SD-WM-TI-707, Rev. 5
Enrichment factor	0.7	Unitless	E_f	NCRP 1999
Inhalation rate when outdoors	8103	m ³ /yr	IR_{out}	HNF-SD-WM-TI-707, Rev. 5
Mass loading factor for outdoor conditions	6.66E-05	g/m ³	M_{out}	ICRP 1994
Fraction of time spent outdoors	0.164	Unitless	t_{out}	HNF-SD-WM-TI-707, Rev. 5

Table 5-6. Parameters Considered in the Inadvertent Intruder Commercial Farm Chronic Exposure Scenario. (2 Pages)

Parameter	Value	Units	Notation	Reference
Inhalation rate when indoors	8103	m ³ /yr	<i>IR_{in}</i>	HNF-SD-WM-TI-707, Rev. 5
Mass loading factor for indoor conditions	6.66E-05	g/m ³	<i>M_{in}</i>	ICRP 1994
Fraction of time spent indoors	0.66	Unitless	<i>t_{in}</i>	NUREG/CR-5512

Concentration in Commercial Farm Soil:

Radionuclide concentration in the commercial farm soil is calculated using the same equations and parameters as in the rural pasture scenario except for the following:

- The diameter of the borehole is a different size because the well is drilled to irrigate a commercial farm instead of a pasture
- The area of the commercial farm is a different size than that of the pasture.

5.2.3.1 Ingestion of Commercial Farm Soil. Dose, D_s in mrem/yr, due to ingestion of soil is given by:

$$D_s = C_{cf} \times IR_s \times EF \times DCF_{ing} \quad \text{Eq. 5-18}$$

where

- C_{cf} = the total radionuclide concentration in the farm soil surface layer (*pCi/g*)
 IR_s = the ingestion rate of soil by exposed individuals (*mg/day*)
 EF = the exposed individual exposure frequency (*days/yr*)
 DCF_{ing} = the dose conversion factor for ingestion (*mrem/pCi*).

5.2.3.2 Inhalation of Commercial Farm Soil. Farm workers will inhale some soil and receive an associated dose. The dose, D_{inh} in mrem/yr, from inhalation is calculated by the following equation:

$$D_{inh} = C_{fs} \times E_f \times (IR_{in} \times M_{in} \times t_{in} + IR_{out} \times M_{out} \times t_{out}) \times DCF_{inh} \quad \text{Eq. 5-19}$$

where

- C_{fs} = the total radionuclide concentration in the farm soil surface layer (*pCi/g*)
 E_f = the enrichment factor (*dimensionless*)
 IR_{in} = the inhalation rate of the farm worker while indoors (*m³/yr*)
 M_{in} = the mass loading factor for indoors conditions (*g/m³*)

- t_{in} = the fraction of time the worker spends outdoors (*dimensionless*)
- IR_{out} = the inhalation rate while outdoors (m^3/yr)
- M_{out} = the mass loading factor for outdoor conditions (g/m^3)
- t_{out} = the fraction of time outdoors (*dimensionless*)
- DCF_{inh} = the dose conversion factor for inhalation ($mrem/pCi$).

5.2.3.3 External Exposure. The external dose, D_{ext} in mrem/yr, from direct radiation from the soil is calculated by:

$$D_{ext} = C_{cf} \times t_{out} \times DCF_{ext} \quad \text{Eq. 5-20}$$

where

- C_{cf} = the total radionuclide concentration in the farm soil surface layer (pCi/g)
- t_{out} = the fraction of time the farmer spends outdoors (*dimensionless*)
- DCF_{ext} = the dose conversion factor for external exposure ($mrem/yr$)/(pCi/g).

5.3 INTRUDER ANALYSIS RESULTS

Sections 5.3.1 and 5.3.2 display the calculated effective dose for each of the four inadvertent intruder scenarios. Graphic displays show the effective dose starting 100 years after closure. Over the compliance time period the relative contribution of radionuclides vary, but the total dose decreases, with highest dose being at 100 years. Table 5-7 summarizes the calculated effective doses for each intruder scenario assuming intrusion at 100 years, when the peak dose occurs (towards demonstrating compliance) and at 500 years to demonstrate rapid decline in dose in a relatively short time period. Total doses and doses for the major radionuclide contributors are presented.

Table 5-7. Effective Dose Equivalent for the Inadvertent Intruder Scenarios at 100 Years and 500 Years Post-Closure Along with Major Dose-Contributing Radionuclides. (2 Pages)

Time (yr)	Total Dose	Cs-137	Ag-108m	Sr-90	Pu-239	Am-241
Well Driller Acute Dose (mrem)						
100	5.51E+00	5.33E+00	1.15E-01	2.79E-02	1.26E-02	6.98E-03
500	8.45E-02	6.09E-04	5.91E-02	2.13E-06	1.25E-02	3.68E-03
Commercial Farm Chronic Dose (mrem/yr)						
100	3.12E-02	2.99E-02	6.42E-04	1.57E-04	2.84E-04	1.27E-04
500	7.90E-04	3.41E-06	3.31E-04	1.20E-08	2.80E-04	6.68E-05
Rural Pasture Chronic Dose (mrem/yr)						
100	1.97E+00	1.11E+00	1.70E-02	8.02E-01	1.37E-02	5.90E-03
500	3.49E-02	1.27E-04	8.76E-03	6.12E-05	1.35E-02	3.11E-03

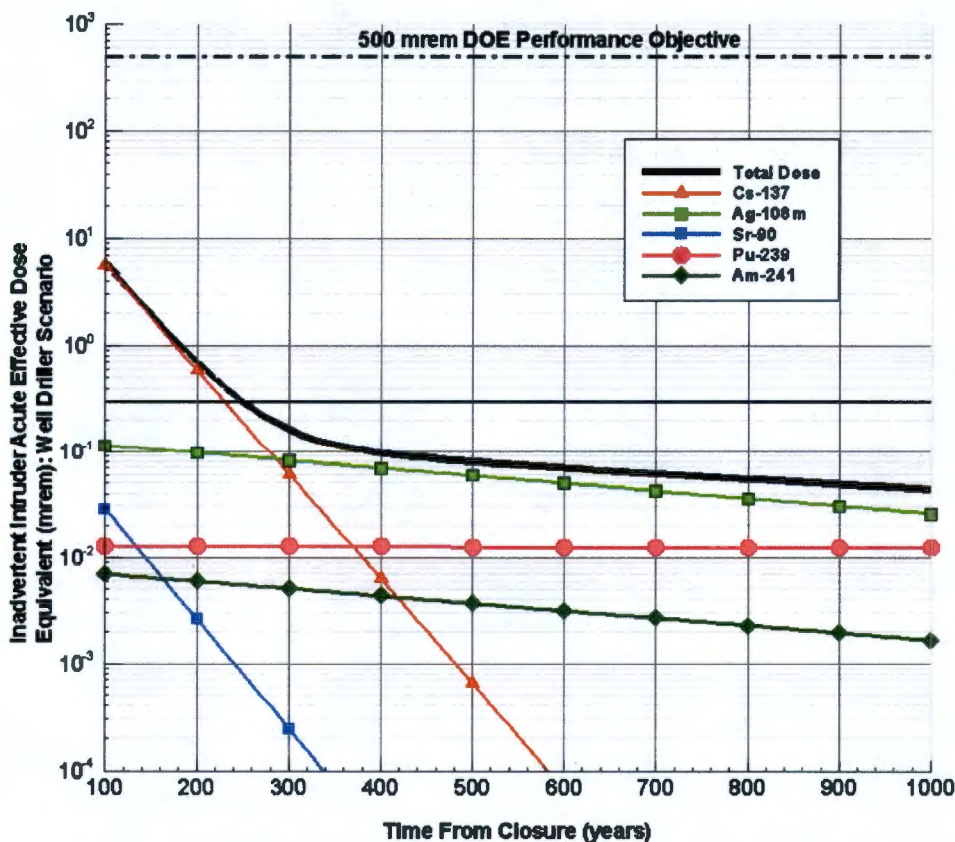
Table 5-7. Effective Dose Equivalent for the Inadvertent Intruder Scenarios at 100 Years and 500 Years Post-Closure Along with Major Dose-Contributing Radionuclides. (2 Pages)

Time (yr)	Total Dose	Cs-137	Ag-108m	Sr-90	Pu-239	Am-241
Suburban Garden Chronic Dose (mrem/yr)						
100	9.27E+00	1.88E+00	2.12E-02	7.01E+00	1.54E-01	6.33E-02
500	3.22E-01	2.15E-04	1.09E-02	5.35E-04	1.52E-01	3.34E-02

5.3.1 Acute Exposure Dose

Figure 5-6 shows the calculated acute dose to the well driller assuming the intrusion takes place 100 years or beyond after ERDF closure. The major contributor to dose to the well driller is cesium-137, and the major pathway is external exposure. If the intrusion were to take place at 500 years after closure, the major dose contributor would be silver-108m and the major pathway would be external exposure.

Figure 5-6. Effective Dose for the Well Driller Acute Exposure Scenario.



5.3.2 Chronic Exposure Dose

Figure 5-7 shows the calculated dose for the rural pasture worker. As in the well driller scenario, cesium-137 is the major contributor up until almost 300 years after closure with major pathways being external exposure and milk ingestion. Strontium-90 through the milk ingestion pathway is also a major contributor to dose at early time period. Plutonium-239 becomes the major contributor after 300 years with major pathway being soil inhalation. Silver-108m resulting from external exposure is also a contributor at late times.

Figure 5-7. Effective Dose for the Rural Pasture Chronic Exposure Scenario.

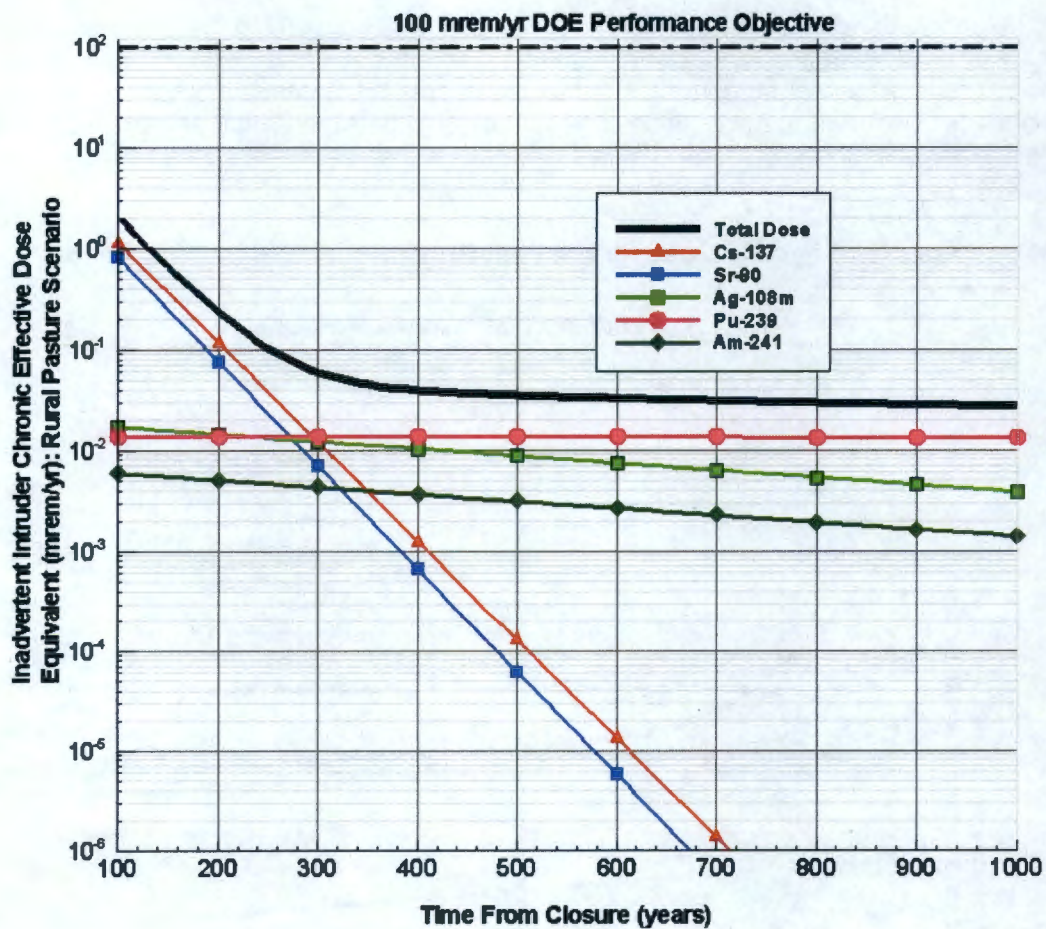


Figure 5-8 displays the expected dose to a suburban gardener with intrusion taking place 100 years or beyond after closure. Strontium-90 is the major contributor, and the vegetable ingestion pathway contributes most to the dose. Cesium-137 through the external exposure pathway is also a large component of the total dose at early on. With time, plutonium-239 becomes the major contributor through the vegetable ingestion pathway.

Figure 5-8. Effective Dose for the Suburban Garden Chronic Exposure Scenario.

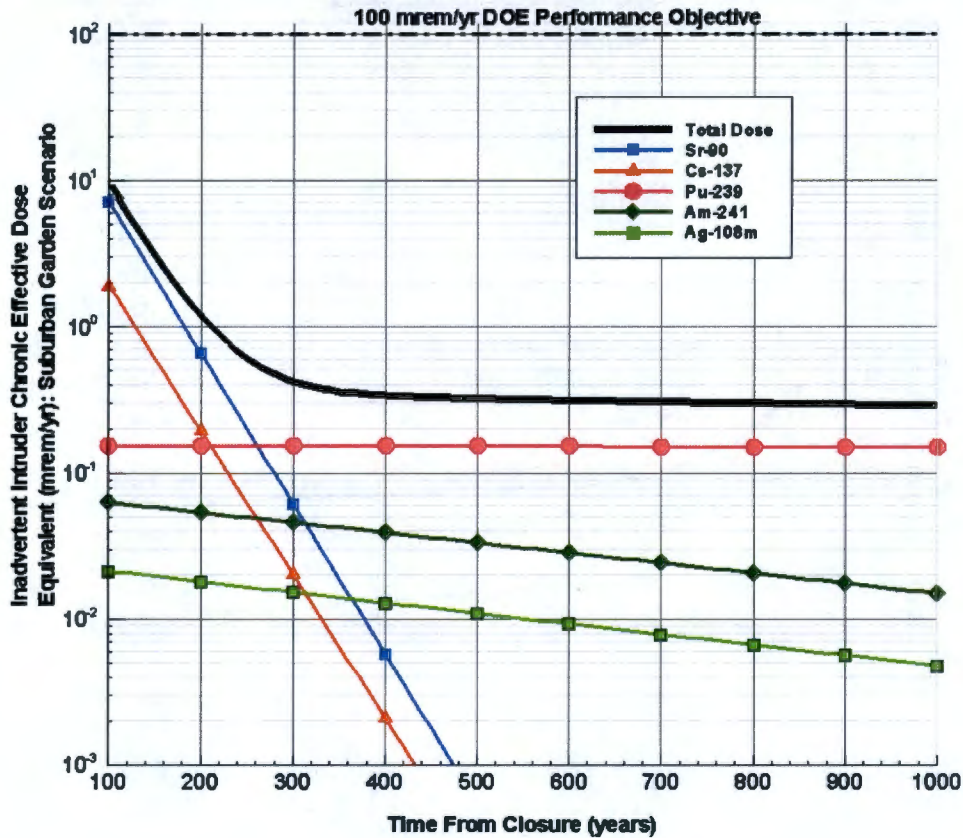
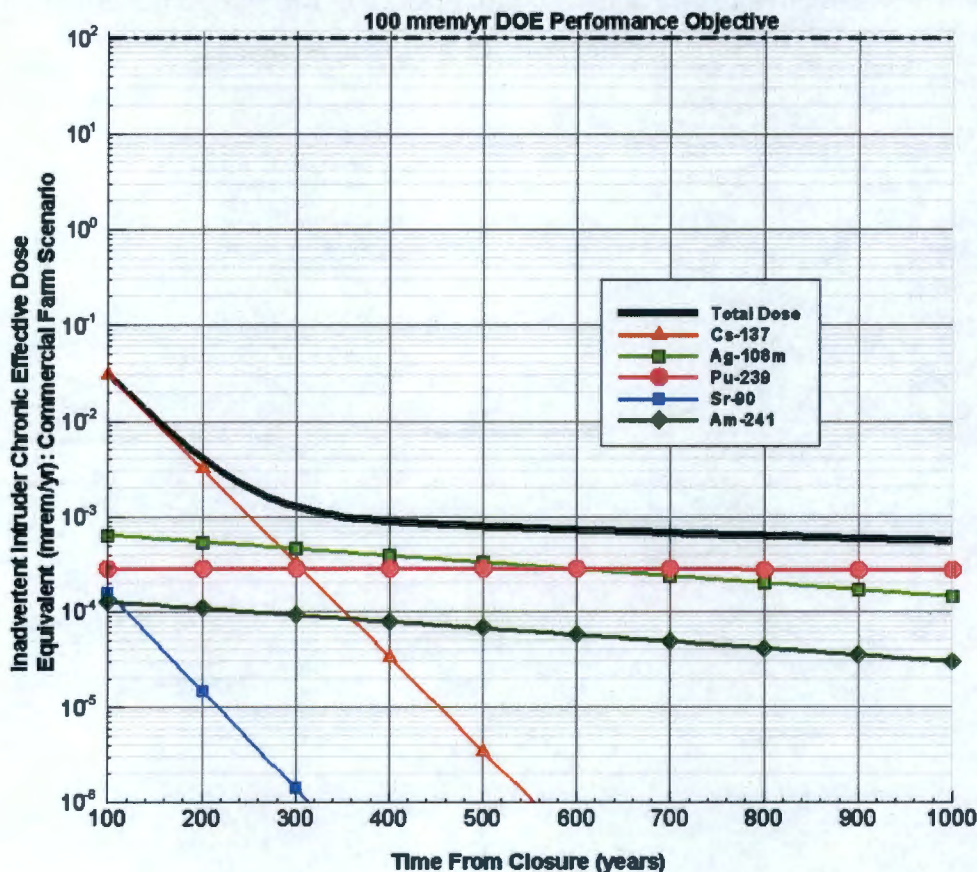


Figure 5-9 illustrates the commercial farm dose. Cesium-137 through the external exposure pathway is the early major dose contributor, with silver-108m becoming the major external exposure contributor as the cesium-137 decays. Over time plutonium-239 becomes a major contributor to total dose through the soil inhalation and soil ingestion pathways.

Figure 5-9. Effective Dose for the Commercial Farm Chronic Exposure Scenario.



5.4 INTRUDER SENSITIVITY/UNCERTAINTY ANALYSIS

Limited sensitivity analysis is performed as the dose calculation equations are linear, and therefore the effect on radionuclide dose will be linear in response to a change in parameter value. For example, the limiting inadvertent intruder scenario is the suburban garden scenario as it leads to the highest dose at 100 (and 500) years. The major dose contributors in this scenario are strontium-90 and cesium-137. Doubling the closure inventory (or concentration) of those two nuclides would result in doubling the suburban garden dose. However, it would produce lesser increases in total dose for the commercial farm and well driller scenarios, as typically strontium-90 dose contribution is minor. The uncertainties in the parameter values are not considered as they are judged to be the best available values given the hypothetical nature of the calculations.

Instead of performing detailed sensitivity analyses on parameter values (which will essentially have a linear effect on dose), the relative importance of various pathways is presented for each scenario in Table 5-8. It provides insight into the group of parameters that will have the greatest impact on the dose, and therefore the uncertainty in dose would be most impacted by the uncertainty in those parameter values. The number "1" indicates the pathway that contributes the most to the scenario (most important), with larger numbers indicating decreasing contribution. Based on the results presented in Table 5-8, the parameters associated with external exposure pathway are deemed to be most important for all scenarios except for the suburban garden, where the parameters associated with vegetable ingestion appear to be the most significant.

Table 5-8. Relative Importance of Pathway Contributions to the Inadvertent Intruder Dose.

Scenario	Pathways				
	External Exposure	Soil Inhalation	Soil Ingestion	Milk Ingestion	Vegetable Ingestion
Well Driller	1	3	2	x	x
Rural Pasture	1	3	4	2	x
Suburban Garden	2	4	3	x	1
Commercial Farm	1	2	3	x	x

X = pathway not considered

1 = Most Important; 4 = Least Important

The base case is consistent with the previous ERDF PA (BHI-00169) in that the drill cuttings were assumed to be spread over an area of 2,500 m² (home construction lot area) and the well diameter was assumed to be 30 cm (12 in.). A sensitivity case was run in which the drill cuttings were conservatively assumed to be spread over only the garden area (100 m²) instead of the entire lot area. In addition, the diameter of the well is reduced from 30 cm (12 in.) to 16.5 cm (6.5 in.), which is a more typical size for domestic wells drilled near the Hanford Site (HNF-SD-WM-TI-707, Rev. 5). All other parameters are left unchanged from the base case. The changes to model parameters are shown in Table 5-9. The impact on dose was calculated using Equation 5-21 (formulated by combining Equations 5-5 and 5-6).

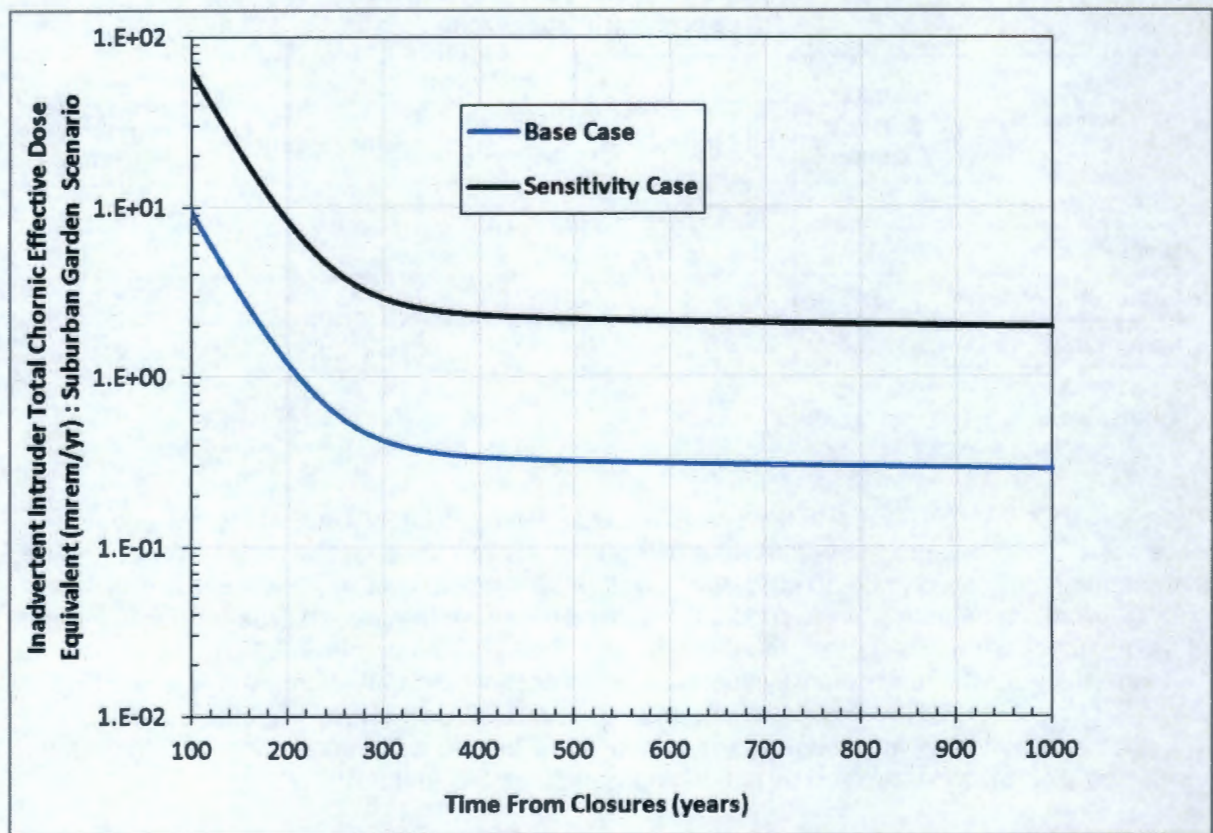
$$C_{garden} = \frac{C_{erd} \times A_{well} / A_{erd}}{A_{targetfield} \times Z_{tilldepth} \times P_{targetfield} + A_{well} \times Z_{gw} \times P_{cuttings}} \quad \text{Eq. 5-21}$$

Table 5-9. Sensitivity Analysis on Well and Garden Size Parameters.

Parameter	Base Case	Sensitivity Case
Target field area (m ²)	2500	100
Well area (cm ²)	706.86	214.08

Figure 5-10 compares the results of the sensitivity case to the base case. The total dose increased significantly in the sensitivity case. By decreasing the target field area the waste is distributed over a smaller area and that increases the waste concentration. Because the well area also decreased, less waste is brought to the target field and that decreases relative waste concentration in the garden soil leading to counteracting effects. Because the target field area was decreased by 25 times and the well area was decreased by about 3.5 times, the base case dose is about a factor of 7 less than the sensitivity case. This indicates that the ratio of target field area and well area are more important than the individual areas in influencing the dose.

Figure 5-10. Sensitivity of Suburban Garden Scenario Dose with Modified Target Field and Well Area.



6.0 INTERPRETATION OF RESULTS

In this chapter, the results presented in Chapters 4.0 and 5.0 are consolidated to provide the basis for evaluating the performance of the ERDF. The goals of the interpretation of results are as follows:

- To provide a rational basis to conclude that the performance of the ERDF has been completely addressed and the results are sufficiently rigorous and provide correct representation of the ERDF performance over the compliance and post-compliance time period
- To address the findings of the sensitivity and uncertainty analyses to provide an overall estimate of the expected performance of ERDF that is defensible for each of the performance criteria for the time of compliance.

The interpretation of the results includes the findings for the following analyses:

- All-pathways analysis
- Radon flux analysis
- Biotic pathways
- Groundwater resource protection analysis
- Inadvertent intruder analysis.

6.1 ALL-PATHWAYS DOSE

All-pathways total EDE are predicted to be well below the 25-mrem/yr standard for all time frames considered in the PA. Table 6-1 summarizes the maximum EDE for the compliance and post-compliance periods at the compliance distance 100 m downgradient of ERDF. As presented in Section 4.5, the predicted peak all-pathway EDE during the 1,000-year compliance time is about 1 mrem/yr, dominated by carbon-14 that peaks at about 120 years post-closure (year 2155). It results from upward gaseous diffusive flux of carbon-14 from ERDF that is evaluated in the air pathway. The dose in the groundwater pathway remains zero within the compliance time period due to slow advective transport in a relatively low-moisture regime through the thick vadose zone underneath ERDF. Since the only dose within the compliance time period is from the air pathway, the peak dose from contributing radionuclides is presented in Table 6-2. As shown in Figure 4-20b the dose declines over time and remains well below the 10-mrem/yr dose limit.

The predicted peak all-pathway total EDE in the post-compliance time period (up to 10,000 years) is approximately 1.88 mrem/yr that is dominated by technetium-99 along the groundwater pathway, which peaks at about 7,200 years post-closure (year 9235). The other dose contributing radionuclides in the groundwater pathway are niobium-94, molybdenum-93, chlorine-36, and iodine-129. The peak dose and time to peak are summarized in Table 6-3. Although the post-compliance peak is greater than the peak during the compliance period, it is still well below the 25-mrem/yr all-pathway EDE objective. Based on the results presented in Chapter 4.0 and Tables 6-1 through 6-3, there is high confidence that the all-pathway peak doses for the compliance (base) case calculations will remain below the dose objective for ERDF.

Table 6-1. Summary of All-Pathway Effective Dose Equivalent for the Compliance and Post-Compliance Periods 100 m Downgradient of ERDF.

Compliance Period ($\leq 1,000$ yr)		Post-Compliance Period ($> 1,000$ yr)	
Maximum Dose (mrem/yr)	Time to Maximum Dose (years)	Maximum Dose (mrem/yr)	Time to Maximum Dose (years)
1.02	120	1.88	7200
Primary Radionuclide(s)			
C-14 (Air pathway)		Tc-99 (Groundwater pathway)	

NOTE: Time is given as simulated time from post-closure (calendar year 2035).

Table 6-2. Summary of Air-Pathway Effective Dose Equivalent for the Compliance Period 100 m Downgradient of ERDF.

Radionuclide	Maximum Air Pathway Dose (mrem/yr)	Time of Maximum Dose (yr)
C-14	0.96	120
H-3	0.069	110
I-129	0.053	120

NOTE: Time is given as simulated time from post-closure (calendar year 2035).

Table 6-3. Summary of Groundwater Pathway Effective Dose Equivalent for the Post-Compliance Period 100 m Downgradient of ERDF.

Radionuclide	Maximum Groundwater Pathway Dose (mrem/yr)	Time of Maximum Dose (yr)
Tc-99	1.83	7200
Nb-94	0.027	7200
Mo-93	0.016	6740
Cl-36	1.46E-3	7200
I-129	1.72E-06	10000

NOTE: Time is given as simulated time from post-closure (calendar year 2035).

For the groundwater pathway, the arrival of radionuclides at the water table does not occur until after approximately 2,200 years from closure (for the compliance calculations). The radionuclides that appear in the saturated zone within the simulated time period of 10,000 years are all long-lived highly mobile radionuclides (with $K_d = 0$ mL/g), except for iodine-129 that appears past 9,500 years and has a small K_d (ranging from 0.1 to 0.2 mL/g). All other radionuclides considered in the inventory are noncontributors to the groundwater pathway as they are either short-lived or have K_d greater than 0.2 mL/g and thus show no breakthrough at the water table within the 10,000 years.

Monte Carlo uncertainty and sensitivity analyses provide a means to evaluate the influence of the uncertainty associated with the number of different parameters on the range of possible all-pathway dose results and also to develop an estimate of the relative importance of

different parameters. The range of groundwater pathway dose results are given in Figure 4-28 and that for the air pathway dose are given in Figure 4-31. The 95th percentile value in both cases when combined remains well below the 25-mrem/yr dose objective for all times. This provides confidence that, for foreseeable conditions, few circumstances would arise leading to a dose in excess of the all-pathways dose objective.

The uncertainty analysis also identified the important parameters that have the largest influence on the results. Tables 4-8 and 4-9 summarize the relative importance of the parameters on the groundwater pathway and air pathway dose contributions, respectively. In the groundwater pathway the peak dose is most sensitive to horizontal saturated hydraulic conductivity in the unconfined aquifer below ERDF. The second and third most important uncertain parameters are the ones that determine the velocity field in the vadose zone (the flow-field selector and the long-term recharge rate). Because of small K_d range selected for technetium-99 it plays a minor role in affecting peak dose. In the air pathway, the important uncertain parameters vary over time. The uncertainty in K_d of carbon-14 influences the uncertainty in total dose at early time (<200 years) as the amount of carbon-14 available in the gas phase is controlled by the amount that can be present in the dissolved state. The tortuosity factor also influences the dose through diffusive flux of carbon-14. At later times (>200 years) the air pathway dose is controlled by the uncertainty in the leach rate of carbon-14 from graphite waste form. The all-pathways dose is relatively insensitive to other parameters.

The sensitivity analyses indicate that a linear relationship exists between the concentration in the vadose zone that enters the water table and the saturated zone concentration at the compliance location 100 m downgradient of ERDF. The amount of dilution in the saturated zone depends upon the parameter values selected but typically varies between a factor of 30 and 60 (Figure 4-36). For the compliance case calculations, this dilution factor is about 44 (Figure 4-35) and about same as the dilution factor of 45 derived for the median case. Similarly, a linear relationship exists between the contaminant flux entering the groundwater from vadose zone and the groundwater concentration at the compliance location 100-m downgradient of ERDF. The lag time between the peak flux at the water table and the peak concentration in the saturated zone varies from about 25 years to greater than 200 years depending upon the parameter values. For the compliance case calculations, this lag time is approximately 80 years (Figure 4-36), which is about the same for the median case calculation. The sensitivity analyses also indicated that of the various recharge time periods considered the only one that can appreciably affect the radionuclide flux is the one that occurs after the surface barrier has failed.

6.2 RADON FLUX RESULTS

As discussed in Section 4.3, the projected waste inventory is not a significant radon source. The initial inventory of radium-226 is estimated to be about 1.7 Ci and is expected to contribute to almost all of the radon-222 flux at early times. The flux is estimated using a conservative set of assumptions, including the assumption of only a 1-m-thick surface barrier (instead of 4.5 m original thickness) throughout the simulated time period. This bounding approach avoids the task of defining release mechanisms and rates of progress of vapors through the overlying soils. The computed outward diffusive flux at the ERDF surface is presented in Figure 4-19.

The peak radon flux for the 1,000-year compliance period is estimated to be about 0.11 pCi/m²/s, which is well below the performance objective of 20 pCi/m²/s. The flux declines as the radium-226 inventory is depleted while the ingrowth from decay of uranium-238 and uranium-234 remains negligibly small. The result, given the conservative nature of the

calculations, provides confidence in the long-term performance of the facility to meet the radon flux performance objective, and indicates that a more complicated analysis of the features and processes of the release mechanism for vapors is unnecessary.

6.3 BIOTIC PATHWAY RESULTS

Biointrusion, i.e., contact of waste by means of plant root penetration or burrowing animals, is not expected to occur because of the 4.5-m-thick RCRA-compliant cover that will be placed over the ERDF. This cover will be placed above the interim compacted soil cover of approximately 0.6 m, leading to a minimum depth of intrusion of over 5 m needed to access the waste. The upper 0.9 m of the soil cover is composed of an admixture of silt and gravels that is intended to enhance the resistance to burrowing animals and long-term wind erosion. Given the features of the surface barrier (as discussed in Section 3.6), it is unlikely to become a viable biotic pathway. The release of radionuclides from this pathway is therefore not modeled.

6.4 GROUNDWATER PROTECTION RESULTS

Groundwater protection is evaluated by comparing predicted concentrations in groundwater 100 m downgradient from the ERDF boundary during the compliance and post-compliance time periods with the National Primary Drinking Water Regulations for MCLs for radionuclides listed in 40 CFR 141, Subpart G, *National Primary Drinking Water Regulation: Maximum Contaminant Levels and Maximum Residual Disinfectant Levels* (40 CFR 141.66). The State of Washington has adopted the federal drinking water regulations (revised as of July 1, 2009) for MCLs for radionuclides in WAC Title 246, Chapter 246-290 (WAC 246-290-025 and WAC 246-290-310).

Peak predicted radionuclide groundwater concentrations are summarized and compared to applicable groundwater protection criteria in Table 6-4. For beta-gamma-emitting radionuclides (technetium-99, niobium-94, molybdenum-93, chlorine-36, and iodine-129), an assessment of compliance with the radionuclides' respective MCLs was conducted by computing the dose equivalent and comparing the sum of the dose over time to the 4-mrem/yr dose equivalent limit. For the man-made radionuclides other than tritium (H-3) and strontium-90, 40 CFR 141.66 requires the maximum concentration limits to be calculated based on 4-mrem total body or organ dose equivalents from 2-L/day drinking water intake using the 168-hour data list in NBS 69 (National Bureau of Standards Handbook 69 as amended August 1963, *Maximum Permissible Body Burdens and Maximum Permissible Concentrations of Radionuclides in Air and in Water for Occupational Exposure*). Using this handbook, the MCLs for technetium-99, chlorine-36, and iodine-129 are derived to be 900 pCi/L, 700 pCi/L, and 1 pCi/L, respectively. The maximum permissible concentrations in water for niobium-94 and molybdenum-93 are not mentioned specifically in the handbook. For the purpose of this document, the MCL for niobium-94 is derived from proxies by evaluating the maximum permissible concentrations in water recommended for niobium-93m and niobium-95 and taking the minimum value among the two ($= 10^{-3} \mu\text{Ci}/\text{cm}^3$) based on 15 rem for individual organs of the body (at 2.2 L/day drinking water intake) and scaling it to the 4 mrem annual limit (at 2 L/day drinking water intake).

Table 6-4. Comparison of Peak Groundwater Concentration Results to Groundwater Protection Criteria.

Groundwater Performance Measure (Based on 40 CFR 141)	Compliance Period (100 m Downgradient) (Years 2035-3035)	Post-Compliance Period (100 m Downgradient) (Years 3035-12035)	Comments
Beta-gamma dose equivalent ≤ 4 mrem/yr	0 mrem/yr	3.3 ^a mrem/yr	Tc-99 accounts for almost all of the dose (>96%) during the post-compliance period. Other minor contributors to dose are Nb-94, Mo-93, and Cl-36.
Gross alpha activity concentration (excluding radon and uranium) ≤ 15 pCi/L	0 pCi/L	1E-10 ^b pCi/L	No arrival at the water table due to high K_d of radionuclides such as Np-237, Pu-239, Pu-240, and Ra-226.
Combined Ra-226 and Ra-228 concentration ≤ 5 pCi/L	0 pCi/L	1E-10 ^b pCi/L	Ingrowth from U-238, U-234, and Th-232. No arrival at the water table.
Uranium concentration ≤ 30 μ g/L MCL	0 μ g/L	1E-10 ^b μ g/L	—
Sr-90 concentration ≤ 8 pCi/L MCL	NA ^c	NA ^c	—
H-3 concentration $\leq 20,000$ pCi/L	0 pCi/L	1E-10 ^b pCi/L	—

^a Calculated using the formula $(C_{Peak}/MCL) \times 4$ mrem/yr. For example, using C_{Peak} (peak concentration for Tc-99) = 731 pCi/L and MCL = 900 pCi/L for Tc-99, which is the most significant dose contributor, the equivalent dose is calculated to be 3.25 mrem/yr.

^b Concentrations less than 1E-10 pCi/L are essentially zero.

^c Not applicable; Sr-90 was screened out during evaluation of the groundwater pathway due to its relatively short half-life and its low mobility in the subsurface.

MCL = maximum contaminant level

NA = not applicable

Similarly, for the purpose of this document, the MCL for molybdenum-93 is derived by considering the maximum permissible concentrations in water recommended for molybdenum-99 ($= 2 \times 10^{-3}$ μ Ci/cm³) based on 15 rem for individual organs of the body (at 2.2 L/day drinking water intake) and scaling it to the 4-mrem annual limit (at 2 L/day drinking water intake). Using this method, the MCLs for niobium-94 and molybdenum-93 are derived to be 293 pCi/L and 597 pCi/L, respectively, which have been rounded up to 300 pCi/L (for niobium-94) and 600 pCi/L (for molybdenum-93).

For beta-gamma-emitting radionuclides, the peak dose equivalent was 0 mrem/yr during the compliance time period. For the post-compliance time period, the peak dose equivalent was about 3.3 mrem/yr and was dominated by technetium-99. This dose is below the 4-mrem/yr dose equivalent limit.

The peak gross alpha activity, combined radium-226 and radium-228 concentration, uranium concentration, strontium-90 concentration, and tritium concentration in the groundwater is zero during the compliance period and is projected to be less than 1E-10 pCi/L or essentially zero during the post-compliance period.

All of the groundwater protection performance metrics are well below the performance objectives, which provide confidence that a reasonable expectation of compliance with the groundwater protection performance objectives can be achieved.

6.5 INADVERTENT INTRUDER ANALYSIS RESULTS

The inadvertent intruder analysis was presented in Chapter 5.0 with the assumption that intrusion occurs immediately following the loss of institutional controls at 100 years after closure. For ERDF, the acute intruder drilling scenario yielded a peak dose of 5.51 mrem at 100 years after closure (Table 5-7). Cesium-137 was the dominant radionuclide (5.33 mrem) with external exposure as the primary pathway. Silver-108m was the next dominant radionuclide, accounting for 0.11 mrem of the total dose with external exposure as the major pathway. Doses declined beyond 100 years. The total dose, 5.51 mrem, is well below the acute exposure standard of 500 mrem.

Of the three chronic intruder scenarios evaluated in Chapter 5.0, the suburban garden scenario yielded the highest dose of 9.27 mrem/yr at 100 years after closure (Table 5-7). Strontium-90 was the dominant radionuclide (7.01 mrem/yr) with vegetable ingestion as the primary pathway. Cesium-137 was the next dominant radionuclide, accounting for 1.88 mrem/yr of the total dose with external exposure as the major pathway. The total dose in all three chronic intruder scenarios declined beyond 100 years and remained below the performance measure of 100 mrem/yr.

7.0 PERFORMANCE EVALUATION

This PA documents the projected radiological impacts associated with the disposal of LLW at ERDF. The projected impacts are used to demonstrate compliance with applicable radiological dose criteria of DOE and EPA for protection of the public and the environment. This chapter compares PA results to applicable performance objectives and measures in the context of compliance. Additionally, it addresses the application of the results of the PA for development of waste acceptance criteria and radionuclide inventory threshold levels.

All of the dose-related performance objectives are based on the EDE. The term "dose" in this chapter is used for convenience, but implies EDE.

7.1 COMPARISON OF RESULTS TO PERFORMANCE OBJECTIVES

Table 7-1 presents the results of the ERDF PA for compliance as well as for post-compliance periods and compares them to the applicable performance objectives and measures. The dose to a hypothetical member of the general public was assessed through reasonable, yet conservative, scenarios. These scenarios reflect the site-specific conditions at ERDF. The PA results (Table 7-1) indicate that the performance objectives and measures are met for both the 1,000-year compliance time period (2035 to 3035) and the post-compliance period (3035 to 12035). Therefore, there is a reasonable expectation that performance objectives and measures established for the long-term protection of the public and the environment will not be exceeded following closure of ERDF.

For the post-compliance time period, Table 7-1 shows the all-pathway dose to be 1.88 mrem/yr and a groundwater protection dose of 3.3 mrem/yr. This apparent difference is due to usage of latest DOE effective dose coefficient for ingested water (DOE-STD-1196-2011) for the all-pathway dose calculation while using the EPA MCL for the groundwater protection calculation.

7.2 USE OF PERFORMANCE ASSESSMENT RESULTS

This chapter uses the inadvertent intruder (Chapter 5.0) and groundwater (Chapter 4.0) calculations to support the generally applied radionuclide concentration thresholds for disposal of wastes at the ERDF. The hypothetical inadvertent intruder scenario is used to establish disposal thresholds for waste concentrations, while the assessment of all-pathways dose (includes both groundwater and air pathway) and the peak groundwater concentration is used to establish inventory thresholds of radionuclides disposed of in ERDF.

Table 7-1. Comparison of Performance Objectives and the ERDF Performance Assessment Results for the Compliance and Post-Compliance Periods.

Performance Objective and/or Measure	Standard	Performance Assessment Results	
		Compliance Period (2035-3035) ^a	Post-Compliance Period (3035-12035) ^a
All pathways (DOE O 435.1 Chg 1)	25 mrem/yr EDE	1.02 mrem/yr	1.88 mrem/yr
Atmospheric (40 CFR 61, Subpart H)	10 mrem/yr EDE	1.02 mrem/yr	0.51 mrem/yr
Atmospheric (40 CFR 61, Subpart Q)	20 pCi.m ⁻² .s ⁻¹ radon flux (at surface of disposal facility)	0.11 pCi.m ⁻² .s ⁻¹	0.08 pCi.m ⁻² .s ⁻¹
Acute inadvertent intruder (DOE O 435.1 Chg 1)	500 mrem EDE ^b	5.51 mrem ^f	NA
Chronic inadvertent intruder (DOE O 435.1 Chg 1)	100 mrem/yr EDE ^b	9.27 mrem/yr ^f	NA
Groundwater protection (40 CFR 141)	Beta-gamma dose equivalent ≤ 4 mrem/yr	0 mrem/yr	3.3 ^c mrem/yr
	Gross alpha activity concentration (excluding radon and uranium) ≤ 15 pCi/L	0 pCi/L	1E-10 ^d pCi/L
	Combined Ra-226 and Ra-228 concentration ≤ 5 pCi/L	0 pCi/L	1E-10 ^d pCi/L
	Uranium concentration ≤ 30 µg/L	0 µg/L	1E-10 ^d µg/L
	Sr-90 concentration ≤ 8 pCi/L ^e	NA	NA
	H-3 concentration ≤ 20,000 pCi/L	0 pCi/L	1E-10 ^d pCi/L

^a Compliance at 100 m downgradient of ERDF except for inadvertent intruder scenarios.

^b Not applicable for the post-compliance time period.

^c Beta-gamma dose equivalent ≤ 4 mrem/yr (based on federal MCL) and calculated as $(C_{Peak}/MCL)^*$ 4 mrem/yr. For Tc-99, which contributes almost all of the dose, $C_{Peak}=731$ pCi/L and $MCL=900$ pCi/L, so the equivalent dose is calculated to be 3.3 mrem/yr.

^d Concentrations less than 1E-10 pCi/L are essentially zero.

^e Not applicable; Sr-90 was screened out during evaluation of the groundwater pathway due to its relatively short half-life and its low mobility in the subsurface.

^f Peak dose based on assumed inadvertent intrusion at 100 years following loss of institutional control. Peak occurs at 100 years after closure.

EDE = effective dose equivalent

MCL = maximum contaminant level

NA = not applicable

7.2.1 Inadvertent Intruder Waste Concentration Disposal Thresholds

The intruder dose assessment described in Chapter 5.0 is used, together with the performance measures for inadvertent intruders (500 mrem EDE for an acute exposure and 100 mrem/yr EDE for a chronic exposure), to derive generally applicable radionuclide concentration thresholds for waste packages to be disposed of in ERDF. Waste concentration thresholds are the maximum concentrations of individual radionuclides within a waste container that lead to a dose equivalent to the performance measure for an inadvertent intrusion scenario. The most limiting of the concentration thresholds from the acute or chronic scenarios are used to define the inadvertent intruder waste concentration disposal thresholds.

7.2.1.1 Derivation of Inadvertent Intruder Waste Concentration Thresholds. The inadvertent intruder scenarios evaluate the dose that might occur if a driller were to drill through the ERDF-emplaced waste, bring radionuclides to the land surface, and suffer an acute exposure (Chapter 5.0). After the radionuclides have been brought to the land surface, they might be spread over an area and tilled into the soil instead of being left in a waste pile or mud pit. People living and working near the area where the radionuclides were placed would suffer chronic exposure to the radiation (e.g., from ingestion or inhalation of the material). The three chronic exposure scenarios considered are (1) rural pasture, (2) suburban garden, and (3) commercial farm.

As described in Chapter 5.0, the source of radionuclide contamination for all inadvertent intruder scenarios is contamination brought to the surface by a drill penetrating the waste to the water table. The drill cuttings are then assumed to be uniformly spread over the drill pad for the acute scenario and uniformly spread over a target field and tilled into the soil for the chronic scenarios. The sizes of the target fields in each inadvertent intruder chronic scenario were chosen to represent typical land use in the Pacific Northwest. The detailed approach, equations, and data used to compute concentrations and dose estimates for the acute and chronic inadvertent intruder scenarios are provided in Chapter 5.0.

DSR represents the dose-per-unit concentration of a given radionuclide in the source (emplaced waste) at the time of exposure including radioactive decay and ingrowth of progeny, as applicable. DSR (mrem/yr per pCi/g) is used to calculate the maximum concentration of a given radionuclide in the source (emplaced waste), $C_s(\text{Threshold})$, that will yield a dose (combined over all pathways considered in a given scenario) equal to the performance measure D_L for the acute (500 mrem) or chronic (100 mrem/yr) intruder scenario. The relationship is expressed as

$$C_s(\text{Threshold}) = \frac{D_L}{DSR} \quad \text{Eq. 7-1}$$

where C_s is the threshold concentration in the source (emplaced waste) that yields a dose equal to the performance measure.

7.2.1.2 Inadvertent Intruder Pathway Inventory Threshold Results. The inventory thresholds for the inadvertent intruder scenarios are presented in Table 7-2 assuming intrusion occurs at 100 years after closure. As discussed in Chapter 1.0 (Section 1.5.3), the 100-year time frame represents the loss of active institutional controls.

Table 7-2. Calculated Radionuclide Concentration Thresholds for Waste Disposal in ERDF for Acute and Chronic Inadvertent Intruder Scenarios Based on Dose after 100 years of ERDF Closure.

Analyte	C ₀ at Closure (pCi/g)	Acute: Well Driller			Chronic: Commercial Farm			Chronic: Rural Pasture			Chronic: Suburban Garden						
		Dose at 100yr (mrem)	DSR (mrem/pCi/g)	C ₀ (Threshold) (pCi/g)	C ₀ (Threshold) (Ci/m ³)	Dose at 100yr (mrem/yr)	DSR (mrem/yr/pCi/g)	C ₀ (Threshold) (pCi/g)	C ₀ (Threshold) (Ci/m ³)	Dose at 100yr (mrem/yr)	DSR (mrem/yr/pCi/g)	C ₀ (Threshold) (pCi/g)	C ₀ (Threshold) (Ci/m ³)				
Ac-227	7.45E-05	2.03E-06	2.73E-02	1.83E+04	3.81E-02	1.48E-08	1.98E-04	5.04E+05	1.05E+00	4.84E-07	6.50E-03	1.54E+04	3.20E-02	2.63E-06	3.53E-02	2.83E+03	5.80E-03
Ag-108m	1.48E+01	1.15E-01	7.72E-03	6.47E+04	1.34E-01	6.42E-04	4.33E-05	2.31E+06	4.80E+00	1.70E-02	1.15E-03	8.73E+04	1.81E-01	2.12E-02	1.43E-03	6.99E+04	1.45E-01
Am-241	5.22E+01	6.98E-03	1.34E-04	3.75E+06	7.78E+00	1.27E-04	2.43E-06	4.12E+07	8.90E+01	5.90E-03	1.13E-04	8.80E+05	1.84E+00	6.33E-02	1.21E-03	8.25E+04	1.71E-01
Am-243	4.96E-02	4.72E-05	9.51E-04	5.26E+05	1.09E+00	3.60E-07	7.26E-06	1.38E+07	2.80E+01	1.22E-05	2.46E-04	4.00E+05	8.44E-01	7.65E-05	1.54E-03	6.49E+04	1.35E-01
C-14	1.45E+02	4.57E-05	3.15E-07	1.50E+00	3.30E+03	2.71E-07	1.87E-09	5.30E+10	1.11E+05	3.30E-03	2.27E-05	4.40E+06	9.14E+00	5.97E-02	4.11E-04	2.43E+05	5.05E-01
Cd-113m	8.50E-02	9.12E-09	1.07E-07	4.60E+06	9.67E+03	5.29E-11	6.23E-10	1.61E+11	3.33E+05	1.68E-07	1.98E-06	5.05E+07	1.05E+02	8.48E-05	9.97E-05	1.00E+06	2.08E+00
Cl-36	1.24E-03	3.55E-09	2.86E-06	1.75E+08	3.64E+02	2.03E-11	1.64E-08	6.10E+09	1.27E+04	1.18E-05	9.55E-03	1.05E+04	2.18E-02	2.87E-05	2.32E-02	4.32E+03	8.97E-03
Cm-243	3.23E-02	1.95E-06	6.06E-05	8.25E+06	1.71E+01	1.56E-08	4.83E-07	2.07E+08	4.30E+02	5.43E-07	1.68E-05	5.95E+06	1.23E+01	3.69E-06	1.11E-04	8.08E+05	1.86E+00
Cm-244	7.33E-01	1.25E-06	1.71E-06	2.92E+08	6.07E+02	2.89E-08	3.94E-08	2.64E+09	5.27E+03	1.39E-06	1.90E-05	5.28E+07	1.09E+02	1.54E-05	2.10E-05	4.70E+06	9.89E+00
Co-60	9.53E+01	6.29E-06	6.60E-08	7.57E+09	1.57E+04	3.53E-08	3.70E-10	2.70E+11	5.61E+05	9.57E-07	1.90E-08	9.98E+09	2.07E+04	1.33E-06	1.39E-06	7.19E+09	1.46E+04
Cs-137	1.59E+04	5.33E+00	3.35E-04	1.49E+08	3.10E+00	2.96E-02	1.89E-06	5.32E+07	1.11E+02	1.11E+00	7.00E-05	1.43E+06	2.97E+00	1.88E+00	1.18E-04	8.47E+05	1.76E+00
Eu-152	8.79E+01	3.89E-03	4.43E-05	1.13E+07	2.35E+01	2.18E-05	2.49E-07	4.03E+08	8.37E+02	5.99E-04	6.47E-06	1.55E+07	3.21E+01	7.17E-04	8.16E-06	1.23E+07	2.55E+01
Eu-154	1.36E+01	4.22E-05	3.09E-06	1.62E+08	3.39E+02	2.36E-07	1.73E-08	5.77E+09	1.20E+04	6.16E-06	4.52E-07	2.21E+08	4.60E+02	7.76E-06	5.71E-07	1.75E+08	3.63E+02
H3	4.94E+02	2.09E-08	4.24E-11	1.18E+13	2.45E+07	1.23E-10	2.48E-13	4.03E+14	8.38E+08	3.92E-08	7.93E-11	1.20E+12	2.62E+06	2.12E-07	4.28E-10	2.34E+11	4.85E+05
I-129	1.24E-03	8.77E-08	7.07E-05	7.07E+06	1.47E+01	4.93E-10	3.97E-07	2.52E+08	5.23E+02	1.74E-06	1.40E-03	7.14E+04	1.48E-01	3.42E-00	2.76E-03	3.63E+04	7.54E-02
K-40	0.00E+00	0.00E+00	N/A	N/A	N/A	0.00E+00	N/A	N/A	N/A	0.00E+00	N/A	N/A	N/A	N/A	N/A	N/A	N/A
Mo-93	3.29E-02	6.97E-08	2.12E-06	2.36E+08	4.90E+02	3.92E-10	1.19E-08	8.39E+09	1.74E+04	4.79E-07	1.46E-05	6.87E+06	1.43E+01	9.81E-06	2.98E-04	3.35E+05	6.97E-01
Nb-93m	1.10E-01	3.00E-10	2.71E-09	1.84E+11	3.83E+05	1.73E-12	1.50E-11	6.40E+12	1.33E+07	6.71E-11	6.07E-10	1.65E+11	3.42E+05	3.92E-09	3.55E-08	2.82E+09	5.85E+03
Nb-94	2.36E-02	2.15E-04	9.11E-03	5.40E+04	1.14E-01	1.20E-06	5.11E-05	1.90E+06	4.07E+00	3.14E-05	1.33E-03	7.51E+04	1.56E-01	3.96E-05	1.69E-03	5.90E+04	1.23E-01
Ni-59	1.86E+01	7.15E-07	3.84E-08	1.30E+10	2.70E+04	4.14E-09	2.22E-10	4.50E+11	9.35E+05	1.36E-04	7.33E-06	1.36E+07	2.83E+01	7.52E-05	4.04E-06	2.48E+07	5.14E+01
Ni-63	7.87E+02	3.80E-05	4.83E-08	1.04E+10	2.15E+04	2.23E-07	2.83E-10	3.53E+11	7.33E+05	7.25E-03	9.21E-06	1.09E+07	2.26E+01	3.99E-03	5.07E-06	1.97E+07	4.09E+01
Np-237	2.67E-02	3.10E-05	1.16E-03	4.30E+05	8.94E-01	2.04E-07	7.65E-06	1.31E+07	2.72E+01	6.24E-06	2.34E-04	4.27E+05	6.88E-01	8.91E-05	3.34E-03	3.00E+04	6.22E-02
Pa-231	2.48E-04	3.04E-06	1.22E-02	4.09E+04	8.49E-02	2.28E-08	6.17E-05	1.00E+06	2.26E+00	7.67E-07	3.99E-03	3.24E+04	6.72E-02	1.08E-05	4.36E-02	2.29E+03	4.78E-03
Pu-238	4.72E+00	2.74E-04	5.81E-05	8.61E+06	1.79E+01	6.21E-06	1.32E-06	7.60E+07	1.58E+02	3.00E-04	6.85E-05	1.57E+06	3.27E+00	3.36E-03	7.11E-04	1.41E+06	2.92E-01
Pu-239	9.05E+01	1.28E-02	1.46E-04	3.58E+06	7.44E+00	2.84E-04	3.13E-06	3.19E+07	6.63E+01	1.37E-02	1.51E-04	6.61E+05	1.37E+00	1.54E-01	1.70E-03	5.87E+04	1.22E-01
Pu-240	2.60E+01	3.60E-03	1.39E-04	3.62E+06	7.51E+00	8.08E-05	3.11E-06	3.22E+07	6.69E+01	3.90E-03	1.50E-04	6.80E+05	1.38E+00	4.39E-02	1.69E-03	5.92E+04	1.23E-01
Pu-241	1.15E+02	2.59E-06	2.25E-08	2.22E+10	4.82E+04	5.74E-08	4.98E-10	2.01E+11	4.17E+05	2.77E-06	2.40E-08	4.16E+09	8.64E+03	3.16E-05	2.74E-07	3.65E+08	7.96E+02
Pu-242	4.47E-02	5.04E-06	1.33E-04	3.78E+06	7.81E+00	1.33E-07	2.99E-06	3.35E+07	6.90E+01	6.44E-06	1.44E-04	6.94E+05	1.44E+00	7.26E-05	1.62E-03	6.15E+04	1.28E-01
Ra-226	1.04E-01	1.08E-03	1.03E-02	4.83E+04	1.00E-01	6.06E-06	5.81E-05	1.72E+06	3.57E+00	2.31E-04	2.21E-03	4.52E+04	9.30E-02	2.07E-03	1.99E-02	5.04E+03	1.05E-02
Ra-228	9.94E-02	1.30E-03	1.45E-02	3.45E+04	7.18E-02	7.27E-06	8.14E-05	1.23E+06	2.55E+00	3.90E-04	4.43E-03	2.26E+04	4.69E-02	5.52E-03	6.24E-02	1.60E+03	3.33E-03
Se-79	9.31E-03	2.12E-08	2.28E-06	2.19E+08	4.58E+02	1.20E-10	1.59E-08	7.75E+09	1.61E+04	5.03E-07	5.41E-05	1.85E+06	3.84E+00	4.24E-06	4.56E-04	2.19E+05	4.56E-01
Sm-151	1.66E+01	5.34E-07	3.22E-08	1.56E+10	3.22E+04	4.58E-09	2.76E-10	3.62E+11	7.52E+05	2.91E-07	1.76E-08	5.69E+09	1.18E+04	6.66E-06	4.02E-07	2.49E+08	5.16E+02
Sn-121m	7.81E-01	3.69E-07	4.72E-07	1.06E+09	2.20E+03	2.10E-09	2.69E-09	3.71E+10	7.71E+04	4.61E-07	5.90E-07	1.70E+08	3.52E+02	2.47E-05	3.16E-05	3.19E+06	6.57E+00
Sn-126	1.68E-02	1.87E-04	1.12E-02	4.47E+04	9.28E-02	1.05E-06	6.27E-05	1.69E+06	3.31E+00	2.79E-05	1.86E-03	6.01E+04	1.25E-01	6.46E-05	3.86E-03	2.59E+04	5.38E-02
Sr-90	7.33E+03	2.79E-02	3.80E-06	1.32E+08	2.73E+02	1.57E-04	2.15E-08	4.66E+09	9.68E+03	8.02E-01	1.09E-04	9.15E+05	1.90E+00	7.01E+00	9.57E-04	1.05E+05	2.17E-01
Tc-99	3.29E+00	1.82E-06	5.53E-07	9.04E+08	1.88E+03	1.09E-08	3.31E-09	3.02E+10	6.28E+04	4.58E-04	1.39E-04	7.19E+05	1.49E+00	1.38E-02	4.20E-03	2.39E+04	4.94E-02
Th-229	1.96E-03	1.76E-05	8.88E-03	5.63E+04	1.17E+01	1.51E-07	7.59E-05	1.32E+06	2.74E+00	5.46E-06	2.75E-03	3.64E+04	7.56E-02	3.87E-05	1.95E-02	5.13E+03	1.07E-02
Th-230	1.43E-03	3.01E-07	2.10E-04	2.38E+06	4.95E+00	6.93E-09	4.62E-06	2.16E+07	4.49E+01	3.22E-07	2.24E-04	4.46E+05	9.29E-01	3.64E-06	2.54E-03	3.94E+04	8.19E-02
Th-232	8.07E-02	1.24E-03	1.54E-02	3.24E+04	6.73E-02	7.15E-06	8.96E-05	1.13E+06	2.34E+00	1.92E-04	2.38E-03	4.21E+04	8.74E-02	3.67E-04	4.43E-03	2.28E+04	4.69E-02
U-233	9.07E-01	2.78E-05	3.04E-05	1.64E+07	3.41E+01	3.20E-07	3.52E-07	2.84E+08	5.89E+02	4.05E-05	4.47E-05	2.24E+06	4.65E+00	3.43E-04	3.79E-04	2.64E+05	5.48E-01
U-234	1.09E+00	3.10E-05	2.85E-05	1.75E+07	3.64E+01	3.68E-07	3.96E-07	2.95E+08	6.13E+02	4.70E-05	4.32E-05	2.31E+06	4.80E+00	3.98E-04	3.67E-04	2.73E+05	5.67E-01
U-235	4.90E-01	3.64E-04	7.42E-04	6.74E+05	1.40E+00	2.12E-06	4.32E-06	2.32E+07	4.81E+01	7.09E-05	1.45E-04	6.91E+05	1.44E+00	2.33E-04	4.75E-04	2.10E+05	4.37E-01
U-236	3.10E-02	8.29E-07	2.67E-05	1.87E+07	3.89E+01	9.73E-09	4.13E-07	3.19E+08	6.63E+02	1.26E-06	4.05E-05	2.47E+06	6.13E+00	1.07E-05	3.45E-04	2.90E+05	6.02E-01
U-238	5.43E+00	7.22E-04	1.33E-04	3.76E+06	7.81E+00	4.84E-06	6.92E-07	1.12E+08	2.33E+02	2.93E-04	5.39E-05	1.85E+06	3.89E+00	1.86E-03	3.48E-04	2.87E+05	5.97E-01
Zr-93	1.12E+00	6.49E-07	5.81E-07	8.60E+06	1.79E+03	4.11E-09	3.68E-09	2.72E+10	5.64E+04	1.96E-07	1.76E-07	5.69E+08	1.18E+03	5.68E-06	5.09E-06	1.07E+07	4.08E+01
Rn-222	0.00E+00	0.00E+00	N/A	N/A	N/A	0.00E+00	N/A	N/A	N/A	0.00E+00	N/A	N/A	N/A	N/A	N/A	N/A	N/A

NA = not applicable

For the acute scenario, the threshold limits are based on calculated dose (mrem), whereas for the chronic scenarios, the limits are based on mrem/yr. Table 7-2 provides the emplaced ERDF waste concentration (C_w) at closure, EDE (dose) at 100-years post-closure, DSR (dose-to-source ratio) and the computed threshold concentrations, $C_s(\text{Threshold})$, for acute and chronic inadvertent intruder scenarios for different radionuclides. Figure 7-1 illustrates, for different scenarios, the dose-based concentration threshold values, for selected radionuclides at 100 years post-closure. Among the various scenarios evaluated, the inventory concentration thresholds calculated from the suburban garden chronic exposure scenario provides the most limiting concentrations (for all except six radionuclides). These concentrations are recommended for developing the waste acceptance criteria as they would be most protective (see Appendix E for additional discussion).

7.2.1.3 Groundwater Pathway Waste Acceptance Criteria. The groundwater pathway dose assessment results for the compliance case radionuclides are presented in Chapter 4.0. These results are used, together with the performance measures for groundwater pathway, to derive generally applicable total inventory thresholds (i.e., waste acceptance criteria) for the ERDF. The total inventory thresholds are only provided for those radionuclides that arrive at the compliance location in the saturated zone within the 10,000-year time period. These radionuclides are technetium-99, niobium-94, molybdenum-93, chlorine-36, and iodine-129. For all other radionuclides emplaced in ERDF, no groundwater pathway dose-based inventory threshold would be imposed.

The total inventory thresholds are determined for the following performance measures for maximum predicted all-pathways dose and concentration:

- Calculated all-pathways dose compared to the 25-mrem/yr performance criteria for the compliance period (2035 to 3035) and post-compliance period (3035 to 12035)
- Calculated peak groundwater concentrations compared to the safe drinking water criteria based on (a) the EPA MCL (40 CFR 141.66) and (b) more recently published DOE effective dose coefficients for ingested water (DOE-STD-1196-2011) by calculating the concentration limits for annual EDE of 4 mrem at ingestion rate of 2 L/day. Calculations are performed for the compliance period (2035 to 3035) and post-compliance period (3035 to 12035).

The total inventory threshold calculation is an extension of the PA dose assessment results and is given by

$$I_T = \frac{P_o}{P_A / I} \quad \text{Eq. 7-2}$$

where

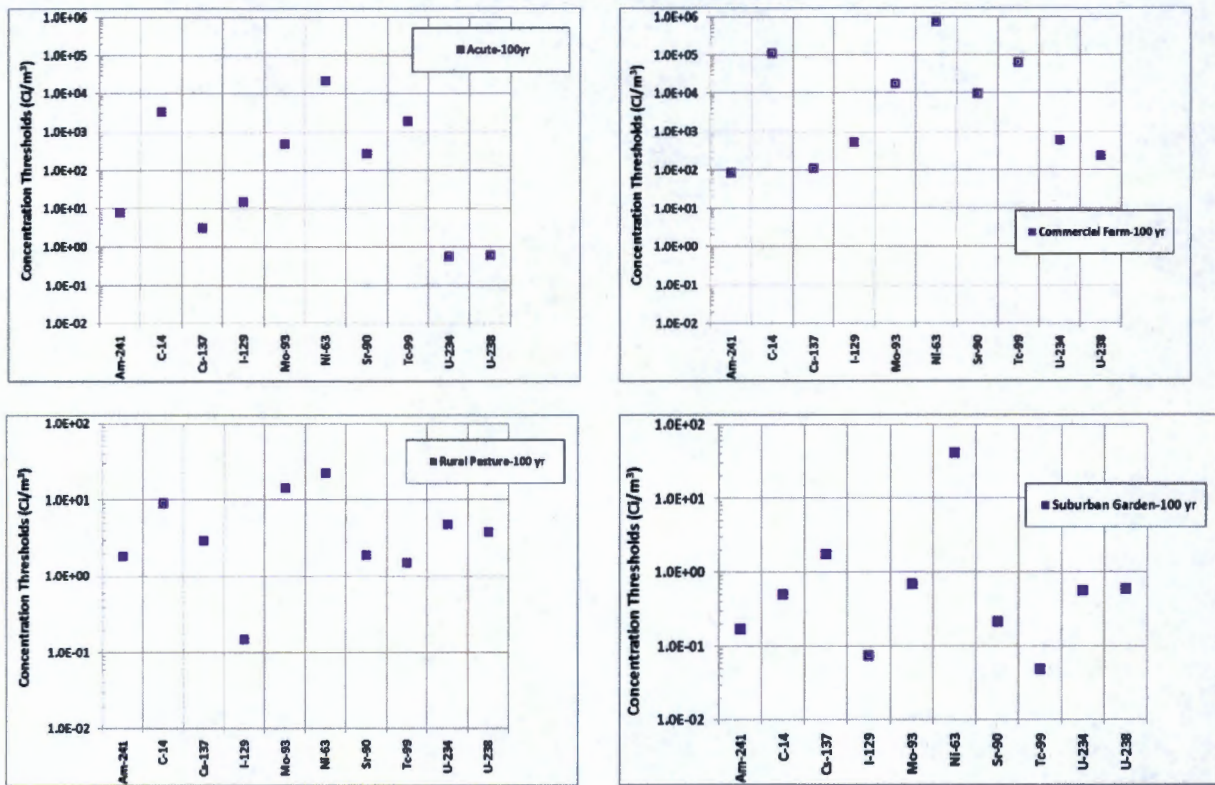
I_T = inventory threshold (Ci)

P_o = performance objective for dose (mrem/yr) or concentration (pCi/L)

P_A = peak radionuclide concentration (pCi/L) or all-pathway dose (mrem/yr) predicted at the compliance location

I = initial radionuclide inventory (Ci).

Figure 7-1. Concentration Threshold Based on Dose after 100 years of ERDF Closures for Different Scenarios.



The predicted concentration and dose are based on the PA compliance case models and analysis. The thresholds are calculated during the compliance and post-compliance periods from the maximum concentrations and doses predicted 100 m downgradient of ERDF.

The inventory threshold provides the maximum allowable inventory for a single radionuclide disposed in the facility. For a mixture of radionuclides, the sum-of-ratios should be computed to ensure that it is <1 and the performance objectives are not exceeded. The sum-of-ratios is given by:

$$SOR = \sum_{i=1}^n \frac{I_i}{I_{Ti}} \quad \text{Eq. 7-3}$$

where I_i is the actual inventory of radionuclide i and I_{Ti} is the inventory threshold for radionuclide i .

7.2.1.4 Groundwater Pathway Inventory Threshold Results. The groundwater pathway total inventory thresholds for the compliance time (2035 to 3035) and post-compliance time (3035-12035) for the ERDF are presented in Table 7-3. The thresholds are based on the predicted maximum concentrations in groundwater and predicted maximum groundwater pathway dose at the compliance location 100-m downgradient of ERDF. Since the groundwater concentrations are practically zero within the compliance time period, no inventory limits are imposed within the compliance time period.

The inventory threshold based on dose for a given radionuclide is calculated by taking the maximum EDE contribution from that radionuclide within the time period of interest and calculating corresponding inventory that is equivalent to 25 mrem/yr effective dose limit. The inventory threshold based on concentration for a given radionuclide is calculated using two different concentration thresholds: one based on the MCLs established by the EPA regulations (EPA MCL) and the other based on more recently published effective dose coefficients for ingested water from DOE derived concentration standards (DOE-STD-1196-2011). Derived concentration standards are quantities used in the design and conduct of radiological environmental protection programs at DOE facilities and sites using the latest biokinetic and dosimetric information and latest information on radiation energies and intensities. The concentration thresholds per EPA MCLs and DOE standards are presented in Table 7-3 from which inventory thresholds are derived.

For EPA MCLs, the current limits for beta-gamma emitters specify that MCLs are to be calculated based upon an annual dose equivalent of 4 mrem to the total body or any internal organ. It is further specified that the calculation is to be performed on the basis of a 2-L/day drinking water intake using the 168-hour data listed in the NBS Handbook 69, *Maximum Permissible Body Burdens and Maximum Permissible Concentrations of Radionuclides in Air or Water for Occupational Exposure*, as amended August 1963. These calculations have been done for most beta emitters and published as part of 40 CFR 141.166. The calculation basis for EPA MCLs for technetium-99, niobium-94, molybdenum-93, chlorine-36, and iodine-129 are discussed in Section 6.4, and the calculated MCLs are presented in Table 7-3. The radionuclide concentration thresholds using the DOE effective dose coefficients for ingested water are calculated by assuming 2 L/day drinking water intake and annual EDE of 4 mrem (Table 7-3).

Note that the State of Washington has adopted the federal drinking water regulations (revised as of July 1, 2009) for maximum contaminant levels for radionuclides in WAC 246-290 (WAC 246-290-025 and WAC 246-290-310).

For LLW management purposes, Table 7-3 provides a range of inventory thresholds. The groundwater pathway dose and the beta-gamma dose are the primary performance measures determining the groundwater pathway inventory thresholds. The thresholds calculated for the mobile radionuclides are limited by the beta-gamma performance measure. The other radionuclides are primarily limited by the groundwater pathway dose performance measure.

Table 7-3. Groundwater Pathway Inventory Thresholds for ERDF.

Radionuclide	Inventory Thresholds (Ci) Based on Dose ^a		Concentration Threshold (pCi/L)		Inventory Thresholds (Ci) Based on Concentration ^d		
	Compliance	Post-Compliance	Based on EPA MCL ^b	Based on DOE Standard ^c	Compliance	Post-Compliance (EPA MCL)	Post-Compliance (DOE Standard)
Tc-99	NL	724	900	1650	NL	65	120
Nb-94	NL	349	300	670	NL	26	58
Mo-93	NL	811	600	480	NL	165	134
Cl-36	NL	342	700	1200	NL	50	86
I-129	NL	2.90E+05	1	12	NL	5.00E+03	6.00E+04

^a Inventory thresholds were calculated based on all-pathway effective dose equivalent limit of 25 mrem/yr based on peak dose.

^b MCL based on EPA regulations.

^c Concentration threshold is based on DOE-STD-1196-2011 effective dose coefficients for ingestion as presented in Table 3-28 by assuming 2 L/day drinking water ingestion and 4 mrem annual effective dose equivalent to a reference person.

^d Peak concentrations for Tc-99, Nb-94, Mo-93, Cl-36, and I-129 occur, respectively, at 7225, 7155, 6740, 7230, and 10,000 years (Chapter 4.0).

MCL = maximum contaminant level

NL = not limiting

7.2.2 Air-Pathway Waste Acceptance Criteria

The air-pathway dose assessment results for the radionuclides are presented in Section 4.5. These results are used, together with the performance measures for the air pathway, to derive generally applicable air-pathway inventory thresholds towards developing waste acceptance criteria for the ERDF. These inventory guidelines are radionuclide-specific. Only radionuclides carbon-14, tritium (H-3), and iodine-129 are considered as they are the only volatile radionuclides considered for air-pathway dose calculations (Section 4.2.4).

The air-pathway inventory thresholds are calculated using Equation 7-2 by taking the maximum predicted air-pathway EDE and 10-mrem/yr performance criteria

Air-Pathway Inventory Threshold Results. The air-pathway inventory thresholds for the ERDF compliance time period are presented in Table 7-4. The thresholds are based on the predicted maximum air-pathway dose. The inventory threshold provides the maximum allowable inventory for a single radionuclide disposed in the facility. For a mixture of radionuclides, the sum-of-ratios should be computed to ensure that it is <1 and the performance objectives are not exceeded.

Table 7-4. Air-Pathway Inventory Thresholds for the ERDF for the Compliance Time Period (Year 2035 to 3035).

Radionuclide	Inventory Thresholds (Ci) ^a
C-14	2.43E+04
H-3	1.15E+06
I-129	4

^a Inventory thresholds were calculated based on DOE air-pathway effective dose limit of 10 mrem/yr.

7.2.3 Summary of Inventory Thresholds

A summary of the calculated and recommended inventory thresholds for the radionuclides of concern is presented in Table 7-5 based on the evaluation of both groundwater and air-pathway inventory thresholds. The calculated inventory thresholds are based on the compliance time period (year 2035 to 3035) as reported in Tables 7-3 and 7-4. Where inventory thresholds are indeterminate within the compliance time period they are recommended based on the post-compliance inventory threshold limits based on an all-pathway EDE limit of 25 mrem/yr. The post-compliance period inventory thresholds based on maintaining safe drinking water concentrations in groundwater are not recommended because (a) the peak concentrations are not likely to occur until after 6,500 years, (b) it is unlikely that the receptor will be drinking water exactly at the time of peak concentrations from the well located 100 m downgradient from ERDF, and (c) the well pumping effects would lead to mixing with uncontaminated water within the cone of depression in the aquifer causing much lower actual concentrations in the borehole than are predicted based on the conservative assumption of no pumping considered in this PA.

Iodine-129 is the only radionuclide that is present in both the groundwater pathway and air-pathway inventory threshold calculations. The air-pathway inventory thresholds for iodine-129 are much lower than for the groundwater pathway inventory thresholds, and it is considered as the final inventory threshold for iodine-129. For a mixture of radionuclides, the sum-of-ratios should be computed to ensure that it is <1 and the performance objectives are not exceeded.

Table 7-5. Calculated and Recommended Inventory Thresholds for Radionuclides of Concern.

Radionuclide	Calculated Inventory Thresholds (Ci)	Recommended Inventory Thresholds (Ci)
Tc-99	NL	724 ^a
Nb-94	NL	349 ^a
Mo-93	NL	811 ^a
Cl-36	NL	342 ^a
I-129	4	4
C-14	2.43E+04	2.43E+04
H-3	1.15E+06	1.15E+06

^a Inventory thresholds based on all-pathway effective dose equivalent limit of 25 mrem/yr (Table 7-3).

NL = not limiting

7.3 ALARA ANALYSIS

The DOE's approach to radiation protection for ERDF disposal is based on two key components. One component is the performance objectives described in Chapter 1.0, which specify maximum doses for various pathways. The other component requires doses to be maintained ALARA.

The goal of the ALARA process is attainment of the lowest practical dose level after taking into account social, technical, economic, and public policy considerations. Therefore, in addition to providing a reasonable expectation that the performance objectives described in Chapter 1.0 will not be exceeded, the PA also needs to show that the ERDF disposal is being conducted in a manner that maintains releases of radionuclides to the environment ALARA.

The ERDF site is in a remote location and the population is nonexistent or sparse in the vicinity of ERDF. No incorporated towns and/or residents of any kind are within miles of the facility. In addition to future institutional control, the substantial depth to the water table makes it difficult to establish a residence near ERDF in the future as well. However, consistent with the assumptions for the PA, for the purposes of the ALARA analysis, it is postulated that one or two families will establish residence 100 m downgradient of the facility.

The background activity from radionuclide that occurs in soils on the Hanford Site is discussed in detail in DOE/RL-96-12 (*Hanford Site Background: Part 2, Soil Background for Radionuclides*, Rev. 0). The soil data used were obtained from samples collected from the surface and from the vadose zone. The background activity results from naturally occurring radionuclides and anthropogenic radionuclides that were deposited by global fallout. An average background dose of 96.9 ± 29.8 mrem/yr is calculated in DOE/RL-96-12 based on residential exposure scenario, with the greatest dose contribution from the radon pathway. In contrast the peak dose within the compliance and post-compliance time period from ERDF is calculated to be 1.88 mrem/yr. This is about a factor of 50 smaller than the background dose level.

Other potential options that have been considered for ALARA include a larger buffer zone, more robust covers, or other engineered measures; but, given the very low collective doses currently estimated and the incremental cost associated with any of these options, it is hard to imagine any of these options being cost effective from the ALARA perspective.

7.4 FUTURE WORK

DOE M 435.1-1 Chg 1 (IV.P.(4)) includes a requirement for PA maintenance to evaluate the impact of design and operational changes and to incorporate any new information regarding waste forms, site characteristics, etc. In addition to a PA maintenance plan, required documentation in support of the DAS for ERDF includes a closure plan, monitoring plan, and annual reports documenting any recent changes to the plans for the LLW facility or changes in the understanding of the environmental impacts from the facility.

An unreviewed disposal evaluation process is required for evaluating proposed or discovered changes in waste management or disposal-related activities throughout the facility's operational life and closure that could impact the PA assumptions and results. The evaluation process must be implemented in a systematic, graded approach.

8.0 PREPARERS

Sunil Mehta

Ph.D., Earth Sciences (Hydrogeology specialization), University of Kentucky
M.S., Geosciences, University of Louisiana at Monroe
M.Sc., Geology, University of Poona, India
B.Sc., Chemistry, Zoology, and Geology, University of Jodhpur, India

Dr. Sunil Mehta has more than 18 years of experience related to groundwater flow and transport modeling, reactive transport modeling, total system performance assessment, uncertainty analysis, geophysical logging, and well testing. He has worked on projects involving geologic isolation of radioactive wastes, environmental restoration activities, and water resources exploration and evaluation. Dr. Mehta has over 10 years of experience in designing, developing, and applying probabilistic tools to assess the long-term performance of radioactive waste storage and disposal facilities. He has performed reactive transport modeling and groundwater flow modeling to study behavior of contaminants such as uranium and hexavalent chromium in periodically rewetted zones influenced by aquifer-river interactions. For this study, Dr. Mehta has been one of the principal investigators, performing the flow and transport abstraction modeling for uncertainty analysis and dose calculations, inadvertent intruder analysis, air-pathway analysis, focusing on project coordination, reviews, and overall document preparation.

William J. McMahon

M.S., Agricultural Engineering, Texas A&M University
B.S., Agricultural Engineering, University of California, Davis

Mr. McMahon specializes in hydrologic data collection, analysis, and interpretation, and groundwater and vadose zone numerical modeling to support groundwater and vadose remedial projects. He has experience with a number of vadose zone and groundwater modeling packages. He also provides technical direction, guidance, and oversight to subcontractors performing numerical modeling in support of the risk assessments associated with accelerated retrieval and closure of single-shell tanks. His other duties include directing hydrologic data collection efforts, analyzing and interpreting hydrologic data, assessing the effectiveness of groundwater remedial actions, developing work plans for data collection and interpretation, and performing numerical modeling to predict facility impacts to the aquifer to support remediation and construction decisions.

For this study, Mr. McMahon has been the one of the principal investigators, focusing on the flow and transport modeling using STOMP code, groundwater pathway compliance calculations, sensitivity analysis, and document preparation.

Raziuddin Khaleel

Ph.D., Soil and Water Engineering, Texas A&M University
M.S., Water Science and Engineering, Asian University of Technology
B.S., Civil Engineering, Bangladesh University of Engineering and Technology

Dr. Khaleel has over 25 years of experience in groundwater hydrology and numerical simulations of subsurface flow and transport. He was a key contributor to the Hanford Site Performance Assessment for the Disposal of Low-Level Waste in the 200 West Area Burial Grounds, the Performance Assessment for the Disposal of Low-Level Waste in the 200 East Area Burial Grounds, and the Hanford Immobilized Low-Activity Tank Waste Performance Assessment, particularly in the area of conceptual model development, direction of modeling, and in writing the document.

For this document, Dr. Khaleel developed the hydraulic parameter sets for the vadose zone, technical basis for conceptual vadose zone flow and transport model discussed in Appendix A, and document preparation.

Steven M. Baker

Ph.D., Mathematics, Oregon State University
M.S., Nuclear Engineering, Oregon State University
B.S., Mathematics, Oregon State University

Dr. Baker has over 50 years work experience in scientific and engineering disciplines. Since 1982 he has focused on technical and policy aspects of high-level nuclear waste management and disposal and environmental cleanup. He has supported DOE in many roles, including: nuclear engineer for the Fast Flux Test Facility at Hanford, manager responsible for groundwater characterization of the Basalt Waste Isolation Project site at Hanford; Environmental, Safety and Health (ES&H) manager for high-level nuclear waste tank design of tanks at the Idaho National Engineering Laboratory chemical processing plant near Idaho Falls, consultant for accelerated cleanup of Rocky Flats; and participant in ES&H audits of DOE facilities, including 11 facilities at Hanford and Tiger Team reviews at Y-12 (Oak Ridge, TN), Pittsburgh Environmental Technology Center (PA), Sandia National Laboratory (NM), and Paducah Gaseous Diffusion Plant (KY).

For this document, Dr. Baker focused on developing dose calculations, exposure pathways, modeling inadvertent intruder scenario, and document preparation.

Benjing Sun

Ph.D., Environmental Analytical/Atmospheric Chemistry, Brigham Young University
M.S., Environmental Sciences, Beijing Normal University
B.S., Physics, Beijing Normal University

Dr. Sun has expertise in managing and conducting projects in the areas of risk assessment, performance assessment, environmental chemistry, and air quality modeling. He also has experience in permitting, regulatory compliance and environmental forensic investigation. He has in-depth knowledge in fate and transport modeling among multiple environmental media, sensitivity and uncertainty analyses, and risk-based remediation goal setup following the

technical guidance under CERCLA and RCRA, and other federal and state regulations. He has managed and performed many risk assessment projects in support of remedial investigation/feasibility study, permit application, regulatory compliance, and risk management.

For this document, Dr. Sun developed exposure scenarios and associated parameters, dose calculation methodologies for various exposure pathways, and validation activities for the air pathway.

Christelle Courbet

Ph.D., Hydrogeology, Pierre & Marie Curie University, Paris VI, UMR Sisyphe, France
M.S., Hydrology and Hydrogeology, Pierre & Marie Curie University, Paris VI, UMR Sisyphe, France
B.S., Geology and Soil Mechanics, Pierre & Marie Curie University, Paris VI, Science And Technology School (CNAM), France

Dr. Courbet has over six years of experience in performing hydrogeologic investigations and applying groundwater flow models for contaminated land remediation, water resource management and mine dewatering. Her past work focused on optimizing pump-and-treat system for removal of chlorinated solvents, studying movement and natural attenuation of these compounds through innovative tools (compound-specific stable isotope analysis and biomolecular measurements on groundwater samples). She has also worked on a uranium mining site (Arlit, Niger) where she was involved in dewatering of open-pit mines and hydraulic testing campaigns to characterize a multi-layer aquifer system.

For this document, Dr. Courbet helped develop the uncertainty distribution for key parameters and abstraction model used for uncertainty analysis, review of exposure scenario parameters, and validation of air pathway calculation methodology.

Nazmul Hasan

M.S., Environmental Engineering, Washington State University
B.S., Civil Engineering, University of Engineering & Technology, Bangladesh

Mr. Hasan has over three years of experience performing numerical modeling in the saturated and unsaturated zones, including model calibration and sensitivity analysis, geostatistical analysis, and programming.

For this document, Mr. Hasan helped in checking flow and transport models, developing the flow-fields for the abstraction model, and performing uncertainty analyses. He also supported document preparation, generation of figures, and waste acceptance criteria.

9.0 REFERENCES

- 0000X-DC-W001, 2008, *Supplemental Waste Acceptance Criteria for the Environmental Restoration Disposal Facility*, Rev. 10 or latest revision, Washington Closure Hanford, Richland, Washington.
- 07-AMRC-0077, 2007, "Transmittal of an Amendment to the Environmental Restoration Disposal Facility (ERDF) Record of Decision (ROD)" (letter to Nicholas Ceto, U.S. Environmental Protection Agency, and Jane A. Hedges, Washington State Department of Ecology, from Keith A. Klein), U.S. Department of Energy, Richland Operations Office, Richland, Washington, January 12. Available at: <http://www.epa.gov/superfund/sites/rods/fulltext/a2007100003141.pdf>
- 09-AMRC-0179, 2009, "Transmittal of Signed Environmental Restoration Disposal Facility (ERDF) Record of Decision (ROD) Amendment Authorizing Supercells 9 & 10" (letter to C. G. Spencer, Washington Closure Hanford, from J. J. Short), U.S. Department of Energy, Richland Operations Office, Richland, Washington, August 13. Available at: <http://www5.hanford.gov/arpir/index.cfm?content=findpage&AKey=0096067>
- 10 CFR 61, "Licensing Requirements for Land Disposal of Radioactive Waste," *Code of Federal Regulations*.
- 10 CFR 830, "Nuclear Safety Management," *Code of Federal Regulations*.
- 40 CFR 61, "National Emission Standards for Hazardous Air Pollutants," *Code of Federal Regulations*. Available at: <http://www.gpo.gov/fdsys/pkg/CFR-2010-title40-vol8/xml/CFR-2010-title40-vol8-part61.xml>
- 40 CFR 141, "National Primary Drinking Water Regulations," *Code of Federal Regulations*, as amended.
- 40 CFR 264, "Standards for Owners and Operators of Hazardous Waste Treatment, Storage, and Disposal Facilities," Subpart N, "Landfills," *Code of Federal Regulations*. Available at: <http://www.gpo.gov/fdsys/pkg/CFR-2010-title40-vol25/xml/CFR-2010-title40-vol25-part264.xml>
- 40 CFR 300, "National Oil and Hazardous Substances Pollution Contingency Plan," *Code of Federal Regulations*. Available at: <http://www.gpo.gov/fdsys/pkg/CFR-2010-title40-vol27/xml/CFR-2010-title40-vol27-part300.xml>
- 64 FR 61615, 1999, "Record of Decision: Hanford Comprehensive Land-Use Plan Environmental Impact Statement (HCP EIS)," *Federal Register*, Vol. 64, No. 218, pp. 61615-61625, November 12.
- 69 FR 39449, 2004, "Record of Decision for the Solid Waste Program, Hanford Site, Richland WA: Storage and Treatment of Low-Level Waste and Mixed Low-Level Waste; Disposal of Low-Level Waste and Mixed Low-Level Waste, and Storage, Processing, and Certification of Transuranic Waste for Shipment to the Waste Isolation Pilot Plan," *Federal Register*, Vol. 69, No. 125, pp. 39449-39455, June 30.

- 65 FR 37253, "Establishment of the Hanford Reach National Monument," *Federal Register*, Vol. 65, No. 114, pp. 37253-37257, June 13, 2000. Available at: <http://www.gpo.gov/fdsys/pkg/FR-2000-06-13/pdf/00-15111.pdf>
- Allen, J. R. and L. Allen, 1982, "Developments in Sedimentology," in *Sedimentary Structures, their Character and Physical Basis*, Elsevier Scientific Publications, Amsterdam, New York, pp. 30A-30B.
- Alwin, J. A., 1970, *Clastic Dikes of the Touchet Beds, Southeastern Washington*, M.S. thesis, Washington State University, Pullman, Washington.
- ARH-CD-775, 1976, *Geohydrologic Study of the West Lake Basin*, Atlantic Richfield Hanford Company, Richland, Washington.
- ARH-LD-137, 1976, *Geology of the 241-U Tank Farm*, Rockwell Hanford Operations, Richland, Washington.
- Audi, G. O. J. Bersillon, J. Blachot, and A. H. Wapstra, 2003, "The NUBASE Evaluation of Nuclear and Decay Properties," *Nuclear Physics A* 729 (2003) 3-128.
- Baker, V. R. and R. C. Bunker, 1985, "Cataclysmic Late Pleistocene Flooding from Glacial Lake Missoula: A Review," *Quat. Sci. Rev.*, Vol. 4, No. 1, pp. 1-41.
- Benson, J. E., R. T. Tveten, M. G. Asher, and P. W. Dunwiddie, 2011, *Shrub-Steppe and Grassland Restoration Manual for the Columbia River Basin*, Washington Department of Fish and Wildlife, 108 p.
- BHI-00007, 1994, *Prototype Hanford Surface Barrier: Design Basis Document*, Rev. 0, Bechtel Hanford, Inc., Richland, Washington.
- BHI-00169, 1995, *Environmental Restoration Disposal Facility Performance Assessment*, Rev. 00, Bechtel Hanford, Inc., Richland, Washington.
- BHI-00270, 1996, *Preoperational Baseline and Site Characterization Report for the Environmental Restoration Disposal Facility*, Rev. 2, Bechtel Hanford, Inc., Richland, Washington.
- BHI-01103, 1999, *Clastic Injection Dikes of the Pasco Basin and Vicinity – Geologic Atlas Series*, Rev. 0, Bechtel Hanford, Inc., Richland, Washington.
- BHI-01573, 2001, *Groundwater/Vadose Zone Integration Project - The Application of Feature, Event, and Process Methodology at the Hanford Site*, Rev. 0, Bechtel Hanford, Inc., Richland, Washington.
- Bjornstad, B. N., K. R. Fecht, and C. J. Pluhar, 2001, "Long History of Pre-Wisconsin, Ice Age Cataclysmic Floods: Evidence from Southeastern Washington State," *Journal of Geology*, Vol. 109, pp. 695-713.
- BNWL-243, 1966, *Soil Survey: Hanford Project in Benton County, Washington*, Pacific Northwest Laboratory, Richland, Washington.

- BNWL-1709, 1973, *Collection and Analysis of Pump Test Data for Transmissivity Values*, Pacific Northwest Laboratory, Richland, Washington.
- BNWL-B-360, 1974, *Selected Water Table Contour Maps and Well Hydrographs for the Hanford Reservation, 1944-1973*, BNWL-B-360, Pacific Northwest Laboratory, Richland, Washington.
- Bretz, J. H., H. T. U. Smith, and G.E. Neff, 1956, "Channeled Scabland of Washington: New Data and Interpretations," *Geol. Soc. of Am. Bul.*, Vol. 67, No. 8, pp. 957-1049.
- Bruckler, L., B. C. Ball, and P. Renault, 1989. "Laboratory Estimation of Gas Diffusion Coefficient and Effective Porosity in Soils," *Soil Science*, Vol. 147, pp. 1-10.
- CP-47631, 2011, *Model Package Report: Central Plateau Groundwater Model Version 3.3*, Rev. 0, CH2M HILL Plateau Remediation Company, Richland, Washington.
- CHPRC-00189, 2012, *CH2M HILL Plateau Remediation Company Environmental Quality Assurance Program Plan*, Rev. 9, CH2M HILL Plateau Remediation Company, Richland, Washington.
- Comprehensive Environmental Response, Compensation, and Liability Act of 1980*, 42 USC 9601, et seq., Pub. L. 107-377, December 31, 2002. Available at: <http://epw.senate.gov/cercla.pdf>
- CP-47631, 2011, *Model Package Report: Central Plateau Groundwater Model Version 3.3*, Rev. 0, CH2MHILL Plateau Remediation Company, Richland, Washington.
- CVP-2001-00002, 2001, *Cleanup Verification Package for the 100-F-19:1 and 100-F-19:3 Reactor Cooling Water Effluent Pipelines, 100-F-34 Biology Facility, French Drain, and 116-F-12 French Drain*, Appendix D, "100-F Area Soil Hexavalent Chromium and Carbon-14 Leachability Study Summary Report," Rev. 0, Washington Closure Hanford, Richland, Washington.
- De Smedt, F. and P. J. Wierenga, 1984, "Solute Transfer through Columns of Glass Beads," *Water Resources Research*, Vol. 20, pp. 225-232.
- Deng, H., M. Ye, M.G. Schaap, and R. Khaleel, 2009, "Quantification of Uncertainty in Pedotransfer Function-Based Parameter Estimation for Unsaturated Flow Modeling," *Water Resources Research*, 45, W04409, doi:10.1029/2008WR007477.
- DNFSB 1994, "Recommendation 94-2 to the Secretary of Energy Pursuant to 42 U.S.C. 2286A(5) Atomic Energy Act of 1954, as Amended," letter from J. T. Conway, Chairman, Defense Nuclear Facility Safety Board, Washington, D.C., to H. O'Leary, Secretary, U.S. Department of Energy, Washington, D.C., dated September 8.
- DOE, 1999a, "Disposal Authorization for the Hanford Site Low-Level Waste Disposal Facilities," memorandum from J. J. Fiore and M. W. Frei, U.S. Department of Energy, Headquarters, to R. T. French, U.S. Department of Energy, Office of River Protection, and K. A. Klein, U.S. Department of Energy, Richland Operations Office, U.S. Department of Energy, Washington, D.C.

- DOE, 1999b, *Format and Content Guide for U.S. Department of Energy Low-Level Waste Disposal Facility Performance Assessments and Composite Analyses*, U.S. Department of Energy, Washington, D.C.
- DOE, 1999c, *Low-Level Waste Disposal Facility Federal Review Group Manual*, Rev. 1, U.S. Department of Energy, Washington, D.C.
- DOE, 2001, "Disposal Authorization for the Hanford Site Low-Level Waste Disposal Facilities – Revision 2," memorandum from R. S. Scott, Acting Deputy Assistant Secretary for Project Completion, Office of Environmental Management, to H. L. Boston, Manager, Office of River Protection, and K. A. Klein, Manager, Department of Energy, Richland Operations Office, U.S. Department of Energy, Washington, D.C., November 1.
- DOE G 435.1-1, 1999, *Implementation Guide for Use with DOE M 435.1-1*, U.S. Department of Energy, Washington, D.C. Available at:
<https://www.directives.doe.gov/directives/current-directives/435.1-EGuide-1ch1/view>
- DOE M 435.1-1, 1999, *Radioactive Waste Management Manual*, U.S. Department of Energy, Washington, D.C. Available at:
<https://www.directives.doe.gov/directives/0435.1-DManual-1admchg2/view>
- DOE O 414.1D, 2011, *Quality Assurance*, U.S. Department of Energy, Washington, D.C. Available at:
<https://www.directives.doe.gov/directives/0414.1-BOrder-d/view>
- DOE O 435.1, 1999, *Radioactive Waste Management*, U.S. Department of Energy, Washington, D.C. Available at:
<https://www.directives.doe.gov/directives/0435.1-BOrder-c1/view>
- DOE Order 5820.2A, *Radioactive Waste Management*, U.S. Department of Energy, Washington, D.C. Superseded by DOE O 435.1.
- DOE/EIS-0113, 1987, *Final Environmental Impact Statement Disposal of Hanford Defense High-Level, Transuranic and Tank Wastes: Hanford Site Richland, Washington*, 5 vols., U.S. Department of Energy, Washington, D.C. Available at:
<http://www5.hanford.gov/arpir/?content=findpage&AKey=D3829331>
<http://www5.hanford.gov/arpir/?content=findpage&AKey=D3829572>
<http://www5.hanford.gov/arpir/?content=findpage&AKey=D3829769>
<http://www5.hanford.gov/arpir/?content=findpage&AKey=D3829970>
<http://www5.hanford.gov/arpir/?content=findpage&AKey=D3830231>
<http://www5.hanford.gov/arpir/?content=findpage&AKey=D3830468>
<http://www5.hanford.gov/arpir/?content=findpage&AKey=D3834099>
<http://www5.hanford.gov/arpir/?content=findpage&AKey=D3834352>
<http://www5.hanford.gov/arpir/?content=findpage&AKey=D3834497>
<http://www5.hanford.gov/arpir/?content=findpage&AKey=D3834724>
<http://www5.hanford.gov/arpir/?content=findpage&AKey=D3834979>
- DOE/EIS-0222-F, 1999, *Final Hanford Comprehensive Land-Use Plan Environmental Impact Statement*, U.S. Department of Energy, Washington, D.C. Available at:
<http://www5.hanford.gov/arpir/?content=findpage&AKey=D199158842>

<http://www5.hanford.gov/arpir/?content=findpage&AKey=D199158843>
<http://www5.hanford.gov/arpir/?content=findpage&AKey=D199158844>
<http://www5.hanford.gov/arpir/?content=findpage&AKey=D199158845>
<http://www5.hanford.gov/arpir/?content=findpage&AKey=D199158846>
<http://www5.hanford.gov/arpir/?content=findpage&AKey=D199158847>

DOE/EIS-0222-SA-01, 2008, *Supplement Analysis: Hanford Comprehensive Land-Use Plan Environmental Impact Statement*, U.S. Department of Energy, Richland Operations Office, Richland, Washington. Available at:
http://www.hanford.gov/files.cfm/SAwith_signed-R1.pdf

DOE/EIS-0286F, 2004, *Final Hanford Site Solid (Radioactive and Hazardous) Waste Program Environmental Impact Statement*, Richland, Washington, U.S. Department of Energy, Richland Operations Office, Richland, Washington.

DOE/EIS-0391, 2012, *Final Tank Closure and Waste Management Environmental Impact Statement for the Hanford Site, Richland, Washington (TC & WM EIS)*, U.S. Department of Energy, Richland Operations Office, Richland, Washington. Available at:
<http://www.hanford.gov/page.cfm/FinalTCWMEIS>

DOE/ORP-2000-24, 2001, *Hanford Immobilized Low-Activity Waste Performance Assessment: 2001 Version*, Rev. 0, U.S. Department of Energy, Office of River Protection, Richland, Washington. Available at:
<http://www2.hanford.gov/arpir/?content=findpage&AKey=D8862887>
<http://www2.hanford.gov/arpir/?content=findpage&AKey=D8862892>

DOE/ORP-2005-01, 2006, *Initial Single-Shell Tank System Performance Assessment for the Hanford Site*, Rev. 0, U.S. Department of Energy, Office of River Protection, Richland, Washington. Available at:
http://www.hanford.gov/orp/uploadfiles/1_DOE-ORP-2005-01_ChapES-Chap1.pdf
http://www.hanford.gov/orp/uploadfiles/2_DOE-ORP-2005-01_Chap2a.pdf
http://www.hanford.gov/orp/uploadfiles/3_DOE-ORP-2005-01_Chap2b.pdf
http://www.hanford.gov/orp/uploadfiles/4_DOE-ORP-2005-01_Chap3.pdf
http://www.hanford.gov/orp/uploadfiles/5_DOE-ORP-2005-01_Chap4-7.pdf
http://www.hanford.gov/orp/uploadfiles/6_DOE-ORP-2005-01_Appendices.pdf

DOE/RL-91-45, 1995, *Hanford Site Risk Assessment Methodology*, Rev. 3, U.S. Department of Energy, Richland Operations Office, Richland, Washington.

DOE/RL-92-94, 1994, *Hanford Site Background: Part 1, Soil Background for Nonradioactive Analytes*, Rev. 2, 2 vols., U.S. Department of Energy, Richland Operations Office, Richland, Washington.

DOE/RL-93-33, 1996, *Focused Feasibility Study of Engineered Barriers for Waste Management Units in the 200 Areas*, Rev. 1, U.S. Department of Energy, Richland Operations Office, Richland, Washington. Available at:
<http://www5.hanford.gov/arpir/?content=findpage&AKey=D197226618>

- DOE/RL-93-99, 1994, *Remedial Investigation and Feasibility Study Report for the Environmental Restoration Disposal Facility*, Rev. 1, U.S. Department of Energy, Richland Operations Office, Richland, Washington. Available at:
<http://www5.hanford.gov/arpir/?content=findpage&AKey=D196061256>
- DOE/RL-94-47, 1994, *Proposed Plan for the Environmental Restoration Disposal Facility (ERDF) at the Hanford Site, Richland, Washington*, Rev. 1, U.S. Department of Energy Richland Operations Office, Richland, Washington. Available at:
http://www5.hanford.gov/pdw/fsd/AR/FSD0001/FSD0034/D196061217/D196061217_5998_14.pdf
- DOE/RL-95-55, 1995, *Hanford Site Background: Evaluation of Existing Soil Radionuclide Data*, Rev. 0, U.S. Department of Energy, Richland Operations Office, Richland, Washington.
- DOE/RL-96-12, 1996, *Hanford Site Background: Part 2, Soil Background for Radionuclides*, Rev. 0, U.S. Department of Energy, Richland Operations Office, Richland, Washington. Available at:
<http://www5.hanford.gov/arpir/index.cfm?content=findpage&AKey=D1808987>
- DOE/RL-96-17, 2009, *Remedial Design Report/Remedial Action Work Plan for the 100 Area*, Rev. 6, U.S. Department of Energy, Richland Operations Office, Richland, Washington. Available at: <http://www5.hanford.gov/arpir/?content=findpage&AKey=0810240391>.
- DOE/RL-2000-29, 2003, *Maintenance Plan for the Composite Analysis of the Hanford Site, Southeast Washington*, Rev. 2, U.S. Department of Energy, Richland Operations Office, Richland, Washington.
- DOE/RL-2001-54, 2005, *Central Plateau Ecological Evaluation*, Rev. 0, U.S. Department of Energy, Richland Operations Office, Richland, Washington.
- DOE/RL-2002-39, 2002, *Standardized Stratigraphic Nomenclature for the Post-Ringold-Formation Sediments Within the Central Pasco Basin*, Rev. 0, U.S. Department of Energy, Richland Operations Office, Richland, Washington.
- DOE/RL-2007-28, 2008, *Feasibility Study for the 200-ZP-1 Operable Unit*, U.S. Department of Energy, Richland Operations Office, Richland, Washington
- DOE/RL-2007-50, 2011, *Central Plateau Ecological Risk Assessment Data Package Report*, Rev. 1, U.S. Department of Energy, Richland Operations Office, Richland, Washington. Available at:
<http://www5.hanford.gov/arpir/index.cfm?content=findpage&AKey=1108100554>
- DOE/RL-2009-10, 2010, *Hanford Site Cleanup Completion Framework*, Rev. 0, U.S. Department of Energy, Richland Operations Office, Richland, Washington. Available at: <http://www5.hanford.gov/arpir/?content=findpage&AKey=1008190506>
- DOE/RL-2011-50, 2012, *Regulatory Basis and Implementation of a Graded Approach to Evaluation of Groundwater Protection*, Rev. 1, U.S. Department of Energy, Richland Operations Office, Richland, Washington. Available at:
<http://www5.hanford.gov/arpir/?content=findpage&AKey=0093361>

- DOE/RL-2011-56, 2011, *Hanford Site Third CERCLA Five-Year Review Report*, Rev. 0, U.S. Department of Energy, Richland Operations Office, Richland, Washington. Available at: http://www.hanford.gov/files.cfm/DOE-RL-2011-56_Hanford_3rd_CERCLA_5-Yr_Review_Rpt_11-4-11.pdf
- DOE/RL-2011-118, 2012, *Hanford Site Groundwater Monitoring for 2011*, Rev. 0, U.S. Department of Energy, Richland Operations Office, Richland, Washington. Available at: <http://www.hanford.gov/c.cfm/sgrp/GWRep11/html/start11.htm>
- DOE/RL-2012-19, 2012, *Radionuclide Air Emissions Report for the Hanford Site, Calendar Year 2011*, Rev. 0, U.S. Department of Energy, Richland Operations Office, Richland, Washington.
- DOE/RW-0070, 1986, *Environmental Assessment: Reference Repository Location, Hanford Site, Washington*, Vols. I – III, U.S. Department of Energy, Washington, D.C. Available at: <http://www5.hanford.gov/arpir/?content=findpage&AKey=D195059580>
<http://www5.hanford.gov/arpir/?content=findpage&AKey=D195059591>
<http://www5.hanford.gov/arpir/?content=findpage&AKey=D195059645>
- DOE/RW-0164, 1988, *Site Characterization Plan: Reference Repository Location, Hanford Site, Washington*, 9 vols., Consultation Draft, U.S. Department of Energy, Washington, D.C. Available at: <http://www5.hanford.gov/arpir/?content=findpage&AKey=D196007701>
<http://www5.hanford.gov/arpir/?content=findpage&AKey=D196007769>
<http://www5.hanford.gov/arpir/?content=findpage&AKey=D196007788>
<http://www5.hanford.gov/arpir/?content=findpage&AKey=D196007871>
<http://www5.hanford.gov/arpir/?content=findpage&AKey=D196007870>
<http://www5.hanford.gov/arpir/?content=findpage&AKey=D196007876>
<http://www5.hanford.gov/arpir/?content=findpage&AKey=D196007901>
<http://www5.hanford.gov/arpir/?content=findpage&AKey=D196007935>
<http://www5.hanford.gov/arpir/?content=findpage&AKey=D196027182>
- DOE-STD-1196-2011, *Derived Concentration Technical Standard*, U.S. Department of Energy, Washington, D.C.
- Dronen, V. R., 1996, "Environmental Restoration Disposal Facility CERCLA/DOE Order 5820.2a Roadmap," letter to O. Robertson, U.S. Department of Energy, Richland Operations Office, Richland, Washington, from V. R. Dronen, Bechtel Hanford, Inc., Richland, Washington, November 8.
- Ecology, EPA, and DOE, 1989, *Hanford Federal Facility Agreement and Consent Order*, 2 vols., as amended, Washington State Department of Ecology, U.S. Environmental Protection Agency, and U.S. Department of Energy, Olympia, Washington. Available at: <http://www.hanford.gov/?page=81>
- EM-QA-001, 2012, *Environmental Management (EM) Quality Assurance Program (QAP)*, Rev. 1, Attachment G – *Software Quality Requirements*; Attachment H – *Model Development, Use, and Validation*, U.S. Department of Energy, Office of Environmental Management, Washington, D.C.

-
- Environment Agency, 2004, *The Likely Medium to Long-term Generation of Defects in Geomembrane Liners*, R&D Technical Report P1-500/1/TR, Almondsbury, Bristol, United Kingdom.
- EPA, 1999, *Data Collection for the Hazardous Waste Identification Rule*.
<http://www.epa.gov/osw/hazard/wastetypes/wasteid/hwirwste/risk.htm>
- EPA, 2010, EPA On-line Tools for Site Assessment Calculation,
<http://www.epa.gov/athens/learn2model/part-two/onsite/estdiffusion-ext.html>. Web site updated January 2012.
- EPA, 2012, User's Guide for Preliminary Remediation Goals for Radionuclides, http://epa-prgs.ornl.gov/radionuclides/prg_guide.html
- EPA/240/B-01/003, 2001, *EPA Requirements for Quality Assurance Project Plans*, EPA QA/R-5, U.S. Environmental Protection Agency, Office of Environmental Information, Washington, D.C.
- EPA/240/R-02/007, 2002, *Guide for Quality Assurance Project Plans for Modeling*, EPA QA/G-5M, U.S. Environmental Protection Agency, Office of Environmental Information, Washington, D.C.
- EPA-402-R-00-004, 2007, *Updated User's Guide For CAP88-PC Version 3.0*, U.S. Environmental Protection Agency, December 2007 (currently available at <http://www.epa.gov/radiation/assessment/CAP88/index.html>)
- EPA/402/R-93/081, 1993, *External Exposure to Radionuclides in Air, Water, and Soil*, Federal Guidance Report 12, prepared by the Oak Ridge National Laboratory for the Office of Radiation and Indoor Air, U.S. Environmental Protection Agency, Washington, D.C.
- EPA 402-R-94-012, 1994, *Technical Guide to Ground-Water Model Selection at Sites Contaminated with Radioactive Substances*, U.S. Environmental Protection Agency, Washington, D.C. Available at:
<http://www.epa.gov/radiation/docs/assessment/402-r-94-012.pdf>
- EPA-402-R-99-004B, 1999, *Understanding Variation in Partition Coefficient, K_d , Values*, Volume II, U.S. Environmental Protection Agency, Office of Solid Waste and Emergency Response, Washington, D.C. Available at:
<http://www.epa.gov/rpdweb00/docs/kdreport/vol2/402-r-99-004b.pdf>
- EPA 530-R-05-006, 2005, *Human Health Risk Assessment Protocol for Hazardous Waste Combustion Facilities, Final*, U.S. Environmental Protection Agency, Washington, D.C. Available at: <http://www.epa.gov/osw/hazard/tsd/td/combust/riskvol.htm#volume1>
- EPA/540/F-95/041, 1996, *Soil Screening Guidance: Fact Sheet*, U.S. Environmental Protection Agency, Office of Solid Waste and Emergency Response, Washington, D.C.
- EPA/540/R-96/018, 1996, *Soil Screening Guidance: User's Guide*, Second Edition, Publication 9355.4-23, U.S. Environmental Protection Agency, Office of Environmental Information, Washington, D.C. Available at:
<http://www.epa.gov/superfund/health/conmedia/soil/pdfs/ssg496.pdf>

- EPA 542-F-11-001, 2011, *Fact Sheet on Evapotranspiration Cover Systems for Waste Containment*, U.S. Environmental Protection Agency, Washington, D.C.
- EPA/600/2-91/065, 1991, *The RETC Code for Quantifying the Hydraulic Functions of Unsaturated Soils*, U.S. Environmental Protection Agency, Washington, D.C.
- EPA/600/P-95/002Fa, *Exposure Factors Handbook*, U.S. Environmental Protection Agency, Washington, D.C. Available at:
http://cfpub.epa.gov/ols/catalog/catalog_display.cfm?&FIELD1=SUBJECT&INPUT1=Hazardous%20substances%20Risk%20assessment%20Handbooks%20manuals%20etc.&TYPE1=EXACT&item_count=14
- EPA/600/R-02/099, 2002, *Assessment and Recommendations for Improving the Performance of Waste Containment Systems*, U.S. Environmental Protection Agency, Office of Research and Development, Cincinnati, Ohio. Available at: <http://tiny.cc/j1hfiw>
- EPA/600/R-05/074, 2005, *Partition Coefficients for Metals in Surface Water, Soil, and Waste*, U.S. Environmental Protection Agency, Office of Research and Development, Washington, D.C. Available at:
<http://www.epa.gov/athens/publications/reports/Ambrose600R05074PartitionCoefficients.pdf>
- EPA/600/R-08/058, 2008, *FOOTPRINT (A Screening Model for Estimating the Area of a Plume Produced from Gasoline Containing Ethanol), Version 1*, U.S. Environmental Protection Agency, Office of Research and Development, National Risk Management Research Laboratory, Ada, Oklahoma.
- EPA/AMD/R10-02/030, 2002, *Record of Decision Amendment: U.S. Department of Energy Environmental Restoration Disposal Facility Hanford Site – 200 Area Benton County, Washington*, U.S. Environmental Protection Agency, Region 10, Washington State Department of Ecology, and U.S. Department of Energy, Seattle, Washington. Available at: <http://www.epa.gov/superfund/sites/rods/fulltext/a1002030.pdf>
- EPA/AMD/R10-97/101, 1997, *Record of Decision Amendment: U.S. Department of Energy Environmental Restoration Disposal Facility Hanford Site – 200 Area Benton County, Washington*, U.S. Environmental Protection Agency, Region 10, Washington State Department of Ecology, and U.S. Department of Energy, Seattle, Washington. Available at: <http://www.epa.gov/superfund/sites/rods/fulltext/a1097101.pdf>
- EPA/AMD/R10-99/038, 1999, *Record of Decision Amendment: U.S. Department of Energy Environmental Restoration Disposal Facility Hanford Site – 200 Area Benton County, Washington*, U.S. Environmental Protection Agency, Region 10, Washington State Department of Ecology, and U.S. Department of Energy, Seattle, Washington. Available at: <http://www.epa.gov/superfund/sites/rods/fulltext/a1099038.pdf>
- EPA/ESD/R10-96/145, 1996, *Explanation of Significant Differences: USDOE Environmental Restoration Disposal Facility, Hanford Site, Benton County, Washington*, U.S. Environmental Protection Agency, Washington State Department of Ecology, and U.S. Department of Energy, Seattle, Washington. Available at:
<http://www.epa.gov/superfund/sites/rods/fulltext/e1096145.pdf>

- EPA/ROD/200CW-PW, 2011, *Declaration of the Record of Decision for USDOE Hanford 200 Area 200-CW-5 and 200-PW-1, 200-PW-3, and 200-PW-6 Operable Units, Hanford Site, Benton County, Washington*, U.S. Environmental Protection Agency, Washington State Department of Ecology, and U.S. Department of Energy, Seattle, Washington. Available at: http://www.epa.gov/region10/pdf/sites/hanford/200/hanford_200_rod.pdf
- EPA/ROD/200UP1, 2012, *Declaration of the Record of Decision for Interim Remedial Action USDOE Hanford 200 Area 200-UP-1 Operable Unit, Hanford Site, Benton County, Washington*, U.S. Environmental Protection Agency, Washington State Department of Ecology, and U.S. Department of Energy, Seattle, Washington. Available at: http://www.epa.gov/region10/pdf/sites/hanford/200/Hanford_200_Area_Interim_ROD_Re_medial_Action_0912.pdf
- EPA/ROD/200ZP1, 2008, *Declaration of the Record of Decision for USDOE Hanford 200 Area 200-ZP-1 Operable Unit, Hanford Site, Benton County, Washington*, U.S. Environmental Protection Agency, Washington State Department of Ecology, and U.S. Department of Energy, Seattle, Washington. Available at: [http://yosemite.epa.gov/r10/CLEANUP.NSF/sites/hanford2/\\$FILE/Hanford-200-ZP-1-ROD.pdf](http://yosemite.epa.gov/r10/CLEANUP.NSF/sites/hanford2/$FILE/Hanford-200-ZP-1-ROD.pdf)
- EPA/ROD/R10-95/100, 1995, *Declaration of the Record of Decision for USDOE Environmental Restoration Disposal Facility, Hanford Site, Benton County, Washington*, U.S. Environmental Protection Agency, Washington State Department of Ecology, and U.S. Department of Energy, Olympia, Washington. Available at: <http://www.epa.gov/superfund/sites/rods/fulltext/r1095100.pdf>
- EPA-SAB-RAC-ADV-99-006, 1999, *AN SAB ADVISORY: Modeling of Radionuclide Releases from Disposal of Low Activity Mixed Waste*, U.S. Environmental Protection Agency, Washington, D.C. Available at: [http://yosemite.epa.gov/sab/sabproduct.nsf/95eac6037dbec075852573a00075f732/fa83e4afdc6f145085257193005937af/\\$FILE/raca9906.pdf](http://yosemite.epa.gov/sab/sabproduct.nsf/95eac6037dbec075852573a00075f732/fa83e4afdc6f145085257193005937af/$FILE/raca9906.pdf)
- ERDA, 1975, *Final Environmental Impact Statement: Waste Management Operations, Hanford Reservation, Richland, Washington*, ERDA-1538, Energy, Research, and Development Administration, Richland, Washington.
- Executive Order 12580, *Superfund Implementation*, EH-231-015/0593, Information Brief, May 1993.
- Fayer, M. J., G. W. Gee, M. L. Rockhold, M. D. Freshley, and T. B. Walters, 1996, "Estimating Recharge Rates for a Groundwater Model Using a GIS," *Journal of Environmental Quality*, Vol. 25, pp. 510-518.
- Fecht, K. R., S. P. Reidel, and A. M. Tallman, 1987, "Paleodrainage of the Columbia River System on the Columbia Plateau of Washington State – A Summary," Washington Division of Geology and Earth Resources Bulletin 77, Washington State Department of Natural Resources, Olympia, Washington.
- Gardner, W. R., 1958, "Some Steady-State Solutions of the Unsaturated Moisture Flow Equation with Applications to Evaporation from a Water Table," *Soil Science*, Vol. 85, pp. 228-232.

- Gee, G. W., M. J. Fayer, M. L. Rockhold, and M. D. Campbell, 1992, "Variations in Recharge at the Hanford Site," *Northwest Science*, Vol. 66, pp. 237-250. Available at: http://www.vetmed.wsu.edu/org_nws/NWSci%20journal%20articles/1992%20files/Issue%204/v66%20p237%20Gee%20et%20al.PDF.
- Gelhar, L. W., 1993, *Stochastic Subsurface Hydrology*, Prentice Hall, New York, New York.
- Gelhar, L. W., C. Welty, and K. R. Rehfeldt, 1992, "A Critical Review of Data on Field Scale Dispersion in Aquifers," *Water Resources Research*, Vol. 28, pp. 1955-1974.
- Giroud, J. P., 1997, "Equations for Calculating the Rate of Liquid Migration Through Composite Liners Due to Geomembrane Defects," *Geosynthetics International*, Vol. 4, Nos. 3-4, pp. 335-348.
- Giroud, J. P., R. Bonaparte, and J. A. McKelvey, 1997, "Leachate Flow in Leakage Collection Layers Due to Geomembrane Defects", *Geosynthetics International*, Vol. 4, Nos. 3-4, pp. 215-292.
- GoldSim Technology Group, 2009a, *GoldSim User's Guide*, GoldSim Technology Group, Issaquah, Washington.
- GoldSim Technology Group, 2009b, *User's Guide: GoldSim Contaminant Transport Module*, GoldSim Technology Group, Issaquah, Washington.
- Hall, E. R., 1981, *The Mammals of North America*, John Wiley and Sons, New York, New York.
- Harr, M. E., 1987, *Reliability-Based Design in Civil Engineering*, McGraw-Hill, New York, New York.
- Haynes, W. M. and D. R. Lide, eds., 2011, *CRC Handbook of Chemistry and Physics*, 92nd Edition, CRC Press, Boca Raton, Florida.
- HFSUWG, 1992a, *The Future for Hanford: Uses and Cleanup, Summary of the Final Report of the Hanford Future Site Uses Working Group*, Hanford Future Site Uses Working Group, Westinghouse Hanford Company, Richland, Washington.
- HFSUWG, 1992b, *The Future for Hanford: Uses and Cleanup, The Final Report of the Hanford Future Site Uses Working Group*, Hanford Future Site Uses Working Group, Westinghouse Hanford Company, Richland, Washington.
- HMS, 2012, Hanford Meteorological Station Web Site, U.S. Department of Energy, Richland Operations Office, Richland Washington. Available at: <http://www.hanford.gov/page.cfm/HMS>
- HNF-5294, 1999, *Computer Code Selection Criteria for Flow and Transport Code(s) to Be Used in Vadose Zone Calculations for Environmental Analyses in the Hanford Site's Central Plateau*, Rev. 0, CH2M HILL Hanford Group, Inc., Richland, Washington. Available at: <http://www2.hanford.gov/arpir/?content=findpage&AKey=0911240802>

- HNF-5507, 2000, *Subsurface Conditions Description for the B-BX-BY Waste Management Area*, Rev. 0A, CH2M HILL Hanford Group, Inc., Richland, Washington. Available at: <http://www5.hanford.gov/arpir/?content=findpage&AKey=0911240519>
- HNF-SD-WM-TI-707, 2007, *Exposure Scenarios and Unit Factors for the Hanford Tank Waste Performance Assessment*, Rev. 5, CH2M HILL Hanford Group, Inc., Richland, Washington.
- Huyakorn, P.S. and S. Panday, 1992, *VAM3DCG: A Variably Saturated Analysis Model in Three Dimensions with Preconditioned Conjugate Gradient Matrix Solvers – Documentation and User's Guide, Version 2.4*, HydroGeologic, Inc., Herndon, Virginia.
- IAEA, 1994, *Handbook of Parameter Values for the Prediction of Radionuclide Transfer in Temperate Environments*, Technical Reports Series No. 364, International Atomic Energy Agency, Vienna, Austria.
- IAEA, 2010, *Handbook of Parameter Values for the Prediction of Radionuclide Transfer in Terrestrial and Freshwater Environments*, Technical Reports Series No. 472, International Atomic Energy Agency, Vienna, Austria.
- ICRP, 1994, *Human Respiratory Tract Model for Radiological Protection*, Publication 66, International Commission on Radiological Protection.
- INEEL/EXT-01-00273, 2006, *Biological Data to Support Operable Unit 7-13/14 Modeling of Plant and Animal Intrusion at Buried Waste Sites*, Revision 1, Project No. 23378. January 2006, 60pp.
- INEEL/EXT-04-01793, 2004, *Multiphase Carbon-14 Transport in a Near-Field-Scale Unsaturated Column of Natural Sediments*, Idaho National Engineering and Environmental Laboratory, Bechtel BWXT Idaho, LLC, Idaho Falls, Idaho.
- Jin, Y. and W. A. Jury, 1996. "Characterizing the Dependence of Gas Diffusion Coefficient on Soil Properties," *Soil Science Society of America Journal*, Vol. 60, pp. 66–71.
- Jury, W. A. and R. Horton, 2004, *Soil Physics*, Wiley and Sons, Inc., Hoboken, New Jersey, 370 p.
- Karimi, A. A., W. J. Farmer, and M. M. Cliath, 1987, "Vapor Phase Diffusion of Benzene in Soil," *J. Environ. Qual.* Vol. 16, pp. 38–43.
- Khaleel, R. and J. F. Relyea, 1997, "Correcting Laboratory-Measured Moisture Retention Data for Gravels," *Water Resources Research*, Vol. 33(8), p. 1875, doi:[10.1029/97WR01068](https://doi.org/10.1029/97WR01068).
- Khaleel, R., J. F. Relyea, and J. L. Conca, 1995, "Evaluation of van Genuchten-Mualem Relationships to Estimate Unsaturated Conductivity at Low Water Contents," *Water Resources Research*, Vol. 31, No. 11, pp. 2659-2668.
- Khaleel R., T.-C.J. Yeh, and Z. Lu, 2002, "Upscaled Flow and Transport Properties for Heterogeneous Unsaturated Media," *Water Resources Research*, Vol. 38(5), p. 1053, doi:[10.1029/2000WR000072](https://doi.org/10.1029/2000WR000072).

- Klein, K. A., 2000, "Environmental Restoration Disposal Facility (ERDF) Crosswalk to DOE Order 435.1 Requirements," letter to J. J. Fiore and M. W. Frei, U.S. Department of Energy, Richland Operations Office, Richland, Washington, from K. A. Klein, U.S. Department of Energy, Richland Operations Office, Richland, Washington, July 17.
- Klute, A., 1986, "Water Retention: Laboratory Methods," in *Methods of Soil Analysis*, part I, edited by A. Klute, pp. 635–660, *American Society of Agronomy*, Madison, Wisconsin.
- Klute, A. and C. Dirksen, 1986, "Hydraulic Conductivity and Diffusivity: Laboratory Methods," in *Methods of Soil Analysis*, part I, edited by A. Klute, pp. 687–734, *American Society of Agronomy*, Madison, Wisconsin.
- Koerner, R. M. and Y. G. Husan, 2003 "Lifetime Prediction of Polymeric Geomembranes Used in New Dam Construction and Dam Rehabilitation," in *Proceedings of the Association of State Dam Safety Officials Conference*, Lake Harmony, Pennsylvania.
- Leary, K. D., 1990, "Analysis of Techniques for Estimating Potential Recharge and Shallow Unsaturated Zone Water Balance near Yucca Mountain," M.S. Thesis, University of Nevada, Reno, Nevada, 334 pages.
- Lindsey, K. A., 1991, *Revised Stratigraphy for the Ringold Formation, Hanford Site, South-Central Washington*, WHC-SD-EN-EE-004, Westinghouse Hanford Company, Richland, Washington.
- Lindsey, K. A., 1995, *Miocene- to Pliocene-Aged Suprabasalt Sediments of the Hanford Site, South-Central Washington*, BHI-00184, Rev. 00, Bechtel Hanford, Inc., Richland, Washington.
- Lindsey, K. A., 1996, "The Miocene to Pliocene Ringold Formation and Associated Deposits of the Ancestral Columbia River System, South-Central Washington and North-Central Oregon," Washington Division of Geology and Earth Resources Open File Report 96-8, Washington State Department of Natural Resources, Olympia, Washington.
- Liu, G., B. Li, K. Hu, and M.T. van Genuchten, 2006, "Simulating the Gas Diffusion Coefficient in Macropore Network Images: Influence of Soil Pore Morphology," *Soil Science Society of America Journal*, Vol. 70, pp.1252–1261.
- Luftig, S. D. and L. Weinstock, 1997, "Establishment of Cleanup Levels for CERCLA Sites with Radioactive Contamination" (memorandum to Addressees), OSWER No. 9200.4-18, Office of Emergency and Remedial Response and Office of Radiation and Indoor Air, U.S. Environmental Protection Agency, Washington, D.C., August 22. Available at: <http://www.epa.gov/oerrpage/superfund/health/contaminants/radiation/pdfs/radguide.pdf>
- Lupher, R. L., 1944, "Clastic Dikes of the Columbia Basin Region, Washington and Idaho," *Geological Society of America Bulletin*, Vol. 55, pp. 1431-1462.
- Malde, H. E., 1968, *The Catastrophic Late Pleistocene Bonneville Flood in the Snake River Plain, Idaho*, Professional Paper 596, U.S. Geological Survey, Washington, D.C.

- Mallants, D., A. Espino, M. Van Hoorick, J. Feyen, N. Vandenberghe, and W. Loy, 2000, "Dispersivity Estimates from a Tracer Experiment in a Sandy Aquifer," *Ground Water*, Vol. 38(2), pp. 304-310.
- Mishra, S., 2002, "Assigning Probability Distributions to Input Parameters of Performance Assessment Models," SKB Technical Report TR-02-11, Swedish Nuclear Fuel and Waste Management Co., Stockholm, 49 p.
- Millington, R.J. and J.M. Quirk, 1960. "Transport in porous media," pp. 97-106. In F. A. Van Beren et al. (ed.), *Trans. 7th Int. Congr. Soil Sci.*, Vol. 1, Madison, Wisconsin, 14-24 August 1960, Elsevier, Amsterdam.
- Millington, R. J. and J. P. Quirk, 1961, "Permeability of Porous Solids," *Trans. Faraday Soc.*, Vol. 57, pp. 1200-1207.
- Moldrup, P., T. Oleson, S. Yoshikawa, T. Komatsu, and D. E. Rolston, 2004. "Three-Porosity Model for Predicting The Gas Diffusion Coefficient in Undisturbed Soil," *Soil Science Society of America Journal*, Vol. 68, pp. 750-759.
- Moldrup, P., S. Yoshikawa, T. Olesen, T. Komatsu, and D. E. Rolston, 2003. "Gas Diffusivity in Undisturbed Volcanic Ash Soils: Test of Soil-Water-Characteristic-Based Prediction Models," *Soil Science Society of America Journal*, Vol. 67, pp. 41-51.
- Mualem, Y., 1976, "A New Model for Predicting the Hydraulic Conductivity of Unsaturated Porous Media," *Water Resources Research*, Vol. 12, No. 3, pp. 513-522.
- Murray C. J., A. L. Ward, and J. Wilson, 2007. "Influence of Clastic Dikes on Vertical Migration of Contaminants at the Hanford Site," *Vadose Zone Journal*, Vol. 6(4), pp. 959-970. doi:10.2136/vzj2007.0004
- National Nuclear Data Center, "NuDat 2.1 database," Brookhaven National Laboratory. <http://www.nndc.bnl.gov/nudat2/>. Retrieved October 2012.
- Nazaroff, W. W. and A. V. Nero, 1988, *Radon and Its Decay Products in Indoor Air*, John Wiley & Sons, New York, New York.
- NBS Handbook 69, 1963, *Maximum Permissible Body Burdens and Maximum Permissible Concentrations of Radionuclides in Air or Water for Occupational Exposure*, National Bureau of Standards, U.S. Department of Commerce, Washington, D.C.
- NCRP, 1987, *Ionizing Radiation Exposure of the Population of the United States*, Report No. 93, National Council on Radiation Protection, Bethesda, Maryland.
- NCRP, 1999, *Recommended Screening Limits for Contaminated Surface Soil and Review of Factors Relevant to Site-Specific Studies*, Report No. 129, National Council on Radiation Protection and Measurements, Bethesda, Maryland.
- Newcomb, R. C., 1958, "Ringold Formation of Pleistocene Age in Type Locality, the White Bluffs, Washington," *American Journal of Science*, Vol. 256, pp. 328-340.

- Newcomb, R. C., 1962, "Hydraulic Injection of Clastic Dikes in the Touchet Beds, Washington, Oregon, and Idaho," *Geological Society of the Oregon Country Geological Newsletter*, Vol. 28(10), p. 70.
- Newcomb, R. C., J. R. Strand, and F. J. Frank, 1972, *Geology and Ground-Water Characteristics of the Hanford Reservation of the U.S. Atomic Energy Commission*, Washington, Professional Paper 717, U.S. Geological Survey, Washington, D.C.
- Nkedi-Kizza, P., J. W. Biggar, M. T. van Genuchten, P. J. Wierenga, H. M. Selim, J. M. Davidson, and D. R. Nielsen, 1983, "Modeling Tritium and Chloride 36 Transport Through an Aggregated Oxisol," *Water Resources Research*, Vol. 19, pp. 691-700.
- NUREG-1573, 2000, *A Performance Assessment Methodology for Low-Level Radioactive Waste Disposal Facilities: Recommendations of NRC's Performance Assessment Working Group*, U.S. Nuclear Regulatory Commission, Washington, D.C.
- NUREG/CR-4122, 1985, *A FORTRAN Program and User's Guide for the Calculations of Partial Correlation and Standardized Regression Coefficients*, SAND85-0044, U.S. Nuclear Regulatory Commission, Washington, D.C.
- NUREG/CR-4461, 2007, *Tornado Climatology of the Contiguous United States*, Revision 2, U.S. Nuclear Regulatory Commission, Washington, D.C.
- NUREG/CR-5512, 1992, *Residual Radioactive Contamination from Decommissioning: Technical Basis for Translating Contamination Levels to Annual Total Effective Dose Equivalent*, Vol. 1, U.S. Nuclear Regulatory Commission, Washington, D.C.
- O'Connor, J. E., 1993, "Hydrology, Hydraulics, and Geomorphology of the Bonneville Flood," *Geol. Soc. Am. Spec. Paper*, Vol. 274, p.83.
- O'Connor, J. E. and V.R. Baker, 1992, "Magnitudes and Implications of Peak Discharges from Glacial Lake Missoula," *Geological Society of America Bulletin*, Vol. 104, No. 3, pp. 267-279.
- Obermeier, S. F., 1996, "Use of Liquefaction-Induced Features for Seismic Analysis – An Overview of How Seismic Liquefaction Features Can be Distinguished from Other Features and How Their Regional Distribution and Properties of Source Sediment Can be Used to Infer the Location and Strength of Holocene Paleo-Earthquakes," *Engineering Geology*, Vol. 44, pp. 1-76.
- OFM, 2011, *2010 Census*, Washington State Office of Financial Management, Olympia, Washington. Available at: <http://www.ofm.wa.gov/pop/april1/>
- OSWER Directive 9285.6-03, 1991, *Risk Assessment for Superfund, Volume 1: Human Health Evaluation Manual Supplemental Guidance - "Standard Default Exposure Factors"* (Interim Final), PB91-921314, U.S. Environmental Protection Agency, Washington, D.C. Available at: http://www.epa.gov/oswer/riskassessment/pdf/oswer_directive_9285_6-03.pdf
- Pasquill, F., 1961, "The Estimation of the Dispersion of Windborne Material," *The Meteorological Magazine*, Vol. 90, No. 1063, pp. 33-49.

-
- Petersen, S. W., 2005, *Silt Borrow Source Field Investigation Report*, D&D-25575, Rev. 0, Fluor Hanford, Inc., Richland, Washington.
- Plummer, M. A., L. C. Hull, and D. T. Fox, 2004, "Transport of Carbon-14 in a Large Unsaturated Soil Column," *Vadose Zone Journal*, Vol. 3, pp. 109-121.
- PNL-2774, 1979, *Characterization of the Hanford 300 Area Burial Grounds: Task IV – Biological Transport*, Pacific Northwest Laboratory, Richland, Washington.
- PNL-5247, 1985, *Rooting Depth and Distributions of Deep-Rooted Plants in the 200 Area Control Zone of the Hanford Site*, Pacific Northwest Laboratory, Richland, Washington.
- PNL-5289, 1984, *Investigation of Ground-Water Seepage from the Hanford Shoreline of the Columbia River*, Pacific Northwest Laboratory, Richland, Washington. Available at: <http://www2.hanford.gov/arpir/?content=findpage&AKey=D196018566>
- PNL-6313, 1987, *An Evaluation of Aquifer Intercommunication Between the Unconfined and Rattlesnake Ridge Aquifers on the Hanford Site*, Pacific Northwest Laboratory, Richland, Washington.
- PNNL-6415, 2007, *Hanford Site National Environmental Policy Act (NEPA) Characterization*, Rev. 18, Pacific Northwest National Laboratory, Richland, Washington. Available at: http://www.pnl.gov/main/publications/external/technical_reports/PNNL-6415Rev18.pdf
- PNL-6769, 1988, *Leaching of ¹⁴C and ³⁶Cl from Hanford Reactor Graphite*, Pacific Northwest Laboratory, Richland, Washington.
- PNL-6989, 1989, *Leaching of ¹⁴C and ³⁶Cl from Irradiated French Graphite*, Pacific Northwest Laboratory, Richland, Washington.
- PNL-7662, 1991, *An Evaluation of the Chemical, Radiological, and Ecological Conditions of West Lake on the Hanford Site*, Pacific Northwest Laboratory, Richland, Washington. Available at: <http://www.osti.gov/energycitations/servlets/purl/5949139-cQnbwy/5949139.pdf>.
- PNL-8337, 1992, *Summary and Evaluation of Available Hydraulic Property Data for the Hanford Site Unconfined Aquifer System*, Pacific Northwest Laboratory, Richland, Washington.
- PNL-8479, 1993, *Soil Erosion Rates Caused by Wind and Saltating Sand Stresses in Wind Tunnel*, Pacific National Laboratory, Richland, Washington.
- PNL-8580, 1993, *Water Level Measurements for Modeling Hydraulic Properties in the 300-FF-5 and 100 Aggregate Area Operable Units*, Pacific Northwest Laboratory, Richland, Washington. Available at: http://www.osti.gov/bridge//product.biblio.jsp?query_id=0&page=0&osti_id=10144261.
- PNL-10195, 1994, *Three-Dimensional Conceptual Model for the Hanford Site Unconfined Aquifer System: FY 1994 Status Report*, Pacific Northwest Laboratory, Richland, Washington. Available at: <http://www5.hanford.gov/arpir/?content=findpage&AKey=D199061222>.

- PNNL-10285, 1995, *Estimated Recharge Rates at the Hanford Site*, Pacific Northwest Laboratory, Richland, Washington.
- PNL-10788, 1995, *The Role of Plants and Animals in Isolation Barriers at Hanford, Washington*, Pacific Northwest National Laboratory, Richland, Washington.
- PNL-10835, 1995, *Comparison of Constant-Rate Pumping Test and Slug Interference Test Results at the Hanford Site B Pond Multilevel Test Facility*, Pacific Northwest National Laboratory, Richland, Washington.
- PNNL-10886, 1995, *Development of a Three-Dimensional Ground-Water Model of the Hanford Site Unconfined Aquifer System: FY 1995 Status Report*, Pacific Northwest National Laboratory, Richland, Washington.
- PNNL-11367, 1996, *Hanford Prototype-Barrier Status Report: FY 1996*, Pacific Northwest National Laboratory, Richland, Washington.
- PNNL-11463, 1997, *A Comprehensive Analysis of Contaminant Transport in the Vadose Zone Beneath Tank SX-109*, Pacific Northwest National Laboratory, Richland, Washington.
- PNNL-11800, 1998, *Composite Analysis for Low-Level Waste Disposal in the 200 Area Plateau of the Hanford Site*, Pacific Northwest National Laboratory, Richland, Washington.
- PNNL-13033, 1999, *Recharge Data Package for the Immobilized Low-Activity Waste 2001 Performance Assessment*, Pacific Northwest National Laboratory, Richland, Washington.
- PNNL-13342, 2000, *Analysis of the Hydrologic Response Associated with Shutdown and Restart of the 200-ZP-1 Pump-and-Treat System*, Pacific Northwest National Laboratory, Richland, Washington.
- PNNL-13378, 2001, *Results of Detailed Hydrologic Characterization Tests – Fiscal Year 1999*, Pacific Northwest National Laboratory, Richland, Washington.
- PNNL-13514, 2001, *Results of Detailed Hydrologic Characterization Tests – Fiscal Year 2000*, Pacific Northwest National Laboratory, Richland, Washington.
- PNNL-13641, 2001, *Uncertainty Analysis Framework – Hanford Site-Wide Groundwater Flow and Transport Model*, Pacific Northwest National Laboratory, Richland, Washington.
- PNNL-13674, 2001, *Zone of Interaction Between Hanford Site Groundwater and Adjacent Columbia River: Progress Report for the Groundwater/River Interface Task Science and Technology Groundwater/Vadose Zone Integration Project*, Pacific Northwest National Laboratory, Richland, Washington. Available at:
http://www.pnl.gov/main/publications/external/technical_reports/pnnl-13674.pdf.
- PNNL-13757-1, 2002, *Characterization of Vadose Zone Sediment: Uncontaminated RCRA Borehole Core Samples and Composite Samples*, Pacific Northwest National Laboratory, Richland, Washington.

- PNNL-14058, 2002, *Prototype Database and User's Guide of Saturated Zone Hydraulic Properties for the Hanford Site*, Pacific Northwest National Laboratory, Richland, Washington.
- PNNL-14113, 2002, *Results of Detailed Hydrologic Characterization Tests – Fiscal Year 2001*, Pacific Northwest National Laboratory, Richland, Washington.
- PNNL-14233, 2003, *Biological Review of the Hanford Solid Waste EIS – Borrow Area C (600 Area), Stockpile and Conveyance Road Area (600 Area), Environmental Restoration Disposal Facility (ERDF) (600 Area), Central Waste Complex (CWC) Expansion (200 West), 218-W-5 Expansion Area (200 West), New Waste Processing Facility (200 West), Undeveloped Portion of 218-W-4C (200 West), Western Half & Northeastern Corner of 218-W-6 (200 West), Disposal Facility Near Plutonium-Uranium Extraction (PUREX) Facility (200 East), ECR #2002-600-012b*, Pacific Northwest National Laboratory, Richland, Washington.
- PNNL-14224, 2003, *Influence of Clastic Dikes on Vertical Migration of Contaminants in the Vadose Zone at Hanford*, Pacific Northwest National Laboratory, Richland, Washington.
- PNNL-14398, 2003, *Transient Inverse Calibration of the Site-Wide Groundwater Flow Model (ACM-2): FY 2003 Progress Report*, Pacific Northwest National Laboratory, Richland, Washington.
- PNNL-14702, 2006, *Vadose Zone Hydrogeology Data Package For Hanford Assessments*, Rev. 1, Pacific Northwest National Laboratory, Richland, Washington.
- PNNL-14725, 2004, *Geographic and Operational Site Parameters List (GOSPL) for the 2004 Composite Analysis*, Rev. 0, Pacific Northwest National Laboratory, Richland, Washington.
- PNNL-14744, 2004, *Recharge Data Package for the 2005 Integrated Disposal Facility Performance Assessment*, Pacific Northwest National Laboratory, Richland, Washington. Available at:
http://www.pnl.gov/main/publications/external/technical_reports/PNNL-14744.pdf
- PNNL-14753, 2006, *Groundwater Data Package for Hanford Assessments*, Rev. 1, Pacific Northwest National Laboratory, Richland, Washington.
- PNNL-15160, 2005, *Hanford Site Climatological Summary 2004 with Historical Data*, Pacific Northwest National Laboratory, Richland, Washington.
- PNNL-15782, 2006, *STOMP Subsurface Transport Over Multiple Phases Version 4.0 User's Guide*, Pacific Northwest National Laboratory, Richland, Washington. Available at:
<http://stomp.pnl.gov/documentation/guides/userguide.pdf>
- PNNL-16663, 2007, *Geochemical Processes Data Package for the Vadose Zone in the Single-Shell Tank Waste Management Areas at the Hanford Site*, Pacific Northwest National Laboratory, Richland, Washington.
- PNNL-16688, 2007, *Recharge Data Package for Hanford Single-Shell Tank Waste Management Areas*, Pacific Northwest National Laboratory, Richland, Washington.

-
- PNNL-17031, 2007, *A Site-Wide Perspective on Uranium Geochemistry at the Hanford Site*, Pacific Northwest National Laboratory, Richland, Washington.
- PNNL-17154, 2008, *Geochemical Characterization Data Package for the Vadose Zone in the Single-Shell Tank Waste Management Areas at the Hanford Site*, Pacific Northwest National Laboratory, Richland, Washington.
- PNNL-18819, 2010, *Hanford Site Guidelines for Preparation and Presentation of Geologic Information*, Rev. 1, Pacific Northwest National Laboratory, Richland, Washington. Available at: http://www.pnl.gov/main/publications/external/technical_reports/PNNL-18819rev1.pdf
- PNNL-19482, 2010, *Slug Test Characterization Results for Multi-Test/Depth Intervals Conducted During the Drilling of CERCLA Operable Unit OU UP-1 Wells 299-W19-48, 699-30-66, and 699-36-70B*, Pacific Northwest National Laboratory, Richland, Washington.
- PNNL-19491, 2010, *Slug Test Characterization Results for Multi-Test/Depth Intervals Conducted During the Drilling of CERCLA Operable Unit OU ZP-1 Wells 299-W11-43, 299-W15-50, and 299-W18-16*, Pacific Northwest National Laboratory, Richland, Washington.
- PNNL-20302, 2011, *First Quarter Hanford Seismic Report for Fiscal Year 2011*, Pacific Northwest National Laboratory, Richland, Washington. Available at: http://www.pnl.gov/main/publications/external/technical_reports/PNNL-20302.pdf
- PNNL-20548, 2011, *Hanford Site Environmental Report for Calendar Year 2010*, Pacific Northwest National Laboratory, Richland, Washington. Available at: <http://msa.hanford.gov/msa/FileDisplay.cfm?FileID=1467&confirm=true>
- PNNL-20631, 2011, *Hanford Site Regional Population – 2010 Census*, Pacific Northwest National Laboratory, Richland, Washington. Available at: http://www.pnnl.gov/main/publications/external/technical_reports/PNNL-20631.pdf
- Pogue, K. R., 1998, "Earthquake-Generated (?) Structures in Missoula Flood Slackwater Sediments (Touchet Beds) of Southeastern Washington," *Geological Society of America Abstracts with Programs*, Vol. 30, No. 7, pp. 398-399.
- Polmann, D. J., 1990, *Application of Stochastic Methods to Transient Flow and Transport in Heterogeneous Unsaturated Soils*, Ph.D. Thesis, Massachusetts Institute of Technology, Cambridge, Massachusetts.
- PRC-PRO-IRM-309, *Controlled Software Management*, Revision 2, Change 0, Administrative Procedure, CH2M Hill Plateau Remediation Company, Richland, Washington.
- PSPL, 1982, *Preliminary Safety Analysis for Skagit/Hanford Nuclear Project*, Amendment 29, Puget Sound Power and Light Company, Bellevue, Washington.
- Reidel, S. P. and P. R. Hooper (editors), 1989, "Volcanism and Tectonism in the Columbia River Flood-Basalt Province," Special Paper 239, Geological Society of America, Boulder, Colorado, p. 386, plate 1.

Reidel, S. P., N. P. Campbell, K. R. Fecht, and K. A. Lindsey, 1994, "Late Cenozoic Structure and Stratigraphy of South-Central Washington," in *Regional Geology of Washington State*, E. Cheney, and R. Lasmanis (editors), Washington Division of Geology and Earth Resources, Bulletin 80, Washington State Department of Natural Resources, pp. 159-180.

Resource Conservation and Recovery Act of 1976, 42 USC 6901, et seq. Available at:
<http://epw.senate.gov/rcra.pdf>

RHO-BWI-C-120/PNL-4219, 1981, *Flood Risk Analysis of Cold Creek near the Hanford Site*, prepared by Pacific Northwest Laboratory for Rockwell Hanford Operations, Richland, Washington.

RHO-BWI-ST-14, 1981, "Suprabasalt Sediments of the Cold Creek Syncline Area," in *Subsurface Geology of the Cold Creek Syncline*, C. W. Myers and S. M. Price (editors), Rockwell Hanford Operations, Richland, Washington.

RHO-RE-ST-12P, 1984, *An Assessment of Aquifer Intercommunication in the B Pond-Gable Mountain Pond Area of the Hanford Site*, Rockwell Hanford Operations, Richland, Washington.

RHO-SA-211, 1981, "Invasion of Radioactive Waste Burial Sites by the Great Basin Pocket Mouse (*Perognathus parvus*)," *International Symposium on Migration in the Terrestrial Environment of Long-Lived Radionuclides from the Nuclear Fuel Cycle*, Knoxville, Tennessee, Rockwell Hanford Operations, Richland, Washington.

RLO-76-4, 1976, *Evaluation of Impact of Potential Flooding Criteria on the Hanford Project*, U.S. Energy Research and Development Administration, Richland, Washington.

Rowe, R. K., 2005, "Long-Term Performance of Contaminant Barrier Systems," *Geotechnique* 55, No. 9, 631-678.

RPP-6296, 2000, *Modeling Data Package for S-SX Field Investigation Report (FIR)*, Rev. 0, CH2M HILL Hanford Group, Inc., Richland, Washington.

RPP-13310, 2006, *Modeling Data Package for an Initial Assessment of Closure of the C Tank Farm*, Rev. 1, CH2M HILL Hanford Group, Inc., Richland, Washington.

RPP-15834, 2003, *Integrated Disposal Facility Risk Assessment*, Rev. 0, CH2M Hill Hanford Group, Inc, Richland, Washington.

RPP-23752, 2005, *Field Investigation Report for Waste Management Areas T and TX-TY*, Rev. 0-A, CH2M HILL Hanford Group, Richland, Washington. Available at:
<http://www5.hanford.gov/arpir/?content=findpage&AKey=1001051156>
<http://www5.hanford.gov/arpir/?content=findpage&AKey=1001051157>
<http://www5.hanford.gov/arpir/?content=findpage&AKey=0911240516>

RPP-23752, 2005, *Field Investigation Report for Waste Management Areas T and TX-TY*, Appendix D, "Digest of Science and Technology Project Evaluations," Rev. 0-A, CH2M HILL Hanford Group, Richland, Washington. Available at:
<http://www5.hanford.gov/arpir/?content=findpage&AKey=1001051157>

- RPP-7884, 2002, *Field Investigation Report for Waste Management Area S-SX*, Rev. 0, CH2M HILL Hanford Group, Inc., Richland, Washington. Available at:
<http://www5.hanford.gov/arpir/?content=findpage&AKey=D8974033>
<http://www5.hanford.gov/arpir/?content=findpage&AKey=D8974041>
<http://www5.hanford.gov/arpir/?content=findpage&AKey=D8974046>
<http://www5.hanford.gov/arpir/?content=findpage&AKey=D8974049>
- Saltelli, A. and S. Tarantola, 2002, "On the Relative Importance of Input Factors in Mathematical Models: Safety Assessment of Nuclear Waste Disposal," *Journal of the American Statistical Association*, Vol. 97, No. 459.
- Sander, R., 1999, *Compilation of Henry's Law Constants for Inorganic and Organic Species of Potential Importance in Environmental Chemistry, Version 3*, Max-Planck Institute of Chemistry, Mainz, Germany, 107 p. Available at: <http://www.rolf-sander.net/henry/henry.pdf>
- Scanlon, B. R., K. E. Keese, A. L. Flint, L. E. Flint, C. B. Gaye, W. M. Edmunds, and I. Simmers, 2006, "Global Synthesis of Groundwater Recharge in Semiarid and Arid Regions," *Hydrological Processes* 20, 3335–3370.
- Seyfried, M. S., S. Schwinning, M. A. Walvoord, W. T. Pockman, B. D. Newman, R. B. Jackson, and F. M. Phillips, 2005, "Ecohydrological Control of Deep Drainage in Arid and Semiarid Regions," *Ecology*, 86(2), pp. 277–287
- Shaw, J., M. Munro-Stasuik, B. Sawyer, C. Beaney, J.-E. Lesemann, A. Musacchio, B. Rains, and R. R. Young, 1999, "The Channeled Scabland: Back to Bretz?," *Geology*, Vol. 27, No. 7, pp. 605-608.
- Slate, J. L., 1996, "Buried Carbonate Paleosols Developed in Pliocene-Pleistocene Deposits of the Pasco Basin, South-Central Washington, U.S.A.," *Quaternary International*, Vol. 34-36, pp. 191-196.
- Swanson, D. A., J. L. Anderson, R. D. Bentley, G. R. Byerly, V. E. Camp, J. N. Gardner, and T. L. Wright, 1979a, "Reconnaissance Geologic Map of the Columbia River Basalt Group in Eastern Washington and Northern Idaho," Open-File Report 79-1363, U.S. Geological Survey, Washington, D.C.
- Swanson, D. A., T. L. Wright, P. R. Hooper, and R. D. Bentley, 1979b, *Revisions in Stratigraphic Nomenclature of the Columbia River Basalt Group*, Bulletin 1457-G, U.S. Geological Survey, Boulder, Colorado.
- Takahashi, R., M. Toyahara, S. Maruki, H. Ueda, and T. Yamamoto, 2001, "Investigation of Morphology and Impurity of Nuclear Grade Graphite and Leaching Mechanism of Carbon-14," *Proceedings of the Technical Committee Meeting about Nuclear Graphite Waste Management*, 18-20 October 1999, International Atomic Energy Agency, Manchester, United Kingdom.
- TNC, 1998, *Biodiversity Inventory and Analysis of the Hanford Site, 1997 Annual Report*, The Nature Conservancy of Washington, Seattle, Washington.

- U.S. Army Corps of Engineers, 1989, *Water Control Manual for McNary Lock and Dam, Columbia River, Oregon and Washington*, U.S. Army Corps of Engineers, Walla Walla District, Walla Walla, Washington.
- U.S. Army Corps of Engineers, 1993, "Engineering Study", Load/Deformation Characteristics of Potential Waste Soils for the Environmental Restoration Disposal Facility, DOE/RL/12074-31, Rev. 0. U.S. Army Corps of Engineers, Walla Walla District, Walla Walla, Washington.
- U.S. Department of Agriculture, Natural Resources Conservation Service, Fact Sheets & Plant Guides, *Artemisia tridentata* ssp. *Tridentata*. Available at http://plants.usda.gov/plantguide/pdf/pg_artrt.pdf
- USGS, 2007, *USGS Water Data for the Nation*, U.S. Geological Survey, Reston, Virginia. Available at: <http://waterdata.usgs.gov/nwis/nwis>
- van Genuchten, M.Th., 1980, "A Closed-Form Equation for Predicting the Hydraulic Conductivity of Unsaturated Soils," *Soil Science Society of America Journal*, Vol. 44, pp. 892-898.
- WAC 173-216, "State Waste Discharge Permit Program," *Washington Administrative Code*, Olympia, Washington. Available at: <http://apps.leg.wa.gov/WAC/default.aspx?cite=173-216>
- WAC 246-290-025, "Adoption by Reference," *Washington Administrative Code*, Olympia, Washington. Available at: <http://apps.leg.wa.gov/wac/default.aspx?cite=246-290-025>
- WAC 246-290-310, "Maximum Contaminant Levels (MCLs) and Maximum Residual Disinfection Levels (MRDLs)." *Washington Administrative Code*, Olympia, Washington. Available at: <http://apps.leg.wa.gov/wac/default.aspx?cite=246-290-310>
- Waite, R. B., 1980, "About Forty Last-Glacial Lake Missoula Jökulhlaups through Southern Washington," *Journal of Geology*, Vol. 88, pp. 653-679.
- Wang, J. S. and T. N. Narasimhan, 1985, "Hydrologic Mechanisms Governing Fluid Flow in Saturated, Fractured Porous Media," *Water Resources Research*, Vol. 21, pp. 1861-74.
- Waste Isolation Pilot Plant Land Withdrawal Act*, Public Law 102-579, as amended.
- WCH, 2009, *Technology Update ERDF Single Cell Design*, File Number 0080871, Washington Closure Hanford, Richland, Washington. Available at: [http://www5.hanford.gov/pdw/fsd/AR/FSD0001/FSD0050/0904290336/\[0904290336\].PDF](http://www5.hanford.gov/pdw/fsd/AR/FSD0001/FSD0050/0904290336/[0904290336].PDF)
- WCH, 2011, *ERDF 5% Final Cover Slope*, Calculation No. 0600X-CA-C0048, Rev. 0, prepared by Weaver Boos Consultants, ILLC, Greenwood Village, Colorado, for Washington Closure Hanford, Richland, Washington.
- WCH-138, 2008, *Waste Management Information System (WMIS) User Guide*, Rev. 2, Washington Closure Hanford, Richland, Washington. Available at: <http://www.osti.gov/bridge/servlets/purl/945220-SM8aor/>

- WCH-178, 2011, *Environmental Disposal Facility Waste and Material Management Plan*, Rev. 4, Washington Closure Hanford, Richland, Washington
- WCH-191, 2010, *Environmental Restoration Disposal Facility Waste Acceptance Criteria*, Rev. 2, Washington Closure Hanford, LLC, Richland, Washington. Available at: <http://www2.hanford.gov/arpir/?content=findpage&AKey=0084183>
- WCH-295, 2008, *Groundwater and Leachate Monitoring and Sampling at ERDF, CY 2007*, Rev. 0, Washington Closure Hanford, Richland, Washington. Available at: <http://www.osti.gov/bridge/servlets/purl/973162-3bu2rf/>
- WCH-315, 2009, *Groundwater and Leachate Monitoring and Sampling at ERDF, CY 2008*, Rev. 0, Washington Closure Hanford, Richland, Washington. Available at: <http://www.osti.gov/bridge/servlets/purl/973165-wGf19E/>
- WCH-382, 2011, *Washington Closure Hanford Evaluation of Wood Waste Settlement, ERDF Landfill, 200 West Area Hanford Site, Washington*, Rev. 0, Washington Closure Hanford, Richland, Washington.
- WCH-399, 2010, *Groundwater and Leachate Monitoring and Sampling at ERDF, CY 2009*, Rev. 0, Washington Closure Hanford, Richland, Washington. Available at: <http://www.osti.gov/bridge/servlets/purl/1017502-vxqllq/>
- WCH-463, 2013, *Hydrogeologic Model for the Environmental Restoration Disposal Facility, Hanford Site*, Rev. 0, Washington Closure Hanford, Richland, Washington.
- WCH-464, 2013, *Hydrologic Data Package in Support of Environmental Restoration Disposal Facility Performance Assessment Modeling*, Rev. 0, Washington Closure Hanford, Richland, Washington.
- WCH-477, 2013, *Conceptual Models for Release and Transport of Environmental Restoration Disposal Facility Waste Contaminants through the Near Field Environment*, Rev. 0, Washington.
- WCH-478, 2013, *Exposure and Inadvertent Scenarios for the Environmental Restoration Disposal Facility*, Rev. 1, Washington Closure Hanford, Richland, Washington.
- WCH-479, 2013, *Inventory Data Package for ERDF Waste Disposal*, Rev. 1, Washington Closure Hanford, Richland, Washington.
- WCH-515, 2013, *Parameter Uncertainty for the ERDF Performance Assessment Uncertainty and Sensitivity Analysis*, Rev. 0, Washington Closure Hanford, Richland, Washington.
- WHC-EP-0332, 1989, *Simulations of Infiltration of Meteoric Water and Contaminant Plume Movement in the Vadose Zone at Single-Shell Tank 241-T-106 at the Hanford Site*, Westinghouse Hanford Company, Richland, Washington.
- WHC-EP-0645, 1995, *Performance Assessment for the Disposal of Low-Level Waste in the 200 West Area Burial Grounds*, Westinghouse Hanford Company, Richland, Washington. Available at: <http://www.osti.gov/bridge/servlets/purl/105099-XRRk1W/webviewable/105099.pdf>

- WHC-EP-0673, 1993, *Permanent Isolation Surface Barrier Development Plan*, Westinghouse Hanford Company, Richland, Washington.
- WHC-MR-0293, 1992, *Legend and Legacy: Fifty Years of Defense Production at the Hanford Site*, Rev. 2, Westinghouse Hanford Company, Richland, Washington.
- WHC-MR-0391, 1992, *Field Trip Guide to the Hanford Site*, Westinghouse Hanford Company, Richland, Washington.
- WHC-SA-1252-S, 1991, *Mammal Occurrence and Exclusion at the Hanford Site*, Westinghouse Hanford Company, Richland, Washington.
- WHC-SD-EN-EV-009, 1994, *Siting Evaluation Report for the Environmental Restoration Disposal Facility*, Rev. 1, Westinghouse Hanford Company, Richland, Washington.
- WHC-SD-EN-TI-014, 1992, *Hydrogeologic Model for the 200 West Groundwater Aggregate Area*, Rev. 0, Westinghouse Hanford Company, Richland, Washington.
- WHC-SD-EN-TI-019, 1992, *Hydrogeologic Model for the 200 East Groundwater Aggregate Area*, Rev. 0, Westinghouse Hanford Company, Richland Washington.
- WHC-SD-GN-DB-003, 1989, *Natural Phenomena Hazards: The Hanford Site, Washington*, Rev. 0, Westinghouse Hanford Company, Richland, Washington.
- WHC-SD-W236A-TI-0002, *Probabilistic Seismic Hazard Analysis for the Hanford Site*, Rev. 0, Westinghouse Hanford Company, Richland, Washington. Available at:
<http://www5.hanford.gov/arpir/index.cfm?content=findpage&AKey=D196005995>
- WHC-SD-WM-EE-004, 1995, *Volume 1: Performance Assessment of Grouted Double-Shell Tank Waste Disposal at Hanford*, Rev. 1, Westinghouse Hanford Company, Richland, Washington. Available at:
<http://www5.hanford.gov/arpir/index.cfm?content=findpage&AKey=D196012502>
<http://www5.hanford.gov/arpir/index.cfm?content=findpage&AKey=D196012512>
- WHC-SD-WM-TI-730, 1996, *Performance Assessment for the Disposal of Low-Level Waste in the 200 East Area Burial Grounds*, Westinghouse Hanford Company, Richland, Washington.
- WHC-EP-0595, 1993, *Groundwater Status Report*, Westinghouse Hanford Company, Richland, Washington.
- WHC-EP-0707, 1994, *216-U-10 Pond and 216-Z19 Ditch Characterization Studies*, (formerly RHO-ST-45), Westinghouse Hanford Company, Richland, Washington.
- WHC-EP-0815, 1995, *Groundwater Impact Assessment Report for the 216-T-4-2 Ditch*, Westinghouse Hanford Company, Richland, Washington.
- Wing, N. R. and G. W. Gee, 1994, "Quest for the Perfect Cap," *Civil Engineering*, Vol. 64, No. 10, pp. 38-41.

- WMP-22922, 2004, *Prototype Hanford Features, Events, and Processes (HFEP) Graphical User Interface*, Rev. 0, Fluor Hanford, Richland, Washington.
- WMT-1, *Waste Management and Transportation*, Washington Closure Hanford, Richland, Washington.
- Xu, X., J. L. Niber, and S. C. Gupta, 1992. "Compaction Effects on the Gas Diffusion Coefficient in Soils," *Soil Science Society of America Journal*, Vol. 56, pp. 1743–1750.
- Ye, M. and R. Khaleel, 2008, "A Markov Chain Model for Characterizing Medium Heterogeneity and Sediment Layering Structure," *Water Resources Research*, Vol. 44, W09427, doi:10.1029/2008WR006924.
- Ye, M., R. Khaleel, M.G. Schaap, and J. Zhu, 2007, "Simulation of Field Injection Experiments in Heterogeneous Unsaturated Media Using Cokriging and Artificial Neural Network," *Water Resources Research*, Vol. 43, W07413, doi:10.1029/2006WR005030.
- Ye, M., R. Khaleel, and T.-C.J. Yeh, 2005, "Stochastic Analysis of Moisture Plume Dynamics of a Field Injection Experiment," *Water Resources Research*, 41, W03013, doi: 10.1029/2004WR003735
- Yeh, T.-C.J. Yeh, M. Ye, and R. Khaleel, 2005, "Estimation of Effective Unsaturated Hydraulic Conductivity Tensor Using Spatial Moments of Observed Moisture Plume," *Water Resources Research*, Vol. 41, W03014, doi:10.1029/2004WR003736.
- Yu, C., A. J. Zielen, J.-J Cheng, D. J LePoire, E. Gnanapragasam, S. Kamboj, J. Arnish, A. Wallo III, W. A. Williams, and H. Peterson, 2001, *User's Manual for RESRAD Version 6*, ANL/EAD-4, Argonne National Laboratory, Argonne, Illinois.
- Zhang, Z. F. and R. Khaleel, 2010, "Simulating Field-Scale Moisture Flow Using a Combined Power-Averaging and Tensorial Connectivity-Tortuosity Approach," *Water Resources Research*, Vol. 46, W09505, doi:10.1029/2009WR008595.

APPENDIX A

TECHNICAL BASIS FOR THE GROUNDWATER PATHWAY CONCEPTUAL MODEL: FIELD DATA AND RELATED INVESTIGATIONS

TABLE OF CONTENTS

APPENDIX A TECHNICAL BASIS FOR THE GROUNDWATER PATHWAY
CONCEPTUAL MODEL: FIELD DATA AND RELATED INVESTIGATIONS A-1

A.1 INTRODUCTION A-1

A.2 INFLUENCE OF MEDIA HETEROGENEITIES ON VADOSE ZONE
MOISTURE FLOW A-2

A.3 FIELD EXPERIMENTS A-4

A.3.1 Controlled Field Experiment A-4

A.3.2 Uncontrolled Field Experiments A-6

A.4 VARIABLE ANISOTROPY A-13

A.5 UPSCALING AND APPLICATIONS USING SISSON AND LU DATA A-15

A.5.1 Equivalent Homogeneous Medium- Based Upscaling A-16

A.5.2 Upscaling Using “Soft” and “Hard” Data A-22

A.6 ERDF PA INTERMEDIATE CALCULATIONS AND COMPARISON TO
SITE DATA AND RELATED INVESTIGATIONS A-27

A.7 CONCLUDING REMARKS A-34

A.8 REFERENCES A-35

FIGURES

A-1. Cross-Sectional View of Heterogeneous Sediments in a 200 East Area Outcrop. A-2

A-2. Typical Moisture Retention (Moisture Content, θ , Versus Pressure Head, h)
Curves for a Fine-Textured (e.g., Silt) and a Coarse-Textured (e.g., Coarse
Sand) Sediment A-3

A-3. Typical Unsaturated Hydraulic Conductivity, $K(h)$ Versus Pressure Head, h ,
Relation for a Fine-Textured (e.g., Silt) and a Coarse-Textured (e.g., Coarse
Sand) Sediment A-3

A-4. (a) Plan View of the Layout of the 200 Area Injection Well (Empty Circle Near the
Center), the Sampling Boreholes (Empty Squares), and the Observation Wells
(Filled Circles at the Sisson and Lu Site); and (b) the A-A' Cross-Section
Showing the Lithostratigraphy (Modified After PNNL-13631). A-5

A-5. Profiles of Moisture Content Difference During Infiltration and Redistribution for
the Field Injection Experiment in the 200 East Area (after Zhang and Khaleel
2010). A-7

A-6. Pre- and Post-Injection Moisture Plumes for the Field Injection Experiment in the
200 East Area A-8

A-7. Vadose Zone Contamination for Cesium-137, Technetium-99, and Sodium near
Tank SX-108 (after PNNL-13757-3). A-9

A-8.	A Comparison of Contaminant Profiles in Boreholes 299-W10-196 and C4104 for (a) Nitrate and (b) Technetium-99 (RPP-23752).....	A-11
A-9.	Observed and Predicted Distributions in Year 2005 at Borehole C4191 for (a) Technetium-99 and (b) Nitrate.....	A-12
A-10.	Observed and Predicted Profile of Sediment Volumetric Moisture Content Through the Center of Trench 216-B-26 in 2004 (after PNNL-14907).....	A-13
A-11.	Schematics Illustrating Comparison of (a) an Observed Plume with Simulations using (b) an Isotropic, and (c) a Variable Moisture Dependent Anisotropy for Unsaturated Hydraulic Conductivity (K); (d) Constant and Variable Anisotropy; K_h is Horizontal Hydraulic Conductivity Parallel to Bedding and K_v is Vertical Hydraulic Conductivity Perpendicular to Bedding; ψ is Matric Potential or Pressure Head (h) (image courtesy of T.-C. Jim Yeh, University of Arizona).....	A-15
A-12.	Schematic Illustrating the Upscaling Concept.....	A-16
A-13.	The Observed and Simulated Center of Mass in the Vertical (z) Direction (after Zhang and Khaleel 2010).....	A-18
A-14.	The Spreading of the Moisture Plume in (a) x (Easting), (b) y (Northing), and (c) z (Vertical) Directions Based on the Diagonal Components of the Second Moments (after Zhang and Khaleel 2010).....	A-19
A-15.	Snapshots of the Observed Moisture Plumes and the Ellipsoids (White, Based on the Observed Plume and Black, the Simulated Plume) (after Yeh et al. 2005).....	A-21
A-16.	Comparison of Mass Centers and Spatial Variances of the Simulated (Dashed Lines) and Observed (Solid Lines) Moisture Plumes (after Yeh et al. 2005).....	A-22
A-17.	(a-1 and b-1) Three-Dimensional Fields of Observed (a-1) and Cokriging/ANN Simulated (b-1) Moisture Content on June 2, 2000; (a-2 and b-2) Three-Dimensional Fields of Observed (a-2) and Cokriging/ANN Simulated (b-2) Moisture Content on July 31, 2000 (after Ye et al. 2007).....	A-24
A-18.	(a-1 and b-1) Three-Dimensional Fields of Observed (a-1) and TP/MC Simulated (b-1) Moisture Content on June 2, 2000; (a-2 and b-2) Three-Dimensional Fields of Observed (a-2) and TP/MC Simulated (b-2) Moisture Content on July 31, 2000 (after Ye and Khaleel 2008).....	A-25
A-19.	(a) Sisson and Lu Site Observed Moisture Plume on July 31, 2000; (b) Upscaling Method-Based Simulated Moisture Plume on July 31, 2000; c) Cokriging/Artificial Neural Network (ANN) Method Based Simulated Moisture Plume on July 31, 2000; and (d) Transition Probability (TP)/Markov Chain (MC) Method Based Simulated Moisture Plume on July 31, 2000.....	A-26
A-20.	Sisson and Lu Site Volumetric Moisture Content Measurements for 5 May 2000	A-30
A-21.	Matric Potentials Measured by Filter Paper Technique on Core Samples from Borehole 299-E27-22 (after PNNL-15503).....	A-31
A-22.	Borehole 299-E27-22 Lithology and Gravimetric Moisture Content Measurements (the shaded areas in light blue and gray are regions of increased moisture) (after PNNL-15503)	A-32
A-23.	Hanford Formation Filter Paper Based Measurements for ERDF Site Characterization Samples (after BHI-00270).....	A-33

TABLE

A-1.	Simulated Volumetric Moisture Contents and Matric Potentials for Various Stratigraphic Units at ERDF.....	A-27
------	---	------

APPENDIX A

TECHNICAL BASIS FOR THE GROUNDWATER PATHWAY CONCEPTUAL MODEL: FIELD DATA AND RELATED INVESTIGATIONS

A.1 INTRODUCTION

An important aspect of the Environmental Restoration Disposal Facility (ERDF) Performance Assessment (PA) is the groundwater pathway analysis, which includes the conceptual model for vadose zone flow and transport, and its technical basis for use in the PA. Vadose zone hydrology of the 200 Areas plays a key role on moisture flow and contaminant migration through the vadose zone to groundwater. The objective of this appendix is to provide a detailed assessment of existing field data, related investigations, and an evaluation of the technical basis for the vadose zone conceptual model used in ERDF PA modeling. Model parameters and data used in numerical modeling for the ERDF vadose zone modeling are discussed and presented in Chapter 3.0.

Moisture (water) flow in the sediments above groundwater (known as the vadose zone) is important because the downward-moving water is the medium in which the contaminants are transported from their source to groundwater.

Within the context of the groundwater pathway for the ERDF PA, key questions addressed in this appendix include, but are not limited to, the following:

- Why subsurface media heterogeneities are important
- What field-scale processes are important for vadose zone moisture flow
- What determines the rate of moisture flow and contaminant migration in relatively dry heterogeneous sediments
- How subsurface media heterogeneities are addressed and handled in ERDF PA vadose zone modeling for moisture flow and transport.

To address the preceding questions, we invoke a two-staged approach. First, we present results of existing "uncontrolled" (unplanned) as well as controlled large-scale field experiments conducted in the 200 Areas. We summarize the salient ubiquitous feature of the field data for both the 200 West and 200 East Areas. Next, we discuss how the information derived from field data is used to formulate a conceptual framework for vadose zone moisture flow and transport for the ERDF PA modeling.

Section A.2 provides a brief summary of the controlling features and processes of the 200 Areas vadose zone. **Section A.3** provides details about controlled and uncontrolled field experiments in the 200 Areas. **Section A.4** introduces an important field-scale process called saturation- or moisture-dependent anisotropy. **Section A.5** introduces the upscaling concept and describes how the media heterogeneities are handled in ERDF PA modeling for vadose

zone moisture flow. **Section A.6** compares the intermediate modeling results with site data or related investigations. **Section A.7** provides the concluding remarks.

A.2 INFLUENCE OF MEDIA HETEROGENEITIES ON VADOSE ZONE MOISTURE FLOW

Figure A-1 illustrates a vertical cross-section of an outcrop in the 200 Areas. As the figure suggests, the Hanford vadose zone contains alternate layering of fine and coarse sands. The heterogeneous nature is manifested in the spatial variability of physical and hydraulic properties of Hanford sediments (WHC-EP-0883, *Variability and Scaling of Hydraulic Properties for 200 Area Soils, Hanford Site*; RPP-RPT-35222, *Far-Field Hydrology Data Package for the RCRA Facility Investigation [RFI] Report*). Subsurface heterogeneity is therefore a rule rather than an exception. Of particular importance is the spatial variability in moisture retention and unsaturated hydraulic conductivity relationships within a geologic unit as well as among different units. As expected, different types of media have different moisture retention characteristics. However, a fundamental porous medium characteristic that influences the retention behavior is the sediment particle size distribution and therefore the pore size distribution for a particular sample. As indicated in Figure A-2, the moisture content (θ) for a sediment sample decreases as the negative pressure head or matric potential (h) becomes more negative. Generally speaking, the rate of reduction in θ as the negative pressure head h becomes more negative depends on the sediment pore size distribution. For instance, sandy sediments tend to have a narrow pore-size distribution (i.e., a relatively large number of large pores and only a few small pores). Therefore, sandy materials tend to have a rapid reduction in θ as h becomes more negative. Conversely, fine-textured materials such as silty sediments have a widespread pore-size distribution, and the reduction in moisture content is therefore much gentler (Figure A-2).

Figure A-1. Cross-Sectional View of Heterogeneous Sediments in a 200 East Area Outcrop.

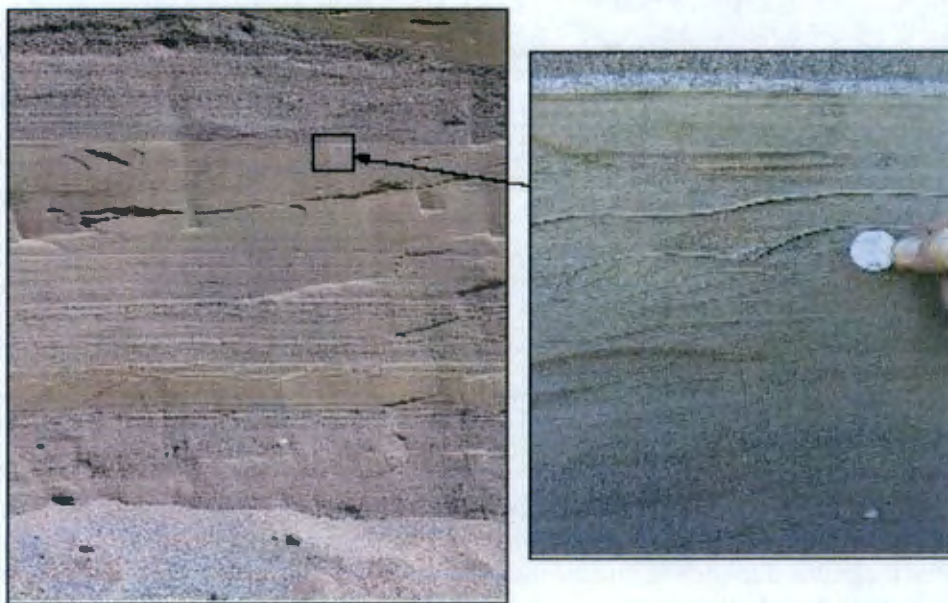
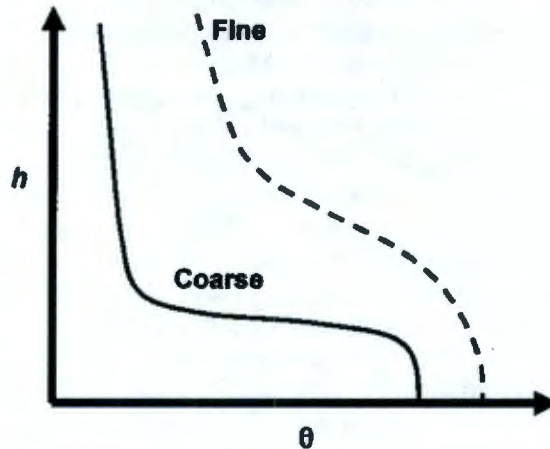


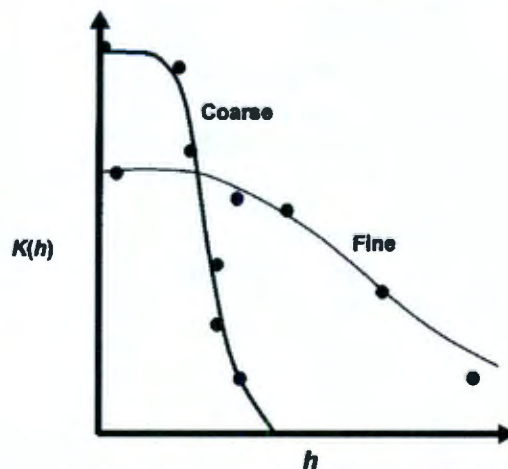
Figure A-2. Typical Moisture Retention (Moisture Content, θ , Versus Pressure Head, h) Curves for a Fine-Textured (e.g., Silt) and a Coarse-Textured (e.g., Coarse Sand) Sediment.



NOTE: The curves represent fit through the experimental data.

Figure A-3 illustrates the unsaturated hydraulic conductivity relations that go with the moisture retention curves for the fine-textured and coarse-textured sediments shown in Figure A-2. For both fine- and coarse-textured media, the unsaturated hydraulic conductivity, K , decreases with a greater decrease in θ ; the reduction in K with a reduction in θ is highly nonlinear. The conductivity will asymptotically approach a limiting value after a threshold value of moisture content (i.e., residual water content) is reached. That is, media with moisture content less than the threshold value virtually cannot transmit any significant amount of remaining moisture, because of its being attached to solids or forming films that are isolated from each other.

Figure A-3. Typical Unsaturated Hydraulic Conductivity, $K(h)$ Versus Pressure Head, h , Relation for a Fine-Textured (e.g., Silt) and a Coarse-Textured (e.g., Coarse Sand) Sediment.



NOTE: The circles represent the experimental data.

To illustrate the effect of media heterogeneity on unsaturated flow, consider the case where a fine-textured material overlies a coarse-textured material. Suppose the pressure heads (matrix potentials) in the two materials are more negative than the cross-over pressure head in their conductivity curves (Figure A-3). For such a case, moisture in the fine-textured material will not be able to flow into the coarse material below because of its lower conductivity (Figure A-3). In other words, there exists a significant presence of air in the coarse-textured material below, and moisture from the fine-textured material cannot enter the coarse-textured material unless the pressure head is built up high enough (toward saturation) in the fine-textured material to expel the air in the underlying coarse-textured material. Such a behavior is counter-intuitive, given the fact that the saturated hydraulic conductivity of the coarse-textured material is larger than the saturated conductivity of the fine-textured material. Nonetheless, during unsaturated flow conditions (i.e., right of the cross-over point in Figure A-3 and towards more negative h), the unsaturated hydraulic conductivity for the underlying coarse-textured material is much smaller than that of the overlying fine-textured material. This phenomenon is called the capillary effect, and it has been used as a fundamental principle in the design of liners and "umbrellas" for facilities such as ERDF to prevent infiltrating moisture migrating below from the surface. When starting from left hand side (lowest negative pressure head) up to the cross-over point, the fine-textured material has lower unsaturated hydraulic conductivity and acts as a barrier to the flow from any overlying coarse-textured material. This situation enhances lateral spreading of fluid and contaminant migration in the coarse-textured material.

A.3 FIELD EXPERIMENTS

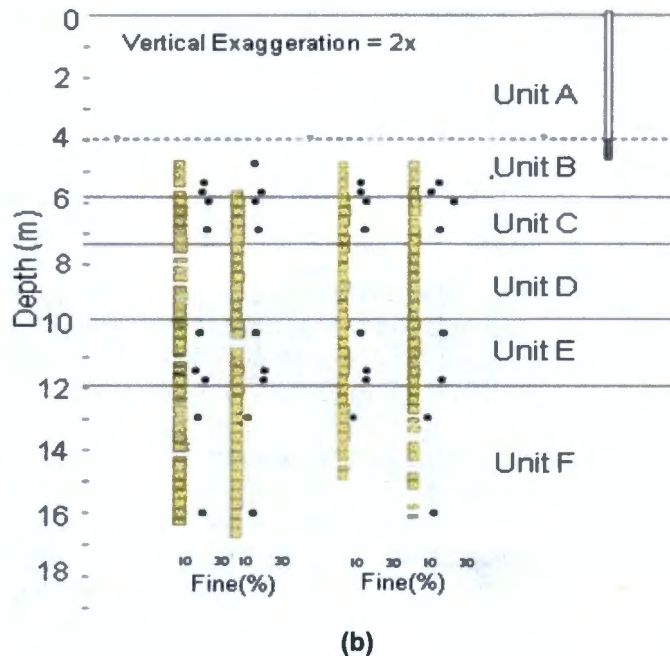
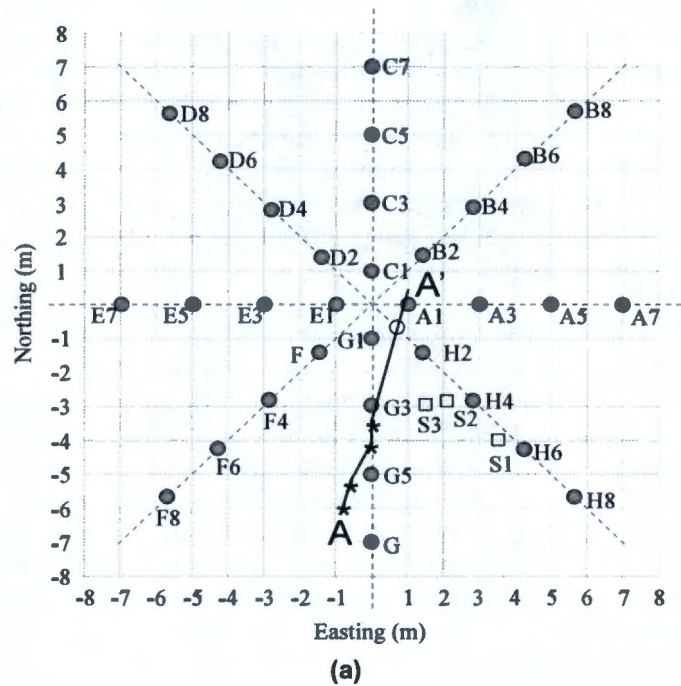
This section summarizes important findings on vadose zone flow and transport based on various studies conducted within the 200 Areas. The field experiments include controlled as well as uncontrolled (unplanned) experiments in the 200 East and 200 West Areas.

A.3.1 Controlled Field Experiment

The controlled field injection site (Sisson and Lu site; a.k.a., vadose zone test facility) (RHO-ST-46P, *Field Calibration of Computer Models for Application to Buried Liquid Discharges: A Status Report*) is located in the 200 East Area and northeast of the ERDF site. The plan view of the Sisson and Lu site and its well numbering scheme are shown in Figure A-4 (a); the injection well is situated near the center. Figure A-4 (b) shows the lithostratigraphy at the Sisson and Lu site.

An infiltration experiment was conducted at the Sisson and Lu site over a 2-month period during the summer of 2000 (PNNL-13679, *Vadose Zone Transport Field Study: Status Report*). Using neutron probes, the pre- and post-injection moisture content (θ) data were collected for 32 radially arranged cased boreholes and 43 depths over an area of 15 m by 15 m (Figure A-4). The pre-injection (i.e., initial) water content distribution was measured on May 5, 2000. Injections began on June 1 (day 154) and 4,000 L of water was metered into an injection point (point source) about 5 m below the land surface over a 6-hour period. Similarly, 4,000 L of water was injected in each subsequent injection on June 8 (day 161), June 15 (day 168), June 22 (day 175), and June 28 (Day 181). During the injection period, neutron logging in 32 wells took place within a day following each of the first four injections. A wildfire close to the test site prevented immediate logging of the moisture content distribution for the fifth injection on June 28. Three additional readings of the 32 wells were subsequently completed on July 7 (day 189), July 17 (day 199), and July 31 (day 213). During each neutron logging, water contents were monitored at 0.305-m (12-in.) depth intervals starting from a depth of 3.97 m and continuing to a

Figure A-4. (a) Plan View of the Layout of the 200 Area Injection Well (Empty Circle Near the Center), the Sampling Boreholes (Empty Squares), and the Observation Wells (Filled Circles at the Sisson and Lu Site); and (b) the A-A' Cross-Section Showing the Lithostratigraphy (Modified After PNNL-13631).



Plot (b) also shows sample locations and the percentage of fine particles (after Zhang and Khaleel 2010).

depth of 16.78 m, resulting in a total of 1,344 measurements for the 8 observation times over the 2-month period. The unique moisture content (θ) database (Figure A-5) was used to identify the lithology at the field site and to interpret, visualize, and quantify the spatio-temporal evolution of the three-dimensional (3-D) moisture plume created by the injection experiment (Ye et al. 2005). The 3-D moisture plume evolution illustrates effects of media heterogeneity (Figure A-5). The May 5 initial moisture content (θ_i) distribution is under a state of natural equilibrium, with a larger θ associated with fine-textured sediments and a smaller θ with coarse-textured sediments. This interpretation of the θ_i pattern is in general agreement with the lithostratigraphy, which below the injection well can be classified into five sediment layers B through F (Figure A-4 (b)). A bottom layer (F) of coarse-textured sediments (~3 m thick) is overlain by a layer (E) of fine-textured sediments (~2 m thick). Another layer (D) of coarse-textured sediments (~3 m thick) appears at a depth of about 10 m and is overlain by a layer (C) of fine-textured sediments (~2 m thick). Finally, a layer (B) of coarse-textured sediments appears at a depth of about 5 m.

Figure A-6 shows the composite moisture content profiles before and after injection. The moisture content profiles (Figure A-5 and Figure A-6) clearly illustrate the impact of media heterogeneities and natural capillary breaks. The capillary breaks created due to textural discontinuities allow flow to occur laterally until the pressure head in the fine layer is sufficient to overcome the entry pressure head of the underlying coarse layer. As indicated in Figure A-6, the pre- and post-injection moisture plumes are essentially confined within three layers (i.e., two fine-textured layers C and E and a coarse-textured layer D that is sandwiched in between the two fine-textured layers). As discussed later, the transient plume behavior (Figure A-5) is enhanced by the saturation- or moisture-dependent anisotropy phenomenon, a large field-scale process (Ye et al. 2005, Yeh et al. 2005). Such field-scale processes are included in ERDF PA vadose zone modeling.

A.3.2 Uncontrolled Field Experiments

We now discuss the site characterization data from uncontrolled (unplanned) experiments in 200 Areas in the vicinity of the ERDF site. These include documented leaks and discharges at three sites: (a) SX-108 tank leak, (b) T-106 tank leak, and (c) BC Cribs and Trenches.

A.3.2.1 SX-108 Tank Leak. The SX-108 tank, situated west of the ERDF site, is part of the S-SX tank farm in 200 West Area. The SX-108 tank leak is estimated to be 57,532 L (15,200 gal), occurring between 1962 and 1967. Figure A-7 shows the technetium-99 profile in borehole 41-09-39 in the vicinity of the tank leak (Khaleel et al. 2007); the vadose zone sampling was done in 1998. The vadose zone profile (Figure A-7) shows that even after >30 years of migration, the contaminant peak concentration for the long-lived mobile radionuclide is contained primarily within the fine-textured horizons well above the water table.

Figure A-7 also illustrates a distinct chromatographic separation with depth of cesium-137 and technetium-99 from sodium ion (Khaleel et al. 2007). Such site characterization data provide circumstantial evidence of predominant porous medium flow. In other words, such data can be used to postulate that contaminant plumes are more likely to travel through the far-field vadose zone sediments in 200 Areas via porous media flow, as opposed to traveling through preferred pathways. If the preferential flow conditions were controlling the plume movement at these sites, it would be unlikely to encounter, for different species, the well-defined distinct solute fronts throughout the borehole profiles (Figure A-7). In addition, under meteoric recharge conditions, precipitation at arid sites is typically too low (in relation to saturated hydraulic conductivity) to invoke preferential flow; much of the moisture in the dry soils is simply adsorbed

Figure A-5. Profiles of Moisture Content Difference During Infiltration and Redistribution for the Field Injection Experiment in the 200 East Area (after Zhang and Khaleel 2010).

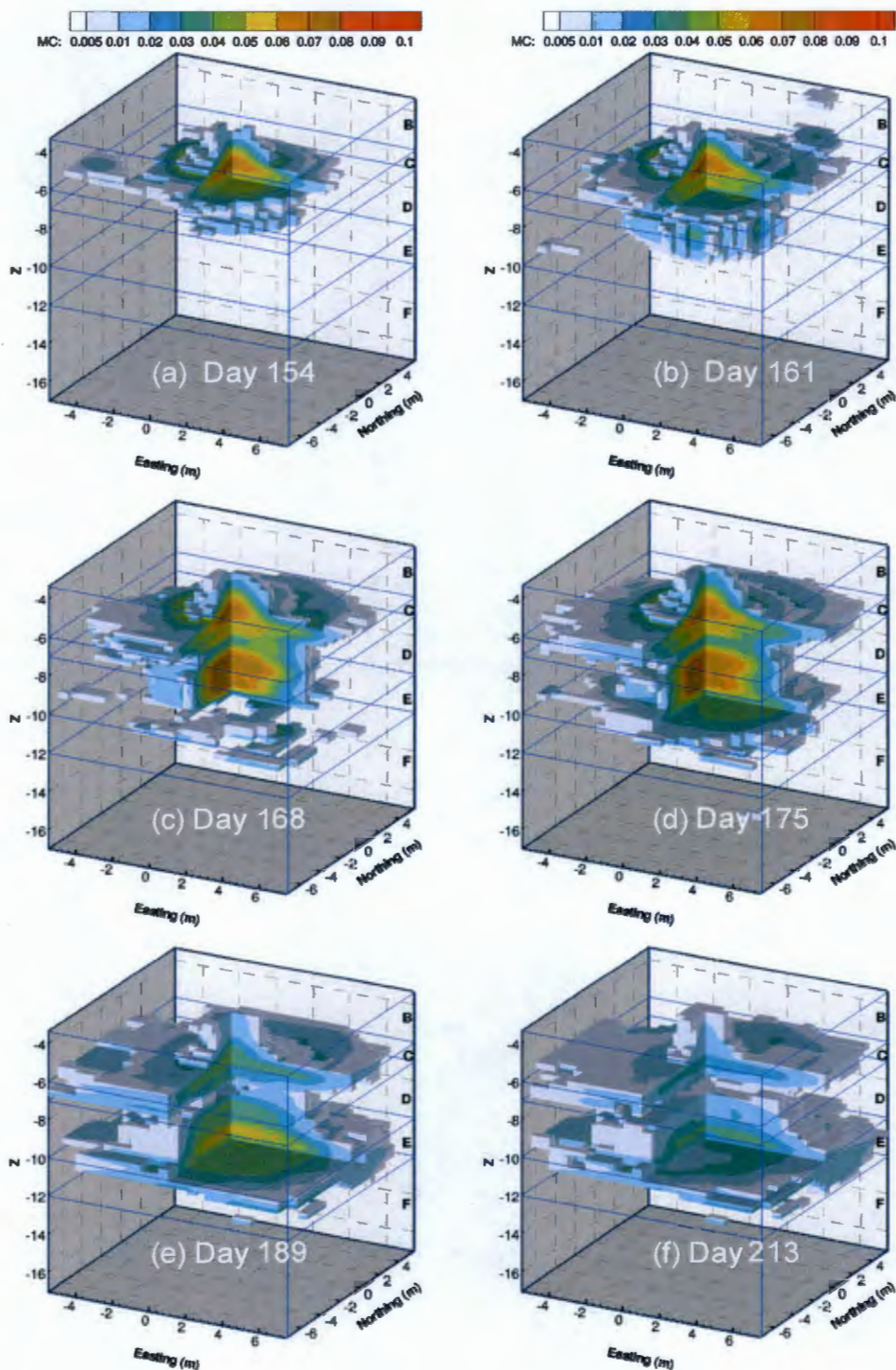
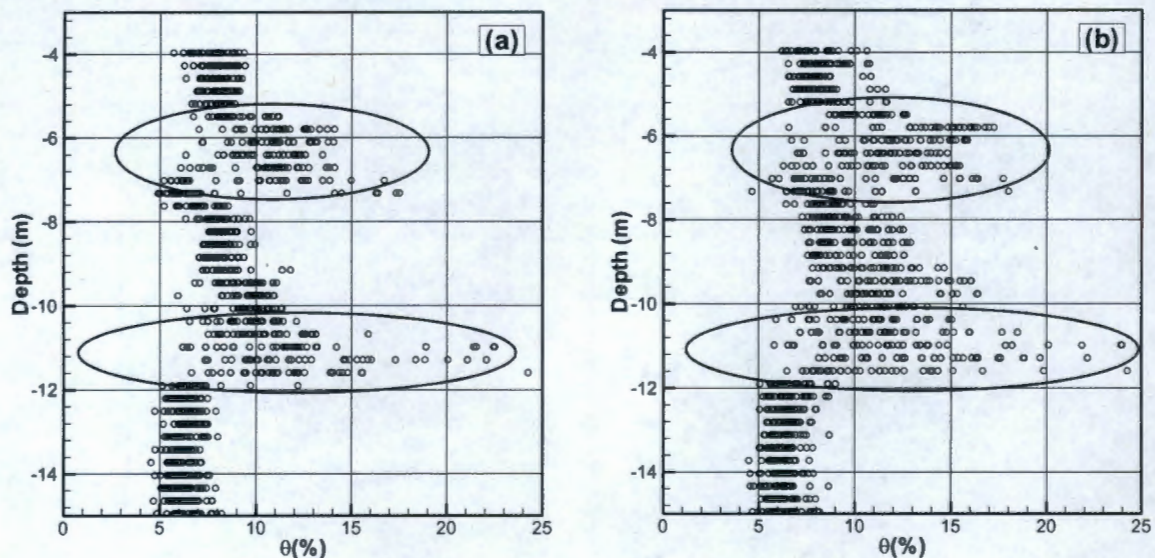


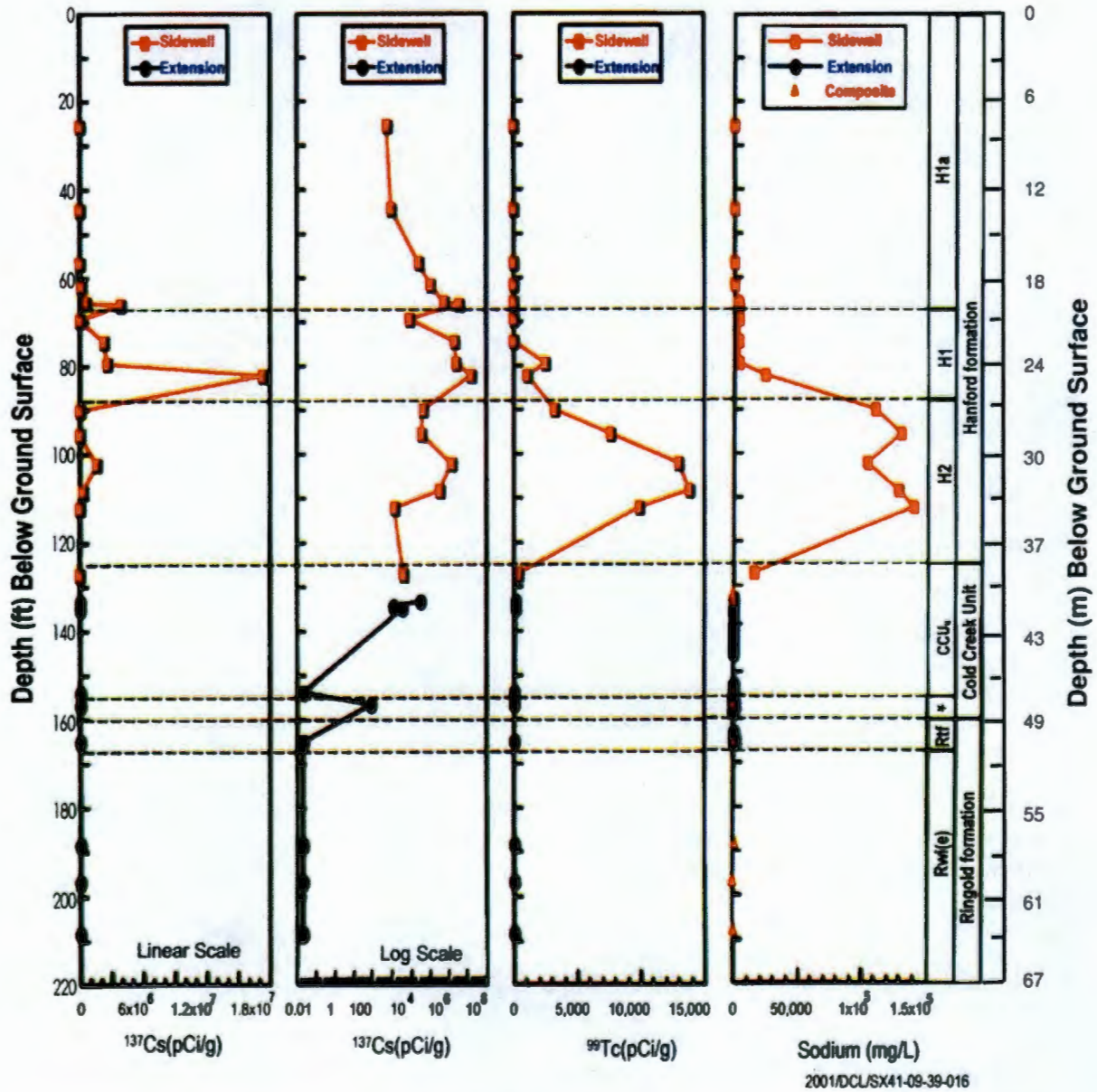
Figure A-6. Pre- and Post-Injection Moisture Plumes for the Field Injection Experiment in the 200 East Area.^(a)



^(a)After Ye et al. (2005).

Profiles of volumetric moisture content (%) measured on (a) May 5, 2000, and (b) July 31, 2000. The figures illustrate the fact that, in the absence of manmade injections, moisture contents at the field site are in equilibrium with natural recharge at the site.

Figure A-7. Vadose Zone Contamination for Cesium-137, Technetium-99, and Sodium near Tank SX-108 (after PNNL-13757-3).



A composite sample was obtained by combining two adjacent sleeves of the borehole liner (Khaleel et al. 2007).

onto the grain surfaces and cannot move along preferred pathways. Chapter 3.0 provides further details on the use of porous medium approximation for ERDF PA.

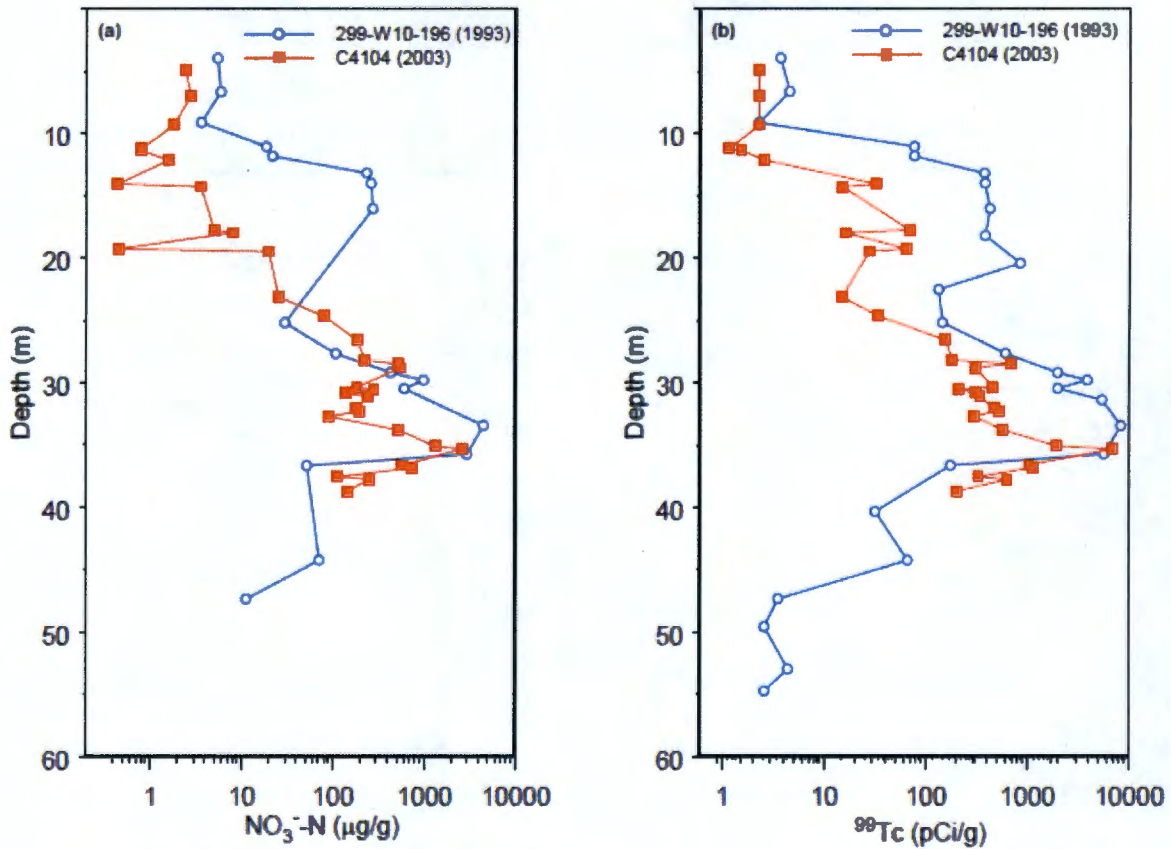
A.3.2.2 T-106 Tank Leak. The T-106 tank is situated northwest of ERDF in the 200 West Area. The T-106 tank leak (30,383L/115,000 gal), occurring in 1973, is the largest known tank leak at the Hanford Site. Figure A-8 (a) and Figure A-8 (b) show the 1993 and 2003 nitrate and technetium-99 profiles in boreholes 299-W10-196 and C4104 in the vicinity of the tank leak (BHI-00061, *Engineering Evaluation of the GAO-RCED-89-157, Tank 241-T-106 Vadose Zone Investigation*; RPP-23752, *Field Investigation Report for Waste Management Areas T and TX-TY*). The vadose zone profile shows that, even after 30 years of migration, the peak concentration profiles for the mobile species are contained primarily within the fine-textured horizons at a depth of 35 m to 40 m below ground surface and well above the water table (Figure A-8). Due to a separation distance of 4 m between the 1993 and 2003 boreholes, differences in the contaminant profiles could be partly due to differences in lithostratigraphy between the two boreholes. However, a comparison of neutron moisture logs and antecedent moisture derived from sediment cores suggest only minor differences in stratigraphy between the two boreholes.

As with SX-108 tank leak, preponderance of lateral migration is also evident at the T-106 tank leak site. The fine-textured Cold Creek unit and the underlying Ringold Formation appear to be quite effective in enhancing lateral migration and in limiting vertical migration of contaminants to the water table. Contaminant concentrations continued to increase with depth, reaching a maximum in finer-textured, wetter sediments corresponding to the Cold Creek and upper Ringold silt units (BHI-00061; RPP-23752). The location of the peak concentrations for both technetium-99 and nitrate (Figure A-8) coincided with the peak in moisture from the neutron logs and laboratory measurements. In addition to borehole data, an apparent capillary break type behavior of the Cold Creek/Ringold interface is also evident from numerical simulations (RPP-23752). The field data for T-106 as well as SX-108 tank leaks suggest that the natural heterogeneity of Hanford vadose zone sediments plays an important role on flow and transport, and the significant lateral migration, which is, in fact, induced by media heterogeneities, is highly effective in containing plumes within the vadose zone for an extended period, and thereby limiting migration toward the water table.

A.3.2.3 BC Cribs and Trenches. A further evidence of media heterogeneities is evident at the 216-B-26 trench site just south of ERDF and the 200 East Area. The BC cribs and trenches received nearly 30 Mgal of scavenged tank waste with possibly the largest inventory of technetium-99 ever disposed to soil at the Hanford Site. There is no indication of groundwater contamination yet. In fact, field measurements suggest that the bulk of the technetium (Figure A-9 (a)) and nitrate (Figure A-9 (b)) plume is concentrated within the fine-textured sediments at a depth of about 30 m to 35 m below ground surface almost 50 years after the high-volume discharge (PNNL-14907, *Vadose Zone Contaminant Fate and Transport Analysis for the 216-B-26 Trench*).

Figure A-10 illustrates the strong correlation of measured moisture content with sediment texture, i.e., a larger θ associated with fine-textured sediments and a smaller θ with coarse-textured sediments. Again, similar to the T-106 tank leak site (Figure A-8), the location of the peak concentrations for both technetium-99 and nitrate (Figure A-9) at the trench site coincided with the peak in moisture content (Figure A-10). These field data once again illustrate the favorable impact of natural heterogeneities and the impact of "built-in" natural capillary breaks in limiting migration toward the water table.

Figure A-8. A Comparison of Contaminant Profiles in Boreholes 299-W10-196 and C4104 for (a) Nitrate and (b) Technetium-99 (RPP-23752).



Boreholes 299-W10-196 and C4104 drilled in April 1993 and February 2003, respectively, (a) nitrate, and (b) technetium-99.

Figure A-9. Observed and Predicted Distributions in Year 2005 at Borehole C4191 for (a) Technetium-99 and (b) Nitrate. (Predicted values are based on STOMP modeling reported in PNNL-14907.)

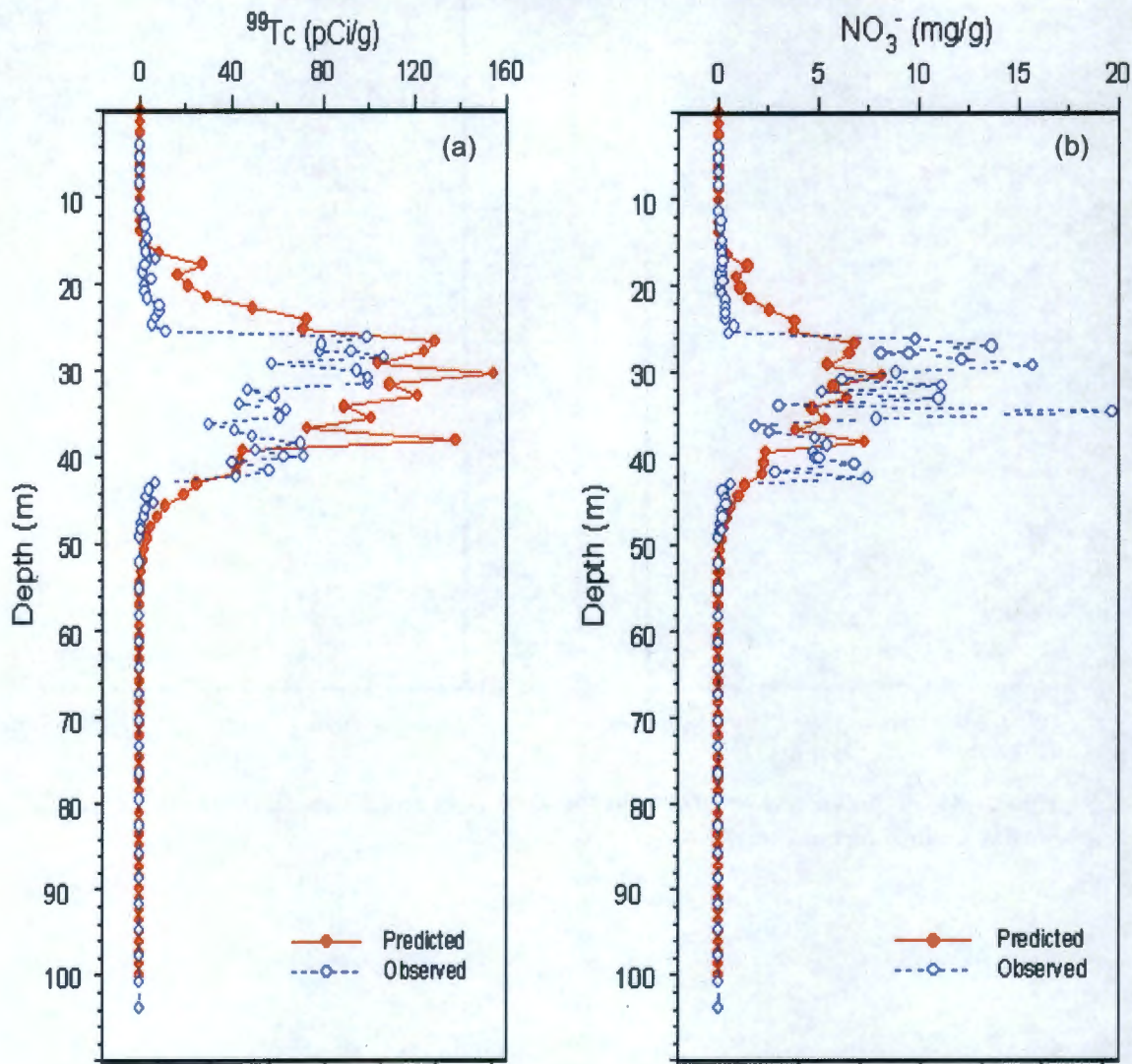
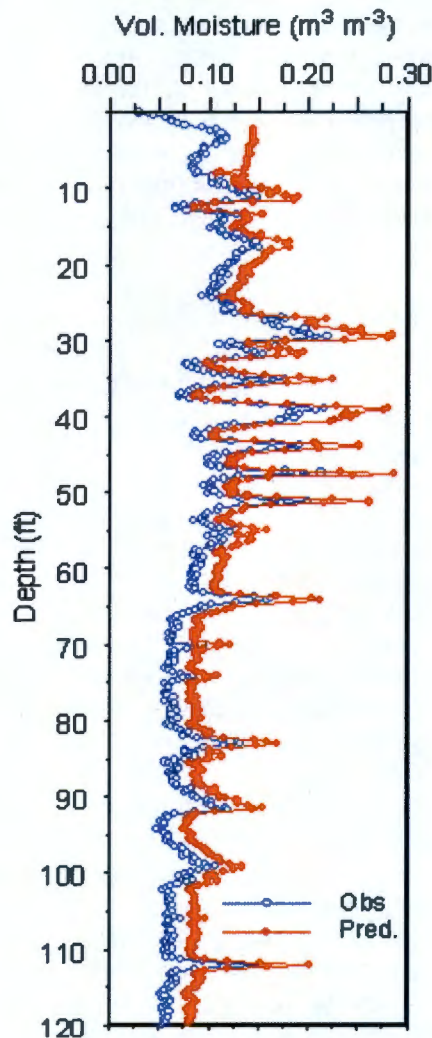


Figure A-10. Observed and Predicted Profile of Sediment Volumetric Moisture Content Through the Center of Trench 216-B-26 in 2004 (after PNNL-14907).



A.4 VARIABLE ANISOTROPY

In addition to heterogeneity and textural discontinuities that are ubiquitous with Hanford sediments and lead to natural capillary breaks, another important characteristic is varying anisotropy (i.e., directional dependence of hydraulic conductivity). As described below, the variable anisotropy in unsaturated hydraulic conductivity and the consequent lateral migration has a significant impact on vadose zone contaminant fate and transport; contaminants travel more in the lateral than in the vertical direction.

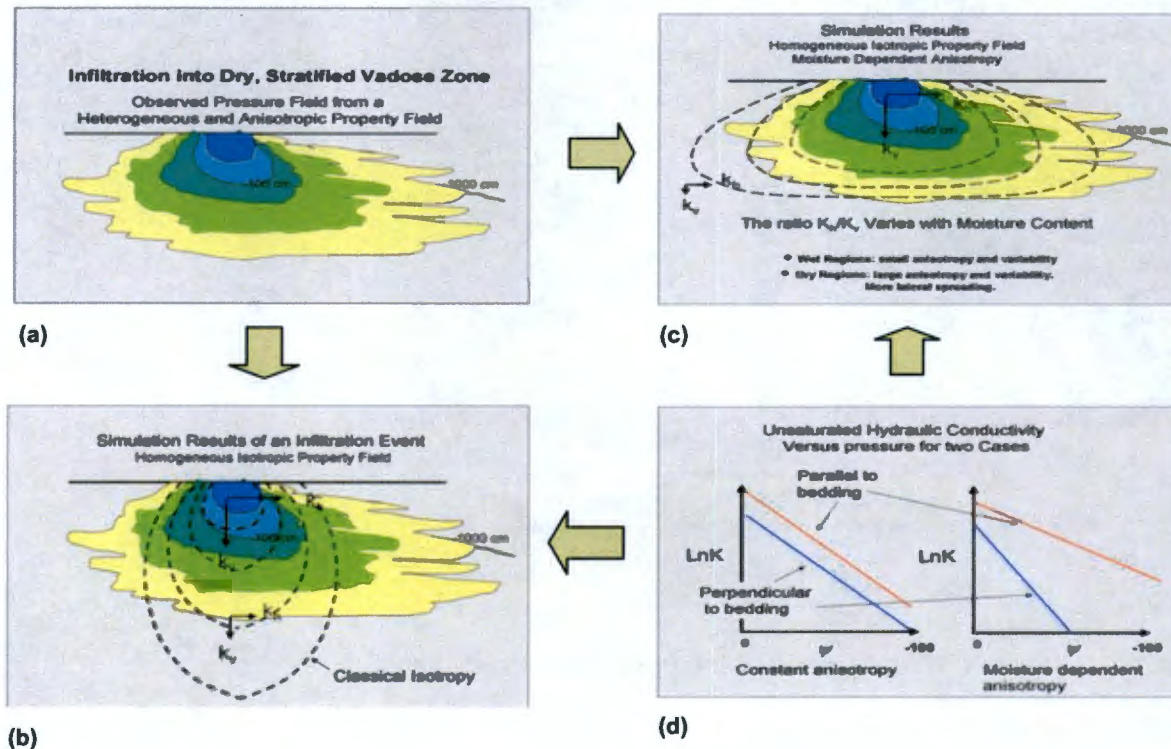
In general, anisotropy in the hydraulic conductivity varies with the observation scale as well as with the scale of heterogeneity within the observation scale. Below we examine the hydraulic conductivity anisotropy at two observation scales, i.e., pore-scale anisotropy and field-scale anisotropy. Pore-scale hydraulic conductivity anisotropy describes the macroscopic hydraulic

conductivity over a certain representative volume (e.g., a sediment core sample). Within the core sample, one likely will find that depositional processes cause flat particles (minerals) to orient themselves with the longest dimension parallel to the plane on which they settle. This produces flow channels parallel to the bedding plane, which allows fluid to flow with little resistance. Fluid flow in the direction perpendicular to the flat surface of particles, however, must detour and take more tortuous and longer paths than for flow parallel to the bedding. Therefore, under the same hydraulic gradient, more flow can occur through a soil core if the gradient is parallel than is perpendicular to the bedding plane. The bulk hydraulic conductivity of the soil core in the direction parallel to the bedding (K_h) is thus greater than in the direction perpendicular to the bedding (K_v). Sediment core samples thus possess pore-scale anisotropy in hydraulic conductivity.

In contrast to pore-scale anisotropy, field-scale anisotropy refers to the fact that when we determine the hydraulic conductivity in a field situation, we often employ the Darcy-Buckingham Law (Jury and Horton 2004), which assumes homogeneity of the medium over a relatively large heterogeneous flow domain. In essence, we seek to describe effective properties for the media in a large control volume (much larger than the sediment core dimension) that likely includes numerous structural heterogeneities (e.g., stratification, cross-bedding, clay lenses, and structural discontinuities). Such anisotropy effects are evident in experimental as well as numerical simulation studies (e.g., Pace et al. 2003, Khaleel et al. 2002), who found, at lower water contents, a greater conductivity for the Hanford sediment cores parallel to bedding than for sediment cores perpendicular to bedding.

To illustrate the impact of field-scale unsaturated hydraulic conductivity anisotropy on simulated moisture movement, let us assume that Figure A-11(a) represents the observed plume due to infiltration into a relatively dry, stratified medium (e.g., Figure A-11) having heterogeneous and anisotropic properties. In Figure A-11(b), the schematic "classical isotropy" indicates the expected, simulated plume behavior for an equivalent homogeneous medium (i.e., if we assume that the heterogeneous medium is replaced by a homogeneous medium) having isotropic properties ($K_h=K_v$). Note that a constant anisotropy implies that the unsaturated hydraulic conductivity (K) as a function of pressure head (or moisture content) maintains the identical ratio for K parallel to bedding to K perpendicular to bedding. This is illustrated in Figure A-11(d), where the K_h/K_v is constant regardless of variability in pressure head, h , or saturation in a partially saturated medium. In case where the media is assumed to be isotropic ($K_h=K_v$), the moisture plume moves predominantly in the vertical than in the lateral direction (Figure A-11(b)). Compared to the observed plume, the vertical extent of the plume is clearly overestimated (Figure A-11(b)). In case where a constant anisotropy ($K_h/K_v=\text{constant}$) in unsaturated hydraulic conductivity is assumed (Figure A-11(d)), the moisture plume travels more in the lateral than in the vertical direction. Illustrated in Figure A-11(c) is the simulated moisture content distribution with a moisture-dependent anisotropy in unsaturated hydraulic conductivity. The moisture content distributions in both Figure A-11(a) (observed plume) and Figure A-11(c) (simulated plume) show significant lateral movement. The anisotropy in unsaturated hydraulic conductivity retards the vertical movement of moisture but enhances lateral spreading (Figure A-11(a) and Figure A-11(c)). With moisture-dependent anisotropy, a greater lateral spreading is evident (Figure A-11(c)) than in an isotropic profile (Figure A-11(b)). As shown in Figure A-11(d), unlike constant anisotropy, for moisture-dependent anisotropy, K_h/K_v is a function of pressure head or moisture content; as the pressure head, h becomes more negative or as the medium gets drier, the K_h/K_v ratio becomes larger. The impact of moisture-dependent anisotropy on moisture plume dynamics is further illustrated for the plume resulting from field injection experiments at the Sisson and Lu site in the 200 East Area. Moisture-dependent anisotropy is included in ERDF PA modeling.

Figure A-11. Schematics Illustrating Comparison of (a) an Observed Plume with Simulations using (b) an Isotropic, and (c) a Variable Moisture Dependent Anisotropy for Unsaturated Hydraulic Conductivity (K); (d) Constant and Variable Anisotropy; K_h is Horizontal Hydraulic Conductivity Parallel to Bedding and K_v is Vertical Hydraulic Conductivity Perpendicular to Bedding; ψ is Matric Potential or Pressure Head (h) (image courtesy of T.-C. Jim Yeh, University of Arizona).

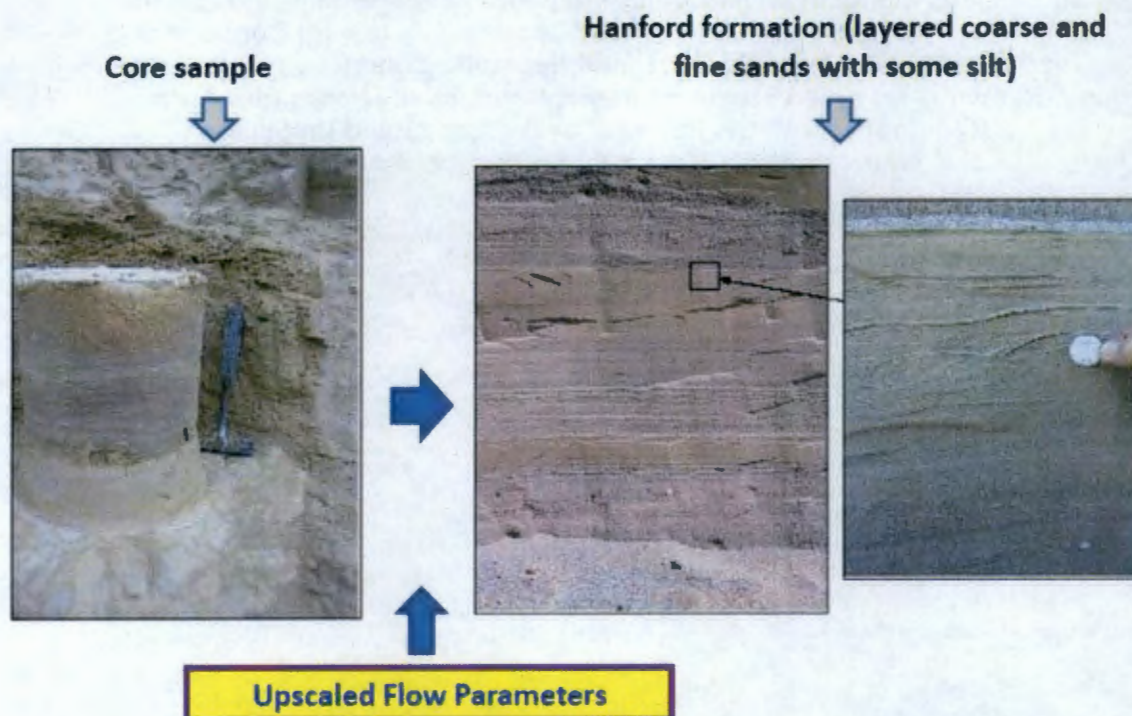


A.5 UPSCALING AND APPLICATIONS USING SISSON AND LU DATA

Upscaling accounts for the fact that the numerical modeling applies to a scale that is much larger than the core scale at which laboratory measurements are available (Figure A-12). To describe the bulk (or mean) flow behavior for ERDF PA modeling, each heterogeneous formation is replaced by its homogeneous equivalent, and effective or upscaled flow parameters are used to represent the equivalent homogeneous medium (Section 3.2.2.4; vadose zone conceptual model). Using a variety of upscaling modeling approaches, we describe below the justification of using the effective parameter approach in ERDF PA vadose zone modeling.

With equivalent homogeneous medium (EHM)-based upscaling, each heterogeneous geologic unit within the vadose zone is replaced by its homogeneous equivalent. Each geologic unit is assigned its upscaled (effective) hydraulic properties.

Figure A-12. Schematic Illustrating the Upscaling Concept.



A.5.1 Equivalent Homogeneous Medium- Based Upscaling

First, we present numerical results using the EHM-based upscaling approach. Two variations of the EHM model are explored. One is a direct, forward method which uses the small-scale core measurements for hydraulic properties to predict the large-scale field behavior (Zhang and Khaleel 2010); the other is an inverse approach which inverts the large-scale unsaturated properties using the temporal evolution of moisture profiles at the Sisson and Lu site (Yeh et al. 2005).

A.5.1.1 Forward Upscaling. For the forward upscaling approach, because of the presence of a rich, extensive hydraulic properties database at the Sisson and Lu site, we could use the small-scale measurements to estimate the three-dimensional effective unsaturated hydraulic conductivity. Each stratigraphic unit at the Sisson and Lu site was treated as an anisotropic equivalent homogeneous medium (EHM), with a set of effective moisture retention and unsaturated hydraulic conductivity, $K^e(h)$ as a function of pressure head, h . For each EHM, the effective $K^e(h)$ values were first obtained by a power averaging method (Ababou 1996); the power p varies between -1 and 1. The use of a larger p yields a larger $K^e(h)$ for a given data set. Such an averaging is equivalent, as in saturated flow, to the arithmetic mean for $p = 1$ and the harmonic mean for $p = -1$; it approaches the geometric mean when p approaches zero. The effective $K_e(h)$, for each EHM, was determined with different combinations of (p_1, p_2, p_3) in the (x, y, z) directions, where z is aligned with the vertical direction. The directional $K^e(h)$ data for each direction and each EHM were described next using a tensorial connectivity-tortuosity (TCT) model (Zhang et al. 2003); the effective tortuosity-connectivity coefficients L_e ("A New Model for Predicting the Hydraulic Conductivity of Unsaturated Porous Media" [Muallem 1976])

were obtained for each anisotropic EHM using a least-square fit for the effective K_e versus h data pairs (Zhang and Khaleel 2010). The hydraulic properties at the core scale for the Sisson and Lu site were derived from two sources: *Laboratory Measurements of the Unsaturated Hydraulic Properties at the Vadose Zone Transport Field Study Site* (PNNL-14284) and "Evaluation of van Genuchten-Mualem Relationships to Estimate Unsaturated Conductivity at Low Water Contents" (Khaleel et al. 1995).

Forward Upscaling

A combined power-averaging and tensorial connectivity-tortuosity (PA-TCT) model (Zhang and Khaleel 2010) is used to derive macroscopic anisotropy in unsaturated hydraulic conductivity at the Sisson and Lu site. A larger difference between the power values in the horizontal and vertical directions indicates a larger macroscopic anisotropy in unsaturated hydraulic conductivity.

Note that the degree of macroscopic anisotropy in hydraulic conductivity at the Sisson and Lu site is not known a priori, except that horizontal stratification was visually observed in each of the stratigraphic units. For comparison purposes, the PA-TCT numerical simulation results using STOMP are reported for four typical cases representing isotropy (ISO), low anisotropy (LA), intermediate anisotropy (IA), and high anisotropy (HA) (Zhang and Khaleel 2010)

A moment analysis (Ye et al. 2005) was used to quantify the center of mass and the spread of the injected water for the observed and simulated moisture plumes. The 1st moments represent the mass center of the plume in different directions at a given time. The 2nd moments reflect spread of the plume about its mass centers.

Figure A-13 shows the observed and simulated centers of the injected fluid plume within the monitored region in the z direction. The low anisotropy (LA) simulations gave the best prediction, while isotropy (ISO) over-estimated, and intermediate anisotropy (IA) and high anisotropy (HA) under-estimated the movement in the vertical direction (Figure A-13). Unlike other cases, the trend in the movement of mass center in the z direction for the low anisotropy (LA) and the observed plumes is similar; the comparison between the two is reasonably good. As both the low anisotropy case and the observed plumes indicate, the mass centers moved most rapidly during the early part of the injection experiment. In the z direction, the mass center for the observed plume traveled downward ~1 m for the first 15 days but ~1.1 m in the following 45 days (Ye et al. 2005).

Figure A-13. The Observed and Simulated Center of Mass in the Vertical (z) Direction (after Zhang and Khaleel 2010).

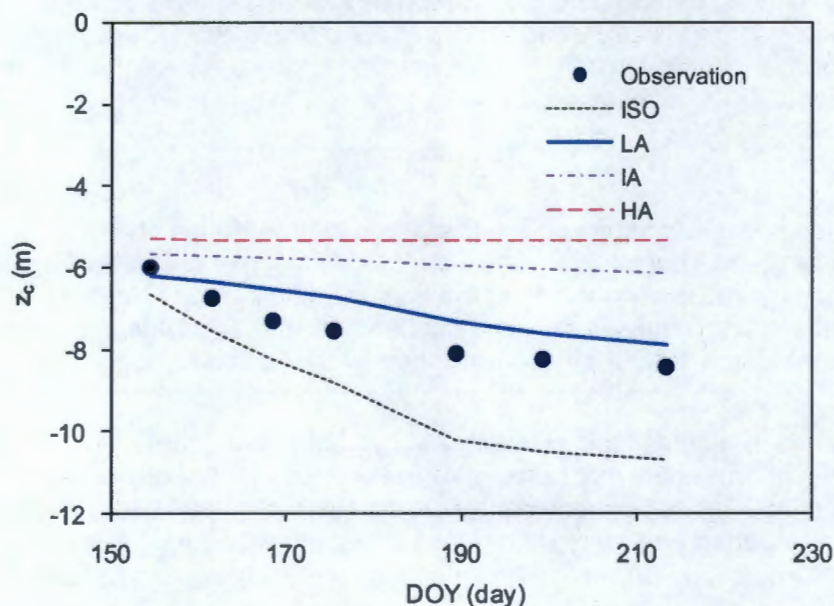
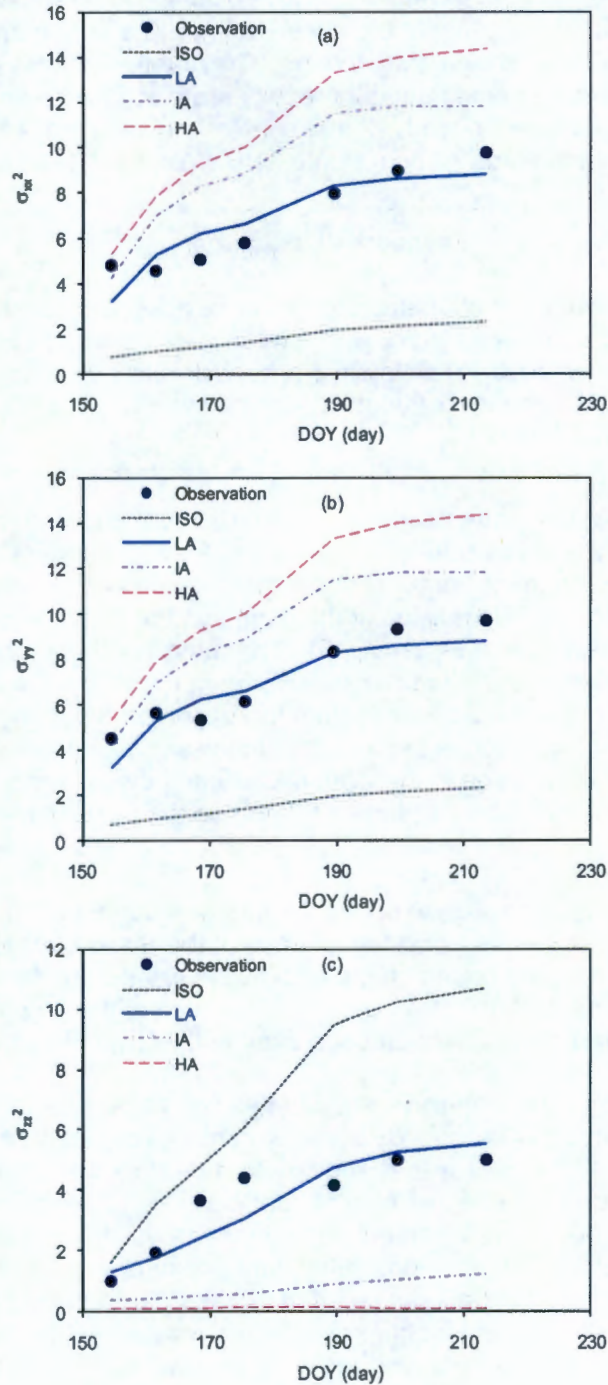


Figure A-14 illustrates the temporal evolution of components of the spatial variance tensor as an indication of the spreading of the injected water. The observed spatial variances (σ_{xx}^2 , σ_{yy}^2 and σ_{zz}^2) of the plume increased with time, indicative of the continuous spreading of the plume around its mass center in the x-, y-, and z-directions during the injection experiment. The larger spatial variances in the x- and y-directions than in the z-direction suggest a greater spreading in the horizontal plane than in the vertical. The cross-covariances (σ_{xy}^2 , σ_{xz}^2 and σ_{yz}^2) are non-zero because the principal directions of the moisture plume were not aligned with the x- y- z coordinate system. Among all cases, the simulation of low anisotropy (LA) predicted the spreading the best. The isotropic case (ISO) overestimated, whereas intermediate anisotropy (IA) and high anisotropy (HA) underestimated the vertical spreading. The opposite is true for the lateral spreading. Note the considerable deviation of high anisotropy (HA) and intermediate anisotropy (IA) based spatial variances, in comparison to observed spatial variances.

Thus, the numerical simulations showed that, if the flow domain was treated as being isotropic, the vertical migration was significantly overestimated while the lateral movement was underestimated. To the contrary, if the media were treated as layered, the lateral moisture movement was considerably overestimated while the vertical movement was underestimated. However, when the flow domain was modeled as being mildly anisotropic with the PA-TCT-based parameters, the model could successfully predict the moisture flow and the simulated plume matched best the center of mass and the spread of the injected water of the observed moisture plume. In summary, an application of the EHM model using the Sisson and Lu data suggests that the model provides a reasonable framework for upscaling core-scale measurements as well as an accurate simulation of moisture flow in a heterogeneous vadose zone. As discussed in Chapter 3.0, such an EHM model-based upscaling is used in ERDF PA modeling.

Figure A-14. The Spreading of the Moisture Plume in (a) x (Easting), (b) y (Northing), and (c) z (Vertical) Directions Based on the Diagonal Components of the Second Moments (after Zhang and Khaleel 2010).



A.5.1.2 Inverse Upscaling. Unlike the PA-TCT approach, where the small-scale core measurements were the basis for upscaling, the inverse approach used snapshots of the moisture plume at the Sisson and Lu site to derive the large-scale macroscopic unsaturated conductivity tensor for the Hanford formation. In short, the θ -based Richards' equation and the temporal evolution of spatial moments of the observed moisture plume are used to estimate the effective unsaturated hydraulic conductivity tensor. The detailed inverse upscaling approach is described in Yeh et al. (2005); some important results are discussed below. Note that, unlike the forward approach that treated each fine- and coarse-horizon as an EHM, the inverse method treated the entire Hanford unit as a single EHM (Yeh et al. 2005).

Inverse Upscaling

The θ -based Richards' equation and snapshots of observed moisture plume under transient flow are used to derive the three-dimensional effective hydraulic properties (Yeh et al. 2005). The inverse approach relies on the temporal evolution of spatial moments of the observed moisture plumes at the Sisson and Lu field injection site.

Figure A-15 shows snapshots of the observed (white ellipsoid) and simulated (black ellipsoid) moisture plume. Note that the moisture profiles (Figure A-15) are based on the difference between the observed θ and the initial θ . The simulated as well as the observed ellipsoids reflect the average location and dimension of the plume on the basis of spatial moments of the respective plume at different times (Figure A-15). The mass centers of the ellipsoids are at the same coordinates as those for the injection well. Compared with the actual plumes and the white ellipses based on moment calculations from the observed data, the black ellipses define remarkably well the spatial variation of the simulated moisture plume. However, the simulations do overestimate the spatial variation in the z direction during the redistribution period and cannot reproduce the dipping of the ellipses calculated on the basis of moments of the observed moisture plume.

Figure A-16 shows a comparison, based on the inverse approach, of spatial (first and second) moments of simulated and observed moisture plumes at the Sisson and Lu site. Spatial moments of the simulated plume based on the effective hydraulic conductivities are in reasonably good agreement with those for the observed plume, thereby providing an evaluation of the upscaling or effective parameter approach used in the ERDF PA modeling.

Also, the inverse modeling-based effective K estimates compared well (not shown here) and agreed mostly within an order of magnitude of measurements based on the core samples. Furthermore, the estimated anisotropy in K appears to reproduce the observed θ field reasonably well. The overall good agreement of conductivities derived from laboratory measurements and the good comparison between the numerically simulated plume and the observed plume demonstrate that moisture-dependent anisotropy is a valid, reproducible phenomenon in the field. We illustrate the fact that, at this particular field site, the effective hydraulic properties of an equivalent homogeneous medium can yield a similar temporal evolution of spatial moment of the observed moisture plume (Figure A-16). The macroscopic anisotropy does indeed vary with decreasing moisture content of the unsaturated medium. Such a large-scale macroscopic process is included in ERDF PA vadose zone modeling (Chapter 3.0).

Figure A-15. Snapshots of the Observed Moisture Plumes and the Ellipsoids (White, Based on the Observed Plume and Black, the Simulated Plume) (after Yeh et al. 2005).

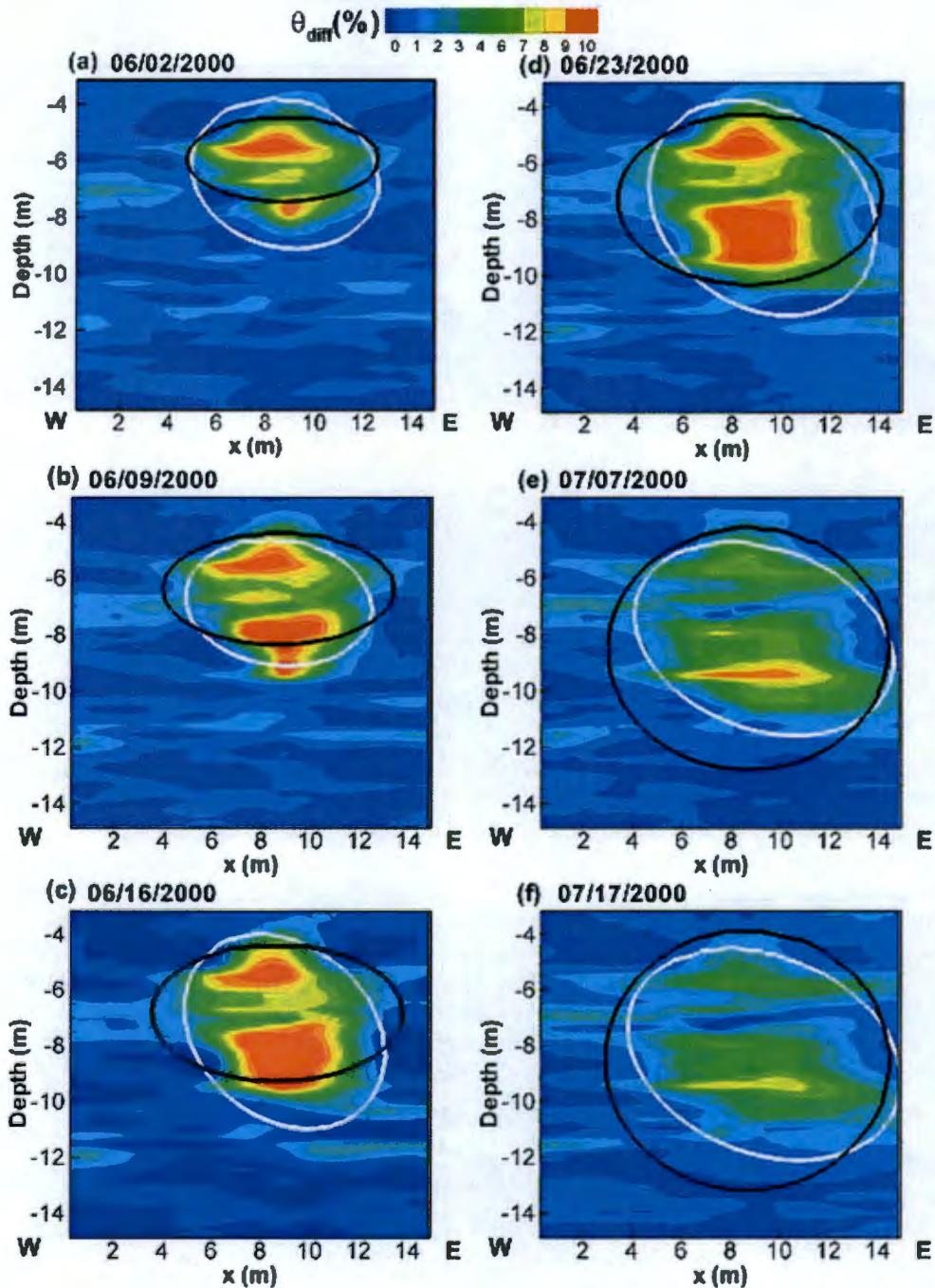
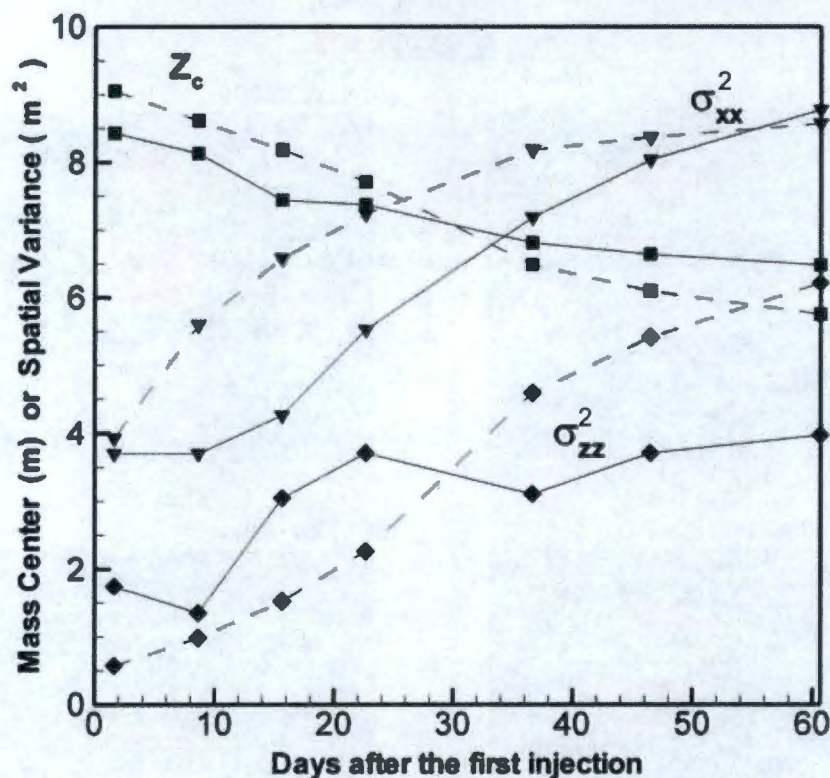


Figure A-16. Comparison of Mass Centers and Spatial Variances of the Simulated (Dashed Lines) and Observed (Solid Lines) Moisture Plumes (after Yeh et al. 2005).



The inverse approach estimates the effective K solely based on the temporal evolution (snapshots) of spatial moments of moisture plumes. Neither our prior knowledge on the unsaturated conductivity of the core samples nor any geologic structure information is used during the estimation. Note that both forward and inverse methods used an equivalent homogeneous medium approach to model the heterogeneous media and thus both methods essentially modeled the mean ensemble behavior. Consequently, they were not able to capture the highly variable nature of the observed moisture plume and its splitting within the coarse-textured layer that is sandwiched between two fine-textured layers (Figure A-4). Nonetheless, the forward as well as the inverse EHM-based upscaling provided a good comparison of first and second moments of observed and simulated moisture plumes. This is an important consideration from the ERDF PA perspective and numerical simulations performed over a long time frame.

A.5.2 Upscaling Using “Soft” and “Hard” Data

The forward and inverse upscaling modeling are based on the EHM approximation. Consequently, they cannot reproduce the observed moisture plume variations, even though the first and second moments, based on simulations, compare well with the observed moments. To address this drawback, we consider alternate approaches (Deng et al. 2009; Ye and Khaleel 2008; Ye et al. 2007) based on an integration of “soft” data (data that can be easily obtained, for example, initial moisture content, bulk density, and soil texture) and “hard” data (data that are more difficult to obtain, for example, soil hydraulic properties).

The data at the Sisson and Lu site are obtained from widely spaced boreholes; they provide relatively adequate information about heterogeneity in the vertical direction, but not necessarily in the horizontal direction. The use of hard as well as soft data allows us to characterize the spatial heterogeneity in the lateral direction by interpolating information between boreholes. We present results below using two methods; first using an integration of cokriging and artificial neural network (ANN) (Ye et al. 2007) and the second using transition probability/Markov Chain (TP/MC) (Ye and Khaleel 2008). Both methods are summarized below; details on the methodology are described in the preceding two articles.

Figure A-17 provides a comparison of observed and simulated moisture plumes on selected dates using the cokriging/ANN methodology, while Figure A-18 provides a comparison using the TP/MC method. As indicated by both figures, unlike the forward and inverse upscaling that used an equivalent homogeneous medium approach to model the heterogeneous media and thus essentially modeled the mean ensemble behavior, both cokriging/ANN and TP/MC simulations were able to model the highly variable nature of the observed moisture plume and its splitting within the coarse-textured layer that is sandwiched between two fine-textured layers (Figure A-17 and Figure A-18). Also, the first and second moments, based on cokriging/ANN and TP/MC simulations, compared well with the observed moments (Ye et al. 2007; Ye and Khaleel 2008). The EHM-based upscaling produces a plume that honors the first and second moments of the observed moisture plume, whereas the upscaling using both hard and soft data, in addition to honoring the observed first and second moments, was able to reproduce the splitting of the observed plume (Figure A-19).

Cokriging and Artificial Neural Network (ANN)

- Geostatistics (cokriging) is first used to generate 3-D heterogeneous fields of bulk density and texture using Sisson and Lu site initial θ distribution (i.e., soft data)
- Bulk density and soil texture data are then mapped onto an ANN-based pedotransfer function to generate 3-D heterogeneous hydraulic parameter field (i.e., hard data)

Transition Probability/Markov Chain (TP/MC)

- Media heterogeneity is first characterized via spatial variability of the geometry of soil textural classes
- Using “soft” data (e.g., initial moisture content), the transition probability (TP) based Markov chain (MC) model is used to characterize the medium heterogeneity and sediment layering structure

Figure A-17. (a-1 and b-1) Three-Dimensional Fields of Observed (a-1) and Cokriging/ANN Simulated (b-1) Moisture Content on June 2, 2000; (a-2 and b-2) Three-Dimensional Fields of Observed (a-2) and Cokriging/ANN Simulated (b-2) Moisture Content on July 31, 2000 (after Ye et al. 2007).

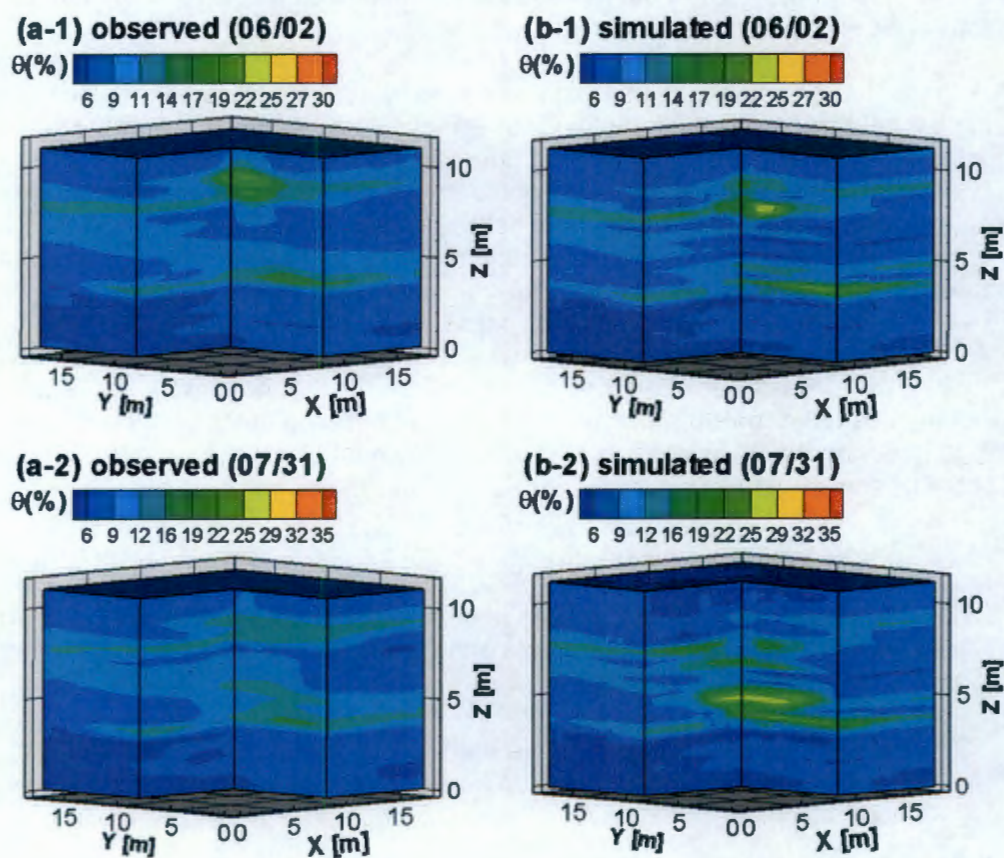


Figure A-18. (a-1 and b-1) Three-Dimensional Fields of Observed (a-1) and TP/MC Simulated (b-1) Moisture Content on June 2, 2000; (a-2 and b-2) Three-Dimensional Fields of Observed (a-2) and TP/MC Simulated (b-2) Moisture Content on July 31, 2000 (after Ye and Khaleel 2008).

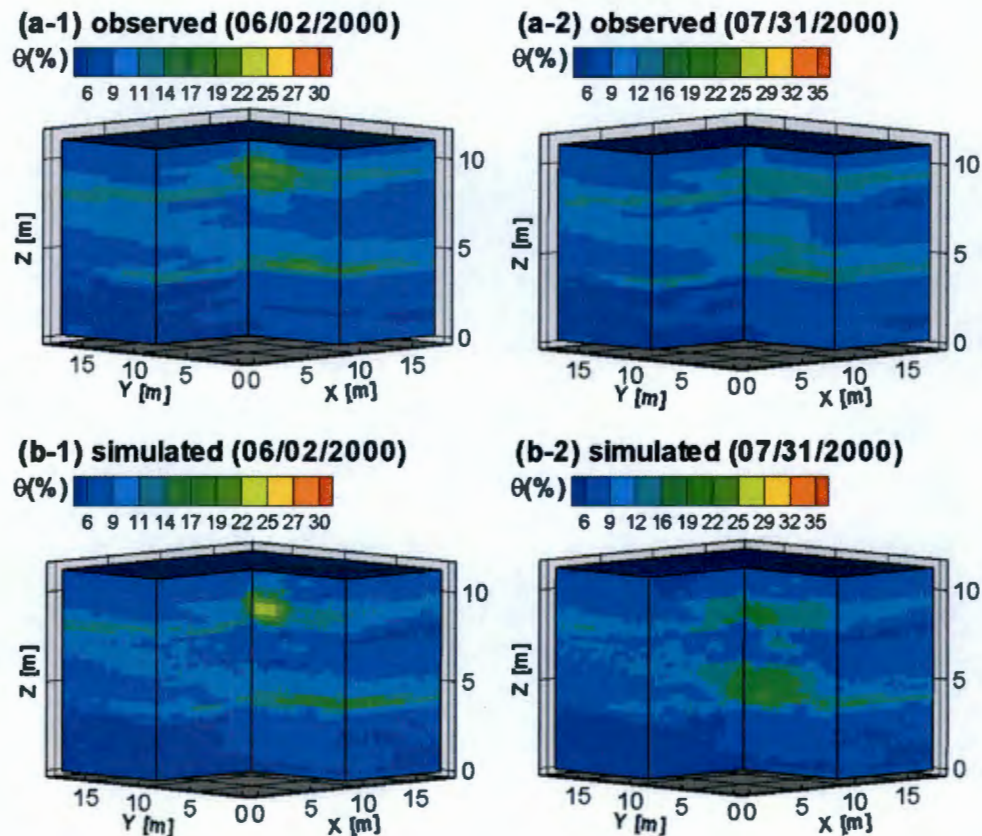
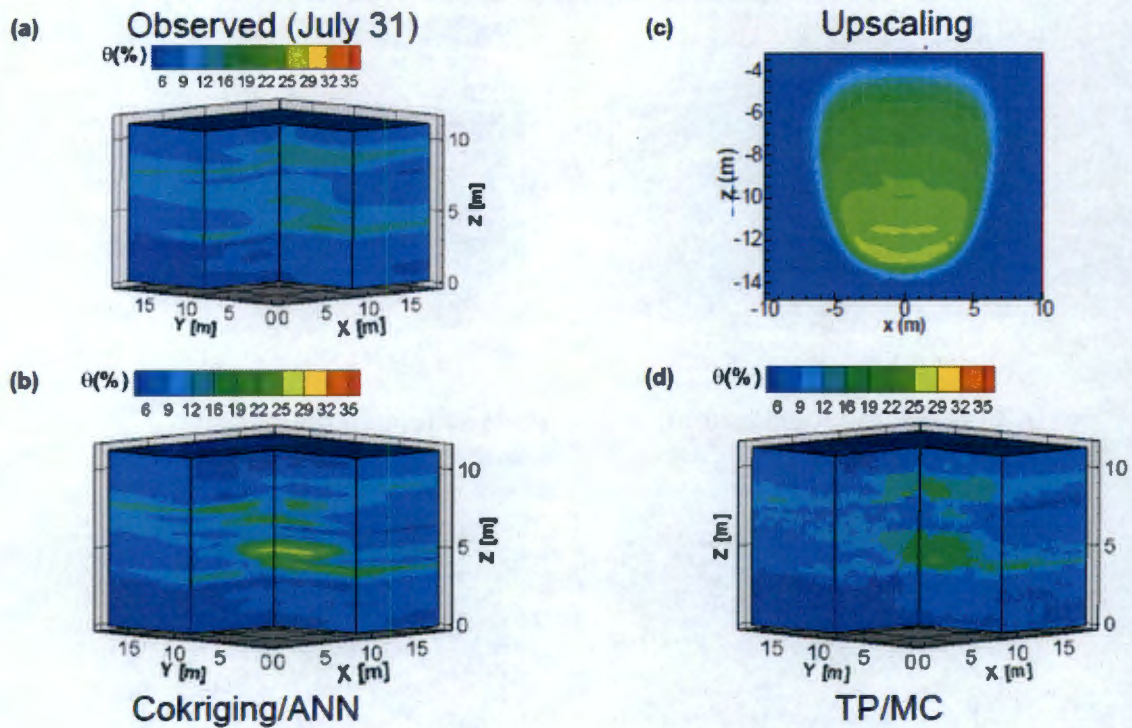


Figure A-19. (a) Sisson and Lu Site Observed Moisture Plume on July 31, 2000; (b) Upscaling Method-Based Simulated Moisture Plume on July 31, 2000; (c) Cokriging/Artificial Neural Network (ANN) Method Based Simulated Moisture Plume on July 31, 2000; and (d) Transition Probability (TP)/Markov Chain (MC) Method Based Simulated Moisture Plume on July 31, 2000.



A.6 ERDF PA INTERMEDIATE CALCULATIONS AND COMPARISON TO SITE DATA AND RELATED INVESTIGATIONS

The preceding sections focused on a detailed assessment of existing field data, related investigations, and an evaluation of the technical basis for the vadose zone conceptual model as well as the upscaling process used in the ERDF PA. The purpose of this section is to summarize some intermediate ERDF PA calculations and compare those to ERDF site data and related investigations. In particular, we compare simulated results with data obtained at nearby sites in 200 East Area as well as ERDF site characterization data on soil matric potential and moisture content for Hanford formation. Hanford formation is the only unit with field data available for comparison.

For the ERDF PA simulations, described in Chapter 4, Table A-1 lists the summary statistics for simulated steady-state moisture contents and matric potentials for various stratigraphic units and for a natural recharge of 1.7 mm/yr. To compare against these model estimates, no direct field measurements are available which are consistent with the ERDF vadose zone modeling scale domain. Nonetheless, field measurements on moisture content and matric potential at nearby sites allow us to evaluate the reliability of the simulated data.

Table A-1. Simulated Volumetric Moisture Contents and Matric Potentials for Various Stratigraphic Units at ERDF.

	Moisture Content		Matric Potential (-cm)	
	Minimum	Maximum	Maximum	Minimum
Ringold Unit E	0.0276	0.0646	2426	262
Ringold Taylor Flat	0.1038	0.1178	2405	528.6
Cold Creek Carbonate	0.0604	0.0720	2722	1606
Cold Creek Silt	0.0594	0.0661	2899	2019
Hanford Hf2	0.1037	0.1420	2439	236.5
Hanford Hf1	0.0653	0.0682	266.9	242.2

First, we consider the initial moisture content (θ_i) data collected on 5 May 2000 at the nearby Sisson and Lu site (Figure A-20). These measurements, using neutron-logging, are all within the imperfectly-stratified Hanford formation. Figure A-20 is essentially a repeat of Figure A-6a, presented earlier. As stated earlier, the θ_i pattern is in general agreement with the stratigraphic cross-section at the Sisson and Lu site, with larger θ values associated with fine-textured media and smaller values with coarse-textured media. In addition to the 2000 field experiment, data also exist on the 1980 field experiment conducted at the same site (RHO-ST-46P). Although not shown here, the 1980 θ_i measurements are nearly identical to the 2000 θ_i measurements. The consistency in the θ_i pattern over the 20-year time interval suggests that, in the absence of man-made injections, the θ_i distribution is under a state of natural equilibrium with meteoric recharge at the Sisson and Lu site. Even though the natural recharge at the ERDF and Sisson and Lu site are not identical and the sediment textural data are different, the ERDF PA simulated steady-state moisture contents for the Hanford unit compare well and show similar trends with field-measured moisture contents at the nearby Sisson and Lu site. For ERDF simulations, volumetric moisture content for the Hanford unit ranges from ~ 0.07 to ~ 0.14 , whereas for the Sisson and Lu site, it ranges from ~ 0.045 to ~ 0.24 . As expected, the Sisson and Lu site field measurements are significantly impacted by small-scale heterogeneities. To the

contrary, the ERDF simulations are based on upscaled (effective) hydraulic properties; each heterogeneous formation is replaced by its homogeneous equivalent, and effective or upscaled flow parameters are used to represent the equivalent homogeneous medium. This effectively results in a smoothing of the model estimates. Therefore, the variability of field-measured moisture contents, induced by media heterogeneities, is inherently larger for the Sisson and Lu site in comparison to that based on ERDF simulations using homogenized upscaled properties.

Note that, for a direct comparison, the measurement scale needs to be consistent with the modeling scale. The measurement volume of the neutron probe varies with θ , but for a soil with specified θ , about 95% of the measured slow neutrons are from a sphere of radius r (cm) (Olgaard 1965):

$$r = 100/(1.4 + \theta)$$

For θ measurements at the Sisson and Lu site, r ranges from about 60 to 70 cm. Further details on the neutron probe calibration are given by Ward et al. (2000).

Unlike the rich moisture content database, matric potential measurements are scarce at the Sisson and Lu site. Matric potential measurements following the 15, 22, and 28 June injections were measured using drive cone tensiometers (Hubbell and Sisson 1998) at well locations A3 at a depth of 5.34 m and H6 at a depth of 5.28 m (Figure A-4a). As expected, the limited field measurements suggest a relatively wet tension regime (generally between 50 cm and 150 cm) during injection and redistribution periods.

Matric potential measurements, using filter paper technique, are available for a number of boreholes in 200 Areas in the vicinity of ERDF. With the filter paper technique, the moisture in a filter material reaches equilibrium with the surrounding environment. Below, we present the filter paper measurements for samples from one nearby borehole as well as from the ERDF site.

Figure A-21 shows the filter paper based matric potentials as a function of depth for nearby WMA C borehole 299-E27-22, with the potentials (MPa) shown as absolute values (PNNL-15503). Matric potentials for three of the samples (27.0, 72.0, and 74.5 ft bgs) suggest very dry conditions; these appear to be erroneous because of inadvertent drying of the samples or weighing errors. The red line, labeled "theoretical value" is the theoretical line that represents the steady-state unit hydraulic gradient condition. Matric potential values to the left of the unit gradient line suggest a draining profile (Figure A-21). The general trend for the data from borehole 299-E27-22 is that the measured potentials are consistent with those of a draining profile similar to ERDF simulations. The matric suction values are generally below 0.5 MPa (~5000 cm) for the sediment profile in borehole 299-E27-22. The simulated matric suction values for ERDF range from ~236 cm to ~2439 cm for Hanford unit. Overall, borehole 299-E27-22 tension regime is consistent with the relatively dry regime that exists for ERDF simulations. Note that, unlike ERDF simulations which are based on averaged, upscaled properties for large numerical grid blocks (and the consequent smoothing effect and less variability), filter paper-based soil matric potentials are point measurements. In addition, the error bar for filter paper measurements is large (0.1-0.2 MPa). Soil moisture measurements are typically more accurate than matric potential measurements, and the matric potential variability is typically larger than the soil moisture variability.

Figure A-22 illustrates the gravimetric moisture content (θ_g) as a function of depth for the same RCRA borehole 299-E27-22 (PNNL-15503). Note that no sediment bulk density measurements are available for the borehole samples. Figure A-22 is based on θ_g measurements of continuously cored (19 to 111 ft bgs) as well as selectively cored (111 to 230 ft bgs) samples

from the borehole. The moisture content profile correlates with the lithology shown in Figure A-22. One region with elevated moisture corresponds with a thin, fine-medium sand to silty fine-sand lens within the Hanford formation at ~48 ft bgs. Most of the profile was rather dry, with a mean θ_g of about 2.6 wt%, which, with an assumed bulk density of 1.7 gcm^{-3} , amounts to a volumetric moisture content of ~0.045. A zone of elevated moisture was at the contact of the Hanford formation units at ~82 ft bgs, with a θ_g of 12.5 wt%, i.e., a volumetric moisture content of ~0.213. The final zone of elevated moisture was at ~98 ft bgs and corresponded to a thin, fine to coarse sand contact. Overall, similar to the tension data, borehole 299-E27-22 moisture regime is consistent with the relatively dry regime that exists for ERDF simulations. Note that below the Hanford formation, the Cold Creek unit is believed to have been penetrated by the final splitspoon core sample collected. The sample was composed of gravel and was quite dry. No core samples were obtained from borehole 299-E27-22 in the lower Cold Creek or Ringold units.

Finally, we present the filter paper based matric potential and volumetric moisture content measurements (Figure A-23) at ERDF for Hanford formation. These data were collected as part of site characterization activity in early 1990s prior to construction of ERDF (BHI-00270). The volumetric moisture content values range from a low of 0.014 to as high as 0.098, with a mean θ of ~0.047. The soil matric suction ranges from ~110,000 cm to ~31 cm, with a mean value of ~22,200 cm. While the moisture content values are consistent with ERDF simulated values, soil matric potential values suggest a much drier regime than predicted by ERDF simulations. Again, as stated earlier, unlike ERDF simulations, the measured matric potentials are essentially point measurements and are not consistent with the smoothing resulting from use of averaged upscaled (effective) properties for the large blocks used in ERDF simulations. Nonetheless, the overall characterization data are consistent with the relatively dry moisture regime predicted by ERDF simulations. The deviations in soil matric potential values are due to a mismatch between the modeling scale and measurement scale.

Figure A-20. Sisson and Lu Site Volumetric Moisture Content Measurements for 5 May 2000. The site consists of alternating layers of fine- and coarse-textured units; the two fine-textured units are marked by ellipse. Moisture content below the bottom ellipse changed very little.

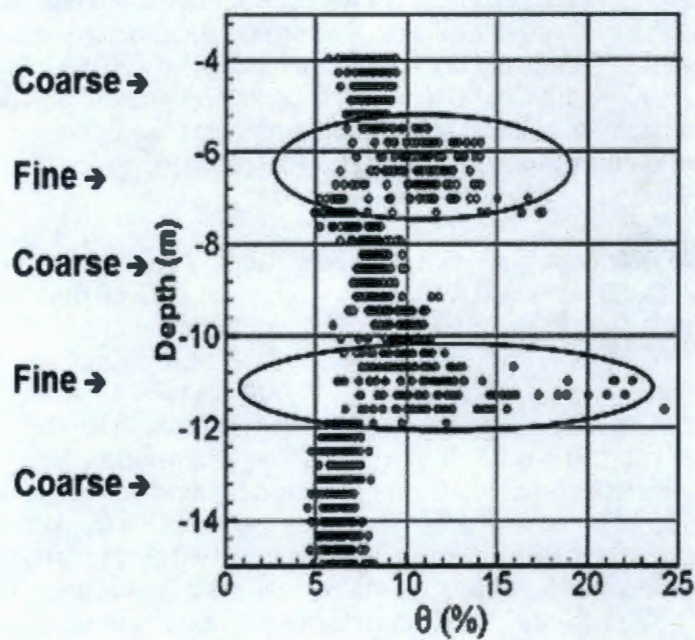
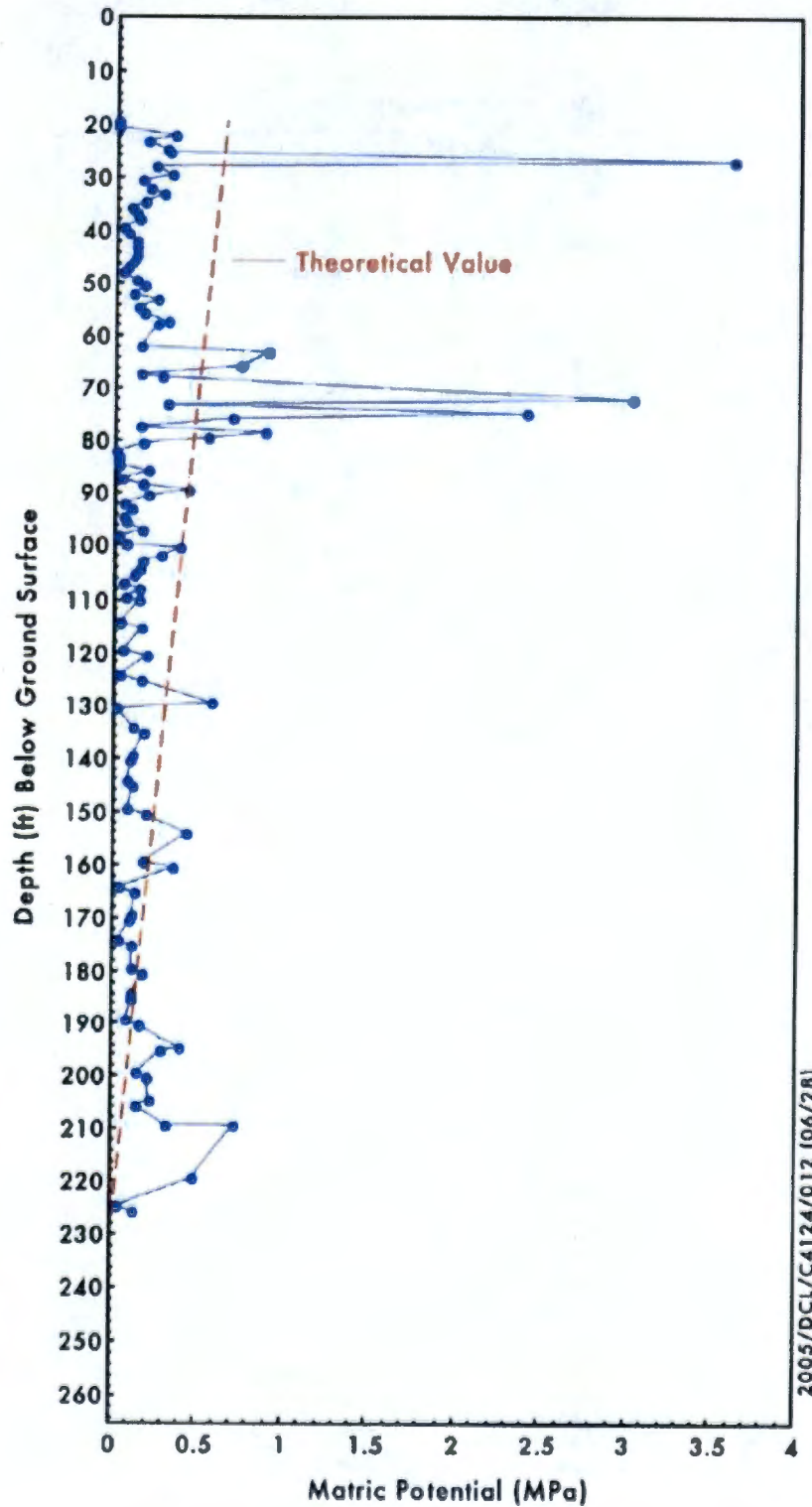


Figure A-21. Matric Potentials Measured by Filter Paper Technique on Core Samples from Borehole 299-E27-22 (after PNNL-15503). Matric potentials are presented as absolute values.



2005/DCL/C4124/012 (06/28)

Figure A-22. Borehole 299-E27-22 Lithology and Gravimetric Moisture Content Measurements (the shaded areas in light blue and gray are regions of increased moisture) (after PNNL-15503)

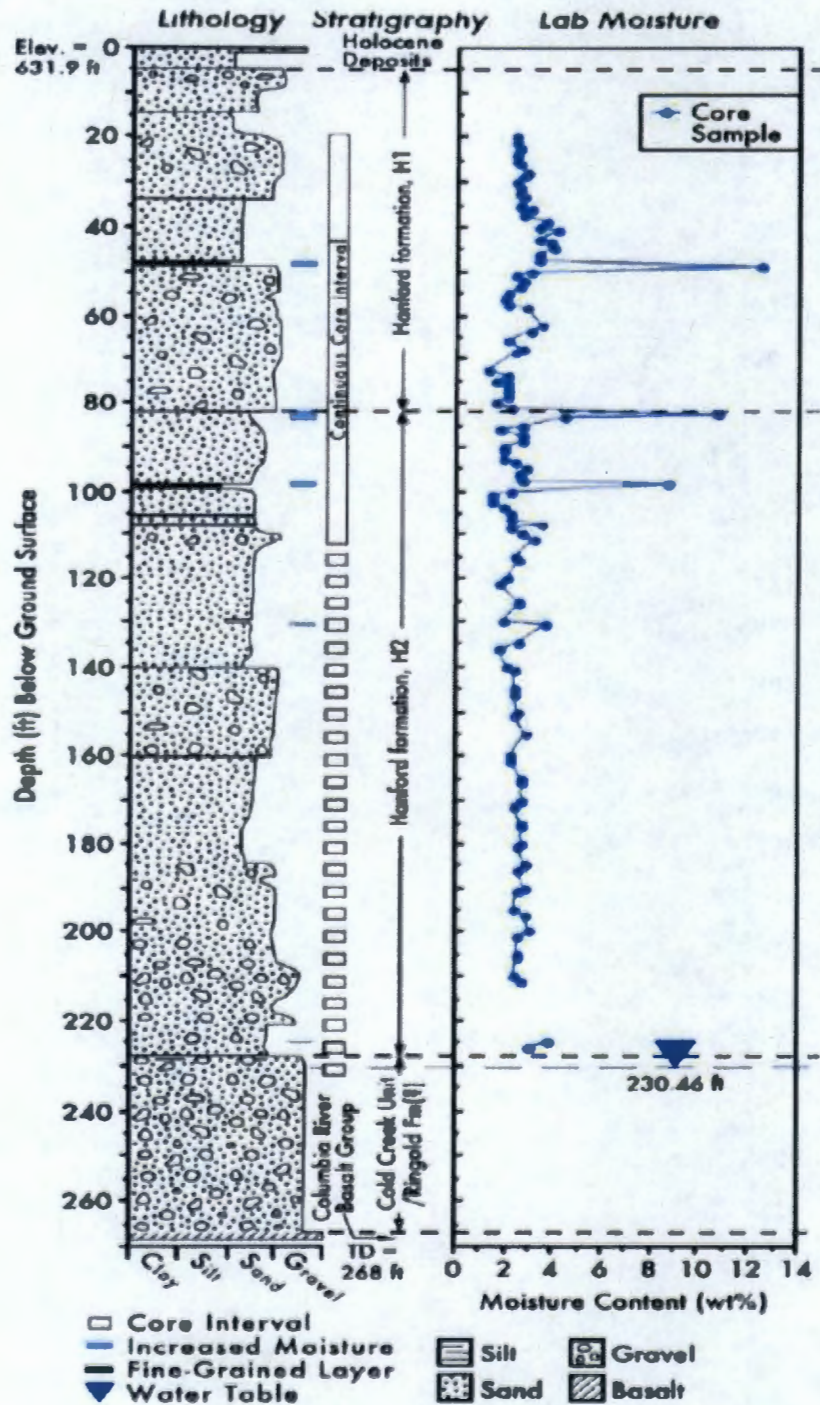
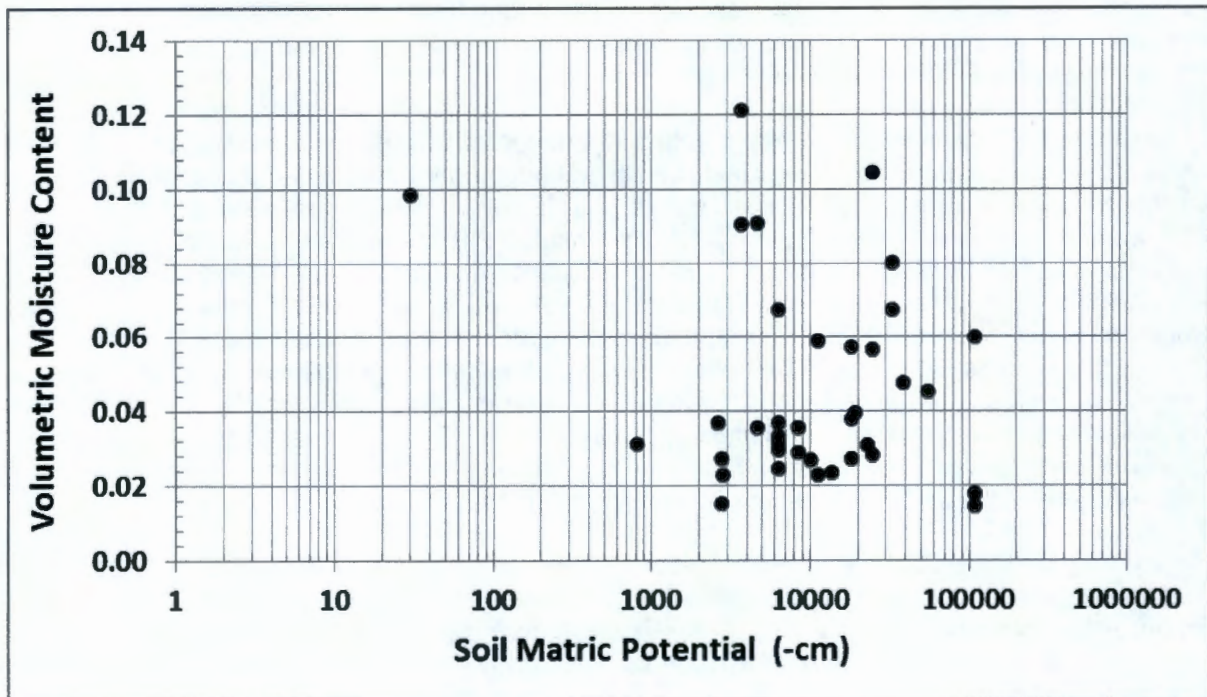


Figure A-23. Hanford Formation Filter Paper Based Measurements for ERDF Site Characterization Samples (after BHI-00270).



A.7 CONCLUDING REMARKS

An important aspect of the ERDF PA groundwater pathway analysis is the conceptual model for vadose zone flow and transport, and its technical basis for use in the PA. The objective of this appendix was to provide a detailed assessment of existing field data, related investigations, and an evaluation of the technical basis for the vadose zone conceptual model as well as the upscaling process used in the ERDF PA.

The site characterization data from controlled and uncontrolled field experiments in the 200 East Area as well as the 200 West Area illustrate several important features and processes for the highly heterogeneous Hanford Site sediments. As illustrated by both controlled and uncontrolled field experiments, heterogeneity in unsaturated geologic media is the rule; the evolving moisture plume and therefore the contaminant transport behavior are significantly impacted by media characteristics. These include (a) presence of capillary breaks, (b) state- or moisture-dependent anisotropy, (c) preponderance of lateral flow, (d) fine-textured sediments having higher moisture contents and coarse-textured sediments having lower moisture contents, and (e) a tendency for the moisture regime in heterogeneous sediments equilibrating with natural recharge, in the absence of man-made discharges. Such large-scale field-scale features that are characteristic of heterogeneous sediments in the 200 Areas are considered and incorporated in ERDF PA vadose zone flow and transport models.

In addition to media heterogeneities, it is important to recognize the multidimensional aspects and the unique differences that exist between field-scale saturated and unsaturated media flow in relatively dry heterogeneous media. For example, for saturated media, macroscopic anisotropy is constant. For unsaturated media, anisotropy is variable and depends on moisture content or matric potential. The horizontal unsaturated hydraulic conductivity for stratified media is typically much greater than the vertical unsaturated hydraulic conductivity. The vertical hydraulic conductivity decreases as the matric potential decreases (i.e., the pressure head becomes more negative). As the sediments become drier, the horizontal conductivity becomes increasingly important relative to the vertical conductivity, thereby enhancing lateral migration, and the contaminant plumes can migrate a substantial horizontal distance within the vadose zone before reaching the water table.

With respect to ERDF PA modeling, because of media heterogeneities and the consequent spatial variability in vadose zone hydraulic properties, it is inappropriate to use measurements from a few small-scale laboratory experiments to model the large, field-scale behavior. A process called upscaling is used to account for the mismatch in scale between small, core-scale measurements and large, field-scale modeling for the ERDF PA. The approach is to define an equivalent homogeneous medium with effective or macroscopic flow properties and thereby predict the bulk or mean flow behavior at the field scale. Each heterogeneous geologic unit is assigned its upscaled or effective hydraulic properties (Chapter 3.0).

As part of testing of the vadose zone conceptual model, the moisture content data that were collected at the Sisson and Lu site (also known as the Vadose Zone Test Facility) in the 200 East Area were analyzed. The rich database at the Sisson and Lu site is an important resource in understanding large-scale moisture movement in imperfectly stratified heterogeneous media and a relatively dry moisture regime such as the ERDF site. We tested EHM-based upscaling methods to derive effective flow properties for the heterogeneous Hanford sediments using the Sisson and Lu site field injection data. For the forward as well as the inverse EHM-based upscaling methods, spatial moments (first and second) of the simulated plume based on the effective hydraulic conductivities were in good agreement with those for the

observed plume. The Sisson and Lu site database also provided a framework for testing a variety of new upscaling modeling approaches (e.g., combining soft and hard data). While the use of both soft and hard data was valuable in producing the detailed moisture plume (i.e., the splitting of the moisture plume sandwiched within the coarse media between two fine layers), the observed and simulated spatial moments (first and second) were not significantly different from those using the EHM medium-based upscaling. With the ERDF PA simulations being conducted over a large flow domain and over a long time frame, this is an important finding because, as the field data from controlled as well as uncontrolled experiments suggest, the vadose zone heterogeneities are effective in smearing out the impact of small-scale heterogeneities over time and space.

Finally, we summarize some intermediate ERDF PA calculations and present results that demonstrate, by comparison to site data or related investigations, the calculations used in the PA are representative of disposal site and facility behavior for important mechanisms represented in the mathematical models. We compare simulated results with data obtained at nearby sites in 200 Area as well as ERDF site characterization data on soil matric potential and moisture content. Overall, ERDF site and nearby borehole sample data are consistent with the relatively dry moisture regime that is predicted by ERDF simulations.

In conclusion, our evaluation using a combination of field data and numerical modeling shows that the ERDF PA vadose zone conceptual model incorporates the dominant macroscopic features and processes controlling vadose zone flow and transport, and is an adequate representation of large-scale moisture flow and transport in heterogeneous Hanford sediments. Through an integrated use of field data and numerical modeling, we demonstrated that the assumptions incorporated into the conceptual model are consistent with the available data, related investigations, and theory related to the conceptual model. Parameters and data used in numerical modeling for the ERDF vadose zone modeling are discussed and presented in Chapter 3.0.

A.8 REFERENCES

- Ababou, R., 1996, "Random Porous Media Flow on Large 3-D grids: Numerics, Performance, and Application to Homogenization," In M. F. Wheeler (ed.), *Environmental Studies Mathematical, Computational, and Statistical Analysis*, Springer-Verlag, New York.
- BHI-00061, 1994, *Engineering Evaluation of the GAO-RCED-89-157, Tank 241-T-106 Vadose Zone Investigation*, Rev. 00, Bechtel Hanford, Inc., Richland, Washington.
- BHI-00270, 1996, *Preoperational Baseline and Site Characterization Report for the Environmental Restoration Disposal Facility*, Vols. 1 and 2, Rev. 2, Bechtel Hanford, Inc., Richland, Washington.
- Deng, H., M. Ye, M.G. Schaap, and R. Khaleel, 2009, "Quantification of Uncertainty in Pedotransfer Function-Based Parameter Estimation for Unsaturated Flow Modeling," *Water Resources Research*, 45, W04409, doi:10.1029/2008WR007477.
- Hubbell, J. M., and J. B. Sisson, 1998, Advanced tensiometer for shallow or deep soil water potential measurements, *Soil Sci.*, 163(4), 271–276.
- Jury, W. A. and R. Horton, 2004, *Soil Physics*, Wiley and Sons, Inc., New York, New York.

- Khaleel, R., M. D. White, M. Oostrom, M. I. Wood, F. M. Mann, and J. G. Kristofzski, 2007, "Impact Assessment of Existing Vadose Zone Contamination at the Hanford Site SX Tank Farm," *Vadose Zone Journal*, Vol. 6, pp. 935–945, doi:10.2136/vzj2006.0176.
- Khaleel, R., T.-C.J. Yeh, and Z. Lu, 2002, "Upscaled Flow and Transport Properties for Heterogeneous Unsaturated Media," *Water Resources Research*, Vol. 38(5), p. 1053, doi:10.1029/2000WR000072.
- Khaleel, R., J.F. Relyea, and J.L. Conca, 1995. "Evaluation of van Genuchten-Mualem Relationships to Estimate Unsaturated Conductivity at Low Water Contents," *Water Resources Research*, Vol. 31, pp. 2659-2668.
- Mualem, Y., 1976. "A New Model for Predicting the Hydraulic Conductivity of Unsaturated Porous Media," *Water Resources Research*, Vol. 12, pp. 513-522.
- Olgaard, P. L., 1965, On the theory of neutron method for measuring the water content in soil, Rep. 97, Danish Atomic Energy Comm., Riso.
- Pace, M. N., M. A. Mayes, P. M. Jardine, T. L. Mehlhorn, J. M. Zachara, and B. N. Bjornstad, 2003, "Quantifying the effects of small-scale heterogeneities on flow and transport in undisturbed cores from the Hanford formation," *Vadose Zone J.* Vol. 2, pp. 664-676.
- PNNL-13631, 2001, *Sampling of Boreholes WL-3A through -12 in Support of the Vadose Zone Transport Field Study*, Pacific Northwest National Laboratory, Richland, Washington.
- PNNL-13679, 2001, *Vadose Zone Transport Field Study: Status Report*, Pacific Northwest National Laboratory, Richland, Washington.
- PNNL-13757-3, 2002, *Characterization of Vadose Zone Sediment: Borehole 41-09-39 in the S-SX Waste Management Area*, Pacific Northwest National Laboratory, Richland, Washington.
- PNNL-14284, *Laboratory Measurements of the Unsaturated Hydraulic Properties at the Vadose Zone Transport Field Study Site*, Pacific Northwest National Laboratory, Richland, Washington.
- PNNL-14907, 2004, *Vadose Zone Contaminant Fate and Transport Analysis for the 216-B-26 Trench*, Pacific Northwest National Laboratory, Richland, Washington.
- PNNL-15503, 2008, *Characterization of Vadose Zone Sediments Below the C Tank Farm: Borehole C4297 and RCRA Borehole 299-E27-22*, Rev. 1, Pacific Northwest National Laboratory, Richland, Washington.
- RHO-ST-46P, 1984, *Field Calibration of Computer Models for Application to Buried Liquid Discharges: A Status Report*, Rockwell Hanford Operations, Richland, Washington.
- RPP-23752, 2005, *Field Investigation Report for Waste Management Areas T and TX-TY*, Rev. 0-A, CH2M HILL Hanford Group, Inc., Richland, Washington.

- RPP-RPT-35222, 2007, *Far- Field Hydrology Data Package for the RCRA Facility Investigation (RFI) Report*, Rev. 1, Prepared for CH2M HILL Hanford Group, Inc. and the U.S. Department of Energy Office of River Protection, Richland, Washington.
- WHC-EP-0883, 1995, *Variability and Scaling of Hydraulic Properties for 200 Area Soils, Hanford Site*, Westinghouse Hanford Company, Richland, Washington.
- Ye, M. and R. Khaleel, 2008, "A Markov chain model for characterizing medium heterogeneity and sediment layering structure," *Water Resources Research*, Vol. 44, W09427, doi:10.1029/2008WR006924.
- Ye, M., R. Khaleel, and T.C.J. Yeh, 2005, "Stochastic analysis of moisture plume dynamics of a field injection experiment," *Water Resources Research*, Vol. 41, W03013, doi: 10.1029/2004WR003735.
- Ye, M., R. Khaleel, M.G. Schaap, and J. Zhu, 2007, "Simulation of Field Injection Experiments in Heterogeneous Unsaturated Media Using Cokriging and Artificial Neural Network," *Water Resour. Res.*, 43, W07413, doi:10.1029/2006WR005030.
- Yeh, T.-C.J., M. Ye, and R. Khaleel, 2005, "Estimation of effective unsaturated hydraulic conductivity tensor using spatial moments of observed moisture plume," *Water Resources Research*, Vol. 41, W03014, doi:10.1029/2004WR003736.
- Ward, A. L., T. G. Caldwell, and G. W. Gee, 2000, *Vadose Zone Transport Field Study: Soil Water Content Distributions by Neutron Moderation*, PNNL-13795, Pacific Northwest National Laboratory, Richland, Washington.
- Zhang, Z. F. and R. Khaleel, 2010, "Simulating Field-Scale Moisture Flow Using a Combined Power-Averaging and Tensorial Connectivity-Tortuosity Approach," *Water Resources Research*, Vol. 46, W09505, doi:10.1029/2009WR008595.
- Zhang, Z. F., A. L. Ward, and G. W. Gee, 2003, "A Tensorial Connectivity-Tortuosity Concept to Describe the Unsaturated Hydraulic Properties of Anisotropic Soils," *Vadose Zone Journal*, Vol. 2, pp. 313-321.

APPENDIX B

**DEVELOPMENT OF THE FATE AND TRANSPORT MODEL FOR THE
ENVIRONMENTAL RESTORATION DISPOSAL FACILITY
PERFORMANCE ASSESSMENT TO EVALUATE THE
IMPACT OF THE GROUNDWATER PATHWAY**

TABLE OF CONTENTS

APPENDIX B DEVELOPMENT OF THE FATE AND TRANSPORT MODEL FOR THE ENVIRONMENTAL RESTORATION DISPOSAL FACILITY PERFORMANCE ASSESSMENT TO EVALUATE THE IMPACT OF THE GROUNDWATER PATHWAY B-1

B.1 PURPOSE B-1

B.2 METHODOLOGY..... B-2

B.3 CONCEPTUAL MODEL COMPONENTS..... B-3

B.4 GROUNDWATER MODELING QUALITY ASSURANCE AND QUALITY CONTROL B-21

B.5 DISTRIBUTION OF MOISTURE AT THE BOUNDARIES B-21

B.6 NUMERICAL SOLUTION LIMITATIONS B-26

B.7 BASIS FOR THE ONE-DIMENSIONAL SCREENING AND SENSITIVITY-UNCERTAINTY MODEL ABSTRACTION..... B-26

B.8 REFERENCES B-46

FIGURES

B-1. Surface Elevation of the ERDF Model Domain (a) During the Pre-Operational Period, (b) During the Operations Period 1996-2035, and (c) After Closure in 2035. B-5

B-2. Plan View of ERDF Model Domain Showing the Horizontal Distribution of the Irregularly Spaced Calculation Nodes. B-7

B-3. Location of Control Points Supplemented to the Lithologic Data Table, Wells 699-35-70 and 699-36-61A, and the ERDF Model Boundary. B-10

B-4. Diagram of the Interpolated Numerical Three-Dimensional Post-Closure Hydrogeologic Model..... B-17

B-5. Time Series Cross-Section Plots of the Change in Moisture Content from the Post-Closure Steady-State Value at the Indicated Time of Interest at the Western Boundary of the Model. B-22

B-6. Time Series Cross-Section Plots of the Change in Moisture Content from the Post-Closure Steady-State Value at the Indicated Time of Interest at the Eastern Boundary of the Model B-23

B-7. Time Series Cross-Section Plots of the Change In Moisture Content from the Post-Closure Steady-State Value at the Indicated Time of Interest at the Southern Boundary of the Model B-24

B-8. Time Series Cross-Section Plots of the Change in Moisture Content from the Post-Closure Steady-State Value at the Indicated Time of Interest at the Northern Boundary of The Model B-25

B-9.	One-Dimensional Transport Model Vadose Zone Templates Used in Screening and Sensitivity-Uncertainty Analysis.	B-28
B-10.	Comparison of the One-Dimensional Transport Model Results to the Comparable Three-Dimensional Transport Model Results of the Breakthrough of a Radionuclide with $K_d = 0$ mL/g (e.g., Technetium-99) to the Water Table for the Individual Hydrologic Parameter Percentile Sets (Results Presented on a per Ci Source Basis).....	B-42
B-11.	Diagram of the Modeling Progression from Three- to One-Dimensional Models.....	B-43
B-12.	Impact of Revision to Hanford Hf1 and Hf2 Contact Depth in the Three-Dimensional Geologic Model.	B-45

TABLES

B-1.	Horizontal and Vertical Spacing of the Finite Difference Cells in the Three-Dimensional ERDF Flow and Transport Model Domain.....	B-6
B-2.	Lithologic Data Table (Excerpted and Adapted from Table B-1 in WCH-463)	B-13
B-3.	Example Identification of Hydrogeologic Units Present at a Particular Horizontal Calculation Node Location in the Three-Dimensional Model (Easting 568310 m, Northing 133850 m).....	B-15
B-4.	Control Points "Tops" Elevation Supplemented to the Lithologic Data Table.....	B-16
B-5.	Identification of Hydrogeologic Units Present at the ERDF Cell Center 1N Location Used in the One-Dimensional Screening Models.	B-29
B-6.	Identification of Hydrogeologic Units Present at the ERDF Cell Center 2S Location Used in the One-Dimensional Screening Models.	B-30
B-7.	Identification of Hydrogeologic Units Present at the ERDF Cell Center 3N Location Used in the One-Dimensional Screening Models.	B-31
B-8.	Identification of Hydrogeologic Units Present at the ERDF Cell Center 4S Location Used in the One-Dimensional Screening Models.	B-32
B-9.	Identification of Hydrogeologic Units Present at the ERDF Cell Center 5N Location Used in the One-Dimensional Screening Models.	B-33
B-10.	Identification of Hydrogeologic Units Present at the ERDF Cell Center 6S Location Used in the One-Dimensional Screening Models	B-34
B-11.	Identification of Hydrogeologic Units Present at the ERDF Cell Center 7N Location Used in the One-Dimensional Screening Models.	B-35
B-12.	Identification of Hydrogeologic Units Present at the ERDF Cell Center 8S Location Used in the One-Dimensional Screening Models.	B-36
B-13.	Identification of Hydrogeologic Units Present at the ERDF Cell Center 9N Location Used in the One-Dimensional Screening Models.	B-37
B-14.	Identification of Hydrogeologic Units Present at the ERDF Cell Center 9S Location Used in the One-Dimensional Screening Models.....	B-38
B-15.	Identification of Hydrogeologic Units Present at the ERDF Cell Center 10N Location Used in the One-Dimensional Screening Models.	B-39
B-16.	Identification of Hydrogeologic Units Present at the ERDF Cell Center 10S Location Used in the One-Dimensional Screening Models.	B-40
B-17.	Results of the One-Dimensional Abstraction Model Vadose Zone Hydrologic and Recharge Parameter Percentile Evaluations for Radionuclides with $K_d = 0$ mL/g (e.g., Technetium-99) Breakthrough to the Water Table (Results Presented on a per Ci Source Basis).....	B-44
B-18.	Revision to Hanford Hf1 and Hf2 Contact Depth Data	B-44

APPENDIX B

DEVELOPMENT OF THE FATE AND TRANSPORT MODEL FOR THE ENVIRONMENTAL RESTORATION DISPOSAL FACILITY PERFORMANCE ASSESSMENT TO EVALUATE THE IMPACT OF THE GROUNDWATER PATHWAY

B.1 PURPOSE

The purpose of the Environmental Restoration Disposal Facility (ERDF) performance assessment (PA) flow and transport modeling is to evaluate the impacts to groundwater associated with waste disposal operations at the ERDF. The modeling is conducted in accordance with the DOE G 435.1 performance assessment guidelines. The modeling includes both a one-dimensional screening phase and a three-dimensional evaluation of the groundwater concentrations and radionuclide arrival times during the 1,000-year compliance and 10,000-year sensitivity-uncertainty periods per DOE O 435.1. This analysis does not consider radionuclide release during facility operations, only the post-closure impacts of the radionuclides to the environment. The intent of the screening phase is to limit the model analysis to those radionuclides sufficiently mobile to impact groundwater within the compliance and sensitivity-uncertainty periods. The screening phase followed the federal soil screening guidance and U.S. Department of Energy (DOE) performance assessment guidelines (EPA/540/F-95/041; DOE G 435.1-1, Chapter 4) that approve of the use of site-specific but simple models for risk assessment screening purposes. For the ERDF PA reference case evaluation, the model incorporates three dimensions to account for the lateral movement of water and radionuclides and maintain comparability with other vadose zone transport analyses conducted at the Hanford Site.

The purpose of this appendix is to provide an explanation, the basis for, and the information necessary to understand the model construction process. Companion data packages have been prepared during the preparation of the ERDF PA that describe in detail the development and basis for the fate and transport model and parameter estimation process. These data packages include a conceptual model description of radionuclide release and transport (WCH-477, *Conceptual Models for Release and Transport of Environmental Restoration Disposal Facility Waste Contaminants through the Near Field Environment*); estimates of life-cycle radionuclide inventory disposed in the ERDF (WCH-479, *Inventory Data Package for ERDF Waste Disposal*); and descriptions of local hydrogeology and soil column hydrologic properties, including net infiltration and recharge (WCH-463, *Hydrogeologic Model for the Environmental Restoration Disposal Facility, Hanford Site*; WCH-464, *Hydrologic Data Package in Support of Environmental Restoration Disposal Facility Performance Assessment Modeling* and WCH-515, *Parameter Uncertainty for the ERDF Performance Assessment Uncertainty and Sensitivity Analysis*). The information contained in the data packages is included and summarized in Chapter 3.0 and not repeated here.

B.2 METHODOLOGY

The methodology for a PA of ERDF is developed based on the following aspects that influence the approach adopted for modeling:

- A compliance case that includes the most likely assumptions about future conditions and best estimate or central tendency parameter estimates is used to assess the performance of ERDF in meeting the post-closure facility performance objectives specified in DOE O 435.1 and to establish waste acceptance criteria.
- Nearly all data, including those for radionuclide inventory, geology, hydrology, and geochemistry, are based on site characterization.
- Field-scale processes that are characteristic of highly heterogeneous Hanford Site sediments (e.g., lateral flow and migration) are simulated using flow and transport models that focus on the radionuclide pathway through the vadose zone and saturated zone.
- All computer codes used have been benchmarked and deemed suitable for undertaking a PA.
- Multiple sensitivity and uncertainty analyses are conducted to provide insight into the impacts that selected assumptions and data choices have on the results.

Key assumptions that limit the scope of this analysis are as follows:

- The engineered cover for ERDF is not yet designed but is considered similar to the Modified *Resource Conservation and Recovery Act of 1976* (RCRA) Subtitle C Barrier that limits infiltration through the waste primarily by evapotranspiration processes (i.e., surface barrier). These processes are not modeled directly. Instead, net infiltration rates applied to the area under the engineered cover are varied spatially and temporally as appropriate according to the estimated or assumed time-dependent performance of a surface barrier.
- The land use and land cover, including the surface barrier, remain shrub-steppe indefinitely.
- The physical and chemical properties of waste material in ERDF are comparable to those of the Hanford Hf1 (gravel-dominated) unit. These properties are not varied during the simulation time.
- For the compliance case, the radionuclide release mechanisms from the source are assumed to be controlled primarily by advection along with equilibrium sorption-desorption processes.
- Calculations are performed for unit curie (Ci) as a source term for the ERDF cells.
- Release and migration from one ERDF cell does not alter similar processes occurring in the other cells.
- The inventory of radionuclides in ERDF is assumed to be uniformly distributed throughout the waste disposal volume.

- Inventories of radionuclides in ERDF are the best available estimates at this time.
- The vadose zone is modeled as an aqueous-gas porous media system where flow and transport through the gas phase is neglected for the purpose of modeling transport to the saturated zone.
- Each heterogeneous geologic unit within the vadose zone is replaced by its homogeneous equivalent. Each geologic unit is assigned its upscaled or effective hydraulic properties.
- Post-closure groundwater flow beneath ERDF is assumed to be west to east and parallel to the long dimension of ERDF.
- A range of distribution coefficient (K_d) values is used to represent sediment-radionuclide chemical interaction. Single values and ranges of values are chosen that are radionuclide-specific. However, the same values are sometimes used for groups of radionuclides that show similar levels of chemical reactivity with Hanford soils and sediments. For known mobile radionuclides, the selected single values are intended to be reasonably conservative or best estimate. For moderate to highly reactive radionuclides, conservative minimum K_d values are used. Ranges of values are provided for mobile radionuclides that best represent plausible levels of reactivity.
- The timeline for human actions used in this assessment is based on requirements in DOE O 435.1 and guidance from supporting documents.
- The point of calculation of the groundwater concentration corresponds to the location 100 m downgradient from the facility per DOE O 435.1.

B.3 CONCEPTUAL MODEL COMPONENTS

The site-specific conceptual model components for the ERDF PA evaluation are as follows:

- Model domain and boundary conditions
- Geologic setting
- Source term
- Groundwater domain and characteristics
- Vadose zone hydrogeology and fluid transport
- Recharge
- Geochemistry.

Although the model domain and boundary conditions are not generally regarded as conceptual model elements, they are included in the list above to emphasize the fundamental nature of boundary conditions in the modeling.

Model Domain and Boundary Conditions

The model domain for flow and transport in the vadose zone is represented numerically in three-dimensional space with the east-west axis aligned in the general direction of groundwater flow. Aligning the east-west axis with the general direction of groundwater flow allows concentrations to be calculated downgradient of the waste sites. The numerical model adapts the physical elements of the conceptual model to a Cartesian grid and also assigns numerical values to the parameters used in algorithms to represent the physical and geochemical systems and processes.

Because of the large size of the ERDF, the grid required a relatively large domain to contain the facility and minimize possible boundary effects in the area of interest (i.e., the point of calculation). The ERDF model domain is 1,880 m (6,170 ft) west to east by 1,235 m (4,050 ft) north to south by 121 m (397 ft), vertically, extending about 15 m (49 ft) below the water table. The western boundary of the model is 568,100 m (Lambert Coordinate system easting, Stem 1989), and the eastern boundary is 569,980 m. The northern boundary is 135,065 m (Lambert Coordinate system northing), and the southern boundary is 133,830 m. The vertical base elevation of the model is 109 m (NAVD88), with the top of the model domain varying spatially according to the surface relief (WCH-463), and also varying depending on the phase of the model. During the pre-operations phase, the undisturbed ground surface establishes the upper boundary of the model and ranges between 208 and 228 m (NAVD88) (see Figure B-1a). During the operations and early post-closure phases, the space representing the ERDF excavation is inactivated and the base of the excavation (194 m NAVD88) becomes the upper boundary of the model within that area (see Figure B-1b). During the late post-closure period, the ERDF excavation is activated and the top of the ERDF trapezoid (218 m NAVD88) becomes the upper boundary of the model within that area (see Figure B-1c).

The horizontal node spacing varies between 10 and 40 m to optimize the discretization in the areas attempting to approximate the slopes associated with construction of ERDF without overwhelming the available computational resources. The vertical spacing was 2 m except around the water table where the spacing increased to 2.25 and 3.0 m to keep the surface of the water table within one numerical layer. The total number of nodes in the modeled rectangular prism equals 493,240. During the pre-operational phase, the number of active nodes equals 443,434 with 49,806 inactive. During the operational phase, the number of active nodes equals 425,319 with 67,921 inactive, the increase in inactive nodes attributed to the inactivation of the nodes within the ERDF excavation. During the post-closure phases, the number of active nodes increases to 444,331, with 48,909 inactive. Table B-1 presents the pattern of the spacing of the finite difference cells, and Figure B-2 shows the plan view distribution of the calculation nodes.

Figure B-1. Surface Elevation of the ERDF Model Domain (a) During the Pre-Operational Period, (b) During the Operations Period 1996-2035, and (c) After Closure in 2035.

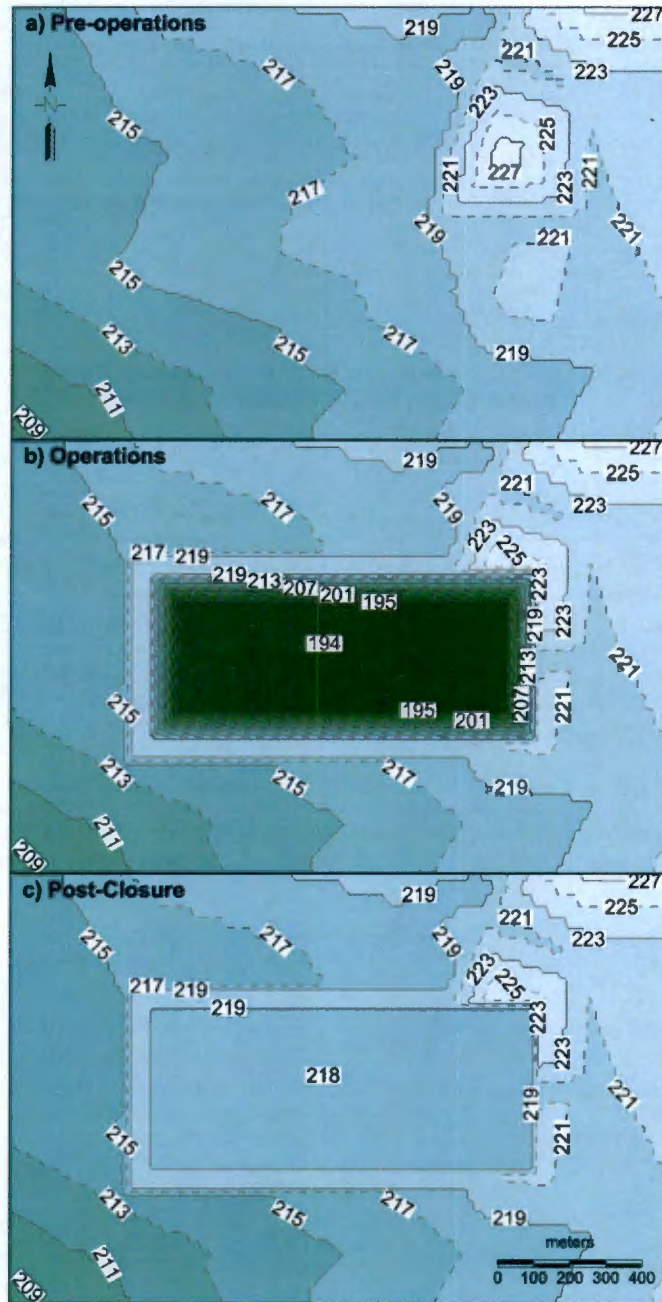
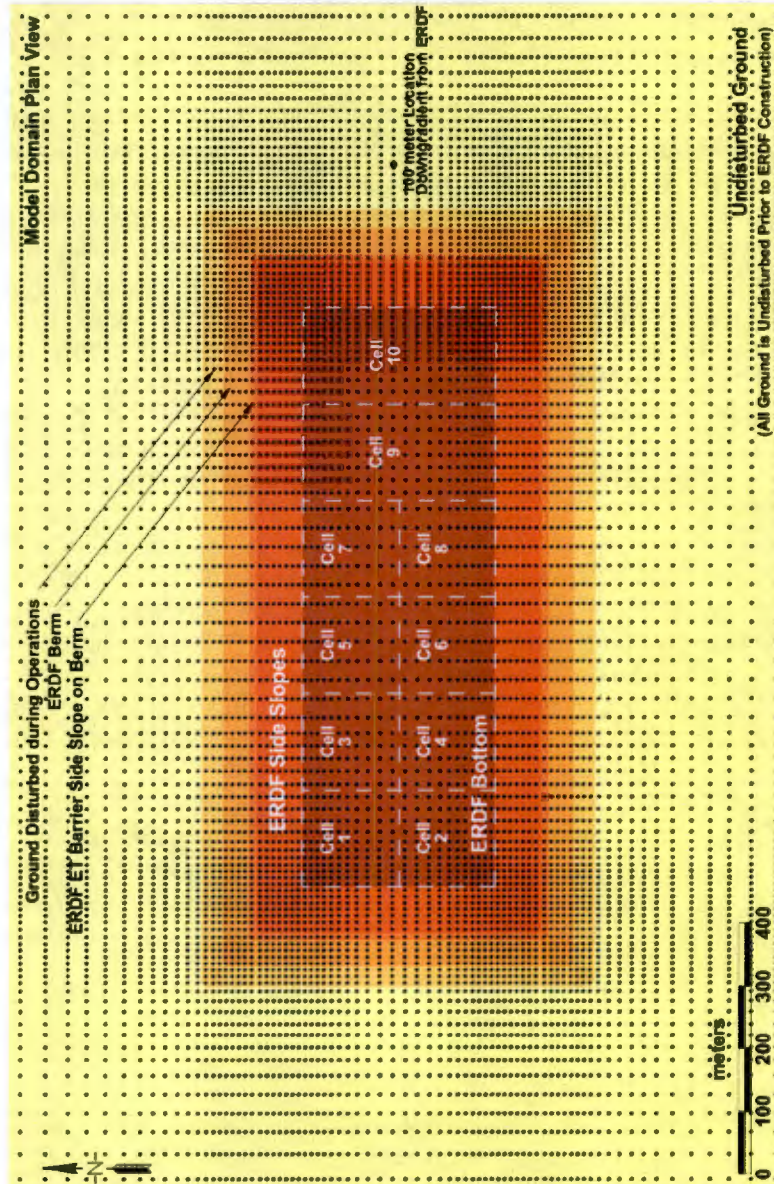


Table B-1. Horizontal and Vertical Spacing of the Finite Difference Cells in the Three-Dimensional ERDF Flow and Transport Model Domain.

West to East Spacing; Western Boundary Coordinate = 568,100 m (Lambert Coordinate System Easting)						
2@40.00 m	4@30.00 m	3@20.00 m	1@19.50 m	1@18.25 m	1@16.00 m	1@13.75 m
1@12.50 m	6@10.00 m	2@12.50 m	10@10.00 m	2@12.50 m	1@13.75 m	1@16.00 m
1@18.25 m	1@19.50 m	6@20.00 m	12@30.00 m	8@20.00 m	1@19.50 m	1@18.25 m
1@16.00 m	1@13.75 m	2@12.50 m	11@10.00 m	2@12.50 m	15@10.00 m	3@12.50 m
1@13.75 m	1@16.00 m	1@18.25 m	1@19.50 m	2@20.00 m	2@30.00 m	1@40.00 m
South to North Spacing; Southern Boundary Coordinate = 133,830 m (Lambert Coordinate System Northing)						
2@40.00 m	4@30.00 m	2@20.00 m	1@19.50 m	1@18.25 m	1@16.00 m	1@13.75 m
1@12.50 m	6@10.00 m	2@12.50 m	10@10.00 m	2@12.50 m	1@13.75 m	1@16.00 m
1@18.25 m	1@19.50 m	2@20.00 m	1@19.50 m	1@18.25 m	1@16.00 m	1@13.75 m
2@12.50 m	10@10.00 m	2@12.50 m	6@10.00 m	1@12.50 m	1@13.75 m	1@16.00 m
1@18.25 m	1@19.50 m	2@20.00 m	4@30.00 m	2@40.00 m	0@40.00 m	0@40.00 m
Vertical Spacing; Bottom Elevation = 109 m (NAVD88)						
2@2.00 m	4@2.25 m	2@3.00 m	1@2.00 m	50@2.00 m		

NOTE: The sequences read left to right. The number preceding the "@" symbol indicates the number of columns (west to east), rows (south to north), or vertical layers (bottom to top) that have the length indicated by the distance following it.

Figure B-2. Plan View of ERDF Model Domain Showing the Horizontal Distribution of the Irregularly Spaced Calculation Nodes.



The resolution increases in the area of the ERDF side slopes and point of calculation 100 m downgradient from the facility.

A specified-flux boundary condition is applied at the surface to simulate recharge. Recharge rates vary spatially and temporally along the upper boundary depending on site conditions, the location and physical dimensions of ERDF, and the time of ERDF operations and surface conditions simulated (Section 3.4.1.3). The bottom boundary of the unsaturated (vadose) zone is the water table, and the bottom of the model (aquifer) is defined as a vertical no-flow boundary condition. Boundary conditions at the sides of the model domain in the vadose zone

are assumed to be no flow. In the aquifer, the boundary conditions are prescribed flux and prescribed head, respectively, on the upgradient and downgradient boundaries, including the capillary fringe. The location of the side boundaries is arbitrary and selected on the basis that the flow field and moisture profile should not change substantially at the side boundaries (confirmation of the validity of this assumption is addressed in Section 5.0).

The boundary condition in the aquifer on the upgradient boundary was assumed to be prescribed flux and independent of recharge. To maintain a constant flux in the aquifer, the prescribed flux boundary condition value must account for the fact that in an unconfined aquifer the flux varies as the hydraulic head varies (assuming that the saturated hydraulic conductivity of the aquifer is constant). To maintain a constant volumetric flux (assuming negligible effect from meteoric recharge), the hydraulic gradient must compensate for the changes in the hydraulic head. Therefore, the hydraulic gradient is not a constant, but is a spatially varying value that maintains mass conservation in the aquifer. Therefore, to determine the upgradient prescribed flux boundary condition requires calculating the volumetric flux in the aquifer, the hydraulic head, and the hydraulic gradient at the upgradient boundary of the model.

The hydraulic heads around ERDF are expected to continue declining slowly until they stabilize around year 2200 at 125.8 m NAVD88 (412.7 ft) in the western part of the facility and 121.6 m NAVD88 (398.9 ft) in the eastern part (CP-47631, as cited in WCH-515 and WCH-462). This stabilization leads to a long-term hydraulic gradient value of 0.0015. Changes in hydraulic gradient are expected to occur within the first 200 years of the post-closure simulation period, which, according to the screening analysis is before the mobile radionuclides reach the water table. Thus, the hydraulic gradient is assumed to be stable for this analysis. Projecting the water-level elevations to the model boundaries according to the hydraulic gradient results in an elevation of 126.5 m NAVD88 at the western boundary and 123.7 m NAVD88 at the eastern boundary of the model.

For the volumetric flux (C) to remain constant in an unconfined aquifer, and assuming unidirectional flow, the product of the saturated hydraulic conductivity, hydraulic gradient, and hydraulic head relative to the base of the model must remain a constant in the aquifer throughout the model domain, i.e.,

$$K_s \frac{\partial h}{\partial x} h = C \quad \text{Equation 1}$$

where $\frac{\partial h}{\partial x}$ and h are the spatially varying hydraulic gradient in the direction of flow and hydraulic head in the aquifer, respectively, and K_s is the aquifer hydraulic conductivity. C is the constant volumetric flux. The gradient across the entire model domain is defined as, with the subscripts u and d used to denote upgradient and downgradient locations, respectively:

$$\nabla H = \frac{h_d - h_u}{x_d - x_u} \quad \text{Equation 2}$$

The definite integral of Equation 1 between the upgradient and downgradient model boundaries, solved for C , assuming K_s is constant and exploiting Equation 2, is

$$C = \frac{K_s(h_d^2 - h_u^2)}{2(x_d - x_u)} = \frac{K_s(h_d - h_u)(h_d + h_u)}{2(x_d - x_u)} = \frac{K_s \nabla H(h_d + h_u)}{2} \quad \text{Equation 3}$$

Inserting the solution for C from Equation 1 into Equation 3 results in the following solution for $\frac{\partial h}{\partial x}$:

$$\frac{\partial h}{\partial x} = \frac{1}{2h} \frac{(h_d^2 - (h_d - \nabla H(x_d - x_u))^2)}{(x_d - x_u)} \quad \text{Equation 4}$$

According to the results of the Central Plateau groundwater model (CP-47631) presented in WCH-515, the hydraulic heads in the western and eastern parts of ERDF will stabilize around year 2200 to post-closure steady-state values of 125.8 m (412.7 ft) and 121.6 m (398.9 ft), respectively, as indicated by the elevation estimated for well 699-35-70 and well 699-36-61A, respectively (see Figure 17 in WCH-515). The hydraulic gradient between the wells after the hydraulic heads have stabilized is estimated to be -0.0015 m/m (see Figure 18 in WCH-515). Figure B-3 shows the location of the wells and the ERDF model boundaries. Extrapolating the projected water level elevation in wells 699-35-70 (125.8 m NAVD88) and 699-36-61A (121.6 m NAVD88) (WCH-464) to the western and eastern boundaries of the model according to the gradient between the wells (-0.0015 m/m) results in projected elevations of 126.5 m and 123.7 m NAVD88, at the two model boundaries, respectively, i.e.:

$$H_u = 125.8 + \frac{(121.6 \text{ m} - 125.8 \text{ m})}{(571395.5 \text{ m} - 568566.5 \text{ m})} * (568100 \text{ m} - 568566.5 \text{ m}) = 126.5 \quad \text{Equation 5}$$

and

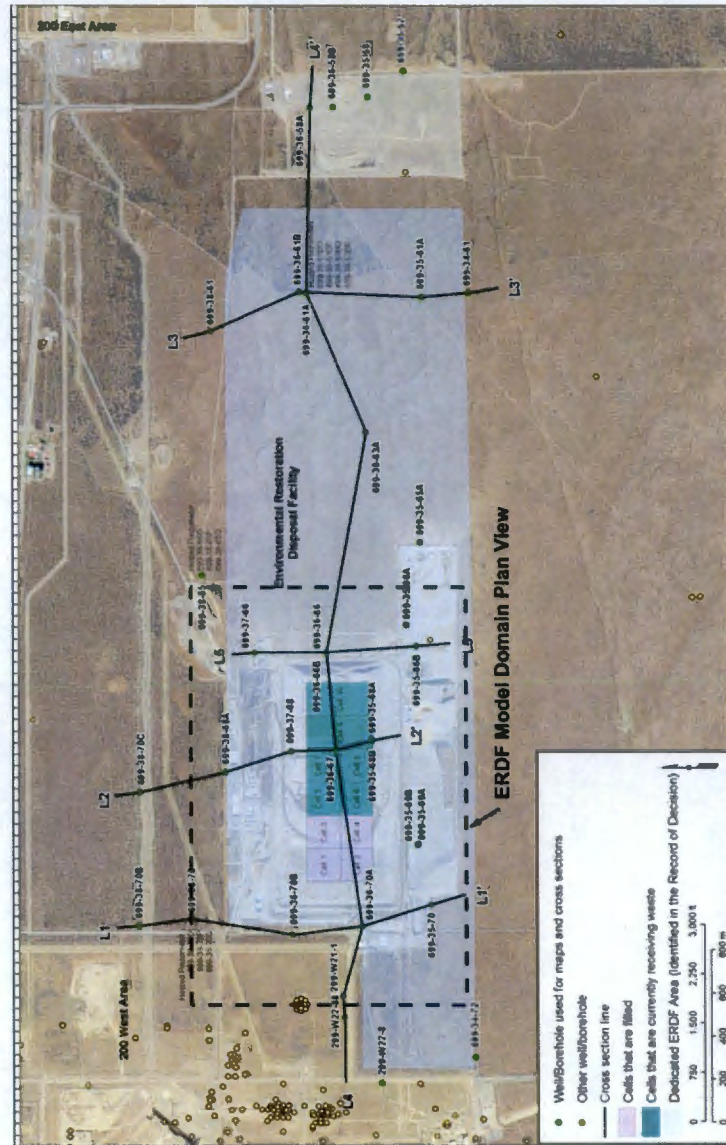
$$H_d = 121.6 + \frac{(121.6 \text{ m} - 125.8 \text{ m})}{(571395.5 \text{ m} - 568566.5 \text{ m})} * (571395.5 \text{ m} - 569980 \text{ m}) = 123.7 \quad \text{Equation 6}$$

With the base of the model defined as 109 m NAVD88, the hydraulic head at the two model boundaries is 17.5 and 14.7 m. The gradient at the western boundary, $\frac{\partial h}{\partial x}[u]$ is equal to 0.00137 m/m at the upgradient boundary for the purpose of calculating the prescribed flux:

$$\frac{\partial h_u}{\partial x} = \frac{1}{2 * 17.5} \frac{(14.7^2 - (14.7 - (-0.0015)(569980 \text{ m} - 568100 \text{ m}))^2)}{(569980 \text{ m} - 568100 \text{ m})} = 0.00137 \quad \text{Equation 7}$$

For the compliance case aquifer hydraulic conductivity value of 5 m/day, the prescribed water flux is calculated to be 2.495 m/yr (per square meter area normal to the flow direction). The prescribed head at the downgradient boundary is 123.7 m NAVD88.

Figure B-3. Location of Control Points Supplemental to the Lithologic Data Table, Wells 699-35-70 and 699-36-61A, and the ERDF Model Boundary.



Geologic Setting

The geologic setting information presented here is a summary and synopsis of the information presented in WCH-463 and Section 3.4.1.4. The vadose zone is approximately 80 to 100 m (262.4 to 328.1 ft) thick, and the ERDF trench excavation is 21.3 m (70 ft) deep (WCH-195), indicating that there is approximately 60 to 80 m between the base of the ERDF and the present-day water table. The suprabasalt aquifer system ranges from 50 to 100 m (164.0 to 328.1 ft) thick. The 10 stratigraphic units recognized in the ERDF area include the following:

- Recent (Holocene) backfill material (Hdb)
- Hanford formation unit 1 – gravel-dominated sequence (Hf1 unit)
- Hanford formation unit 2 – sand-dominated sequence (Hf2 unit)
- Cold Creek unit silt – fine grained (CCu_z)
- Cold Creek unit calcic geosol – coarser grained (CCu_c)
- Ringold Formation member Taylor Flat – fine grained (RFtf)
- Ringold Formation unit E – silty, sandy gravel (RFwie)
- Ringold Formation lower mud unit – fine-grained sequence (RFIm)
- Ringold Formation unit A – silty, sandy gravel (RFwia)
- Columbia River Basalt Group.

The ERDF waste disposal cells penetrate through the Hf1 unit and lie within the sand-dominated Hf2 unit in the thick vadose zone. The Cold Creek unit lies directly beneath the Hanford formation and is subdivided into two subunits, the CCu_z and CCu_c. The CCu_z and CCu_c are laterally continuous throughout most of the 200 West Area, but truncate to the east beyond the existing trench but within the ERDF dedicated area. East of this truncation, Hf2 sediment directly overlies Ringold Formation sediment. The deepest geologic units within the vadose zone consist of the Ringold Formation upper fine-grained unit (RFtf) and the upper portion of the fluvial-silty sandy gravel RFwie. The other Ringold Formation subunits occur deeper in the suprabasalt aquifer and are below the base of the numerical model.

Development of the Numerical Hydrogeologic Model

The hydrogeologic conceptual model developed for the ERDF PA (WCH-463) provides the information basis and data necessary to prepare the three-dimensional geologic inputs used in the three-dimensional numerical model. Each calculation node representing a unique set of horizontal (x, and y) coordinates and vertical (z) elevation is assigned the hydrogeologic properties associated with hydrostratigraphic unit identified as existing in the space represented by the node coordinates and elevation. To translate the hydrogeologic conceptual model presented in WCH-463 to the three-dimensional finite difference numerical grid requires a multistep process. First, every horizontal calculation node location shown in Figure B-2 has a top elevation interpolated to it for each geologic unit that is present at that location. To accomplish this, the "tops" (top of geologic unit) data presented in Table B-2 are linearly interpolated according to a three-point scheme to the coordinates of the calculation nodes. The elevation of each node is then compared to the interpolated tops elevations, and the node is designated by the hydrostratigraphic unit that apparently exists at that elevation (Table B-3).

Table B-2. Lithologic Data Table (Excerpted and Adapted from Table B-1 in WCH-463). (2 Pages)

Well Name	Well ID	Total Depth (ft bgs)	Elevation (m)	Elevation Type	Elevation Source	Geophysical Log	Borehole Log	As-Built	Driller's Log	PMML (08-30-2010)	Top H1 (ft bgs)	Top H2 (ft bgs)	Top H3 (ft bgs)	Top CC1 (ft bgs)	Top CC2 (ft bgs)	Top RFD (ft bgs)	Cross Section Line	Notes						
699-36-06	C5705	285.0	220.04	Ground surface (assumed)	HEIS		X				0	NP?	NP	NP	NP	NP	NP						Undifferentiated Hanford	
699-36-06B	C6219	338.0	220.45	Disc_Z	(BAW 11/2010)	X	X	X			0	40	NP	NP	NP	255	264						L5-L5', L4-L4'	
699-36-67	B2733	303.5	218.96	Disc_Z	(BAW 11/2010)		X	X			NP	0	NP	100	202	237	255						L2-L2', L4-L4'	
699-36-70A	A0601	440.0	215.23	Disc_Z	(BAW 11/2010)		X	X		X	0	30	NP	176	204	139	265	432					L1-L1', L4-L4'	
699-36-70B	C4299	427.0	214.49	Disc_Z	(BAW 11/2010)	X	X	X		X	0	46	NP	167	193	230	250	420					L1-L1'	
699-37-66	C5704	340.8	221.20	Disc_Z	(BAW 11/2010)	X	X	X			0	50	NP	NP	NP	NP	258						L5-L5'	
699-37-68	B2732	297.0	217.80	Disc_Z	(BAW 11/2010)		X	X			NP	0	NP	183	180	225	241						L2-L2'	
699-38-61	A5464	358.1	227.36	Disc_Z	(BAW 11/2010)		X	X			0	57	NP	NP	NP	NP	330						L3-L3'	
699-38-65	A5148	536.0	230.71	Top of casing, north edge, stamped	HEIS					X	0	NP	NP	241	NP?	NP	282						Undifferentiated Cold Creek unit	
699-38-68A	A9516	307.0	218.21	Disc_Z	(BAW 11/2010)		X	X			NP	0	NP	172	215	230	245						L2-L2'	
699-38-70	A5149	413.0	217.70	Top of casing, north edge, stamped	HEIS			X		X	0	30	NP	170	165	235	260	395					L1-L1'	
699-38-70B	C4236	478.5	221.82	Disc_Z	(BAW 11/2010)	X	X	X		X	0	32	NP	170	190	225	255	448	487				L1-L1'	
699-38-70C	C4259	419.0	225.93	Disc_Z	(BAW 11/2010)	X	X	X			0	45	NP	191	196	221	250						L2-L2'	

BAW = subject matter expert (Bruce A. Williams) contact elevation pick
 bgs = below ground surface
 HEIS = Hanford Environmental Information System
 NP = not present

Table B-3. Example Identification of Hydrogeologic Units Present at a Particular Horizontal Calculation Node Location in the Three-Dimensional Model (Easting 568310 m, Northing 133850 m).

Grid Node Easting: 568,310 m				Grid Node Northing: 133,850 m			
Hydrologic Unit:		Top of RFwie	Top of RFtf	Top of CCuc	Top of CCuz	Top of Hf2	Top of Hf1
Interpolated Elevation (m NAVD88)		135.3883	142.4335	149.1833	159.2196	199.573	209.8229
Grid Node Elevation	Hydrologic Unit	Grid Node Elevation	Hydrologic Unit	Grid Node Elevation	Hydrologic Unit	Grid Node Elevation	Hydrologic Unit
110	RFwie	143	CCuc	173	Hf2	203	Hf1
112	RFwie	145	CCuc	175	Hf2	205	Hf1
114	RFwie	147	CCuc	177	Hf2	207	Hf1
116.125	RFwie	149	CCuc	179	Hf2	209	Hf1
118.375	RFwie	151	CCuz	181	Hf2	211	None
120.625	RFwie	153	CCuz	183	Hf2	213	None
123.25	RFwie	155	CCuz	185	Hf2	215	None
126.25	RFwie	157	CCuz	187	Hf2	217	None
128.875	RFwie	159	CCuz	189	Hf2	219	None
131	RFwie	161	Hf2	191	Hf2	221	None
133	RFwie	163	Hf2	193	Hf2	223	None
135	RFwie	165	Hf2	195	Hf2	225	None
137	RFtf	167	Hf2	197	Hf2	227	None
139	RFtf	169	Hf2	199	Hf2	229	None
141	RFtf	171	Hf2	201	Hf1		

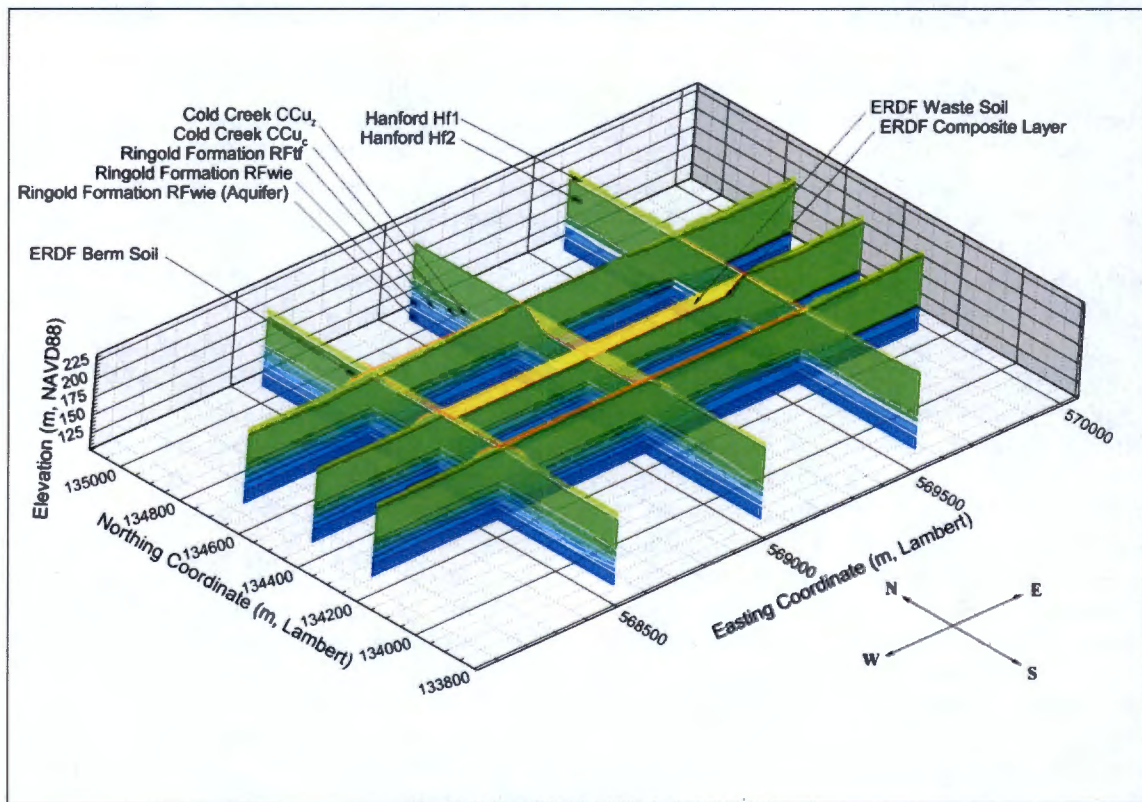
Because the rectangular area of calculation nodes shown in Figure B-2 extends outside the area containing the wells listed in Table B-2, certain control points have been included with the tops data set. The location where the Cold Creek and Ringold RFtf units begin truncating appears to occur approximately midway between lines L2-L2' and L5-L5' shown in Figure B-3. Control points have been added to approximate the location of the truncation. The control points are shown in Figure B-3 and listed in Table B-4. Tops for these control points were estimated according to trends identified in nearby wells, or inferred from the structure and isopach figures presented in Appendix C of WCH-463. The tops values of the control points are presented in Table B-4. A fence-style diagram of the resulting three-dimensional finite difference numerical grid is shown in Figure B-4.

Table B-4. Control Points "Tops" Elevation Supplemented to the Lithologic Data Table.

Control Point	Area of Extrapolation	Easting (m)	Northing (m)	Top Hf1 (m NAVD88)	Top Hf2 (m NAVD88)	Top CCu _z (m NAVD88)	Top CCu _c (m NAVD88)	Top RFFf (m NAVD88)	Top RFw _e (m NAVD88)
L5 North	North of L5-5'	569729	135125	229.50	204.39	NP	NP	NP	144.15
L5 South	South of L5-5'	569788	133636	NP	220.65	NP	NP	NP	146.12
L2 South	South of L2-2'	569344	133994	216.74	216.26	161.47	148.02	144.55	143.24
699-38-70C L2-5	Between L2-2' and L5-5'	569375	135326	227.84	205.36	165.09	160.56	155.98	148.79
699-38-68A L2-5	Between L2-2' and L5-5'	569433	134932	219.87	212.24	163.50	147.78	145.85	142.71
699-37-68 L2-5	Between L2-2' and L5-5'	569478	134629	228.70	212.98	160.18	156.23	147.40	143.68
699-36-67 L2-5	Between L2-2' and L5-5'	569505	134447	220.45	213.61	159.00	153.00	144.70	140.50
699-35-68A L2-5	Between L2-2' and L5-5'	569534	134258	222.27	208.73	159.59	153.82	146.51	142.79
L5 North L2-5	Between L2-2' and L5-5'	569424	134997	217.26	214.39	160.76	146.48	143.84	142.98
Northwest Corner	North of L4, West of L1	568047	135089	213.00	200.00	170.00	160.00	150.00	140.00

NOTE: Water level contours and groundwater flow direction reproduced from DOE/RL-2011-01, 2011, *Hanford Site Groundwater Monitoring Report for 2010*.

Figure B-4. Diagram of the Interpolated Numerical Three-Dimensional Post-Closure Hydrogeologic Model.



Radionuclide Source Distribution

The ERDF waste disposal volume consists of a 21.3-m (70-ft)-deep trench divided into a series of 10 cells. The term "cell" refers to the disposal area, leachate collection sump, and associated piping and crest pad building (BHI-00355, *Design Analysis: Construction of W-296 Environmental Restoration Disposal Facility*). Also, depth is a relative measure and the floor of ERDF has been maintained reasonably flat even though the surface elevation increases toward the east (WCH-195). The first eight cells each measure 152.4 by 152.4 m (500 by 500 ft) at the base, with two cells aligned side-by-side in the north-south direction, and four cells aligned side-by-side in the west-east direction (BHI-00355; WCH-195). Two newer "super cells" located in the eastern end of the trench are equivalent in size to a north-south cell pair and are aligned with the other cells in the west-east direction (WCH-195). The side slopes of the trench are 3:1 horizontal to vertical (BHI-00355). The surface of the waste in the trench is graded 2% upwards from the edges to the center (WCH-195). To approximate the volume of ERDF, the facility is assumed to occupy the space of a trapezoidal prism. While this neglects the waste surface grading and ground surface elevation change, these gradual features are not likely to be expressed meaningfully in a numerical grid with spacing no finer than 10 m (33 ft) x 10 m (33 ft) x 2 m (6.6 ft). The depth dimension is rounded to the nearest even integer (22 m [72 ft]) to make that measurement consistent with the 2-m vertical spacing in the model.

In the model approximation, the extent of the trench at the bottom is 915 m (3,000 ft) in the west-east direction and 305 m (1,000 ft) in the north-south direction (WCH-195). With 3:1 horizontal to vertical side slopes to the trench and a depth of 22 m (72 ft), the extent of the trench at ground surface is 1,050 m (3,440 ft) in the west-east direction and 440 m (1,430 ft) in the north-south direction. According to the exact solution for a trapezoidal prism, the ERDF disposal volume approximation is $8.04 \times 10^6 \text{ m}^3$ ($2.84 \times 10^8 \text{ ft}^3$). Interpolating the trapezoidal volume to the three-dimensional finite difference grid results in the following approximations of the dimensions. At the bottom of the trench, the dimensions are unchanged, but the surface dimensions in the west-east and north south directions measure 1,035 m (3,400 ft) and 425 m (1,390 ft) in the numerical grid, respectively. Summing the volume of the numerical grid cells representing ERDF waste soil in the three-dimensional finite difference model grid produces a volume of $7.76 \times 10^6 \text{ m}^3$ ($2.74 \times 10^8 \text{ ft}^3$), which is within 4% of the exact solution.

The radionuclides within the waste material (such as bulk soil) are assumed to be distributed homogeneously within the ERDF waste volume. The distribution of waste in ERDF is highly uncertain as is the quantification of currently disposed radionuclides (WCH-479). Detailed characterization of the waste has not been performed. While the chronology of waste site disposal at ERDF and the historical availability of the ERDF cells to receive the waste are known, ERDF operations make no effort to segregate waste received from the particular waste sites after disposal (WCH-479). When new cells have opened, waste from existing cells is often spread to the new cells to level the surface of the overall disposal area. Such mixing and redistribution of waste in the cells greatly diminishes the ability to approximate the spatial distribution of the radionuclides (WCH-479). Therefore, all grid nodes identified as ERDF waste material are assigned a volumetric concentration of $1.28878\text{E-}07$, Ci/m³ to produce an initial inventory quantity of 1 Ci, which allows the easy scaling of results to any initial inventory quantity.

For the purpose of this evaluation, the conceptual model considers only the advective release of radionuclides from the waste material. The release of radionuclides is unlimited by any mechanisms that would restrain the release, such as solubility limits, metal precipitation, corrosion rates of activated metals, diffusion limited control of radionuclides from solid form, or

radionuclide sequestration from the advective flow path. All of the radionuclides in the source area are available for advective transport, and the release occurs according to the equilibrium K_d . The waste material itself and any actions taken to stabilize it, such as grouting, are assumed not to affect the hydraulic properties of the ERDF waste and backfill material.

Groundwater Domain and Characteristics

The model domain limits the depth of aquifer to approximately 15 m (49 ft), although the thickness of the uppermost aquifer beneath ERDF generally appears to range from 20 to 70 m (65 to 230 ft). The model results represent concentrations in the upper 5 m (16.4 ft) of the aquifer, which corresponds to a conceptual groundwater monitoring well with the 4.6-m (15-ft) well screen length (and mixing zone dimension) according to state monitoring well descriptions (e.g., see *Washington Administrative Code [WAC] 173-340-747*). The aquifer, identified as Ringold RFWie – aquifer, is separated from that portion of the Ringold RFWie in the vadose zone, reflecting the distinctly different saturation conditions.

Vadose Zone Hydrogeology and Transport

The porous media continuum assumption and the soil relative permeability/saturation/capillary pressure relations provide the basis for vadose zone flow and transport modeling (PNNL-11217, *STOMP Subsurface Transport Over Multiple Phases Theory Guide*; PNNL-11216, *STOMP Subsurface Transport Over Multiple Phases Application Guide*). In the model domain, the hydraulic properties describing fluid transport characteristics associated with each geologic layer are approximated by average upscaled values, with each unit having different flow and transport parameter values (hydraulic conductivity, bulk density, and dispersivity). The model describes bulk (or mean) flow and radionuclide transport behavior in the vadose zone, limiting the evaluation to estimating overall and eventual radionuclide impacts to groundwater.

A stochastic model of variable moisture or tension-dependent anisotropy provides the framework for upscaling small-scale measurements to the effective (upscaled) properties for the large-scale vadose zone (Polmann, 1990, *Application of Stochastic Methods to Transient Flow and Transport in Heterogeneous Unsaturated Soils*; “Stochastic analysis of moisture plume dynamics of a field injection experiment” [Ye et al. 2005]; “Estimation of effective unsaturated hydraulic conductivity tensor using spatial moments of observed moisture plume” [Yeh et al. 2005]). Specific upscaled flow parameters include moisture retention, saturated, and unsaturated hydraulic conductivity. Upscaled transport parameters include bulk density, diffusivity, sorption coefficients, and macrodispersivity. The Gelhar and Axness model (Gelhar and Axness, 1983, “Three-dimensional Analysis of Macrodispersion in a Stratified Aquifer”) provides a method to estimate values of macrodispersivity, which according to Dagan, 1984, “Solute Transport in Heterogeneous Porous Formations,” reaches a constant, asymptotic value after the solute travels a few tens of correlation scales (~50 cm) of the hydraulic conductivity field (WCH-464).

Recharge

The magnitude of recharge for soils at the Hanford Site varies as a function of the soil type, condition of the vegetation cover, and soil integrity (e.g., disturbed versus undisturbed). The recharge values and timelines presented in Section 3.4.1.3 quantify and delimit the applicable recharge rate according to the surface conditions identified in Figure B-2 and the timeline presented in Table 3-5 (Section 3.4.1.3).

Sorption Characteristics

The basis and rationale for the K_d values used to approximate the transport of the radionuclides is presented in DOE/RL-2011-50, *Regulatory Basis and Implementation of a Graded Approach to Evaluation of Groundwater Protection*, and WCH-515. The radionuclides evaluated are limited to those with K_d values less than 1 mL/g because the results of the screening analysis indicated that radionuclides with K_d values greater than 1 mL/g did not impact groundwater within the 10,000-year sensitivity-uncertainty time frame (see Screening Analysis Results in Section 4.2.1).

Point of Calculation, Protectiveness Metric, and Time Frame Considerations

The point of calculation for the groundwater impact analysis is 100 m from the edge of the ERDF berm. The point of calculation is intended to effectively serve as the point where exposure point groundwater concentrations are evaluated in the model for the purpose of evaluating the achievement of the groundwater protection performance objectives. The point of calculation for the protection of groundwater is related to "Point of Compliance" in federal performance assessment requirements (DOE M 435.1; DOE G 435.1-1, Chapter 4) and described as follows,

The point of compliance shall correspond to the point of highest projected dose or concentration beyond a 100 meter buffer zone surrounding the disposed waste. A larger or smaller buffer zone may be used if adequate justification is provided.

The aquifer mixing zone extends into the upper 5 m of the aquifer for the purpose of the evaluations. DOE M 435.1-1 does not specify the level of protection required for water resources, and there are no applicable parameterization requirements or guidelines indicated in DOE G 435.1-1, Chapter 4. The format and content guide (U.S. Department of Energy, *Format and Content Guide for U.S. Department of Energy Low-Level Waste Disposal Facility Performance Assessments and Composite Analyses*, December 7, 1999) indicates that the aquifer mixing must be consistent with state or local laws, regulations, or agreements. While the WAC does not specify a mixing zone, the 5-m vertical interval corresponds to a conceptual groundwater monitoring well with the 4.6-m (15-ft) well screen length (and mixing zone dimension) associated with state monitoring well descriptions (e.g., see WAC 173-340-747).

The compliance time frame is defined as 1,000 years following closure of the facility (DOE M 435.1; DOE G 435.1-1, Chapter 4). The sensitivity/uncertainty analysis extends the evaluation to 10,000 years, which is sufficient to evaluate the peak dose from all of the radionuclides that the screening analysis indicates may impact groundwater within the compliance period. DOE M 435.1 and DOE G 435.1-1, Chapter 4, state that the sensitivity/uncertainty analysis time frame should include calculation of the maximum dose regardless of the time at which the maximum occurs as a means of increasing confidence in the outcome of the modeling and increasing the understanding of the models used. However, EPA-SAB-RAC-ADV-99-006, *AN SAB ADVISORY: Modeling of Radionuclide Releases from Disposal of Low Activity Mixed Waste*, warns that extending the modeling time frame beyond 10,000 years could make the results irrelevant and hinder public acceptance of the results because of the inherent scientific and social uncertainties associated with such an extended time frame. The 10,000-year time frame is sufficient to address uncertainty associated with radionuclides that impact groundwater during the compliance period (NUREG-1573).

The protectiveness metrics determined to be most appropriate for the evaluation of impacts to groundwater from the radionuclide inventory in ERDF are the maximum contaminant levels as indicated in Table 1-1 (Section 1.0). DOE G 435.1-1, Chapter 4 states that DOE low-level waste disposal facilities must comply with legally applicable requirements for water resource protection.

B.4 GROUNDWATER MODELING QUALITY ASSURANCE AND QUALITY CONTROL

The vadose zone fate and transport calculations are performed using the STOMP Version 3.2 code, HISI identification number 2471. STOMP is executed on the RANSAC Linux¹ Cluster (ransac-0.pnl.gov) that is managed by Pacific Northwest National Laboratory (PNNL) and the Green cluster managed by INTERA, Inc. The PNNL computer property tag identifier for the front-end node is WD56054 (PNNL Property System). The front-end hardware (controller node) is a Dell² PowerEdge[®] 2550 with dual 3.00-GHz (Intel³ Xeon[®]) processors and 2 GB of RAM loaded with the Red Hat[®] Enterprise Linux[®] Client release 5.5 (Tikanga) operating system. The INTERA property tag number for Green is 469, and the hardware is Dell³ PowerEdge[®] R510 with two 6-core Intel⁴ Xeon[®] X5660 processors @ 2.80GHz and 48 GB of RAM loaded with Ubuntu⁴ Linux[®] operating system 10.04, kernel 2.6.32-32-server.

The results of the code evaluation in DOE/RL-2011-50 show that the STOMP code is capable of meeting or exceeding the main model attributes and code selection criteria that serve as the basis for the demonstration of the adequacy of the STOMP code for use in vadose zone modeling at the Hanford Site. DOE/RL-2011-50, Appendix C, addresses code selection criteria including quality assurance documentation of verification studies for specific model attributes (e.g., unsaturated flow, solute transport, infiltration, and drainage) and includes a discussion of other code-related criteria (i.e., inter-code comparisons, hardware requirements, solution methodology, dimensionality, and output capability).

The results of CH2M HILL Plateau Remediation Company (CHPRC) acceptance testing demonstrate that the STOMP software is acceptable for its intended use by the CHPRC. Installations of the software are operating correctly, as demonstrated by the RANSAC Linux Cluster systems producing the same results as those presented for selected problems from the STOMP Application Guide (PNNL-11216). The Software Installation and Checkout forms for the Green cluster indicate that the installations of the software on that cluster are operating correctly (Attachment 1).

B.5 DISTRIBUTION OF MOISTURE AT THE BOUNDARIES

The side boundaries of the model domain are located far enough away to avoid interfering with the solution of the model in the area of interest. This premise is confirmed by the results of the modeling from the period 2035 through 4135, after which the results appear to reach steady state. Figures B-5, B-6, B-7, and B-8 present a time series of five times of interest of cross-section plots of moisture content at the four vertical model boundary planes.

¹ Linux is the registered trademark of Linus Torvalds in the U.S. and other countries.

² Dell, PowerEdge, and Optiplex are registered trademarks of Dell Products, Inc. Dell Precision is a trademark of Dell Products, Inc.

³ Intel, Xeon, and Intel Core are trademarks of Intel Corporation in the U.S. and other countries.

⁴ Ubuntu is a registered trademark of Canonical, Ltd.

Figure B-5. Time Series Cross-Section Plots of the Change in Moisture Content from the Post-Closure Steady-State Value at the Indicated Time of Interest at the Western Boundary of the Model.

(The area in red delineates where the moisture content changes by more than 0.0001, the maximum change is indicated on the plots.)

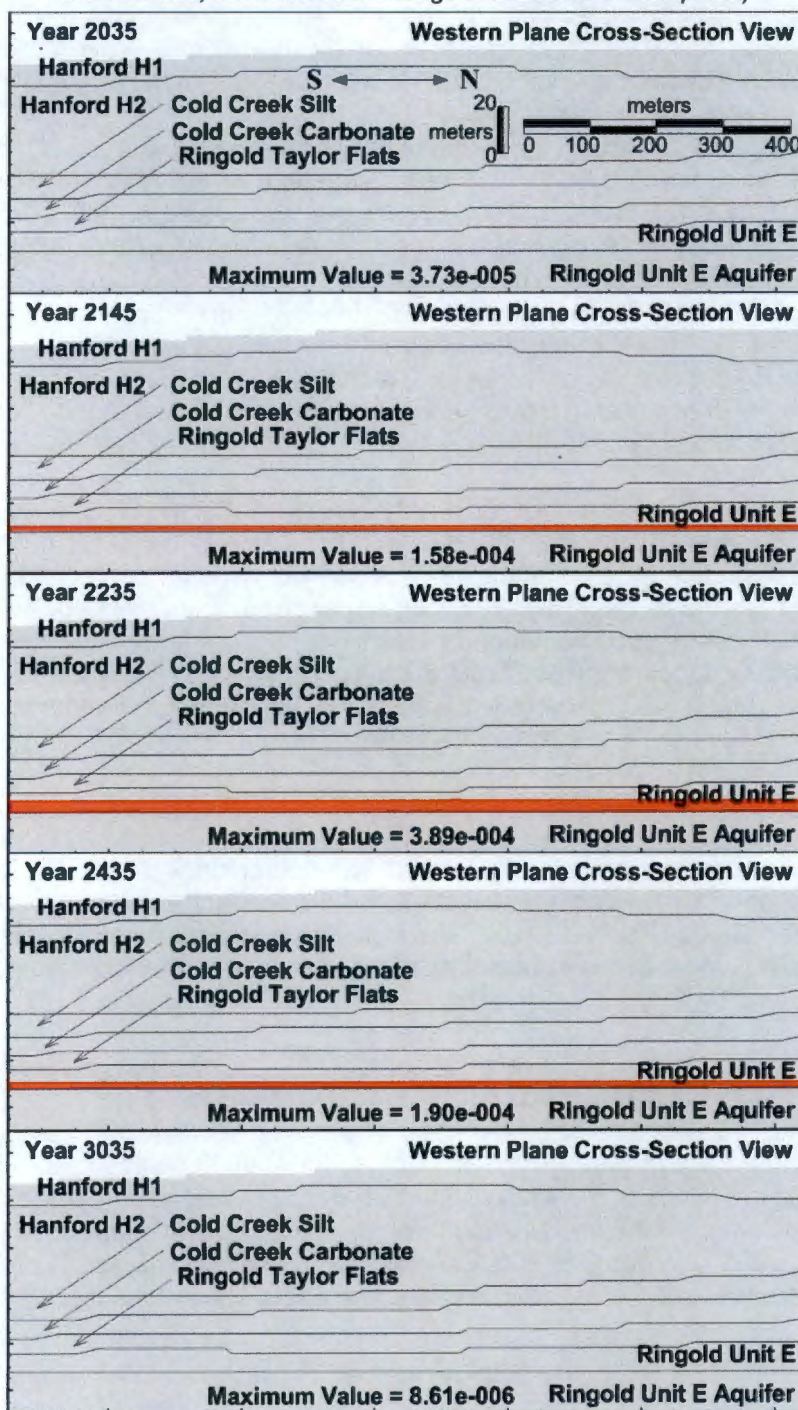


Figure B-6. Time Series Cross-Section Plots of the Change in Moisture Content from the Post-Closure Steady-State Value at the Indicated Time of Interest at the Eastern Boundary of the Model. No change exceeds 0.0001. The maximum change is indicated on the plots.

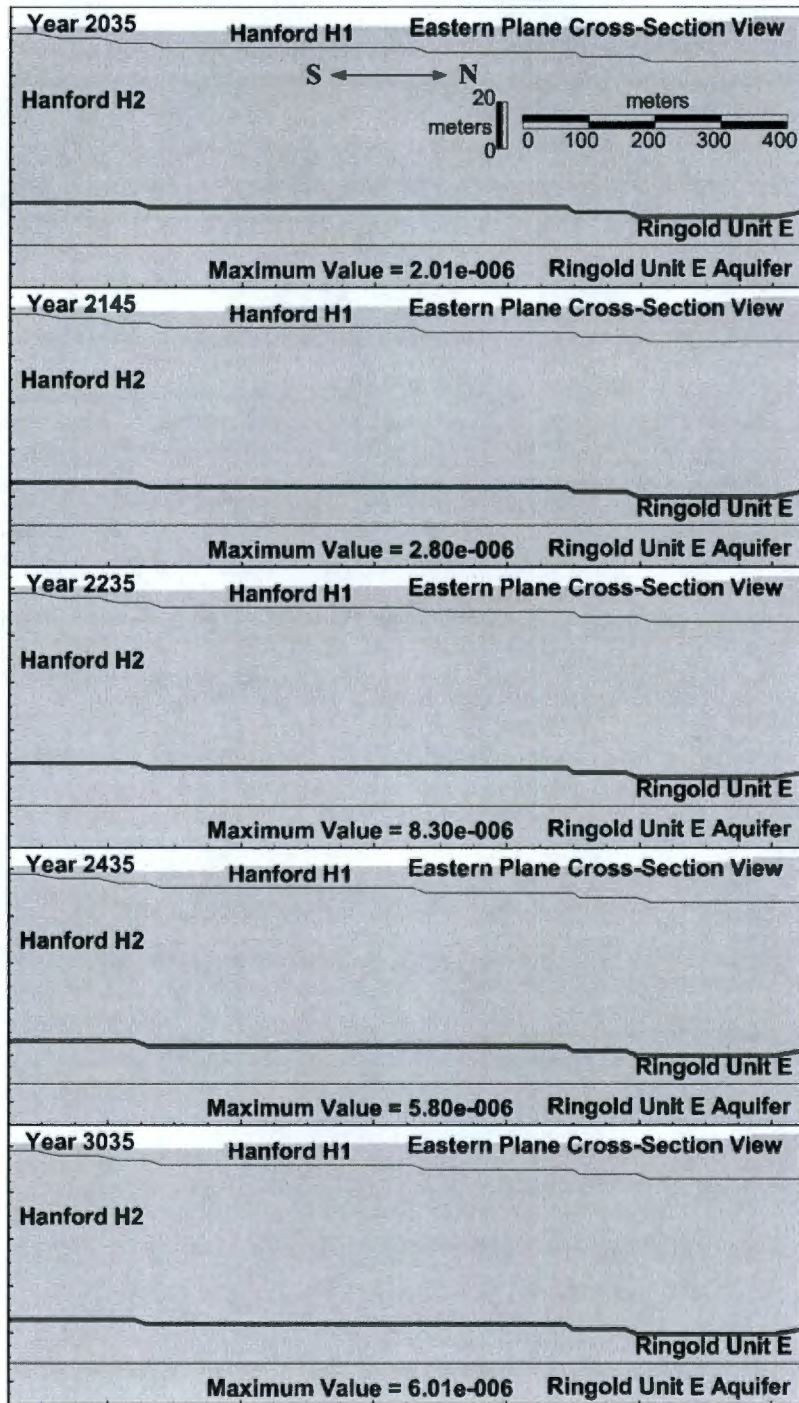


Figure B-7. Time Series Cross-Section Plots of the Change In Moisture Content from the Post-Closure Steady-State Value at the Indicated Time of Interest at the Southern Boundary of the Model. The area in red delineates where the moisture content changes by more than 0.0001, the maximum change is indicated on the plots.

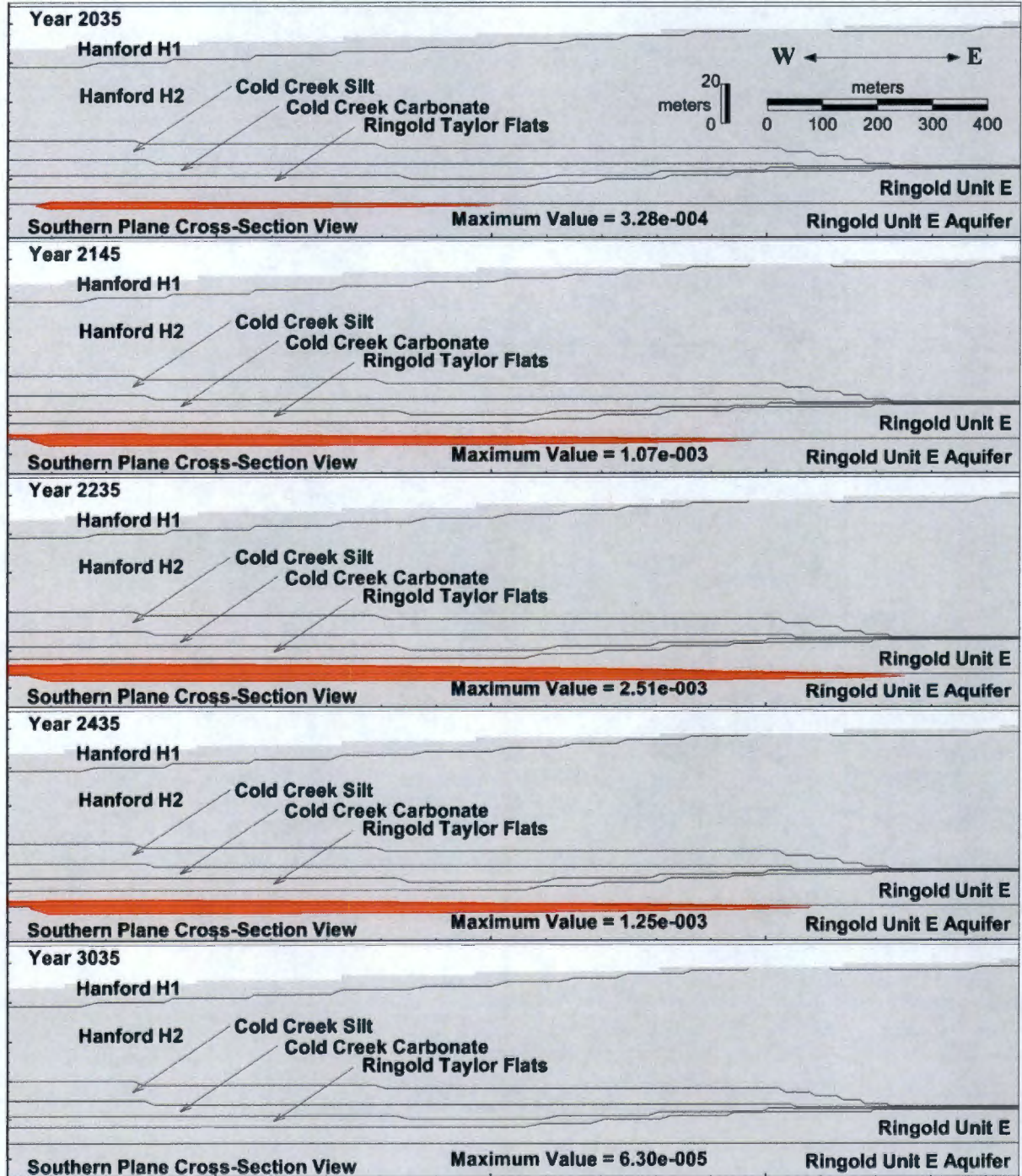
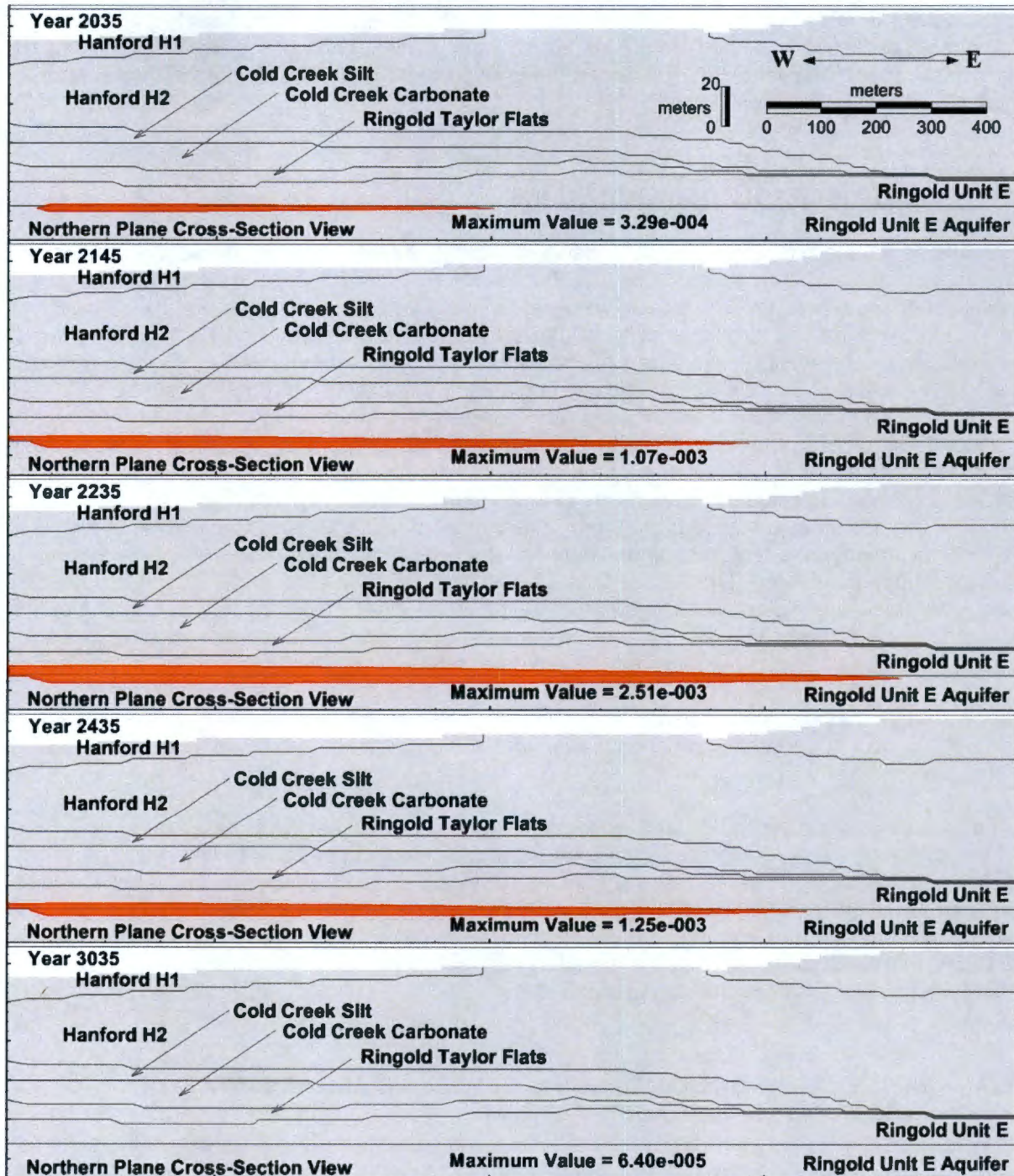


Figure B-8. Time Series Cross-Section Plots of the Change in Moisture Content from the Post-Closure Steady-State Value at the Indicated Time of Interest at the Northern Boundary of The Model. The area in red delineates where the moisture content changes by more than 0.0001, the maximum change is indicated on the plots.



The results presented in the time series plots indicate that the calculations may have included some boundary effects at the southern, northern, and western boundaries. The cross-section plots indicate that the changes in the moisture content at the boundary of the model occur relatively early during the simulation period relative to the time of radionuclide arrival at the water table. The effects are contained within a relatively small segment along the boundary near the water table and appear to be minor. These effects are considered negligible and have dissipated by the year 3050 in the model calculations. Consequently, they are not considered to adversely affect the evaluation of radionuclide transport and groundwater impacts associated with the radionuclide inventory in ERDF.

B.6 NUMERICAL SOLUTION LIMITATIONS

Results determined using numerical models will possibly be influenced by numerical dispersion, which is an artifact of the errors caused by the numerical discretization of the flow domain. To minimize these errors, the grid should be designed ideally so that the Peclet number, the ratio of the grid cell length and the dispersivity, is less than 2 (EPA/600/R-97/102, 1997, *NAPL: Simulator Documentation*). However, maintaining this criterion can lead to grid spacing and an overall domain size that are not practical to implement, especially in three dimensions. Acceptable solutions have been obtained with the Peclet Number as high as 10 (Huyakorn and Pinder 1983, *Computational Methods in Subsurface Flow*). Dispersivity is also scale dependent and increases as the travel distance of the solute increases (Gelhar et al. 1992), so common practice is simply to scale the dispersivity to the size of the model domain (EPA/600/R-97/102, 1997). The grid size selected for the three-dimensional model and the dispersivity coefficients appear to provide an adequate balance between the two demands of solution integrity and practical implementation. The 2-m vertical spacing in the vadose zone and 3-m spacing near the water table is sufficient to allow delineation of the major geologic units and the sloping of the contacts and accommodate the 5-m well screen intervals used to evaluate the impacts to groundwater. The Peclet number for the Hanford and Ringold Formation geologic units is not greater than 1.33 vertically in the vadose zone and not greater than 1.9 horizontally in the aquifer within the boundary of ERDF and the point of calculation located 100 m downgradient from the berm. The Peclet number increases to 4 vertically in the Cold Creek units, but these units are relatively thin.

Another consideration is the discretization of simulation time so that the Courant number ($Cr = \text{porewater velocity} \times \text{time interval}/\text{grid spacing}$) is less than or equal to one (EPA/600/R-97/102). The time step should be selected so that it is less than the value obtained by the ratio of grid spacing to porewater velocity, which is less than the time it takes for the solute to move one grid spacing. Time step control is provided by an internal algorithm in STOMP that reduces the time step associated with the contaminant transport iterations such that the specified Courant criterion is satisfied.

B.7 BASIS FOR THE ONE-DIMENSIONAL SCREENING AND SENSITIVITY-UNCERTAINTY MODEL ABSTRACTION

The modeling results indicate that the groundwater concentration appears to be the product of a simple scalar and the contaminant mass flux into the aquifer (see Figures 4-36 and 4-37 in Section 4.6.2.1). Thus, the variability in the groundwater concentrations is equivalent to the

variability in the flux of radionuclides into the aquifer, and these fluxes can be computed using a one-dimensional abstraction of the three-dimensional model.

The conceptual model components of the one-dimensional abstraction are the same as for the three-dimensional modeling identified in Section B.3, but the contents of those components must be revised to account for the reduction in the number of dimensions. The model domain of the one-dimensional abstraction for flow and transport in the vadose zone consists of a vertical column of 59 nodes. The domain is 152.4 m (500 ft) west to east x 152.4 m (500 ft) north to south (to approximate the area of a standard ERDF cell) x 121 m (397 ft), vertically, extending about 15 m (49 ft) below the water table. To construct the one-dimensional abstractions of the three-dimensional model, the geologic profiles associated with the centers of the first eight ERDF cells and the northern and southern halves of super cells 9 and 10 were extracted from the three-dimensional geologic model. The resulting profiles are shown in Figure B-9, and the listing of the hydrostratigraphic units that occur at the calculation nodes for all of the templates are shown in Tables B-5 through B-16. During the pre-operations phase, the undisturbed ground surface establishes the upper boundary of the model. During the operations and early post-closure phases, the space representing the ERDF excavation is inactivated, and the base of the excavation (194 m NAVD88) becomes the upper boundary of the model. During the late post-closure period, the ERDF excavation is activated and the top of the ERDF trapezoid where it intersects the one-dimensional profiles (218 m NAVD88) defines the upper boundary of the model.

A specified-flux boundary condition is applied at the surface to simulate recharge. Recharge rates vary temporally along the upper boundary depending on site conditions represented in the phases of the modeling. Because the one-dimensional columns represent the center of the ERDF cells, the top boundary represents undisturbed shrub-steppe during the pre-ERDF operations phase, the bottom liner during the operations and early post-closure phases, and the surface barrier during the late post-closure phase. The bottom boundary of the unsaturated (vadose) zone is the water table, and the bottom of the model (aquifer) is defined as a constant head boundary condition. Boundary conditions at the sides of the model domain in the vadose zone and aquifer are no flow. The groundwater domain and flow characteristics are not applicable because there is no lateral flow in the one-dimensional abstraction.

The source term component of the one-dimensional abstraction is essentially the same as the source term of the three-dimensional model, except that the waste volume is approximated by a rectangular cube 152.4 m on a side and 22 m in height. All grid nodes identified as ERDF waste material are assigned a volumetric concentration of $1.96\text{E-}06$ Ci/m³ to produce the easily scalable initial inventory quantity of 1 Ci. The geochemistry conceptual model component for the one-dimensional abstraction is the same as it is for the three-dimensional model. The vadose zone hydrogeology and fluid transport properties of the one-dimensional abstraction are the same as those in the three-dimensional model, although anisotropy is not applicable to one-dimensional calculations.

Figure B-9. One-Dimensional Transport Model Vadose Zone Templates Used in Screening and Sensitivity-Uncertainty Analysis.

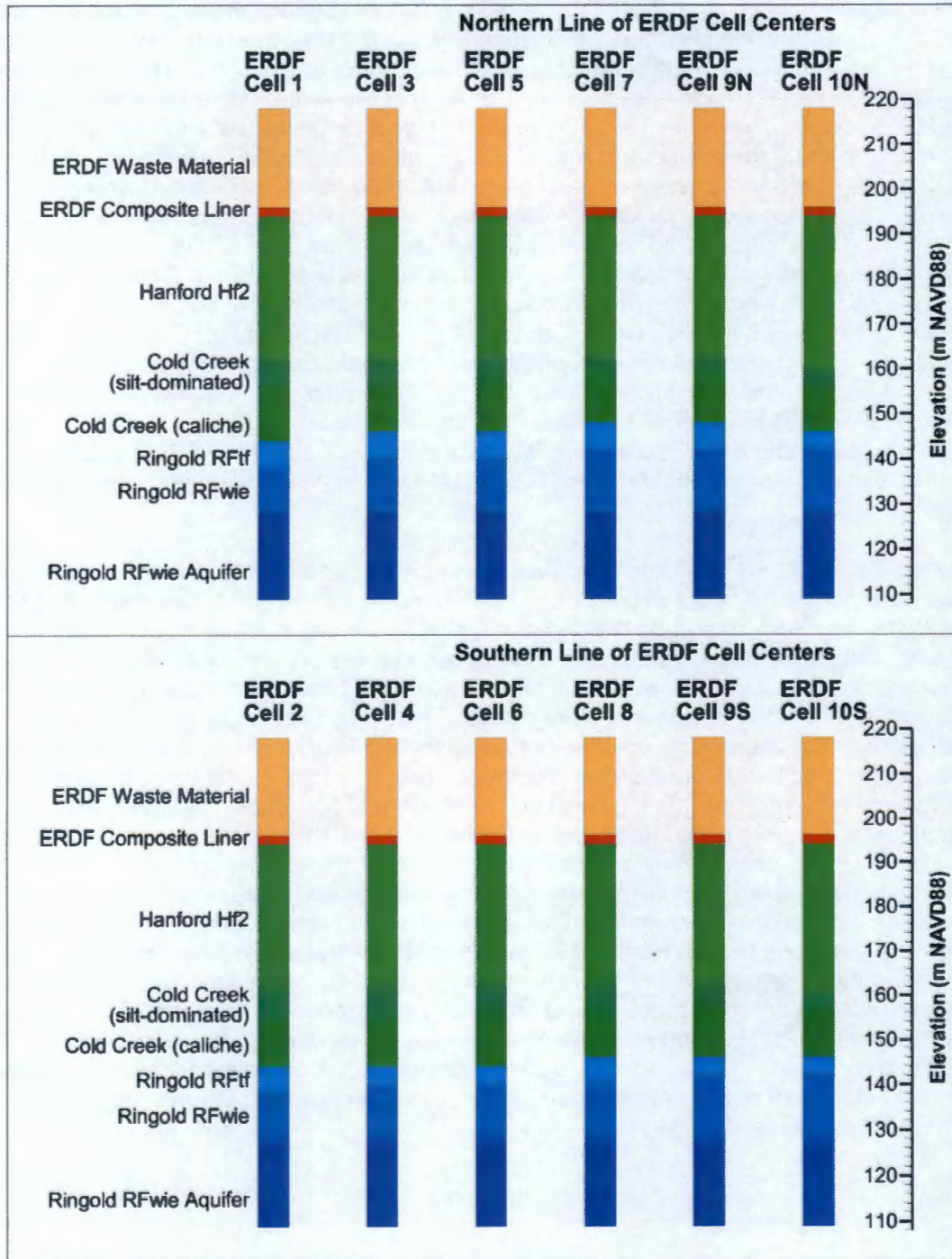


Table B-5. Identification of Hydrogeologic Units Present at the ERDF Cell Center 1N Location Used in the One-Dimensional Screening Models.

ERDF Cell 1N		Grid Node Easting: 568657m			Grid Node Northing: 134528m		
Hydrologic Unit:		Top of RFwie	Top of RFtf	Top of CCu _c	Top of CCu _z	Top of Hf2	Top of Hf1
Interpolated Elevation (m NAVD88):		138.9517	144.7142	155.7451	162.6367	206.1213	215.7685
Grid Node Elevation	Hydrologic Unit	Grid Node Elevation	Hydrologic Unit	Grid Node Elevation	Hydrologic Unit	Grid Node Elevation	Hydrologic Unit
110	RFwie	143	RFtf	173	Hf2	203	Hf2
112	RFwie	145	CCu _c	175	Hf2	205	Hf2
114	RFwie	147	CCu _c	177	Hf2	207	Hf1
116.125	RFwie	149	CCu _c	179	Hf2	209	Hf1
118.375	RFwie	151	CCu _c	181	Hf2	211	Hf1
120.625	RFwie	153	CCu _c	183	Hf2	213	Hf1
123.25	RFwie	155	CCu _c	185	Hf2	215	Hf1
126.25	RFwie	157	CCu _z	187	Hf2	217	None
128.875	RFwie	159	CCu _z	189	Hf2	219	None
131	RFwie	161	CCu _z	191	Hf2	221	None
133	RFwie	163	Hf2	193	Hf2	223	None
135	RFwie	165	Hf2	195	Hf2	225	None
137	RFwie	167	Hf2	197	Hf2	227	None
139	RFtf	169	Hf2	199	Hf2	229	None
141	RFtf	171	Hf2	201	Hf2		
	Indicates that the nodes become or remain inactive during the operations and early post-closure phases, and the hydrogeologic unit becomes composite during the late post-closure phase.						
	Indicates that the nodes become or remain inactive during the operations and early post-closure phases, and the hydrogeologic unit becomes ERDF waste during the late post-closure phase.						
	Indicates that the nodes become or remain inactive during the operations, early post-closure, and late post-closure phases.						

Table B-6. Identification of Hydrogeologic Units Present at the ERDF Cell Center 2S Location Used in the One-Dimensional Screening Models.

ERDF Cell 2S		Grid Node Easting: 568657 m			Grid Node Northing: 134367 m		
Hydrologic Unit:		Top of Rfwie	Top of RFtf	Top of CCu _c	Top of CCu _z	Top of Hf2	Top of Hf1
Interpolated Elevation (m NAVD88):		138.4708	143.6095	154.3358	161.6485	208.6203	216.0491
Grid Node Elevation	Hydrologic Unit	Grid Node Elevation	Hydrologic Unit	Grid Node Elevation	Hydrologic Unit	Grid Node Elevation	Hydrologic Unit
110	RFwie	143	RFtf	173	Hf2	203	Hf2
112	RFwie	145	CCu _c	175	Hf2	205	Hf2
114	RFwie	147	CCu _c	177	Hf2	207	Hf2
116.125	RFwie	149	CCu _c	179	Hf2	209	Hf1
118.375	RFwie	151	CCu _c	181	Hf2	211	Hf1
120.625	RFwie	153	CCu _c	183	Hf2	213	Hf1
123.25	RFwie	155	CCu _z	185	Hf2	215	Hf1
126.25	RFwie	157	CCu _z	187	Hf2	217	None
128.875	RFwie	159	CCu _z	189	Hf2	219	None
131	RFwie	161	CCu _z	191	Hf2	221	None
133	RFwie	163	Hf2	193	Hf2	223	None
135	RFwie	165	Hf2	195	Hf2	225	None
137	RFwie	167	Hf2	197	Hf2	227	None
139	RFtf	169	Hf2	199	Hf2	229	None
141	RFtf	171	Hf2	201	Hf2		
Indicates that the nodes become or remain inactive during the operations and early post-closure phases, and the hydrogeologic unit becomes composite during the late post-closure phase.							
Indicates that the nodes become or remain inactive during the operations and early post-closure phases, and the hydrogeologic unit becomes ERDF waste during the late post-closure phase.							
Indicates that the nodes become or remain inactive during the operations, early post-closure, and late post-closure phases.							

Table B-7. Identification of Hydrogeologic Units Present at the ERDF Cell Center 3N Location Used in the One-Dimensional Screening Models.

ERDF Cell 3N		Grid Node Easting: 568808m			Grid Node Northing: 134528m		
Hydrologic Unit:		Top of RFwie	Top of RFtf	Top of CCu _c	Top of CCu _z	Top of Hf2	Top of Hf1
Interpolated Elevation (m NAVD88):		139.5787	145.371	156.3612	162.4052	208.8406	216.4971
Grid Node Elevation	Hydrologic Unit	Grid Node Elevation	Hydrologic Unit	Grid Node Elevation	Hydrologic Unit	Grid Node Elevation	Hydrologic Unit
110	RFwie	143	RFtf	173	Hf2	203	Hf2
112	RFwie	145	RFtf	175	Hf2	205	Hf2
114	RFwie	147	CCu _c	177	Hf2	207	Hf2
116.125	RFwie	149	CCu _c	179	Hf2	209	Hf1
118.375	RFwie	151	CCu _c	181	Hf2	211	Hf1
120.625	RFwie	153	CCu _c	183	Hf2	213	Hf1
123.25	RFwie	155	CCu _c	185	Hf2	215	Hf1
126.25	RFwie	157	CCu _z	187	Hf2	217	None
128.875	RFwie	159	CCu _z	189	Hf2	219	None
131	RFwie	161	CCu _z	191	Hf2	221	None
133	RFwie	163	Hf2	193	Hf2	223	None
135	RFwie	165	Hf2	195	Hf2	225	None
137	RFwie	167	Hf2	197	Hf2	227	None
139	RFwie	169	Hf2	199	Hf2	229	None
141	RFtf	171	Hf2	201	Hf2		
	Indicates that the nodes become or remain inactive during the operations and early post-closure phases, and the hydrogeologic unit becomes composite during the late post-closure phase.						
	Indicates that the nodes become or remain inactive during the operations and early post-closure phases, and the hydrogeologic unit becomes ERDF waste during the late post-closure phase.						
	Indicates that the nodes become or remain inactive during the operations, early post-closure, and late post-closure phases.						

Table B-8. Identification of Hydrogeologic Units Present at the ERDF Cell Center 4S Location Used in the One-Dimensional Screening Models.

ERDF Cell 4S		Grid Node Easting: 568808 m			Grid Node Northing: 134367 m		
Hydrologic Unit:		Top of R _{Fwie}	Top of R _{Ftf}	Top of CC _{uc}	Top of CC _{uz}	Top of H _{f2}	Top of H _{f1}
Interpolated Elevation (m NAVD88):		139.0978	144.2663	154.9519	161.4171	211.3396	216.7778
Grid Node Elevation	Hydrologic Unit	Grid Node Elevation	Hydrologic Unit	Grid Node Elevation	Hydrologic Unit	Grid Node Elevation	Hydrologic Unit
110	R _{Fwie}	143	R _{Ftf}	173	H _{f2}	203	H _{f2}
112	R _{Fwie}	145	CC _{uc}	175	H _{f2}	205	H _{f2}
114	R _{Fwie}	147	CC _{uc}	177	H _{f2}	207	H _{f2}
116.125	R _{Fwie}	149	CC _{uc}	179	H _{f2}	209	H _{f2}
118.375	R _{Fwie}	151	CC _{uc}	181	H _{f2}	211	H _{f2}
120.625	R _{Fwie}	153	CC _{uc}	183	H _{f2}	213	H _{f1}
123.25	R _{Fwie}	155	CC _{uz}	185	H _{f2}	215	H _{f1}
126.25	R _{Fwie}	157	CC _{uz}	187	H _{f2}	217	None
128.875	R _{Fwie}	159	CC _{uz}	189	H _{f2}	219	None
131	R _{Fwie}	161	CC _{uz}	191	H _{f2}	221	None
133	R _{Fwie}	163	H _{f2}	193	H _{f2}	223	None
135	R _{Fwie}	165	H _{f2}	195	H _{f2}	225	None
137	R _{Fwie}	167	H _{f2}	197	H _{f2}	227	None
139	R _{Fwie}	169	H _{f2}	199	H _{f2}	229	None
141	R _{Ftf}	171	H _{f2}	201	H _{f2}		
	Indicates that the nodes become or remain inactive during the operations and early post-closure phases, and the hydrogeologic unit becomes composite during the late post-closure phase.						
	Indicates that the nodes become or remain inactive during the operations and early post-closure phases, and the hydrogeologic unit becomes ERDF waste during the late post-closure phase.						
	Indicates that the nodes become or remain inactive during the operations, early post-closure, and late post-closure phases.						

Table B-9. Identification of Hydrogeologic Units Present at the ERDF Cell Center 5N Location Used in the One-Dimensional Screening Models.

ERDF Cell 5N		Grid Node Easting: 568972m			Grid Node Northing: 134528m		
Hydrologic Unit:		Top of RFwie	Top of RFtf	Top of CCu _c	Top of CCu _z	Top of Hf2	Top of Hf1
Interpolated Elevation (m NAVD88):		140.6463	146.2598	157.1929	162.1081	212.1387	217.1782
Grid Node Elevation	Hydrologic Unit	Grid Node Elevation	Hydrologic Unit	Grid Node Elevation	Hydrologic Unit	Grid Node Elevation	Hydrologic Unit
110	RFwie	143	RFtf	173	Hf2	203	Hf2
112	RFwie	145	RFtf	175	Hf2	205	Hf2
114	RFwie	147	CCu _c	177	Hf2	207	Hf2
116.125	RFwie	149	CCu _c	179	Hf2	209	Hf2
118.375	RFwie	151	CCu _c	181	Hf2	211	Hf2
120.625	RFwie	153	CCu _c	183	Hf2	213	Hf1
123.25	RFwie	155	CCu _c	185	Hf2	215	Hf1
126.25	RFwie	157	CCu _c	187	Hf2	217	Hf1
128.875	RFwie	159	CCu _z	189	Hf2	219	None
131	RFwie	161	CCu _z	191	Hf2	221	None
133	RFwie	163	Hf2	193	Hf2	223	None
135	RFwie	165	Hf2	195	Hf2	225	None
137	RFwie	167	Hf2	197	Hf2	227	None
139	RFwie	169	Hf2	199	Hf2	229	None
141	RFtf	171	Hf2	201	Hf2		
	Indicates that the nodes become or remain inactive during the operations and early post-closure phases, and the hydrogeologic unit becomes composite during the late post-closure phase.						
	Indicates that the nodes become or remain inactive during the operations and early post-closure phases, and the hydrogeologic unit becomes ERDF waste during the late post-closure phase.						
	Indicates that the nodes become or remain inactive during the operations, early post-closure, and late post-closure phases.						

**Table B-10. Identification of Hydrogeologic Units Present at the ERDF Cell Center 6S
Location Used in the One-Dimensional Screening Models**

ERDF Cell 6S		Grid Node Easting: 568972 m			Grid Node Northing: 134367 m		
Hydrologic Unit:		Top of RFWie	Top of RFtf	Top of CCu _c	Top of CCu _z	Top of Hf2	Top of Hf1
Interpolated Elevation (m NAVD88):		139.4901	144.8208	155.5147	161.2729	213.8681	217.4084
Grid Node Elevation	Hydrologic Unit	Grid Node Elevation	Hydrologic Unit	Grid Node Elevation	Hydrologic Unit	Grid Node Elevation	Hydrologic Unit
110	RFwie	143	RFtf	173	Hf2	203	Hf2
112	RFwie	145	CCu _c	175	Hf2	205	Hf2
114	RFwie	147	CCu _c	177	Hf2	207	Hf2
116.125	RFwie	149	CCu _c	179	Hf2	209	Hf2
118.375	RFwie	151	CCu _c	181	Hf2	211	Hf2
120.625	RFwie	153	CCu _c	183	Hf2	213	Hf2
123.25	RFwie	155	CCu _c	185	Hf2	215	Hf1
126.25	RFwie	157	CCu _z	187	Hf2	217	Hf1
128.875	RFwie	159	CCu _z	189	Hf2	219	None
131	RFwie	161	CCu _z	191	Hf2	221	None
133	RFwie	163	Hf2	193	Hf2	223	None
135	RFwie	165	Hf2	195	Hf2	225	None
137	RFwie	167	Hf2	197	Hf2	227	None
139	RFwie	169	Hf2	199	Hf2	229	None
141	RFtf	171	Hf2	201	Hf2		
Indicates that the nodes become or remain inactive during the operations and early post-closure phases, and the hydrogeologic unit becomes composite during the late post-closure phase.							
Indicates that the nodes become or remain inactive during the operations and early post-closure phases, and the hydrogeologic unit becomes ERDF waste during the late post-closure phase.							
Indicates that the nodes become or remain inactive during the operations, early post-closure, and late post-closure phases.							

Table B-11. Identification of Hydrogeologic Units Present at the ERDF Cell Center 7N Location Used in the One-Dimensional Screening Models.

ERDF Cell 7N		Grid Node Easting: 569122 m			Grid Node Northing: 134528 m		
Hydrologic Unit:		Top of RFwie	Top of RFtf	Top of CCu _c	Top of CCu _z	Top of Hf2	Top of Hf1
Interpolated Elevation (m NAVD88):		141.7102	147.1093	157.9875	161.8273	215.2151	217.7686
Grid Node Elevation	Hydrologic Unit	Grid Node Elevation	Hydrologic Unit	Grid Node Elevation	Hydrologic Unit	Grid Node Elevation	Hydrologic Unit
110	RFwie	143	RFtf	173	Hf2	203	Hf2
112	RFwie	145	RFtf	175	Hf2	205	Hf2
114	RFwie	147	RFtf	177	Hf2	207	Hf2
116.125	RFwie	149	CCu _c	179	Hf2	209	Hf2
118.375	RFwie	151	CCu _c	181	Hf2	211	Hf2
120.625	RFwie	153	CCu _c	183	Hf2	213	Hf2
123.25	RFwie	155	CCu _c	185	Hf2	215	Hf2
126.25	RFwie	157	CCu _c	187	Hf2	217	Hf2
128.875	RFwie	159	CCu _z	189	Hf2	219	None
131	RFwie	161	CCu _z	191	Hf2	221	None
133	RFwie	163	Hf2	193	Hf2	223	None
135	RFwie	165	Hf2	195	Hf2	225	None
137	RFwie	167	Hf2	197	Hf2	227	None
139	RFwie	169	Hf2	199	Hf2	229	None
141	RFwie	171	Hf2	201	Hf2		
		Indicates that the nodes become or remain inactive during the operations and early post-closure phases, and the hydrogeologic unit becomes composite during the late post-closure phase.					
		Indicates that the nodes become or remain inactive during the operations and early post-closure phases, and the hydrogeologic unit becomes ERDF waste during the late post-closure phase.					
		Indicates that the nodes become or remain inactive during the operations, early post-closure, and late post-closure phases.					

Table B-12. Identification of Hydrogeologic Units Present at the ERDF Cell Center 8S Location Used in the One-Dimensional Screening Models.

ERDF Cell 8S		Grid Node Easting: 569122 m			Grid Node Northing: 134367 m		
Hydrologic Unit:		Top of Rfwie	Top of RFtf	Top of CCu _c	Top of CCu _z	Top of Hf2	Top of Hf1
Interpolated Elevation (m NAVD88):		139.6718	145.227	155.9599	161.207	215.8992	217.8822
Grid Node Elevation	Hydrologic Unit	Grid Node Elevation	Hydrologic Unit	Grid Node Elevation	Hydrologic Unit	Grid Node Elevation	Hydrologic Unit
110	RFwie	143	RFtf	173	Hf2	203	Hf2
112	RFwie	145	RFtf	175	Hf2	205	Hf2
114	RFwie	147	CCu _c	177	Hf2	207	Hf2
116.125	RFwie	149	CCu _c	179	Hf2	209	Hf2
118.375	RFwie	151	CCu _c	181	Hf2	211	Hf2
120.625	RFwie	153	CCu _c	183	Hf2	213	Hf2
123.25	RFwie	155	CCu _c	185	Hf2	215	Hf2
126.25	RFwie	157	CCu _z	187	Hf2	217	Hf2
128.875	RFwie	159	CCu _z	189	Hf2	219	None
131	RFwie	161	CCu _z	191	Hf2	221	None
133	RFwie	163	Hf2	193	Hf2	223	None
135	RFwie	165	Hf2	195	Hf2	225	None
137	RFwie	167	Hf2	197	Hf2	227	None
139	RFwie	169	Hf2	199	Hf2	229	None
141	RFtf	171	Hf2	201	Hf2		
	Indicates that the nodes become or remain inactive during the operations and early post-closure phases, and the hydrogeologic unit becomes composite during the late post-closure phase.						
	Indicates that the nodes become or remain inactive during the operations and early post-closure phases, and the hydrogeologic unit becomes ERDF waste during the late post-closure phase.						
	Indicates that the nodes become or remain inactive during the operations, early post-closure, and late post-closure phases.						

Table B-13. Identification of Hydrogeologic Units Present at the ERDF Cell Center 9N Location Used in the One-Dimensional Screening Models.

ERDF Cell 9N		Grid Node Easting: 569268 m			Grid Node Northing: 134528 m		
Hydrologic Unit:		Top of RFwie	Top of RFtf	Top of CCu _c	Top of CCu _z	Top of Hf2	Top of Hf1
Interpolated Elevation (m NAVD88):		142.7386	147.9305	158.7556	161.556	218.189	218.3393
Grid Node Elevation	Hydrologic Unit	Grid Node Elevation	Hydrologic Unit	Grid Node Elevation	Hydrologic Unit	Grid Node Elevation	Hydrologic Unit
110	RFwie	143	RFtf	173	Hf2	203	Hf2
112	RFwie	145	RFtf	175	Hf2	205	Hf2
114	RFwie	147	RFtf	177	Hf2	207	Hf2
116.125	RFwie	149	CCu _c	179	Hf2	209	Hf2
118.375	RFwie	151	CCu _c	181	Hf2	211	Hf2
120.625	RFwie	153	CCu _c	183	Hf2	213	Hf2
123.25	RFwie	155	CCu _c	185	Hf2	215	Hf2
126.25	RFwie	157	CCu _c	187	Hf2	217	Hf2
128.875	RFwie	159	CCu _z	189	Hf2	219	None
131	RFwie	161	CCu _z	191	Hf2	221	None
133	RFwie	163	Hf2	193	Hf2	223	None
135	RFwie	165	Hf2	195	Hf2	225	None
137	RFwie	167	Hf2	197	Hf2	227	None
139	RFwie	169	Hf2	199	Hf2	229	None
141	RFwie	171	Hf2	201	Hf2		
	Indicates that the nodes become or remain inactive during the operations and early post-closure phases, and the hydrogeologic unit becomes composite during the late post-closure phase.						
	Indicates that the nodes become or remain inactive during the operations and early post-closure phases, and the hydrogeologic unit becomes ERDF waste during the late post-closure phase.						
	Indicates that the nodes become or remain inactive during the operations, early post-closure, and late post-closure phases.						

Table B-14. Identification of Hydrogeologic Units Present at the ERDF Cell Center 9S Location Used in the One-Dimensional Screening Models.

ERDF Cell 9S		Grid Node Easting: 569268 m			Grid Node Northing: 134367 m		
Hydrologic Unit:		Top of RFWie	Top of RFtf	Top of CCu _c	Top of CCu _z	Top of Hf2	Top of Hf1
Interpolated Elevation (m NAVD88):		141.4175	146.7896	157.1658	161.1823	216.9958	218.674
Grid Node Elevation	Hydrologic Unit	Grid Node Elevation	Hydrologic Unit	Grid Node Elevation	Hydrologic Unit	Grid Node Elevation	Hydrologic Unit
110	RFwie	143	RFtf	173	Hf2	203	Hf2
112	RFwie	145	RFtf	175	Hf2	205	Hf2
114	RFwie	147	CCu _c	177	Hf2	207	Hf2
116.125	RFwie	149	CCu _c	179	Hf2	209	Hf2
118.375	RFwie	151	CCu _c	181	Hf2	211	Hf2
120.625	RFwie	153	CCu _c	183	Hf2	213	Hf2
123.25	RFwie	155	CCu _c	185	Hf2	215	Hf2
126.25	RFwie	157	CCu _c	187	Hf2	217	Hf2
128.875	RFwie	159	CCu _z	189	Hf2	219	None
131	RFwie	161	CCu _z	191	Hf2	221	None
133	RFwie	163	Hf2	193	Hf2	223	None
135	RFwie	165	Hf2	195	Hf2	225	None
137	RFwie	167	Hf2	197	Hf2	227	None
139	RFwie	169	Hf2	199	Hf2	229	None
141	RFwie	171	Hf2	201	Hf2		
	Indicates that the nodes become or remain inactive during the operations and early post-closure phases, and the hydrogeologic unit becomes composite during the late post-closure phase.						
	Indicates that the nodes become or remain inactive during the operations and early post-closure phases, and the hydrogeologic unit becomes ERDF waste during the late post-closure phase.						
	Indicates that the nodes become or remain inactive during the operations, early post-closure, and late post-closure phases.						

Table B-15. Identification of Hydrogeologic Units Present at the ERDF Cell Center 10N Location Used in the One-Dimensional Screening Models.

ERDF Cell 10N		Grid Node Easting: 569418 m			Grid Node Northing: 134528m		
Hydrologic Unit:		Top of R _{Fwie}	Top of R _{Ftf}	Top of CC _{uc}	Top of CC _{uz}	Top of H _{f2}	Top of H _{f1}
Interpolated Elevation (m NAVD88):		142.2809	146.6695	156.0075	160.2414	215.0595	223.9562
Grid Node Elevation	Hydrologic Unit	Grid Node Elevation	Hydrologic Unit	Grid Node Elevation	Hydrologic Unit	Grid Node Elevation	Hydrologic Unit
110	R _{Fwie}	143	R _{Ftf}	173	H _{f2}	203	H _{f2}
112	R _{Fwie}	145	R _{Ftf}	175	H _{f2}	205	H _{f2}
114	R _{Fwie}	147	CC _{uc}	177	H _{f2}	207	H _{f2}
116.125	R _{Fwie}	149	CC _{uc}	179	H _{f2}	209	H _{f2}
118.375	R _{Fwie}	151	CC _{uc}	181	H _{f2}	211	H _{f2}
120.625	R _{Fwie}	153	CC _{uc}	183	H _{f2}	213	H _{f2}
123.25	R _{Fwie}	155	CC _{uc}	185	H _{f2}	215	H _{f2}
126.25	R _{Fwie}	157	CC _{uz}	187	H _{f2}	217	H _{f1}
128.875	R _{Fwie}	159	CC _{uz}	189	H _{f2}	219	H _{f1}
131	R _{Fwie}	161	H _{f2}	191	H _{f2}	221	H _{f1}
133	R _{Fwie}	163	H _{f2}	193	H _{f2}	223	H _{f1}
135	R _{Fwie}	165	H _{f2}	195	H _{f2}	225	None
137	R _{Fwie}	167	H _{f2}	197	H _{f2}	227	None
139	R _{Fwie}	169	H _{f2}	199	H _{f2}	229	None
141	R _{Fwie}	171	H _{f2}	201	H _{f2}		
	Indicates that the nodes become or remain inactive during the operations and early post-closure phases, and the hydrogeologic unit becomes liner composite during the late post-closure phase.						
	Indicates that the nodes become or remain inactive during the operations and early post-closure phases, and the hydrogeologic unit becomes ERDF waste during the late post-closure phase.						
	Indicates that the nodes become or remain inactive during the operations, early post-closure, and late post-closure phases.						

Table B-16. Identification of Hydrogeologic Units Present at the ERDF Cell Center 10S Location Used in the One-Dimensional Screening Models.

ERDF Cell 10S		Grid Node Easting: 569418 m			Grid Node Northing: 134367 m		
Hydrologic Unit:		Top of RFWie	Top of RFtf	Top of CCu _c	Top of CCu _z	Top of Hf2	Top of Hf1
Interpolated Elevation (m NAVD88):		141.7736	146.3343	155.258	160.1397	213.9181	219.6472
Grid Node Elevation	Hydrologic Unit	Grid Node Elevation	Hydrologic Unit	Grid Node Elevation	Hydrologic Unit	Grid Node Elevation	Hydrologic Unit
110	RFwie	143	RFtf	173	Hf2	203	Hf2
112	RFwie	145	RFtf	175	Hf2	205	Hf2
114	RFwie	147	CCu _c	177	Hf2	207	Hf2
116.125	RFwie	149	CCu _c	179	Hf2	209	Hf2
118.375	RFwie	151	CCu _c	181	Hf2	211	Hf2
120.625	RFwie	153	CCu _c	183	Hf2	213	Hf2
123.25	RFwie	155	CCu _c	185	Hf2	215	Hf1
126.25	RFwie	157	CCu _z	187	Hf2	217	Hf1
128.875	RFwie	159	CCu _z	189	Hf2	219	Hf1
131	RFwie	161	Hf2	191	Hf2	221	None
133	RFwie	163	Hf2	193	Hf2	223	None
135	RFwie	165	Hf2	195	Hf2	225	None
137	RFwie	167	Hf2	197	Hf2	227	None
139	RFwie	169	Hf2	199	Hf2	229	None
141	RFwie	171	Hf2	201	Hf2		
		Indicates that the nodes become or remain inactive during the operations and early post-closure phases, and the hydrogeologic unit becomes composite during the late post-closure phase.					
		Indicates that the nodes become or remain inactive during the operations and early post-closure phases, and the hydrogeologic unit becomes ERDF waste during the late post-closure phase.					
		Indicates that the nodes become or remain inactive during the operations, early post-closure, and late post-closure phases.					

To test the applicability of the one-dimensional transport models to approximate the performance of the three-dimensional, the percentile results of the one-dimensional transport models are compared to the three-dimensional transport model results. Because the results of the screening analysis indicated that radionuclide breakthrough occurs soonest in northern half of ERDF cell 9N (Table 4-1 in Section 4.2.1), that geologic template was selected for the one-dimensional benchmarking and sensitivity-uncertainty evaluations. Figure B-10 shows the breakthrough of technetium-99 with an assumed 1 Ci inventory within the ERDF volume from the vadose zone to the aquifer for the various percentile flow and transport parameter values. The results indicate good comparison between the one-dimensional abstraction model and the three-dimensional model results for the minimum, 25th percentile, median, and 75th percentile parameter sets (Figure B-10). The relative difference between the one-dimensional and the three-dimensional model results is somewhat larger for the compliance and maximum parameter sets. The larger difference in the compliance and maximum parameter set results appears to be caused by amount of anisotropic lateral flow calculated to occur in the three-dimensional model.

Some anisotropic lateral flow appears to contribute to the downward flow beneath ERDF calculated in the three-dimensional model, and this is especially apparent when the compliance and maximum parameter sets are used. The water flux at the water table calculated in the three-dimensional model is 67% higher than the surface barrier post-design life recharge rate in the case with the maximum parameter set, and 16% higher in the case with the compliance parameter set (Section 4.6.2.1 and Table 4-10). The water flux at the water table at the arrival time of the maximum radionuclide flux is no more than 10% higher than the surface barrier post-design life recharge rate in any of the other percentile cases. In all of the cases, the recharge rate outside the surface barrier exceeds the recharge rate through the barrier and provides the source of the additional flux. The water flux at the water table calculated in the one-dimensional model abstraction is equal to the surface barrier post-design life recharge rate for the compliance and all of the percentile cases. Thus, while the three-dimensional simulations allow for anisotropic lateral flow, which typically attenuates a maximum or peak radionuclide flux, the dry vadose zone and conditions of the surface barrier introduce moisture from the outside that increases the downward flux of water and radionuclides. The anisotropic lateral flow also appears to affect the calculated maximum radionuclide flux. With the exception of the compliance case results, the maximum radionuclide flux in the percentile case results in the three-dimensional model calculations, when the radionuclide flux in the area under the berm is included, exceeds the maximum flux in the one-dimensional model results (Table 4-10 in Section 4.6.2.1, Table B-17, and Figure B-10).

The difference in the maximum radionuclide flux calculated in the one- and three-dimensional models for the minimum percentile case is negligibly small, and within 11% to 14% for the 25th percentile, median, and 75th percentile cases. The difference in the maximum radionuclide flux calculated in the one- and three-dimensional models is 26% greater for the compliance parameter case, and 26% less for the maximum parameter case. These differences are considered acceptable because the one-dimensional sensitivity-uncertainty evaluations address vadose zone hydraulic property variability and the "what if" postulations. The results of the vadose zone hydraulic property sensitivity analysis are intended primarily to identify the possible impact of the individual parameters' variability on the results, and identify the parameters that exert the greatest influence over the results. The "what if" analysis is intended for relative comparison purposes of conceivable but unexpected conditions, but not for quantifying absolutely the consequences of the assumed or postulated event occurring. The modeling progression from three- to one-dimensional models is depicted in Figure B-11.

Figure B-10. Comparison of the One-Dimensional Transport Model Results to the Comparable Three-Dimensional Transport Model Results of the Breakthrough of a Radionuclide with $K_d = 0$ mL/g (e.g., Technetium-99) to the Water Table for the Individual Hydrologic Parameter Percentile Sets (Results Presented on a per Ci Source Basis).

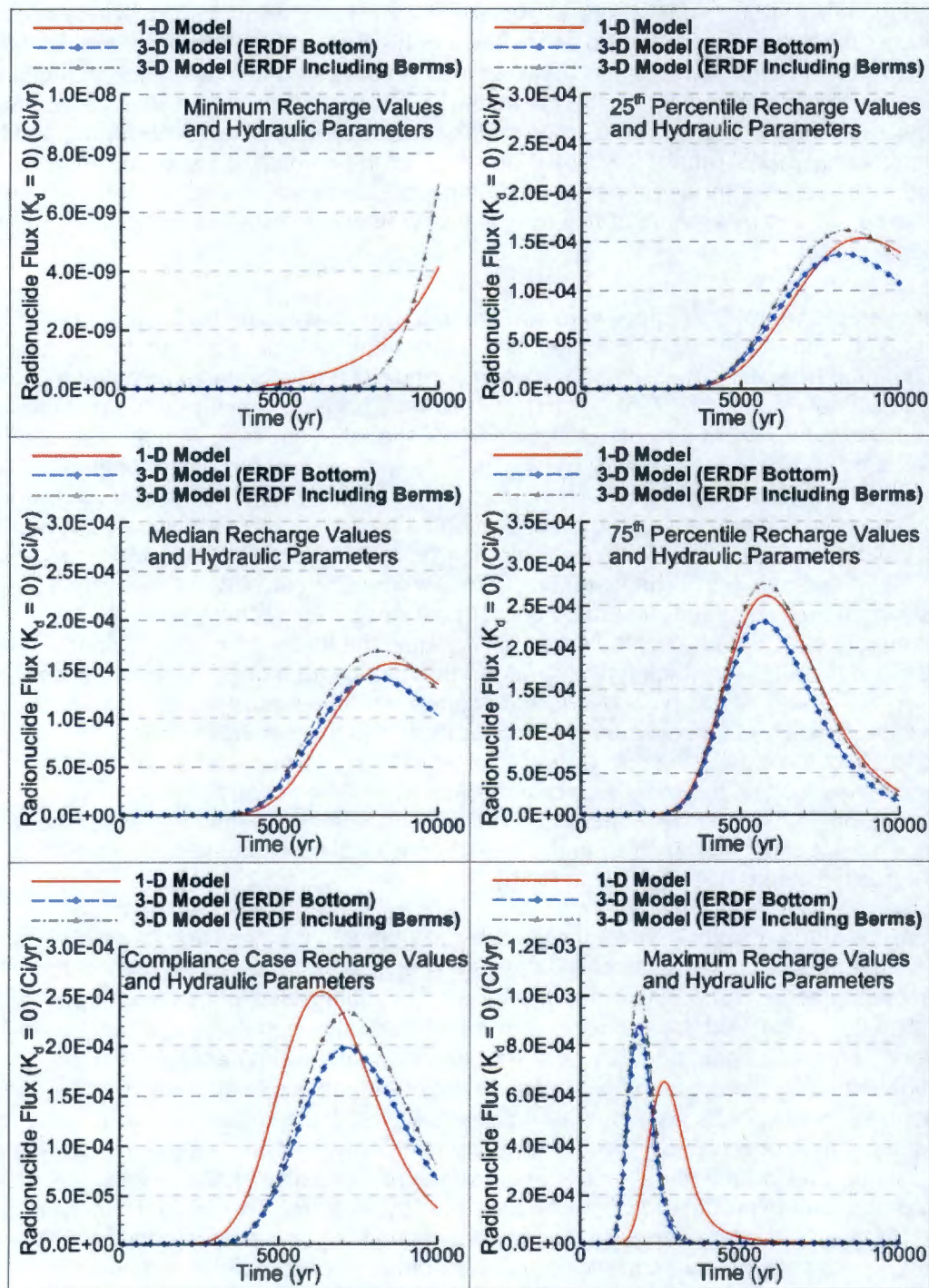


Figure B-11. Diagram of the Modeling Progression from Three- to One-Dimensional Models.

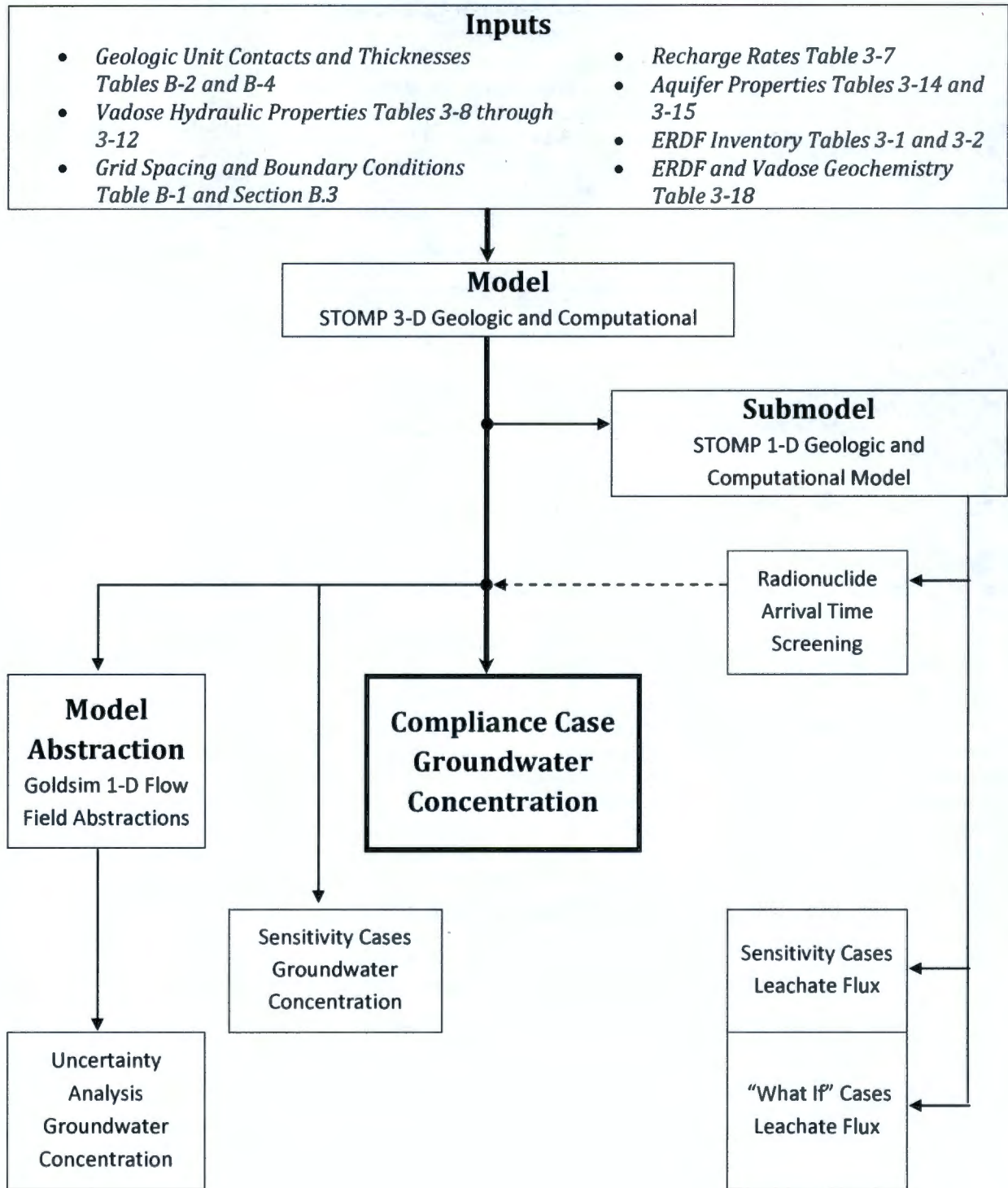


Table B-17. Results of the One-Dimensional Abstraction Model Vadose Zone Hydrologic and Recharge Parameter Percentile Evaluations for Radionuclides with $K_d = 0$ mL/g (e.g., Technetium-99) Breakthrough to the Water Table (Results Presented on a per Ci Source Basis).

Flow and Transport Parameter Percentile Values	Arrival Time of Maximum Radionuclide Flux at Water Table (Years Post-Closure)	Maximum Radionuclide Flux at Water Table (Ci/yr)	Water Flux at Water Table (mm/yr)	Surface Barrier Post-Design Life Recharge Rate (mm/yr)	Pre-ERDF Construction Recharge Rate (mm/yr)
Minimum	10000	4.16E-09	0.10	0.10	0.26
25 th Percentile	8795	1.53E-04	0.75	0.75	1.05
Median	8590	1.56E-04	1.03	1.03	1.59
Compliance	6345	2.54E-04	1.00	1.00	1.70
75 th Percentile	5810	2.62E-04	1.31	1.31	2.30
Maximum	2620	6.53E-04	2.00	2.00	4.00

B.8 REVISION TO GEOLOGIC DATA IN TABLE B-2

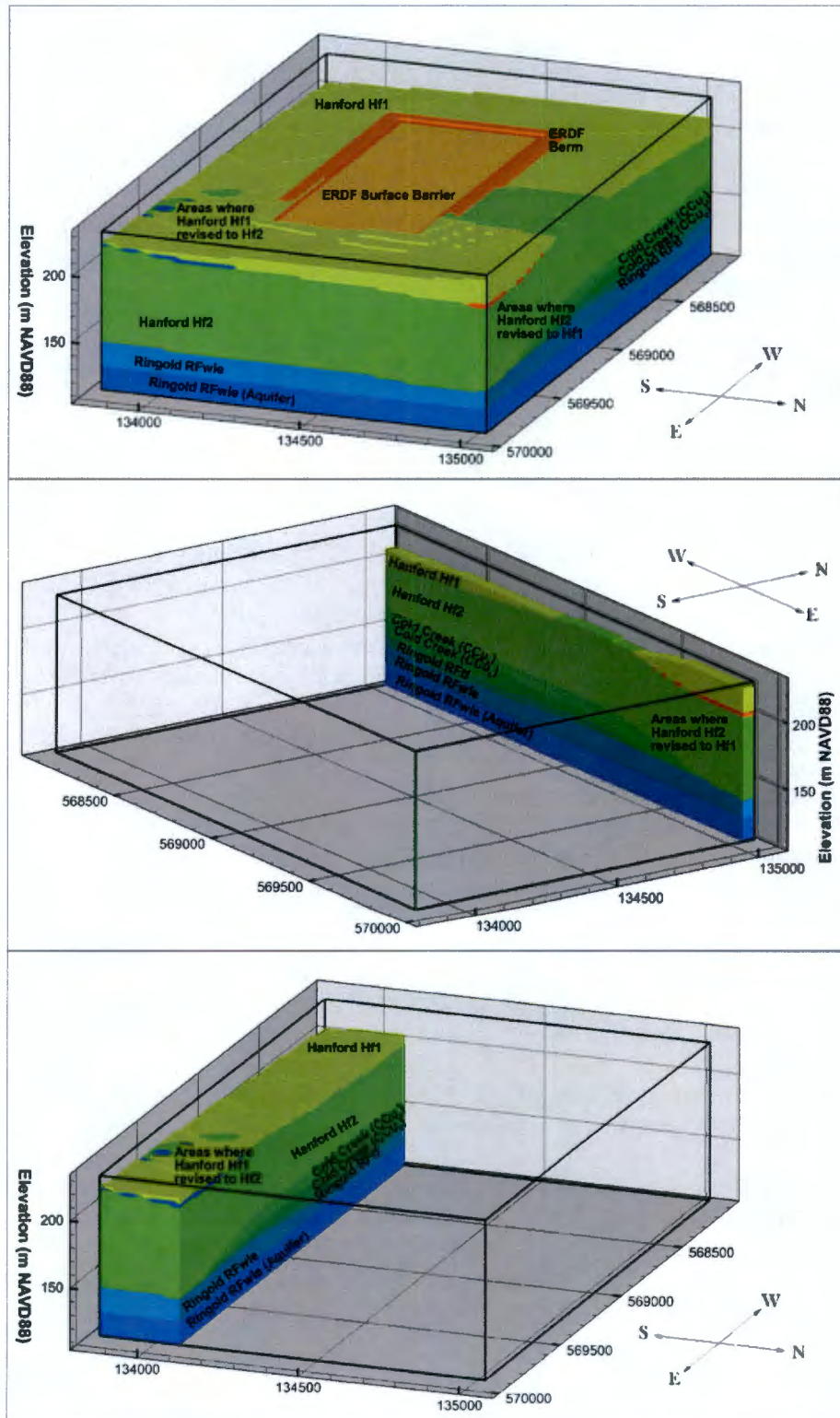
During review of the geological data but after completion of the three-dimensional modeling evaluations, the estimates of the Hanford Hf1 and Hf2 contact depth in three wells used to develop the three-dimensional geologic model were revised. The data contained in Table B-1 of WCH-463 and Table B-2 of this appendix were changed as shown in Table B-18. Although the data from all three wells were used to develop the three-dimensional geologic model that was interpolated onto the numerical model grid, two of the wells, 699-35-61A and 699-36-61B, are located far outside of the model domain, and well 699-35-66B is located near the eastern boundary of the model domain (Figure B-3). The Hanford Hf1 and Hf2 contact is located fairly shallow in the vadose zone, and the areas impacted by the revision are well outside the vertical flow path from the bottom of ERDF to the water table. The impact of the revisions appears to be minor. These revisions were not implemented in the development of the numerical model geologic conceptual model because the changes associated with the revision to the geologic contact information appear to be limited to small areas located near the model domain boundaries and not consequential to the results of the model.

Table B-18. Revision to Hanford Hf1 and Hf2 Contact Depth Data

Well Name	Revised Estimate of Hanford Hf1 and Hf2 Contact		Estimate of Hanford Hf1 and Hf2 Contact Listed in Table B-2	
	Top Hf1 (ft bgs)	Top Hf2 (ft bgs)	Top Hf1 (ft bgs)	Top Hf2 (ft bgs)
699-35-61A	0	36	NP	0
699-35-66B	0	20	NP	0
699-36-61B	0	64	NP	0

NP = Not present

Figure B-12. Impact of Revision to Hanford Hf1 and Hf2 Contact Depth in the Three-Dimensional Geologic Model.



B.9 REFERENCES

- BHI-00355, 1995, *Design Analysis: Construction of W-296 Environmental Restoration Disposal Facility*, Rev. 00, Bechtel Hanford, Inc., Richland, Washington.
- CP-47631, 2011, *Model Package Report: Central Plateau Groundwater Model Version 3.3*, CH2M Hill Plateau Remediation Company, Richland, Washington.
- Dagan, G., 1984, "Solute Transport in Heterogeneous Porous Formations," *Journal of Fluid Mechanics*, Vol. 145, pp. 151-157.
- DOE, 1999, *Format and Content Guide for U.S. Department of Energy Low-Level Waste Disposal Facility Performance Assessments and Composite Analyses*, U.S. Department of Energy, Washington, D.C.
- DOE G 435.1-1, Chapter 4, 1999. *Radioactive Waste Management Implementation Guide for use with DOE M 435.1-1, Chapter IV: Low-Level Waste Requirements*, U.S. Department of Energy, Washington, D.C.
- DOE M 435.1-1, 2001, *Radioactive Waste Management Manual*, U.S. Department of Energy, Washington, D.C.
- DOE O 435.1, 2001, *Radioactive Waste Management*, U.S. Department of Energy, Washington, D.C.
- DOE/RL-2011-01, 2011, *Hanford Site Groundwater Monitoring Report for 2010*, Rev. 0, U.S. Department of Energy, Richland Operations Office, Richland, Washington.
- DOE/RL-2011-50, 2012, *Regulatory Basis and Implementation of a Graded Approach to Evaluation of Groundwater Protection*, Rev. 01, U.S. Department of Energy, Richland Operations Office, Richland, Washington.
- Appendix A: "Regulatory Requirements, Guidelines, and Criteria Associated with the Selection and Use of Fate and Transport Models for Vadose zone Modeling at the Hanford Site"
- Appendix B: "Application of the Model Selection, Use, and Documentation Criteria to the Hanford Site Vadose zone System: Conceptual Model; Features, Events, and Processes; and Identification of Model Attributes"
- Appendix C: "Application of the Code Selection Process for Vadose zone Fate and Transport Modeling at the Hanford Site"
- EPA/540/F-95/041, 1989, *Soil Screening Guidance: Fact Sheet*, U.S. Environmental Protection Agency, Washington, D.C.
- EPA/600/R-97/102, 1997, *NAPL: Simulator Documentation*, U.S. Environmental Protection Agency, National Risk Management Research Laboratory, Ada, Oklahoma.

-
- EPA-SAB-RAC-ADV-99-006, 1999, *AN SAB ADVISORY: Modeling of Radionuclide Releases from Disposal of Low Activity Mixed Waste*, U.S. Environmental Protection Agency, Science Advisory Board, Washington, D.C.
- Gelhar, L. W. and C. L. Axness, 1983, "Three-Dimensional Analysis of Macrodispersion in a Stratified Aquifer," *Water Resources Research*, Vol. 19, pp. 161-180.
- Gelhar, L. W., C. Welty, and K. R. Rehfeldt, 1992, "A Critical Review of Data on Field Scale Dispersion in Aquifers," *Water Resources Research*, Vol. 28, pp. 1955-1974.
- Huyakorn, P. S. and G. F. Pinder, 1993, *Computational Methods in Subsurface Flow*, Academic Press, Salt Lake City, Utah.
- NAVD88, North American Vertical Datum of 1988, National Geodetic Survey, U.S. Department of Commerce, Silver Spring, Maryland.
- NUREG-1573, 2000, "A Performance Assessment Methodology for Low-Level Radioactive Waste Disposal Facilities – Recommendations of NRC's Performance Assessment Working Group," U.S. Nuclear Regulatory Commission, Washington, D.C.
- PNNL-11216, 1997, *STOMP Subsurface Transport Over Multiple Phases: Application Guide*, Pacific Northwest National Laboratory, Richland, Washington.
- PNNL-11217, 1997, *STOMP Subsurface Transport Over Multiple Phases Theory Guide*, Pacific Northwest National Laboratory, Richland, Washington.
- Polmann, D. J., 1990, *Application of Stochastic Methods to Transient Flow and Transport in Heterogeneous Unsaturated Soils*, Thesis, Massachusetts Institute of Technology, Department of Civil Engineering, Cambridge, Massachusetts.
- RCRA Subtitle C *Hazardous Waste Management, Resource Conservation and Recovery Act of 1976*, 42 U.S.C. 6901 et seq.
- WAC 173-340-747, "Deriving Soil Concentrations for Ground Water Protection," *Washington Administrative Code*, as amended.
- WCH-195, 2007, *Design Analysis Variance Report ERDF Cells 7-10*, Rev. 0, Washington Closure Hanford, Richland, Washington.
- WCH-462, 2013, *ERDF Performance Assessment Modeling Approach*, Rev. 0, Washington Closure Hanford, Richland, Washington.
- WCH-463, 2013, *Hydrogeologic Model for the Environmental Restoration Disposal Facility, Hanford Site*, Rev. 0, Washington Closure Hanford, Richland, Washington.
- WCH-464, 2013, *Hydrologic Data Package in Support of Environmental Restoration Disposal Facility Performance Assessment Modeling*, Rev. 0, Washington Closure Hanford, Richland, Washington.

WCH-477, 2013, *Conceptual Models for Release and Transport of Environmental Restoration Disposal Facility Waste Contaminants through the Near Field Environment*, Rev. 0, Washington Closure Hanford, Richland, Washington.

WCH-479, 2013, *Inventory Data Package for ERDF Waste Disposal*, Rev. 1, Washington Closure Hanford, Richland, Washington.

WCH-515, 2013, *Parameter Uncertainty for the ERDF Performance Assessment Uncertainty and Sensitivity Analysis*, Rev. 0, Washington Closure Hanford, Richland, Washington.

Ye, M., R. Khaleel, and T.-C.J. Yeh, 2005. "Stochastic Analysis of Moisture Plume Dynamics of a Field Injection Experiment," *Water Resources Research*, Vol. 41, W03013.

Yeh, T.-C.J., M. Ye, and R. Khaleel, 2005. "Estimation of Effective Unsaturated Hydraulic Conductivity Tensor Using Spatial Moments of Observed Moisture Plume," *Water Resources Research*, Vol. 41, W03014.

APPENDIX C
VALIDATION OF THE AIR-PATHWAY MODELING APPROACH

TABLE OF CONTENTS

APPENDIX C VALIDATION OF THE AIR-PATHWAY MODELING APPROACH	C-1
C.1 COMPARISON WITH ANALYTICAL SOLUTIONS	C-1
C.1.1 Gas Diffusion Through Semi-Infinite Porous Medium	C-2
C.1.2 Gas Diffusion from Porous Medium to the Atmosphere	C-4
C.2 COMPARISON AGAINST EPA CAP88-PC SOFTWARE.....	C-6
C.3 COMPARISON AGAINST HANFORD SITE NATIONAL ENVIRONMENTAL POLICY ACT CHARACTERIZATION REPORT	C-11
C.4 REFERENCES	C-11

FIGURES

C-1. Comparison of GoldSim Results Against the General Diffusion Equation Through a Semi-Infinite Porous Medium.....	C-4
C-2. Comparison of GoldSim Results Against Mathews and Walker (1970) Analytical Solution for a 1-m-thick Porous Medium in Contact with the Atmosphere.	C-5
C-3. 2011 Wind Rose for Hanford Meteorological Station (Left) and Yakima Airport (Right) Showing the Incoming Wind Direction.....	C-9

TABLES

C-1. Physical Properties of ERDF Soils for Comparison with Analytical Solutions.....	C-3
C-2. Diffusion Coefficients in Air at 20 °C and 1 Atm.....	C-3

APPENDIX C

VALIDATION OF THE AIR-PATHWAY MODELING APPROACH

As a part of the performance assessment (PA) requirements, potential gas emissions (e.g., radon flux) and the resulting air concentrations of radionuclides originating from the Environmental Restoration Disposal Facility (ERDF) need to be modeled for calculating exposure dose via the atmospheric pathway. Among the radionuclides contained in the wastes in ERDF at closure, four of them can potentially emanate in gaseous form. These radionuclides are carbon-14 (as CO₂), hydrogen-3 (as H₂), iodine-129 (as I₂), and radon-222 (as radon gas). It was assumed that the wastes are uniformly disposed at ERDF and mixed with soils so that gases could slowly emanate and diffuse through the porous medium. Using the ERDF PA model, the diffusive fluxes and concentrations for the four radionuclides over the ERDF facility are predicted. The ERDF PA model conceptualization for air-pathway modeling is discussed in Chapter 3.0.

This section provides validation of the air-pathway modeling approach by building confidence that diffusive flux can be adequately modeled to meet the performance requirements of the PA. First, the ERDF PA model methodology for air-pathway calculations is compared to the analytical solution for similar boundary conditions and assumptions, and then the modeling results are compared to the U.S. Environmental Protection Agency (EPA) CAP88-PC model based results and those calculated from the recent Hanford Site National Environmental Policy Act (NEPA) Characterization Report (PNNL-6415, *Hanford Site National Environmental Policy Act [NEPA] Characterization*) for a given receptor location and given set of inputs. The comparison of results indicate that the ERDF PA model built for the air-pathway calculation is valid for its intended purpose.

C.1 COMPARISON WITH ANALYTICAL SOLUTIONS

In order to build confidence in the gas diffusion modeling performed using the GoldSim®¹ Pro software package, the results of the GoldSim-based models are compared against the following two analytical solutions that represent the following:

- Diffusion through a semi-infinite porous medium from a source where the gas concentration is kept constant over time
- Diffusion through a porous medium with fixed far-field boundary concentration from a source where the gas concentration is kept constant over time.

¹ GoldSim® Pro is a registered trademark of GoldSim Technologies, Issaquah, Washington, in the United States and other countries.

C.1.1 Gas Diffusion Through Semi-Infinite Porous Medium

The analytical solution for calculating the concentration from gaseous diffusion over a semi-infinite porous medium (Ogata and Banks 1961) where the gas concentration at the source is held constant and the concentration at the far-field boundary is zero is given as:

$$\frac{C(x,t)}{C_0} = \operatorname{erfc} \left(\frac{x}{2 \sqrt{\frac{D_{ef}}{\theta_a} t}} \right)$$

where:

$C(x,t)$ = the air concentration (kg/m^3) in the pore network of a given gas at the distance x (m) from the source and time t (s)

C_0 (kg/m^3) = the air concentration in the pore network at the source

D_{ef} (m^2/s) = the effective diffusion coefficient of a given gas through the tortuous air pathway of the porous medium

θ_a (-) = the air content of the porous medium reported in Table C-1.

For the following initial and boundary conditions:

$$C(x,0) = 0, \text{ for all } x$$

$$C(0,t) = C_0, \text{ for } t > 0$$

$$C(\infty,t) = 0, \text{ for all } t$$

The effective diffusion coefficient through the tortuous air pathway of the porous medium (D_{ef}) is given by:

$$D_{ef} = D_0 \tau$$

where D_0 (m^2/s) is the diffusion coefficient of the gas of concern in the air (Table C-2), and τ (-) is the tortuosity of the porous medium reported in Table C-1.

Table C-1. Physical Properties of ERDF Soils for Comparison with Analytical Solutions.

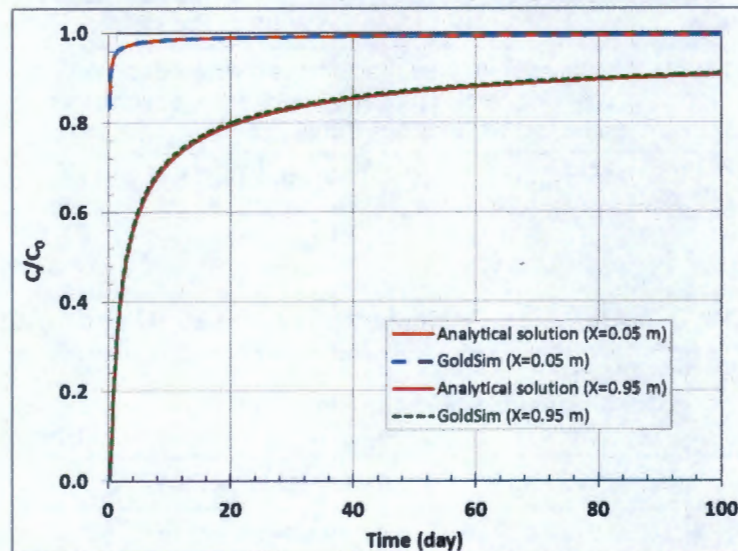
Parameter	Value	Origin of the value
θ_a	0.2094	Calculated from subtracting residual water content of 0.0032 (compliance value for Hf1 unit) from total porosity of 0.2126 (compliance value for Hf1 unit); see Table 3-8
τ	0.0509	Millington and Quirk (1960) model for $\phi = 0.8$ (see Section 3.4.2.2)

Table C-2. Diffusion Coefficients in Air at 20 °C and 1 Atm.

Radionuclide	Gas Form	Diffusion Coefficient in Air (cm ² s ⁻¹)	Reference	Boiling Point (°C) Used in EPA Calculations (Haynes and Lide 2011)
¹⁴ C	CO ₂	0.1600	EPA 2010 (average method)	-78.55
³ H	H ₂	0.8190	EPA 2010 (average method)	-252.76
¹²⁹ I	I ₂	0.0897	EPA 2010 (FSG/LaBas method)	184.45
²²² Rn	Rn	0.1100	Nazaroff and Nero (1988) cited in Yu et al. (2001)	(-)

The concentrations given by this analytical solution have been compared with a simple GoldSim model built to represent these initial and boundary conditions through a semi-infinite porous medium. The first meter of the porous medium is discretized into 10 cells, and the calculations are performed using the diffusion coefficient of carbon-14 (Table C-2) and properties of ERDF soils (Table C-1). Figure C-1 presents the simulated air concentrations over time at two given distances (0.05 m and 0.95 m) from the source. The agreement between GoldSim and the analytical solution is deemed satisfactory.

Figure C-1. Comparison of GoldSim Results Against the General Diffusion Equation Through a Semi-Infinite Porous Medium.



C.1.2 Gas Diffusion from Porous Medium to the Atmosphere

Carslaw and Jaeger (1959) and Mathews and Walker (1970) provide an analytical solution for diffusion through a fixed length of a porous medium, where the concentration in the far-field boundary is constant (such as in contact with the atmosphere). The analytical solution for the following initial and boundary conditions:

$$C(x, 0) = 0, \text{ for all } x$$

$$C(0, t) = C_0, \text{ for } t > 0$$

$$\frac{\partial C(l_0, t)}{\partial x} = 0, \text{ at } x = l_0 \text{ for } t > 0$$

is given below:

$$\frac{C(x, t)}{C_0} = 1 - \frac{4}{\pi} \sum_{n=0}^{\infty} \frac{1}{2n+1} \exp\left(-\frac{(n+\frac{1}{2})^2 \pi^2 \frac{D_{ef}}{\theta_a} t}{l_0^2}\right) \sin\left(\frac{(n+\frac{1}{2})\pi x}{l_0}\right)$$

where:

$C(x, t)$ = the air concentration (kg/m^3) in the pore network of a given gas at the distance x (m) from the source and time t (s)

C_0 (kg/m^3) = the air concentration in the pore network at the source

l_0 (m) = the length of the porous medium (distance between the source and the atmosphere)

D_{ef} (m²/s) = the effective diffusion coefficient of the given gas through the tortuous air pathway of the porous medium

θ_a (-) = the air content of the porous medium (Table C-1).

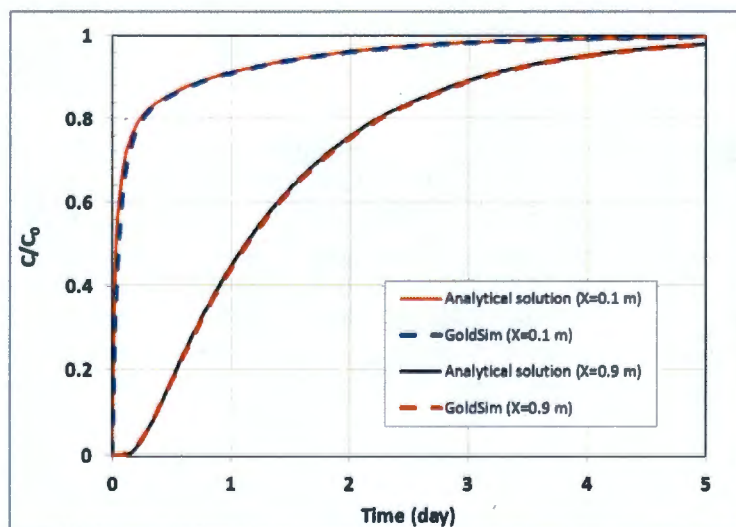
The effective diffusion coefficient through the tortuous air pathway of the porous medium is given by:

$$D_{ef} = D_0\tau$$

where D_0 (m²/s) is the diffusion coefficient of the gas of concern in the air (Table C-2), and τ (-) is the tortuosity of the porous medium (Table C-1).

This analytical solution has been calculated using Excel[®] considering the diffusion coefficient of carbon-14 and the porous medium properties reported in Table C-1. These results have been compared with a simple GoldSim model built to represent these initial and boundary conditions. A 1-m-thick porous medium ($l_0 = 1$ m) has been spatially discretized into five cells between the source ($C_0 = 1$ g/L) and the atmosphere, considering the diffusion coefficient of carbon-14 (Table C-2) and properties of ERDF soils. Figure C-2 presents the results at two given distances (0.1 and 0.9 m) from the source. The agreement between GoldSim results and the analytical solution was deemed satisfactory.

Figure C-2. Comparison of GoldSim Results Against Mathews and Walker (1970) Analytical Solution for a 1-m-thick Porous Medium in Contact with the Atmosphere.



[®] Excel is a registered trademark of Microsoft Corporation.

C.2 COMPARISON AGAINST EPA CAP88-PC SOFTWARE

To verify the modeled radionuclide concentrations by the ERDF PA model, a comparative modeling study was performed using the CAP88-PC Version 3 (EPA 402-R-00-004) computer program. The CAP88 (which stands for Clean Air Act Assessment Package – 1988) computer model is a set of computer programs, databases, and associated utility programs for estimation of concentrations, dose, and risk from radionuclide emissions to the air.

CAP88-PC uses a modified Gaussian plume equation to estimate the average dispersion of radionuclides released from up to six emitting sources. The sources may be either elevated stacks (such as a smoke stack) or uniform area sources (such as a landfill or a pile of uranium mill tailings). Plume rise can be calculated assuming either a momentum or buoyant-driven plume. Assessments are done for a circular grid of distances and directions for a radius of up to 80 km (50 mi) around the facility. The Gaussian plume model produces results that agree with experimental data as well as other similar regulatory models. CAP88-PC has the capability of generating dry and wet deposition rates for dose estimation and risk calculation. The calculation of deposition velocity and the default scavenging coefficient is defined by current EPA policy. Version 3 of CAP88-PC is also modified to do either "Radon-only" or "Non-Radon" runs, to conform to the format of the 1988 Clean Air Act NESHAPS Rulemaking.

The CAP88-PC model requires the following inputs:

- Facility data
- Source data
- Receptor location and population
- Meteorological data
- Nuclide data
- Agriculture data (for dose estimation and risk calculation).

For this comparative study, the CAP88-PC modeling was conducted using the following options and input parameters:

Run Options

The CAP88-PC modeling was set up for "individual assessment" (rather than for "population assessment"). The modeled receptor distance was the distance from the center of ERDF to the edge plus 100 m. The edge of the ERDF facility was estimated by the effective radius of the source. The source area of ERDF, for the purpose of input to the CAP88-PC model, is approximated as 451,180 m² based on approximate top surface dimensions of 1,042 m by 433 m, assuming the waste is spread on the side slopes of ERDF. The effective radius was calculated using the following equation:

$$R = \sqrt{\frac{1042 \times 433}{\pi}} = 379 \text{ m}$$

Subsequently, the receptor distance for the CAP88 modeling is set to be 479 m (adjusted for the additional 100-m receptor distance).

Nuclide Data

Carbon-14 was the selected radionuclide for the comparative modeling run, and it was modeled as CO₂ in gas form.

Source Data

The emissions from ERDF were modeled as a single point source (stack) at ground level (i.e., source height is zero) with an effective diameter of 758 m (effective radius is 379 m). An emission rate of 1.7 Ci/yr for carbon-14 was chosen for comparative modeling, based on the calculated diffusive flux over the entire ERDF at a post-closure time of 110 years by the ERDF PA model. Plume rise was set to zero for each Pasquill stability category based on the source emission characteristics.

Meteorological Data

The following site-specific meteorological input parameters for the comparative modeling were determined based on the average of 30 years of meteorological data collected at the Hanford Meteorological Station (HMS). The HMS is located near the center of the Hanford Site, just outside the northeast corner of the 200 West Area:

- Annual ambient temperature: 12.17 °C
- Annual precipitation: 18.14 cm/yr
- Height of the mixing layer: 1000 m (default)
- Absolute humidity: 8.00 g/m³ (default, similar to the HMS value)

In addition to the meteorological parameters described above, a wind file is required for the execution of CAP88 model. Two wind files were considered in the calculations:

1. The wind files from meteorological station at Yakima Airport were used as it is the closest meteorological station to the ERDF site that is originally included in the CAP88-PC Wind File Library. The Yakima Airport is located at 46.568 N and 120.544 W with an elevation of 1,099 ft (Airport-Data.com, 2013).
2. A Hanford Site-specific wind file for the 200 Area was used based on wind data collected by HMS for the 200 Area between 1983 and 2006 (at the 10-m level). Wind file from HMS in joint frequency distributions (JFD) format was derived from the National Environmental Policy Act characterization report (PNNL-6415). Using this wind file, a site-specific meteorological file was created inside the WindLib subdirectory of CAP88 software for dispersion modeling runs. The "Custom Wind File" option was selected to use this wind file.

Figure C-3 compares the wind rose diagram for the HMS and Yakima Airport for 2011, indicating that the prevailing wind direction is from the west-northwest towards the east-southeast. The variability in wind direction is similar in the two data sets with minor differences in the predominant directions. For the purpose of this calculation these small differences can be ignored as they are unlikely to cause any appreciable differences in dispersion of plume and therefore the magnitude of the maximum concentration downwind.

CAP88 Modeling Results

Using the wind file from Yakima Airport, the CAP88 modeling results show that the maximum concentration of carbon-14 at the receptor location (479 m from the center of ERDF and 100 m from the edge) is 1.8 pCi/m³. In comparison, the ERDF PA model calculated the air-pathway concentration at a 100-m downgradient receptor location of about 16 pCi/m³ using the same set of parameters.

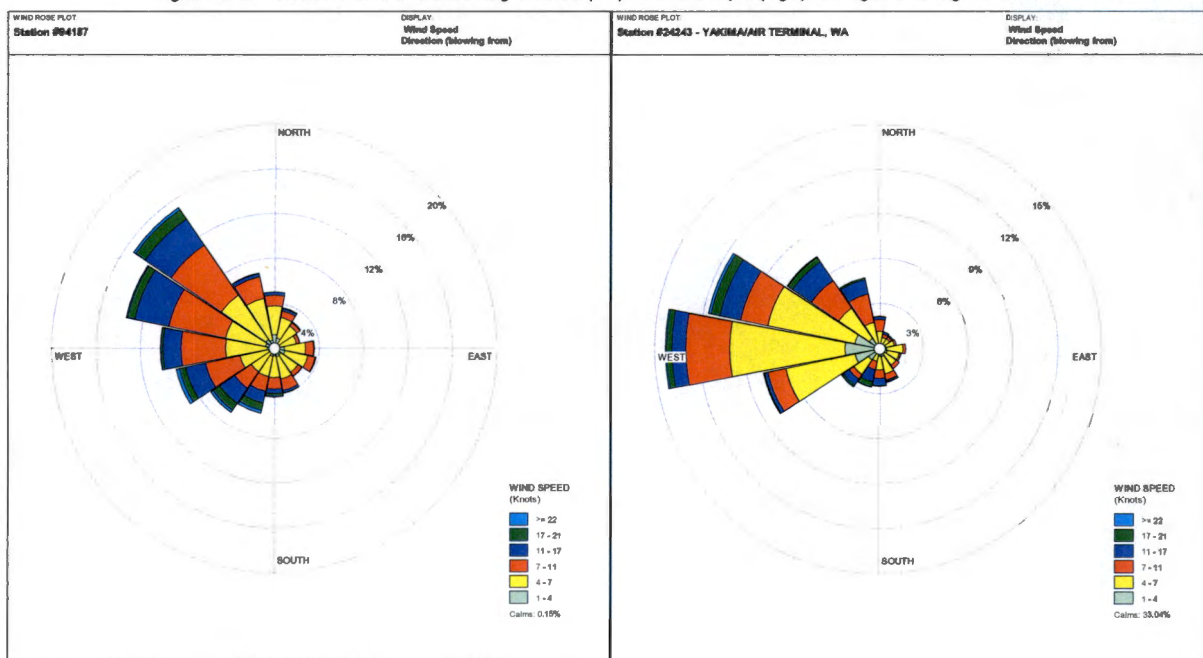
Using the wind file from HMS (200 Area), and based on the same input parameters and modeling setup described previously, the CAP88 model generated the maximum concentration of 1.4 pCi/m³ for carbon-14 at the receptor location (479 m from the center of ERDF and 100 m from the edge).

When comparing CAP88 modeling results using the HMS wind file with that using the wind file from the Yakima Airport, the following were observed:

- The maximum modeled concentration based on the HMS wind file decreased by 24% when compared with that based on wind file from Yakima Airport;
- The maximum modeled concentrations were generated in east-southeast direction for both the HMS wind file and the wind file from Yakima Airport;
- Small wind direction changes between the Yakima meteorological data and HMS meteorological data were observed from the modeling concentrations in East direction (3rd highest using HMS data; 2nd highest using Yakima Airport data) and a southeast direction (2nd highest using HMS data and 3rd highest using Yakima Airport data).

The comparative modeling results of using wind files from the HMS (1.4 pCi/m³) and Yakima Airport (1.8 pCi/m³) demonstrate that the CAP88-PC modeling system generates a lower concentration when compared with the concentration predicted by the ERDF PA model (16 pCi/m³), indicating that the model applied for the compliance calculation is conservative and therefore more protective.

Figure C-3. 2011 Wind Rose for Hanford Meteorological Station (Left) and Yakima Airport (Right) Showing the incoming Wind Direction.



C.3 COMPARISON AGAINST HANFORD SITE NATIONAL ENVIRONMENTAL POLICY ACT CHARACTERIZATION REPORT

As part of the annual Hanford Site NEPA Characterization Report, atmospheric dispersion analysis is performed to characterize the distribution of the identified radionuclides in the ambient air and to estimate the potential exposure. These are presented in PNNL-6415, Rev. 18. The annual sector average dispersion coefficients for the major Hanford Site areas are tabulated and presented in the appendix of this report by taking into account the wind-related data from 1983 through 2006 from various meteorological stations on the Hanford Site. These dispersion factors are presented as a function of direction and distance from the release point.

The atmospheric dispersion analysis in the PNNL-6415 report was conducted using simple dispersion models and the joint frequency distribution of atmospheric stability, wind speed, and wind direction to compute diffusion factors for both chronic and acute releases. Joint frequency distributions for atmospheric stability, wind speed, and transport direction have been estimated and presented for the meteorological data collected from the 100-N, 200, 300, and 400 Areas at two release heights (9.1 m [30 ft] and 60 m [197 ft]).

To verify the ERDF PA air-pathway modeling results, a comparative evaluation was performed by comparing the ERDF PA modeled concentrations at a selected distance with the derived air concentrations for the similar distance using the reported annual sector average dispersion coefficients (X/Q' , where X is the air concentration [Ci/m^3] and Q' is the emission rate) in PNNL-6415 for a given ERDF gas emission rate.

For this comparison analysis, joint frequency distributions for the 200 Area were used. The atmospheric dispersion coefficient (X/Q') of $2.0 \text{ E-}5 \text{ s}\cdot\text{m}^{-3}$ for the ground level release is selected based on a distance of 500 m (approximate effective distance of receptor from the center of ERDF) in the southeast direction (the predominant direction of flow) from Table A11 of PNNL-6415. Based on this X/Q' value and using an ERDF emission rate of $1.7 \text{ Ci}/\text{m}^3$, the ground level concentration is calculated to be $1.1 \text{ pCi}/\text{m}^3$. In comparison, the ERDF PA model calculated a value of about $16 \text{ pCi}/\text{m}^3$, indicating that the model applied for the compliance calculation is conservative and therefore more protective.

C.4 REFERENCES

Airport-Data.com, 2013, Yakima Air Terminal/Mcallister Field Airport (YKM) Information.
<http://www.airport-data.com/airport/YKM/>

Carslaw, H. S. and J. C. Jaeger, 1959, *Conduction of Heat in Solids (Second ed.)*, Oxford, University Press.

EPA 402-R-00-004, 2007, *Updated User's Guide for CAP88-PC Version 3.0*, U.S. Environmental Protection Agency, Washington, D. C. Currently available at
<http://www.epa.gov/radiation/assessment/CAP88/index.html>

EPA, 2010, *EPA On-line Tools for Site Assessment Calculation*,
<http://www.epa.gov/athens/learn2model/part-two/onsite/estdiffusion-ext.html>. Web site updated January 2012.

- Haynes, W. M. and D.R. Lide (Ed.), 2011, *CRC Handbook of Chemistry and Physics*, 92nd Edition, CRC Press, Boca Raton, Florida.
- Mathews, J. and R. L. Walker, 1970, *Mathematical Methods of Physics*, p. 226–239. In *Partial Differential Equations*. 2nd ed. W.A. Benjamin, New York.
- Millington, R. J. and J. P. Quirk, 1960, "Transport in Porous Media," In Van Beren, F. A. (ed.), *Transactions of the 7th International Congress of Soil Science*, Vol. 1, 14–24. p. 97–106.
- Nazaroff, W. W. and A. V. Nero, 1988, *Radon and Its Decay Products in Indoor Air*, John Wiley & Sons, New York, New York.
- Ogata A. and R. B. Banks, 1961, *A Solution of the Differential Equation of Longitudinal Dispersion in Porous Media*, USGS Professional Paper 411-A.
- PNNL-6415, 2007, *Hanford Site National Environmental Policy Act (NEPA) Characterization*, Rev. 18, Pacific Northwest National Laboratory, Richland, Washington. Available at: http://www.pnl.gov/main/publications/external/technical_reports/PNNL-6415Rev18.pdf.
- WCH-515, 2013, *Parameter Uncertainty for the ERDF Performance Assessment Uncertainty and Sensitivity Analysis*, Rev. 0, Washington Closure Hanford, Richland, Washington.
- Yu, C., A. J. Zielen J.-J. Cheng, D. J. LePoire, E. Gnanapragasam, S. Kamboj, J. Arnish, A. III Wallo, W. A. Williams, and H. Peterson 2001, *User's Manual for RESRAD Version 6*, ANL/EAD-4, Argonne National Laboratory, Argonne, Illinois.

APPENDIX D

**SURFACE BARRIER AND LINER PERFORMANCE AND WATER
ACCUMULATION IN THE ERDF ENGINEERED STRUCTURE**

TABLE OF CONTENTS

APPENDIX D SURFACE BARRIER AND LINER PERFORMANCE AND WATER ACCUMULATION IN THE ERDF ENGINEERED STRUCTURE.....	D-1
D.1 INTRODUCTION	D-1
D.2 HANFORD PROTOTYPE BARRIER PERFORMANCE	D-1
D.3 WATER ACCUMULATION "WHAT IF" SCENARIOS.....	D-9
D.3.1 Diffuse Recharge Sharp Wetting-Front Model and Vertical Movement	D-13
D.3.2 Diffuse Recharge Horizontal Movement	D-16
D.3.3 Buried Point Source Model and Travel Times.....	D-17
D.3.4 BC Cribs and Trenches Site	D-22
D.4 DUST-SUPPRESSION MOISTURE PERSISTENCE.....	D-29
D.5 ALTERNATE SURFACE BARRIER AND LINER DEGRADATION CONCEPTUAL MODEL EVALUATION	D-30
D.6 CONCLUDING REMARKS	D-33
D.7 REFERENCES	D-34

FIGURES

D-1. Plan View of the Prototype Hanford Barrier Showing Monitoring Stations (PNNL-18845).	D-4
D-2. Plan View of the Prototype Hanford Barrier Showing the Layout of the 12 Surface Soil Plots (1W to 6W and 1E to 6E) and Horizontal Neutron Access Tubes (AA Above Asphalt; BA Below Asphalt) (PNNL-18845).	D-5
D-3. Distribution of Long-Term Average Natural Precipitation and Irrigation Used During the Treatability Test (Ward et al. 2010).	D-6
D-4. Cross Section of the Prototype Hanford Barrier (PNNL-18845; Ward et al. 2010).	D-6
D-5. Temporal Variation in Soil-Water Storage in Northwest Plot 6W at the Prototype Hanford Barrier, October 1994 Through September 2009 (Design Water Storage Capacity is 600 mm) (PNNL-18845).	D-7
D-6. Cumulative Amounts of Water Diverted by the Asphalt Pad (Drainage) from the Silt-Loam Plots at the Prototype Hanford Barrier in September 1994 Through August 2009 (PNNL-18845).	D-7
D-7. Evapotranspiration on the Silt-Covered Plots Calculated Using the Water Balance Equation (PNNL-18845).....	D-8
D-8. Measured Moisture Content Profile (PNNL-18845).....	D-8
D-9. ERDF Leachate Liner Collection System.....	D-9
D-10. ERDF Simulated Steady-State Moisture Content (Chapter 4.0).....	D-10
D-11. ERDF Moisture Retention and Unsaturated Hydraulic Conductivities (Chapter 3.0).....	D-11

D-12.	ERDF Disposal Facility Moisture Regime.	D-12
D-13.	ERDF Diffuse Recharge Sharp Wetting-Front Model.	D-15
D-14.	ERDF Diffuse Recharge Horizontal Movement Model.	D-17
D-15.	ERDF Buried Point Source Model (a) Plan View and (b) Vertical Cross Section.	D-20
D-16.	ERDF Buried Point Source Model (a) Spherical Coordinate System and (b) Dimensionless Travel Time T - Dimensionless R Graphical Solution, B= Buried Source, S=Surface Source (after Philip 1984).	D-21
D-17.	Measured Saturated and Unsaturated Hydraulic Conductivity for (a) a Sandy Sample and (b) a Gravelly Sample (after Khaleel and Relyea 2001).	D-22
D-18.	BC Cribs and Trenches Site Location in the 200 East Area.	D-23
D-19.	BC Cribs and Trenches in the 200 East Area.	D-24
D-20.	BC Cribs and Trenches North-South Profile for Cross-Section Dissecting Trenches 216-B-34 Through 216-B-28.	D-25
D-21.	Observed and Predicted Profile of Sediment Volumetric Moisture Content Through the Center of Trench 216-B-26 in 2004 (after PNNL-14907).	D-26
D-22.	Observed and Predicted Distributions in Year 2005 at Borehole C4191 for (a) Technetium-99, and (b) Nitrate. (Predicted values are based on STOMP modeling reported in PNNL-14907.)	D-27
D-23.	Pre- and Post-Injection (May 5, 2000 and July 31, 2000) Moisture Plumes for the Sisson and Lu Field Injection Experiment in the 200 East Area (Ye et al. 2005).	D-30
D-24.	Net and Cumulative Infiltration Through the ERDF Surface Barrier and Liner System for the Gradual Failure and Instantaneous Failure Conceptual Models.	D-32

TABLES

D-1.	Evaluation of the Net and Cumulative Infiltration Through the ERDF Surface Barrier and Liner System Using Equation 1.	D-32
------	--	------

APPENDIX D

SURFACE BARRIER AND LINER PERFORMANCE AND WATER ACCUMULATION IN THE ERDF ENGINEERED STRUCTURE

D.1 INTRODUCTION

The application of defense-in-depth principles provides insights into the closure design of the Environmental Restoration Disposal Facility (ERDF). Key elements of the defense-in-depth philosophy are the use of multiple barriers (engineered and natural) to isolate waste in the disposal environment and the establishment of institutional controls to prevent or limit human access to the waste. The use of multiple barriers improves confidence in the adequacy of closure actions by mitigating intrinsic uncertainties associated with any single barrier. With this approach, even if one or more parts of the system fail or function at less than optimum levels than projected, the overall system performance remains at sufficiently protective levels.

The ERDF is composed of manmade as well as natural components (Figure ES-4). The manmade components of the system that provide defense in depth and influence contaminant migration include a closure surface barrier, a double-liner leachate collection system, the ERDF cells and infrastructure, and the distribution of waste in the subsurface. The natural components of the system that influence contaminant migration are multiple underlying nearly horizontal stratigraphic layers within the vadose zone and the unconfined aquifer.

The ERDF performance assessment (PA) modeling considered reduction of net infiltration from the presence of a double leachate collection liner system at the base and an engineered cover (surface barrier) over the top. The liner system is installed during construction of the cells, and the surface barrier is assumed to be installed on ERDF at closure in 2035. Although the actual performance of the surface barrier cannot be known prior to construction, its efficacy can be inferred from the monitoring data collected at the Prototype Hanford Barrier that was constructed in the 200 East Area in 1994.

The primary objectives of this appendix are to provide additional supporting material for ERDF closure barrier recharge estimates as well as an evaluation of "what if" scenarios for water accumulation within the ERDF waste disposal facility. We evaluate water accumulation scenarios using a combination of analytical solutions and neighboring field data.

Section D.2 summarizes results of 15 years of continuous performance monitoring for the 200-BP-1 Prototype Hanford Barrier in the 200 East Area. **Section D.3** presents detailed equations and results of bounding solutions for "what if" water accumulation scenarios. Section D.3 also provides an overview of field data on contaminant plumes resulting from large-scale discharges at the neighboring BC Cribs and Trenches site. **Section D.4** provides an evaluation of moisture buildup from ERDF dust-suppression operations. **Section D.5** presents the concluding remarks.

D.2 HANFORD PROTOTYPE BARRIER PERFORMANCE

An engineered surface barrier (Chapter 2.0) is an integral component of ERDF closure. In August 1994, a prototype Hanford barrier, a multilayered capillary barrier with an evapotranspiration (ET) surface layer, was constructed over the 216 B-57 liquid waste disposal

crib in the 200 East Area of the Hanford Site. The 5-m-thick barrier covers an area of 2.5 ha (6.2 acres) and was designed with objectives that included the ability to (1) limit recharge to 0.5 mm/yr (1.6×10^{-9} cm/s); (2) be maintenance free, (3) resist plant animal and human intrusion, (4) limit the exhalation of noxious gases, (5) minimize erosion, (6) meet or exceed *Resource Conservation and Recovery Act of 1976* (RCRA) cover performance requirements, (7) be accepted by regulators and the public, and (8) isolate wastes for at least 1,000 years. Additional details are presented in PNNL-18845 (*200-BP-1 Prototype Hanford Barrier – 15 Years of Performance Monitoring, Rev.1*).

The barrier performance was monitored almost continuously for 15 years to document structural stability, erosion, and components of the water balance including precipitation, surface runoff, water storage, percolation out of the root zone, and ET. To monitor the water-balance components in the top 2-m silt-loam layer of the barrier, the surface was fitted with 14 water-balance monitoring stations (S1 through S14; Figure D-1). The stations were arranged with three monitoring stations in each of the four silt-loam-covered plots (3W, 3E, 6W, and 6E) and one monitoring station in each of the two gravel-covered plots (1W and 4W).

Figure D-2 shows the layout of the 12 surface soil plots (1W to 6W and 1E to 6E) and horizontal neutron access tubes (AA above asphalt; BA below asphalt). The 2-m-thick silt-loam layer is heavily instrumented. A treatability test conducted from 1994-1998 irrigated the northern half of the barrier such that it received approximately 480 mm/yr (i.e., more than three times the long-term average [LTA] precipitation) and included a simulated 1,000-year return storm each March from 1995 to 1997 in which 68 mm of water was applied over an 8-hour period (Figure D-3). In September 2008, one-half of the barrier was burned to gain an improved understanding of the response of engineered ecosystems to wild fire (PNNL-18845).

The prototype barrier is similar in concept to the RCRA subtitle C design for ERDF and consists of a 2-m-thick silt-loam layer overlying other, coarser materials including sand, gravel, and basalt riprap with each layer serving a distinct purpose (Figure D-4). The silt-loam layer acts as a medium in which moisture is stored until the ET processes recycle any excess water back to the atmosphere. The design storage capacity, the amount of water that can be stored before drainage occurs, for the 2-m-thick silt-loam layer is 600 mm (23.6 in.), which is over three times the LTA precipitation for the site. The silt loam also provides a medium for establishing vegetation, which is necessary to recycle water to the atmosphere. In addition, the top 1 m (3.3 ft) of silt loam was amended with 15% by weight of pea gravel as a guard against erosion. The entire silt-loam layer is a medium for plant growth and therefore forms the ET layer. Coarser materials (sand overlying gravel) placed directly below the silt-loam layer create a capillary break that inhibits the downward percolation of water through the silt and prevents fine soil from migrating into the coarser layers. The basalt riprap layer is intended to act as a biointrusion layer to deter root penetration, animal burrowing, and inadvertent human intrusion. An asphalt layer at the base of the barrier provides redundancy in infiltration and biointrusion control. The entire barrier was constructed with a 2% slope to promote movement of water towards the edges.

Detailed monitoring results for the prototype barrier during the treatability test and through the first 15 years of operation are presented in DOE/RL-99-11, *200-BP-1 Prototype Barrier Treatability Test Report*, and PNNL-18845, respectively. As an illustration, Figure D-5 shows the temporal pattern in water storage on plot 6W in the northwestern quadrant of the barrier. Note the elevated water storage observed during the treatability test. This is expected because the northern half of the barrier was irrigated from fiscal year (FY) 1995 through FY 1997 as part of a 4-year *Comprehensive Environmental Response, Compensation, and Liability Act of 1980*

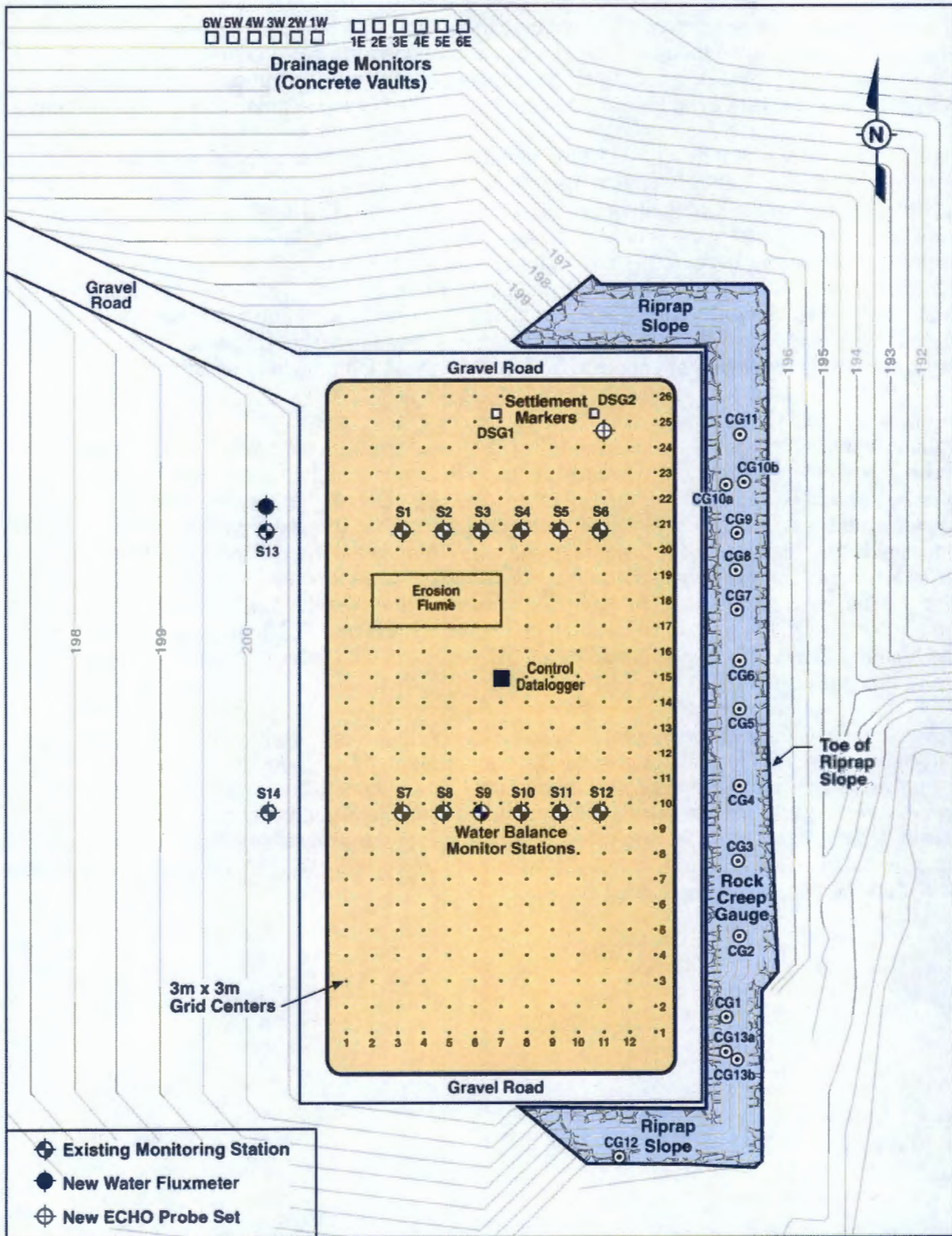
(CERCLA) treatability test. The northern half of the barrier showed the largest values of storage during this period and for almost 2 years after the cessation of irrigation. The cumulative precipitation and irrigation during the treatability test was 1462 mm, with an annual average rate of 487 mm/yr, which is approximately equal to three times the LTA precipitation for the Hanford Site. Nonetheless, even though water storage approached the design storage capacity in 1997, the wettest year on record, the design capacity was never exceeded and no drainage occurred from the fine-soil layers even for considerably higher than average precipitation (PNNL-18845).

Figure D-6 shows that, through FY 2009, cumulative drainage from each of the soil covered plots remained significantly less than the 0.5-mm yr^{-1} drainage criterion; the 600-mm storage capacity of the 2-m-thick silt-loam layer was never exceeded (PNNL-18845). The mean cumulative drainage from the four soil plots over the 15-year monitoring period is only 0.116 mm with a standard deviation of 0.093 mm. This is equivalent to a percolation rate of only 0.0075 mm/yr or 1.5% of the annual drainage criterion of 0.5 mm. These results clearly illustrate the effectiveness of the capacitive barriers constructed of fine soil materials in minimizing percolation. The 2-m-thick silt-loam cover essentially cut off percolation because these small amounts of water collected from under the silt-loam have been attributed to condensation in the drainage system (PNNL-18845).

Data collected at the barrier were used to solve the water-balance equation and to calculate ET for each soil-covered plot on the two precipitation treatments at the barrier. Figure D-7 shows a plot of calculated ET from 1994 through 2009. During the 3-year treatability test, calculated ET showed essentially no intra-plot difference but showed significant treatment differences; the highest amounts came from the north plots. In the first year of monitoring, a mean ET of 744 mm was calculated for the north plots, whereas only 396 mm was calculated for the south plots. The total ET declined sharply over time, reaching a minimum of 156 mm on the north half and 124 mm on the south half in 1999. Since then, ET from both treatment plots has hovered around a mean value of about 167 ± 40 mm each year, thus exceeding the LTA precipitation (PNNL-18845).

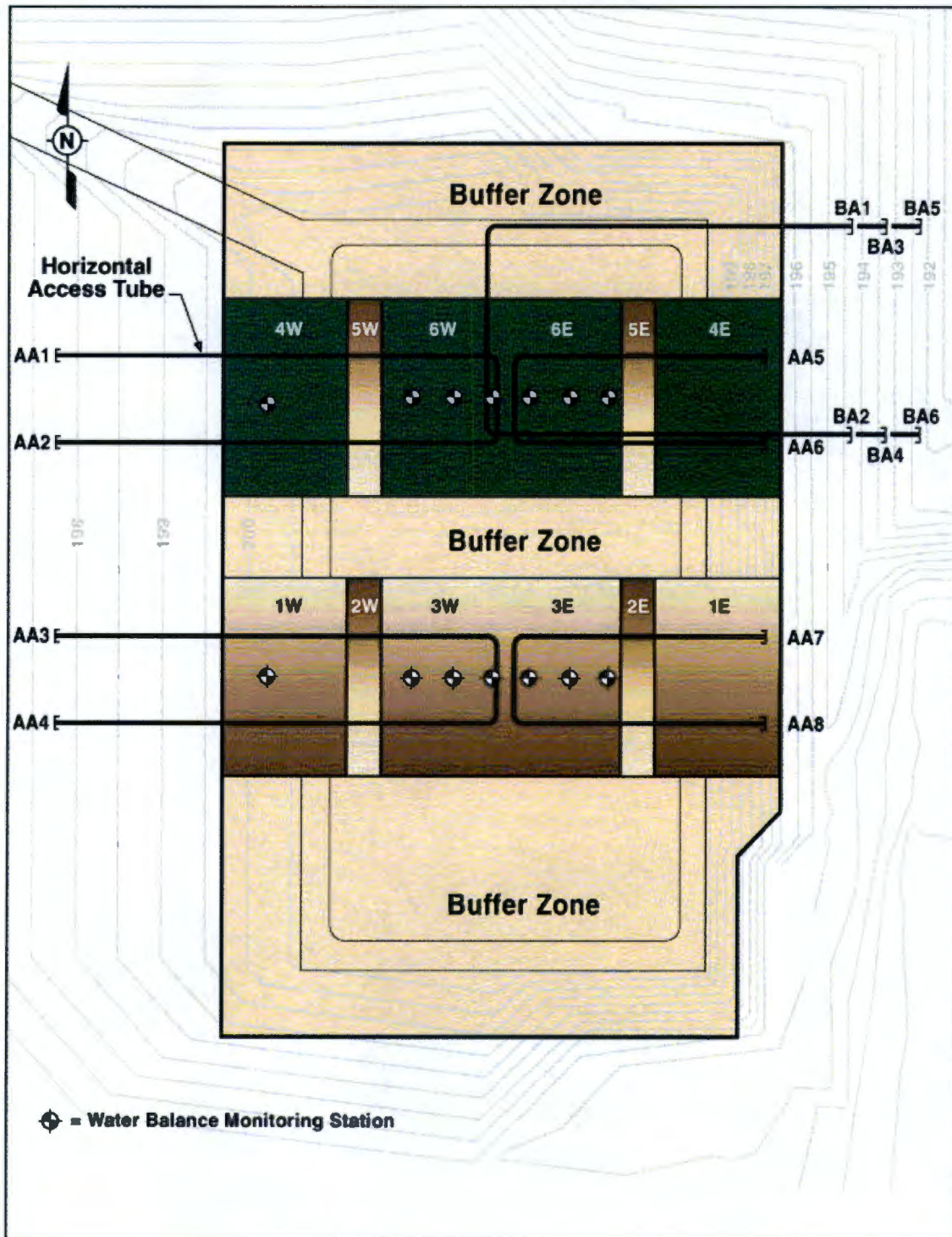
Figure D-8 shows the water content profiles for the northern and southern halves, illustrating a moisture content of about 5% on a volume basis. In September 2008, the northern half of the barrier was burned to remove vegetation and study the effects of fire on barrier performance. The most immediate effects have been on water storage patterns; the bare surface showed a slower accumulation of water, a smaller peak storage, and a delayed release relative to the unburned side due to evaporation. Nonetheless, the residual storage at the end of the year was similar for the burned and unburned sides.

Figure D-1. Plan View of the Prototype Hanford Barrier Showing Monitoring Stations (PNNL-18845).



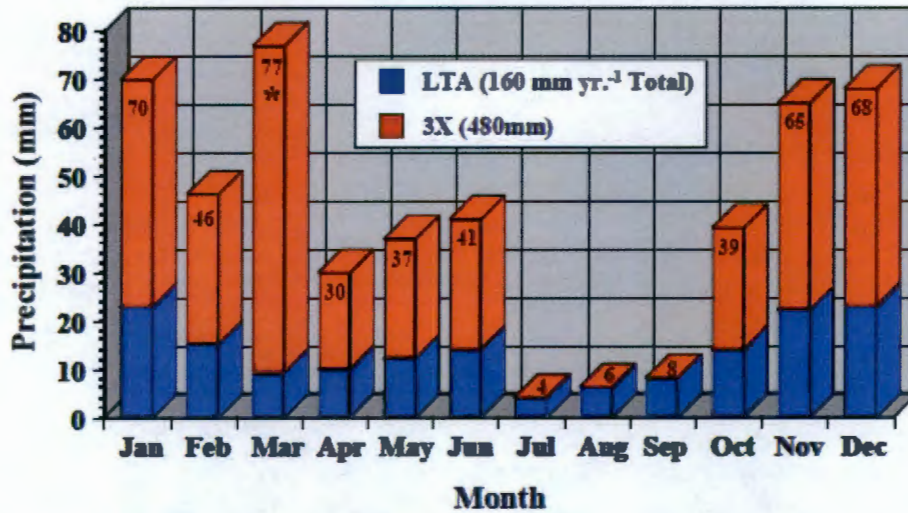
E0302002_1

Figure D-2. Plan View of the Prototype Hanford Barrier Showing the Layout of the 12 Surface Soil Plots (1W to 6W and 1E to 6E) and Horizontal Neutron Access Tubes (AA Above Asphalt; BA Below Asphalt) (PNNL-18845).



E9805023.2c

Figure D-3. Distribution of Long-Term Average Natural Precipitation and Irrigation Used During the Treatability Test (Ward et al. 2010).



*Simulated 1,000-yr. storm (68 mm in 8 hrs.)

Figure D-4. Cross Section of the Prototype Hanford Barrier (PNNL-18845; Ward et al. 2010).

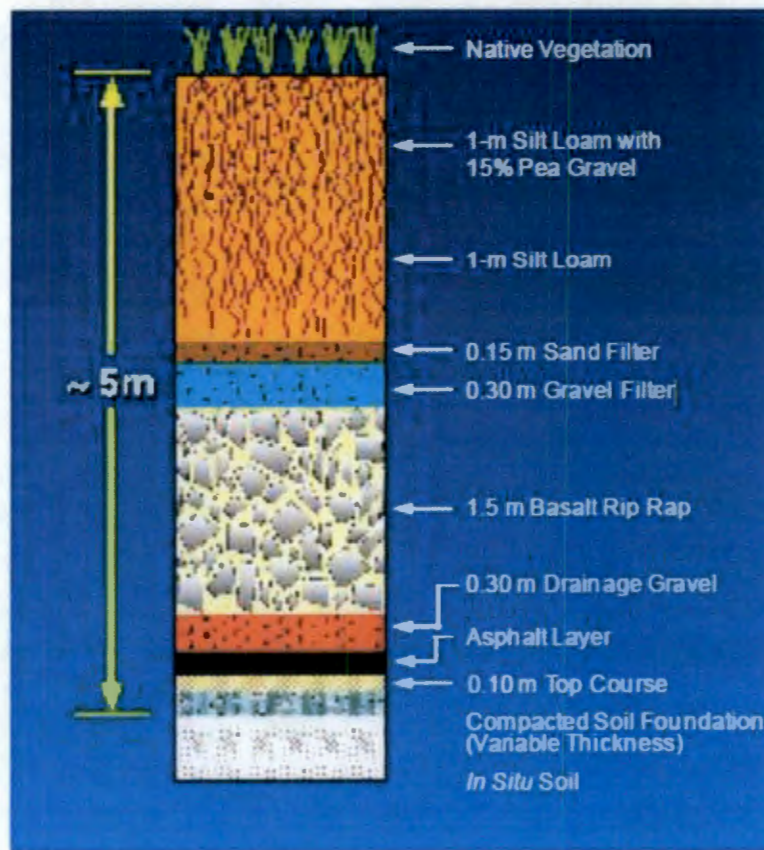


Figure D-5. Temporal Variation in Soil-Water Storage in Northwest Plot 6W at the Prototype Hanford Barrier, October 1994 Through September 2009 (Design Water Storage Capacity is 600 mm) (PNNL-18845).

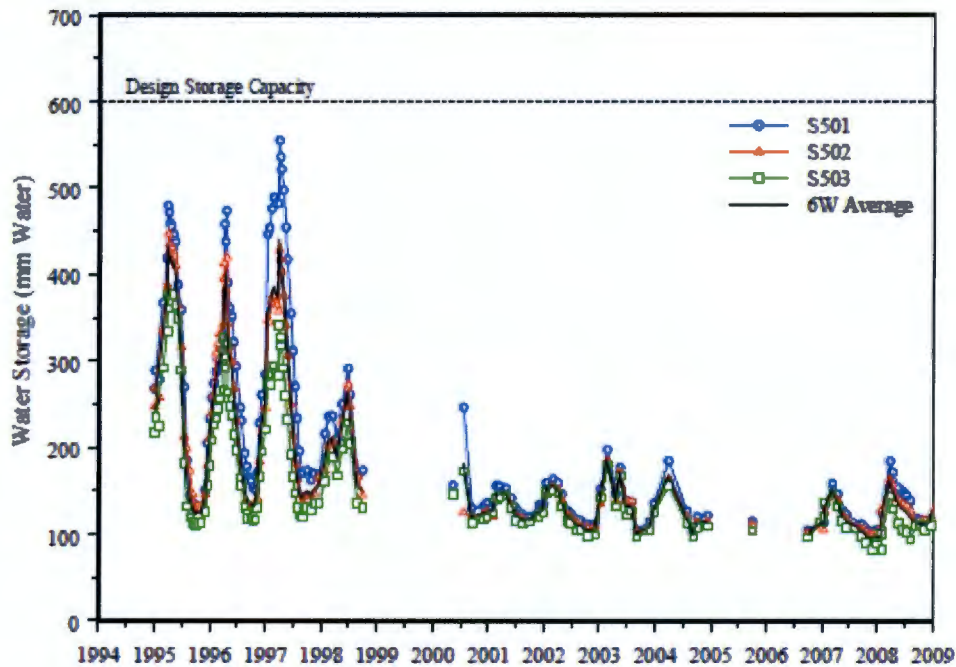


Figure D-6. Cumulative Amounts of Water Diverted by the Asphalt Pad (Drainage) from the Silt-Loam Plots at the Prototype Hanford Barrier in September 1994 Through August 2009 (PNNL-18845).

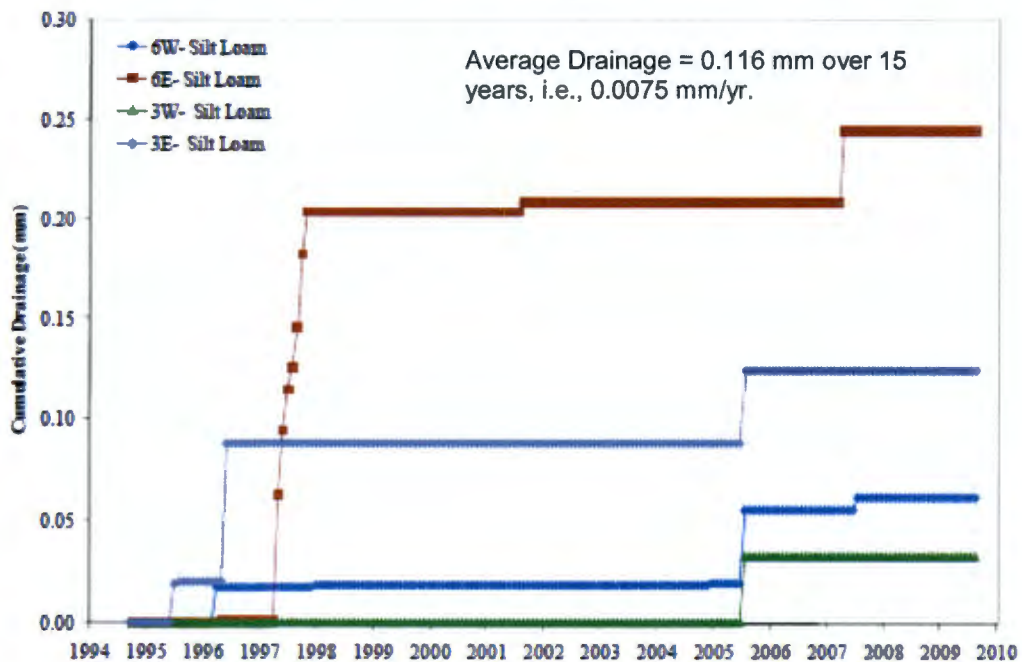


Figure D-7. Evapotranspiration on the Silt-Covered Plots Calculated Using the Water-Balance Equation (PNNL-18845).

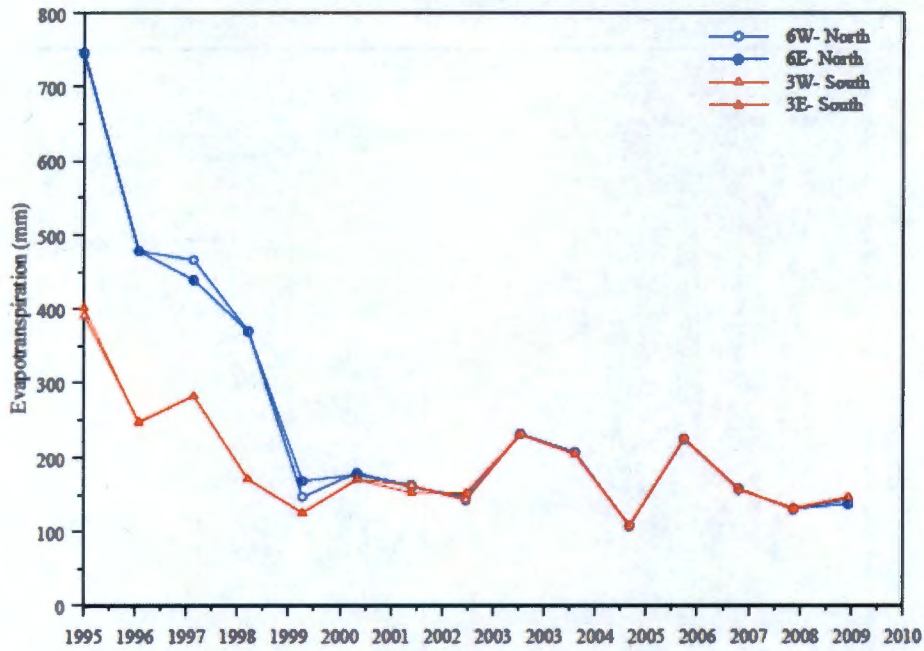
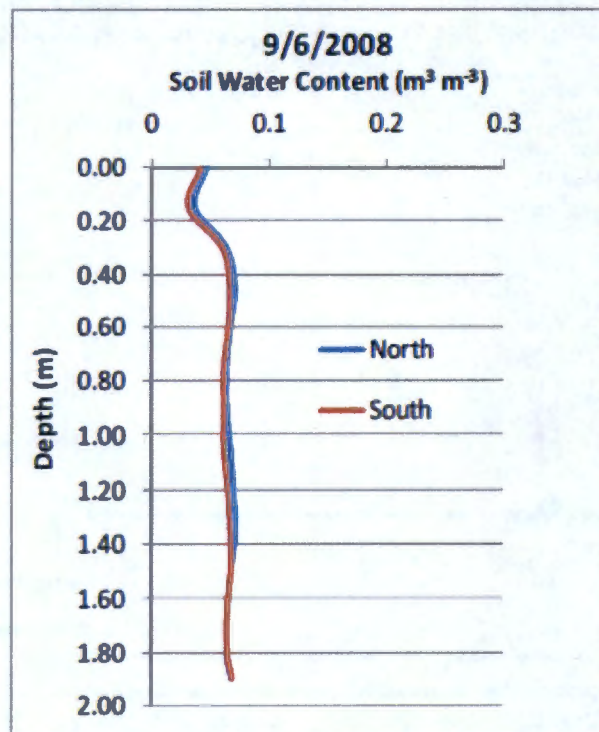


Figure D-8. Measured Moisture Content Profile (PNNL-18845).

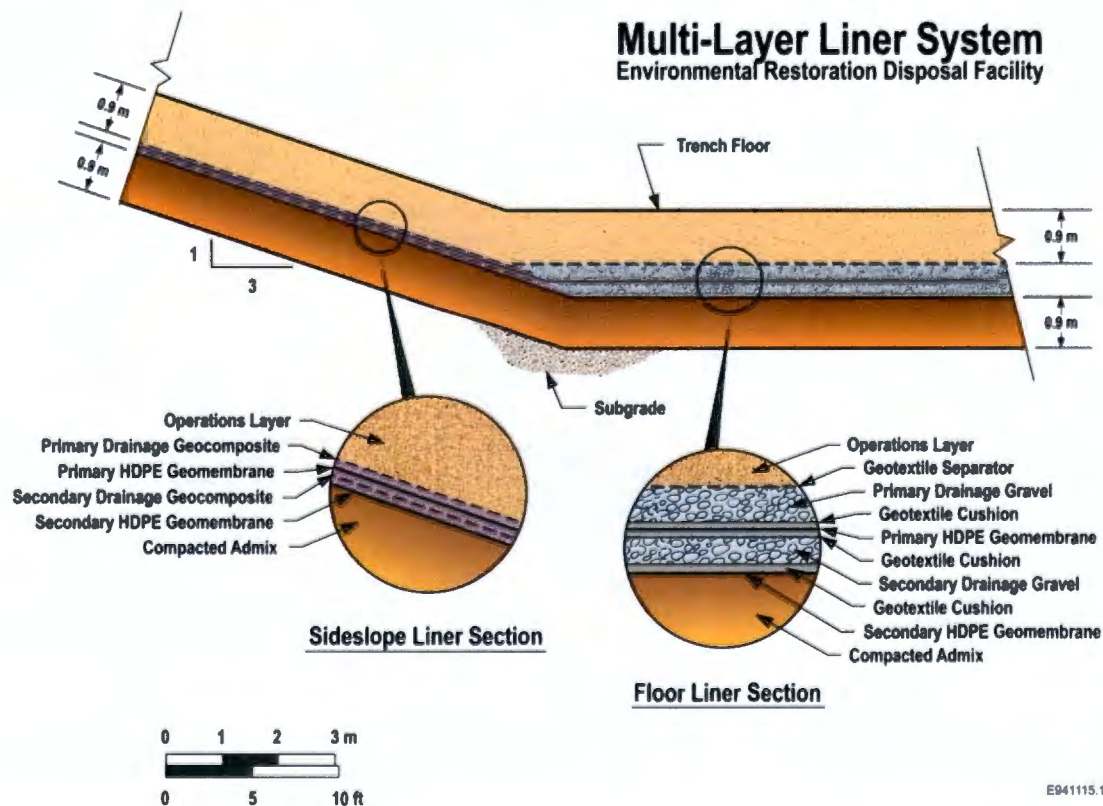


D.3 WATER ACCUMULATION “WHAT IF” SCENARIOS

The preceding data on Hanford prototype barrier performance suggest that a 2-m-thick silt-loam layer is sufficient to reduce deep infiltration to negligible levels. With multiple defense-in-depth as well as capillary break construction, and with a low-moisture regime due to negligible infiltration, water accumulation within the ERDF is not a likely scenario. Nonetheless, we consider the following scenarios whereby water somehow manages to get to the sump over an ERDF cell and accumulates. This assumes that the closure surface barrier is not functioning and the liner fails under the accumulated water, and the numerous capillary breaks throughout the disposal facility are ineffective.

As discussed in Chapter 2.0, the ERDF manmade engineered system is composed of (a) a modified RCRA-compliant closure cover (5 m thick) over (b) 22 m of compacted waste (soil) over (c) a double leachate liner collection system (d) underlain by 0.9 m of compacted admix (clay mixture). Figure D-9 illustrates the ERDF leachate liner collection system. The primary liner is designed to keep leachate from leaking into the underlying primary leak detection recovery system. The secondary liner provides a means of identifying a leak from the primary system and provides an enhanced absorptive capacity for contaminants. The composite liner system thus provides an added protection from leaks. The lower liner at the composite will mitigate leaks from the upper layer, reducing flow through a hole or defect by keeping the hole or defect from becoming larger over time.

Figure D-9. ERDF Leachate Liner Collection System.



E941115.1

For ERDF PA modeling, the 22 m of compacted waste (primarily bulk soil from remediation sites) underneath the ERDF closure barrier was assigned the Hf1 (sandy gravel) hydraulic properties. As described in WCH-464, *Hydrologic Data Package in Support of Environmental Restoration Disposal Facility Performance Assessment Modeling*, and Chapter 3.0, the hydraulic properties were based on laboratory experiments and upscaling. Figure D-10 illustrates the steady-state moisture contents for ERDF PA simulations (Chapter 4.0). Figure D-11 shows the fitted moisture retention and unsaturated conductivity relations used in ERDF PA modeling (Chapter 3). Under steady-state conditions the unsaturated hydraulic conductivity for Hf1 is expected to be about $\sim 2 \times 10^{-8}$ cm/s, which is about 0.006 m/yr (Figure D-11). For a relatively wet volumetric moisture content of 0.09 (Figure D-11), the average linear velocity would be about 0.067 m/yr. Thus, it will take as a minimum about 330 years for a parcel of water to travel from the top to the bottom of ERDF (22 m).

Figure D-10. ERDF Simulated Steady-State Moisture Content (Chapter 4.0).

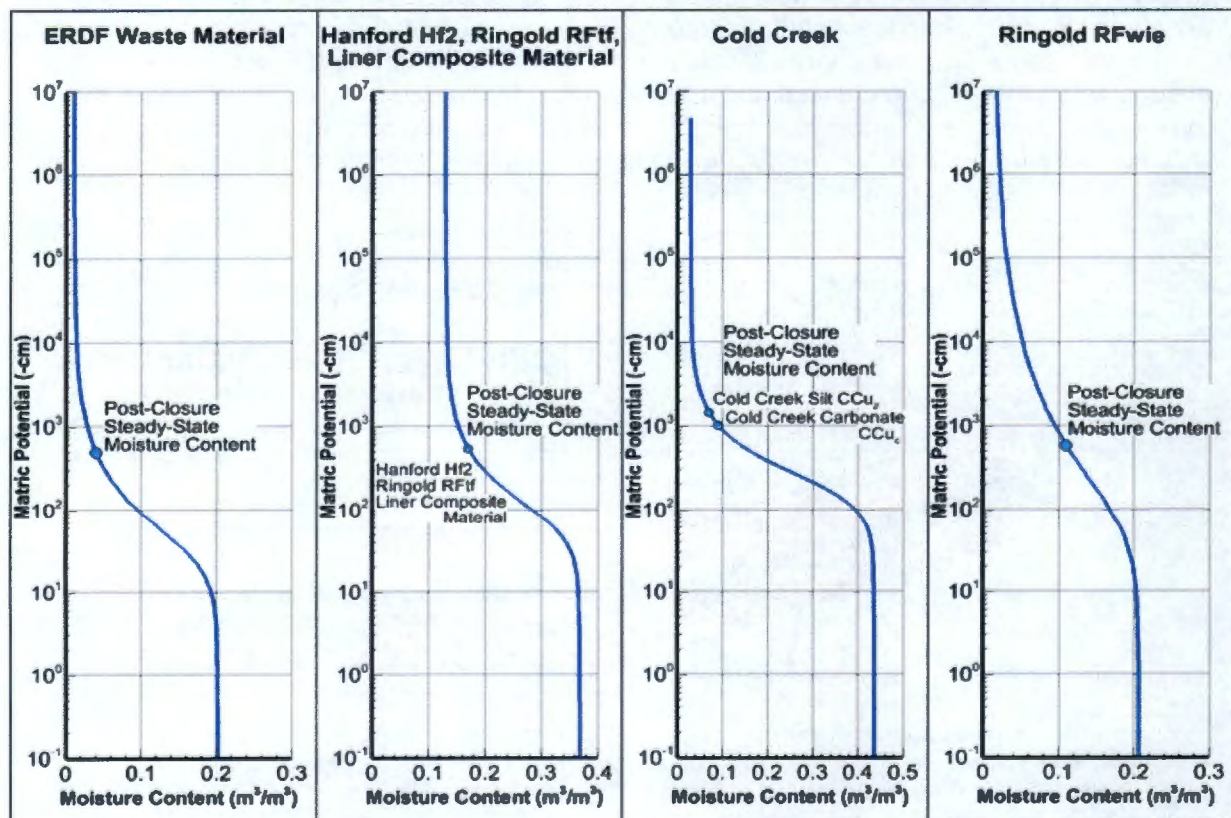
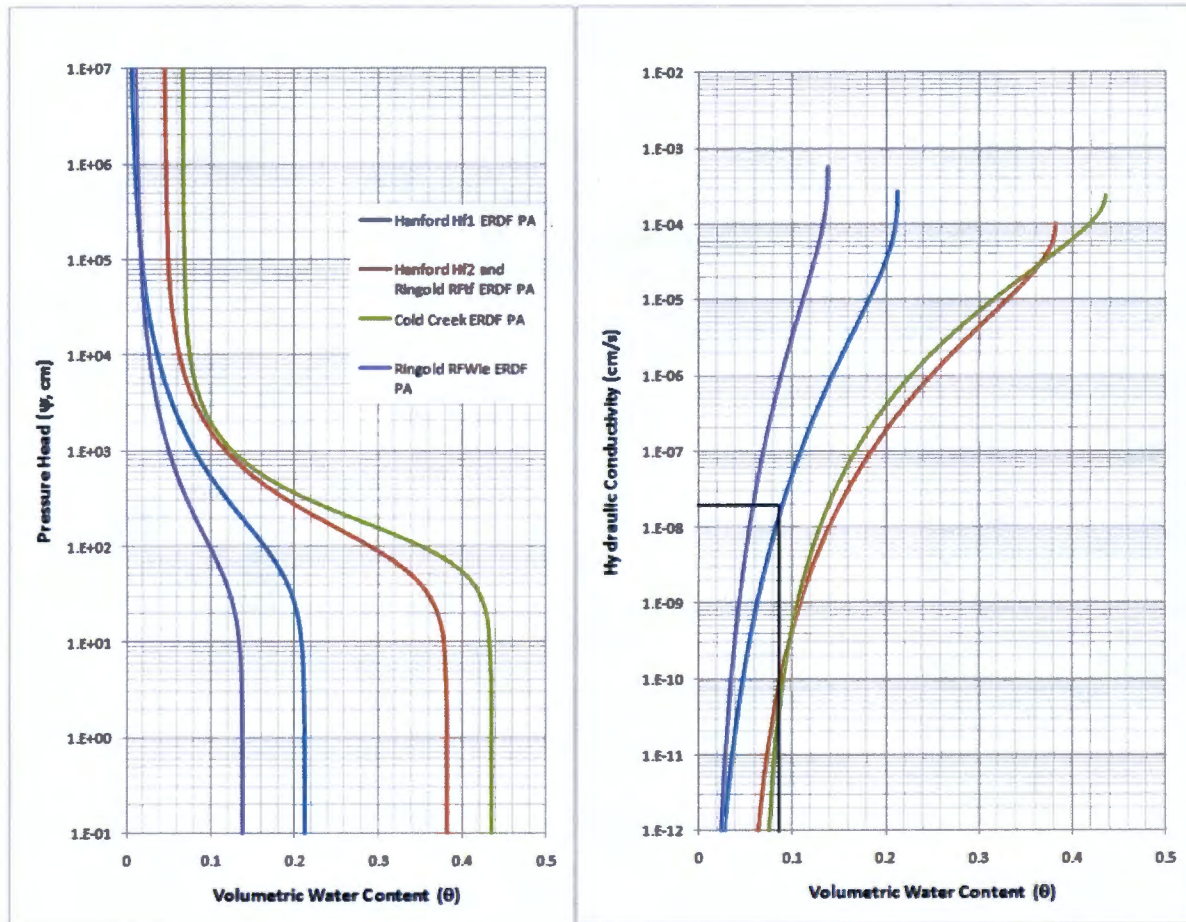
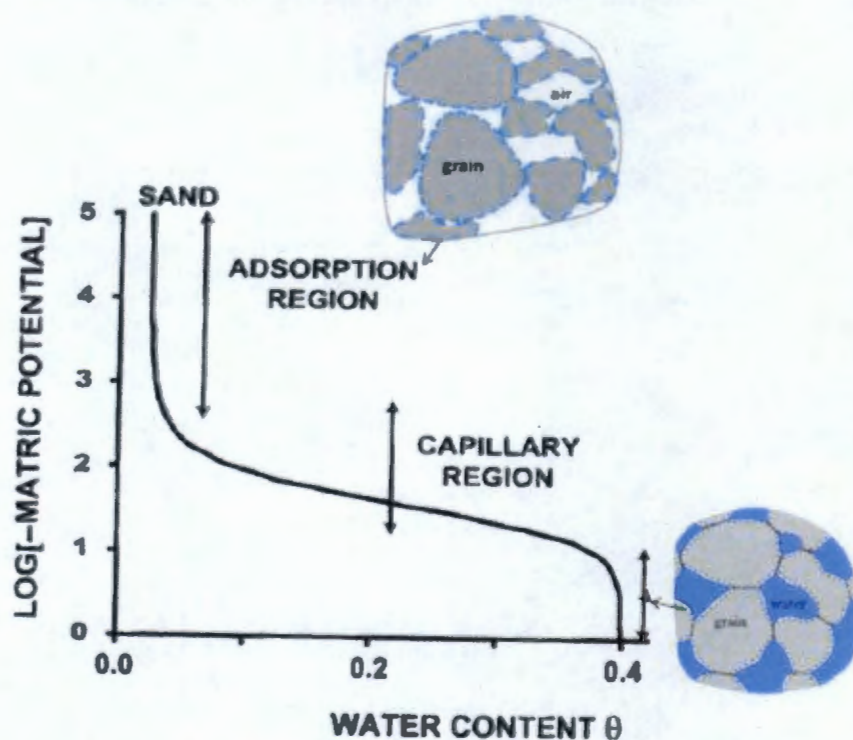


Figure D-11. ERDF Moisture Retention and Unsaturated Hydraulic Conductivities (Chapter 3.0).



The preceding scenario of one-dimensional vertical migration under unit gradient conditions is, however, overly idealized and grossly conservative for the heterogeneous flow domain. This is due to the fact that the bulk of the 22-m ERDF is under a low-moisture regime and only the tightly bound water adsorbed to solid particles constitutes the low-moisture adsorption region (Figure D-12). Large changes in matric potential in the adsorption region are associated with small changes in moisture content. On the contrary, the capillary region is active for a high-moisture regime near air entry suction or near saturation. The two regions are different enough that different laboratory techniques are needed to describe the soil moisture retention curve for the adsorption region (pressure plate method) versus the capillary region (hanging water column method).

Figure D-12. ERDF Disposal Facility Moisture Regime.



For the double-leachate liner system, note the change in particle-size distribution between the liner gravels and the material above and below it, thus resulting in effective capillary breaks and retention of moisture within the finer grained portion (soil physics principle). For example, the operations layer overlying the primary drainage gravel layer works as a capillary break; moisture will accumulate and stay within the finer operations layer because the unsaturated hydraulic conductivity of the underlying coarse-textured material will be much smaller than that of the overlying fine-textured material under low (more negative) matric potential (dry) conditions.

The 0.9-m compacted admix layer composed of clay and native soil (liner floor) is designed to have a minimum saturated hydraulic conductivity of about 1×10^{-7} cm/s. This material has a much smaller pore size compared to the overlying gravel in the liner. Given the unlikely scenario of water accumulating on the liner and subsequent failure of the liner system overlying the admix layer, the admix layer will retain most of the moisture. Again, this is because of capillary break at the contact with the underlying relatively coarser grained Hf2 sand unit. With the unsaturated hydraulic conductivity of the underlying coarse-textured (Hf2 unit) material being much smaller than that of the overlying fine-textured (admix layer) material, the moisture will be largely retained within the admix layer resulting in limited drainage potential.

With multiple defense-in-depth as well as capillary break construction, and with moisture held primarily in the adsorption region of the retention curve for the relatively low-moisture regime, water accumulation within the ERDF is not a likely scenario on the basis of soil physics principles. Nonetheless, we have considered "what if"-type water accumulation and liner failure scenarios. We consider scenarios whereby water somehow manages to get to the sump over an ERDF cell and accumulates. This assumes that the closure surface barrier is not functioning

(e.g., blown away by wind). Such a scenario further assumes that the liner fails under the accumulated water, and the numerous capillary breaks are ineffective throughout the disposal facility.

We considered two “what if” water accumulation and release scenarios, one with water ponding leading to diffuse recharge and other assuming a point source leak. The water accumulation scenario assumptions are as follows.

- The ERDF liner remains intact for 500 years (instead of 100 years for the compliance case).
- The surface barrier fails and the net infiltration increases to 1 mm/yr; the amount of water entering the ERDF waste volume is 500 mm in 500 years.
- For diffuse recharge, bounding calculations are conducted for downward (vertical only) migration and lateral (horizontal only) migration.
- For both diffuse recharge and point source leak scenarios, calculations are based on the θ -based Richards’ equation and mass balance considerations.
- Calculations are based on Hanford Hf2 (sand-dominated) unit hydraulic properties (i.e., unsaturated hydraulic conductivity, soil moisture diffusivity, and longitudinal dispersivity estimates).

Because of limitations of analytical approach, macroscopic, large field-scale processes induced by media heterogeneities are not considered. As described later by contrast to field characterization data, field-scale heterogeneities significantly impact the evolving vadose zone moisture plume and contaminant transport.

D.3.1 Diffuse Recharge Sharp Wetting-Front Model and Vertical Movement

With gravity effects greater than the capillary effects, the moisture content (θ)-based one-dimensional Richards’ equation is:

$$\frac{\partial \theta}{\partial t} + \frac{dK}{d\theta} \frac{\partial \theta}{\partial z} = 0$$

where t is time, K is unsaturated hydraulic conductivity, and z is distance in the vertical direction. The differential equation is similar to the conventional advective-dispersive equation. Figure D-13 illustrates the sharp wetting-front model. The solution for the characteristic curves on the θ - z plane for large times (t) is given by Warrick (2003); z_f is the wetting-front depth.

$$\frac{dz_f}{dt} = \frac{dK}{d\theta}$$

The wetting-front velocity for a given θ at large t is:

$$V = \frac{dz_f}{dt} \approx \frac{K_{wet} - K_{dry}}{\theta_{wet} - \theta_{dry}}$$

With a unit hydraulic gradient model, the wetting-front velocity V_z , at large t , is:

$$V_z = \frac{dz_f}{dt} = \frac{K_{wet} - K_{dry}}{\theta_{wet} - \theta_{dry}} = \frac{q_{in} - K_{dry}}{\Delta\theta}$$

For the Hanford Hf2 (sand-dominated) unit (Chapter 3.0):

$$\theta_{dry} = 0.0443$$

$$\theta_{wet} = 0.3819$$

$$\Delta\theta = \theta_{wet} - \theta_{dry} = 0.34$$

$$K_{dry} = 8E-11 \text{ cm/s} = 0.03 \text{ mm/y}$$

$$K_{wet} = q_{in} = 1.0 \text{ mm/y}$$

The calculated vertical wetting-front velocity is:

$$V_z = \frac{dz_f}{dt} \approx \frac{K_{wet} - K_{dry}}{\theta_{wet} - \theta_{dry}} = 2.89 \text{ mm/y}$$

The vadose zone residence time within the Hf2 unit (medium homogeneity limitation) is:

$$t = \frac{L}{V_z} = \frac{30.5 \text{ m}}{3 \text{ mm/y}} \approx > 10,000 \text{ y}$$

The one-dimensional (1-D) advective-dispersive equation (ADE) for $C(z,t)$ is:

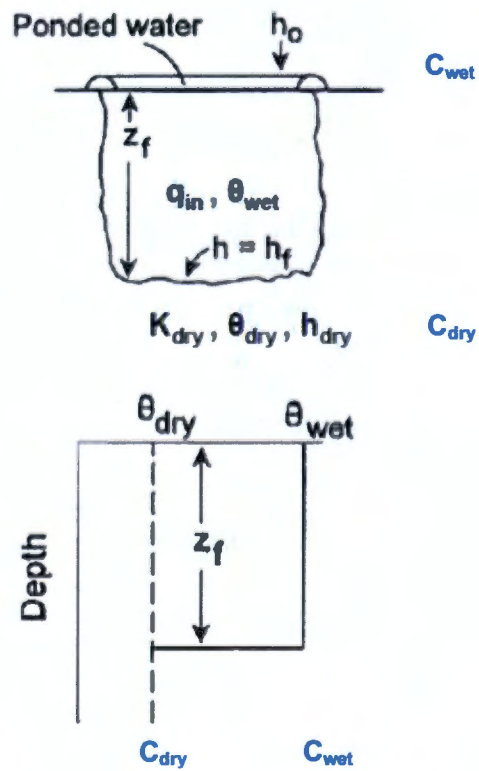
$$\frac{\partial C(z,t)}{\partial t} = D_L \frac{\partial^2 C(z,t)}{\partial z^2} - V \frac{\partial C(z,t)}{\partial z}$$

With C_{wet} =leachate concentration and C_{dry} =initial concentration, the solution for 1-D ADE is:

$$\frac{C(z,t) - C_{dry}}{C_{wet} - C_{dry}} = 0.5 \left\{ \operatorname{erfc} \left[\frac{z - Vt}{2\sqrt{D_L t}} \right] + \exp \left(\frac{Vz}{D_L} \right) \operatorname{erfc} \left[\frac{z + Vt}{2\sqrt{D_L t}} \right] \right\}$$

For the velocity estimate, the predicted relative concentration ratio ~ 0 at 1,000 years at the Hf2 bottom.

Figure D-13. ERDF Diffuse Recharge Sharp Wetting-Front Model.



D.3.2 Diffuse Recharge Horizontal Movement

We now consider the horizontal movement (Figure D-14). The θ -based Richards' equation for moisture movement, without the gravity term, is:

$$\frac{d\theta}{dt} = D(\theta) \frac{\partial^2 \theta}{\partial x^2}$$

where x is the horizontal distance and the soil moisture diffusivity is

$$D(\theta) = K(\theta) \frac{dh}{d\theta}$$

and h is matric potential and the soil moisture capacity is given by

$$\frac{dh}{d\theta}$$

The solution for $\theta(x,t)$ is (Warrick 2003):

$$\frac{\theta(x,t) - \theta_{dry}}{\theta_{wet} - \theta_{dry}} = \left\{ \operatorname{erfc} \left[\frac{x}{2\sqrt{D(\theta)t}} \right] \right\}$$

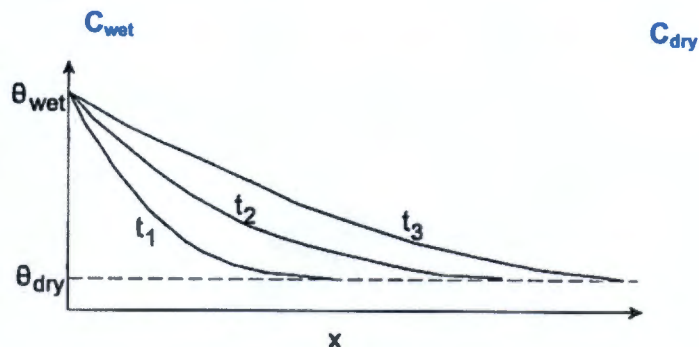
For Hf2, at $\theta=0.05$, $K(\theta)=9.4E-16 \text{ cm s}^{-1}$, $dh/d\theta=4.8E+06 \text{ cm}$, and $D(\theta)\sim 4.51E-09 \text{ cm}^2\text{s}^{-1}$. The estimated normalized $\theta \sim 0$ at $x=10 \text{ m}$ and $t=1000 \text{ yr}$. Without gravity, the penetration distance laterally for the sharp front is $< 1.5 \text{ m}$. The solution for $C(x,t)$ is (Freeze and Cherry 1979):

$$\frac{C(x,t) - C_{dry}}{C_{wet} - C_{dry}} = \left\{ \operatorname{erfc} \left[\frac{x}{2\sqrt{D_{diff}t}} \right] \right\}$$

For a diffusion coefficient of $10^{-10} \text{ m}^2/\text{s}$, the predicted normalized concentration ~ 0 at $x = 10 \text{ m}$ and $t = 1,000 \text{ years}$.

The preceding calculations show that, for a diffuse recharge of 1 mm/yr for 500 years , the moisture accumulation within the ERDF facility has a negligible impact on flow and contaminant transport in a low-moisture environment.

Figure D-14. ERDF Diffuse Recharge Horizontal Movement Model.



D.3.3 Buried Point Source Model and Travel Times

Figure D-15 illustrates the buried point source model. The basic equation of the quasi-linear analysis of three-dimensional (3-D) steady unsaturated flow is (Philip 1984):

$$\nabla^2 \Theta = \alpha_{Gardner} \frac{\partial \Theta}{\partial z}$$

where the vertical z coordinate is positive downward, and the matric flux potential Θ is:

$$\Theta = \int_{-\infty}^{\psi} K d\psi$$

where K is the unsaturated hydraulic conductivity and ψ is the matric potential, consistent with Philip's notation. The parameter $\alpha_{Gardner}$ enters through the Gardner (1958) exponential approximation to $K(\psi)$

$$K(\psi) = K_0 \exp(\alpha_{Gardner} \psi)$$

which is an essential ingredient of the quasi-linear approximation. We locate a point source of strength Q at $(s, z) = (0, 0)$, with s denoting the horizontal radial coordinate. As indicated in Figure D-16(a), we use spherical polar coordinates r, ϕ , where

$$r \sin \phi = s \quad r \cos \phi = z.$$

The dimensionless solution (Figure D-16(b)) for travel times is (Philip 1984):

$$T(R, Z) = \frac{R \exp[R-Z]}{R+Z} \cdot \left\{ R^2 - R + 0.5 \left[\ln \frac{R+Z}{2R} - (R-Z) + 1 \right] \cdot \ln \frac{2R(\exp[R-Z] - [R+Z])}{R-Z} + 0.5 \left[L \left(\frac{2R}{R+Z} \exp[R-Z] \right) - L \left(\frac{2R}{R+Z} \right) \right] \right\} \quad |Z| < R$$

where the dimensionless T , R and Z , and the dilogarithm L are given by

$$T = \frac{\alpha_{\text{Gardner}}^3 Q t}{16 \pi \Delta \theta}$$

$$R = \frac{\alpha_{\text{Gardner}} r}{2}$$

$$Z = \frac{\alpha_{\text{Gardner}} z}{2}$$

$$L(x) = \int_1^x \frac{\ln x}{x-1} dx$$

The bounding solutions, i.e., the maximum and minimum travel times for fixed R lie on $\phi = \pi$ and $\phi = 0$, respectively, or, equivalently, $Z = \mp R$.

For $\phi = 0$

$$\frac{\partial T}{\partial R} = \frac{2R^2}{1+2R}$$

With the integral

$$T = \frac{1}{2}(R^2 - R) + \frac{1}{4} L_n(1+2R)$$

For $\phi = \pi$

$$\frac{\partial T}{\partial R} = 2R^2 e^{2R}$$

With the integral

$$T = \frac{1}{2} [e^{2R}(1-2R+2R^2) - 1]$$

The Gardner α is the slope of the unsaturated hydraulic conductivity (K) - matric potential relation (Figure D-17). The dimensionless travel time T is proportional to the third power of Gardner α , and is therefore a key parameter in Philip's model. A Hanford Site database exists for Gardner α ; the database consists of 79 sandy and gravelly samples (Khaleel and Relyea 2001).

The calculations below are for dimensionless travel time T , $\phi=0$, $Q=Q_{max}/2$, where $Q_{max}=68.3 \text{ m}^3/\text{yr}$; the Gardner α estimate is based on values reported in Khaleel and Relyea (2001). The Q_{max} estimate is for an ERDF cell size of 7.3 ha (18 acres), leak area being 7.6 by 7.6 m (25 by 25 ft), and an infiltration rate of 1 mm/yr for 500 years yielding a leachate volume of 9×10^6 gal.

$$T = \frac{\alpha_{Gardner}^3 Q t}{16 \pi \Delta \theta}$$

$$R = \frac{\alpha_{Gardner} r}{2}$$

$$T = \frac{1}{2}(R^2 - R) + \frac{1}{4} \text{Ln}(1 + 2R)$$

$$r \cos \phi = z \quad \phi = 0 \quad r = z$$

$$\alpha_{Gardner} = 0.00131 / \text{cm} = 0.131 / \text{m}$$

$$Q = (1/2) 68.3 \text{ m}^3 / \text{yr}$$

$$\Delta \theta = 0.34$$

$$VZ_{Thickness} = 60 \text{ m}$$

$$t_{VZ} \approx 1412 \text{ yr}$$

Results were checked against Philip's graphical solution (Figure D-16(b)). The above travel time of 1,412 years represents the minimum residence time; the mass center (first moment) is therefore further up in the vadose zone. Equations are linear for Q so we can scale up or down. For example, for Q_{max} , the minimum residence time is 706 years. The three-dimensional point source model accounts for dimensionality but does not include, as discussed later, the impact of large field-scale processes induced by media heterogeneities. As discussed in Section D.3.4, the field-scale heterogeneities ignored in Philip's solution control the evolving moisture plume originating from a point source leak.

Figure D-15. ERDF Buried Point Source Model (a) Plan View and (b) Vertical Cross Section.

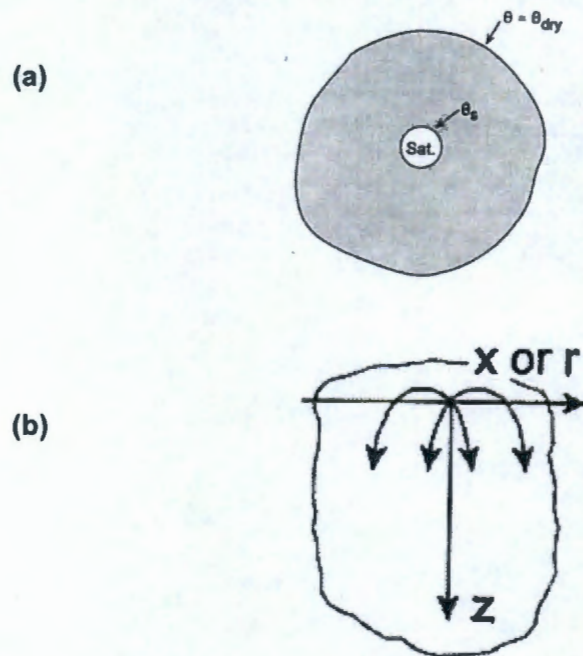


Figure D-16. ERDF Buried Point Source Model (a) Spherical Coordinate System and (b) Dimensionless Travel Time T - Dimensionless R Graphical Solution, B= Buried Source, S=Surface Source (after Philip 1984).

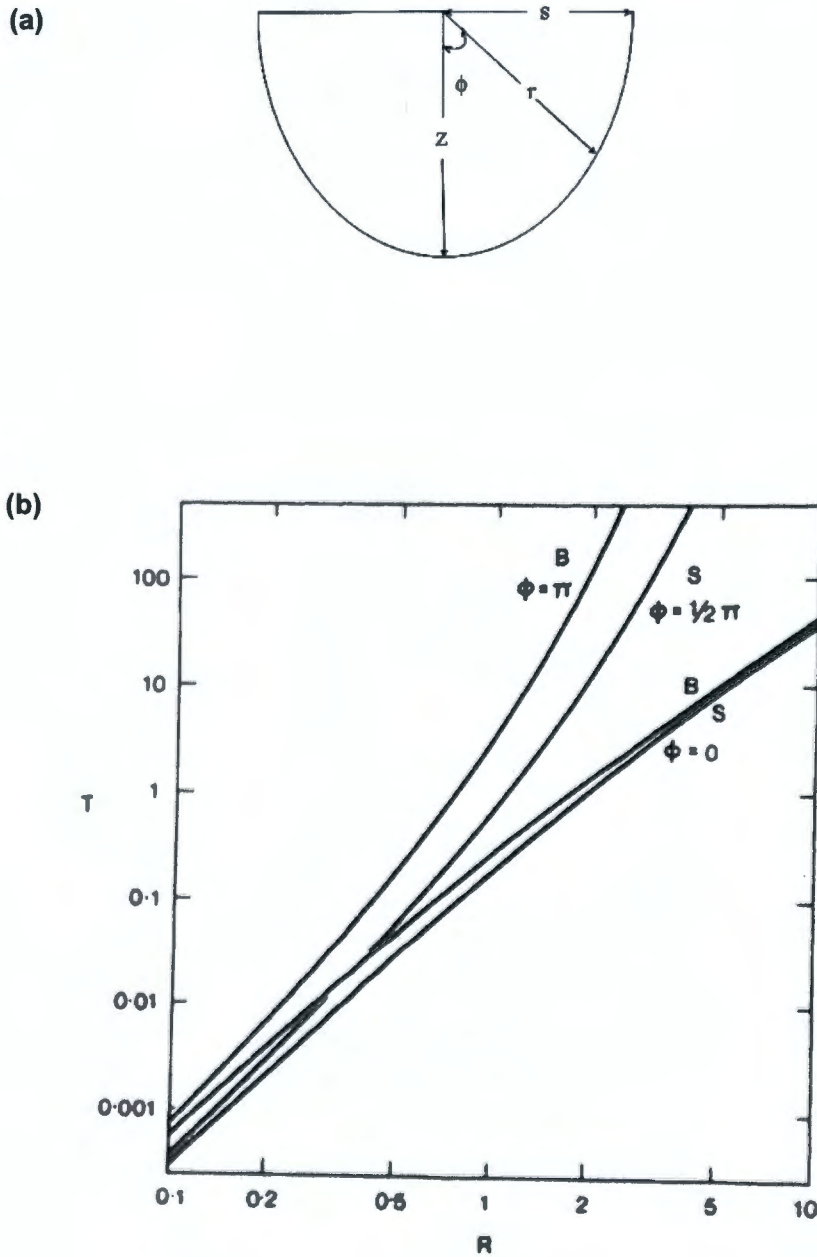
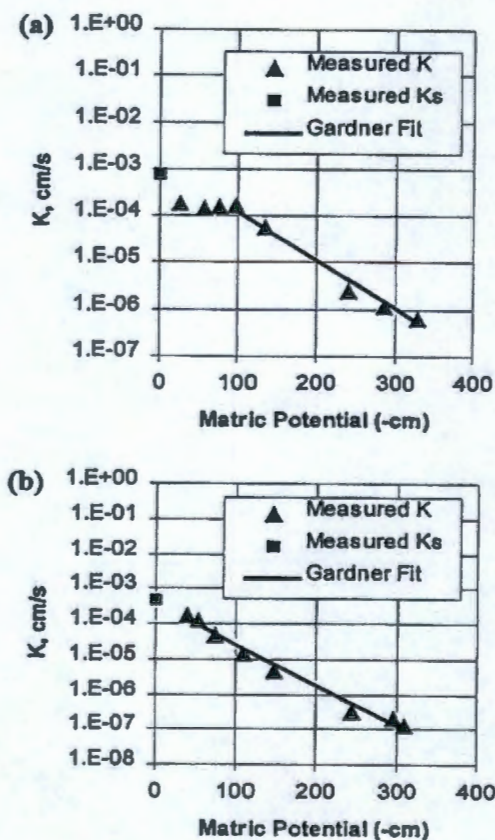


Figure D-17. Measured Saturated and Unsaturated Hydraulic Conductivity for (a) a Sandy Sample and (b) a Gravelly Sample (after Khaleel and Relyea 2001).



D.3.4 BC Cribs and Trenches Site

The BC Cribs and Trenches, directly east of ERDF in the 200 East Area (Figures D-18 and D-19), are believed to have received about 30 Mgal of scavenged tank waste containing an estimated 400 Ci of technetium-99. The BC Cribs and Trenches site is composed of 20 trenches and 6 cribs over an area of approximately 20 ha. Of particular interest is the 216-B-26 trench (Figure D-19) because of its relatively heavy loads of both highly mobile contaminant (nitrate and technetium) and those of low mobility (plutonium, strontium, and cesium). The trench was operated from February to April 1957 and received approximately 5,880 m³ of liquid. The discharges from multiple trenches appear to have comeingled to form a single plume and behaved as discharge from a point source away from the source area (PNNL-14907).

Figure D-18. BC Cribs and Trenches Site Location in the 200 East Area.

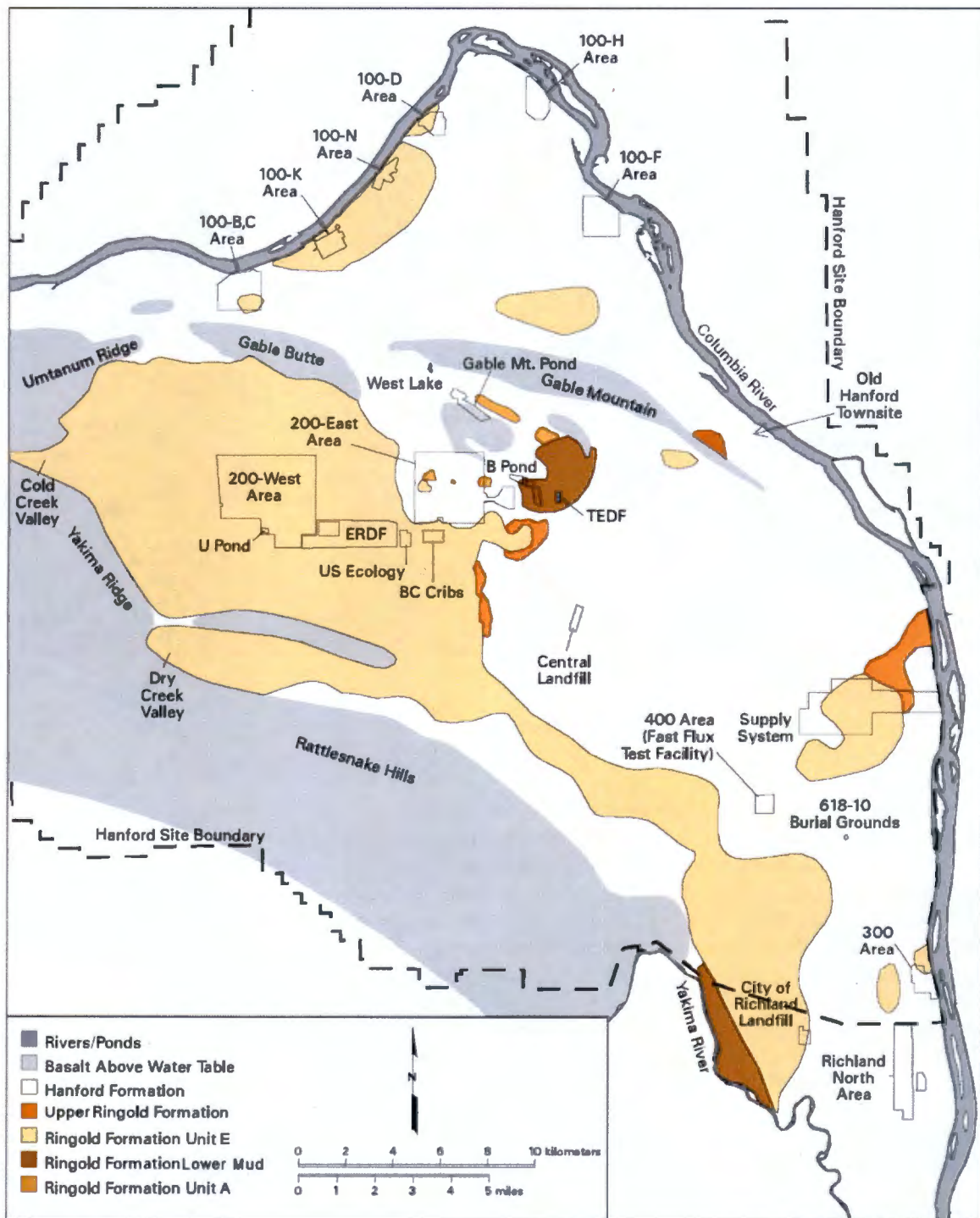
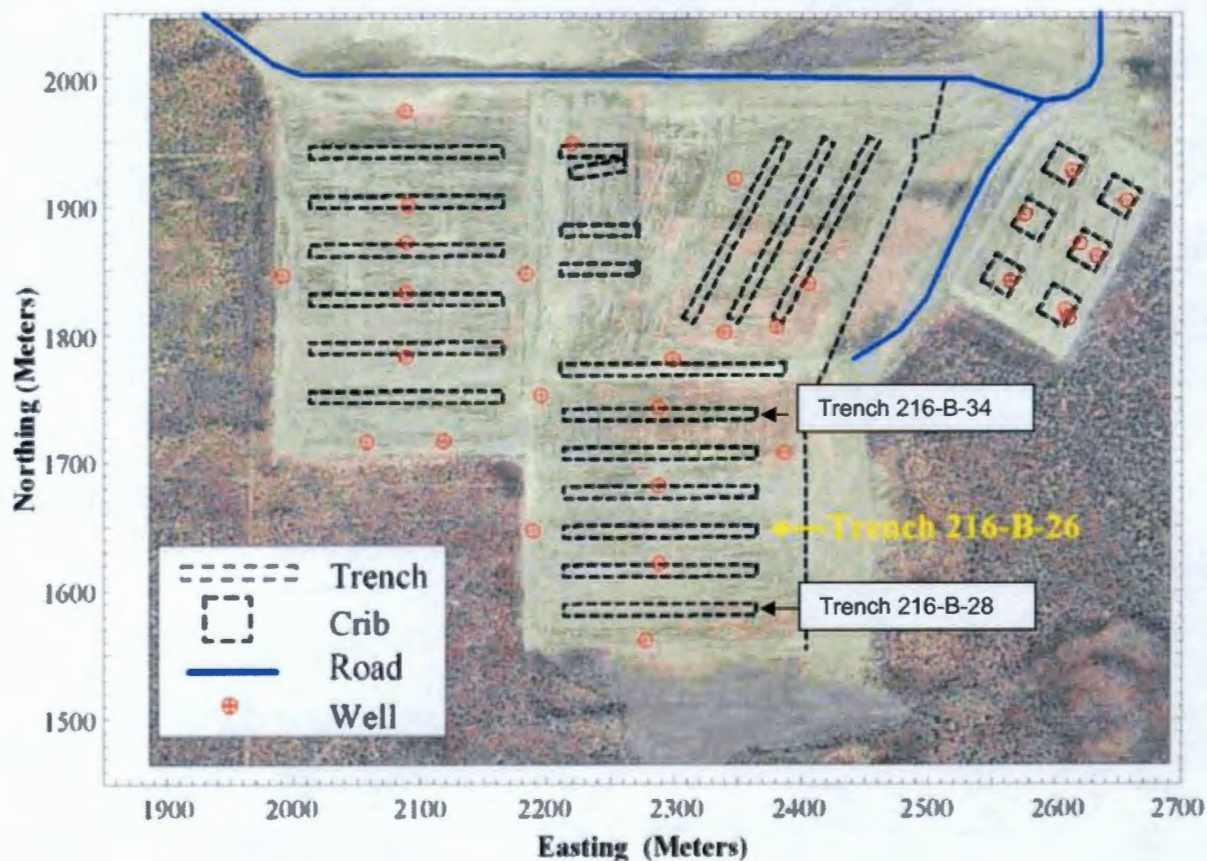


Figure D-19. BC Cribs and Trenches in the 200 East Area.



In February 2004 a characterization borehole, labeled C4191, was drilled near the 216-B-26 trench (Figure D-19); the borehole characterization data provided significant insight on the impact of media heterogeneities and the spatial distribution of contamination within the vadose zone. A fine-scale three-dimensional STOMP model was developed for the BC Cribs and Trenches site (PNNL-14907). The STOMP vadose zone model included (1) small-scale media heterogeneities and changes in lithostratigraphy (Figure D-20), (2) tilted layers to accommodate the natural slope for different geologic units, and (3) lateral spreading along multiple strata with contrasting physical and hydraulic properties. The STOMP modeling predictions of the current plume distribution are remarkably similar to field observations (Figure D-22). Both site characterization data (Figure D-21) as well as STOMP modeling results (Figure D-22) suggest considerable lateral migration and contamination residing well within the vadose zone, and high above the water table, even after 47 years since disposal.

The plumes illustrate the impact of “built-in” capillary breaks and macroscopic field-scale processes which Philip’s solution ignores. Consequently, Philip’s analytical solution significantly overestimates the vertical movement for the catastrophic point source leak albeit providing sufficiently long vadose zone residence times. The field data as well as the STOMP modeling results show a strong correlation of moisture content (θ) and contaminant concentration (C) with sediment texture, i.e., a higher θ and a higher C for the fine-textured sediments and a smaller θ and a smaller C for the coarse-textured sediments (Figures D-21 and D-22).

Figure D-21. Observed and Predicted Profile of Sediment Volumetric Moisture Content Through the Center of Trench 216-B-26 in 2004 (after PNNL-14907).

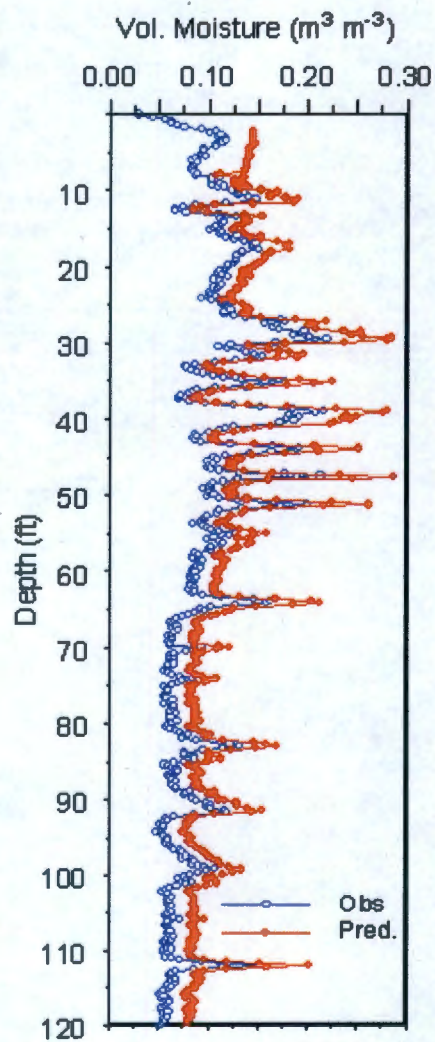
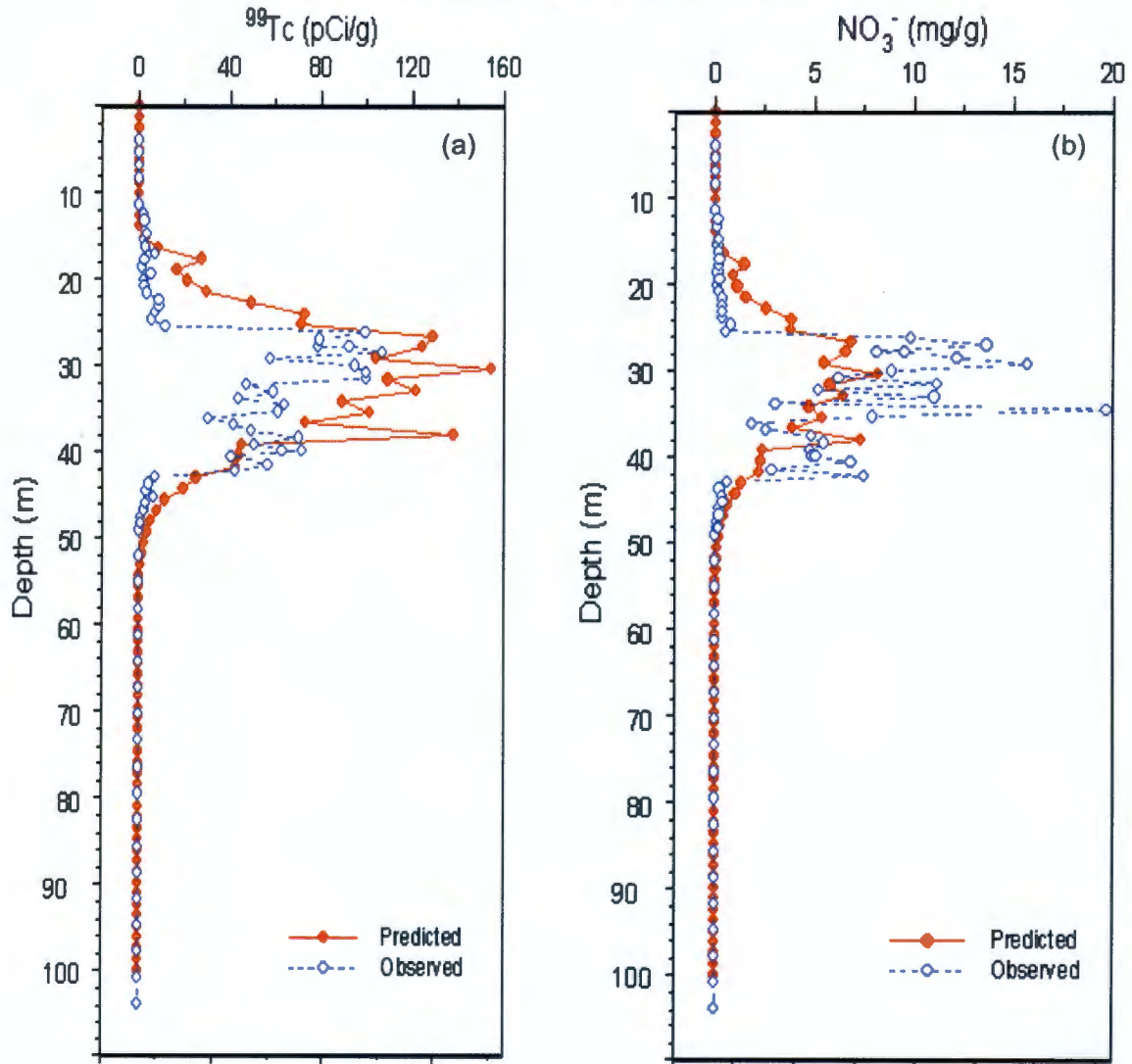


Figure D-22. Observed and Predicted Distributions in Year 2005 at Borehole C4191 for (a) Technetium-99, and (b) Nitrate. (Predicted values are based on STOMP modeling reported in PNNL-14907.)



Note that even though Philip's 3-D solution does not account for field-scale media heterogeneities, it does account for dimensionality. Philip's solution, however, is also linear with respect to source strength (Q). Using a combination of ERDF PA analytical solution results and the BC Cribs and Trenches characterization data (which incorporate field-scale processes), we can scale the BC Cribs center of mass data for the ERDF scenario. Such a scaling on the basis of comparison of source strength (Q) for the BC Cribs and Trenches with the ERDF water accumulation point source solution (which ignores field-scale processes) suggests a center of mass for the ERDF scenario to be of the order of approximately 10 m below the leak site.

At the BC Cribs and Trenches site, the presence of small-scale textural discontinuities (Figure D-20) is responsible for the variations in moisture contents observed in the neutron-probe measurements (Figure D-21). These heterogeneities led to the development of complex flow networks whose impacts dominate flow and transport at the field scale. Changes in saturation can impact the subsurface flow network, thereby influencing the spatial correlation structure of relative permeability and the location of fast paths. This suggests that, unlike Philip's point source model, contaminant transport is much more strongly dependent on saturation and in a way more complicated than the simple effect on the pore-water velocity. In such systems, the magnitude of lateral spreading observed would strongly depend on the flow regime and have important consequences for field-scale transport (PNNL-14907).

In addition, the BC Cribs and Trenches site characterization data as well as the STOMP modeling results provide valuable insight on the long-term persistence of ERDF "what if" water accumulation scenarios. A massive ERDF leak scenario or discharge, as with the BC Cribs and Trenches, would show preferential lateral movement initially due to a combination of large lateral matric potential gradients and large horizontal saturated conductivities. Even though saturation- or moisture-dependent anisotropy (Appendix A) predicts an increased tendency for lateral migration, the unsaturated hydraulic conductivity at low moisture contents can eventually be too low to significantly affect redistribution at the low matric potential gradients. This is of particular importance for the fine-textured lenses that show higher moisture contents in the field (Figure D-21). Even though the unsaturated hydraulic conductivity is higher in such cases than that of drier adjacent sands, the actual values of conductivity are such that continued lateral migration would be at very low rates (PNNL-14907). However, at the same time, significant vertical migration would also require conditions that are wet enough to overcome the natural capillary breaks. The BC Cribs and Trenches site flow domains that were accessible during the initial high-flux discharges may thus become relatively inaccessible with desaturation (PNNL-14907). These flow domains may again become accessible to infiltrating moisture only if saturations and fluxes similar to those at the time of trench operations reoccur. Like ERDF, this appears unlikely under current and expected recharge scenarios for the BC Cribs and Trenches site. This combination of factors explains why technetium-99, 47 years after being discharged to the shallow subsurface, is still over 50 m above the water table at the BC Cribs and Trenches site.

Thus, unlike the ERDF point source model in which heterogeneities and stratigraphic changes are ignored, the mobile species (technetium-99 and nitrate) migrated laterally and remained high above the water table, even after 47 years since disposal (PNNL-14907). Unlike the STOMP model, the three-dimensional point source model assumed that the geologic units were homogeneous and isotropic, although in reality, these units display a complex small-scale structure. As documented and described in Appendix A, the dominant effect of these complex structures and structural heterogeneities is to enhance lateral spreading and impede downward migration. Thus, unlike the point source modeling, an accurate simulation of flow and transport

must account for the small-scale stratigraphy with adequate description of moisture-dependent anisotropy mechanisms (Appendix A).

D.4 DUST-SUPPRESSION MOISTURE PERSISTENCE

The application of dust-suppression water is an integral component of ERDF operations. Using a combination of a wetting-front model as well as field data, we evaluate the long-term persistence of moisture profiles from application of dust-suppression water.

As discussed in Section D.3.1, for a one-dimensional sharp wetting-front model (gravity > capillary effects) and a unit hydraulic gradient condition, the wetting-front velocity V_z , at large t , is:

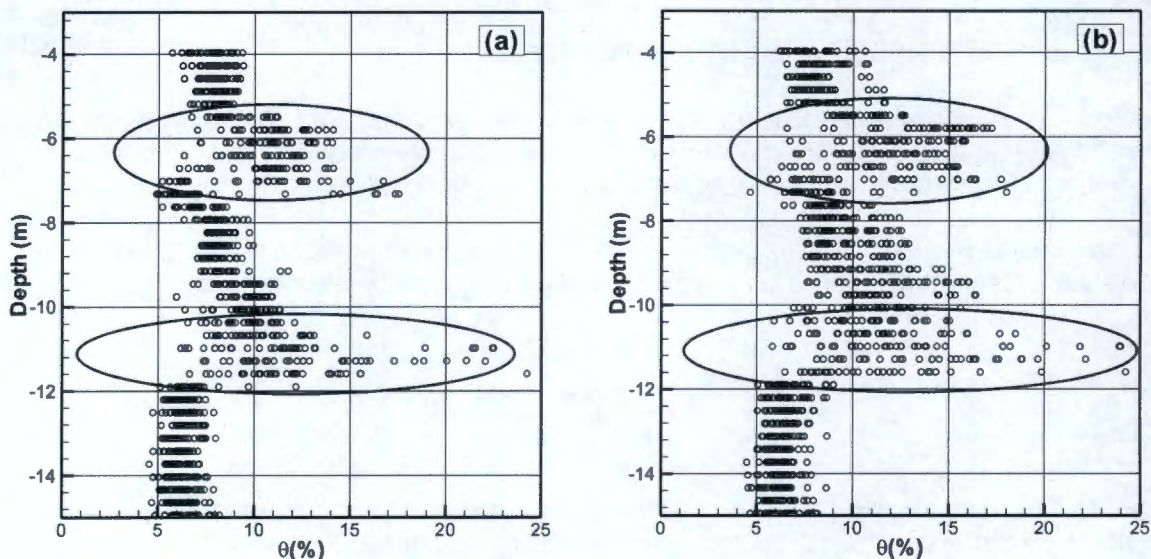
$$V_z = \frac{dz_f}{dt} = \frac{K_{wet} - K_{dry}}{\theta_{wet} - \theta_{dry}} = \frac{q_{in} - K_{dry}}{\Delta\theta}$$

Figure D-11 shows the fitted moisture retention and unsaturated conductivity relations used in ERDF PA modeling (Chapter 3.0). Using the preceding equation and Figure D-11 Hf1 (sandy gravel) properties, for an average application rate of 1 cm/yr, the steady-state vertical velocity for the wetting front is 5 cm/yr. This suggests that the residence time for the wetting front within the ERDF (22 m depth and within the Hf1 unit) is about 440 years.

The preceding scenario of one-dimensional vertical migration under a unit gradient condition is, however, overly idealized and grossly conservative for the highly heterogeneous flow domain. As discussed in Section D.3.4 (BC Cribs and Trenches), the one-dimensional wetting-front model ignores the impact of "built-in" capillary breaks and macroscopic field-scale processes including the ubiquitous lateral migration. Any moisture buildup from dust suppression, however, will be significantly impacted by the overwhelming macroscopic field-scale processes. As discussed earlier, because of the macroscopic field-scale processes, the center of mass due to massive discharges from the BC Cribs and Trenches, for example, resides way up in the vadose zone, even 47 years since disposal.

In addition to the BC Cribs and Trenches site characterization data, a further corroboration of negligible long-term persistence of moisture buildup from dust-suppression water is provided by the extensive moisture profile database for the Sisson and Lu field injection site in the 200 East Area (Appendix A). Figure D-23 shows the moisture profiles before and after weekly field injections. The pre- and post-injection moisture plumes are essentially confined within three layers (i.e., two fine-textured layers and a coarse-textured layer that is sandwiched in between the two fine-textured layers). The moisture content profile is in general agreement with the stratigraphic cross-section at the Sisson and Lu site, with larger θ values associated with fine-textured media and smaller values with coarse-textured media. Again, because of natural capillary breaks, there is very little noticeable change in moisture profiles before and after weekly injections and virtually no moisture movement below the bottom ellipse (Figure D-23).

Figure D-23. Pre- and Post-Injection (May 5, 2000 and July 31, 2000) Moisture Plumes for the Sisson and Lu Field Injection Experiment in the 200 East Area (Ye et al. 2005).



The site consists of alternating layers of fine- and coarse-textured units; the two fine-textured units are marked by ellipse.

D.5 ALTERNATE SURFACE BARRIER AND LINER DEGRADATION CONCEPTUAL MODEL EVALUATION

Appendix C of DOE/LX/07-0099&D2/R1, *Work Plan for CERCLA Waste Disposal Alternatives Evaluation Remedial Investigation/Feasibility Study at the Paducah Gaseous Diffusion Plant, Paducah, Kentucky*, applies a gradual failure function to surface barrier and liner failure. For the gradual failure scenario, all components of the waste disposal facility remain intact for 200 years after which the high-density polyethylene (HDPE) geomembrane components of the cap and liner are assumed to begin degrading. Degradation of the HDPE geomembrane is assumed to continue for 400 years (600 years total) after which the compacted clay liners, with a hydraulic conductivity of 1×10^{-6} cm/s, provide the only control on net infiltration out of the liner system. The net infiltration during the period between 200 and 600 years is estimated according to the following equation:

$$F(t) = \frac{f_1 \times f_2}{f_2 + (f_2 - f_1) \times e^{-\alpha(t-t_0)}} \quad \text{Equation 1}$$

where

- $F(t)$ = net infiltration rate at any time t during the gradual failure of the barrier and liner system (m/yr)
- f_1 = average groundwater recharge during the initial period (m/yr)
- f_2 = final groundwater recharge during the new period (m/yr)
- t = time (yr) at which $F(t)$ is estimated
- t_0 = time (yr) at the end of the initial period
- α = barrier/liner degradation constant (1/yr).

In DOE/LX/07-0099&D2/R1, the barrier/liner degradation constant, α , is equal to 0.064 1/yr, which results in net infiltration of the engineered barrier system equaling the failure rate in 400 years. This value was used in this analysis too. Because Equation 1 is not valid if f_1 or f_2 are zero, the average groundwater recharge in the institutional control period for the ERDF evaluation was assigned a value of 1.0E-06 m/yr to approximate zero.

In the ERDF PA analysis, failure of the liner and surface barrier are assumed to occur instantaneously. After 100 years, the liner system stops collecting leachate and net infiltration is controlled only by the surface barrier. After 500 years, the surface barrier is assumed to degrade and allow twice the design net infiltration rate to pass through it. Net infiltration according to two gradual failure scenarios is evaluated and compared to the net infiltration according to the instantaneous failure scenario used in the ERDF PA. The first gradual failure scenario assumes that the net infiltration rate gradually increases from 0 mm/yr to 0.5 mm/yr during the period from 100 years to 500 years after closure, and from 0.5 mm/yr to 1.0 mm/yr during the period from 500 years to 1,000 years after closure. The second gradual failure scenario assumes that the net infiltration rate gradually increases from 0 mm/yr to 1.0 mm/yr during the period from 200 years to 600 years after closure, comparable to the timing of the evaluation in DOE/LX/07-0099&D2/R1.

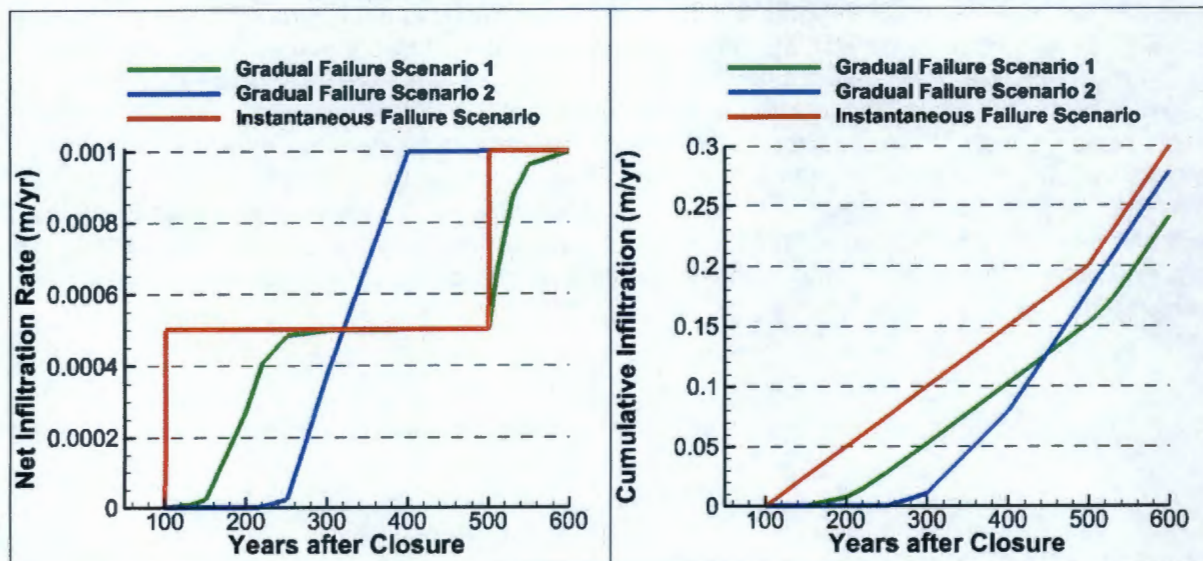
Table D-1 and Figure D-24 display the failure scenario net infiltration rates and cumulative infiltration during the first 600 years after ERDF closure. The differences between the net infiltration rates of the gradual failure scenarios and the instantaneous failure scenario appear to be minor. The increases in net infiltration rates calculated for gradual failure scenario 1 lag the instantaneous jumps observed in the instantaneous failure scenario, but the net infiltration rate during the design life for both scenarios becomes equal approximately 300 years after closure. After the second jump in the instantaneous failure scenario net infiltration rate at the end of the barrier design life, the rates become equal again after approximately 100 years. The increases in net infiltration rates calculated for gradual failure scenario 2 lag the instantaneous jumps observed in the instantaneous failure scenario during the design life of the surface barrier, but lead the instantaneous jumps after its design life. The differences in cumulative infiltration during the first 600 years after closure between gradual failure scenario 1 and gradual failure scenario 2 and the instantaneous failure scenario are 0.06 and 0.02 m, respectively.

The 2-m vertical spacing of the grid and the compliance case value of porosity of the composite material (0.382) used in the STOMP fate and transport model represent a moisture capacity of 0.764 m. Thus, the difference in infiltration rates represents less than 10% of the moisture capacity of the composite layer, with the accumulation of this difference spread over 600 years. Travel time through the vadose zone for the moisture and peak radionuclide flux of the most mobile radionuclides required over 7,000 years; thus, the net infiltration rates have equalized in less than 10% of the time required for transport. Therefore, differences in the results associated with the peak radionuclide concentration in groundwater introduced by gradual failure scenarios are expected to be negligible and further evaluation of gradual failure scenarios is not warranted.

Table D-1. Evaluation of the Net and Cumulative Infiltration Through the ERDF Surface Barrier and Liner System Using Equation 1.

Year of Evaluation	Gradual Failure Scenario 1		Gradual Failure Scenario 2		Instantaneous Failure Scenario	
	Net Infiltration (m/yr)	Cumulative Infiltration (m)	Net Infiltration (m/yr)	Cumulative Infiltration (m)	Net Infiltration (m/yr)	Cumulative Infiltration (m)
0 - 100	0	0	0	0	0	0
101	1.07E-06	1.03E-06	0	0	0.0005	0.0005
110	1.89E-06	1.43E-05	0	0	0.0005	0.005
130	6.74E-06	1.01E-04	0	0	0.0005	0.015
150	2.34E-05	4.02E-04	0	0	0.0005	0.025
200	0.000273	0.00782	0	0	0.0005	0.05
220	0.000406	0.0146	3.59E-06	4.59E-05	0.0005	0.06
250	0.000484	0.0280	2.40E-05	0.000459	0.0005	0.075
300	0.000499	0.0525	0.000376	0.0105	0.0005	0.1
400	0.0005	0.103	0.000997	0.0791	0.0005	0.15
410	0.0005	0.108	0.000999	0.0891	0.0005	0.155
500	0.0005	0.153	0.001	0.179	0.001	0.2
501	0.000516	0.153	0.001	0.180	0.001	0.201
510	0.000655	0.158	0.001	0.189	0.001	0.21
530	0.000872	0.174	0.001	0.209	0.001	0.23
550	0.000961	0.192	0.001	0.229	0.001	0.25
600	0.000998	0.241	0.001	0.279	0.001	0.3

Figure D-24. Net and Cumulative Infiltration Through the ERDF Surface Barrier and Liner System for the Gradual Failure and Instantaneous Failure Conceptual Models.



D.6 CONCLUDING REMARKS

The ERDF is composed of manmade as well as natural components. The manmade components of the system that provide defense in depth and influence contaminant migration include a closure surface barrier, a double-liner leachate collection system, the ERDF cells and infrastructure, and the distribution of waste in the subsurface. The natural components of the system that influence contaminant migration are the several underlying nearly horizontal stratigraphic layers within the vadose zone and the unconfined aquifer. The primary objectives of this appendix were to provide additional supporting material for ERDF closure barrier recharge estimates as well as an evaluation of "what if" scenarios for water accumulation within the ERDF waste disposal facility.

In August 1994, a prototype Hanford barrier, a multilayered capillary barrier with an ET surface layer, was constructed over the 216 B-57 liquid waste disposal crib in the 200 East Area of the Hanford Site. The 15-year continuously collected data and their subsequent analysis for the prototype barrier performance suggests that a 2-m-thick silt-loam layer is sufficient to reduce deep infiltration to negligible levels. With multiple defense in depth as well as capillary break construction, and with moisture held primarily in the adsorption region of the retention curve for the relatively low-moisture regime, water accumulation within the ERDF is not a likely scenario on the basis of soil physics principles. In fact, on the basis of ERDF pore volume considerations, an infiltration of 1 mm/yr for 500 years amounts to an average moisture content (θ) of about 0.025 on a volume basis. Such a θ value is below the residual θ for Hanford Site sediments. In theory, the unsaturated hydraulic conductivity is essentially negligible at or near the residual θ . Nonetheless, we consider "what if" water accumulation and liner failure scenarios. We consider scenarios whereby water somehow manages to get to the sump over an ERDF cell and accumulates. This also assumes the additional unlikely scenario that the ERDF closure barrier is not functioning (e.g., blown away by wind). The catastrophic scenario thus assumes that the liner fails under the accumulated water, and the numerous engineered capillary breaks throughout the disposal facility are ineffective. Results based on water accumulation diffuse recharge as well as point source leak scenarios suggest sufficiently long vadose zone residence times.

The analytical solutions used in "what if" analyses incorporate dimensionality aspects but do not include the impact of large field-scale processes induced by media heterogeneities. As discussed in Appendix A, site characterization data from controlled and uncontrolled field experiments in the 200 East Area as well as the 200 West Area illustrate several important features and processes for the highly heterogeneous Hanford Site sediments. As illustrated by both controlled and uncontrolled field experiments, heterogeneity in unsaturated geologic media is the rule; the evolving moisture plume and therefore the contaminant transport behavior are significantly impacted by media characteristics. These include (a) presence of capillary breaks, (b) state- or moisture-dependent anisotropy, (c) preponderance of lateral flow, (d) fine-textured sediments having higher moisture contents and coarse-textured sediments having lower moisture contents, and (e) a tendency for the moisture regime in heterogeneous sediments equilibrating with natural recharge, in the absence of man-made discharges. Such large-scale field-scale features that are characteristic of heterogeneous sediments in the 200 Areas are considered and incorporated in ERDF PA vadose zone flow and transport models. These field-scale processes are not included, for example, in Philip's analytical solution, and the analytical solutions significantly overestimate the vertical migration albeit providing sufficiently long vadose zone residence times even for catastrophic leaks. Using a combination of ERDF PA analytical solution results and the nearby BC Cribs and Trenches characterization data (which incorporate field-scale processes), we can scale the BC Cribs center of mass for the ERDF water

accumulation scenario. Such scaling on the basis of comparison of source strength for the BC Cribs and Trenches with the ERDF "what if" scenario suggests a center of mass for the "what if" scenario to be less than approximately 10 m below the leak site.

The application of dust-suppression water is an integral component of ERDF operations. Using a combination of a wetting-front analytical model as well as field data, we evaluated the long-term persistence of moisture profiles from application of dust-suppression water. Both analytical solution results and field data (Sisson and Lu field injection site and BC Cribs and Trenches site) suggest that the long-term persistence of moisture buildup from dust suppression within the ERDF facility is negligible.

The assumptions concerning liner and barrier failure appear to be conservative with respect to evaluating radionuclide transport through the vadose zone. Liner and barrier longevity may extend to hundreds of years, and as shown, the potential for excessive water accumulation in ERDF during this time does not appear to exist. There does not appear to be any benefit in evaluating gradual failure scenarios. The differences between the net infiltration rates of the gradual failure scenarios and the instantaneous failure scenario appear to be negligible.

D.7 REFERENCES

- Comprehensive Environmental Response, Compensation, and Liability Act of 1980*,
42 U.S.C. 9601, et seq.
- DOE/LX/07-0099&D2/R1, 2011, *Work Plan for CERCLA Waste Disposal Alternatives Evaluation Remedial Investigation/Feasibility Study at the Paducah Gaseous Diffusion Plant, Paducah, Kentucky*, Appendix C, "Proposed Groundwater Modeling Methodology," U.S. Department of Energy, Paducah, Kentucky.
- DOE/RL-99-11, 1999, *200-BP-1 Prototype Barrier Treatability Test Report*, Rev. 0, U.S. Department of Energy, Richland Operations Office, Richland, Washington.
- Freeze, R. A., and Cherry, J. A., 1979, *Groundwater*, Prentice-Hall, Inc., Englewood Cliffs, New Jersey.
- Gardner, W. R., 1958. "Some Steady State Solutions of the Unsaturated Moisture Flow Equation with Application to Evaporation from Water Table," *Soil Science*, Vol. 85, pp. 228-232.
- Khaleel, R., and J. F. Relyea, 2001. "Variability of Gardner's α for Coarse-Textured Sediments," *Water Resources Research*, Vol. 37, pp. 1567-1576.
- Philip, J. R., 1984, "Travel Times from Buried and Surface Infiltration Point Sources," *Water Resources Research*, Vol. 20, pp. 990-994.
- PNNL-14907, 2004, *Vadose Zone Contaminant Fate and Transport Analysis for the 216-B-26 Trench*, Pacific Northwest National Laboratory, Richland, Washington.
- PNNL-18845, 2011, *200-BP-1 Prototype Hanford Barrier -- 15 Years of Performance Monitoring*, Rev. 1, Pacific Northwest National Laboratory, Richland, Washington.

Resource Conservation and Recovery Act of 1976, 42 U.S.C. 6901, et seq.

Ye, M., R. Khaleel, and T.C.J. Yeh, 2005, "Stochastic Analysis of Moisture Plume Dynamics of a Field Injection Experiment," *Water Resources Research*, Vol. 41, W03013, doi: 10.1029/2004WR003735.

Ward, A., S. Link, C. Wittreich, K. Leary, G. Berlin, and G. Gee, 2010, "Quest for The Perfect Cap: The Prototype Hanford Barrier 15 Years Later -10419," Waste Management Symposium 2010, Phoenix, Arizona.

Warrick, A. W., 2003, *Soil Water Dynamics*, Oxford University Press, New York, New York.

WCH-464, 2013, *Hydrologic Data Package in Support of Environmental Restoration Disposal Facility Performance Assessment Modeling*, Rev. 0, Washington Closure Hanford, Richland, Washington.

APPENDIX E
RECOMMENDATIONS FOR WASTE ACCEPTANCE CRITERIA

TABLE OF CONTENTS

APPENDIX E RECOMMENDATIONS FOR WASTE ACCEPTANCE CRITERIA	E-1
E.1 RECOMMENDED WASTE CONCENTRATION THRESHOLDS FOR RADIONUCLIDES CONSIDERED IN THE DOSE CALCULATION.....	E-1
E.2 RECOMMENDED WASTE CONCENTRATION THRESHOLDS FOR RADIONUCLIDES NOT CONSIDERED IN THE DOSE CALCULATION	E-5
E.3 RECOMMENDED INVENTORY THRESHOLDS FOR RADIONUCLIDES BASED ON GROUNDWATER PATHWAY AND AIR-PATHWAY CALCULATIONS	E-6
E.4 REFERENCES	E-8

TABLES

E-1. Recommended Radionuclide Concentration Thresholds for Waste Disposal in ERDF For Radionuclides Analyzed in the Dose Calculations	E-2
E-2. Radionuclide Concentration Thresholds Calculated at 500-Year Intruder Time (For Information Purpose Only)	E-4
E-3. Recommended Radionuclide Concentration Thresholds for Waste Disposal in ERDF For Radionuclides Not Analyzed in the Dose Calculations With Small Initial Inventory	E-5
E-4. Calculated and Recommended Inventory Thresholds for Radionuclides of Concern.....	E-7

APPENDIX E

RECOMMENDATIONS FOR WASTE ACCEPTANCE CRITERIA

All low-level waste management facilities, such as the Environmental Restoration Disposal Facility (ERDF), are required to have established waste acceptance criteria (WAC) specifying the radionuclide concentration limits and total inventory limits that must be met for all waste being managed in the facility. Based on the performance evaluations presented in Chapter 7.0, the following WAC are recommended for various radionuclides.

E.1 RECOMMENDED WASTE CONCENTRATION THRESHOLDS FOR RADIONUCLIDES CONSIDERED IN THE DOSE CALCULATION

As discussed in Chapter 3.0, a total of 46 radionuclides are considered in the dose calculations. These radionuclides were chosen based on a careful screening process described in WCH-479, *Inventory Data Package for ERDF Waste Disposal*, and Section 3.3. In essence, all radionuclides that were deemed important dose contributors were considered while those that had relatively short half-lives (less than 6 years) or small inventories (less than 1 Ci at closure) were screened out.

The waste concentration thresholds that are recommended for ERDF WAC are based on the inadvertent intruder suburban garden chronic exposure scenario. This scenario provides the most limiting (lowest) concentrations among the various inadvertent intruder scenarios for all radionuclides except for six radionuclides (Ag-108m, Eu-152, Eu-154, Nb-94, Ni-59, and Ni-63). Upon further evaluation it was found that the concentration limits based on suburban garden scenario were only marginally higher, but within the same order of magnitude, as the lowest concentration limit derived from other inadvertent intruder scenarios. Therefore, for the purpose of simplification, only suburban garden scenario-based concentration thresholds are used.

Table E-1 summarizes the waste concentration thresholds for those radionuclides that were considered in the dose calculations. A 100-year inadvertent intruder time was chosen for developing the WAC consistent with the assumption of loss of institutional controls 100 years after closure and the peak dose occurring at 100 years. Note that this table is a subset of Table 7-2, and the calculation methodology is presented in Section 7.2.1.

Most of the radionuclide inventory is present in untreated (bulk soil) waste with minor fraction of some radionuclide inventory associated with activated metal or insoluble material (Table 3-3). The only exception is carbon-14, where the primary inventory resides as insoluble material (graphite). For all radionuclides the threshold concentrations presented in Table E-1, derived from the inadvertent intruder suburban garden chronic exposure scenario, are based on the conservative assumption that all radionuclides are present in the bulk soil (irrespective of the waste form). As a result, the recommended radionuclide concentrations for WAC do not vary by the waste form type.

Waste concentration thresholds presented in Table E-1 are the maximum concentrations of individual radionuclides that lead to a 100 mrem/yr dose, equivalent to the performance measure for an inadvertent intruder chronic scenario. For a mixture of radionuclides, the sum-of-ratios should be computed by calculating the ratio of concentration for a given radionuclide in a given waste stream by the threshold concentration and then summing all the ratios to ensure that it is <1 and the performance objectives are not exceeded.

Although waste concentration thresholds based on 100-year intruder time are recommended for developing WAC, it is possible that more robust waste forms that are different from those assumed in the PA (bulk soil) will be disposed at ERDF. These may include grouted waste forms or macroencapsulated waste forms or those that are disposed in high-integrity containers (HICs). Such waste forms or special packaging may provide enhanced protection to the inadvertent intruder, and therefore increased deterrence time can be used for the purpose of developing WAC for such waste forms or specially packaged material. Assuming a 500-year time period for the intrusion, the concentration thresholds are calculated in Table E-2. These are presented for information purposes only.

Table E-1. Recommended Radionuclide Concentration Thresholds for Waste Disposal in ERDF For Radionuclides Analyzed in the Dose Calculations. (2 Pages)

Analyte ^a	Threshold Concentration	
	(pCi/g)	(Ci/m ³)
Ac-227	2.83E+03	5.89E-03
Ag-108m	6.99E+04	1.45E-01
Am-241	8.25E+04	1.71E-01
Am-243	6.49E+04	1.35E-01
C-14	2.43E+05	5.05E-01
Cd-113m	1.00E+06	2.08E+00
Cl-36	4.32E+03	8.97E-03
Cm-243	8.98E+05	1.86E+00
Cm-244	4.76E+06	9.89E+00
Co-60	7.18E+09	1.49E+04
Cs-137	8.47E+05	1.76E+00
Eu-152	1.23E+07	2.55E+01
Eu-154	1.75E+08	3.63E+02
H3	2.34E+11	4.85E+05
I-129	3.63E+04	7.54E-02
Mo-93	3.35E+05	6.97E-01
Nb-93m	2.82E+09	5.85E+03
Nb-94	5.90E+04	1.23E-01
Ni-59	2.48E+07	5.14E+01
Ni-63	1.97E+07	4.09E+01
Np-237	3.00E+04	6.22E-02
Pa-231	2.29E+03	4.76E-03
Pu-238	1.41E+05	2.92E-01
Pu-239	5.87E+04	1.22E-01

Table E-1. Recommended Radionuclide Concentration Thresholds for Waste Disposal in ERDF For Radionuclides Analyzed in the Dose Calculations. (2 Pages)

Analyte ^a	Threshold Concentration	
	(pCi/g)	(Ci/m ³)
Pu-240	5.92E+04	1.23E-01
Pu-241	3.65E+08	7.59E+02
Pu-242	6.15E+04	1.28E-01
Ra-226	5.04E+03	1.05E-02
Ra-228	1.60E+03	3.33E-03
Se-79	2.19E+05	4.56E-01
Sm-151	2.49E+08	5.16E+02
Sn-121m	3.16E+06	6.57E+00
Sn-126	2.59E+04	5.38E-02
Sr-90	1.05E+05	2.17E-01
Tc-99	2.38E+04	4.94E-02
Th-229	5.13E+03	1.07E-02
Th-230	3.94E+04	8.19E-02
Th-232	2.26E+04	4.69E-02
U-233	2.64E+05	5.48E-01
U-234	2.73E+05	5.67E-01
U-235	2.10E+05	4.37E-01
U-236	2.90E+05	6.02E-01
U-238	2.87E+05	5.97E-01
Zr-93	1.97E+07	4.08E+01

^a Calculations based on inadvertent intrusion occurring at 100 years after closure (assumed loss of institutional controls) for the suburban garden scenario. For K-40 and Rn-222 there is no limit calculated because K-40 occurs naturally in the soils (it was not generated during the Hanford reactor operations) and for Rn-222 (and progeny) there is no dose limit requirement as per DOE O 435.1.

For six radionuclides the threshold concentrations from other inadvertent intruder scenarios were slightly lower than the suburban garden scenario. These radionuclides and their lowest threshold concentrations (given in parenthesis in Ci/m³) are as follows: Ag-108m (1.34E-01); Eu-152 (2.35E+01); Eu-154 (3.36E+02); Nb-94 (1.14E-01); Ni-59 (2.83E+01); and Ni-63 (2.26E+01). These concentrations are marginally different but in the same order of magnitude than the suburban garden-based concentration thresholds presented in this table.

Table E-2. Radionuclide Concentration Thresholds Calculated at 500-Year Intruder Time (For Information Purpose Only). (2 Pages)

Analyte ^a	Threshold Concentration	
	(pCi/g)	(Ci/m ³)
Ac-227	5.37E+02	1.12E-03
Ag-108m	1.36E+05	2.82E-01
Am-241	1.57E+05	3.25E-01
Am-243	6.74E+04	1.40E-01
C-14	2.55E+05	5.30E-01
Cd-113m	2.18E+14	4.52E+08
Cl-36	4.32E+03	8.98E-03
Cm-243	1.10E+10	2.29E+04
Cm-244	1.61E+13	3.34E+07
Co-60	1.06E+27	2.21E+21
Cs-137	7.41E+09	1.54E+04
Eu-152	6.12E+15	1.27E+10
Eu-154	5.29E+21	1.10E+16
H3	7.67E+20	1.59E+15
I-129	3.63E+04	7.54E-02
Mo-93	3.63E+05	7.54E-01
Nb-93m	5.92E+16	1.23E+11
Nb-94	5.97E+04	1.24E-01
Ni-59	2.49E+07	5.16E+01
Ni-63	3.04E+08	6.31E+02
Np-237	2.60E+04	5.41E-02
Pa-231	5.44E+02	1.13E-03
Pu-238	3.28E+06	6.81E+00
Pu-239	5.94E+04	1.23E-01
Pu-240	6.17E+04	1.28E-01
Pu-241	5.87E+16	1.22E+11
Pu-242	6.16E+04	1.28E-01
Ra-226	5.94E+03	1.23E-02
Ra-228	1.60E+03	3.33E-03
Se-79	2.20E+05	4.56E-01
Sm-151	4.42E+09	9.18E+03
Sn-121m	1.64E+09	3.41E+03
Sn-126	2.60E+04	5.39E-02
Sr-90	1.37E+09	2.84E+03
Tc-99	2.38E+04	4.95E-02
Th-229	1.24E+03	2.59E-03
Th-230	1.49E+04	3.10E-02
Th-232	2.26E+04	4.69E-02
U-233	2.64E+05	5.49E-01
U-234	2.71E+05	5.64E-01

Table E-2. Radionuclide Concentration Thresholds Calculated at 500-Year Intruder Time (For Information Purpose Only). (2 Pages)

Analyte ^a	Threshold Concentration	
	(pCi/g)	(Ci/m ³)
U-235	2.10E+05	4.37E-01
U-236	2.87E+05	5.97E-01
U-238	2.87E+05	5.97E-01
Zr-93	1.97E+07	4.08E+01

^a Calculations based on inadvertent intrusion occurring at 500 years after closure for suburban garden scenario. For K-40 and Rn-222 there is no limit calculated because K-40 occurs naturally in the soils (it was not generated during Hanford reactor operations) and for Rn-222 (and progeny) there is no dose limit requirement as per DOE O 435.1.

E.2 RECOMMENDED WASTE CONCENTRATION THRESHOLDS FOR RADIONUCLIDES NOT CONSIDERED IN THE DOSE CALCULATION

For those radionuclides that were screened out from the dose calculations for which a small inventory is estimated at closure (WCH-479), the waste concentration thresholds are considered to be not limiting. Table E-3 summarizes the projected inventory for screened-out radionuclides at the time of closure (derived from WCH-479). The inventory is further decayed by 100 years, the earliest time of inadvertent intrusion, to demonstrate the negligibly small inventory that would be available for any dose calculation. Since the average soil concentrations are calculated by distributing the inventory over the full volume of ERDF, the concentrations are expected to remain negligibly small resulting in a practically zero intruder dose and thereby a very large threshold concentration, which is practically not limiting.

Table E-3. Recommended Radionuclide Concentration Thresholds for Waste Disposal in ERDF For Radionuclides Not Analyzed in the Dose Calculations With Small Initial Inventory. (2 Pages)

Analyte	Half-Life (years) ^a	Projected Inventory (Ci) at Closure (Year 2035) ^b	Projected Inventory (Ci) at Time of Intrusion (Year 2135) ^b	Threshold Concentration
Am-242m	1.41E+02	2.67E-01	1.63E-01	Not Limiting
Ba-133	1.05E+01	1.03E+00	1.40E-03	
Be-7	1.46E-01	0.00E+00	0.00E+00	
Bi-207	3.16E+01	0.00E+00	0.00E+00	
Ca-41 ^c	1.02E+05	3.00E-01	3.00E-01	
Ce-144	8.00E-01	0.00E+00	0.00E+00	
Cf-249	3.51E+02	8.58E-04	7.04E-04	
Cf-252	2.65E+00	0.00E+00	0.00E+00	
Cm-242	4.46E-01	0.00E+00	0.00E+00	
Cm-245	8.48E+03	0.00E+00	0.00E+00	
Cm-246	4.76E+03	0.00E+00	0.00E+00	
Cm-247	1.56E+07	0.00E+00	0.00E+00	
Cm-248	3.48E+05	0.00E+00	0.00E+00	
Co-58	1.94E-01	0.00E+00	0.00E+00	

Table E-3. Recommended Radionuclide Concentration Thresholds for Waste Disposal in ERDF For Radionuclides Not Analyzed in the Dose Calculations With Small Initial Inventory. (2 Pages)

Analyte	Half-Life (years) ^a	Projected Inventory (Ci) at Closure (Year 2035) ^b	Projected Inventory (Ci) at Time of Intrusion (Year 2135) ^b	Threshold Concentration
Cs-134	2.07E+00	2.51E-03	0.00E+00	Not Limiting (cont.)
Cs-135	2.30E+06	3.00E-02	3.00E-02	
Eu-150	3.60E+01	1.26E-04	1.84E-05	
Eu-155	4.76E+00	5.77E+00	2.74E-06	
Fe-55	2.73E+00	4.06E-02	0.00E+00	
Fe-59	1.23E-01	0.00E+00	0.00E+00	
Kr-85	1.07E+01	8.49E-02	1.31E-04	
Mn-54	8.54E-01	0.00E+00	0.00E+00	
Na-22	2.61E+00	0.00E+00	0.00E+00	
Pb-210	2.26E+01	0.00E+00	0.00E+00	
Pd-107	6.50E+06	9.00E-03	9.00E-03	
Pm-147	2.62E+00	1.09E-01	0.00E+00	
Po-209	1.28E+02	0.00E+00	0.00E+00	
Pu-244	8.00E+07	0.00E+00	0.00E+00	
Re-187	4.16E+10	0.00E+00	0.00E+00	
Ru-103	1.07E-01	0.00E+00	0.00E+00	
Ru-106	1.02E+00	0.00E+00	0.00E+00	
Sb-125	2.76E+00	3.60E-02	0.00E+00	
Sb-126	3.30E-02	0.00E+00	0.00E+00	
Sn-113	3.15E-01	0.00E+00	0.00E+00	
Th-228	1.91E+00	3.34E-05	0.00E+00	
Th-234	6.60E-02	0.00E+00	0.00E+00	
Ti-44	5.90E+01	1.51E-05	4.67E-06	
U-232	7.00E+01	0.00E+00	0.00E+00	
Zn-65	6.68E-01	0.00E+00	0.00E+00	

^a Source: Haynes and Lide, 2011, *CRC Handbook of Chemistry and Physics 92nd Edition*, CRC Press, Boca Raton, Florida.

^b When projected inventory is estimated to be less than 1E-06 Ci then it is set to zero.

^c Calcium-41 is screened out as it is associated with impurities present in graphite and silica gel desiccant in trace quantities and will not be available freely.

E.3 RECOMMENDED INVENTORY THRESHOLDS FOR RADIONUCLIDES BASED ON GROUNDWATER PATHWAY AND AIR-PATHWAY CALCULATIONS

A summary of the calculated and recommended inventory thresholds for the radionuclides of concern is presented in Table E-4 based on the evaluation of both groundwater and air-pathway inventory thresholds. The calculated inventory thresholds are based on the compliance time period (year 2035 to 3035) as reported in Tables 7-3 and 7-4. Since the dose calculated within the compliance time period is derived only from the air pathway, the threshold concentrations for carbon-14, iodine-129, and hydrogen-3 are calculated based on effective dose equivalent limit of 10 mrem/yr for the air pathway.

The dose contribution along the groundwater pathway within the compliance time period is zero, and thus the inventory thresholds for groundwater contributing radionuclides is indeterminate and therefore "not limiting." Where inventory thresholds are indeterminate within the compliance time period they are recommended based on the post-compliance inventory threshold limits based on all-pathway effective dose equivalent limit of 25 mrem/yr. The post-compliance period inventory thresholds based on maintaining safe drinking water concentrations in groundwater are not recommended because (a) the peak concentrations are not likely to occur until after 6,500 years, (b) it is unlikely that the receptor will be drinking water exactly at the time of peak concentrations from the well located 100 m downgradient from ERDF, and (c) the well pumping effects would lead to mixing with uncontaminated water within the cone of depression in the aquifer causing much lower actual concentrations in the borehole than are predicted based on the conservative assumption of no pumping considered in this PA.

Iodine-129 is the only radionuclide that is present in both the groundwater pathway and air-pathway inventory threshold calculations. The air-pathway inventory thresholds for iodine-129 are much lower than for the groundwater pathway inventory thresholds and it is considered as the final inventory threshold for iodine-129.

The peak concentrations for radionuclides in the two pathways (air and groundwater) are separated by a significant amount of time and therefore inventory thresholds should not be combined. For a mixture of radionuclides, the sum-of-ratios should be computed separately for each pathway to ensure that it is <1 and the performance objectives for each pathway are not exceeded.

Table E-4. Calculated and Recommended Inventory Thresholds for Radionuclides of Concern.

Radionuclide	Calculated Inventory Thresholds (Ci)	Recommended Inventory Thresholds (Ci)
Tc-99	Not Limiting	724 ^a
Nb-94	Not Limiting	349 ^a
Mo-93	Not Limiting	811 ^a
Cl-36	Not Limiting	342 ^a
I-129	4	4 ^b
C-14	2.43E+04	2.43E+04 ^b
H-3	1.15E+06	1.15E+06 ^b

^a Inventory thresholds based on all-pathway effective dose equivalent limit of 25 mrem/yr (Table 7-3).

^b Inventory thresholds based on air-pathway effective dose equivalent limit of 10 mrem/yr (Table 7-4).

E.4 REFERENCES

Haynes, W. M. and D. R. Lide, eds., 2011, *CRC Handbook of Chemistry and Physics*, 92nd Edition, CRC Press, Boca Raton, Florida.

WCH-479, 2013, *Inventory Data Package for ERDF Waste Disposal*, Rev. 1, Washington Closure Hanford, Richland, Washington.

DISTRIBUTION

U.S. Department of Energy
Richland Operations Office

R. D. Hildebrand (1 CD only)	A6-38
O. C. Robertson (1 CD only)	A3-04

Washington Closure Hanford

J. F. Armatrout	T2-03
W. A. Borlaug	T2-03
M. A. Casbon	T2-03
R. J. Landon	H4-21
B. L. Lawrence	T2-03

CH2MHILL Plateau Remediation Company

S. Mehta (1 CD only)	H8-51
----------------------	-------

Document Control	H4-11
------------------	-------

